Discovery of BUB1 kinase inhibitors for the treatment of cancer

Bosman, R.E.J.

Discovery of BUB1 kinase inhibitors for the treatment of cancer

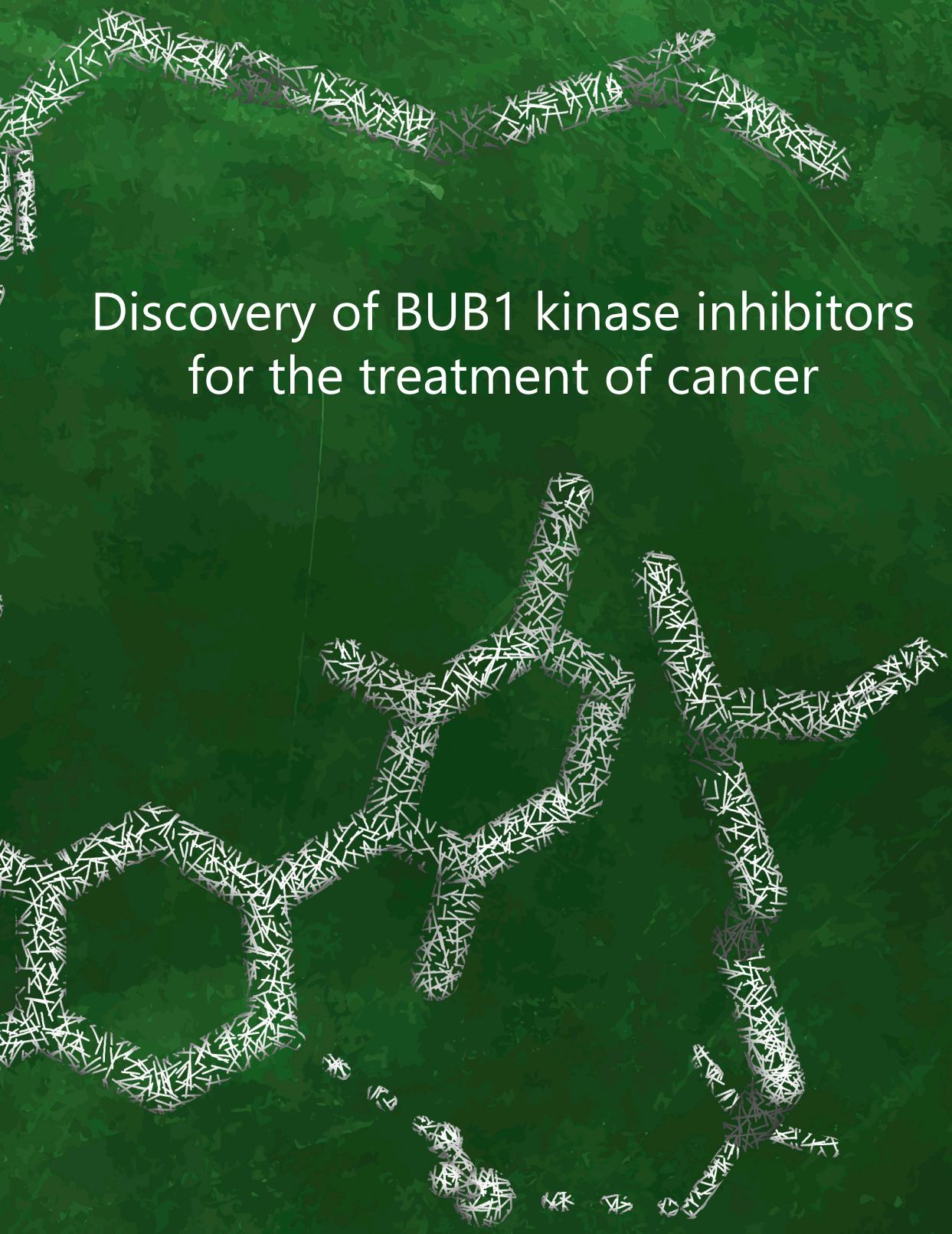

Robertus E.J. Bosman

Discovery of BUB1 kinase inhibitors for the treatment of cancer

Proefschrift

ter verkrijging van
de graad van doctor aan de Universiteit Leiden,
op gezag van rector magnificus prof.dr.ir. H. Bijl,
volgens besluit van het college voor promoties
te verdedigen op donderdag 29 september 2022
klokke 10:00 uur

door

Robertus Eduardus Johannes Bosman

geboren te Delft
in 1993

Promotiecommissie

Promotores:	Prof. dr. M. van der Stelt
	Prof. dr. C.A.A. van Boeckel
Co-promotor:	Dr. R.C. Buijsman *Netherlands Translational Research Center (NTRC)*
Promotiecommissie:	Prof. dr. H.S. Overkleeft
	Prof. dr. J.D.C. Codee
	Dr. M.E. Artola Perez de Azanza
	Prof. dr. A. Perrakis *Netherlands Cancer Institute (NKI)*
	Prof. dr. G.J.P.L. Kops *Hubrecht Institute*

ISBN: 978-94-6423-965-2
Cover pattern: www.freepik.com
Printed by: ProefschriftMaken BV

Table of contents

1

General introduction

The spindle assembly checkpoint (SAC)

Eukaryotic cell division is divided into four phases: gap 1 (G_1), synthesis (S), gap 2 (G_2) and mitosis (M) (**Figure 1.1**). In the G_1 phase, cells are metabolically active and grow. In order for a cell to divide, all genetic information needs to be copied and this process occurs during the S phase. In subsequent G_2 phase, cells prepare for mitosis in which duplicated chromosomes are equally divided between the two daughter cells after which the cell cycle starts over. Mitosis itself is subdivided into five distinct phases: prophase, prometaphase, metaphase, anaphase and telophase (**Figure 1.1**). During prophase, chromosomes are highly condensed, centrosomes separate and nuclear envelope breakdown occurs.[1] During prometaphase, the spindle poles are connected to kinetochores, which are located at the centromeres of sister chromatids, and chromosomes align at the spindle equator, which is referred to as the metaphase.[1] Sister chromatids are separated and pulled towards opposite spindle poles during anaphase and in the final stage, the telophase, new nuclear envelopes are formed and DNA decondenses.[1]

The spindle assembly checkpoint (SAC) is one of the cell cycle checkpoints and is active during the prometaphase of mitosis.[2] During this mitotic phase, microtubules must form stable connections between the kinetochores of sister chromatids and spindle poles in a bi-oriented fashion (**Figure 1.2**). Proper kinetochore-microtubule connections are crucial for genomic integrity since mitotic progression with erroneous connections may lead to aneuploid cells which, in turn, might contribute to tumorigenesis.[3] The SAC is responsible for monitoring unattached kinetochores and prevents mitotic progression to the anaphase until fully satisfied (**Figure 1.2**). The anaphase is initiated by the anaphase-promoting complex/cyclosome (APC/C) which requires co-factor CDC20 (cell-division-cycle 20 homologue) to be active.[4] Once activated, APC/CDC20 targets Cyclin B and Securin for proteasomal degradation.[5] Cyclin B degradation inactivates CDK1 (cyclin-dependent kinase 1), which promotes mitotic exit, and destruction of Securin activates Separase, which in turn is required for cleaving Cohesin that holds sister chromatids together. The mitotic checkpoint complex (MCC), consisting of BUBR1 (budding uninhibited by benzimidazole-related 1), BUB3 (budding uninhibited by benzimidazole 3), MAD2 (mitotic arrest deficient 2) and CDC20, inhibits APC/C activation and is therefore crucial for inducing a mitotic arrest.[6] During this arrest, incorrect kinetochore-microtubule attachments can be corrected and unattached kinetochores can be attached to the mitotic spindle. SAC activation by unattached kinetochores results in the recruitment of SAC proteins and kinetochores might act as catalytic platforms to accelerate the production of the MCC.[2] Due to the importance of the MCC to arrest mitosis, the proteins of this complex belong to the core SAC proteins in addition to MAD1, which forms a stable complex with MAD2, as well as several kinases that are required to amplify SAC signaling and rate of MCC formation, including Aurora B, MPS1 (monopolar spindle 1) and BUB1 (budding uninhibited by benzimidazole 1).[2] Other important mitotic proteins that regulate SAC activity include proteins of the RZZ (ROD-ZW10-ZWILCH) complex as well as kinases CDK1-cyclin-B and PLK1 (polo-like kinase 1), among others.[2]

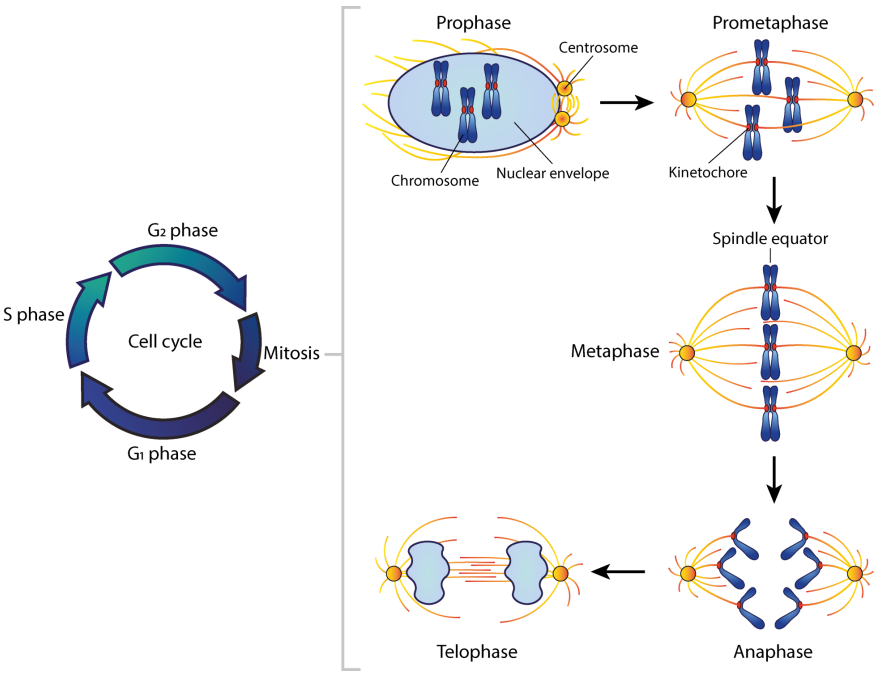

Figure 1.1 | Phases of the eukaryotic cell cycle (left) and schematic representation of mitotic phases (right).

Targeting the SAC has been suggested as potential strategy to kill cancer cells, since many cancer cells suffer from a weakened checkpoint.[3,7] Interference with these diminished checkpoints further disrupts SAC signaling which eventually results in cell death due to severe chromosomal instability.[3] Previously, it has been shown that small interfering RNA (siRNA)-mediated interference with SAC kinases BUBR1 and MPS1 sensitized cancer cells to low doses of paclitaxel in a synergistic fashion.[8,9] MPS1 depletion did not sensitize untransformed human fibroblasts, suggesting a preference for killing cancer cells.[9] Potential SAC kinase targets for small molecule inhibitors include Aurora B, MPS1 and BUB1.

Kinases as drug target

Protein kinases are required for proper SAC functioning and are therefore key players of mitosis.[10] Protein kinases are part of a large enzyme family of over 500 members, referred to as the human kinome[11], which catalyze the transfer of the γ-phosphate of ATP to side chains of serine, threonine and tyrosine residues of substrate proteins. Physiological functions of phosphorylation include enzyme activation, enzyme inhibition, protein localization, protein stabilization and protein degradation.[12] Protein kinases are therefore key regulators of cellular processes. The catalytic domain of kinases, referred to as the kinase domain, is structurally similar across the kinome and contains several conserved elements. The kinase domain consists of two major subdomains, the N-terminal lobe (N-lobe) and C-terminal lobe (C-lobe), which are connected via the so called hinge region (**Figure 1.3**).[12] Whereas the N-lobe predominantly consists of β-strands (β1-β5) and an α-helix (αC-helix), the C-lobe

primarily consists of α-helices.[13] ATP binds in the active site of a kinase which is located in between the two lobes. Binding interactions include hydrogen bonds between the adenine core of ATP and the amide backbone of the hinge region, ionic interactions with a conserved lysine from β3 which is the link between the α- and β-phosphate of ATP and a conserved glutamate present in the αC-helix, additional ionic interactions between the β- and γ-phosphate and the Mg^{2+} ion which is bound to the aspartate of the conserved DFG (Asp-Phe-Gly) motif as well as ionic interactions between the β- and γ-phosphate with glycine residues of the glycine-rich loop present between β1 and β2 (**Figure 1.3**).[14]

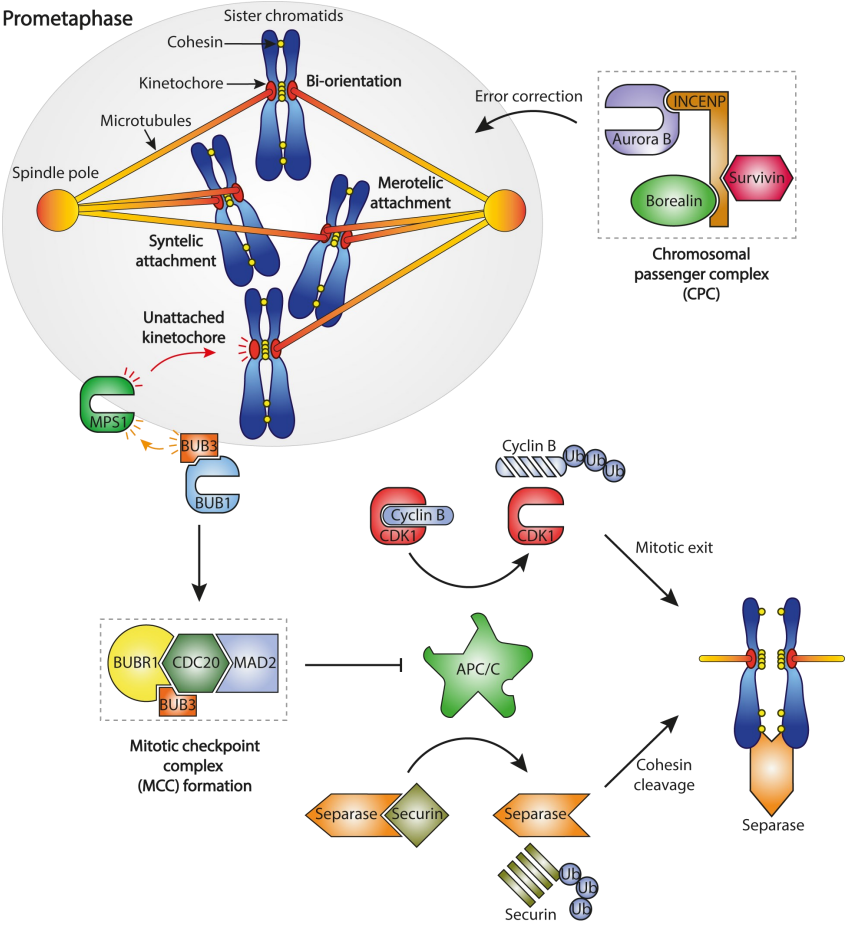

Figure 1.2 | Simplified representation of the prometaphase with different types of kinetochore-microtubule attachments. Unattached kinetochores trigger the recruitment of MPS1, which in turn recruits the BUB1-BUB3 complex. Multiple SAC proteins are subsequently recruited to unattached kinetochores resulting in the formation of the mitotic checkpoint complex (MCC) which consists of BUBR1, BUB3, CDC20 and MAD2. The MCC inhibits the activation of APC/C (which requires CDC20 to be active) thereby causing a mitotic arrest required to correct syntelic and merotelic attachment errors and connect unattached kinetochores to the spindle poles in a bi-oriented fashion. Upon activation of APC/CDC20, Cyclin B and Securin are targeted for proteasomal degradation by polyubiquitination. Cyclin B degradation inactivates CDK1 which promotes mitotic exit. Degradation of Securin activates Separase which cleaves Cohesin that holds sister chromatids together. The chromosomal passenger complex (CPC), consisting of Aurora B, INCENP, Borealin and Survivin, is responsible for correcting attachment errors.[2,15,16]

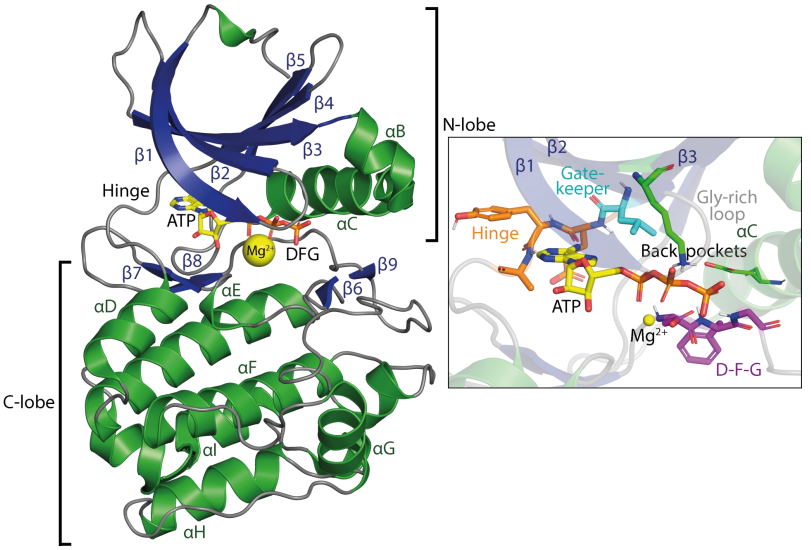

Figure 1.3 | Representation of the general structure of kinases (left) and an enlarged view of ATP binding (right). The crystal structure used for this figure represents Aurora A in complex with ATP (PDB code: 5dn3).[17] Figure generated using PyMOL.[18]

Deregulation of kinase activity, for example due to gene alterations, kinase overexpression or mutations that enhance kinase activity, has been implicated in the pathogenesis of human diseases, including cancer.[19] Counteracting undesired kinase signaling can be achieved by small molecule kinase inhibitors. The majority of kinase inhibitors developed to date bind the ATP-binding pocket and selectivity for a particular kinase can be achieved by exploiting small structural differences to other kinases as well as occupation of kinase back pockets.[20,21] The access to these back pockets is dependent on the conserved lysine in β3 as well as the size of the gatekeeper residue, which resides next to the hinge region (**Figure 1.3**).[12] Off-target activity may contribute to pharmacological side-effects, however, targeting multiple kinases, an phenomenon known as polypharmacology, can also favor efficacy. Kinases have been shown to be prominent drug targets with currently more than 70 kinase inhibitors approved for clinical use.[22] Since the approval of Gleevec, the first kinase inhibitor, in 2001, approval of drugs targeting kinases have steadily increased from about one per year in the period 2001-2006 to almost nine per year in the period 2017-2020.[22] The majority of these kinase inhibitors, about 84%, is used for the treatment of cancer.[22] Besides established kinase targets, new kinase targets have emerged for clinical evaluation, among which are kinases of the spindle assembly checkpoint, including Aurora B and MPS1.[23–26]

Aurora kinase B (Aurora B)

Aurora kinase B belongs to the aurora kinase family which consists of aurora kinase (Aurora) A, B and C. Despite their homology, aurora kinases have distinctive functions.[27,28] Whereas Aurora A functions in centrosome maturation, separation and bipolar spindle assembly, Aurora C is hypothesized to more closely resemble functions of Aurora B, but Aurora C is present in germ cells.[29] Aurora B is the enzymatic component of the chromosomal passenger

complex (CPC) which fulfills important roles in mitotic progression.[16] In addition to Aurora B, the CPC is formed by INCENP (inner centromere protein), Borealin and Survivin. The CPC is, via Aurora B activity, responsible for correcting erroneous, i.e. syntelic[30] and merotelic[31], kinetochore-microtubule attachments (**Figure 1.2**). In addition, Aurora B activity is required for the recruitment of key SAC proteins to kinetochores, among which are MPS1, BUBR1, BUB1.[16,32–34] Aurora B is hypothesized to function upstream of the SAC and is suggested to contribute to SAC activity which is independent from its function in error correction.[35,36] Furthermore, in late mitosis, Aurora B has been shown to be involved in cytokinesis.[37]

Aurora B has been found to be overexpressed in a multitude of cancers which is associated with poor prognoses.[38] Therefore, inhibition of its kinase function is thought to have therapeutic potential. Several aurora kinase inhibitors have reached clinical trials, however, only a limited number of these compounds are selective for Aurora B over Aurora A.[39–41] Barasertib (AZD-1152, a prodrug, **Figure 1.4**)[42], which shows over 3,000-fold selectivity over Aurora A, potently inhibited proliferation of several hematologic malignant cell lines, which could be enhanced by tubulin depolymerizing agent vincristine.[43] In addition, barasertib potently inhibited growth of human colon, lung and hematologic tumors in mouse xenografts by inducing polyploidy and concurrent apoptosis.[44] Although lacking efficacy in solid tumors during phase I[45], the inhibitor reached a phase II clinical trial for the treatment of acute myeloid leukemia (AML) and showed an improved objective complete response rate.[46] However, due to an inconvenient route of administration (7-day infusion), a nanoparticle encapsulating AZD-2811 (the active inhibitor of prodrug AZD-1152, **Figure 1.4**) was developed which allowed for continuous drug release for over a week, showed lower toxicity and increased efficacy in multiple xenograft models.[23] AZD-2811 is currently in clinical trials for small-cell lung cancer (phase II) and AML (phase I/II). Overall, these data support clinical proof of concept for Aurora B inhibition, however, with neutropenia being the most common on-target dose-limiting toxicity, the therapeutic window for Aurora B inhibition may be small.[47]

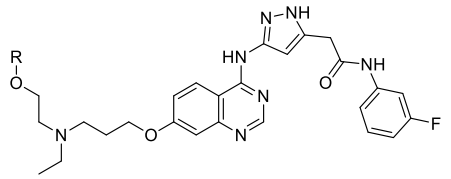

AZD-1152 R = PO_3H_2
AZD-2811 R = H

Figure 1.4 | Chemical structure of barasertib (AZD-1152, a prodrug) and corresponding Aurora B inhibitor AZD-2811.

Monopolar spindle 1 (MPS1)

MPS1, also known as TTK (threonine tyrosine kinase), is recruited to unattached kinetochores and initiates the SAC response.[48,49] MPS1 phosphorylates KNL1 (kinetochore scaffold 1), a member of the KMN (KNL1-MIS12-NDC80) network[50] which is essential for both microtubule binding and SAC signaling.[51] Phosphorylated KNL1 is recognized by BUB3, which in complex with BUB1, results in kinetochore recruitment of BUB1 (**Figure 1.2**).[52] In addition, like Aurora B, MPS1 is thought to be involved in correction of kinetochore-microtubule attachments errors.[34,53] Furthermore, MPS1 catalytic activity is required for the formation and/or stability of the MCC[53–55] and is important for maintaining SAC signaling.[36,56]

MPS1 is overexpressed in several tumors and its gene is part of a genetic signature associated with chromosomal instability in human cancers.[57,58] MPS1 inhibition with small molecule inhibitors is therefore studied as a potential strategy to kill cancer cells. Several MPS1 inhibitors have been developed of which a few reached phase I or phase I/II clinical trials.[59] In multiple studies of animal models, single agent therapy using MPS1 inhibitors only showed efficacy when administered near the maximum tolerated dose (MTD), indicating a small therapeutic window.[60–63] However, doses below the MTD synergistically enhanced the efficacy of taxanes (i.e. docetaxel, paclitaxel) in mouse xenograft models and this combination therapy was better tolerated.[25,62] Similarly, MPS1 inhibitors currently in clinical trials, including BOS-172722[24], BAY-1161909[25], BAY-1217389[25] and CFI-402257[26], are investigated in combination with paclitaxel.

Budding uninhibited by benzimidazole 1 (BUB1)

BUB1 was first identified in mutant strains of budding yeast *Saccharomyces cerevisiae* in which cell cycles at mitosis failed to arrest upon loss of microtubule function by benzimidazole.[64] Three years later, the *BUB1* gene and its product were characterized.[65] Human BUB1 is a 1085-residue protein which contains several structural elements, some of which are highly important for SAC function of BUB1, whereas the contribution to SAC signaling of others are not yet fully understood. These elements include the TPR (tetratricopeptide repeat) motif, BUB3-binding domain, R1LM (BUBR1 localization motif), RZZ binding domain, CD1 (conserved domain 1) region, ABBA (present in Cyclin A, BUBR1, BUB1 and Acm1) motif, KEN (lysine(K)-glutamate(E)-asparagine(N)) boxes, N-terminal extension and the kinase domain (**Figure 1.5**). The TPR motif[15], which although allows for the interaction with KNL1 (a kinetochore protein required for BUB1 localization[66]), is dispensable for kinetochore localization of BUB1.[67] The BUB3-binding domain, also known as the GLEBS (Gle20-binding site) motif, is responsible for binding BUB3 which is crucial for kinetochore recruitment of BUB1.[67] The R1LM was found to recruit BUBR1 to kinetochores, however, this domain was not found to be essential for SAC signaling.[68] In contrast, removal of the R1LM was found to increase SAC strength, suggesting BUB1-mediated BUBR1 recruitment to kinetochores might be required for SAC silencing.[68] CD1 is phosphorylated by MPS1 which enables the binding of MAD1.[69] Disturbance of MAD1 binding to BUB1 is detrimental for the

SAC, suggesting that this interaction is important for kinetochore localization of MAD1.[70] The RZZ binding domain is important for efficient kinetochore localization of the RZZ complex.[68] This domain has overlap with the CD1 domain of BUB1 (**Figure 1.5**) and it is thought that BUB1-mediated MAD1 recruitment is highly integrated with the RZZ complex, since the RZZ complex has been shown to localize MAD1-MAD2 to kinetochores.[68,71] The ABBA motif (also called Phe box) is required to activate the SAC by proper recruitment of CDC20 to unattached kinetochores.[72] Since the ABBA motif is close to CD1 of BUB1 (**Figure 1.5**), BUB1-mediated recruitment of CDC20 to kinetochores might bring CDC20 close to MAD1-MAD2 which may facilitate MCC formation.[73] BUB1 contains two KEN boxes which, together with the ABBA motif, are important for binding of CDC20 and is required for CDC20 phosphorylation to inhibit APC/C.[74,75] In addition, BUB1 facilitates binding of PLK1 to CDC20 allowing both kinases to phosphorylate several residues of CDC20 which, in turn, inhibits APC/CDC20 and thereby contribute to SAC signaling.[76] The N-terminal extension is required for BUB1 kinase activity[74] and the kinase domain was found to interact with CENP-F (centromere protein F) which is necessary for kinetochore recruitment of CENP-F.[77] The C-terminal tail of BUB1's kinase domain, but not its kinase activity, was reported to be important for chromosome alignment.[78] Kinase activity of BUB1 was found to phosphorylate histone H2A at threonine 120 which results in the centromere localization of Shugoshin 1 (SGO1).[79] SGO1 localization, in turn, recruits the CPC subunit Borealin.[80] CPC recruitment is enhanced by Haspin-mediated phosphorylation of histone H3 at threonine 3, resulting in the binding of CPC subunit Survivin which is important for activation of Aurora B and checkpoint signaling.[81,82] In addition, SGO1 protects centromeric cohesion which reveals a role of BUB1 in controlling sister chromatid cohesion through SGO1.[83,84] Despite histone H2A being a clear phosphorylation target of BUB1, the importance of the kinase function of BUB1 in the SAC is still under debate.[10,85,86] Therefore, the current hypothesis is that BUB1's kinase activity contributes to the strength of SAC signaling.[10,85,86]

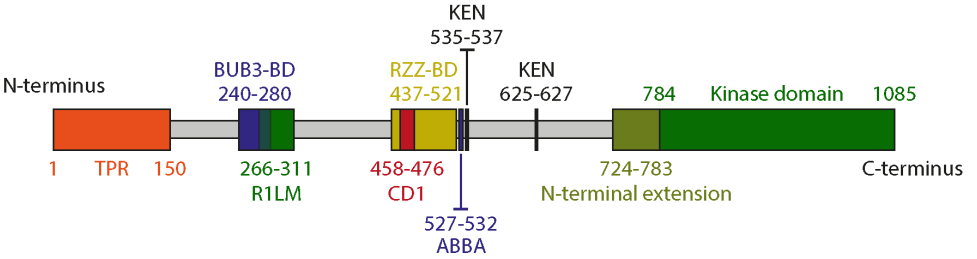

Figure 1.5 | Schematic representation of structural domains and motifs of human BUB1. TRP, tetratricopeptide repeat; BUB3-BD, BUB3 binding domain (also known as GLEBS (Gle20-binding site) motif); R1LM, BUBR1 localization motif; RZZ-BD, RZZ-binding domain; CD1, conserved domain 1; ABBA, also present in Cyclin A, BUBR1, BUB1 and yeast Acm1; KEN, lysine(K)-glutamate(E)-asparagine(N).[67–69,72,74,85]

Like Aurora B and MPS1, BUB1 is overexpressed in numerous human cancers and often correlates with poorer prognoses.[87–91] Recently, two structurally related BUB1 inhibitors were published, BAY-320 and BAY-524 (**Figure 1.6**), which were the first optimized BUB1 inhibitors reported.[92] The effect of BUB1 inhibition was compared to siRNA-mediated BUB1 depletion in aneuploid HeLa and diploid RPE1 cells. BAY-320 (3 μM) or BAY-524 (7 μM) resulted in

about 80% reduction of both H2A phosphorylation and centromeric levels of SGO1 and SGO2. In addition, BUB1 inhibition reduced centromeric levels of CPC components Aurora B, Borealin and INCENP by about 50% and also the activity of Aurora B was reduced. In contrast to siRNA-mediated BUB1 depletion, BUB1 inhibition did not significantly alter MAD1, MAD2 and BUBR1 kinetochore levels, which is in line with reports mentioned above and indicates that kinetochore recruitment of these proteins is independent on BUB1 kinase activity. Based on all data, Baron *et al*. hypothesized that BUB1 protein is predominantly required for the SAC and that its kinase activity is largely dispensable.[92] However, they found that BUB1 inhibition sensitized cells to low doses (1–4 nM) paclitaxel, which particularly affected the aneuploid HeLa cells, whereas diploid RPE1 cells were less affected. More recently, BAY1816032 (**Figure 1.6**) was published as an optimized lead BUB1 inhibitor.[93] BAY1816032 was found to synergistically inhibit cell proliferation of several cancer cell lines, including triple-negative breast cancer (TNBC) cells, when combined with paclitaxel or docetaxel. In addition, cell proliferation was synergistically inhibited when combined with ATR kinase inhibitor AZ20[94] in ATM-proficient cells, which are both protein kinases involved in the DNA damage response.[95] Furthermore, a synergistic effect on cell proliferation was observed when BAY1816032 was combined with several PARP inhibitors. Efficacy of BAY1816032, with or without paclitaxel, was investigated in mouse xenografts using TNBC cells (SUM-149) as a model system. Whereas paclitaxel initially reduced tumor growth, BAY1816032 did not show efficacy as single agent. In contrast, BAY1816032 combined with paclitaxel outperformed the efficacy of paclitaxel single agent therapy. Treatments were found to be well tolerated and no treatment related effects were observed in toxicologic studies on rats and dogs at concentrations up to 20-fold (rat) and 7-fold (dog) above efficacious concentrations in mice. Overall, these data suggest a clinical proof of concept for BUB1 inhibition combined with taxanes.

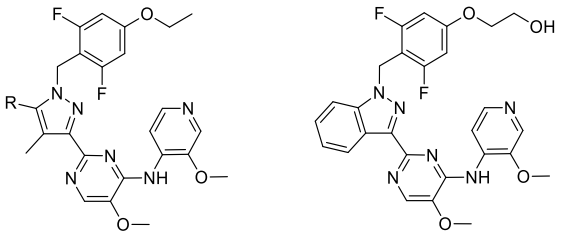

Figure 1.6 | Chemical structure of BUB1 inhibitors BAY-320, BAY-524 and BAY1816032.

Unlike Aurora B and MPS1 inhibitors, BUB1 kinase inhibition seems to be much better tolerated with respect to adverse effects in preclinical models. However, BUB1 inhibition by BAY1816032 lacked *in vivo* efficacy as single agent. The reasons for this lack of efficacy are unclear at the moment, but could be due to the extent of BUB1 inhibition which may be below the threshold required to induce a significant effect. The spindle assembly checkpoint

has been found to be extraordinarily sensitive and even a single unattached kinetochore allows for a mitotic arrest in vertebrate cells.[96] In addition, it was recently found that knocking-out BUB1 by CRISPR/Cas9 could induce alternatively spliced BUB1 mRNA which recovered SAC function.[97,98] CRISPR/Cas9-mediated BUB1 knockout was estimated to still express about 4% of BUB1, which was suggested to be sufficient for normal checkpoint activity.[71,98] Only when CRISPR/Cas9 knockout was combined with BUB1 siRNA, the SAC was significantly impaired.[71,98] Although these observations probably impacts the scaffolding function of BUB1 more significantly, the same might be true for its kinase activity. Therefore, more potent BUB1 inhibitors may be required to allow for single agent efficacy. In addition, targeted therapy may result in acquired resistance, in which mutations in the target protein can prevent inhibitor binding.[99] Alternative chemotypes may still be active on the mutated protein, which therefore supports the need for drug discovery (**Box 1.1**) of new BUB1 inhibitors. Finally, single agent efficacy may also be obtained by a mixed inhibition profile of BUB1 and other kinases.

Box 1.1 | Drug discovery.

The development of a small molecule drug (or a new chemical entity) is a laborious and expensive trajectory. The average costs for a successful drug discovery program is estimated to be $1.8 billion and requires approximately 13.5 years.[100] The drug discovery process follows several sequential phases starting with target selection and progresses towards clinical evaluation of the drug candidate (**Figure 1.7**). The first phase, target selection, requires a target that is 'druggable', meaning that it should be accessible to a potential drug molecule which, upon binding, can induce a biological response.[101] The strategy of target selection can be categorized into two subclasses: a speculative research target and innovative improvement.[102] A speculative research target is a new target for which therapeutic utility has not yet been proven by existing drugs. The speculative target is based on, for example, information obtained from samples derived from patients with a particular disease or targets hypothesized to be drivers of human diseases. In contrast, the innovative improvement approach aims to improve the performance of an existing drug by focusing on a target that is already known to have therapeutic utility. Protein families currently targeted by drugs include G-protein coupled receptors (GPCRs), nuclear receptors, ion channels and enzymes such as kinases.[103] Target selection is followed by hit identification which aims to find an appropriate starting point for further drug discovery. Hit identification strategies are diverse[101] and the choice for a particular strategy depends on the available information about the target of interest and molecules that are known to bind this target, as well as available assays to determine binding affinity, accessibility to the protein target and expertise of the people contributing to the project. Identified hits are subsequently resynthesized and evaluated to confirm their activity. Confirmed hits, in turn, are subjected to extensive hit to lead optimization during which the structure-activity relationship is investigated by iterative rounds of designing and synthesizing new molecules followed by evaluation of their activity.[104] Hits are initially optimized on *in vitro* activity while keeping properties such as molecular weight, lipophilicity, number of hydrogen bond donors/acceptors, rotatable bonds and polar surface area into account.[105,106] Once sufficient *in vitro* potency is achieved, optimized hits are further profiled for selectivity, cellular target engagement and cellular activity. In addition, pharmacokinetic properties such as absorption, distribution, metabolism and excretion (ADME) are investigated by *in vitro* assays which allow for assessment of plasma- and metabolic stability, aqueous solubility, plasma protein binding, cell permeability, among others.[104] ADME properties can subsequently be optimized, when required, to obtain lead compounds. Lead compounds are subsequently investigated *in vivo* during which the pharmacokinetic (PK) profile is investigated. The PK parameters investigated include

clearance, volume of distribution, half-life and bioavailability.[104] When required, lead optimization is used to address unfavorable PK profiles. Once acceptable PK profiles are achieved, optimized leads can proceed to animal models representative for the disease under investigation. In these models proof of efficacy and safety are required before drug candidates may enter clinical evaluation in humans.[104] During clinical evaluation drug candidates are tested in humans for the first time and evaluation is divided into four clinical phases (phase I – IV).[104] Phase I clinical trials are aimed at determining safety, maximum tolerated doses and to assess dose limiting toxicities in a small group of healthy or diseased volunteers. Phase II trials are usually performed on a larger group of patients who have the disease under investigation and aim to investigate preliminary efficacy of the candidate drug as well as to determine the dose for phase III studies. Safety is still carefully monitored due to higher exposures to the drug. Usually, phase III clinical trials consist of two or three studies in which efficacy and safety need to be confirmed on a broad patient population. Once successfully completed, marketing approval will be provided. Marketing approval commonly requires additional surveillance studies which are referred to as phase IV trials.

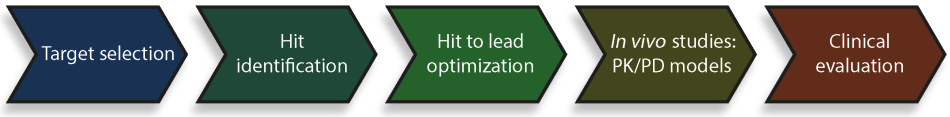

Figure 1.7 | Simplified scheme of the different phases in drug discovery.

Aim and outline

The aim of the research described in this thesis is to discover and optimize novel inhibitors of the spindle assembly checkpoint kinase BUB1 to study its biological role in cancer cell proliferation.

Chapter 2 describes the results of a high-throughput screen which was used as hit identification strategy in the search for novel chemical scaffolds as BUB1 inhibitors. The activity of over 50,000 compounds was assessed in a primary screen and subsequent confirmation screen, deselection assay and dose-response measurements yielded a qualified hit list of 25 compounds. Resynthesis of four prioritized hits confirmed their activity and provided excellent starting points for further drug discovery.

Chapter 3 continues with hit optimization of one of the confirmed hits: OSI-420. Synthesis and biochemical evaluation of structural analogues provided insight into the structure-activity relationship and resulted in optimization of lipophilicity (cLogP) as well as lipophilic efficiency (LipE).

Chapter 4 describes the hit optimization of another confirmed hit, AT-9283. A comprehensive investigation of the structure-activity relationship by synthesis and biochemical evaluation of AT-9283 derivatives resulted in highly potent BUB1 inhibitors with sub-nanomolar biochemical activity, good lipophilicity and excellent lipophilic efficiency. In addition, a co-crystal structure of one of the inhibitors revealed the binding mode of this molecule in the kinase domain of BUB1.

Chapter 5 presents the development of an assay which allows for assessment of cellular BUB1 target engagement. A previously published chloro-fluoroacetamide probe,

reported to show off-target activity on BUB1, as well as structural analogues were synthesized and investigated for their potential as BUB1 probes. Probe binding was studied by mutating the proposed nucleophilic cysteine of BUB1 and provided evidence for the amino acid responsible for covalent bond formation. One of the probes allowed for dose- and time-dependent BUB1 labeling in living cells. Labeling could dose-dependently be outcompeted with published BUB1 inhibitor BAY1816032 which provided proof of principle for the use of this assay to study cellular BUB1 target engagement.

Chapter 6 focusses on the biological profiling of the most potent benzimidazole-based inhibitors discovered in Chapter 4. Several *in vitro* absorption, distribution, metabolism and excretion (ADME) assays were performed to study drug-likeness. Cellular BUB1 target engagement was measured and activities of the compounds on cell proliferation was assessed. In addition, the *in vitro* selectivity profile was studied in a broad panel of kinases and, finally, the antiproliferative activity in a large panel of cancer cell lines was investigated of the most promising inhibitor. Overall, these assays revealed two lead BUB1 inhibitors, ROB433 and ROB464, with favorable drug-like properties.

Chapter 7 summarizes the research described in this thesis and provides future directions.

References

1. Walczak, C. E., Cai, S. & Khodjakov, A. Mechanisms of chromosome behaviour during mitosis. *Nat. Rev. Mol. Cell Biol.* **11**, 91–102 (2010).
2. Musacchio, A. & Salmon, E. D. The spindle-assembly checkpoint in space and time. *Nat. Rev. Mol. Cell Biol.* **8**, 379–393 (2007).
3. Kops, G. J. P. L., Weaver, B. A. A. & Cleveland, D. W. On the road to cancer: aneuploidy and the mitotic checkpoint. *Nat. Rev. Cancer* **5**, 773–785 (2005).
4. Peters, J.-M. The anaphase promoting complex/cyclosome: a machine designed to destroy. *Nat. Rev. Mol. Cell Biol.* **7**, 644–656 (2006).
5. Peters, J.-M. The Anaphase-Promoting Complex: Proteolysis in Mitosis and Beyond. *Mol. Cell* **9**, 931–943 (2002).
6. Sudakin, V., Chan, G. K. T. & Yen, T. J. Checkpoint inhibition of the APC/C in HeLa cells is mediated by a complex of BUBR1, BUB3, CDC20, and MAD2. *J. Cell Biol.* **154**, 925–936 (2001).
7. Dominguez-Brauer, C., Thu, K. L., Mason, J. M., Blaser, H., Bray, M. R. & Mak, T. W. Targeting Mitosis in Cancer: Emerging Strategies. *Mol. Cell* **60**, 524–536 (2015).
8. Lee, E. A., Keutmann, M. K., Dowling, M. L., Harris, E., Chan, G. & Kao, G. D. Inactivation of the mitotic checkpoint as a determinant of the efficacy of microtubule-targeted drugs in killing human cancer cells. *Mol. Cancer Ther.* **3**, 661–669 (2004).
9. Janssen, A., Kops, G. J. P. L. & Medema, R. H. Elevating the frequency of chromosome mis-segregation as a strategy to kill tumor cells. *Proc. Natl. Acad. Sci.* **106**, 19108–19113 (2009).
10. Funabiki, H. & Wynne, D. J. Making an effective switch at the kinetochore by phosphorylation and dephosphorylation. *Chromosoma* **122**, 135–158 (2013).
11. Manning, G. The Protein Kinase Complement of the Human Genome. *Science* **298**, 1912–1934 (2002).
12. Schwartz, P. A. & Murray, B. W. Protein kinase biochemistry and drug discovery. *Bioorganic Chem.* **39**, 192–210 (2011).
13. Taylor, S. S. & Kornev, A. P. Protein kinases: evolution of dynamic regulatory proteins. *Trends Biochem. Sci.* **36**, 65–77 (2011).
14. Kornev, A. P., Haste, N. M., Taylor, S. S. & Ten Eyck, L. F. Surface comparison of active and inactive protein kinases identifies a conserved activation mechanism. *Proc. Natl. Acad. Sci.* **103**, 17783–17788 (2006).
15. Lara-Gonzalez, P., Westhorpe, F. G. & Taylor, S. S. The Spindle Assembly Checkpoint. *Curr. Biol.* **22**, R966–R980 (2012).
16. Carmena, M., Wheelock, M., Funabiki, H. & Earnshaw, W. C. The chromosomal passenger complex (CPC): from easy rider to the godfather of mitosis. *Nat. Rev. Mol. Cell Biol.* **13**, 789–803 (2012).
17. Janeček, M., Rossmann, M., Sharma, P., Emery, A., Huggins, D. J., Stockwell, S. R., Stokes, J. E., Tan, Y. S., Almeida, E. G., Hardwick, B., Narvaez, A. J., Hyvönen, M., Spring, D. R., McKenzie, G. J. & Venkitaraman, A. R. Allosteric modulation of AURKA kinase activity by a small-molecule inhibitor of its protein-protein interaction with TPX2. *Sci. Rep.* **6**, 28528 (2016).
18. The PyMOL Molecular Graphics System, Version 2.3.0 Schrödinger, LLC.
19. Du, Z. & Lovly, C. M. Mechanisms of receptor tyrosine kinase activation in cancer. *Mol. Cancer* **17**, 58 (2018).
20. Dar, A. C. & Shokat, K. M. The Evolution of Protein Kinase Inhibitors from Antagonists to Agonists of Cellular Signaling. *Annu. Rev. Biochem.* **80**, 769–795 (2011).
21. Liao, J. J.-L. Molecular Recognition of Protein Kinase Binding Pockets for Design of Potent and Selective Kinase Inhibitors. *J. Med. Chem.* **50**, 409–424 (2007).
22. Cohen, P., Cross, D. & Jänne, P. A. Kinase drug discovery 20 years after imatinib: progress and future directions. *Nat. Rev. Drug Discov.* **20**, 551–569 (2021).
23. Ashton, S., Song, Y. H., Nolan, J., Cadogan, E., Murray, J., Odedra, R., Foster, J., Hall, P. A., Low, S., Taylor, P., Ellston, R., Polanska, U. M., Wilson, J., Howes, C., Smith, A., Goodwin, R. J. A., Swales, J. G., Strittmatter, N., Takáts, Z., Nilsson, A., Andren, P., Trueman, D., Walker, M., Reimer, C. L., Troiano, G., Parsons, D., De Witt, D., Ashford, M., Hrkach, J., Zale, S., Jewsbury, P. J. & Barry, S. T. Aurora kinase inhibitor nanoparticles target tumors with favorable therapeutic index in vivo. *Sci. Transl. Med.* **8**, 325ra17-325ra17 (2016).
24. Anderhub, S. J., Mak, G. W.-Y., Gurden, M. D., Faisal, A., Drosopoulos, K., Walsh, K., Woodward, H. L., Innocenti, P., Westwood, I. M., Naud, S., Hayes, A., Theofani, E., Filosto, S., Saville, H., Burke, R., van Montfort, R. L. M., Raynaud, F. I., Blagg, J., Hoelder, S., Eccles, S. A. & Linardopoulos, S. High Proliferation Rate and a Compromised Spindle Assembly Checkpoint Confers Sensitivity to the MPS1 Inhibitor BOS172722 in Triple-Negative Breast Cancers. *Mol. Cancer Ther.* **18**, 1696–1707 (2019).
25. Wengner, A. M., Siemeister, G., Koppitz, M., Schulze, V., Kosemund, D., Klar, U., Stoeckigt, D., Neuhaus, R., Lienau, P., Bader, B., Prechtl, S., Raschke, M., Frisk, A.-L., von Ahsen, O., Michels, M., Kreft, B., von Nussbaum, F., Brands, M., Mumberg, D. & Ziegelbauer, K. Novel Mps1 Kinase Inhibitors with Potent Antitumor Activity. *Mol. Cancer Ther.* **15**, 583–592 (2016).

26. Mason, J. M., Wei, X., Fletcher, G. C., Kiarash, R., Brokx, R., Hodgson, R., Beletskaya, I., Bray, M. R. & Mak, T. W. Functional characterization of CFI-402257, a potent and selective Mps1/TTK kinase inhibitor, for the treatment of cancer. *Proc. Natl. Acad. Sci.* **114**, 3127–3132 (2017).
27. Carmena, M., Ruchaud, S. & Earnshaw, W. C. Making the Auroras glow: regulation of Aurora A and B kinase function by interacting proteins. *Curr. Opin. Cell Biol.* **21**, 796–805 (2009).
28. Willems, E., Dedobbeleer, M., Digregorio, M., Lombard, A., Lumapat, P. N. & Rogister, B. The functional diversity of Aurora kinases: a comprehensive review. *Cell Div.* **13**, 7 (2018).
29. Vader, G. & Lens, S. M. A. The Aurora kinase family in cell division and cancer. *Biochim. Biophys. Acta BBA - Rev. Cancer* **1786**, 60–72 (2008).
30. Lampson, M. A., Renduchitala, K., Khodjakov, A. & Kapoor, T. M. Correcting improper chromosome–spindle attachments during cell division. *Nat. Cell Biol.* **6**, 232–237 (2004).
31. Knowlton, A. L., Lan, W. & Stukenberg, P. T. Aurora B Is Enriched at Merotelic Attachment Sites, Where It Regulates MCAK. *Curr. Biol.* **16**, 1705–1710 (2006).
32. Ditchfield, C., Johnson, V. L., Tighe, A., Ellston, R., Haworth, C., Johnson, T., Mortlock, A., Keen, N. & Taylor, S. S. Aurora B couples chromosome alignment with anaphase by targeting BubR1, Mad2, and Cenp-E to kinetochores. *J. Cell Biol.* **161**, 267–280 (2003).
33. Hauf, S., Cole, R. W., LaTerra, S., Zimmer, C., Schnapp, G., Walter, R., Heckel, A., van Meel, J., Rieder, C. L. & Peters, J.-M. The small molecule Hesperadin reveals a role for Aurora B in correcting kinetochore–microtubule attachment and in maintaining the spindle assembly checkpoint. *J. Cell Biol.* **161**, 281–294 (2003).
34. Santaguida, S., Tighe, A., D'Alise, A. M., Taylor, S. S. & Musacchio, A. Dissecting the role of MPS1 in chromosome biorientation and the spindle checkpoint through the small molecule inhibitor reversine. *J. Cell Biol.* **190**, 73–87 (2010).
35. Santaguida, S., Vernieri, C., Villa, F., Ciliberto, A. & Musacchio, A. Evidence that Aurora B is implicated in spindle checkpoint signalling independently of error correction: Aurora B is directly implicated in spindle checkpoint. *EMBO J.* **30**, 1508–1519 (2011).
36. Maldonado, M. & Kapoor, T. M. Constitutive Mad1 targeting to kinetochores uncouples checkpoint signalling from chromosome biorientation. *Nat. Cell Biol.* **13**, 475–482 (2011).
37. Ruchaud, S., Carmena, M. & Earnshaw, W. C. Chromosomal passengers: conducting cell division. *Nat. Rev. Mol. Cell Biol.* **8**, 798–812 (2007).
38. Tang, A., Gao, K., Chu, L., Zhang, R., Yang, J. & Zheng, J. Aurora kinases: novel therapy targets in cancers. *Oncotarget* **8**, 23937–23954 (2017).
39. Carles, F., Bourg, S., Meyer, C. & Bonnet, P. PKIDB: A Curated, Annotated and Updated Database of Protein Kinase Inhibitors in Clinical Trials. *Molecules* **23**, 908 (2018).
40. Borisa, A. C. & Bhatt, H. G. A comprehensive review on Aurora kinase: Small molecule inhibitors and clinical trial studies. *Eur. J. Med. Chem.* **140**, 1–19 (2017).
41. Borah, N. A. & Reddy, M. M. Aurora Kinase B Inhibition: A Potential Therapeutic Strategy for Cancer. *Molecules* **26**, 1981 (2021).
42. Mortlock, A. A., Foote, K. M., Heron, N. M., Jung, F. H., Pasquet, G., Lohmann, J.-J. M., Warin, N., Renaud, F., De Savi, C., Roberts, N. J., Johnson, T., Dousson, C. B., Hill, G. B., Perkins, D., Hatter, G., Wilkinson, R. W., Wedge, S. R., Heaton, S. P., Odedra, R., Keen, N. J., Crafter, C., Brown, E., Thompson, K., Brightwell, S., Khatri, L., Brady, M. C., Kearney, S., McKillop, D., Rhead, S., Parry, T. & Green, S. Discovery, Synthesis, and *in Vivo* Activity of a New Class of Pyrazoloquinazolines as Selective Inhibitors of Aurora B Kinase. *J. Med. Chem.* **50**, 2213–2224 (2007).
43. Yang, J., Ikezoe, T., Nishioka, C., Tasaka, T., Taniguchi, A., Kuwayama, Y., Komatsu, N., Bandobashi, K., Togitani, K., Koeffler, H. P., Taguchi, H. & Yokoyama, A. AZD1152, a novel and selective aurora B kinase inhibitor, induces growth arrest, apoptosis, and sensitization for tubulin depolymerizing agent or topoisomerase II inhibitor in human acute leukemia cells in vitro and in vivo. *Blood* **110**, 2034–2040 (2007).
44. Wilkinson, R. W., Odedra, R., Heaton, S. P., Wedge, S. R., Keen, N. J., Crafter, C., Foster, J. R., Brady, M. C., Bigley, A., Brown, E., Byth, K. F., Barrass, N. C., Mundt, K. E., Foote, K. M., Heron, N. M., Jung, F. H., Mortlock, A. A., Boyle, F. T. & Green, S. AZD1152, a Selective Inhibitor of Aurora B Kinase, Inhibits Human Tumor Xenograft Growth by Inducing Apoptosis. *Clin. Cancer Res.* **13**, 3682–3688 (2007).
45. Boss, D. S., Witteveen, P. O., van der Sar, J., Lolkema, M. P., Voest, E. E., Stockman, P. K., Ataman, O., Wilson, D., Das, S. & Schellens, J. H. Clinical evaluation of AZD1152, an i.v. inhibitor of Aurora B kinase, in patients with solid malignant tumors. *Ann. Oncol.* **22**, 431–437 (2011).
46. Kantarjian, H. M., Martinelli, G., Jabbour, E. J., Quintás-Cardama, A., Ando, K., Bay, J.-O., Wei, A., Gröpper, S., Papayannidis, C., Owen, K., Pike, L., Schmitt, N., Stockman, P. K., Giagounidis, A., & SPARK-AML1 Investigators. Stage I of a phase 2 study assessing the efficacy, safety, and tolerability of barasertib (AZD1152) versus low-dose cytosine arabinoside in elderly patients with acute myeloid leukemia: Barasertib vs LDAC in AML. *Cancer* **119**, 2611–2619 (2013).
47. Kollareddy, M., Zheleva, D., Dzubak, P., Brahmkshatriya, P. S., Lepsik, M. & Hajduch, M. Aurora kinase inhibitors: Progress towards the clinic. *Invest. New Drugs* **30**, 2411–2432 (2012).
48. Ji, Z., Gao, H. & Yu, H. Kinetochore attachment sensed by competitive Mps1 and microtubule binding to Ndc80C. *Science* **348**, 1260 (2015).

49. Hiruma, Y., Sacristan, C., Pachis, S. T., Adamopoulos, A., Kuijt, T., Ubbink, M., von Castelmur, E., Perrakis, A. & Kops, G. J. P. L. Competition between MPS1 and microtubules at kinetochores regulates spindle checkpoint signaling. *Science* **348**, 1264–1267 (2015).
50. Foley, E. A. & Kapoor, T. M. Microtubule attachment and spindle assembly checkpoint signalling at the kinetochore. *Nat. Rev. Mol. Cell Biol.* **14**, 25–37 (2013).
51. Yamagishi, Y., Yang, C.-H., Tanno, Y. & Watanabe, Y. MPS1/Mph1 phosphorylates the kinetochore protein KNL1/Spc7 to recruit SAC components. *Nat. Cell Biol.* **14**, 746–752 (2012).
52. Primorac, I., Weir, J. R., Chiroli, E., Gross, F., Hoffmann, I., van Gerwen, S., Ciliberto, A. & Musacchio, A. Bub3 reads phosphorylated MELT repeats to promote spindle assembly checkpoint signaling. *eLife* **2**, e01030 (2013).
53. Sliedrecht, T., Zhang, C., Shokat, K. M. & Kops, G. J. P. L. Chemical Genetic Inhibition of Mps1 in Stable Human Cell Lines Reveals Novel Aspects of Mps1 Function in Mitosis. *PLoS ONE* **5**, e10251 (2010).
54. Tipton, A. R., Ji, W., Sturt-Gillespie, B., Bekier, M. E., Wang, K., Taylor, W. R. & Liu, S.-T. Monopolar Spindle 1 (MPS1) Kinase Promotes Production of Closed MAD2 (C-MAD2) Conformer and Assembly of the Mitotic Checkpoint Complex*. *J. Biol. Chem.* **288**, 35149–35158 (2013).
55. Faesen, A. C., Thanasoula, M., Maffini, S., Breit, C., Müller, F., van Gerwen, S., Bange, T. & Musacchio, A. Basis of catalytic assembly of the mitotic checkpoint complex. *Nature* **542**, 498–502 (2017).
56. Kuijt, T. E. F., Omerzu, M., Saurin, A. T. & Kops, G. J. P. L. Conditional targeting of MAD1 to kinetochores is sufficient to reactivate the spindle assembly checkpoint in metaphase. *Chromosoma* **123**, 471–480 (2014).
57. Carter, S. L., Eklund, A. C., Kohane, I. S., Harris, L. N. & Szallasi, Z. A signature of chromosomal instability inferred from gene expression profiles predicts clinical outcome in multiple human cancers. *Nat. Genet.* **38**, 1043–1048 (2006).
58. Xie, Y., Wang, A., Lin, J., Wu, L., Zhang, H., Yang, X., Wan, X., Miao, R., Sang, X. & Zhao, H. Mps1/TTK: a novel target and biomarker for cancer. *J. Drug Target.* **25**, 112–118 (2017).
59. Wang, S., Zhang, M., Liang, D., Sun, W., Zhang, C., Jiang, M., Liu, J., Li, J., Li, C., Yang, X. & Zhou, X. Molecular design and anticancer activities of small-molecule monopolar spindle 1 inhibitors: A Medicinal chemistry perspective. *Eur. J. Med. Chem.* **175**, 247–268 (2019).
60. Kusakabe, K., Ide, N., Daigo, Y., Itoh, T., Yamamoto, T., Hashizume, H., Nozu, K., Yoshida, H., Tadano, G., Tagashira, S., Higashino, K., Okano, Y., Sato, Y., Inoue, M., Iguchi, M., Kanazawa, T., Ishioka, Y., Dohi, K., Kido, Y., Sakamoto, S., Ando, S., Maeda, M., Higaki, M., Baba, Y. & Nakamura, Y. Discovery of Imidazo[1,2- *b*]pyridazine Derivatives: Selective and Orally Available Mps1 (TTK) Kinase Inhibitors Exhibiting Remarkable Antiproliferative Activity. *J. Med. Chem.* **58**, 1760–1775 (2015).
61. Martinez, R., Blasina, A., Hallin, J. F., Hu, W., Rymer, I., Fan, J., Hoffman, R. L., Murphy, S., Marx, M., Yanochko, G., Trajkovic, D., Dinh, D., Timofeevski, S., Zhu, Z., Sun, P., Lappin, P. B. & Murray, B. W. Mitotic Checkpoint Kinase Mps1 Has a Role in Normal Physiology which Impacts Clinical Utility. *PLOS ONE* **10**, e0138616 (2015).
62. Maia, A. R. R., de Man, J., Boon, U., Janssen, A., Song, J.-Y., Omerzu, M., Sterrenburg, J. G., Prinsen, M. B. W., Willemsen-Seegers, N., de Roos, J. A. D. M., van Doornmalen, A. M., Uitdehaag, J. C. M., Kops, G. J. P. L., Jonkers, J., Buijsman, R. C., Zaman, G. J. R. & Medema, R. H. Inhibition of the spindle assembly checkpoint kinase TTK enhances the efficacy of docetaxel in a triple-negative breast cancer model. *Ann. Oncol.* **26**, 2180–2192 (2015).
63. Schulze, V. K., Klar, U., Kosemund, D., Wengner, A. M., Siemeister, G., Stöckigt, D., Neuhaus, R., Lienau, P., Bader, B., Prechtl, S., Holton, S. J., Briem, H., Marquardt, T., Schirok, H., Jautelat, R., Bohlmann, R., Nguyen, D., Fernández-Montalván, A. E., Bömer, U., Eberspaecher, U., Brüning, M., Döhr, O., Raschke, M., Kreft, B., Mumberg, D., Ziegelbauer, K., Brands, M., von Nussbaum, F. & Koppitz, M. Treating Cancer by Spindle Assembly Checkpoint Abrogation: Discovery of Two Clinical Candidates, BAY 1161909 and BAY 1217389, Targeting MPS1 Kinase. *J. Med. Chem.* **63**, 8025–8042 (2020).
64. Hoyt, M. A., Totis, L. & Roberts, B. T. S. cerevisiae genes required for cell cycle arrest in response to loss of microtubule function. *Cell* **66**, 507–517 (1991).
65. Roberts, B. T., Farr, K. A. & Hoyt, M. A. The Saccharomyces cerevisiae checkpoint gene BUB1 encodes a novel protein kinase. *Mol Cell Biol* **14**, 10 (1994).
66. Kiyomitsu, T., Obuse, C. & Yanagida, M. Human Blinkin/AF15q14 Is Required for Chromosome Alignment and the Mitotic Checkpoint through Direct Interaction with Bub1 and BubR1. *Dev. Cell* **13**, 663–676 (2007).
67. Krenn, V., Wehenkel, A., Li, X., Santaguida, S. & Musacchio, A. Structural analysis reveals features of the spindle checkpoint kinase Bub1–kinetochore subunit Knl1 interaction. *J. Cell Biol.* **196**, 451–467 (2012).
68. Zhang, G., Lischetti, T., Hayward, D. G. & Nilsson, J. Distinct domains in Bub1 localize RZZ and BubR1 to kinetochores to regulate the checkpoint. *Nat. Commun.* **6**, 7162 (2015).
69. Ji, Z., Gao, H., Jia, L., Li, B. & Yu, H. A sequential multi-target Mps1 phosphorylation cascade promotes spindle checkpoint signaling. *eLife* **6**, e22513 (2017).
70. Zhang, G., Kruse, T., López-Méndez, B., Sylvestersen, K. B., Garvanska, D. H., Schopper, S., Nielsen, M. L. & Nilsson, J. Bub1 positions Mad1 close to KNL1 MELT repeats to promote checkpoint signalling. *Nat. Commun.* **8**, 15822 (2017).

71. Zhang, G., Kruse, T., Guasch Boldú, C., Garvanska, D. H., Coscia, F., Mann, M., Barisic, M. & Nilsson, J. Efficient mitotic checkpoint signaling depends on integrated activities of Bub1 and the RZZ complex. *EMBO J.* **38**, (2019).
72. Di Fiore, B., Davey, N. E., Hagting, A., Izawa, D., Mansfeld, J., Gibson, T. J. & Pines, J. The ABBA Motif Binds APC/C Activators and Is Shared by APC/C Substrates and Regulators. *Dev. Cell* **32**, 358–372 (2015).
73. Kim, T. & Gartner, A. Bub1 kinase in the regulation of mitosis. *Anim. Cells Syst.* **25**, 1–10 (2021).
74. Kang, J., Yang, M., Li, B., Qi, W., Zhang, C., Shokat, K. M., Tomchick, D. R., Machius, M. & Yu, H. Structure and Substrate Recruitment of the Human Spindle Checkpoint Kinase Bub1. *Mol. Cell* **32**, 394–405 (2008).
75. Tang, Z., Shu, H., Oncel, D., Chen, S. & Yu, H. Phosphorylation of Cdc20 by Bub1 Provides a Catalytic Mechanism for APC/C Inhibition by the Spindle Checkpoint. *Mol. Cell* **16**, 387–397 (2004).
76. Jia, L., Li, B. & Yu, H. The Bub1–Plk1 kinase complex promotes spindle checkpoint signalling through Cdc20 phosphorylation. *Nat. Commun.* **7**, 10818 (2016).
77. Ciossani, G., Overlack, K., Petrovic, A., Huis in 't Veld, P. J., Koerner, C., Wohlgemuth, S., Maffini, S. & Musacchio, A. The kinetochore proteins CENP-E and CENP-F directly and specifically interact with distinct BUB mitotic checkpoint Ser/Thr kinases. *J. Biol. Chem.* **293**, 10084–10101 (2018).
78. Raaijmakers, J. A., van Heesbeen, R. G. H. P., Blomen, V. A., Janssen, L. M. E., van Diemen, F., Brummelkamp, T. R. & Medema, R. H. BUB1 Is Essential for the Viability of Human Cells in which the Spindle Assembly Checkpoint Is Compromised. *Cell Rep.* **22**, 1424–1438 (2018).
79. Kawashima, S. A., Yamagishi, Y., Honda, T., Ishiguro, K. & Watanabe, Y. Phosphorylation of H2A by Bub1 Prevents Chromosomal Instability Through Localizing Shugoshin. *Science* **327**, 172–177 (2010).
80. Tsukahara, T., Tanno, Y. & Watanabe, Y. Phosphorylation of the CPC by Cdk1 promotes chromosome bi-orientation. *Nature* **467**, 719–723 (2010).
81. Yamagishi, Y., Honda, T., Tanno, Y. & Watanabe, Y. Two Histone Marks Establish the Inner Centromere and Chromosome Bi-Orientation. *Science* **330**, 239–243 (2010).
82. Kelly, A. E., Ghenoiu, C., Xue, J. Z., Zierhut, C., Kimura, H. & Funabiki, H. Survivin Reads Phosphorylated Histone H3 Threonine 3 to Activate the Mitotic Kinase Aurora B. *Science* **330**, 235–239 (2010).
83. Kitajima, T. S., Hauf, S., Ohsugi, M., Yamamoto, T. & Watanabe, Y. Human Bub1 Defines the Persistent Cohesion Site along the Mitotic Chromosome by Affecting Shugoshin Localization. *Curr. Biol.* **15**, 353–359 (2005).
84. Liu, H., Jia, L. & Yu, H. Phospho-H2A and Cohesin Specify Distinct Tension-Regulated Sgo1 Pools at Kinetochores and Inner Centromeres. *Curr. Biol.* **23**, 1927–1933 (2013).
85. Bolanos-Garcia, V. M. & Blundell, T. L. BUB1 and BUBR1: multifaceted kinases of the cell cycle. *Trends Biochem. Sci.* **36**, 141–150 (2011).
86. Elowe, S. Bub1 and BubR1: at the Interface between Chromosome Attachment and the Spindle Checkpoint. *Mol. Cell. Biol.* **31**, 3085–3093 (2011).
87. Essegian, D., Khurana, R., Stathias, V. & Schürer, S. C. The Clinical Kinase Index: A Method to Prioritize Understudied Kinases as Drug Targets for the Treatment of Cancer. *Cell Rep. Med.* **1**, 100128 (2020).
88. Piao, J., Zhu, L., Sun, J., Li, N., Dong, B., Yang, Y. & Chen, L. High expression of CDK1 and BUB1 predicts poor prognosis of pancreatic ductal adenocarcinoma. *Gene* **701**, 15–22 (2019).
89. Moreno-Bueno, G., Sánchez-Estévez, C., Cassia, R., Rodríguez-Perales, S., Díaz-Uriarte, R., Domínguez, O., Hardisson, D., Andujar, M., Prat, J., Matias-Guiu, X., Cigudosa, J. C. & Palacios, J. Differential Gene Expression Profile in Endometrioid and Nonendometrioid Endometrial Carcinoma. *Cancer Res.* **63**, 5697–5702 (2003).
90. Grabsch, H., Takeno, S., Parsons, W. J., Pomjanski, N., Boecking, A., Gabbert, H. E. & Mueller, W. Overexpression of the mitotic checkpoint genesBUB1, BUBR1, andBUB3 in gastric cancer?association with tumour cell proliferation. *J. Pathol.* **200**, 16–22 (2003).
91. Wang, Z., Katsaros, D., Shen, Y., Fu, Y., Canuto, E. M., Benedetto, C., Lu, L., Chu, W.-M., Risch, H. A. & Yu, H. Biological and Clinical Significance of MAD2L1 and BUB1, Genes Frequently Appearing in Expression Signatures for Breast Cancer Prognosis. *PLOS ONE* **10**, e0136246 (2015).
92. Baron, A. P., von Schubert, C., Cubizolles, F., Siemeister, G., Hitchcock, M., Mengel, A., Schröder, J., Fernández-Montalván, A., von Nussbaum, F., Mumberg, D. & Nigg, E. A. Probing the catalytic functions of Bub1 kinase using the small molecule inhibitors BAY-320 and BAY-524. *eLife* **5**, e12187 (2016).
93. Siemeister, G., Mengel, A., Fernández-Montalván, A. E., Bone, W., Schröder, J., Zitzmann-Kolbe, S., Briem, H., Prechtl, S., Holton, S. J., Mönning, U., von Ahsen, O., Johanssen, S., Cleve, A., Pütter, V., Hitchcock, M., von Nussbaum, F., Brands, M., Ziegelbauer, K. & Mumberg, D. Inhibition of BUB1 Kinase by BAY 1816032 Sensitizes Tumor Cells toward Taxanes, ATR, and PARP Inhibitors *In Vitro* and *In Vivo*. *Clin. Cancer Res.* **25**, 1404–1414 (2019).
94. Foote, K. M., Blades, K., Cronin, A., Fillery, S., Guichard, S. S., Hassall, L., Hickson, I., Jacq, X., Jewsbury, P. J., McGuire, T. M., Nissink, J. W. M., Odedra, R., Page, K., Perkins, P., Suleman, A., Tam, K., Thommes, P., Broadhurst, R. & Wood, C. Discovery of 4-{4-[(3 *R*)-3-Methylmorpholin-4-yl]-6-[1-(methylsulfonyl)cyclopropyl]pyrimidin-2-yl}-1 *H* -indole (AZ20): A Potent and Selective Inhibitor of ATR Protein Kinase with Monotherapy in Vivo Antitumor Activity. *J. Med. Chem.* **56**, 2125–2138 (2013).
95. Cimprich, K. A. & Cortez, D. ATR: an essential regulator of genome integrity. *Nat. Rev. Mol. Cell Biol.* **9**, 616–627 (2008).

96. Rieder, C. L., Schultz, A., Cole, R. & Sluder, G. Anaphase onset in vertebrate somatic cells is controlled by a checkpoint that monitors sister kinetochore attachment to the spindle. *J. Cell Biol.* **127**, 1301–1310 (1994).
97. Rodriguez-Rodriguez, J.-A., Lewis, C., McKinley, K. L., Sikirzhytski, V., Corona, J., Maciejowski, J., Khodjakov, A., Cheeseman, I. M. & Jallepalli, P. V. Distinct Roles of RZZ and Bub1-KNL1 in Mitotic Checkpoint Signaling and Kinetochore Expansion. *Curr. Biol.* **28**, 3422-3429.e5 (2018).
98. Meraldi, P. Bub1—the zombie protein that CRISPR cannot kill. *EMBO J.* **38**, (2019).
99. Lovly, C. M. & Shaw, A. T. Molecular Pathways: Resistance to Kinase Inhibitors and Implications for Therapeutic Strategies. *Clin. Cancer Res.* **20**, 2249–2256 (2014).
100. Paul, S. M., Mytelka, D. S., Dunwiddie, C. T., Persinger, C. C., Munos, B. H., Lindborg, S. R. & Schacht, A. L. How to improve R&D productivity: the pharmaceutical industry's grand challenge. *Nat. Rev. Drug Discov.* **9**, 203–214 (2010).
101. Hughes, J., Rees, S., Kalindjian, S. & Philpott, K. Principles of early drug discovery: Principles of early drug discovery. *Br. J. Pharmacol.* **162**, 1239–1249 (2011).
102. Knowles, J. & Gromo, G. Target selection in drug discovery. *Nat. Rev. Drug Discov.* **2**, 63–69 (2003).
103. Santos, R., Ursu, O., Gaulton, A., Bento, A. P., Donadi, R. S., Bologa, C. G., Karlsson, A., Al-Lazikani, B., Hersey, A., Oprea, T. I. & Overington, J. P. A comprehensive map of molecular drug targets. *Nat. Rev. Drug Discov.* **16**, 19–34 (2017).
104. Blass, B. E. Basic principles of drug discovery and development. (Academic Press, 2015).
105. Lipinski, C. A., Lombardo, F., Dominy, B. W. & Feeney, P. J. Experimental and computational approaches to estimate solubility and permeability in drug discovery and development settings. *Adv. Drug Deliv. Rev.* **46**, 3–26 (2001).
106. Veber, D. F., Johnson, S. R., Cheng, H.-Y., Smith, B. R., Ward, K. W. & Kopple, K. D. Molecular Properties That Influence the Oral Bioavailability of Drug Candidates. *J. Med. Chem.* **45**, 2615–2623 (2002).

2

Discovery of novel BUB1 inhibitors by high-throughput screening

Introduction

Breast cancer is the most common cancer among women worldwide, with an estimated 2.2 million new cases in 2020.[1] In addition, breast cancer was the leading cause of cancer related deaths among women in 2020.[1] There are three main subtypes of breast cancer and assessment of breast cancer subtype is predominantly based on the expression of the estrogen receptor alpha (ERα), progesterone receptor (PR) and human epidermal growth factor receptor 2 (HER2).[2] Clinical decisions for breast cancer therapy rely on the expression of these receptors and breast cancer subtypes therefore include: hormone receptor positive/HER2 negative ($HR^+/HER2^-$), HER2 positive ($HER2^+$) and triple-negative.[3] The $HR^+/HER2^-$ subtype, which represents the majority of the patient group (~73%)[4], is treated with endocrine therapy. Endocrine therapy counteracts estrogen-promoted tumor growth by, for example, tamoxifen, which is an ER modulator[5], or by aromatase inhibitors (i.e. anastrozole, exemestane, letrozole), which decrease estrogen levels.[6] $HR^+/HER2^-$ breast cancers showing high expression of ER and PR are usually of lower grade, show low proliferation rates and therefore have good prognosis.[7] $HER2^+$ tumors (~15%)[4], which can either be HR^+ or HR^-, have intermediate prognosis[7] and are treated with a combination of chemotherapy and HER2-targeted therapies.[3] Chemotherapy includes DNA binding drugs, such as doxorubicin, cyclophosphamide or carboplatin, or microtubule targeting drugs, such as taxanes (i.e. docetaxel, paclitaxel). HER2 can be targeted by anti-HER2 antibodies, such as trastuzumab or pertuzumab.[8] Alternatively, the intracellular kinase domain of HER2 can be inhibited by small molecule inhibitors like lapatinib and neratinib, thereby inhibiting downstream signal transduction.[9] $HER2^+$ tumors that stain positive for hormone receptors may also be treated with endocrine therapy. Triple-negative breast cancer (TNBC), which accounts for ~12% of all breast cancers[4], shows high proliferation and has poor prognosis.[7] TNBC is characterized by the lack of expression of both hormone receptors as well as HER2 expression, which limits therapeutic options to only general chemotherapy due to the lack of a molecular target. Therefore, new treatments for TNBC based on novel molecular targets are urgently needed. Targeting kinases of the spindle assembly checkpoint has emerged as a potential strategy.[10–12]

The spindle assembly checkpoint (SAC) is a safety mechanism during mitosis which prevents mitotic progression when chromosomes are not correctly attached to the mitotic spindle.[13] The SAC is active during the prometaphase of mitosis and prevents anaphase initiation by inhibiting the anaphase-promoting complex/cyclosome (APC/C).[13] SAC signaling involves a multitude of proteins, including kinases such as BUB1. Many cancer cells suffer from a diminished SAC and interference with these weakened checkpoints is thought to cause severe chromosomal instability which eventually results in cell death.[10,11] Targeting kinases of the SAC by small molecule inhibitors has therefore emerged as a new strategy to kill cancer cells.

BUB1 fulfills important roles in the SAC by recruiting numerous of proteins to kinetochores which are important for SAC signaling.[14–17] The importance of the kinase function of BUB1, however, has been subject of debate.[18–20] Until recently, no optimized BUB1 inhibitors had been published, which hindered the investigation of the kinase function of BUB1 in cancer cell proliferation. In 2019, Siemeister *et al.*[12] published the first optimized BUB1 inhibitor, BAY1816032 (**Figure 2.1**), which was based on their earlier report from Baron *et al.*[21] BAY1816032 was evaluated *in vivo* using a human TNBC mouse xenograft model and synergistically inhibited tumor growth when combined with paclitaxel.[12] Tumor growth inhibition with this combined treatment outperformed the efficacy of treatment with paclitaxel alone. However, BAY1816032 did not show efficacy as single agent. The reason for this lack of efficacy remains unclear, but might be due to incomplete BUB1 inhibition. Recently, it was suggested that about 4% of BUB1 levels remain after CRISPR/Cas9-mediated BUB1 knockout and this amount was hypothesized to be sufficient for normal SAC activity.[22] Therefore, more potent BUB1 inhibitors are required.

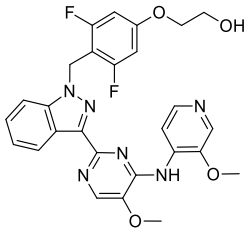

Figure 2.1 | Chemical structure of BUB1 inhibitor BAY1816032.

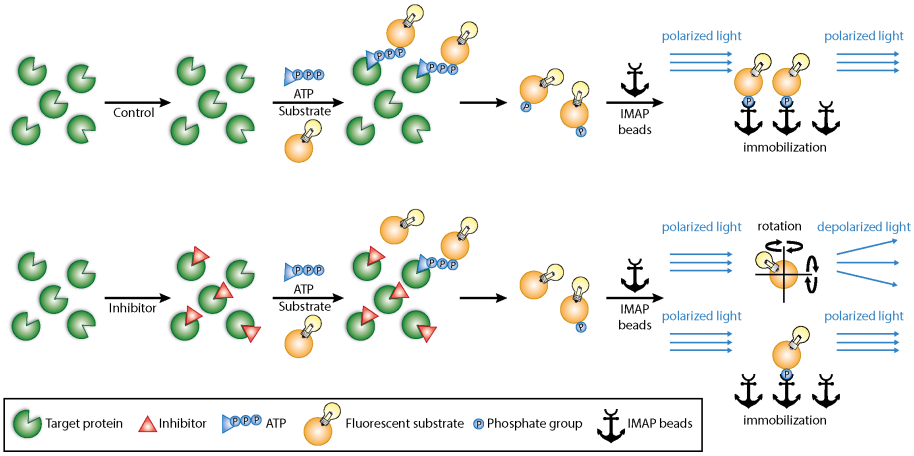

Figure 2.2 | Schematic representation of the fluorescence polarization assay to measure the kinase activity of BUB1. Control samples (top) are incubated with ATP and a fluorescent peptide substrate that can be phosphorylated by BUB1. Addition of IMAP (immobilized metal affinity for phosphochemicals) beads[23] causes immobilization of the phosphorylated substrate fraction. Immobilization of the fluorescent substrate reduces its rotational speed and thereby retaining the polarized light. For inhibitor treated samples (bottom), only a fraction of the peptide substrate is phosphorylated. The unphosphorylated fraction remains free in solution and due to its rotational freedom, depolarization of the light occurs. Depolarization of the light is therefore related to inhibitor potency.

In this chapter, the results of a high-throughput screen (HTS)[24,25], using a fluorescence polarization assay[26,27] (**Figure 2.2**), to identify new chemotypes as BUB1 inhibitors are described (see **Box 2.1** for alternative hit identification strategies). A hit list of 25 molecules was obtained and resynthesis of four prioritized hits resulted in the confirmation of their activity.

Box 2.1 | Hit identification

In drug discovery, target selection (**Chapter 1**) is followed by hit identification. Several hit identification strategies can provide the basis for a drug discovery program, such as selective optimization of side activities (SOSA) of drug molecules[28], fragment-based drug discovery (FBDD)[29], virtual screening[30] or high-throughput screening.[24,25] SOSA is based on the observation that approved drugs might suffer from one or several pharmacological side effects due to binding of the drug with unintended protein targets. These off-target activities can be used as starting point for drug discovery for a new biological target. In FBDD a relatively small library (~1000 compounds) of diverse molecules with low molecular weights (typically 100 – 250 Da) is screened on purified kinases.[29] This results in inhibitors with low binding affinities (μM – mM range), but with high ligand efficiencies[31], a metric that describes the average binding energy per atom. Sensitive screening technologies are required for FBDD as well as significant amounts of purified protein. Virtual screening can be categorized into two major approaches: ligand-based screening and structure-based screening.[30] For ligand-based screening known active molecules are used to build pharmacophore models or are transformed into molecular fingerprints. Screening a virtual molecular library in these models or similarity searches using the fingerprints may yield novel hits. Structure-based screening can be performed in case three-dimensional structural information of the protein of interest is available. High-throughput screening (HTS)[24,25] is an automated way of screening large compound libraries (~10^4 – 10^6 molecules) which include historical compound collections, natural products and/or combinatorial chemistry libraries.[32] Initiating a HTS campaign requires an assay that can distinguish active compounds from inactive ones. These assays have to be miniaturized, usually in 384- or 1536-well plates, to save reagents and compounds, thereby reducing costs.

Results & Discussion

High-throughput screen

High-throughput screening was performed at the Pivot Park Screening Centre (PPSC) (Oss, The Netherlands). A fluorescence polarization assay was miniaturized from a 384- to a 1536-well plate format. A library, enriched with kinase inhibitors and consisting of 53,408 compounds, was screened at a concentration of 10 μM. The quality of the data throughout the screening campaign was evaluated by monitoring the Z′-factor[33] and assay window (in ΔmP) for each assay plate. Active compounds (actives) were distinguished by Z-scores[34] for which Z-score < –4 was used as cutoff. For the primary screen, Z′-factor ≥ 0.67 and ΔmP ≥ 91 were obtained (**Supplementary Figure 1**, p. 46), indicating good quality. The complete library was screened in one day, after which 704 primary actives were found (~13% effect) (**Figure 2.3A,C**). All primary actives were screened again at a concentration of 10 μM, which resulted in 214 confirmed actives (Z′-factor ≥ 0.57 and ΔmP ≥ 99) (**Figure 2.3B,C**). These compounds were investigated for potential interference with the fluorescence polarization assay by applying a different experimental setup. Briefly, BUB1 was mixed with ATP and

fluorescent peptide substrate to allow for maximum phosphorylation of the peptide substrate. Instead of pre-incubating BUB1 with the compounds, compounds were added at this stage. Compounds that still decreased polarization of light, interfered with the assay and were therefore deselected. In total, 57 compounds were found to interfere with the assay (Z-score < –4, Z'-factor ≥ 0.69 and ΔmP ≥ 102). Of the remaining 157 compounds, 74 molecules were selected and dose-response curves were determined. Based on potency, the shape of the IC_{50} curves, drug-likeness (molecular weight <450 g/mol and logP <4 (with a few exceptions for compounds with favorable potency)) and removal of pan-assay interference compounds (PAINS), a hit list of compounds (**1** – **25**) was obtained (**Table 2.1**). Purity and molecular weight of these compounds were confirmed by liquid chromatography-mass spectrometry (LCMS) analysis.

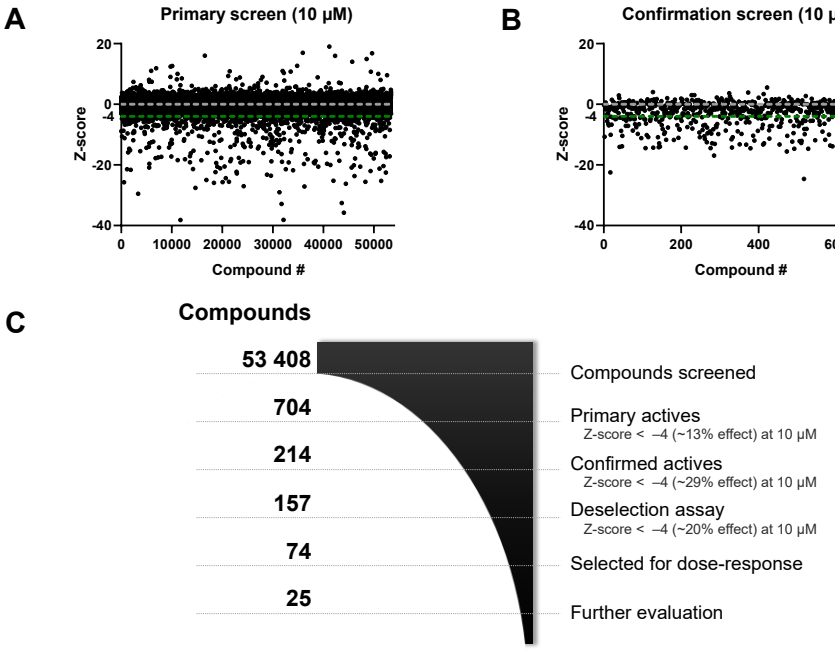

Figure 2.3 | Summary of the high-throughput screen. (A) Z-scores obtained from the primary screen. Z-score < –4 was used as cutoff for primary actives. **(B)** Z-scores obtained from the confirmation screen. Z-score < –4 was used as cutoff for confirmed actives. **(C)** Summary of the high-throughput screen.

Table 2.1 | Qualified hit list and corresponding physicochemical parameters.

ID	Name[a]	Structure	pIC_{50}[b]	App. K_i (nM)[c]	MW[d]	LE[e]	cLogP[f]	LipE[g]	Ref.[h]
1	AT-9283	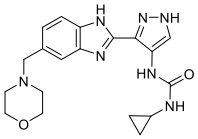	6.78	103	381	0.34	0.4	6.5	[35]
2	CYC-116	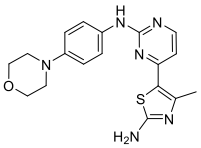	6.75	110	368	0.37	3.0	4.0	[36]
3	OSI-420	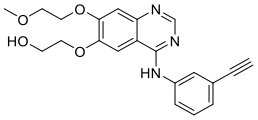	6.59	159	379	0.33	2.6	4.2	[37]
4	PP-121	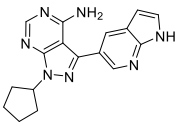	6.32	296	319	0.37	2.0	4.5	[38]
5	PF-00477736	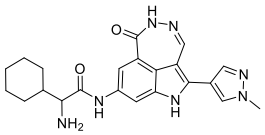	6.51	191	419	0.30	0.9	5.8	[39,40]
6	Ralimetinib (LY-2228820)	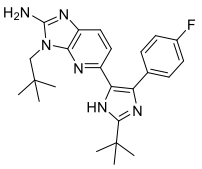	6.17	419	421	0.28	5.2	1.2	[41]
7	Momelotinib (CYT-387)	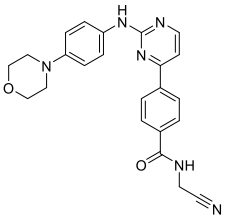	6.10	492	414	0.28	2.5	3.8	[42,43]
8	BCC0044301	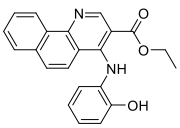	6.04	565	358	0.32	4.7	1.6	–
9	Erlotinib	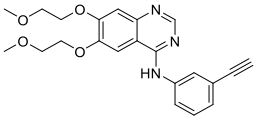	5.79	1004	393	0.28	3.1	2.9	[44,45]

Table 2.1 | Qualified hit list and corresponding physicochemical parameters (continued).

ID	Name[a]	Structure	pIC_{50}[b]	App. K_i (nM)[c]	MW[d]	LE[e]	cLogP[f]	LipE[g]	Ref.[h]
10	NP_000412	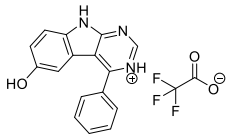	5.65	1386	261	0.40	3.1	2.7	[46,47]
11	BCC0090688	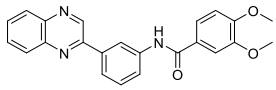	5.58	1629	385	0.27	3.9	1.9	–
12	SPCE000468_01	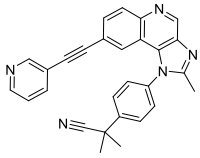	5.53	1827	428	0.24	5.3	0.5	[48]
13	AZD-5438	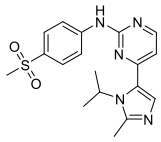	5.44	2248	371	0.30	2.1	3.5	[49]
14	BCC0114359	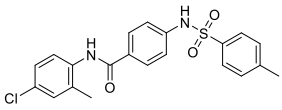	5.42	2354	415	0.28	4.4	1.2	–
15	CP-466722	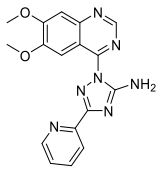	5.41	2409	349	0.30	2.2	3.4	[50,51]
16	SPCE000116_01	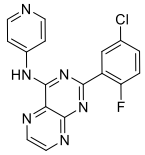	5.41	2409	353	0.31	3.0	2.6	[52]
17	BCC0049010	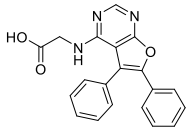	5.39	2522	345	0.30	3.4	2.2	[53]
18	PF-4800567	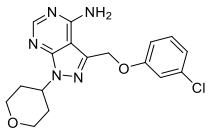	5.31	3033	360	0.30	2.1	3.4	[54]
19	BCC0104036	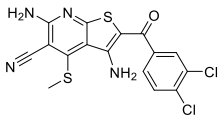	5.21	3818	409	0.30	3.4	2.0	–

Table 2.1 | Qualified hit list and corresponding physicochemical parameters (continued).

ID	Name[a]	Structure	pIC_{50}[b]	App. K_i (nM)[c]	MW[d]	LE[e]	cLogP[f]	LipE[g]	Ref.[h]
20	Reversine	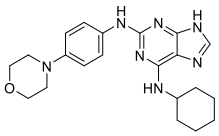	5.20	3907	393	0.26	3.1	2.3	[55]
21	BCC0088074	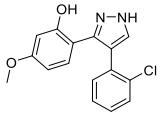	5.17	4186	301	0.35	3.2	2.2	–
22	BCC0075829	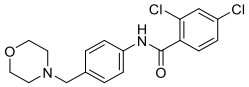	5.16	4284	365	0.31	3.6	1.8	–
23	TWS-119	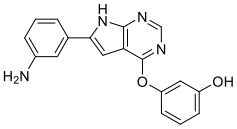	5.08	5150	318	0.30	2.9	2.4	[56,57]
24	Silmitasertib (CX-4945)	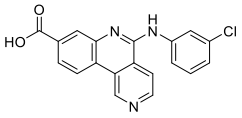	5.06	5393	350	0.29	4.0	1.3	[58]
25	Axitinib (AG-013736)	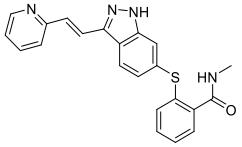	5.03	5778	386	0.26	3.4	1.8	[59,60]

[a] Published compound name or code, otherwise compound code from HTS library; [b] Half maximal inhibitory concentrations (expressed as pIC_{50}) from high-throughput dose-response assay; [c] app. K_i: apparent K_i as determined by the Cheng-Prusoff equation[61]; [d] MW: molecular weight (g/mol); [e] LE: ligand efficiency[31], defined as: $\mathrm{LE} = (-RT * \ln(\mathrm{app.}\,K_i))/\mathrm{HA}$, where HA stands for the number of 'heavy atoms' (non-hydrogen atoms); [f] cLogP: LogP calculated by DataWarrior (v.5.2.1); [g] LipE: lipophilic efficiency[31], defined as: $\mathrm{LipE} = \mathrm{app.}\,pK_i - \mathrm{cLogP}$; [h] reference.

Hit prioritization

The main compound properties considered for hit prioritization included half maximal inhibitory concentrations (pIC_{50}), ligand efficiency (LE, calculated as defined in **Table 2.1**), calculated LogP (cLogP), lipophilic efficiency (LipE, calculated as defined in **Table 2.1**) and molecular weight (MW). Additionally, synthetic accessibility was taken into account as well as the availability of co-crystallized structures with kinases. Hits **8** – **25** have pIC_{50} values below 6 or a high cLogP, which resulted in a low to moderate LipE. Compounds **5** – **7** have a molecular weight above 413 Da, which resulted in a low LE, which is undesirable in view of the fact that MW generally increases during hit optimization.[62] In addition, the synthetic accessibility of hit **5** was deemed low.[63] The remaining hits, **1** – **4**, had an acceptable molecular weight (MW ≤ 381) as well as good activity (pIC_{50} > 6.3), ligand efficiency (LE ≥ 0.33), lipophilicity (cLogP ≤ 3.0) and lipophilic efficiency (LipE ≥ 4.0). In addition, co-crystal

structures with kinases have been published for hits **1**, **2**, **4** as well as for an analogue of compound **3**.[35,36,64,65] Taken together, compounds **1** – **4** were prioritized for hit confirmation. In the following sections a short description of each hit, their resynthesis and biochemical evaluation is described.

Resynthesis of hit 1

The discovery of compound **1** (1-cyclopropyl-3-(3-(5-(morpholinomethyl)-1*H*-benzo[*d*]imidazol-2-yl)-1*H*-pyrazol-4-yl)urea, or AT-9283) was first reported in 2009.[35] AT-9283 (**1**) is a potent inhibitor of multiple kinases including Aurora A, Aurora B, JAK2 and JAK3. In addition, high activities (pIC_{50} > 7) were also reported for over 30 other kinases.[35] AT-9283 (**1**) has been investigated in several phase I clinical trials in patients with leukemia, solid tumors and non-Hodgkin's lymphoma[66–69] and as such may represent an excellent starting point for a new drug discovery program. Synthesis of **1** (AT-9283) was performed by using previously published procedures[35] with minor modifications (**Scheme 2.1**). In short, 3,4-dinitrobenzoic acid was converted into its acyl chloride, followed by a peptide bond formation with morpholine. Amide **26** was reduced to amine **27** of which the nitro groups were subsequently reduced to their corresponding amines to form **28**. A peptide coupling was performed with 4-nitro-1*H*-pyrazole-3-carboxylic acid and subsequent cyclization resulted in benzimidazole **29**. The nitro group of **29** was reduced to amine **30** which was used to form the cyclopropyl urea of AT-9283 (**1**).

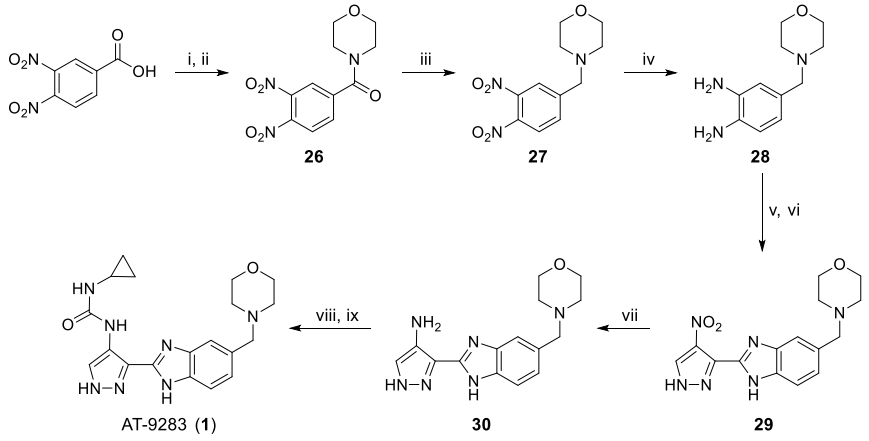

Scheme 2.1 | Synthesis of hit AT-9283. Reagents and conditions: **i)** $SOCl_2$, DMF, THF, 70°C. **ii)** Et_3N, morpholine, 0°C → RT, 93%. **iii)** $NaBH_4$, $BF_3{\cdot}OEt_2$, THF, 0°C → RT, 77%. **iv)** 10% Pd/C, EtOH, 81%. **v)** 4-nitro-1*H*-pyrazole-3-carboxylic acid, EDC·HCl, HOBt, DMF. **vi)** AcOH, 118°C, 55%. **vii)** 10% Pd/C, MeOH, 72%. **viii)** CDI, THF, 66°C. **ix)** cyclopropylamine, DMF, 100°C, 33%.

Resynthesis of hit 2

CYC-116 (**2**), or 4-methyl-5-(2-((4-morpholinophenyl)amino)pyrimidin-4-yl)thiazol-2-amine, was identified by investigation of the structure-activity relationship of a similar compound found through cell-based screens.[36] CYC-116 (**2**) is a potent inhibitor of Aurora A and B with sub-nanomolar activity, inhibited proliferation of multiple cancer cell lines and reduced

tumor growth in several *in vivo* tumor models.[36] The compound was evaluated in phase I clinical trials, however, this study was terminated by the sponsor for unknown reasons.[70] Hit **2** (CYC-116) was synthesized employing previously described procedures (**Scheme 2.2**).[36,71] In brief, 1-fluoro-4-nitrobenzene was used for a nucleophilic aromatic substitution with morpholine to obtain **31**.[72] Palladium catalyzed reduction of the nitro group was performed to form **32**. The amine of **32** was converted into a guanidine under acidic conditions.[73] In parallel, 3-chloropentane-2,4-dione was reacted with thiourea to form thiazole **34**, which was subsequently transformed into enaminone **35** by using DMF-DMA. Guanidine **33** and enaminone **35** were condensed to form a pyrimidine and afforded CYC-116 (**2**).

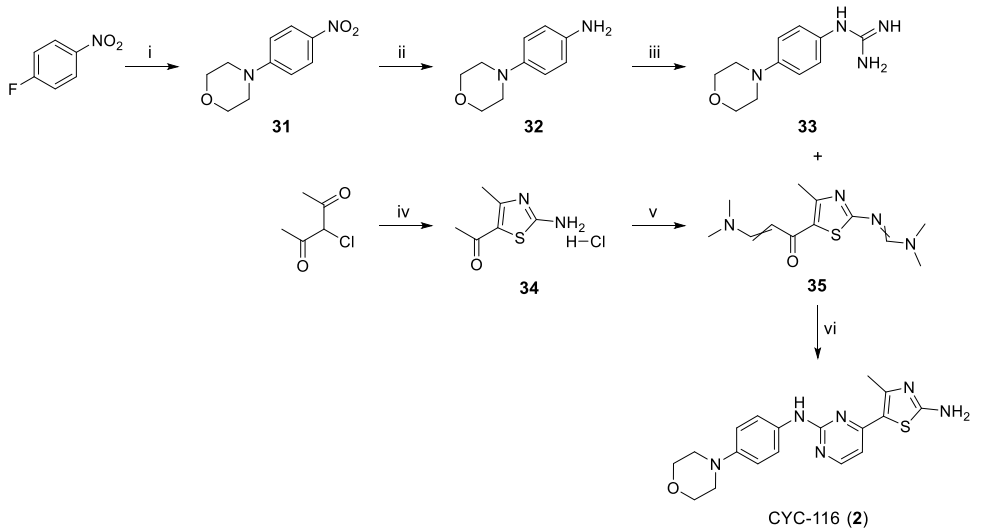

Scheme 2.2 | Synthesis of hit CYC-116. Reagents and conditions: **i)** morpholine, Et_3N, MeCN, 82°C, 93%. **ii)** 10% Pd/C, MeOH, 91%. **iii)** conc. HCl (aq.), cyanamide (aq.), EtOH, 0 → 78°C, 96%. **iv)** thiourea, pyridine, MeOH, 0°C → RT, 89%. **v)** DMF-DMA, 105°C, 70%. **vi)** Na_2CO_3, 2-methoxyethanol, 124°C, 46%.

Resynthesis of hit 3

Compound **3** (2-((4-((3-ethynylphenyl)amino)-7-(2-methoxyethoxy)quinazolin-6-yl)oxy)ethan-1-ol, or OSI-420) is a metabolite of approved drug erlotinib.[37] Erlotinib is an inhibitor of the human epidermal growth factor receptor (EGFR), a membrane receptor tyrosine kinase, and is used in the treatment of non-small cell lung cancer.[74] Interestingly, in addition to OSI-420, erlotinib was identified as one of the hits (**9**) (**Table 2.1**). However, erlotinib (**9**) showed a 6-fold reduced potency, suggesting that the free hydroxyl of OSI-420 (**3**) is an important structural feature for its activity. Hit **3** was synthesized according to published procedures[75–77] (**Scheme 2.3**). Ethyl 3,4-dihydroxybenzoate was subjected to a Mitsunobu reaction with benzyl alcohol to selectively protect the alcohol *para* to the ester (regioselectivity was confirmed by 1H-1H-ROESY NMR).[76] The free alcohol of **36** was subsequently alkylated with 2-bromoethyl acetate, after which the benzyl protecting group was removed and the resulting free alcohol was alkylated with 1-bromo-2-methoxyethane to afford **39**. The nitro group was regioselectively introduced[77] by a Menke nitration to afford

40 (regioselectivity was confirmed by 1H-1H-ROESY NMR). The nitro group was reduced and the obtained free amine was used for a Niementowski reaction to obtain quinazolinone **42**. The quinazolinone was chlorinated to form 4-chloroquinazoline **43** which was used for a nucleophilic aromatic substitution with 3-ethynylaniline to obtain **44**. Deacetylation finally led to the formation of **3**.

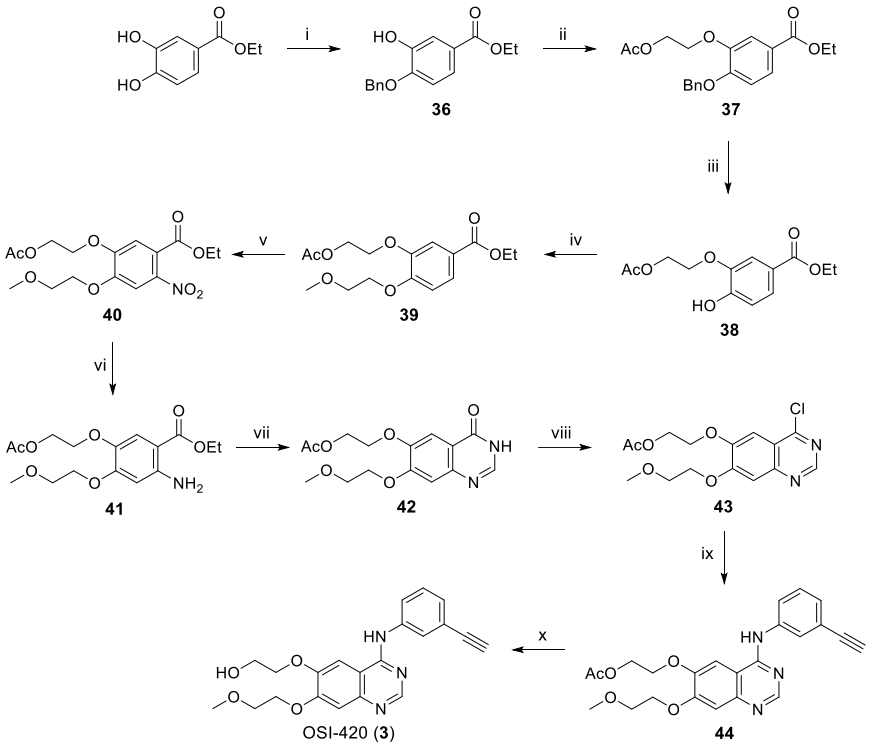

Scheme 2.3 | Synthesis of hit OSI-420. Reagents and conditions: **i)** Ph_3P, DIAD, BnOH, THF, 0°C → RT, 41%. **ii)** 2-bromoethyl acetate, K_2CO_3, DMF, 100°C, 72%. **iii)** 10% Pd/C, MeOH, 98%. **iv)** 1-bromo-2-methoxyethane, K_2CO_3, DMF, 100°C, 96%. **v)** $Cu(NO_3)_2 \cdot 3H_2O$, Ac_2O, 0°C → RT, 73%. **vi)** 5% Pt/C, MeOH, 66%. **vii)** NH_4HCO_2, formamide, 160°C, 60%. **viii)** $POCl_3$, 105°C, 80%. **ix)** 3-ethynylaniline, 2-propanol, 82°C, quant. **x)** 0.4 M NaOH in MeOH, 27%.

Resynthesis of hit 4

Compound **4** (1-cyclopentyl-3-(1*H*-pyrrolo[2,3-*b*]pyridin-5-yl)-1*H*-pyrazolo[3,4-*d*]pyrimidin-4-amine, or PP-121), is a multitargeted kinase inhibitor which inhibits several members of the phosphatidylinositol-3-OH kinase (PI(3)K) family of lipid kinases.[38] In addition, high activities were observed for multiple tyrosine kinases, including ABL, HCK, SRC, VEGFR2 and PDGFR, among others.[38] PP-121 (**4**) was found to inhibit proliferation of several cancer cell lines which was attributed to direct inhibition of oncogenic tyrosine kinases and PI(3)Ks.[38] Compound **4** was synthesized as depicted in **Scheme 2.4** using published procedures.[78] 1*H*-pyrazolo[3,4-*d*]pyrimidin-4-amine was halogenated by using *N*-iodosuccinimide to obtain **45**. The endocyclic amine was alkylated by bromocyclopentane to afford **46**.

Subsequent Suzuki coupling with 7-azaindole-5-boronic acid pinacol ester resulted in the formation of PP-121 (**4**).

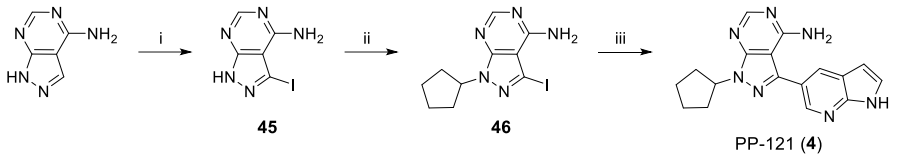

Scheme 2.4 | Synthesis of hit PP-121. Reagents and conditions: **i)** *N*-iodosuccinimide, DMF, 85°C, 63%. **ii)** bromocyclopentane, K_2CO_3, DMF, 80°C, 59%. **iii)** 7-azaindole-5-boronic acid pinacol ester, Na_2CO_3, $Pd(PPh_3)_4$, DMF:H_2O (10:1), 100°C, 70%.

Table 2.2 | Hit confirmation results. Half maximal inhibitory concentrations (expressed as pIC_{50} (± SEM)) and corresponding apparent K_i values from high-throughput screening (HTS) hits and resynthesized hits determined by a biochemical fluorescence polarization assay on BUB1 kinase activity.

ID	Name	pIC_{50} (HTS)	App. K_i (nM)	pIC_{50} ± SEM	App. K_i (nM)
1	AT-9283	6.78	103	6.66 ± 0.02	77
2	CYC-116	6.75	110	6.34 ± 0.05	162
3	OSI-420	6.59	159	6.28 ± 0.05	185
4	PP-121	6.32	296	6.22 ± 0.05	214

Resynthesized hits **1** – **4** were evaluated in the fluorescence polarization assay and observed activities correspond with the potencies obtained from the high-throughput screen (Table 2.2).

Conclusion

High-throughput screening was successfully used to screen over 50,000 compounds and led to the identification of 25 novel BUB1 inhibitors with pIC_{50} values ranging from 5.03 – 6.78. Based on potency and physicochemical properties, hits **1** – **4** were prioritized and subsequently resynthesized. Biochemical evaluation confirmed their activity and these hits, therefore, provide excellent starting points for drug discovery of BUB1 inhibitors. The binding modes of hit **1**, **2**, **4** and the analogue of compound **3** (erlotinib (**9**)) (Figure 2.4) revealed that the cyclopropyl urea of **1**, the aminothiazole of **2**, the phenylacetylene of **3** and azaindole of **4** provide opportunities to reach back pockets of their respective kinases.[35,36,64,65] Since occupation of kinase back pockets contributes to selectivity of inhibitors[79,80] and assuming that these inhibitors may bind similarly in BUB1, modifications of hits **1** – **4** may therefore be aimed at aforementioned part of their structure. For the modification of these groups, reactions with an amino pyrazole (compound **30**, Scheme 2.1) or a chloroquinazoline (compound **43**, Scheme 2.3) were favored over the condensation reaction between compound **33** and **35** (Scheme 2.2) and the Suzuki coupling with **46** (Scheme 2.4). Hit **1** and **3** were therefore selected for hit optimization which will be described in Chapters 4 and 3, respectively.

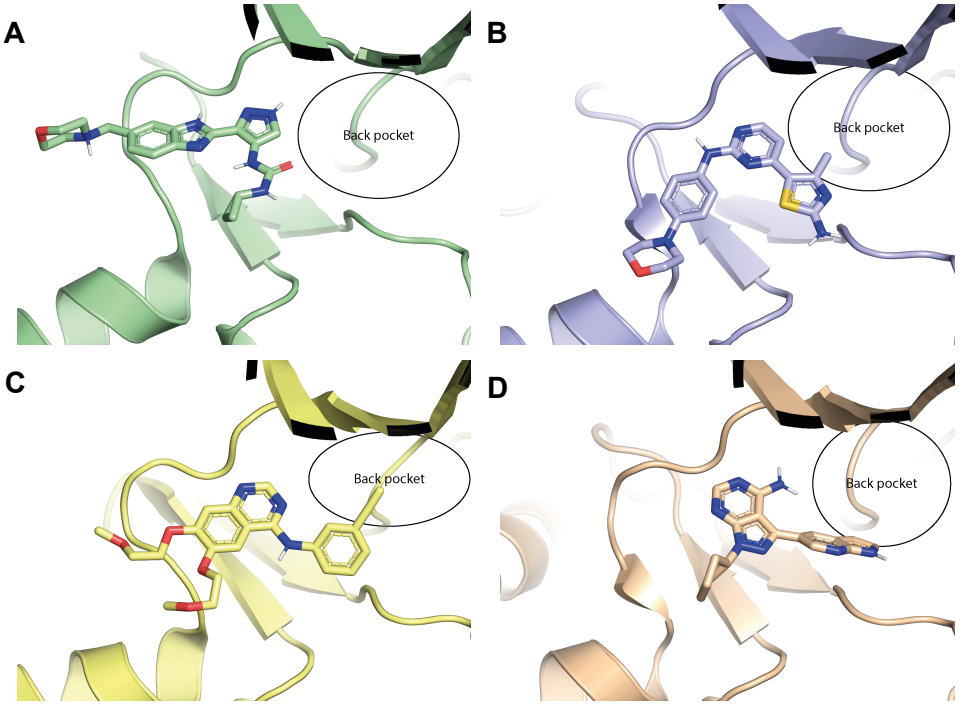

Figure 2.4 | Crystal structures of hits 1, 2, 9 and 4. Crystal structures of **(A)** AT-9283 (**1**) in Aurora A (PDB code: 2W1G)[35], **(B)** CYC-116 (**2**) in CDK2/cyclin A (PDB code: 2UUE)[36], **(C)** Erlotinib (**9**) in EGFR (PDB code: 1M17)[65] and **(D)** PP-121 (**4**) in STK24 (PDB code: 4QMW)[64]. Figures were generated using PyMOL.[81]

Acknowledgements

From Netherlands Translational Research Center (NTRC), Martine Prinsen is kindly acknowledged for the development of the fluorescence polarization assay to measure BUB1 kinase activity and Rogier Buijsman for supervision. Willemijn Wouters, Helma Rutjes and Stan van Boeckel from the Pivot Park Screening Centre (PPSC) are kindly acknowledged for assay miniaturization and conducting the high-throughput screen. Titia Rixt Oppewal is kindly acknowledged for her contribution on AT-9283 (**1**) resynthesis, Julian Clijncke for resynthesizing OSI-420 (**3**) and confirming its activity, and Hans van den Elst for measuring HRMS.

Experimental – Biochemistry

High-throughput screening

All assays were performed in 1536-well plates (Corning, black polystyrene not treated microplate). The primary screen and active confirmation assay were performed by sequential addition (indicated as: volume, final assay concentration, x working solution) of compound (5 or 10 nL, 10 µM, as 400x or 200x working solutions, respectively), BUB1/BUB3 (1 µL, 27 nM, as 2x working solution, Carna Biosciences (05-187), lot: 16CBS-0204) and a mixture of ATP and BUB1/BUB3 substrate (Carna Biosciences (05-187MS-C11)) (1 µL, 5 µM ATP/100 nM substrate, as 2x working solution). Assay reactions were stopped by addition of IMAP progressive binding reagent (2 µL, 1200x diluted (see below), as 2x working solution, Molecular Devices (R7284)).

For each assay, assay buffer (AB) was freshly prepared and consisted of 20 mM HEPES (prepared by diluting 200 mM HEPES, pH 7.4), 5 mM $MgCl_2$, 0.01% (v/v) Tween-20 and 2 mM L-cysteine. Stocks of compounds (in DMSO) were added to the assay plate by using an Echo Liquid Handler. For controls, DMSO was added instead. BUB1/BUB3 (5 µM in storage buffer) was diluted in AB to obtain 54 nM of which 1 µL was added to the assay plate by using a Certus dispenser. For controls, 1 µL of AB was added instead. The assay plate was centrifuged (1 min, 200 *g*) and incubated at RT for 30 min. ATP (40 mM in MilliQ) and BUB1/BUB3 substrate (1 mM) were diluted in AB such to obtain a solution of 10 µM ATP and 200 nM BUB1/BUB3 substrate of which 1 µL was added to each well of the assay plate. The assay plate was centrifuged (1 min, 200 *g*) and incubated at RT in the dark for 120 min. IMAP progressive binding buffer A (5x) and IMAP progressive binding buffer B (5x) were mixed in a ratio to obtain 30% buffer A and 70% buffer B, which was subsequently diluted 5x in MilliQ. IMAP progressive binding reagent was diluted 600x in aforementioned mixture of buffer A and B (to obtain a 2x working solution) of which 2 µL was added to each well of the assay plate. The assay plate was centrifuged (1 min, 200 *g*) and incubated at RT in the dark for 60 min. Fluorescence polarization was measured on an EnVision plate reader (excitation FITC FP 480, 1st emission FITC FP P-pol 535, 2nd emission FITC FP S-pol 535). ActivityBase (IDBS) software was used to analyze data and to calculate quality parameters (Z'-factor and ΔmP). For the deselection assay, in a tube, BUB1/BUB3 (or AB) was first incubated with the mixture of ATP and BUB1/BUB3 substrate for 120 min in the dark. 30 min prior to the end of the incubation time, compounds (or DMSO) were added to an assay plate and aforementioned solution of IMAP progressive binding reagent (2 µL) was added. The assay plate was centrifuged (1 min, 200 *g*) and incubated at RT for 30 min. Subsequently, 2 µL of the mixture of BUB1/BUB3 (or AB), ATP and BUB1/BUB3 substrate (after incubation of 120 min) was added to corresponding wells. The assay plate was centrifuged (1 min, 200 *g*), incubated at RT in the dark for 60 min and fluorescence polarization was measured. For the dose-response assay, stock solutions of compounds (in DMSO) were serially diluted ($\sqrt{10}$ dilutions) in DMSO obtain 10 concentrations (final concentrations of 6.32 nM – 20 µM) as 100x working solutions. 20 nL of compound (or DMSO) was added to the assay plate after which the protocol of the primary screen was followed. ActivityBase was used to calculate pIC_{50} values using the four parameter fitting protocol.

Biochemical evaluation of BUB1 inhibitors

Assays were performed in 384-well plates (Greiner, black, flat bottom, 781076) by sequential addition (indicated as: volume, final assay concentration) of inhibitor (5 µL, 3 nM – 10 µM), BUB1/BUB3 (5 µL, 3.26 nM, Carna Biosciences (05-187), lot: 15CBS-0644 D), ATP (5 µL, 15 µM) and BUB1/BUB3 substrate (5 µL, 75 nM, Carna Biosciences (05-187MSSU)), all as 4x working solutions. The final concentration of DMSO was 1%. Assay reactions were stopped by addition of IMAP progressive binding reagent (20 µL, 1200x diluted (see below), Molecular Devices (R8155), lot: 3117896). Each assay included the following controls: (i) a background control (treated with vehicle instead of inhibitor and BUB1/BUB3 substrate), (ii) MIN controls (treated with 5 µM BAY1816032 (MedChem Express) as inhibitor, defined as 0% BUB1 activity) and (iii) MAX controls (treated with vehicle instead of inhibitor, defined as 100% BUB1 activity). All inhibitors were tested in two separate assays and all inhibitor concentrations were tested in duplicate per assay (N=2, n=2).

For each assay, assay buffer (AB) was freshly prepared and consisted of 20 mM HEPES (prepared by diluting 1 M HEPES, pH 7.2), 5 mM $MgCl_2$, 0.01% (v/v) Tween-20 and 1 mM DTT. Stocks of inhibitors (in DMSO) were diluted in AB to obtain 4x working solutions (4% DMSO) and 5 µL was added to the assay plate. BUB1/BUB3 (3.26 µM (486 µg/mL) in storage buffer) was diluted in AB to obtain 13.0 nM of which 5 µL was added to all wells of the assay plate. The assay plate was centrifuged (1 min, 200 *g*) and incubated at RT for 30 min. ATP (4 mM in MilliQ) was diluted in AB to obtain 60 µM of which 5 µL was added to each well. BUB1/BUB3 substrate (1 mM) was diluted in 20 mM HEPES (prepared by diluting 1 M HEPES (pH 7.2) in MilliQ) to obtain 80 µM (this solution was freshly prepared every assay) and further diluted in AB to obtain 300 nM after which 5 µL was added to each well of the assay plate except for background control wells. The assay plate was centrifuged (1 min, 200 *g*) and incubated at RT in the dark for 180 min. IMAP progressive binding buffer A (5x) and IMAP progressive binding buffer B (5x) were mixed in a ratio to obtain 30% buffer A and 70% buffer B, which was subsequently diluted 5x in MilliQ. IMAP progressive binding reagent was diluted 600x in aforementioned mixture of buffer A and B (to obtain a 2x working solution) of which 20 µL was added to each well of the assay plate. The assay plate was centrifuged (1 min, 200 *g*) and incubated at RT in the dark for 90 min. Fluorescence polarization was measured on a CLARIOstar plate reader using the following settings: (i) optic settings → excitation = F: 482-16, dichroic = F: LP 504, emission = F: 530-40, (ii) optic = top optic, (iii) speed/precision = maximum precision, (iv) focus adjustment was performed for every assay and (v) gain adjustment was done by setting the target mP value to 35 mP for one of the MIN control wells. Data was normalized between MIN and MAX controls and data was plotted using GraphPad Prism 8.0 using "Nonlinear regression (curve fit)" and "log(inhibitor) vs. normalized response – Variable slope" to determine pIC_{50} values. For determining the apparent K_M for ATP, the assay was performed as described above, but with variable ATP concentrations (20 nM – 100 µM final concentrations). K_M determination was performed in triplicate and the apparent K_M for ATP was determined to be 8.13 µM. This value was used in the Cheng-Prusoff equation to calculate K_i values.

Experimental – Chemistry

General synthetic procedures

All reagents were purchased from chemical suppliers (Fluorochem, Sigma-Aldrich, Merck, Fisher Scientific) and used without further purification. Solvents (Honeywell, VWR, Biosolve) indicated with "dry" were stored on activated 4 Å molecular sieves (8 to 12 mesh, Acros Organics). Solvents indicated by "degassed" were sonicated while bubbling N_2 through the solvent for 20 min. All reactions were performed at room temperature (RT) under a nitrogen atmosphere, unless stated otherwise. Reactions were monitored by thin layer chromatography (TLC, silica gel 60, UV_{254}, Macherey-Nagel, ref: 818333) and compounds were visualized by UV absorption (254 nm and/or 366 nm) or spray reagent (permanganate (5 g/L $KMnO_4$, 25 g/L K_2CO_3)) followed by heating. Alternatively, reactions were monitored by liquid chromatography-mass spectrometry (LCMS), either on a Thermo Finnigan (Thermo Finnigan LCQ Advantage MAX ion-trap mass spectrometer (ESI+) coupled to a Surveyor HPLC system (Thermo Finnigan) equipped with a Nucleodur C18 Gravity column (50x4.6 mm, 3 µm particle size, Macherey-Nagel)) or a Thermo Fleet (Thermo LCQ Fleet ion-trap mass spectrometer (ESI+) coupled to a Vanquish UHPLC system). LCMS eluent consisted of MeCN in 0.1% TFA (aq.) and LCMS methods were as follows: 0.5 min cleaning with starting gradient, 8 min using specified gradient (linear), 2 min cleaning with 90% MeCN in 0.1% TFA (aq.). LCMS data is reported as follows: instrument (Finnigan or Fleet), gradient (% MeCN in 0.1% TFA (aq.)), retention time (t_r) and mass (as m/z: $[M+H]^+$). Purity of final compounds was determined to be ≥ 95% by integrating UV intensity of spectra generated by either of the LCMS instruments. ^1H and ^{13}C NMR spectra were recorded on a Bruker AV400 (400 and 101 MHz, respectively), Bruker AV500 (500 and 126 MHz, respectively) or Bruker AV600 (600 and 150 MHz, respectively) NMR spectrometer. NMR samples were prepared in deuterated chloroform, methanol or DMSO. Chemical shifts are given in ppm (δ) relative to residual protonated solvent signals ($CDCl_3$ → δ 7.260 (^1H), δ 77.160 (^{13}C), MeOD → δ 3.310 (^1H), δ 49.000 (^{13}C), DMSO → δ 2.500 (^1H), δ 39.520 (^{13}C)). Data was processed by using MestReNova (v. 14) and is reported as follows: chemical shift (δ), multiplicity, coupling constant (*J* in Hz) and integration. Multiplicities are abbreviated as follows: s = singlet, br s = broad singlet, d = doublet, dd = doublet of doublets, ddd = doublet of doublet of

doublets, dt = doublet of triplets, t = triplet, q = quartet, p = pentet, m = multiplet. Purification was done either by manual silica gel column chromatography (using 40-63 µm, 60 Å silica gel, Macherey-Nagel) or automated column chromatography on a Biotage Isolera machine (using pre-packed cartridges with 40-63 µm, 60 Å silica gel (4, 12, 25 or 40 g), Screening Devices). High resolution mass spectrometry (HRMS) spectra were recorded through direct injection of a 1 µM sample either on a Thermo Scientific Q Exactive Orbitrap equipped with an electrospray ion source in positive mode coupled to an Ultimate 3000 system (source voltage = 3.5 kV, capillary temperature = 275°C, resolution R = 240,000 at m/z 400, external lock, mass range m/z = 150-2000) or on a Synapt G2-Si high definition mass spectrometer (Waters) equipped with an electrospray ion source in positive mode (ESI-TOF) coupled to a NanoEquity system with Leu-enkephalin (m/z = 556.2771) as internal lock mass. The eluent for HRMS measurements consisted of a 1:1 (v/v) mixture of MeCN in 0.1% formic acid (aq.) using a flow of 25 mL/min. Compound names were generated by ChemDraw (v. 19.1.21).

1-Cyclopropyl-3-(3-(5-(morpholinomethyl)-1*H*-benzo[*d*]imidazol-2-yl)-1*H*-pyrazol-4-yl)urea (1)

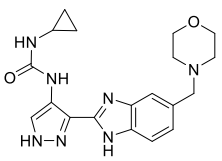

30 (42.1 mg, 141 µmol) and CDI (45.8 mg, 282 µmol) were mixed in dry THF (1.1 mL) and stirred at 66°C for 2.5 h. The obtained solids were collected by filtration, washed with THF (0.5 mL) and dried under reduced pressure. The solids were transferred to a microwave vial, suspended in DMF (0.3 mL) and cyclopropylamine (40 µL, 577 µmol) was added. The vial was sealed and the mixture was stirred at 100°C for 1.5 h. The crude was concentrated at 60°C and purified by automated column chromatography (4 – 15% MeOH/DCM) to afford the product (17.5 mg, 141 µmol, 33%). ^{1}H NMR (500 MHz, MeOD) δ 8.07 (s, 1H), 7.69 – 7.39 (m, 2H), 7.21 (d, *J* = 8.1 Hz, 1H), 3.70 – 3.65 (m, 4H), 3.60 (s, 2H), 2.72 – 2.65 (m, 1H), 2.53 – 2.40 (m, 4H), 1.04 – 0.84 (m, 2H), 0.72 – 0.57 (m, 2H). ^{13}C NMR (126 MHz, MeOD) δ 158.77, 149.31, 144.81, 144.20, 134.95, 134.38, 133.02, 132.04, 131.87, 126.01, 125.07, 123.69, 120.56, 120.00, 119.04, 113.32, 111.86, 67.66, 64.71, 54.59, 23.47, 7.80. LCMS (Finnigan, 0 → 50%): t_r = 5.21 min, m/z: 382.1. HRMS [$C_{19}H_{23}N_7O_2$ + H]$^+$: 382.19860 calculated, 382.1993 found.

4-Methyl-5-(2-((4-morpholinophenyl)amino)pyrimidin-4-yl)thiazol-2-amine (2)

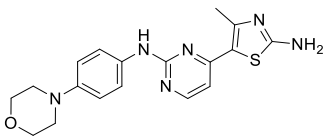

35 (145 mg, 545 µmol) was mixed with **33** (150 mg, 681 µmol) and Na_2CO_3 (57.7 mg, 545 µmol) in 2-methoxyethanol (0.3 mL) and stirred at 124°C for 16 h. The mixture was concentrated at 70°C, brought onto Celite and purified by silica gel chromatography (2 – 5% MeOH/DCM). The impure product was subsequently suspended in MeOH (3 mL), sonicated, filtered and the solids were washed with MeOH (3 mL). The solids were collected and dried to afford the product (91.0 mg, 248 µmol, 46%). ^{1}H NMR (500 MHz, DMSO) δ 9.19 (s, 1H), 8.27 (d, *J* = 5.4 Hz, 1H), 7.65 – 7.58 (m, 2H), 7.47 (s, 2H), 6.91 – 6.83 (m, 2H), 6.80 (d, *J* = 5.5 Hz, 1H), 3.76 – 3.70 (m, 4H), 3.05 – 3.00 (m, 4H), 2.42 (s, 3H). ^{13}C NMR (126 MHz, DMSO) δ 168.72, 159.59, 158.62, 157.56, 151.70, 145.93, 133.13, 120.02, 118.22, 115.55, 106.26, 66.20, 49.34, 18.43. LCMS (Finnigan, 0 → 50%): t_r = 5.79 min, m/z: 369.3. HRMS [$C_{18}H_{20}N_6OS$ + H]$^+$: 369.14921 calculated, 369.14794 found.

2-((4-((3-Ethynylphenyl)amino)-7-(2-methoxyethoxy)quinazolin-6-yl)oxy)ethan-1-ol (3)

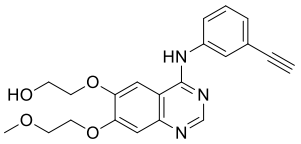

44 (41 mg, 98 µmol) was dissolved in 0.4 M NaOH in MeOH (370 µL) and stirred for 2 h. The mixture was diluted in a mixture of H_2O (30 mL) and brine (2 mL) and the product extracted with $CHCl_3$ (30 mL). The organic layer was concentrated as such and purified by automated column chromatography (4 – 20% MeOH/DCM) to afford the product (10 mg, 27 µmol, 27%). ^{1}H NMR (600 MHz, MeOD) δ 8.41 (s, 1H), 7.91 (t, *J* = 1.9 Hz, 1H), 7.76 (ddd, *J* = 8.2, 2.3, 1.1 Hz, 1H), 7.73 – 7.69 (m, 1H), 7.36 (t, *J* = 7.9 Hz, 1H), 7.25 (dt, *J* = 7.7, 1.2 Hz, 1H), 7.15 – 7.13 (m, 1H), 4.30 – 4.27 (m, 2H), 4.27 – 4.24 (m, 2H), 4.01 – 3.96 (m, 2H), 3.86 – 3.83 (m, 2H), 3.51 (s, 1H), 3.46 (s, 3H). ^{13}C NMR (151 MHz, MeOD) δ 158.44, 155.95, 153.93, 150.54, 147.58, 140.62, 129.89, 128.72, 127.05, 124.29, 124.15, 110.68, 108.31, 103.98, 84.32, 78.71, 72.14,

71.68, 69.49, 61.54, 59.37. LCMS (Finnigan, 10 → 90%): t_r = 5.02 min, m/z: 380.2. HRMS [$C_{21}H_{21}N_3O_4$ + H]$^+$: 380.16048 calculated, 380,1615 found.

1-Cyclopentyl-3-(1*H*-pyrrolo[2,3-*b*]pyridin-5-yl)-1*H*-pyrazolo[3,4-*d*]pyrimidin-4-amine (4)

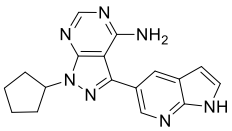

46 (20 mg, 61 µmol), 7-azaindole-5-boronic acid pinacol ester (17.8 mg, 72.9 µmol) and Na_2CO_3 (12.9 mg, 122 µmol) were mixed in degassed DMF (0.5 mL) and H_2O (50 µL). $Pd(PPh_3)_4$ (4.9 mg, 4.3 µmol) was added and the mixture was stirred at 100°C for 17 h. The mixture was poured into H_2O (20 mL) and the product extracted with EtOAc (3x20 mL). The combined organic layers were washed with brine (60 mL), dried over Na_2SO_4, filtered and concentrated. The crude was purified by automated column chromatography (0 – 40% MeOH/DCM) to afford the product (13.5 mg, 42.3 µmol, 70%). ^{1}H NMR (500 MHz, MeOD) δ 8.50 (d, *J* = 2.0 Hz, 1H), 8.25 (d, *J* = 2.0 Hz, 1H), 8.24 (s, 1H), 7.46 (d, *J* = 3.5 Hz, 1H), 6.59 (d, *J* = 3.5 Hz, 1H), 5.27 (p, *J* = 7.6 Hz, 1H), 2.21 – 2.13 (m, 4H), 2.04 – 1.94 (m, 2H), 1.79 – 1.69 (m, 2H). ^{13}C NMR (126 MHz, MeOD) δ 159.47, 156.07, 154.48, 149.11, 143.89, 143.02, 129.89, 128.13, 122.13, 121.78, 101.76, 99.57, 58.73, 32.94, 25.38. LCMS (Finnigan, 0 → 50%): t_r = 7.34 min, m/z: 320.2. HRMS [$C_{17}H_{17}N_7$ + H]$^+$: 320.16182 calculated, 320.1627 found.

(3,4-Dinitrophenyl)(morpholino)methanone (26)

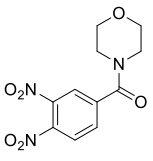

3,4-Dinitrobenzoic acid (15.0 g, 70.7 mmol) was dissolved in dry THF (150 mL) after which dry DMF (0.15 mL) and $SOCl_2$ (7.2 mL, 99 mmol) were added. The mixture was heated to 70°C and stirred for 2.5 h after which the mixture was cooled down to 0°C. Et_3N (14.9 mL, 107 mmol) was added dropwise over 15 min and subsequently morpholine (10.7 mL, 124 mmol) was added dropwise over 10 min. The mixture was allowed to warm up to RT and stirred overnight. H_2O (375 mL) was added and stirring was continued vigorously for 1 h after which the mixture was cooled down to 0°C and filtered. The solids were washed with ice cold H_2O (100 mL), collected and traces of water were removed by coevaporation with MeOH several times to afford the product (18.4 g, 65.4 mmol, 93%). ^{1}H NMR (400 MHz, DMSO) δ 8.31 (d, *J* = 1.7 Hz, 1H), 8.30 (d, *J* = 8.2 Hz, 1H), 8.01 (dd, *J* = 8.3, 1.7 Hz, 1H), 3.71 – 3.60 (m, 4H), 3.59 – 3.49 (m, 2H), 3.37 – 3.27 (m, 2H). ^{13}C NMR (101 MHz, DMSO) δ 165.09, 142.04, 141.35, 132.85, 126.22, 124.30, 65.91, 65.75, 47.41, 42.10.

4-(3,4-Dinitrobenzyl)morpholine (27)

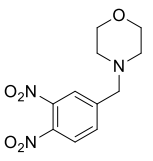

$NaBH_4$ (5.25 g, 139 mmol) was suspended in dry THF (193 mL) and cooled down to 0°C after which boron trifluoride etherate (17.1 mL, 139 mmol) was added. Subsequently, solid **26** (18.4 g, 65.4 mmol) was added after which the mixture was allowed to warm to RT and stirred for 3.5 h. The mixture was cooled down to 0°C and MeOH (160 mL) was added dropwise over 20 min (H_2 evolution). The resulting suspension was allowed to warm to RT, further heated to 70°C and stirred for 75 min (H_2 evolution). The mixture was concentrated, redissolved in EtOAc (200 mL) and poured into half sat. $NaHCO_3$ (200 mL). The organic layer was isolated and the water layer extracted with EtOAc (200 mL). The combined organic layers were washed with H_2O (200 mL), the organic layer was separated and the water layer extracted with EtOAc (100 mL). The combined organic layers were washed with brine (300 mL), dried over Na_2SO_4, filtered and concentrated. The obtained powder was grounded, suspended in MeOH (55 mL) and warmed up until fully dissolved. The solution was slowly cooled down to RT, further cooled on ice and kept on ice for 25 min. The mixture was filtered and the solids were washed with ice cold MeOH (40 mL) to afford the product (13.5 g, 50.4 mmol, 77%). ^{1}H NMR (400 MHz, $CDCl_3$) δ 7.87 (d, *J* = 1.6 Hz, 1H), 7.84 (d, *J* = 8.3 Hz, 1H), 7.71 (dd, *J* = 8.3, 1.6 Hz, 1H), 3.66 – 3.61 (m, 4H), 3.59 (s, 2H), 2.45 – 2.39 (m, 4H). ^{13}C NMR (101 MHz, $CDCl_3$) δ 146.54, 143.01, 141.09, 132.98, 125.06, 124.66, 66.65, 61.35, 53.36. LCMS (Finnigan, 10 → 90%): t_r = 4.03 min, m/z: 268.1.

4-(Morpholinomethyl)benzene-1,2-diamine (28)

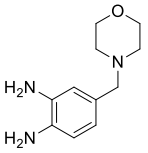

27 (2.50 g, 9.35 mmol) was suspended in absolute EtOH (75 mL) and this mixture was subsequently degassed by bubbling N_2 through the mixture while sonicating for 20 min. 10% Pd/C (250 mg) was added and the atmosphere was exchanged for H_2. The reaction was vigorously stirred for 2 h while bubbling H_2 through the mixture. The atmosphere was exchanged for N_2, the mixture was filtered over Celite and subsequently concentrated to afford the product (1.58 g, 9.35 mmol, 81%). ^{1}H NMR (400 MHz, MeOD) δ 6.63 (d, *J* = 1.8 Hz, 1H), 6.60 (d, *J* = 7.8 Hz, 1H), 6.51 (dd, *J* = 7.9, 1.8 Hz, 1H), 3.63 – 3.58 (m, 4H), 3.27 (s, 2H), 2.41 – 2.31 (m, 4H). ^{13}C NMR (101 MHz, MeOD) δ 135.81, 135.32, 128.48, 122.11, 119.00, 117.20, 67.51, 64.25, 54.39. LCMS (Fleet, 0 → 50%): t_r = 0.86 min, m/z: 208.1.

4-((2-(4-Nitro-1*H*-pyrazol-3-yl)-1*H*-benzo[*d*]imidazol-5-yl)methyl)morpholine (29)

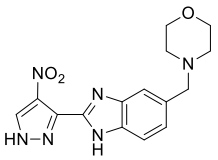

28 (3.55 g, 17.1 mmol), 4-nitro-1*H*-pyrazole-3-carboxylic acid (2.53 g, 16.1 mmol), EDC·HCl (3.38 g, 17.7 mmol) and HOBt (2.32 g, 17.1 mmol) were mixed in dry DMF (39 mL) and stirred for 20 h. The mixture was concentrated at 60°C after which AcOH (49 mL) was added. The mixture was heated to 118°C and stirred for 2.5 h. The mixture was concentrated at 80°C and traces of AcOH were removed by coevaporated with toluene (4x20 mL). The crude was brought onto Celite and purified by silica gel chromatography (5 – 9% MeOH/DCM) to afford the product (3.07 g, 9.35 mmol, 55%). ^{1}H NMR (400 MHz, MeOD) δ 8.60 (s, 1H), 7.68 (s, 1H), 7.60 (d, *J* = 8.3 Hz, 1H), 7.28 (d, *J* = 8.4 Hz, 1H), 3.98 (s, 2H), 3.78 – 3.66 (m, 4H), 2.89 – 2.78 (m, 4H). ^{13}C NMR (101 MHz, MeOD) δ 144.63, 139.63, 139.44, 136.69, 134.62, 133.79, 128.93, 126.95, 118.88, 116.50, 66.10, 63.04, 53.34. LCMS (Finnigan, 0 → 50%): t_r = 4.60 min, m/z: 329.1.

3-(5-(Morpholinomethyl)-1*H*-benzo[*d*]imidazol-2-yl)-1*H*-pyrazol-4-amine (30)

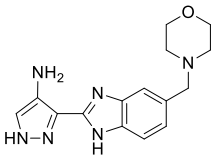

29 (398 mg, 1.21 mmol) was suspended in degassed MeOH (14 mL). 10% Pd/C (56 mg) was added and the atmosphere was exchanged for H_2. The reaction was vigorously stirred for 100 min while bubbling H_2 through the mixture. The atmosphere was exchanged for N_2, the mixture was filtered over Celite and subsequently concentrated. The crude was purified by silica gel chromatography (6 – 9% MeOH (containing 10% sat. NH_4OH (aq.))/DCM) to afford the product (260 mg, 1.21 mmol, 72%). ^{1}H NMR (500 MHz, MeOD) δ 7.53 – 7.40 (m, 2H), 7.31 (s, 1H), 7.10 (dd, *J* = 8.3, 1.3 Hz, 1H), 3.61 – 3.54 (m, 4H), 3.45 (s, 2H), 2.38 – 2.30 (m, 4H). ^{13}C NMR (126 MHz, MeOD) δ 149.40 (br), 139.52 (br), 132.38 (br), 132.14, 130.90, 125.30, 118.67 (br), 116.01 (br), 67.49, 64.48, 54.33. LCMS (Finnigan, 0 → 50%): t_r = 0.92 min, m/z: 299.1.

4-(4-Nitrophenyl)morpholine (31)

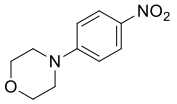

1-Fluoro-4-nitrobenzene (510 mg, 3.61 mmol) was dissolved in MeCN (8 mL) after which morpholine (350 µL, 4.00 mmol) and Et_3N (555 µL, 3.98 mmol) were added. The mixture was heated to 82°C, stirred for 15 h and subsequently poured into H_2O (100 mL). The product was extracted with EtOAc (3x75 mL) after which the combined organic layers were washed with brine (200 mL), dried over Na_2SO_4, filtered and concentrated. The crude was purified by silica gel chromatography (0 – 1% MeOH (containing 10% sat. NH_4OH (aq.))/DCM) to afford the product (701 mg, 3.37 mmol, 93%). ^{1}H NMR (400 MHz, $CDCl_3$) δ 8.10 – 8.04 (m, 2H), 6.82 – 6.75 (m, 2H), 3.87 – 3.79 (m, 4H), 3.38 – 3.31 (m, 4H). ^{13}C NMR (101 MHz, $CDCl_3$) δ 155.00, 138.78, 125.85, 112.55, 66.35, 47.04.

4-Morpholinoaniline (32)

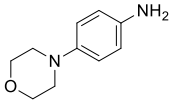

31 (2.51 g, 12.1 mmol) was suspended in MeOH (150 mL) and this mixture was subsequently degassed by bubbling N_2 through the mixture while sonicating for 20 min. 10% Pd/C (251 mg) was added and the atmosphere was exchanged for H_2. The reaction was vigorously stirred for 5 h while bubbling H_2 through the mixture. The atmosphere was exchanged for N_2, the mixture was filtered over Celite and subsequently concentrated. The crude was purified by silica gel chromatography (6 – 20% MeOH (containing 10% sat. NH_4OH

(aq.))/DCM) to afford the product (1.97 g, 11.0 mmol, 91%). ^{1}H NMR (400 MHz, $CDCl_3$) δ 6.81 – 6.76 (m, 2H), 6.66 – 6.61 (m, 2H), 3.87 – 3.80 (m, 4H), 3.46 (s, 2H), 3.05 – 2.97 (m, 4H). ^{13}C NMR (101 MHz, $CDCl_3$) δ 144.21, 140.37, 118.07, 116.07, 66.98, 51.01.

1-(4-Morpholinophenyl)guanidine (33)

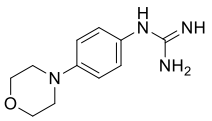

32 (800 mg, 4.49 mmol) was suspended in EtOH (2.65 mL) and cooled down to 0°C. Concentrated HCl (aq.) (300 µL, 3.73 mmol) and cyanamide (50% w/w aq.) (660 µL, 16.6 mmol) were added and the mixture was heated to 78°C and stirred for 4 h. The reaction was allowed to cool down to RT after which concentrated HCl (aq.) (300 µL, 3.73 mmol) was added and the mixture was heated to 78°C and stirred for 4 h. The reaction was cooled to RT and concentrated HCl (466 µL, 5.70 mmol) was added after which the mixture was heated to 78°C and stirred overnight. The crude was carefully poured into a mixture of DCM (100 mL) and 1 M $NaHCO_3$ (100 mL) and stirred. The formed precipitate was collected by filtration of the two layers. The solids were collected, suspended in H_2O (10 mL) and sonicated for a few minutes. The suspension was filtered, washed with acetone (20 mL) after which the solids were collected and concentrated to afford the product (948 mg, 4.31 mmol, 96%). ^{1}H NMR (400 MHz, DMSO) δ 7.29 (br s, 4H), 6.89 (s, 4H), 3.76 – 3.69 (m, 4H), 3.08 – 3.01 (m, 4H). ^{13}C NMR (101 MHz, DMSO) δ 160.18, 155.01 (br), 147.78 (br), 124.73, 116.16, 66.19, 48.99.

1-(2-Amino-4-methylthiazol-5-yl)ethan-1-one hydrochloride (34)

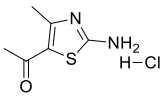

Thiourea (250 mg, 3.28 mmol) was dissolved in MeOH (2.5 mL) and cooled down to 0°C. Pyridine (106 µL, 1.31 mmol) and 3-chloropentane-2,4-dione (372 µL, 3.29 mmol) were added after which the mixture was allowed to warm to RT and stirred for 2 h. The mixture was concentrated, subsequently suspended in EtOAc (3 mL) and filtered. The solids were washed with EtOAc (5 mL), collected and dried to afford the product (562 mg, 2.91 mmol, 89%). ^{1}H NMR (400 MHz, DMSO) δ 7.83 (s, 2H), 2.40 (s, 3H), 2.32 (s, 3H). ^{13}C NMR (101 MHz, DMSO) δ 188.27, 170.51, 157.72, 121.30, 29.49, 18.35.

N'-(5-(3-(Dimethylamino)acryloyl)-4-methylthiazol-2-yl)-*N*,*N*-dimethylformimidamide (35)

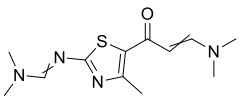

34 (500 mg, 2.60 mmol) was mixed with DMF-DMA (1.5 mL, 11 mmol) and stirred at 105°C for 18 h. The mixture was concentrated and subsequently purified by silica gel chromatography (1 – 6% MeOH/DCM) to afford the product (484 mg, 1.82 mmol, 70%). ^{1}H NMR (400 MHz, $CDCl_3$) δ 8.16 (s, 1H), 7.61 (d, *J* = 12.2 Hz, 1H), 5.28 (d, *J* = 12.2 Hz, 1H), 3.05 (s, 3H), 3.03 (br s, 3H), 3.02 (s, 3H), 2.81 (br s, 3H), 2.57 (s, 3H). ^{13}C NMR (101 MHz, $CDCl_3$) δ 181.50, 173.60, 155.89, 153.98, 152.89, 126.60, 95.03, 40.90, 35.00, 18.28. LCMS (Finnigan, 0 → 50%): t_r = 5.33 min, m/z: 267.1.

Ethyl 4-(benzyloxy)-3-hydroxybenzoate (36)

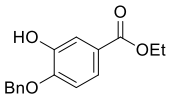

Ph_3P (6.00 g, 23.1 mmol) and DIAD (4.8 mL, 23 mmol) were dissolved in dry THF (147 mL) and cooled down to 0°C. Benzyl alcohol (2.3 mL, 22 mmol) was added and the mixture was stirred for 5 min. A solution of ethyl 3,4-dihydroxybenzoate (4.00 g, 22.0 mmol) in THF (37 mL) was added and the mixture was stirred for 30 min after which the reaction was allowed to warm to RT and continued to stir for 70 h. The mixture was concentrated, loaded onto Celite and purified by automated column chromatography (twice, 5 – 40% Et_2O/pentane) to afford the product (2.43 g, 8.93 mmol, 41%). ^{1}H NMR (400 MHz, $CDCl_3$) δ 7.63 (d, *J* = 2.1 Hz, 1H), 7.60 (dd, *J* = 8.4, 2.1 Hz, 1H), 7.47 – 7.33 (m, 5H), 6.94 (d, *J* = 8.5 Hz, 1H), 5.78 (s, 1H), 5.16 (s, 2H), 4.33 (q, *J* = 7.1 Hz, 2H), 1.37 (t, *J* = 7.1 Hz, 3H). ^{13}C NMR (101 MHz, $CDCl_3$) δ 166.41, 149.59, 145.51, 135.70, 128.75, 128.24, 127.98, 124.10, 122.74, 115.93, 111.29, 71.19, 60.91, 14.45. Regioselectivity was confirmed by ^{1}H-^{1}H-ROESY NMR analysis. LCMS (Finnigan, 10 → 90%): t_r = 7.66 min, m/z: not observed.

Ethyl 3-(2-acetoxyethoxy)-4-(benzyloxy)benzoate (37)

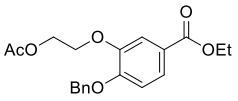

36 (2.40 g, 8.81 mmol) was dissolved in dry DMF (8.8 mL). K_2CO_3 (2.44 g, 17.6 mmol) and 2-bromoethyl acetate (1.5 mL, 13 mmol) were added and the mixture was stirred at 100°C for 3 h. The mixture was poured into H_2O (200 mL) and the product extracted with DCM (3x150 mL). The combined organic layers were washed with brine (200 mL), dried over Na_2SO_4, filtered and concentrated. The crude was purified by silica gel chromatography (10 – 20% Et_2O/pentane) to afford the product (2.26 g, 6.30 mmol, 72%). ^{1}H NMR (400 MHz, $CDCl_3$) δ 7.66 (dd, *J* = 8.4, 2.0 Hz, 1H), 7.61 (d, *J* = 2.0 Hz, 1H), 7.46 – 7.41 (m, 2H), 7.41 – 7.35 (m, 2H), 7.34 – 7.29 (m, 1H), 6.93 (d, *J* = 8.5 Hz, 1H), 5.19 (s, 2H), 4.49 – 4.41 (m, 2H), 4.34 (q, *J* = 7.1 Hz, 2H), 4.31 – 4.27 (m, 2H), 2.07 (s, 3H), 1.37 (t, *J* = 7.1 Hz, 3H). ^{13}C NMR (101 MHz, $CDCl_3$) δ 171.14, 166.32, 152.90, 148.18, 136.57, 128.73, 128.17, 127.25, 124.47, 123.59, 115.71, 113.41, 70.92, 67.65, 62.97, 60.99, 21.00, 14.52. LCMS (Finnigan, 10 → 90%): t_r = 8.27 min, m/z: not observed.

Ethyl 3-(2-acetoxyethoxy)-4-hydroxybenzoate (38)

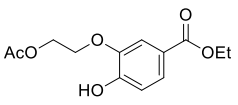

37 (2.26 g, 6.30 mmol) was dissolved in degassed MeOH (63 mL). 10% Pd/C (226 mg) was added and the atmosphere was exchanged for H_2. The reaction was vigorously stirred for 2.5 h while bubbling H_2 through the mixture. The atmosphere was exchanged for N_2, the mixture was filtered over Celite and subsequently concentrated to afford the product (1.65 g, 6.14 mmol, 98%). ^{1}H NMR (400 MHz, $CDCl_3$) δ 7.66 (dd, *J* = 8.3, 1.9 Hz, 1H), 7.55 (d, *J* = 1.9 Hz, 1H), 6.95 (d, *J* = 8.4 Hz, 1H), 6.32 (s, 1H), 4.50 – 4.43 (m, 2H), 4.33 (q, *J* = 7.2 Hz, 2H), 4.31 – 4.27 (m, 2H), 2.10 (s, 3H), 1.37 (t, *J* = 7.1 Hz, 3H). ^{13}C NMR (101 MHz, $CDCl_3$) δ 171.29, 166.38, 150.50, 145.23, 124.95, 122.68, 114.64, 113.60, 67.92, 62.63, 60.97, 21.00, 14.50. LCMS (Finnigan, 10 → 90%): t_r = 6.23 min, m/z: not observed.

Ethyl 3-(2-acetoxyethoxy)-4-(2-methoxyethoxy)benzoate (39)

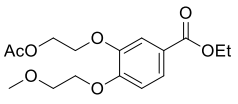

38 (1.62 g, 6.03 mmol) was dissolved in dry DMF (6 mL). K_2CO_3 (1.67 g, 12.1 mmol) and 1-bromo-2-methoxyethane (850 µL, 9.04 mmol) were added and the mixture was stirred at 100°C for 2 h. The mixture was poured into H_2O (200 mL) and the product extracted with DCM (3x150 mL). The combined organic layers were washed with brine (200 mL), dried over Na_2SO_4, filtered and concentrated. The crude was purified by silica gel chromatography (25 – 50% EtOAc/pentane) to afford the product (1.89 g, 5.80 mmol, 96%). ^{1}H NMR (400 MHz, $CDCl_3$) δ 7.68 (dd, *J* = 8.4, 2.0 Hz, 1H), 7.58 (d, *J* = 2.0 Hz, 1H), 6.91 (d, *J* = 8.5 Hz, 1H), 4.48 – 4.41 (m, 2H), 4.34 (q, *J* = 7.1 Hz, 2H), 4.28 – 4.23 (m, 2H), 4.22 – 4.17 (m, 2H), 3.82 – 3.75 (m, 2H), 3.45 (s, 3H), 2.09 (s, 3H), 1.37 (t, *J* = 7.1 Hz, 3H). ^{13}C NMR (101 MHz, $CDCl_3$) δ 171.06, 166.27, 153.06, 148.00, 124.44, 123.49, 115.62, 112.85, 70.87, 68.64, 67.53, 62.95, 60.90, 59.39, 20.95, 14.46.

Ethyl 5-(2-acetoxyethoxy)-4-(2-methoxyethoxy)-2-nitrobenzoate (40)

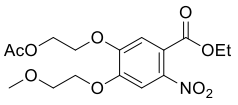

39 (1.86 g, 5.71 mmol) was dissolved in Ac_2O (15 mL) and cooled down to 0°C. $Cu(NO_3)_2{\cdot}3H_2O$ (3.45 g, 14.3 mmol) was added and the mixture was stirred at 0°C for 1 h. The mixture was allowed to warm to RT and stirred until the mild exothermic reaction had occurred. The reaction was cooled down to 0°C, diluted with H_2O (200 mL) and the product extracted with DCM (3x150 mL). The combined organic layers were washed with 1 M $NaHCO_3$ (aq.) (200 mL), brine (200 mL) and subsequently dried over Na_2SO_4, filtered and concentrated. The crude was purified by silica gel chromatography (30 – 60% Et_2O/pentane) to afford the product (1.55 g, 4.17 mmol, 73%). ^{1}H NMR (400 MHz, $CDCl_3$) δ 7.49 (s, 1H), 7.11 (s, 1H), 4.50 – 4.43 (m, 2H), 4.36 (q, *J* = 7.2 Hz, 2H), 4.34 – 4.27 (m, 2H), 4.26 – 4.20 (m, 2H), 3.83 – 3.76 (m, 2H), 3.45 (s, 3H), 2.09 (s, 3H), 1.34 (t, *J* = 7.2 Hz, 3H). ^{13}C NMR (101 MHz, $CDCl_3$) δ 170.94, 165.72, 151.90, 150.26, 141.74, 122.09, 113.21, 109.31, 70.68, 69.45, 67.67, 62.58, 62.40, 59.47, 20.92, 13.90.

Ethyl 5-(2-acetoxyethoxy)-2-amino-4-(2-methoxyethoxy)benzoate (41)

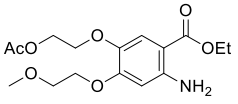

40 (657 mg, 1.77 mmol) was dissolved in degassed MeOH (5 mL). 5% Pt/C (66 mg) was added and the atmosphere was exchanged for H_2. The reaction was vigorously stirred for 1 h while bubbling H_2 through the mixture. The atmosphere was exchanged for N_2, the mixture was filtered over Celite and

subsequently concentrated. The crude was brought onto Celite and purified by automated column chromatography (50 – 100% Et_2O/pentane) to afford the product (396 mg, 1.16 mmol, 66%). ^{1}H NMR (400 MHz, $CDCl_3$) δ 7.41 (s, 1H), 6.13 (s, 1H), 4.38 – 4.34 (m, 2H), 4.27 (q, *J* = 7.1 Hz, 2H), 4.13 – 4.07 (m, 4H), 3.77 – 3.73 (m, 2H), 3.42 (s, 3H), 2.08 (s, 3H), 1.35 (t, *J* = 7.1 Hz, 3H) (the –NH_2 was not observed). ^{13}C NMR (101 MHz, $CDCl_3$) δ 171.17, 167.68, 155.38, 148.04, 139.31, 118.98, 103.06, 100.76, 70.74, 69.16, 68.06, 63.39, 60.20, 59.32, 21.00, 14.52.

2-((7-(2-Methoxyethoxy)-4-oxo-3,4-dihydroquinazolin-6-yl)oxy)ethyl acetate (42)

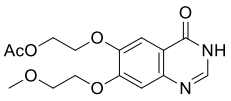

41 (629 mg, 1.84 mmol) and NH_4HCO_2 (117 mg, 1.85 mmol) were mixed in formamide (1.9 mL) and stirred at 160°C for 3.5 h. The mixture was poured into H_2O (25 mL) and the product extracted with DCM (3x25 mL). The combined organic layers were washed with brine (25 mL), dried over Na_2SO_4, filtered and concentrated. The crude was purified by automated column chromatography (1 – 10% MeOH/DCM) to afford the product (357 mg, 1.11 mmol, 60%). ^{1}H NMR (400 MHz, $CDCl_3$) δ 7.99 (s, 1H), 7.51 (s, 1H), 7.07 (s, 1H), 4.47 – 4.42 (m, 2H), 4.30 – 4.25 (m, 2H), 4.25 – 4.19 (m, 2H), 3.82 – 3.75 (m, 2H), 3.41 (s, 3H), 2.05 (s, 3H) (the –NH was not observed). ^{13}C NMR (101 MHz, $CDCl_3$) δ 171.08, 162.23, 154.88, 148.35, 145.45, 142.95, 115.67, 109.15, 107.06, 70.48, 68.60, 67.08, 62.51, 59.31, 20.84. LCMS (Finnigan, 10 → 90%): t_r = 3.86 min, m/z: 323.1.

2-((4-Chloro-7-(2-methoxyethoxy)quinazolin-6-yl)oxy)ethyl acetate (43)

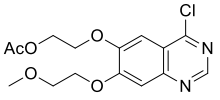

42 (332 mg, 1.03 mmol) was dissolved in $POCl_3$ (2 mL) and the mixture was stirred at 105°C for 1.5 h. The mixture was poured into H_2O (50 mL) and the product extracted with DCM (3x50 mL). The combined organic layers were washed with brine (50 mL), dried over Na_2SO_4, filtered and concentrated. The crude was purified by automated column chromatography (1 – 10% MeOH/DCM) to afford the product (280 mg, 820 µmol, 80%). ^{1}H NMR (400 MHz, $CDCl_3$) δ 8.86 (s, 1H), 7.42 (s, 1H), 7.34 (s, 1H), 4.57 – 4.53 (m, 2H), 4.41 – 4.37 (m, 2H), 4.35 – 4.30 (m, 2H), 3.91 – 3.85 (m, 2H), 3.49 (s, 3H), 2.12 (s, 3H). ^{13}C NMR (101 MHz, $CDCl_3$) δ 171.04, 159.30, 156.45, 152.74, 150.71, 149.19, 119.55, 107.99, 104.48, 70.46, 69.09, 67.34, 62.41, 59.59, 21.00. LCMS (Finnigan, 10 → 90%): t_r = 5.62 min, m/z: 341.0.

2-((4-((3-Ethynylphenyl)amino)-7-(2-methoxyethoxy)quinazolin-6-yl)oxy)ethyl acetate (44)

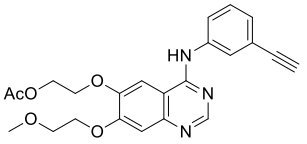

43 (30 mg, 87 µmol) was dissolved in 2-propanol (0.6 mL). 3-Ethynylaniline (10 µL, 96 µmol) was added and the mixture was stirred at 82°C for 1.5 h. The mixture was concentrated and purified by automated column chromatography (1 – 10% MeOH/DCM) to afford the product (36 mg, 87 µmol, quant.). ^{1}H NMR (400 MHz, MeOD) δ 8.44 (s, 1H), 7.90 (d, *J* = 1.9 Hz, 1H), 7.80 (s, 1H), 7.75 (d, *J* = 8.1 Hz, 1H), 7.36 (t, *J* = 7.9 Hz, 1H), 7.26 (d, *J* = 7.6 Hz, 1H), 7.18 (s, 1H), 4.54 – 4.49 (m, 2H), 4.40 (t, *J* = 4.6 Hz, 2H), 4.32 – 4.27 (m, 2H), 3.88 – 3.82 (m, 2H), 3.47 (d, *J* = 1.9 Hz, 4H), 2.09 (s, 3H). LCMS (Finnigan, 0 → 50%): t_r = 8.25 min, m/z: 422.2.

3-Iodo-1*H*-pyrazolo[3,4-*d*]pyrimidin-4-amine (45)

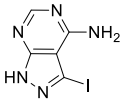

1*H*-Pyrazolo[3,4-*d*]pyrimidin-4-amine (157 mg, 1.16 mmol) and *N*-iodosuccinimide (287 mg, 1.28 mmol) were suspended in dry DMF (0.65 mL), heated to 85°C and stirred for 18 h. The mixture was filtered and the solids washed with ice cold EtOH (2 mL). The solids were collected and concentrated to afford the product (191 mg, 0.733 mmol, 63%).^{1}H NMR (400 MHz, DMSO) δ 8.17 (s, 1H), 7.62 (br s, 1H), 6.69 (br s, 1H) (the –NH was not observed).

1-Cyclopentyl-3-iodo-1*H*-pyrazolo[3,4-*d*]pyrimidin-4-amine (46)

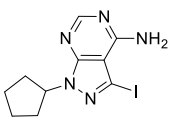

45 (100 mg, 0.383 mmol) and K_2CO_3 (212 mg, 1.53 mmol) were suspended in dry DMF (2.5 mL) after which bromocyclopentane (45 µL, 0.42 mmol) was added and the mixture was stirred at 80°C for 4 h. The mixture was filtered and the solids dissolved in a mixture of H_2O (40 mL) and EtOAc (40 mL). The organic layer was separated and the water layer extracted with EtOAc (40 mL). The combined organic layers were

washed with brine (80 mL), dried over Na_2SO_4, filtered and concentrated. The crude was purified by automated column chromatography (0 – 100% MeOH/DCM) to afford the product (74.7 mg, 0.227 mmol, 59%). ^{1}H NMR (400 MHz, MeOD) δ 8.18 (s, 1H), 5.13 (p, *J* = 7.6 Hz, 1H), 2.16 – 1.99 (m, 4H), 1.99 – 1.85 (m, 2H), 1.79 – 1.60 (m, 2H). ^{13}C NMR (101 MHz, MeOD) δ 158.20, 155.70, 153.39, 104.41, 86.64, 58.78, 32.63, 24.84. LCMS (Finnigan, 0 → 50%): t_r = 7.48 min, m/z: 330.0.

Supplementary information

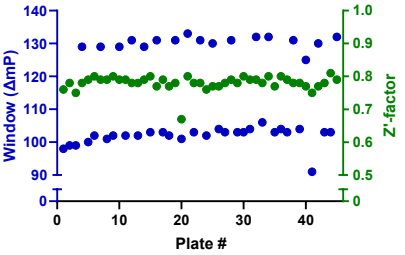

Supplementary Figure 1 | Quality parameters during primary screen. In blue, the assay window (ΔmP) per plate. In green, the Z'-factor per plate.

References

1. Sung, H., Ferlay, J., Siegel, R. L., Laversanne, M., Soerjomataram, I., Jemal, A. & Bray, F. Global Cancer Statistics 2020: GLOBOCAN Estimates of Incidence and Mortality Worldwide for 36 Cancers in 185 Countries. *CA. Cancer J. Clin.* **71**, 209–249 (2021).
2. Duffy, M. J., Harbeck, N., Nap, M., Molina, R., Nicolini, A., Senkus, E. & Cardoso, F. Clinical use of biomarkers in breast cancer: Updated guidelines from the European Group on Tumor Markers (EGTM). *Eur. J. Cancer* **75**, 284–298 (2017).
3. Waks, A. G. & Winer, E. P. Breast Cancer Treatment: A Review. *JAMA* **321**, 288 (2019).
4. Howlader, N., Altekruse, S. F., Li, C. I., Chen, V. W., Clarke, C. A., Ries, L. A. G. & Cronin, K. A. US Incidence of Breast Cancer Subtypes Defined by Joint Hormone Receptor and HER2 Status. *JNCI J. Natl. Cancer Inst.* **106**, (2014).
5. Jordan, V. C. Selective Estrogen Receptor Modulation: A Personal Perspective. *Cancer Res.* **61**, 5683–5687 (2001).
6. Johnston, S. R. D. & Dowsett, M. Aromatase inhibitors for breast cancer: lessons from the laboratory. *Nat. Rev. Cancer* **3**, 821–831 (2003).
7. Harbeck, N., Penault-Llorca, F., Cortes, J., Gnant, M., Houssami, N., Poortmans, P., Ruddy, K., Tsang, J. & Cardoso, F. Breast cancer. *Nat. Rev. Dis. Primer* **5**, 66 (2019).
8. Hudis, C. A. Trastuzumab — Mechanism of Action and Use in Clinical Practice. *N. Engl. J. Med.* **357**, 39–51 (2007).
9. Xuhong, J.-C., Qi, X.-W., Zhang, Y. & Jiang, J. Mechanism, safety and efficacy of three tyrosine kinase inhibitors lapatinib, neratinib and pyrotinib in HER2-positive breast cancer. *Am. J. Cancer Res.* **9**, 2103–2119 (2019).
10. Dominguez-Brauer, C., Thu, K. L., Mason, J. M., Blaser, H., Bray, M. R. & Mak, T. W. Targeting Mitosis in Cancer: Emerging Strategies. *Mol. Cell* **60**, 524–536 (2015).
11. Kops, G. J. P. L., Weaver, B. A. A. & Cleveland, D. W. On the road to cancer: aneuploidy and the mitotic checkpoint. *Nat. Rev. Cancer* **5**, 773–785 (2005).
12. Siemeister, G., Mengel, A., Fernández-Montalván, A. E., Bone, W., Schröder, J., Zitzmann-Kolbe, S., Briem, H., Prechtl, S., Holton, S. J., Mönning, U., von Ahsen, O., Johanssen, S., Cleve, A., Pütter, V., Hitchcock, M., von Nussbaum, F., Brands, M., Ziegelbauer, K. & Mumberg, D. Inhibition of BUB1 Kinase by BAY 1816032 Sensitizes Tumor Cells toward Taxanes, ATR, and PARP Inhibitors *In Vitro* and *In Vivo*. *Clin. Cancer Res.* **25**, 1404–1414 (2019).
13. Musacchio, A. & Salmon, E. D. The spindle-assembly checkpoint in space and time. *Nat. Rev. Mol. Cell Biol.* **8**, 379–393 (2007).
14. Zhang, G., Kruse, T., López-Méndez, B., Sylvestersen, K. B., Garvanska, D. H., Schopper, S., Nielsen, M. L. & Nilsson, J. Bub1 positions Mad1 close to KNL1 MELT repeats to promote checkpoint signalling. *Nat. Commun.* **8**, 15822 (2017).
15. Zhang, G., Lischetti, T., Hayward, D. G. & Nilsson, J. Distinct domains in Bub1 localize RZZ and BubR1 to kinetochores to regulate the checkpoint. *Nat. Commun.* **6**, 7162 (2015).
16. Di Fiore, B., Davey, N. E., Hagting, A., Izawa, D., Mansfeld, J., Gibson, T. J. & Pines, J. The ABBA Motif Binds APC/C Activators and Is Shared by APC/C Substrates and Regulators. *Dev. Cell* **32**, 358–372 (2015).
17. Ciossani, G., Overlack, K., Petrovic, A., Huis in 't Veld, P. J., Koerner, C., Wohlgemuth, S., Maffini, S. & Musacchio, A. The kinetochore proteins CENP-E and CENP-F directly and specifically interact with distinct BUB mitotic checkpoint Ser/Thr kinases. *J. Biol. Chem.* **293**, 10084–10101 (2018).
18. Bolanos-Garcia, V. M. & Blundell, T. L. BUB1 and BUBR1: multifaceted kinases of the cell cycle. *Trends Biochem. Sci.* **36**, 141–150 (2011).
19. Elowe, S. Bub1 and BubR1: at the Interface between Chromosome Attachment and the Spindle Checkpoint. *Mol. Cell. Biol.* **31**, 3085–3093 (2011).
20. Funabiki, H. & Wynne, D. J. Making an effective switch at the kinetochore by phosphorylation and dephosphorylation. *Chromosoma* **122**, 135–158 (2013).
21. Baron, A. P., von Schubert, C., Cubizolles, F., Siemeister, G., Hitchcock, M., Mengel, A., Schröder, J., Fernández-Montalván, A., von Nussbaum, F., Mumberg, D. & Nigg, E. A. Probing the catalytic functions of Bub1 kinase using the small molecule inhibitors BAY-320 and BAY-524. *eLife* **5**, e12187 (2016).
22. Zhang, G., Kruse, T., Guasch Boldú, C., Garvanska, D. H., Coscia, F., Mann, M., Barisic, M. & Nilsson, J. Efficient mitotic checkpoint signaling depends on integrated activities of Bub1 and the RZZ complex. *EMBO J.* **38**, (2019).
23. Gaudet, E. A., Huang, K.-S., Zhang, Y., Huang, W., Mark, D. & Sportsman, J. R. A Homogeneous Fluorescence Polarization Assay Adaptable for a Range of Protein Serine/Threonine and Tyrosine Kinases. *J. Biomol. Screen.* **8**, 164–175 (2003).
24. Mayr, L. M. & Bojanic, D. Novel trends in high-throughput screening. *Curr. Opin. Pharmacol.* **9**, 580–588 (2009).
25. Cronk, D. Chapter 8 - High-throughput screening. in *Drug Discovery and Development (Second Edition)* (eds. Hill, R. & Rang, H.) 95–117 (Churchill Livingstone, 2013).
26. Hall, M. D., Yasgar, A., Peryea, T., Braisted, J. C., Jadhav, A., Simeonov, A. & Coussens, N. P. Fluorescence polarization assays in high-throughput screening and drug discovery: a review. *Methods Appl. Fluoresc.* **4**, 022001 (2016).
27. Jameson, D. M. & Ross, J. A. Fluorescence Polarization/Anisotropy in Diagnostics and Imaging. *Chem. Rev.* **110**, 2685–2708 (2010).

28. Wermuth, C. G. Selective optimization of side activities: the SOSA approach. *Drug Discov. Today* **11**, 160–164 (2006).
29. Kirsch, P., Hartman, A. M., Hirsch, A. K. H. & Empting, M. Concepts and Core Principles of Fragment-Based Drug Design. *Molecules* **24**, 4309 (2019).
30. Gimeno, A., Ojeda-Montes, M., Tomás-Hernández, S., Cereto-Massagué, A., Beltrán-Debón, R., Mulero, M., Pujadas, G. & Garcia-Vallvé, S. The Light and Dark Sides of Virtual Screening: What Is There to Know? *Int. J. Mol. Sci.* **20**, 1375 (2019).
31. Hopkins, A. L., Keserü, G. M., Leeson, P. D., Rees, D. C. & Reynolds, C. H. The role of ligand efficiency metrics in drug discovery. *Nat. Rev. Drug Discov.* **13**, 105–121 (2014).
32. Bleicher, K. H., Böhm, H.-J., Müller, K. & Alanine, A. I. Hit and lead generation: beyond high-throughput screening. *Nat. Rev. Drug Discov.* **2**, 369–378 (2003).
33. Zhang, J.-H., Chung, T. D. Y. & Oldenburg, K. R. A Simple Statistical Parameter for Use in Evaluation and Validation of High Throughput Screening Assays. *J. Biomol. Screen.* **4**, 67–73 (1999).
34. Brideau, C., Gunter, B., Pikounis, B. & Liaw, A. Improved Statistical Methods for Hit Selection in High-Throughput Screening. *J. Biomol. Screen.* **8**, 634–647 (2003).
35. Howard, S., Berdini, V., Boulstridge, J. A., Carr, M. G., Cross, D. M., Curry, J., Devine, L. A., Early, T. R., Fazal, L., Gill, A. L., Heathcote, M., Maman, S., Matthews, J. E., McMenamin, R. L., Navarro, E. F., O'Brien, M. A., O'Reilly, M., Rees, D. C., Reule, M., Tisi, D., Williams, G., Vinković, M. & Wyatt, P. G. Fragment-Based Discovery of the Pyrazol-4-yl Urea (AT9283), a Multitargeted Kinase Inhibitor with Potent Aurora Kinase Activity. *J. Med. Chem.* **52**, 379–388 (2009).
36. Wang, S., Midgley, C. A., Scaërou, F., Grabarek, J. B., Griffiths, G., Jackson, W., Kontopidis, G., McClue, S. J., McInnes, C., Meades, C., Mezna, M., Plater, A., Stuart, I., Thomas, M. P., Wood, G., Clarke, R. G., Blake, D. G., Zheleva, D. I., Lane, D. P., Jackson, R. C., Glover, D. M. & Fischer, P. M. Discovery of *N* -Phenyl-4-(thiazol-5-yl)pyrimidin-2-amine Aurora Kinase Inhibitors. *J. Med. Chem.* **53**, 4367–4378 (2010).
37. Ling, J., Johnson, K. A., Miao, Z., Rakhit, A., Pantze, M. P., Hamilton, M., Lum, B. L. & Prakash, C. Metabolism and excretion of erlotinib, a small molecule inhibitor of epidermal growth factor receptor tyrosine kinase, in healthy male volunteers. *Drug Metab. Dispos.* **34**, 420–426 (2006).
38. Apsel, B., Blair, J. A., Gonzalez, B., Nazif, T. M., Feldman, M. E., Aizenstein, B., Hoffman, R., Williams, R. L., Shokat, K. M. & Knight, Z. A. Targeted polypharmacology: discovery of dual inhibitors of tyrosine and phosphoinositide kinases. *Nat. Chem. Biol.* **4**, 691–699 (2008).
39. Blasina, A., Hallin, J., Chen, E., Arango, M. E., Kraynov, E., Register, J., Grant, S., Ninkovic, S., Chen, P., Nichols, T., O'Connor, P. & Anderes, K. Breaching the DNA damage checkpoint via PF-00477736, a novel small-molecule inhibitor of checkpoint kinase 1. *Mol. Cancer Ther.* **7**, 2394–2404 (2008).
40. Ninkovic, S., Bennett, M. J., Rui, E. Y., Wang, F., Benedict, S. P., Teng, M., Wang, Y. & Zhu, J. Diazepinoindole derivatives as kinase inhibitors. WO2004063198A1 (2004).
41. Mader, M., de Dios, A., Shih, C., Bonjouklian, R., Li, T., White, W., de Uralde, B. L., Sánchez-Martinez, C., del Prado, M., Jaramillo, C., de Diego, E., Martín Cabrejas, L. M., Dominguez, C., Montero, C., Shepherd, T., Dally, R., Toth, J. E., Chatterjee, A., Pleite, S., Blanco-Urgoiti, J., Perez, L., Barberis, M., Lorite, M. J., Jambrina, E., Nevill, C. R., Lee, P. A., Schultz, R. C., Wolos, J. A., Li, L. C., Campbell, R. M. & Anderson, B. D. Imidazolyl benzimidazoles and imidazo[4,5-b]pyridines as potent p38α MAP kinase inhibitors with excellent in vivo antiinflammatory properties. *Bioorg. Med. Chem. Lett.* **18**, 179–183 (2008).
42. Pardanani, A., Lasho, T., Smith, G., Burns, C. J., Fantino, E. & Tefferi, A. CYT387, a selective JAK1/JAK2 inhibitor: in vitro assessment of kinase selectivity and preclinical studies using cell lines and primary cells from polycythemia vera patients. *Leukemia* **23**, 1441–1445 (2009).
43. Burns, C. J., Donohue, A. C., Feutrill, J. T., Nguyen, T. L. T., Wilks, A. F. & Zeng, J. Phenyl amino pyrimidine compounds and uses thereof. WO2008109943A1 (2008).
44. Moyer, J. D., Barbacci, E. G., Iwata, K. K., Arnold, L., Boman, B., Cunningham, A., DiOrio, C., Doty, J., Morin, M. J., Moyer, M. P., Neveu, M., Pollack, V. A., Pustilnik, L. R., Reynolds, M. M., Sloan, D., Theleman, A. & Miller, P. Induction of Apoptosis and Cell Cycle Arrest by CP-358,774, an Inhibitor of Epidermal Growth Factor Receptor Tyrosine Kinase. *Cancer Res.* **57**, 4838–4848 (1997).
45. Schnur, R. C. & Arnold, L. D. Quinazoline derivatives. WO1996030347A1 (1996).
46. Dotzauer, B., Grünert, R., Bednarski, P. J., Lanig, H., Landwehr, J. & Troschütz, R. 2,4-Diamino-9H-pyrimido[4,5-b]indol-5-ols: Synthesis, in vitro cytotoxic activity, and QSAR investigations. *Bioorg. Med. Chem.* **14**, 7282–7292 (2006).
47. Sato, H., Inoue, T., Ly, T.-W., Muramatsu, A., Shimazaki, M., Urbahns, K., Gantner, F., Okigami, H., Bacon, K. B., Komura, H., Yoshida, N. & Tsuno, N. 4-phenyl-pyrimido [4,5-b] indole derivatives. WO2004058764A1 (2004).
48. Stauffer, F., Maira, S.-M., Furet, P. & García-Echeverría, C. Imidazo[4,5-c]quinolines as inhibitors of the PI3K/PKB-pathway. *Bioorg. Med. Chem. Lett.* **18**, 1027–1030 (2008).
49. Anderson, M., Andrews, D. M., Barker, A. J., Brassington, C. A., Breed, J., Byth, K. F., Culshaw, J. D., Finlay, M. R. V., Fisher, E., McMiken, H. H. J., Green, C. P., Heaton, D. W., Nash, I. A., Newcombe, N. J., Oakes, S. E., Pauptit, R. A., Roberts, A., Stanway, J. J., Thomas, A. P., Tucker, J. A., Walker, M. & Weir, H. M. Imidazoles: SAR and development of a potent class of cyclin-dependent kinase inhibitors. *Bioorg. Med. Chem. Lett.* **18**, 5487–5492 (2008).

50. Rainey, M. D., Charlton, M. E., Stanton, R. V. & Kastan, M. B. Transient Inhibition of ATM Kinase Is Sufficient to Enhance Cellular Sensitivity to Ionizing Radiation. *Cancer Res.* **68**, 7466–7474 (2008).
51. Min, J., Guo, K., Suryadevara, P. K., Zhu, F., Holbrook, G., Chen, Y., Feau, C., Young, B. M., Lemoff, A., Connelly, M. C., Kastan, M. B. & Guy, R. K. Optimization of a Novel Series of Ataxia-Telangiectasia Mutated Kinase Inhibitors as Potential Radiosensitizing Agents. *J. Med. Chem.* **59**, 559–577 (2016).
52. Dugar, S., Chakravarty, S., Murphy, A., Mcenroe, G., Conte, A. & Perumattam, J. J. Quinazoline derivatives as medicaments. WO2005032481A2 (2005).
53. Foloppe, N., Fisher, L. M., Howes, R., Kierstan, P., Potter, A., Robertson, A. G. S. & Surgenor, A. E. Structure-Based Design of Novel Chk1 Inhibitors: Insights into Hydrogen Bonding and Protein−Ligand Affinity. *J. Med. Chem.* **48**, 4332–4345 (2005).
54. Walton, K. M., Fisher, K., Rubitski, D., Marconi, M., Meng, Q.-J., Sládek, M., Adams, J., Bass, M., Chandrasekaran, R., Butler, T., Griffor, M., Rajamohan, F., Serpa, M., Chen, Y., Claffey, M., Hastings, M., Loudon, A., Maywood, E., Ohren, J., Doran, A. & Wager, T. T. Selective Inhibition of Casein Kinase 1ϵ Minimally Alters Circadian Clock Period. *J. Pharmacol. Exp. Ther.* **330**, 430–439 (2009).
55. Chen, S., Zhang, Q., Wu, X., Schultz, P. G. & Ding, S. Dedifferentiation of Lineage-Committed Cells by a Small Molecule. *J. Am. Chem. Soc.* **126**, 410–411 (2004).
56. Ding, S., Wu, T. Y. H., Brinker, A., Peters, E. C., Hur, W., Gray, N. S. & Schultz, P. G. Synthetic small molecules that control stem cell fate. *Proc. Natl. Acad. Sci.* **100**, 7632–7637 (2003).
57. Ding, S., WU, T.-H., Gray, N. S. & Schultz, P. G. Compounds that induce neuronal differentiation in embryonic stem cells. WO2004093812A2 (2004).
58. Pierre, F., Chua, P. C., O'Brien, S. E., Siddiqui-Jain, A., Bourbon, P., Haddach, M., Michaux, J., Nagasawa, J., Schwaebe, M. K., Stefan, E., Vialettes, A., Whitten, J. P., Chen, T. K., Darjania, L., Stansfield, R., Anderes, K., Bliesath, J., Drygin, D., Ho, C., Omori, M., Proffitt, C., Streiner, N., Trent, K., Rice, W. G. & Ryckman, D. M. Discovery and SAR of 5-(3-Chlorophenylamino)benzo[*c*][2,6]naphthyridine-8-carboxylic Acid (CX-4945), the First Clinical Stage Inhibitor of Protein Kinase CK2 for the Treatment of Cancer. *J. Med. Chem.* **54**, 635–654 (2011).
59. Hu-Lowe, D. D., Zou, H. Y., Grazzini, M. L., Hallin, M. E., Wickman, G. R., Amundson, K., Chen, J. H., Rewolinski, D. A., Yamazaki, S., Wu, E. Y., McTigue, M. A., Murray, B. W., Kania, R. S., O'Connor, P., Shalinsky, D. R. & Bender, S. L. Nonclinical Antiangiogenesis and Antitumor Activities of Axitinib (AG-013736), an Oral, Potent, and Selective Inhibitor of Vascular Endothelial Growth Factor Receptor Tyrosine Kinases 1, 2, 3. *Clin. Cancer Res.* **14**, 7272–7283 (2008).
60. Kania, R. S., Bender, S. L., Borchardt, A. J., Cripps, S. J., Hua, Y., Johnson, M. D., Jr, T. O. J., Luu, H. T., Palmer, C. L., Reich, S. H., Tempczyk-Russell, A. M., Teng, M., Thomas, C., Varney, M. D., Wallace, M. B. & Collins, M. R. Indazole compounds and pharmaceutical compositions for inhibiting protein kinases, and methods for their use. US6534524B1 (2003).
61. Cheng, Y.-C. & Prusoff, W. H. Relationship between the inhibition constant (KI) and the concentration of inhibitor which causes 50 per cent inhibition (I50) of an enzymatic reaction. *Biochem. Pharmacol.* **22**, 3099–3108 (1973).
62. Young, R. J. & Leeson, P. D. Mapping the Efficiency and Physicochemical Trajectories of Successful Optimizations. *J. Med. Chem.* **61**, 6421–6467 (2018).
63. Ninkovic, S. & Rynberg, R. Polymorphic forms of (2r,z)-2-amino-2-cyclohexyl-n-(5-(1-methyl-1h-pyrazol-4ʊl)-1-oxo-2,6-dihydro-1h-[1,2]diazepino[4,5,6-cd]indol-8-yl)acetamide. WO2007113647A1 (2007).
64. Olesen, S. H., Zhu, J.-Y., Martin, M. P. & Schönbrunn, E. Discovery of Diverse Small-Molecule Inhibitors of Mammalian Sterile20-like Kinase 3 (MST3). *ChemMedChem* **11**, 1137–1144 (2016).
65. Stamos, J., Sliwkowski, M. X. & Eigenbrot, C. Structure of the Epidermal Growth Factor Receptor Kinase Domain Alone and in Complex with a 4-Anilinoquinazoline Inhibitor. *J. Biol. Chem.* **277**, 46265–46272 (2002).
66. Foran, J., Ravandi, F., Wierda, W., Garcia-Manero, G., Verstovsek, S., Kadia, T., Burger, J., Yule, M., Langford, G., Lyons, J., Ayrton, J., Lock, V., Borthakur, G., Cortes, J. & Kantarjian, H. A Phase I and Pharmacodynamic Study of AT9283, a Small-Molecule Inhibitor of Aurora Kinases in Patients With Relapsed/Refractory Leukemia or Myelofibrosis. *Clin. Lymphoma Myeloma Leuk.* **14**, 223–230 (2014).
67. Dent, S. F., Gelmon, K. A., Chi, K. N., Jonker, D. J., Wainman, N., Capier, C. A., Chen, E. X., Lyons, J. F. & Seymour, L. NCIC CTG IND.181: Phase I study of AT9283 given as a weekly 24 hour infusion in advanced malignancies. *Invest. New Drugs* **31**, 1522–1529 (2013).
68. Arkenau, H.-T., Plummer, R., Molife, L. R., Olmos, D., Yap, T. A., Squires, M., Lewis, S., Lock, V., Yule, M., Lyons, J., Calvert, H. & Judson, I. A phase I dose escalation study of AT9283, a small molecule inhibitor of aurora kinases, in patients with advanced solid malignancies. *Ann. Oncol.* **23**, 1307–1313 (2012).
69. Moreno, L., Marshall, L. V., Pearson, A. D. J., Morland, B., Elliott, M., Campbell-Hewson, Q., Makin, G., Halford, S. E. R., Acton, G., Ross, P., Kazmi-Stokes, S., Lock, V., Rodriguez, A., Lyons, J. F., Boddy, A. V., Griffin, M. J., Yule, M. & Hargrave, D. A Phase I Trial of AT9283 (a Selective Inhibitor of Aurora Kinases) in Children and Adolescents with Solid Tumors: A Cancer Research UK Study. *Clin. Cancer Res.* **21**, 267–273 (2015).
70. Cyclacel Pharmaceuticals, Inc. A Phase I Pharmacologic Study of CYC116, an Oral Aurora Kinase Inhibitor, in Patients With Advanced Solid Tumors. Identifier: NCT00560716, https://clinicaltrials.gov/ct2/show/NCT00560716 (Accessed 5 July 2021) (2007).

71. Wang, S., Meades, C., Wood, G., Osnowski, A., Anderson, S., Yuill, R., Thomas, M., Mezna, M., Jackson, W., Midgley, C., Griffiths, G., Fleming, I., Green, S., McNae, I., Wu, S.-Y., McInnes, C., Zheleva, D., Walkinshaw, M. D. & Fischer, P. M. 2-Anilino-4-(thiazol-5-yl)pyrimidine CDK Inhibitors: Synthesis, SAR Analysis, X-ray Crystallography, and Biological Activity. *J. Med. Chem.* **47**, 1662–1675 (2004).
72. Masse, C. E. Substituted oxazolidinone derivatives. WO2009023233A1 (2009).
73. Kompella, A., Adibhatla, B. R. K., Muddasani, P. R., Rachakonda, S., Gampa, V. K. & Dubey, P. K. A Facile Total Synthesis for Large-Scale Production of Imatinib Base. *Org. Process Res. Dev.* **16**, 1794–1804 (2012).
74. Dowell, J., Minna, J. D. & Kirkpatrick, P. Erlotinib hydrochloride. *Nat. Rev. Drug Discov.* **4**, 13–14 (2005).
75. Zhang, Y., Ding, K., Liao, J., Wang, Y. & Chen, P. Coupling compounds of nsaid anti-inflammatory and analgesic drugs and egfr kinase inhibitors, synthesis methods and applications thereof. US20160175453A1 (2016).
76. Wang, X., Ju, T., Li, X. & Cao, X. Regioselective Alkylation of Catechols via Mitsunobu Reactions. *Synlett* **2010**, 2947–2949 (2010).
77. Gregson, S. J., Howard, P. W., Gullick, D. R., Hamaguchi, A., Corcoran, K. E., Brooks, N. A., Hartley, J. A., Jenkins, T. C., Patel, S., Guille, M. J. & Thurston, D. E. Linker Length Modulates DNA Cross-Linking Reactivity and Cytotoxic Potency of C8/C8′ Ether-Linked C2- *exo* -Unsaturated Pyrrolo[2,1- *c*][1,4]benzodiazepine (PBD) Dimers. *J. Med. Chem.* **47**, 1161–1174 (2004).
78. Knight, Z., Apsel, B. & Shokat, K. Kinase antagonists. US20070293516A1 (2007).
79. Dar, A. C. & Shokat, K. M. The Evolution of Protein Kinase Inhibitors from Antagonists to Agonists of Cellular Signaling. *Annu. Rev. Biochem.* **80**, 769–795 (2011).
80. Liao, J. J.-L. Molecular Recognition of Protein Kinase Binding Pockets for Design of Potent and Selective Kinase Inhibitors. *J. Med. Chem.* **50**, 409–424 (2007).
81. The PyMOL Molecular Graphics System, Version 2.3.0 Schrödinger, LLC.

3

Hit optimization of quinazolines as BUB1 inhibitors

Introduction

Many types of cancer cells suffer from a diminished spindle assembly checkpoint (SAC) and further weakening of these checkpoints has emerged as a potential strategy to kill cancer cells.[1,2] During mitosis, the SAC prevents anaphase initiation before all chromosomes are properly attached to the mitotic spindle.[3] Proper SAC functioning is essential for genomic integrity, since mitotic progression in the presence of unattached or incorrectly attached chromosomes may lead to aneuploidy.[3] It has been hypothesized that reducing SAC integrity contributes to the killing of malignant cells.[1] Kinases of the SAC, in particular budding uninhibited by benzimidazole 1 (BUB1), are, therefore, considered interesting drug targets.[1] To date, only one chemotype as BUB1 inhibitor, BAY1816032 (**Figure 3.1A**), has been published.[4] BAY1816032 was evaluated *in vivo* using mouse xenograft models of human triple-negative breast cancer and synergistically inhibited tumor growth when co-treated with a microtubule targeting drug (paclitaxel) or PARP inhibitor olaparib.[4] Of note, BAY1816032 did not show efficacy as single agent which suggests that more potent BUB1 inhibitors are required.

In the search for novel inhibitors for SAC kinase BUB1, quinazoline OSI-420 (**1**) (**Figure 3.1A**) was identified as a hit via high-throughput screening (**Chapter 2**) and showed a half maximum inhibitory concentration (IC_{50}) of 525 nM. Compound **1** is a metabolite of FDA-approved drug erlotinib (**2**) (**Figure 3.1A**), which inhibits the epidermal growth factor receptor (EGFR, also known as HER1 or ERBB1).[5] EGFR is part of the ERBB family of receptor tyrosine kinases and contains an extracellular ligand binding domain.[6] Ligand binding induces receptor dimerization, which in turn activates the intracellular kinase domain.[6] Subsequent autophosphorylation results in receptor activation which initiates a signaling cascade that, among other physiological processes, involves cell proliferation and inhibition of apoptosis.[7] Erlotinib blocks the intracellular kinase domain and thereby inhibits cell proliferation. Erlotinib is used for the treatment of advanced non-small cell lung cancer since 2004.[8] Of note, also erlotinib (**2**) was identified as a BUB1 inhibitor in the high-throughput screen, albeit, with lower potency (IC_{50} = 1072 nM). This may suggest that the free hydroxyl group of compound **1** plays a role in the binding activity. The binding mode of erlotinib (**2**) in EGFR (PDB code: 4HJO)[9] (**Figure 3.1B**) shows that the molecule forms a hydrogen bond between one of the quinazoline nitrogens and the amide backbone of the hinge region in EGFR. The substituents at R_1 and R_2 are solvent exposed and the phenylacetylene substituent at R_3 binds the so-called gate area of EGFR and contributes to selectivity (**Figure 3.1A, B**).[10,11] In this chapter, the structure-activity relationship of compound **1** on BUB1 kinase activity was investigated by systematically changing three distinct regions of its structure (R_1 – R_3, **Figure 3.1A**).

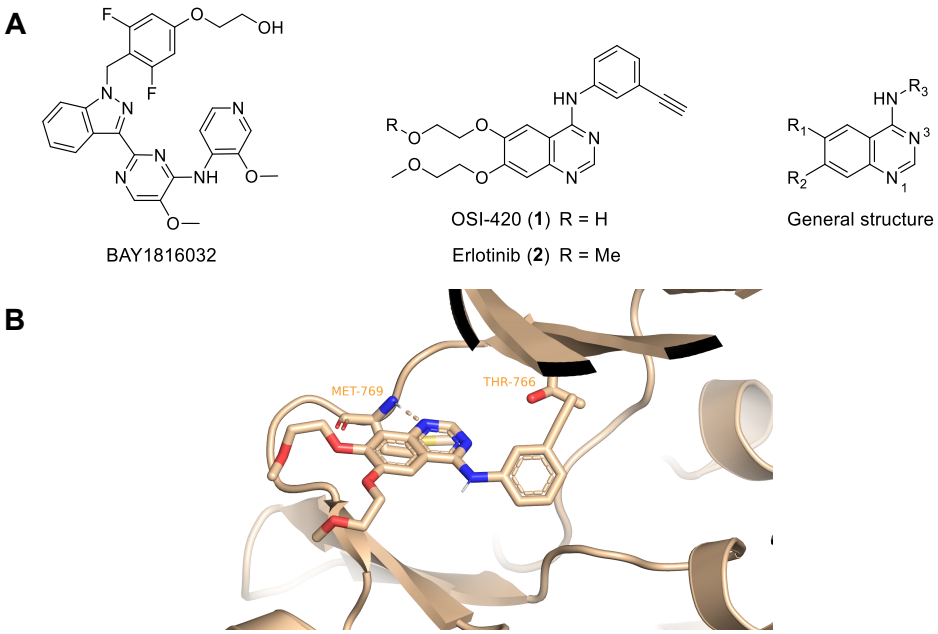

Figure 3.1 | (A) Left: chemical structure of BAY1816032. Middle: chemical structure of OSI-420 (**1**) and erlotinib (**2**). Right: regions R_1 – R_3 of the quinazoline scaffold used to investigate the structure-activity relationship of OSI-420. **(B)** Crystal structure of erlotinib (**2**) in EGFR (PDB code: 4HJO).[9] A hydrogen bond (dashed line) is formed between the quinazoline and the amide backbone of hinge amino acid Met769.

Results & Discussion

Biochemical evaluation of structural analogues 2 – 49 of hit 1

To study the structure-activity relationship (SAR) of compound **1**, analogues **2** – **49** were synthesized according to the routes reported in the Experimental section. Compounds **2** – **49** were subsequently evaluated in a biochemical fluorescence polarization assay to determine the half maximal inhibitory concentrations (IC_{50}) as described in Chapter 2. The data are reported in Table 3.1 – Table 3.6 and activities are expressed as pIC_{50} ± SEM (N=2, n=2).

First, a disjunctive approach was used to identify substituents contributing to BUB1 inhibitory activity. Compound **3**, which lacked the acetylene on the R_3-phenyl group, showed a more than 10-fold loss in potency compared to compound **1** (Table 3.1). Substitution of the phenylacetylene with a naphthyl group (**4**), to probe the size of the binding pocket, also resulted in a loss of potency. These results suggested that the acetylene group may form an important interaction with BUB1 in a relatively small hydrophobic pocket. Next, it was found methylation of the alcohol at R_1 (**2**, erlotinib) reduced potency about 4-fold, which was in agreement with data obtained from the high-throughput screen (Chapter 2). This suggests that a hydrogen bond donating property may be important. Of note, removing the methyl group at R_2 to obtain two hydroxyl groups (**6**) slightly reduced potency as well, which points towards a different role of the two solubilizers. In contrast, shortening R_1 and R_2 to methoxy

groups (**8**) retained potency compared to compound **1**, whereas complete removal of either R_1 or R_2 (**11**, **12**) reduced potency on average about 10-fold. In line, removal of both R_1 and R_2 (**13**), reduced potency at least 20-fold. Substituting the acetylene on the R_3-phenyl ring for a chlorine (**5**, **7**, **9**), reduced potency to a similar extent (on average about 6-fold) compared to analogues **2**, **6**, **8**, respectively. This observation suggested that the acetylene may form a specific contact and its activity is not due to only hydrophobic interactions. Alternatively, the electron withdrawing properties of the chlorine may be detrimental for the binding activity. Of note, an additional fluorine (**10**) did not further reduce potency.

Table 3.1 | Half maximal inhibitory concentrations (expressed as pIC_{50} ± SEM) of **1** – **13** determined by a fluorescence polarization assay on BUB1 kinase activity (N=2, n=2).

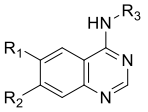

	ID	R_3	pIC_{50} ± SEM	ID	R_3	pIC_{50} ± SEM	ID	R_3	pIC_{50} ± SEM
R_1 HO, R_2 O	**1**	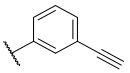	6.28 ± 0.05	**3**		< 5	**4**	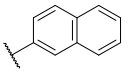	< 5
R_1 O, R_2 O	**2**	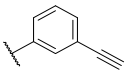	5.67 ± 0.04	**5**	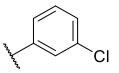	< 5			
R_1 HO, R_2 HO	**6**	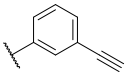	5.94 ± 0.04	**7**	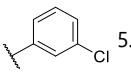	5.27 ± 0.05			
R_1 O, R_2 O	**8**	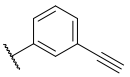	6.17 ± 0.05	**9**	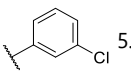	5.31 ± 0.05	**10**	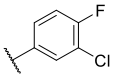	5.37 ± 0.03
R_1 H, R_2 O	**11**	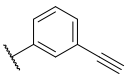	5.10 ± 0.02						
R_1 O, R_2 H	**12**	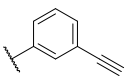	5.35 ± 0.03						
R_1 H, R_2 H	**13**	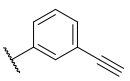	< 5						

Next, the importance of the nitrogens of the quinazoline scaffold was investigated. Removal of the *N*1 nitrogen (**14**, Table 3.2), reduced potency by more than 10-fold, suggesting that this nitrogen might be involved in hydrogen bond formation with the hinge region of BUB1. In contrast, removal of the *N*3 nitrogen (**15**), barely affected potency. Changing the quinazoline scaffold to a pyrrolopyrimidine (**16**), reduced potency significantly.

To further investigate the scope of the R_3 substituents (**Figure 3.1**), compounds **17** – **29** were evaluated (**Table 3.3**). Compared to **6**, substituting the acetylene by an ethyl (**17**) or isopropyl (**18**), reduced potency by at least 10-fold (**Table 3.3**). In contrast, replacing the acetylene for a phenyl (**19**) as bioisostere only slightly reduced potency. Subsequent substitution of this phenyl ring in compounds **20** – **24** with electron donating substituents (*o*, *m*, or *p*-methyl (**20**, **21**, **23**)) was not allowed. An electron withdrawing group, such as a *m*- or *p*-cyano group (**22**, **24**), was tolerated, but did not improve potency. Modification of the phenyl ring of **6** with both small (**25**, **27**) and large (**26**, **28**, **29**) ether substituents reduced potency as well.

Table 3.2 | Half maximal inhibitory concentrations (expressed as pIC_{50} ± SEM) of **14** – **16** determined by a fluorescence polarization assay on BUB1 kinase activity (N=2, n=2).

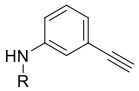

ID	R =	pIC_{50} ± SEM	app. K_i (nM)[a]	cLogP[b]	LipE[c]
8	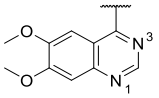	6.17 ± 0.05	236	3.3	3.4
14	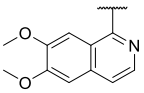	< 5	–	3.7	–
15	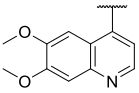	5.97 ± 0.03	373	3.5	3.0
16	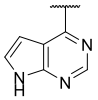	< 5	–	2.4	–

[a] Apparent K_i ; [b] cLogP was calculated by DataWarrior (v.5.2.1); [c] Lipophilic efficiency, defined as $\mathrm{LipE} = \mathrm{app.\ p}K_i - \mathrm{cLogP}$.

Due to the observed decrease in potency for biphenyl and phenyl ether analogues (**Table 3.3**), a small series of substituted pyrazoles (**30** – **41**) was evaluated (**Table 3.4**). The different size and exit vectors of a pyrazole may allow substituents to address different subpockets of the enzyme. In addition, the different electronic properties of a pyrazole ring may affect the binding affinity and its nitrogens may form additional hydrogen bonds. Changing the phenylacetylene of **6** for a pyrazole (**30**) decreased potency significantly. Compared to unsubstituted phenyl **3** (**Table 3.1**), compound **30** still showed some activity. In addition, due to lower lipophilicity, the lipophilic efficiency (LipE, calculated as defined in **Table 3.4**) of **30** was significantly improved when compared to **6**. Alkylation of the pyrazole by methyl (**31**) or ethyl (**32**) further decreased potency. In contrast, substitution with a benzyl group (**33**) showed similar activity compared to **6**, but improved in LipE. Extending the alkyl linker between pyrazole and phenyl (**34**, **35**) decreased potency, indicating that a methylene is the most optimal linker. Based on the activity of **33**, different electron donating and withdrawing substituents on the phenyl ring were explored (**36** – **41**), but none of them improved potency.

Table 3.3 | Half maximal inhibitory concentrations (expressed as pIC_{50} ± SEM) of **17** – **29** determined by a fluorescence polarization assay on BUB1 kinase activity (N=2, n=2).

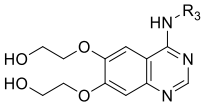

ID	R_3 =	pIC_{50} ± SEM	app. K_i (nM)[a]	cLogP[b]	LipE[c]
6	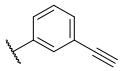	5.94 ± 0.04	407	2.2	4.2
17	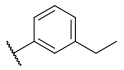	< 5	–	2.9	–
18	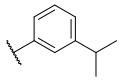	< 5	–	3.3	–
19	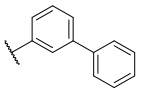	5.63 ± 0.03	828	3.8	2.3
20	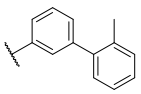	< 5	–	4.1	–
21	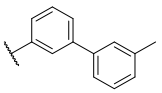	5.00 ± 0.03	–	4.1	–
22	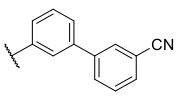	5.66 ± 0.03	769	3.6	2.5
23	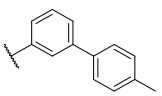	< 5	–	4.1	–
24	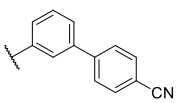	5.52 ± 0.04	1064	3.6	2.4
25	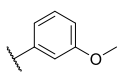	< 5	–	2.0	–
26	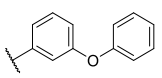	< 5	–	3.5	–
27	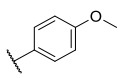	< 5	–	2.0	–
28	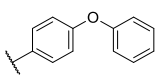	< 5	–	3.5	–
29	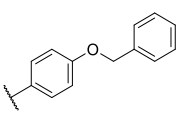	< 5	–	3.5	–

[a] Apparent K_i ; [b] cLogP was calculated by DataWarrior (v.5.2.1); [c] Lipophilic efficiency, defined as $\mathrm{LipE} = \mathrm{app.\,p}K_\mathrm{i} - \mathrm{cLogP}$.

Table 3.4 | Half maximal inhibitory concentrations (expressed as pIC_{50} ± SEM) of **30** – **41** determined by a fluorescence polarization assay on BUB1 kinase activity (N=2, n=2).

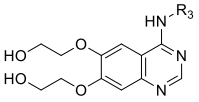

ID	R_3 =	pIC_{50} ± SEM	app. K_i (nM)[a]	cLogP[b]	LipE[c]
6	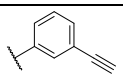	5.94 ± 0.04	407	2.2	4.2
30		5.09 ± 0.05	2877	0.0	5.5
31		< 5	–	0.2	–
32	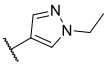	< 5	–	0.4	–
33	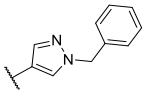	5.92 ± 0.04	420	1.5	4.8
34	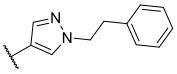	5.18 ± 0.09	2322	1.9	3.8
35	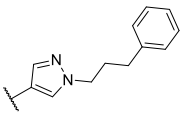	< 5	–	2.3	–
36	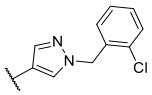	5.04 ± 0.03	3198	2.1	3.4
37	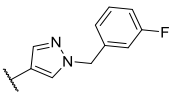	5.87 ± 0.02	474	1.6	4.7
38	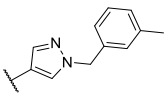	5.19 ± 0.03	2274	1.9	3.8
39	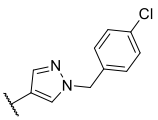	< 5	–	2.1	–
40	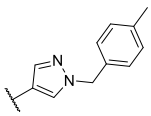	< 5	–	1.9	–
41	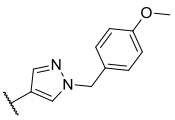	< 5	–	1.5	–

[a] Apparent K_i ; [b] cLogP was calculated by DataWarrior (v.5.2.1); [c] Lipophilic efficiency, defined as $\mathrm{LipE} = \mathrm{app.\,p}K_i - \mathrm{cLogP}$.

Since pyrazoles at R_3 resulted in an active compound with lower lipophilicity, other heterocycles were explored at this position (**42** – **47**, Table 3.5). Indazole or benzimidazole at R_3 (**42** – **44**) were not found to be tolerated. In contrast, chloropyrimidine **45** showed similar activity compared to its chlorophenyl analogue (**9**), which may indicate that the pyrimidine nitrogens do not form additional hydrogen bonds with the enzyme. Substituting the chlorine of **45** for a pyrazole (**46**) significantly improved potency (over 15-fold), and this compound had the highest LipE (5.1) of this study. Substituting the chlorine for a pyrrole (**44**) abolished activity, suggesting that the *N*2 nitrogen of the pyrazole of **46** interacts with the protein via a hydrogen bond. Overall, compound **46** was the most potent BUB1 inhibitor identified in this study with a pIC_{50} of 6.4.

Table 3.5 | Half maximal inhibitory concentrations (expressed as pIC_{50} ± SEM) of **42** – **47** determined by a fluorescence polarization assay on BUB1 kinase activity (N=2, n=2).

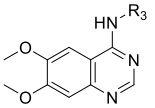

ID	R_3 =	pIC_{50} ± SEM	app. K_i (nM)[a]	cLogP[b]	LipE[c]
8	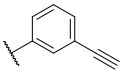	6.17 ± 0.05	236	3.3	3.4
9	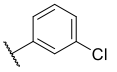	5.31 ± 0.05	1733	3.8	2.0
42	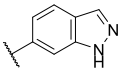	< 5	–	2.4	–
43	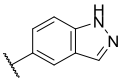	< 5	–	2.4	–
44	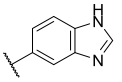	< 5	–	2.8	–
45	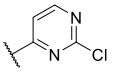	5.18 ± 0.04	2333	2.8	2.8
46	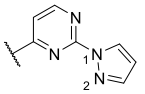	6.41 ± 0.04	136	1.7	5.1
47	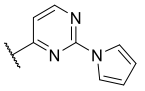	< 5	–	2.8	–

[a] Apparent K_i ; [b] cLogP was calculated by DataWarrior (v.5.2.1); [c] Lipophilic efficiency, defined as $\mathrm{LipE} = \mathrm{app.\,p}K_i - \mathrm{cLogP}$.

Table 3.6 | Half maximal inhibitory concentrations (expressed as pIC_{50} ± SEM) of **48** and **49** determined by a fluorescence polarization assay on BUB1 kinase activity (N=2, n=2).

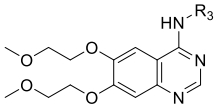

ID	R_3 =	pIC_{50} ± SEM	app. K_i (nM)[a]	cLogP[b]	LipE[c]
2	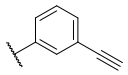	5.67 ± 0.04	746	3.1	3.1
48	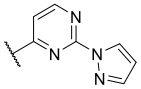	6.25 ± 0.04	197	1.6	5.1
49	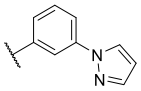	5.43 ± 0.02	1306	2.1	3.7

[a] Apparent K_i ; [b] cLogP was calculated by DataWarrior (v.5.2.1); [c] Lipophilic efficiency, defined as $\mathrm{LipE} = \mathrm{app.\,p}K_i - \mathrm{cLogP}$.

Finally, the R_3 substituent of **46** was grafted on the original scaffold of erlotinib (**2**) , thereby providing compound **48** (Table 3.6). Pyrazole-pyrimidine **48** showed improved potency compared to phenylacetylene **2** (Table 3.6), but was less active than compound **46** (Table 3.5). Strikingly, removal of the pyrimidine nitrogens (**49**) decreased the potency significantly, even below the activity of compound **2**, which indicated the importance of the pyrimidine nitrogens. The observed activities of chlorophenyl **9** and chloropyrimidine **45** (Table 3.5), for which the pyrimidine nitrogens were not found to increase activity, suggests a different binding mode for pyrazole-pyrimidines **46** and **48**.

Proposed binding mode of compound 1 and 46 in BUB1

Based on the obtained biochemical data, a binding model of compound **1** and **46** was generated by docking these molecules into the crystal structure of the kinase domain of human BUB1 (in complex with BAY1816032 (PDB code: 6F7B)[4]). Docking was performed using a published plugin[12] of AutoDock Vina[13] for PyMOL[14]. The proposed binding mode of compound **1** (Figure 3.2A) closely resembled the binding mode of erlotinib (**2**) in EGFR (PDB code: 4HJO) (Figure 3.1B).[9] Like erlotinib, R_1 and R_2 of compound **1** are solvent exposed, R_3 is positioned near the gatekeeper residue and the quinazoline of compound **1** is proposed to form a hydrogen bond between the *N*1 nitrogen and the amide backbone of hinge amino acid Tyr869 (Figure 3.2A). The proposed hydrogen bond is supported by the 15-fold decrease in potency when this nitrogen is removed (**14** vs. **8**, Table 3.2). The acetylene is hypothesized to interact with Val819, Lys821 and Leu864 (Figure 3.2A), which is supported by the observation that removal of this acetylene dropped potency by more than 10-fold (**3** vs. **1**, Table 3.1). The difference in activity between compound **1** and erlotinib (**2**) could not be explained based on the proposed binding mode. The position of the quinazoline ring of compound **1** is in line with the binding mode of the hinge binding pyridine ring of BAY1816032 and the acetylene of compound **1** points in the direction where the indazole

phenyl of BAY1816032 is located (**Figure 3.2B**). Molecular docking of **46** revealed a binding mode in which one of the pyrimidine nitrogens forms a hydrogen bond with Lys821 and the *N*2 nitrogen of the pyrazole forms a hydrogen bond with both Lys821 and Asp946 (**Figure 3.2C**). These proposed hydrogen bonds are supported by the 6-fold potency drop upon removal of both pyrimidine nitrogens (**49** vs. **48**, **Table 3.6**) as well as by the more than 25-fold decrease in potency upon removal of the corresponding pyrazole nitrogen (**47** vs. **46**, **Table 3.5**). When compared to the proposed binding mode of compound **1**, the quinazoline of **46** is slightly shifted and this shift hinders the formation of a hydrogen bond with Tyr869 (**Figure 3.2C**). In addition, this shift in position might explain why the activities of chlorophenyl **9** and chloropyrimidine **45** (**Table 3.5**) indicated no hydrogen bond interactions with the pyrimidine nitrogens of **45**, whereas the activities of compound **48** and **49** suggested that at least one of these nitrogens are involved in the formation of a hydrogen bond. The proposed binding mode of **46** closely resembles part of BAY1816032 which also forms two hydrogen bonds with Lys821 and one hydrogen bond with Asp946 (**Figure 3.2D**).

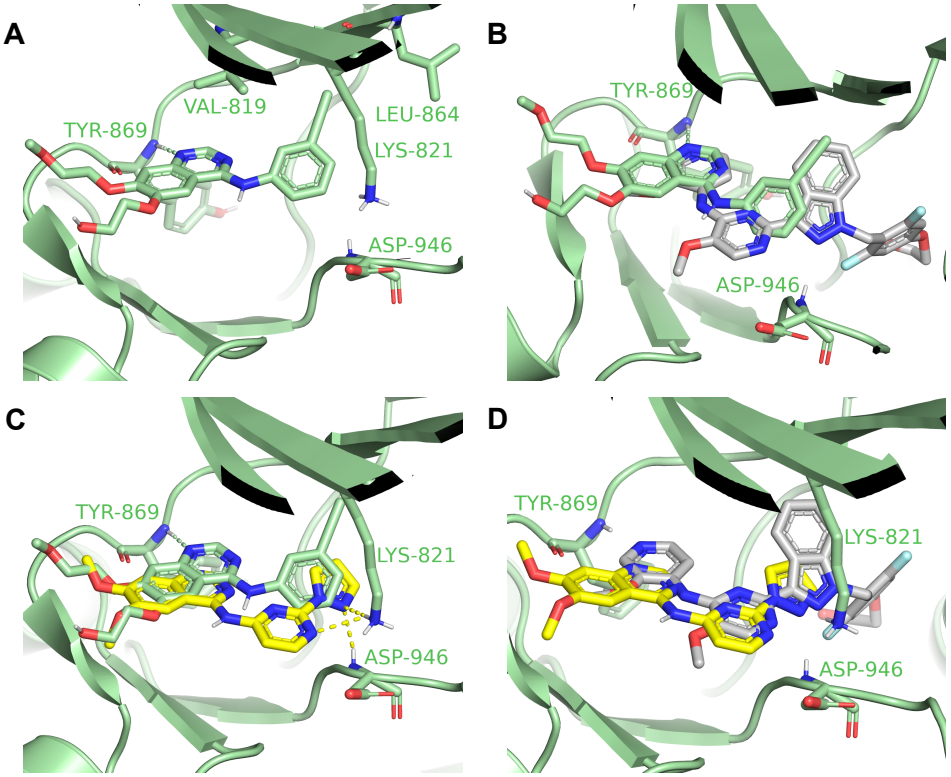

Figure 3.2 | Proposed binding mode of hit 1 and compound 46 in BUB1. (A) Proposed binding mode of compound **1** in BUB1. A hydrogen bond is formed with the amide backbone of hinge amino acid Tyr869 (dashed line). **(B)** Proposed binding mode of compound **1** compared to the binding mode of BAY1816032 (grey). **(C)** Proposed binding mode of compound **46** (yellow) compared with the proposed binding mode of compound **1**. Hydrogen bonds are indicated with dashed lines (green for compound **1**, yellow for compound **46**). **(D)** Proposed binding mode of compound **46** compared to the binding mode of BAY1816032 (grey).

Conclusion

In this chapter, the structure-activity relationship of compound **1** on BUB1 inhibition was investigated by synthesizing 48 analogues. The size of the substituents at R_1 and R_2 (**Figure 3.1A**) could significantly be reduced without losing much potency. The *N*1 nitrogen of the quinazoline scaffold was found to be crucial for activity, since its removal reduced potency over 10-fold. This nitrogen is hypothesized to form a hydrogen bond with hinge amino acid Tyr869 of BUB1. Modifications at R_3 showed that the acetylene is crucial for activity as well and optimization of potency in this region was found to be challenging. A summary of the activity and physicochemical properties of most active inhibitor **46** is shown in **Table 3.7**. A pyrazole-pyrimidine group at R_3 (**46**) was found to show the best activity (pIC_{50} = 6.41) which increased compared to compound **1**. In addition, **46** showed an almost 10-fold decrease in lipophilicity which contributed to the 10-fold increase in lipophilic efficiency. Furthermore, the molecular weight of **46** was reduced which contributed to better ligand efficiency.

Table 3.7 | Properties of initial hit **1** and optimized hit **46**.

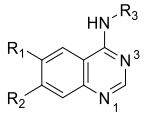

ID	R_1/R_2	R_3 =	pIC_{50} ± SEM	app. K_i (nM)[a]	cLogP[b]	LipE[c]	LE[d]	tPSA[e]	MW[f]
1	R_1 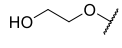 R_2 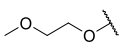	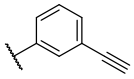	6.28 ± 0.05	185	2.6	4.1	0.33	85	379
46	R_1  R_2 	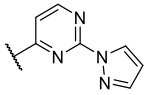	6.41 ± 0.04	136	1.7	5.1	0.36	96	349

[a] Apparent K_i ; [b] cLogP, calculated by DataWarrior (v.5.2.1); [c] Lipophilic efficiency, defined as $\mathrm{LipE} = \mathrm{app.\,p}K_i - \mathrm{cLogP}$; [d] Ligand efficiency, defined as: $\mathrm{LE} = (-RT * \ln(\mathrm{app.}\,K_i))/\mathrm{HA}$, where HA stands for the number of 'heavy atoms' (non-hydrogen atoms); [e] Topological surface area (Å^2), calculated by Chemdraw (v.19.1); [f] Molecular weight (g/mol).

Acknowledgements

Julian Clijncke, Jessica Domínguez Alfaro, Na Zhu, Bas de Man and Joel Rüegger are kindly acknowledged for their contribution with regard to compound synthesis and biochemical testing. Anthe Janssen is kindly acknowledged for his help in molecular docking and Hans van den Elst for HRMS measurements.

Experimental – Biochemistry

Molecular docking

The crystal structure of human BUB1 kinase domain in complex with BAY1816032 (PDB code: 6F7B)[4] was fetched into PyMOL[14]. Reduce[15] was used to add hydrogens to the protein structure and the ligand (BAY1816032) was extracted to a new object. The published plugin[12] of AutoDock Vina[13] for PyMOL was used for molecular docking. The AutoDock Vina grid box was based on the position of BAY1816032 and modified to obtain the following settings: grid size X = 54, Y = 34 and Z = 42 Å (grid spacing = 0.375 Å) centered at X = 12.68 Y = -31.93 and Z = -12.25. The number of docking poses was arbitrarily set to 60 to generate the maximum number of docking poses. Only docking poses which resembled the binding mode of erlotinib (**2**) in EGFR (PDB code: 4HJO)[9] were evaluated.

Biochemical evaluation of BUB1 inhibitors

Assays were performed in 384-well plates (Greiner, black, flat bottom, 781076) by sequential addition (indicated as: volume, final assay concentration) of inhibitor (5 µL, 3 nM – 10 µM), BUB1/BUB3 (5 µL, 3.26 nM, Carna Biosciences (05-187), lot: 15CBS-0644 D), ATP (5 µL, 15 µM) and BUB1/BUB3 substrate (5 µL, 75 nM, Carna Biosciences (05-187MSSU)), all as 4x working solutions. The final concentration of DMSO was 1%. Assay reactions were stopped by addition of IMAP progressive binding reagent (20 µL, 1200x diluted (see below), Molecular Devices (R8155), lot: 3117896). Each assay included the following controls: (i) a background control (treated with vehicle instead of inhibitor and BUB1/BUB3 substrate), (ii) MIN controls (treated with 5 µM BAY1816032 (MedChem Express) as inhibitor, defined as 0% BUB1 activity) and (iii) MAX controls (treated with vehicle instead of inhibitor, defined as 100% BUB1 activity). All inhibitors were tested in two separate assays and all inhibitor concentrations were tested in duplicate per assay (N=2, n=2).

For each assay, assay buffer (AB) was freshly prepared and consisted of 20 mM HEPES (prepared by diluting 1 M HEPES, pH 7.2), 5 mM $MgCl_2$, 0.01% (v/v) Tween-20 and 1 mM DTT. Stocks of inhibitors (in DMSO) were diluted in AB to obtain 4x working solutions (4% DMSO) and 5 µL was added to the assay plate. BUB1/BUB3 (3.26 µM (486 µg/mL) in storage buffer) was diluted in AB to obtain 13.0 nM of which 5 µL was added to all wells of the assay plate. The assay plate was centrifuged (1 min, 200 *g*) and incubated at RT for 30 min. ATP (4 mM in MilliQ) was diluted in AB to obtain 60 µM of which 5 µL was added to each well. BUB1/BUB3 substrate (1 mM) was diluted in 20 mM HEPES (prepared by diluting 1 M HEPES (pH 7.2) in MilliQ) to obtain 80 µM (this solution was freshly prepared every assay) and further diluted in AB to obtain 300 nM after which 5 µL was added to each well of the assay plate except for background control wells. The assay plate was centrifuged (1 min, 200 *g*) and incubated at RT in the dark for 180 min. IMAP progressive binding buffer A (5x) and IMAP progressive binding buffer B (5x) were mixed in a ratio to obtain 30% buffer A and 70% buffer B, which was subsequently diluted 5x in MilliQ. IMAP progressive binding reagent was diluted 600x in aforementioned mixture of buffer A and B (to obtain a 2x working solution) of which 20 µL was added to each well of the assay plate. The assay plate was centrifuged (1 min, 200 *g*) and incubated at RT in the dark for 90 min. Fluorescence polarization was measured on a CLARIOstar plate reader using the following settings: (i) optic settings → excitation = F: 482-16, dichroic = F: LP 504, emission = F: 530-40, (ii) optic = top optic, (iii) speed/precision = maximum precision, (iv) focus adjustment was performed for every assay and (v) gain adjustment was done by setting the target mP value to 35 mP for one of the MIN control wells. Data was normalized between MIN and MAX controls and data was plotted using GraphPad Prism 8.0 using "Nonlinear regression (curve fit)" and "log(inhibitor) vs. normalized response – Variable slope" to determine pIC_{50} values. The Cheng-Prusoff equation was used to calculate K_i values using 8.13 µM as the apparent K_M of ATP (determined as described in the experimental section of **Chapter 2**).

Experimental – Chemistry

Synthetic routes

The synthesis of OSI-420 (**1**), **3** and **4** (**Scheme 3.1**) involved the synthesis of **50** as described in **Chapter 2**.[16–18] From **50**, three groups were introduced at R_3 (**Figure 3.1A**) by nucleophilic aromatic

substitutions to afford **51** – **53**. Deacetylation resulted in the formation of the desired compounds. Erlotinib (**2**) and **5**, in which the free hydroxyl of R_1 (**Figure 3.1A**) was methylated, were synthesized from commercially available 4-chloro-6,7-bis(2-methoxyethoxy)quinazoline by nucleophilic aromatic substitutions (**Scheme 3.2**).

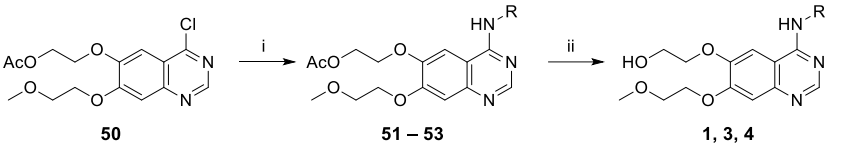

Scheme 3.1 | Synthesis of 1, 3 and 4. Reagents and conditions: **i)** 3-ethynylaniline (for **51**), aniline (for **52**) or naphthalen-2-amine (for **53**), 2-propanol, 82°C, 95% – quant. **ii)** 0.4 M NaOH in MeOH, 27 – 89%.

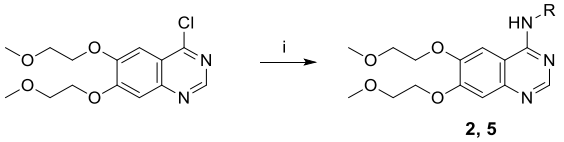

Scheme 3.2 | Synthesis of 2 and 5. Reagents and conditions: **i)** 3-ethynylaniline (for **2**) or 3-chloroaniline (for **5**), 2-propanol, 82°C, 97 – 98%.

Next, several analogues were prepared which either contained methoxy (**8** – **10**) or glycol groups (**6**, **7** and **17** – **41**) at R_1 and R_2 (**Figure 3.1A**, **Scheme 3.3**, **Scheme 3.4**). In addition, this small array of compounds contained derivatives involving R_3 (**Figure 3.1A**). Synthesis of these compounds started from 3,4-dihydroxybenzoate which was alkylated with either 2-bromoethyl acetate or iodomethane to yield **54** and **55**, respectively (**Scheme 3.3**). Compounds **56** – **63** were subsequently synthesized analogous to the synthetic route as described for OSI-420 (**1**) (**Chapter 2**). Compounds **8** – **10** were prepared from **63** via nucleophilic aromatic substitutions. Similarly, nucleophilic aromatic substitutions with **62** resulted in the formation of intermediates **64** – **73** and yielded **6**, **7**, **17**, **18**, **25** – **29** after deacetylation. Synthesis of analogues **19** – **24** involved a Suzuki coupling with **74** and subsequent deacetylation or *vice versa*, which saved one synthetic step per final compound. To obtain pyrazole derivatives **30** – **41**, aminopyrazoles **90** – **101** were first prepared as depicted in **Scheme 3.4**. Protection or alkylation of 4-nitro-1*H*-pyrazole resulted in the formation intermediates **78** – **89**. Nitro group reduction yielded aminopyrazoles **90** – **101** which were subsequently coupled to **62** to form intermediates **102** – **113** (**Scheme 3.4**). Deacetylation resulted in the formation of compounds **30** – **41**.

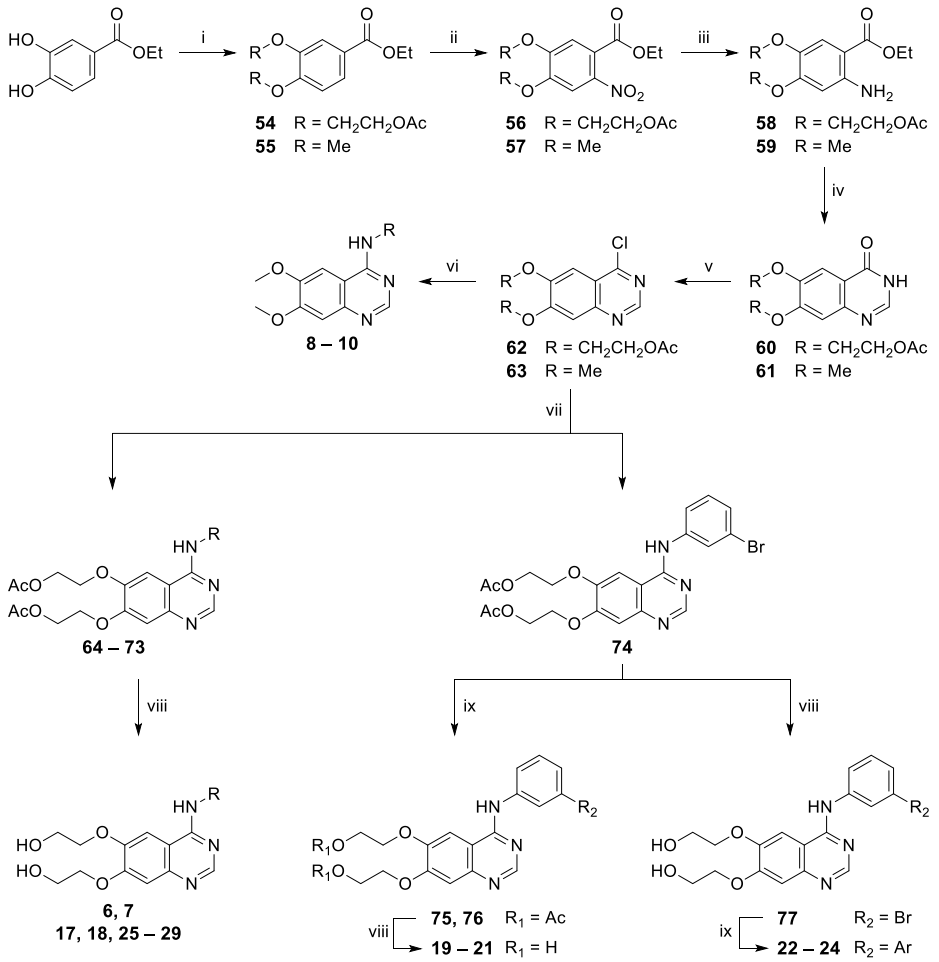

Scheme 3.3 | Synthesis of 6 – 10 and 17 – 29. Reagents and conditions: **i)** 2-bromoethyl acetate (for **54**) or iodomethane (for **55**), K_2CO_3, DMF, 100°C, 62 – 97%. **ii)** $Cu(NO_3)_2 \cdot 3H_2O$, Ac_2O, 0°C → RT, 62 – 71%. **iii)** 5% Pt/C, MeOH, 69 – 95%. **iv)** NH_4HCO_2, formamide, 160°C, 27 – 39%. **v)** $POCl_3$, 105°C, 14 – 84%. **vi)** 3-ethynylaniline (for **8**), 3-chloroaniline (for **9**) or 3-chloro-4-fluoroaniline (for **10**), 2-propanol, 82°C, 68 – 95%. **vii)** corresponding amine, 2-propanol, 82°C, 71 – 99%. **viii)** 0.4 M NaOH in MeOH, 45 – 97%. **ix)** corresponding boronic acid, K_2CO_3, Pd(dppf)Cl_2·DCM, dioxane/H_2O (4:1), 100°C, 55 – 80%.

Further reducing the size of the substituents at R_1 and R_2 (**Figure 3.1A**) involved the synthesis of **11** – **13** (**Scheme 3.5**) which only required a nucleophilic aromatic substitution from commercial building blocks. Similarly, analogues involving the quinazoline scaffold were synthesized from commercial building blocks to obtain compound **14** – **16** (**Scheme 3.6**).[19] Compound **42** – **47**, which contained different heterocycles at R_3 (**Figure 3.1A**), were synthesized as depicted in **Scheme 3.7**. Nucleophilic aromatic substitutions with commercially available 4-chloro-6,7-dimethoxyquinazoline yielded compound **42** – **44**.[20] For the synthesis of **45**, a chloropyrimidine was coupled using a Buchwald-Hartwig amination and this compound also served as building block for the synthesis of **46** and **47** by using nucleophilic aromatic substitutions. Similarly, the R_3 substituent of **46** was attached to the scaffold of erlotinib (**2**) using 4-chloro-6,7-bis(2-methoxyethoxy)quinazoline (**Scheme 3.8**) to form **114** and yielded **48** after an nucleophilic aromatic substitution. To investigate the importance of the pyrimidine nitrogens in this molecule, compound **49** was synthesized (**Scheme 3.8**) and required the synthesis of **116** via an Ullmann reaction[21,22] and subsequent reduction of the nitro group.

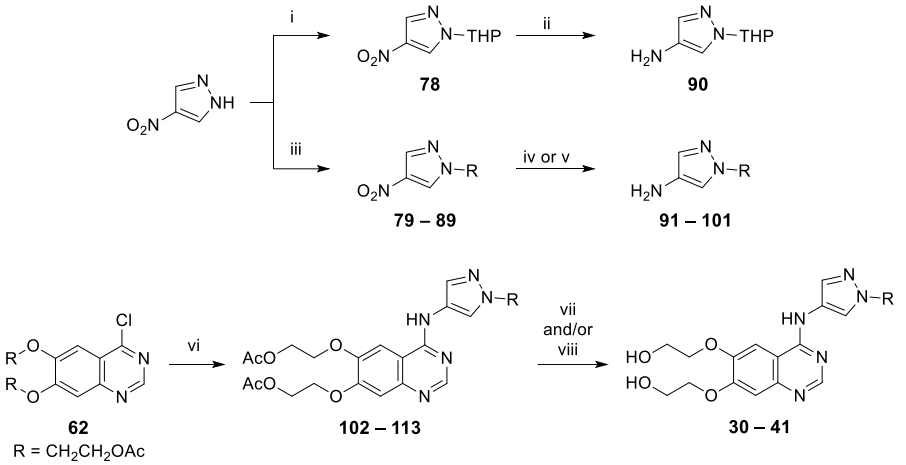

Scheme 3.4 | Synthesis of 30 – 41. Reagents and conditions: **i)** 3,4-dihydro-2*H*-pyran, *p*-TsOH·H_2O, DCM. **ii)** 5% Pt/C, MeOH, 74% over two steps. **iii)** corresponding halide, K_2CO_3, DMF, RT – 90°C, 97% – quant. **iv)** 10% Pd/C, MeOH, 68% – quant. **v)** Fe, NH_4Cl, H_2O/EtOH (1:1), 60°C, 34 – 99%. **vi)** corresponding amine, 2-propanol, 82°C, 73 – 97%. **vii)** 0.16 M HCl (aq.), MeOH. **viii)** 0.4 M NaOH in MeOH, 68 – 92%.

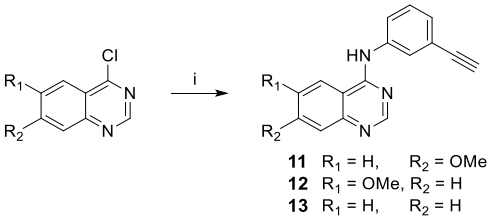

Scheme 3.5 | Synthesis of 11 – 13. Reagents and conditions: **i)** 3-ethynylaniline, 2-propanol, 82°C, 66 – 98%.

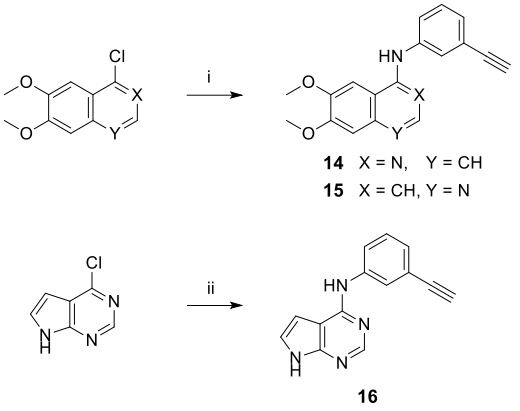

Scheme 3.6 | Synthesis of 14 – 16. Reagents and conditions: **i)** 3-ethynylaniline, cat. HCl (aq.), 2-propanol, 82°C, 32 – 43%. **ii)** 3-ethynylaniline, 2-propanol, 82°C, 35%.

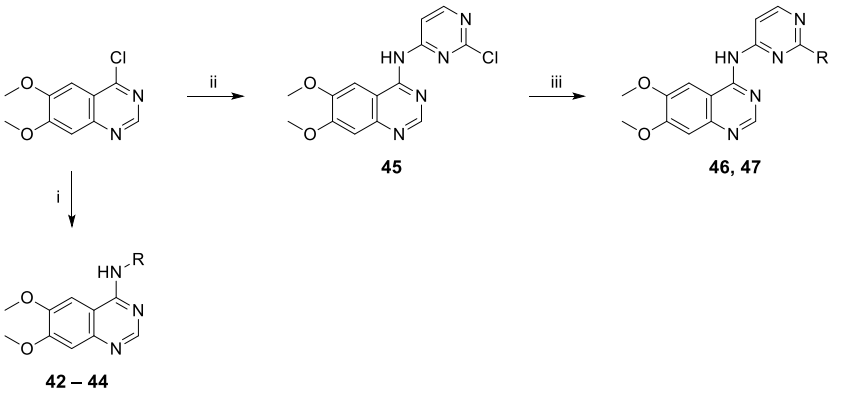

Scheme 3.7 | Synthesis of 42 – 47. Reagents and conditions: **i)** 1*H*-indazol-6-amine (for **42**), 1*H*-indazol-5-amine (for **43**) or 1*H*-benzo[*d*]imidazole-5-amine (for **44**), MeCN, 80°C, 48 – 74%. **ii)** 2-chloropyrimidin-4-amine, Cs_2CO_3, xantphos, $Pd(OAc)_2$, DMF, 90°C, 67%. **iii)** 1*H*-pyrazole (for **46**) or 1*H*-pyrrole (for **47**), NaH, dioxane, 90 – 100°C, 38 – 70%.

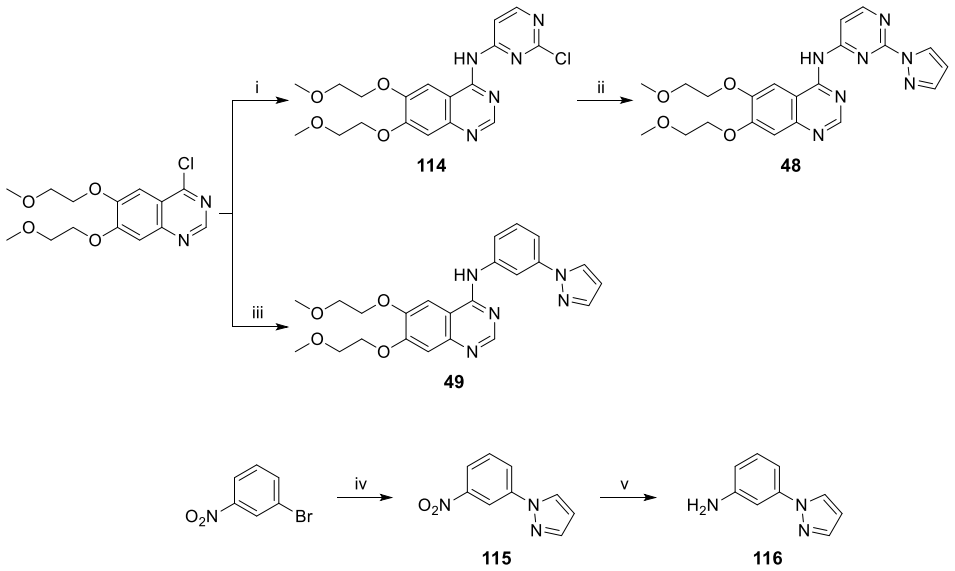

Scheme 3.8 | Synthesis of 48 and 49. Reagents and conditions: **i)** 2-chloropyrimidin-4-amine, Cs_2CO_3, xantphos, $Pd(OAc)_2$, DMF, 90°C, 63%. **ii)** 1*H*-pyrazole, K_2CO_3, dioxane, 95°C, 19%. **iii)** **116**, 2-propanol, 82°C, 45%. **iv)** 1*H*-pyrazole, ethyl 2-oxocyclohexane-1-carboxylate, Cs_2CO_3, Cu_2O, MeCN, 82°C, 55%. **v)** NH_4Cl, Fe, $EtOH/H_2O$ (30:1), 80°C, 98%.

General procedures

All reagents were purchased from chemical suppliers (Fluorochem, Sigma-Aldrich, Merck, Fisher Scientific) and used without further purification. Solvents (Honeywell, VWR, Biosolve) indicated with "dry" were stored on activated 3 Å (MeCN) or 4 Å (other solvents) molecular sieves (8 to 12 mesh, Acros Organics). Solvents indicated by "degassed" were sonicated while bubbling N_2 through the solvent for 20 min. All reactions were performed at room temperature (RT) under a nitrogen atmosphere, unless stated otherwise. Reactions were monitored by thin layer chromatography (TLC, silica gel 60, UV_{254}, Macherey-Nagel, ref: 818333) and compounds were visualized by UV absorption (254 nm and/or 366 nm) or spray reagent (permanganate (5 g/L $KMnO_4$, 25 g/L K_2CO_3)) followed by heating. Alternatively, reactions were monitored by liquid chromatography-mass spectrometry (LCMS), either on a Thermo Finnigan (Thermo Finnigan LCQ Advantage MAX ion-trap mass spectrometer (ESI+) coupled to a

Surveyor HPLC system (Thermo Finnigan) equipped with a Nucleodur C18 Gravity column (50x4.6 mm, 3 µm particle size, Macherey-Nagel)) or a Thermo Fleet (Thermo LCQ Fleet ion-trap mass spectrometer (ESI+) coupled to a Vanquish UHPLC system). LCMS eluent consisted of MeCN in 0.1% TFA (aq.) and LCMS methods were as follows: 0.5 min cleaning with starting gradient, 8 min using specified gradient (linear), 2 min cleaning with 90% MeCN in 0.1% TFA (aq.). LCMS data is reported as follows: instrument (Finnigan or Fleet), gradient (% MeCN in 0.1% TFA (aq.)), retention time (t_r) and mass (as m/z: $[M+H]^+$). Purity of final compounds was determined to be ≥ 95% by integrating UV intensity of spectra generated by either of the LCMS instruments. ^1H and ^{13}C NMR spectra were recorded on a Bruker AV300 (300 and 75 MHz, respectively), Bruker AV400 (400 and 101 MHz, respectively) or Bruker AV500 (500 and 126 MHz, respectively) NMR spectrometer. NMR samples were prepared in deuterated chloroform, water, methanol or DMSO. Chemical shifts are given in ppm (δ) relative to residual protonated solvent signals ($CDCl_3$ → δ 7.260 (^1H), δ 77.160 (^{13}C), D_2O → δ 4.790 (^1H), MeOD → δ 3.310 (^1H), δ 49.000 (^{13}C), DMSO → δ 2.500 (^1H), δ 39.520 (^{13}C)). Data was processed by using MestReNova (v. 14) and is reported as follows: chemical shift (δ), multiplicity, coupling constant (*J* in Hz) and integration. Multiplicities are abbreviated as follows: s = singlet, br s = broad singlet, app. s = apparent singlet, d = doublet, dd = doublet of doublets, ddd = doublet of doublet of doublets, td = triplet of doublets, t = triplet, dt = doublet of triplets, tt = triplet of triplets, q = quartet, p = pentet, hept = heptet, m = multiplet, br m = broad multiplet. Purification was done either by manual silica gel column chromatography (using 40-63 µm, 60 Å silica gel, Macherey-Nagel) or automated flash column chromatography on a Biotage Isolera machine (using pre-packed cartridges with 40-63 µm, 60 Å silica gel (4, 12, 25 or 40 g), Screening Devices). High resolution mass spectrometry (HRMS) spectra were recorded through direct injection of a 1 µM sample either on a Thermo Scientific Q Exactive Orbitrap equipped with an electrospray ion source in positive mode coupled to an Ultimate 3000 system (source voltage = 3.5 kV, capillary temperature = 275 °C, resolution R = 240,000 at m/z 400, external lock, mass range m/z = 150-2000) or on a Synapt G2-Si high definition mass spectrometer (Waters) equipped with an electrospray ion source in positive mode (ESI-TOF) coupled to a NanoEquity system with Leu-enkephalin (m/z = 556.2771) as internal lock mass. The eluent for HRMS measurements consisted of a 1:1 (v/v) mixture of MeCN in 0.1% formic acid (aq.) using a flow of 25 mL/min. Compound names were generated by ChemDraw (v. 19.1.21).

General procedure A – Aromatic substitution

4-Chloroquinazoline analogue (1 eq.) was dissolved in 2-propanol (~0.18 M) after which corresponding aniline or amine analogue (1 – 1.2 eq.) was added. DIPEA (2 eq.) was added only if the aniline or amine analogue was an HCl salt. The mixture was heated to 82°C, stirred for indicated time and subsequently poured into 0.1 M $NaHCO_3$ (aq.) (30 mL). The product was extracted with DCM (3x30 mL) or EtOAc (3x30 mL), the combined organic layers washed with brine (100 mL) and subsequently dried over Na_2SO_4, filtered and concentrated. Purification was performed as indicated.

General procedure B – Acetyl deprotection

Acetyl-protected alcohol starting material was dissolved in a solution of 0.4 M NaOH in MeOH (2.7 eq.) and the mixture was stirred for indicated time. The mixture was diluted in H_2O (30 mL) and the product extracted with EtOAc (3x30 mL) or 20% MeOH in DCM (3x30 mL) and brine was added when required. The combined organic layers were washed with brine (100 mL), dried over Na_2SO_4, filtered and concentrated. For water soluble products, the mixture was concentrated directly and purified as indicated.

General procedure C – Suzuki coupling

A microwave tube was charged with 3-bromoaniline analogue (1 eq.), corresponding boronic acid (1.2 eq.), K_2CO_3 (4 eq.) and 4:1 dioxane/H_2O (~0.15 M). N_2 was bubbled through the mixture for 1 min after which Pd(dppf)Cl_2·DCM (0.07 eq.) was added. N_2 was bubbled through the mixture for 30 sec after which the vial was sealed. The mixture was heated to 100°C, stirred for 1.5 h and subsequently poured into H_2O (20 mL). The product was extracted with EtOAc (3x20 mL) and the combined organic layers were washed with brine (50 mL). The organic layer was dried over Na_2SO_4, filtered and concentrated. Purification was performed as indicated.

General procedure D – Nucleophilic aromatic substitution

4-Chloro-6,7-dimethoxyquinazoline (50.0 mg, 223 µmol) was suspended in MeCN (0.11 M) after which corresponding amine analogue (1 eq.) was added. The mixture was heated to 80°C, stirred for indicated time and subsequently poured into 1 M $NaHCO_3$ (aq.) (20 mL). The product was extracted with EtOAc (3x20 mL) and the combined organic layers were concentrated as such. Purification was performed as indicated.

General procedure E – Alkylation

4-Nitro-1*H*-pyrazole (1 eq.) and K_2CO_3 (1.2 eq.) were mixed in dry DMF (at indicated reaction molarity). Corresponding halide (1 – 1.2 eq.) was added and the mixture was stirred for 16 h at indicated temperature. The mixture was poured into H_2O (30 mL) and the product extracted with EtOAc (3x20 mL). The combined organic layers were washed with brine (30 mL), dried over Na_2SO_4, filtered and concentrated. The crude was purified by silica gel column chromatography (5 – 30% EtOAc/pentane) to afford the product.

General procedure F – Reduction

4-Nitropyrazole analogue (1 eq.) was dissolved in degassed MeOH (3 mL). 10% Pd/C (10 mass%) was added and the atmosphere was exchanged for H_2. The mixture was vigorously stirred for indicated time while bubbling H_2 through the mixture. The atmosphere was exchanged for N_2, after which the mixture was filtered over Celite and concentrated to afford the product.

General procedure G – Reduction

4-Nitropyrazole analogue (1 eq.) and NH_4Cl (4 eq.) were mixed in a 1:1 mixture of H_2O/EtOH (~0.1 M). Iron powder (3 eq.) was added and the mixture was stirred at 60°C for 2 h. The hot mixture was filtered over Celite and concentrated. The residue was diluted in DCM (20 mL) and poured into H_2O (20 mL). The organic layer was separated and the water layer washed with DCM (20 mL). The combined organic layers were washed with brine (20 mL), dried over Na_2SO_4, filtered and concentrated to afford the product.

2-((4-((3-Ethynylphenyl)amino)-7-(2-methoxyethoxy)quinazolin-6-yl)oxy)ethan-1-ol (1)

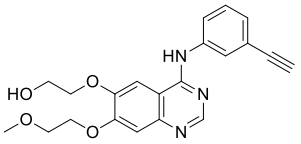

The title compound was synthesized as described in **Chapter 2** (compound 3)

N-(3-Ethynylphenyl)-6,7-bis(2-methoxyethoxy)quinazolin-4-amine (2)

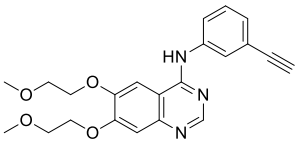

The title compound was synthesized from 4-chloro-6,7-bis(2-methoxyethoxy)quinazoline (40.0 mg, 128 µmol) and 3-ethynylaniline (15.9 µL, 141 µmol) according to general procedure A (reaction time: 1.5 h). The crude was purified by silica gel column chromatography (1 – 10% MeOH/DCM) to afford the product (49.0 mg, 125 µmol, 97%). ^{1}H NMR (400 MHz, $CDCl_3$) δ 8.63 (s, 1H), 7.84 (t, *J* = 1.9 Hz, 1H), 7.72 (dd, *J* = 8.1, 1.2 Hz, 1H), 7.64 (s, 1H), 7.32 (t, *J* = 7.9 Hz, 1H), 7.28 – 7.21 (m, 2H), 7.14 (s, 1H), 4.24 – 4.13 (m, 4H), 3.80 – 3.73 (m, 4H), 3.41 (s, 3H), 3.40 (s, 3H), 3.08 (s, 1H). ^{13}C NMR (101 MHz, $CDCl_3$) δ 156.43, 154.60, 153.70, 148.88, 147.63, 138.96, 129.10, 127.85, 125.23, 122.88, 122.49, 109.26, 108.74, 102.56, 83.48, 77.58, 71.05, 70.48, 69.17, 68.36, 59.42, 59.34. LCMS (Finnigan, 10 → 90%): t_r = 5.38 min, m/z: 394.2. HRMS $[C_{22}H_{23}N_3O_4 + H]^+$: 394.17613 calculated, 394.1764 found.

2-((7-(2-Methoxyethoxy)-4-(phenylamino)quinazolin-6-yl)oxy)ethan-1-ol (3)

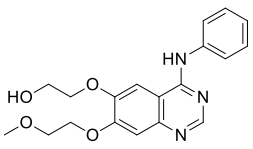

The title compound was synthesized from **52** (36.1 mg, 90.8 µmol) according to general procedure B (reaction time: 3 h). The crude was purified by automated column chromatography (4 – 20% MeOH/DCM) to afford the product (28.7 mg, 80.8 µmol, 89%). ^{1}H NMR (500 MHz, MeOD) δ 8.36 (s, 1H), 7.70 (s, 1H), 7.69 (d, *J* = 7.6 Hz, 2H), 7.37 (t, *J* = 7.9 Hz, 2H), 7.18 – 7.11 (m, 2H), 4.31 – 4.27 (m, 2H), 4.27 – 4.24 (m, 2H), 3.98 – 3.94 (m, 2H), 3.85 – 3.81 (m, 2H), 3.45 (s, 3H). LCMS (Finnigan, 10 → 90%): t_r = 4.50 min, m/z: 356.2. HRMS $[C_{19}H_{21}N_3O_4 + H]^+$: 356.16048 calculated, 356.1613 found.

2-((7-(2-Methoxyethoxy)-4-(naphthalen-2-ylamino)quinazolin-6-yl)oxy)ethan-1-ol (4)

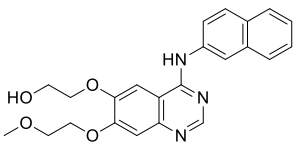

The title compound was synthesized from **53** (36.7 mg, 82.0 µmol) according to general procedure B (reaction time: 3 h). The crude was purified by automated column chromatography (4 – 20% MeOH/DCM) to afford the product (28.8 mg, 71.0 µmol, 87%). ^{1}H NMR (500 MHz, MeOD) δ 8.45 (s, 1H), 8.17 (s, 1H), 7.83 (d, *J* = 8.8 Hz, 1H), 7.81 – 7.72 (m, 4H), 7.43 (t, *J* = 7.4 Hz, 1H), 7.39 (t, *J* = 7.3 Hz, 1H), 7.15 (s, 1H), 4.31 – 4.27 (m, 2H), 4.26 – 4.21 (m, 2H), 4.00 – 3.95 (m, 2H), 3.87 – 3.82 (m, 2H), 3.46 (s, 3H). ^{13}C NMR (126 MHz, MeOD) δ 157.97, 154.88, 153.33, 149.49, 146.41, 136.76, 134.41, 131.50, 128.86, 127.99, 127.95, 126.74, 125.57, 123.25, 120.24, 110.27, 107.64, 103.74, 71.39, 70.88, 68.55, 60.92, 59.27. LCMS (Finnigan, 0 → 50%): t_r = 8.31 min, m/z: 406.2. HRMS $[C_{23}H_{23}N_3O_4 + H]^+$: 406.17613 calculated, 406.1764 found.

***N*-(3-Chlorophenyl)-6,7-bis(2-methoxyethoxy)quinazolin-4-amine (5)**

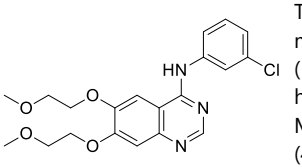

The title compound was synthesized from 4-chloro-6,7-bis(2-methoxyethoxy)quinazoline (41.0 mg, 131 µmol) and 3-chloroaniline (15.3 µL, 144 µmol) according to general procedure A (reaction time: 1.5 h). The crude was purified by silica gel column chromatography (1 – 4% MeOH/DCM) to afford the product (52.0 mg, 129 µmol, 98%). ^{1}H NMR (400 MHz, MeOD) δ 8.39 (s, 1H), 7.88 (s, 1H), 7.63 (dd, *J* = 8.2, 1.0 Hz, 1H), 7.60 (d, *J* = 1.5 Hz, 1H), 7.30 (t, *J* = 8.1 Hz, 1H), 7.09 (dd, *J* = 8.0, 1.0 Hz, 1H), 7.03 (s, 1H), 4.26 (t, *J* = 4.7 Hz, 2H), 4.25 – 4.18 (m, 2H), 3.86 – 3.77 (m, 4H), 3.46 (s, 3H), 3.44 (s, 3H). ^{13}C NMR (101 MHz, MeOD) δ 157.88, 155.63, 153.48, 150.03, 147.16, 141.47, 134.99, 130.61, 124.66, 123.14, 121.31, 110.33, 107.87, 103.71, 71.69, 71.44, 69.68, 69.31, 59.53, 59.48. LCMS (Finnigan, 10 → 90%): t_r = 5.43 min, m/z: 404.1. HRMS $[C_{20}H_{22}ClN_3O_4 + H]^+$: 404.13716 calculated, 404.1378 found.

2,2'-((4-((3-Ethynylphenyl)amino)quinazoline-6,7-diyl)bis(oxy))bis(ethan-1-ol) (6)

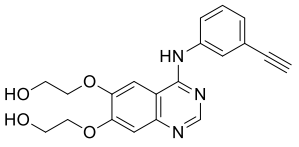

The title compound was synthesized from **64** (36 mg, 80 µmol) according to general procedure B (reaction time: 1 h). The crude was purified by silica gel column chromatography (4 – 20% MeOH/DCM) to afford the product (22.9 mg, 62.7 µmol, 78%). ^{1}H NMR (400 MHz, MeOD) δ 8.42 (s, 1H), 7.91 (t, *J* = 1.9 Hz, 1H), 7.77 (ddd, *J* = 8.2, 2.3, 1.1 Hz, 1H), 7.73 (s, 1H), 7.37 (t, *J* = 7.9 Hz, 1H), 7.25 (dt, *J* = 7.7, 1.3 Hz, 1H), 7.15 (s, 1H), 4.28 – 4.24 (m, 2H), 4.24 – 4.20 (m, 2H), 4.02 – 3.97 (m, 4H), 3.52 (s, 1H). ^{13}C NMR (101 MHz, MeOD) δ 158.47, 156.08, 153.92, 150.57, 147.63, 140.62, 129.91, 128.74, 127.06, 124.30, 124.18, 110.61, 108.04, 103.69, 84.30, 78.72, 72.01, 71.71, 61.45, 61.25. LCMS (Finnigan, 10 → 90%): t_r = 4.54 min, m/z: 366.3. HRMS $[C_{20}H_{19}N_3O_4 + H]^+$: 366.14483 calculated, 366.1448 found.

2,2'-((4-((3-Chlorophenyl)amino)quinazoline-6,7-diyl)bis(oxy))bis(ethan-1-ol) (7)

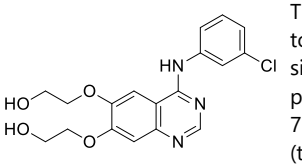

The title compound was synthesized from **65** (39 mg, 85 µmol) according to general procedure B (reaction time: 1 h). The crude was purified by silica gel column chromatography (10% MeOH/DCM) to afford the product (30 mg, 80 µmol, 94%). ^{1}H NMR (400 MHz, MeOD) δ 8.43 (s, 1H), 7.87 – 7.80 (m, 1H), 7.69 (s, 1H), 7.60 (ddd, *J* = 8.2, 2.1, 1.0 Hz, 1H), 7.30 (t, *J* = 8.1 Hz, 1H), 7.13 – 7.06 (m, 2H), 4.27 – 4.17 (m, 4H), 4.02 – 3.96 (m,

4H). ^{13}C NMR (101 MHz, MeOD) δ 157.79, 155.29, 153.30, 149.77, 146.93, 140.99, 134.84, 130.40, 124.68, 123.14, 121.23, 110.23, 107.49, 103.22, 71.33, 71.06, 60.91, 60.68. LCMS (Finnigan, 10 → 90%): t_r = 4.77 min, m/z: 376.2. HRMS $[C_{18}H_{18}ClN_3O_4 + H]^+$: 376.10586 calculated, 376.1064 found.

N-(3-Ethynylphenyl)-6,7-dimethoxyquinazolin-4-amine (8)

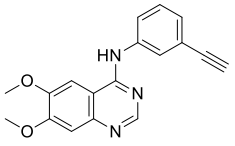

The title compound was synthesized from **63** (16.7 mg, 74.3 µmol) and 3-ethynylaniline (8.4 µL, 74.3 µmol) according to general procedure A (reaction time: 1.5 h). The crude was purified by silica gel column chromatography (1 – 10% MeOH/DCM) to afford the product (21 mg, 69 µmol, 93%). ^{1}H NMR (400 MHz, MeOD) δ 8.42 (s, 1H), 7.84 (t, *J* = 1.8 Hz, 1H), 7.75 – 7.67 (m, 2H), 7.34 (t, *J* = 7.9 Hz, 1H), 7.25 (dt, *J* = 7.7, 1.3 Hz, 1H), 7.14 (s, 1H), 4.03 (s, 3H), 4.01 (s, 3H), 3.33 (s, 1H). ^{13}C NMR (101 MHz, MeOD) δ 158.15, 155.97, 153.37, 150.58, 147.03, 139.86, 129.54, 128.67, 126.98, 124.17, 123.69, 110.32, 106.67, 102.18, 83.94, 78.24, 56.77, 56.57. LCMS (Finnigan, 10 → 90%): t_r = 5.15 min, m/z: 306.3. HRMS $[C_{18}H_{15}N_3O_2 + H]^+$: 306.12370 calculated, 306.1244 found.

N-(3-Chlorophenyl)-6,7-dimethoxyquinazolin-4-amine (9)

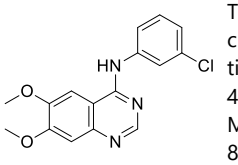

The title compound was synthesized from **63** (15.8 mg, 70.3 µmol) and 3-chloroaniline (7.4 µL, 70.3 µmol) according to general procedure A (reaction time: 1.5 h). The crude was purified by silica gel column chromatography (0 – 4% MeOH/DCM) to afford the product (21 mg, 67 µmol, 95%). ^{1}H NMR (400 MHz, MeOD) δ 8.45 (s, 1H), 7.83 (t, *J* = 2.1 Hz, 1H), 7.71 (s, 1H), 7.61 (ddd, *J* = 8.2, 2.1, 1.0 Hz, 1H), 7.31 (t, *J* = 8.1 Hz, 1H), 7.13 (s, 1H), 7.10 (ddd, *J* = 8.0, 2.1, 1.0 Hz, 1H), 4.03 (s, 3H), 4.01 (s, 3H). ^{13}C NMR (101 MHz, MeOD) δ 157.82, 155.74, 153.25, 150.38, 147.03, 140.96, 134.82, 130.37, 124.68, 123.18, 121.26, 110.24, 106.65, 101.95, 56.71, 56.54, 49.86. LCMS (Finnigan, 10 → 90%): t_r = 5.26 min, m/z: 316.3. HRMS $[C_{16}H_{14}ClN_3O_2 + H]^+$: 316.08473 calculated, 316.0852 found.

N-(3-Chloro-4-fluorophenyl)-6,7-dimethoxyquinazolin-4-amine (10)

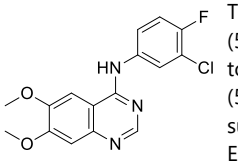

The title compound was synthesized from 4-chloro-6,7-dimethoxyquinazoline (50.0 mg, 223 µmol) and 3-chloro-4-fluoroaniline (32.4 mg, 223 µmol) according to general procedure A (reaction time: 16 h). The crude was suspended in DCM (5 mL) and filtered. The solids were collected, loaded onto Celite and subsequently purified by automated column chromatography (50 – 100% EtOAc/DCM) to afford the product (50.7 mg, 152 µmol, 68%). ^{1}H NMR (400 MHz, DMSO) δ 9.50 (s, 1H), 8.49 (s, 1H), 8.11 (dd, *J* = 6.9, 2.6 Hz, 1H), 7.79 (ddd, *J* = 9.0, 4.3, 2.7 Hz, 1H), 7.75 (s, 1H), 7.42 (t, *J* = 9.1 Hz, 1H), 7.16 (s, 1H), 3.94 (s, 3H), 3.92 (s, 3H). ^{13}C NMR (101 MHz, DMSO) δ 156.00, 154.36, 152.62, 151.94, 149.01, 147.04, 136.87 (d, $J_{(C–F)}$ = 3.0 Hz), 123.39, 122.21 (d, $J_{(C–F)}$ = 6.7 Hz), 118.80 (d, $J_{(C–F)}$ = 18.3 Hz), 116.50 (d, $J_{(C–F)}$ = 21.6 Hz), 108.78, 107.19, 101.62, 56.20, 55.82. LCMS (Fleet, 10 → 90%): t_r = 4.68 min, m/z: 334.3. HRMS $[C_{16}H_{13}ClFN_3O_2 + H]^+$: 334.07531 calculated, 334.07508 found.

N-(3-Ethynylphenyl)-7-methoxyquinazolin-4-amine (11)

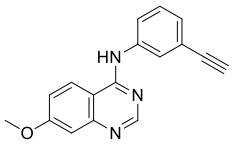

The title compound was synthesized from 4-chloro-7-methoxyquinazoline (50.0 mg, 257 µmol) and 3-ethynylaniline (26.9 µL, 257 µmol) according to general procedure A (reaction time: 3 h). The crude was purified by automated column chromatography (20 – 60% EtOAc/DCM) to afford the product (69.2 mg, 251 µmol, 98%). ^{1}H NMR (400 MHz, DMSO) δ 9.68 (s, 1H), 8.58 (s, 1H), 8.43 (d, *J* = 9.2 Hz, 1H), 8.09 (t, *J* = 1.9 Hz, 1H), 7.91 (ddd, *J* = 8.4, 2.3, 1.1 Hz, 1H), 7.38 (t, *J* = 7.9 Hz, 1H), 7.26 – 7.19 (m, 2H), 7.18 (d, *J* = 2.6 Hz, 1H), 4.19 (s, 1H), 3.90 (s, 3H). ^{13}C NMR (101 MHz, DMSO) δ 162.76, 157.25, 154.90, 152.18, 139.74, 128.87, 126.50, 124.78, 124.55, 122.56, 121.77, 117.74, 109.42, 107.00, 83.63, 80.51, 55.61. LCMS (Fleet, 10 → 90%): t_r = 4.39 min, m/z: 276.3. HRMS $[C_{17}H_{13}N_3O + H]^+$: 276.11314 calculated, 276.11296 found.

_N_-(3-Ethynylphenyl)-6-methoxyquinazolin-4-amine (12)

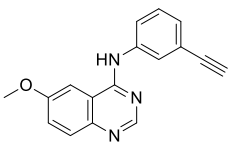

The title compound was synthesized from 4-chloro-6-methoxyquinazoline (50.0 mg, 257 µmol) and 3-ethynylaniline (26.9 µL, 257 µmol) according to general procedure A (reaction time: 3 h). The crude was purified by automated column chromatography (20 – 60% EtOAc/DCM) to afford the product (58.1 mg, 211 µmol, 82%). ^{1}H NMR (500 MHz, DMSO) δ 9.62 (s, 1H), 8.54 (s, 1H), 8.05 (t, *J* = 1.9 Hz, 1H), 7.94 (ddd, *J* = 8.3, 2.3, 1.1 Hz, 1H), 7.88 (d, *J* = 2.7 Hz, 1H), 7.72 (d, *J* = 9.0 Hz, 1H), 7.47 (dd, *J* = 9.1, 2.7 Hz, 1H), 7.41 (t, *J* = 7.9 Hz, 1H), 7.24 (dt, *J* = 7.6, 1.3 Hz, 1H), 4.19 (s, 1H), 3.93 (s, 3H). ^{13}C NMR (126 MHz, DMSO) δ 157.42, 156.77, 152.18, 145.18, 139.64, 129.45, 128.88, 126.62, 124.98, 124.23, 122.75, 121.79, 115.66, 102.10, 83.51, 80.54, 55.99. LCMS (Fleet, 10 → 90%): t_r = 4.42 min, m/z: 276.3. HRMS [$C_{17}H_{13}N_3O$ + H]$^+$: 276.11314 calculated, 276.11305 found.

_N_-(3-Ethynylphenyl)quinazolin-4-amine (13)

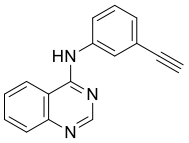

The title compound was synthesized from 4-chloroquinazoline (50.0 mg, 304 µmol) and 3-ethynylaniline (34.2 µL, 257 µmol) according to general procedure A (reaction time: 3 h). The crude was purified by automated column chromatography (1 – 10% MeOH/DCM) to afford the product (49.3 mg, 201 µmol, 66%). ^{1}H NMR (500 MHz, MeOD) δ 8.52 (s, 1H), 8.31 (dd, *J* = 8.4, 0.7 Hz, 1H), 7.93 (t, *J* = 1.9 Hz, 1H), 7.81 (ddd, *J* = 8.3, 6.9, 1.3 Hz, 1H), 7.79 – 7.72 (m, 2H), 7.58 (ddd, *J* = 8.3, 6.9, 1.3 Hz, 1H), 7.34 (t, *J* = 7.9 Hz, 1H), 7.25 (dt, *J* = 7.7, 1.3 Hz, 1H), 3.50 (s, 1H). ^{13}C NMR (126 MHz, MeOD) δ 159.83, 155.49, 150.31, 140.17, 134.54, 129.86, 129.09, 128.03, 128.01, 127.20, 124.42, 124.15, 123.51, 116.61, 84.23, 78.81. LCMS (Fleet, 0 → 50%): t_r = 6.61 min, m/z: 246.1. HRMS [$C_{16}H_{11}N_3$ + H]$^+$: 246.10257 calculated, 246.10253 found.

_N_-(3-Ethynylphenyl)-6,7-dimethoxyisoquinolin-1-amine (14)

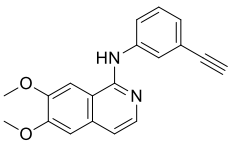

A microwave tube charged with 1-chloro-6,7-dimethoxyisoquinoline (100 mg, 447 µmol) was mixed in 2-propanol (3 mL) after which 3-ethynylaniline (50 µL, 447 µmol) and a catalytic amount of 2 M HCl (aq., 50 µL) were added. The vial was sealed and the mixture was stirred at 82°C for 16 h. This mixture was poured into sat. $NaHCO_3$ (aq.) (20 mL) and the product extracted with $CHCl_3$/MeOH (4:1) (3x20 mL). The combined organic layers were washed with H_2O (30 mL), dried over Na_2SO_4, filtered and concentrated. The crude was purified by silica gel column chromatography (0 – 5% MeOH/DCM) to afford the product (44.0 mg, 145 µmol, 32%). ^{1}H NMR (400 MHz, DMSO) δ 8.96 (s, 1H), 8.00 (t, *J* = 1.9 Hz, 1H), 7.92 – 7.87 (m, 2H), 7.78 (s, 1H), 7.32 (t, *J* = 7.9 Hz, 1H), 7.25 (s, 1H), 7.12 (d, *J* = 5.7 Hz, 1H), 7.07 (dt, *J* = 7.5, 1.3 Hz, 1H), 4.15 (s, 1H), 3.97 (s, 3H), 3.91 (s, 3H). ^{13}C NMR (101 MHz, DMSO) δ 152.11, 151.03, 149.24, 141.86, 138.85, 133.51, 128.73, 124.38, 122.85, 121.57, 120.76, 113.30, 112.64, 105.99, 102.87, 84.02, 80.04, 56.06, 55.61. LCMS (Fleet, 10 → 90%): t_r = 4.50 min, m/z: 305.3. HRMS [$C_{19}H_{16}N_2O_2$ + H]$^+$: 305.12845 calculated, 305.12840 found.

_N_-(3-Ethynylphenyl)-6,7-dimethoxyquinolin-4-amine (15)

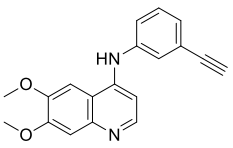

A microwave tube charged with 1-chloro-6,7-dimethoxyisoquinoline (100 mg, 447 µmol) was mixed in 2-propanol (3 mL) after which 3-ethynylaniline (50 µL, 447 µmol) and a catalytic amount of 2 M HCl (aq., 50 µL) were added. The vial was sealed and the mixture was stirred at 82°C for 16 h. This mixture was poured into sat. $NaHCO_3$ (aq.) (20 mL) and the product extracted with $CHCl_3$/MeOH (4:1) (3x20 mL). The combined organic layers were washed with H_2O (30 mL), dried over Na_2SO_4, filtered and concentrated. The crude was purified by silica gel column chromatography (0 – 5% MeOH/DCM) to afford the product (58.3 mg, 192 µmol, 43%). ^{1}H NMR (400 MHz, DMSO) δ 8.88 (br s, 1H), 8.33 (d, *J* = 5.4 Hz, 1H), 7.65 (s, 1H), 7.42 – 7.39 (m, 3H), 7.27 (s, 1H), 7.24 – 7.18 (m, 1H), 6.89 (d, *J* = 5.4 Hz, 1H), 4.22 (s, 1H), 3.93 (s, 3H), 3.91 (s, 3H). ^{13}C NMR (101 MHz, DMSO) δ 151.91, 148.42, 147.88, 146.02, 145.48, 141.36, 129.85, 126.34, 124.46, 122.76, 122.17, 114.21, 107.84, 101.57, 101.02, 83.28, 80.97, 55.94, 55.57. LCMS (Fleet, 10 → 90%): t_r = 4.66 min, m/z: 305.3. HRMS [$C_{19}H_{16}N_2O_2$ + H]$^+$: 305.12845 calculated, 305.12831 found.

_N_-(3-Ethynylphenyl)-7H-pyrrolo[2,3-d]pyrimidin-4-amine (16)

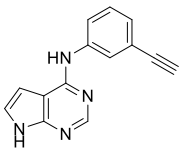

The title compound was synthesized from 4-chloro-7*H*-pyrrolo[2,3-*d*]pyrimidine (50.0 mg, 326 µmol) and 3-ethynylaniline (36.6 µL, 326 µmol) according to general procedure A, using 5% MeOH/$CHCl_3$ for the extraction (reaction time 18 h). The crude was purified by automated column chromatography (1 – 10% MeOH/DCM) to afford the product (26.6 mg, 114 µmol, 35%). ^{1}H NMR (500 MHz, MeOD) δ 8.26 (s, 1H), 7.89 (t, *J* = 1.8 Hz, 1H), 7.70 (ddd, *J* = 8.2, 2.2, 1.0 Hz, 1H), 7.28 (t, *J* = 7.9 Hz, 1H), 7.17 (dt, *J* = 7.6, 1.2 Hz, 1H), 7.14 (d, *J* = 3.5 Hz, 1H), 6.66 (d, *J* = 3.5 Hz, 1H), 3.40 (s, 1H). ^{13}C NMR (126 MHz, MeOD) δ 155.43, 151.61, 151.36, 141.02, 129.72, 127.73, 125.68, 123.93, 123.29, 122.94, 105.41, 99.87, 84.39, 78.29. LCMS (Fleet, 0 → 50%): t_r = 6.19 min, m/z: 235.1. HRMS $[C_{14}H_{10}N_4 + H]^+$: 235.09782 calculated, 235.09760 found.

2,2'-((4-((3-Ethylphenyl)amino)quinazoline-6,7-diyl)bis(oxy))bis(ethan-1-ol) (17)

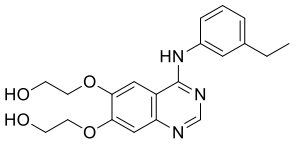

The title compound was synthesized from **66** (28 mg, 62 µmol) according to general procedure B (reaction time: 1 h). The crude was purified by silica gel column chromatography (5 – 8% MeOH/DCM) to afford the product (19 mg, 51 µmol, 83%). ^{1}H NMR (400 MHz, MeOD) δ 8.34 (s, 1H), 7.68 (s, 1H), 7.55 – 7.49 (m, 2H), 7.29 (t, *J* = 7.7 Hz, 1H), 7.09 (s, 1H), 7.02 (dt, *J* = 7.6, 1.2 Hz, 1H), 4.26 – 4.21 (m, 2H), 4.21 – 4.17 (m, 2H), 4.01 – 3.94 (m, 4H), 2.67 (q, *J* = 7.6 Hz, 2H), 1.27 (t, *J* = 7.6 Hz, 3H). ^{13}C NMR (101 MHz, MeOD) δ 158.64, 155.92, 153.87, 150.39, 147.20, 146.24, 140.11, 129.73, 125.20, 123.72, 121.71, 110.50, 107.86, 103.81, 71.97, 71.65, 61.45, 61.24, 29.89, 16.11. LCMS (Finnigan, 10 → 90%): t_r = 4.92 min, m/z: 370.2. HRMS $[C_{20}H_{23}N_3O_4 + H]^+$: 370.17613 calculated, 370.17599 found.

2,2'-((4-((3-Isopropylphenyl)amino)quinazoline-6,7-diyl)bis(oxy))bis(ethan-1-ol) (18)

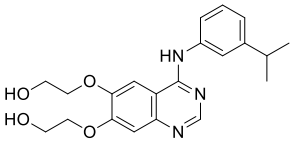

The title compound was synthesized from **67** (28.8 mg, 61.6 µmol) according to general procedure B (reaction time: 1 h). The crude was purified by silica gel column chromatography (5 – 8% MeOH/DCM) to afford the product (20 mg, 52 µmol, 85%). ^{1}H NMR (400 MHz, MeOD) δ 8.34 (s, 1H), 7.70 (s, 1H), 7.57 (ddd, *J* = 8.1, 2.2, 1.1 Hz, 1H), 7.53 (t, *J* = 1.9 Hz, 1H), 7.30 (t, *J* = 7.8 Hz, 1H), 7.10 (s, 1H), 7.05 (dt, *J* = 7.8, 1.1 Hz, 1H), 4.26 – 4.22 (m, 2H), 4.22 – 4.17 (m, 2H), 4.02 – 3.94 (m, 4H), 2.93 (hept, *J* = 6.9 Hz, 1H), 1.29 (d, *J* = 6.9 Hz, 6H). ^{13}C NMR (101 MHz, MeOD) δ 158.64, 155.90, 153.96, 150.91, 150.38, 147.38, 140.14, 129.72, 123.73, 122.28, 121.90, 110.54, 107.97, 103.81, 71.97, 71.65, 61.45, 61.25, 35.45, 24.43. LCMS (Fleet, 10 → 90%): t_r = 4.46 min, m/z: 384.3. LCMS (Fleet, 10 → 90%): t_r = 4.46 min, m/z: 384.3. HRMS $[C_{21}H_{25}N_3O_4 + H]^+$: 384.19178 calculated, 384.19186 found.

2,2'-((4-([1,1'-Biphenyl]-3-ylamino)quinazoline-6,7-diyl)bis(oxy))bis(ethan-1-ol) (19)

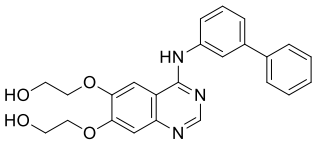

The title compound was synthesized from **68** (39 mg, 78 µmol) according to general procedure B (reaction time: 1 h). The crude was purified by silica gel column chromatography (5 – 8% MeOH/DCM) to afford the product (28.8 mg, 69.0 µmol, 89%). ^{1}H NMR (400 MHz, DMSO) δ 9.57 (s, 1H), 8.47 (s, 1H), 8.06 (t, *J* = 1.9 Hz, 1H), 7.90 (s, 1H), 7.87 (ddd, *J* = 8.0, 2.0, 0.9 Hz, 1H), 7.72 – 7.67 (m, 2H), 7.52 – 7.46 (m, 3H), 7.42 – 7.36 (m, 2H), 7.22 (s, 1H), 4.99 (t, *J* = 5.4 Hz, 1H), 4.96 (t, *J* = 5.4 Hz, 1H), 4.24 – 4.16 (m, 4H), 3.89 – 3.79 (m, 4H). ^{13}C NMR (101 MHz, DMSO) δ 156.36, 153.83, 152.89, 148.38, 146.95, 140.53, 140.24, 140.07, 129.05, 129.01, 127.57, 126.72, 121.72, 121.35, 120.57, 108.93, 108.15, 103.06, 70.78, 70.40, 59.39, 59.26. LCMS (Finnigan, 10 → 90%): t_r = 5.45 min, m/z: 418.2. HRMS $[C_{24}H_{23}N_3O_4 + H]^+$: 418.17613 calculated, 418.17623 found.

2,2'-((4-((2'-Methyl-[1,1'-biphenyl]-3-yl)amino)quinazoline-6,7-diyl)bis(oxy))bis(ethan-1-ol) (20)

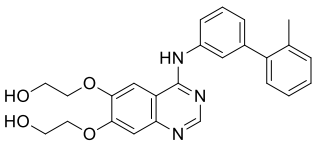

The title compound was synthesized from **75** (26 mg, 50 µmol) according to general procedure B (reaction time: 1 h). The crude was purified by silica gel column chromatography (5 – 8% MeOH/DCM) to afford the product (20 mg, 46 µmol, 92%). ^{1}H NMR (400 MHz, MeOD) δ 8.36 (s, 1H), 7.74 – 7.70 (m, 2H), 7.67 (t, *J* = 1.8 Hz, 1H), 7.42 (t, *J* = 7.9 Hz, 1H), 7.28 – 7.21 (m, 4H), 7.12 – 7.07 (m, 2H), 4.24 (t, 2H), 4.20 (t, 2H), 4.00 – 3.94 (m, 4H), 2.31 (s, 3H). ^{13}C NMR (101 MHz, MeOD) δ 158.61, 155.94, 153.99, 150.43, 147.49, 143.99, 142.99, 140.12, 136.37, 131.37, 130.63, 129.53, 128.43, 126.85, 126.24, 124.84, 122.49, 110.60, 108.00, 103.77, 71.98, 71.66, 61.45, 61.25, 20.69. LCMS (Finnigan, 10 → 90%): t_r = 5.74 min, m/z: 432.3. HRMS $[C_{25}H_{25}N_3O_4 + H]^+$: 432.19178 calculated, 432.19188 found.

2,2'-((4-((3'-Methyl-[1,1'-biphenyl]-3-yl)amino)quinazoline-6,7-diyl)bis(oxy))bis(ethan-1-ol) (21)

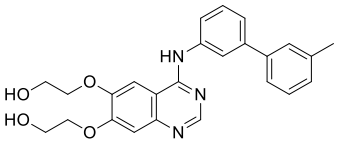

The title compound was synthesized from **76** (24.5 mg, 47.5 µmol) according to general procedure B (reaction time: 1 h). The crude was purified by silica gel column chromatography (4 – 8% MeOH/DCM) to afford the product (18 mg, 42 µmol, 88%). ^{1}H NMR (400 MHz, DMSO) δ 9.56 (s, 1H), 8.47 (s, 1H), 8.01 (t, *J* = 1.8 Hz, 1H), 7.92 – 7.85 (m, 2H), 7.54 – 7.43 (m, 3H), 7.42 – 7.33 (m, 2H), 7.22 (s, 1H), 7.20 (d, *J* = 7.5 Hz, 1H), 5.00 (t, *J* = 5.4 Hz, 1H), 4.96 (t, *J* = 5.4 Hz, 1H), 4.25 – 4.15 (m, 4H), 3.86 (q, *J* = 5.3 Hz, 2H), 3.82 (q, *J* = 5.3 Hz, 2H), 2.39 (s, 3H). ^{13}C NMR (101 MHz, DMSO) δ 156.37, 153.83, 152.90, 148.38, 146.95, 140.63, 140.19, 140.02, 138.12, 128.98, 128.90, 128.20, 127.37, 123.84, 121.71, 121.31, 120.53, 108.93, 108.15, 103.06, 70.79, 70.40, 59.40, 59.27, 21.16. LCMS (Fleet, 10 → 90%): t_r = 4.94 min, m/z: 432.3. HRMS $[C_{25}H_{25}N_3O_4 + H]^+$: 432.19178 calculated, 432.19157 found.

3'-((6,7-Bis(2-hydroxyethoxy)quinazolin-4-yl)amino)-[1,1'-biphenyl]-3-carbonitrile (22)

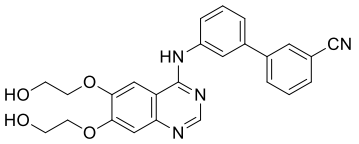

The title compound was synthesized from **77** (50.0 mg, 119 µmol) according to general procedure C using (3-cyanophenyl)boronic acid. The crude was purified by silica gel column chromatography (2 – 8% MeOH/DCM) to afford the product (39 mg, 88 µmol, 74%). ^{1}H NMR (400 MHz, DMSO) δ 9.59 (s, 1H), 8.48 (s, 1H), 8.16 (t, *J* = 1.5 Hz, 1H), 8.11 (t, *J* = 1.7 Hz, 1H), 8.04 (dt, *J* = 7.9, 1.4 Hz, 1H), 7.93 (dt, *J* = 7.8, 1.5 Hz, 1H), 7.88 (s, 1H), 7.85 (dt, *J* = 7.7, 1.3 Hz, 1H), 7.70 (t, *J* = 7.8 Hz, 1H), 7.52 (t, *J* = 7.7 Hz, 1H), 7.48 (dt, *J* = 7.7, 1.6 Hz, 1H), 7.22 (s, 1H), 5.01 (t, *J* = 5.4 Hz, 1H), 4.97 (t, *J* = 5.4 Hz, 1H), 4.25 – 4.15 (m, 4H), 3.86 (q, *J* = 5.4 Hz, 2H), 3.82 (q, *J* = 5.2 Hz, 2H). ^{13}C NMR (101 MHz, DMSO) δ 156.34, 153.88, 152.88, 148.41, 146.98, 141.34, 140.27, 138.35, 131.54, 131.19, 130.26, 129.29, 122.24, 121.91, 120.76, 118.83, 112.17, 108.93, 108.14, 103.01, 70.80, 70.42, 59.40, 59.28. LCMS (Fleet, 10 → 90%): t_r = 4.45 min, m/z: 443.3. HRMS $[C_{25}H_{22}N_4O_4 + H]^+$: 443.17138 calculated, 443.17105 found.

2,2'-((4-((4'-Methyl-[1,1'-biphenyl]-3-yl)amino)quinazoline-6,7-diyl)bis(oxy))bis(ethan-1-ol) (23)

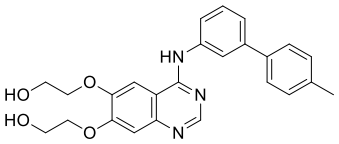

The title compound was synthesized from **77** (34 mg, 81 µmol) according to general procedure C using *p*-tolylboronic acid. The crude was purified by silica gel column chromatography (4 – 8% MeOH/DCM) to afford the product (28 mg, 65 µmol, 80%). ^{1}H NMR (400 MHz, DMSO) δ 9.55 (s, 1H), 8.47 (s, 1H), 8.02 (t, *J* = 1.8 Hz, 1H), 7.89 (s, 1H), 7.87 – 7.83 (m, 1H), 7.61 – 7.57 (m, 2H), 7.46 (t, *J* = 7.9 Hz, 1H), 7.37 (ddd, *J* = 7.7, 1.8, 1.1 Hz, 1H), 7.31 – 7.27 (m, 2H), 7.22 (s, 1H), 5.00 (t, *J* = 5.4 Hz, 1H), 4.96 (t, *J* = 5.4 Hz, 1H), 4.24 – 4.16 (m, 4H), 3.86 (q, *J* = 5.5 Hz, 2H), 3.82 (q, *J* = 5.3 Hz, 2H), 2.35 (s, 3H). ^{13}C NMR (101 MHz, DMSO) δ 156.38, 153.83, 152.90, 148.38, 146.95, 140.42, 140.03, 137.32, 136.85, 129.60, 128.98, 126.53, 121.48, 121.12, 120.30, 108.94, 108.15, 103.08, 70.79, 70.40, 59.40, 59.27, 20.71. LCMS (Fleet, 10 → 90%): t_r = 4.96 min, m/z: 432.3. HRMS $[C_{25}H_{25}N_3O_4 + H]^+$: 432.19178 calculated, 432.19187 found.

3'-((6,7-Bis(2-hydroxyethoxy)quinazolin-4-yl)amino)-[1,1'-biphenyl]-4-carbonitrile (24)

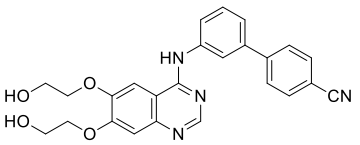

The title compound was synthesized from **77** (45.0 mg, 107 µmol) according to general procedure C using (4-cyanophenyl)boronic acid. The crude was purified by silica gel column chromatography (2 – 8% MeOH/DCM) to afford the product (26 mg, 59 µmol, 55%). ^{1}H NMR (400 MHz, DMSO) δ 9.61 (s, 1H), 8.48 (s, 1H), 8.15 (t, *J* = 1.7 Hz, 1H), 7.99 – 7.86 (m, 6H), 7.53 (t, *J* = 7.8 Hz, 1H), 7.48 (dt, *J* = 8.2, 1.4 Hz, 1H), 7.22 (s, 1H), 5.00 (t, *J* = 5.2 Hz, 1H), 4.96 (t, *J* = 5.3 Hz, 1H), 4.24 – 4.16 (m, 4H), 3.86 (q, *J* = 5.3 Hz, 2H), 3.81 (q, *J* = 5.2 Hz, 2H). ^{13}C NMR (101 MHz, DMSO) δ 156.31, 153.89, 152.84, 148.42, 146.99, 144.73, 140.32, 138.59, 132.97, 129.35, 127.60, 122.51, 121.99, 120.78, 118.91, 110.14, 108.93, 108.15, 103.02, 70.78, 70.42, 59.39, 59.27. LCMS (Fleet, 10 → 90%): t_r = 4.45 min, m/z: 443.3. HRMS $[C_{25}H_{22}N_4O_4 + H]^+$: 443.17138 calculated, 443.17117 found.

2,2'-((4-((3-Methoxyphenyl)amino)quinazoline-6,7-diyl)bis(oxy))bis(ethan-1-ol) (25)

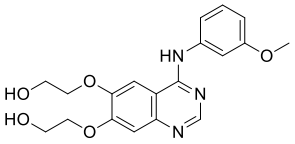

The title compound was synthesized from **69** (49.5 mg, 109 µmol) according to general procedure B (reaction time: 1 h). The crude was purified by silica gel column chromatography (5 – 20% MeOH/DCM) to afford the product (32.5 mg, 87.5 µmol, 81%). ^{1}H NMR (400 MHz, MeOD) δ 8.34 (s, 1H), 7.63 (s, 1H), 7.39 (s, 1H), 7.31 – 7.22 (m, 2H), 7.03 (s, 1H), 6.71 (d, *J* = 7.6 Hz, 1H), 4.22 (t, 2H), 4.15 (t, 2H), 4.03 – 3.91 (m, 4H), 3.81 (s, 3H). ^{13}C NMR (101 MHz, MeOD) δ 161.47, 158.39, 155.78, 154.31, 150.28, 147.21, 141.38, 130.40, 116.14, 110.83, 110.49, 109.78, 107.81, 103.62, 71.91, 71.58, 61.41, 61.20, 55.73. LCMS (Finnigan, 10 → 90%): t_r = 4.39 min, m/z: 372.2. HRMS $[C_{19}H_{21}N_3O_5 + H]^+$: 372.15540 calculated, 372.1557 found.

2,2'-((4-((3-Phenoxyphenyl)amino)quinazoline-6,7-diyl)bis(oxy))bis(ethan-1-ol) (26)

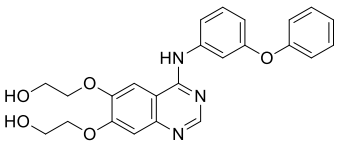

The title compound was synthesized from **70** (32 mg, 62 µmol) according to general procedure B (reaction time: 1 h). The crude was purified by silica gel column chromatography (4 – 10% MeOH/DCM) to afford the product (22 mg, 51 µmol, 82%). ^{1}H NMR (400 MHz, MeOD) δ 8.32 (s, 1H), 7.60 (s, 1H), 7.51 (ddd, *J* = 8.1, 2.0, 0.8 Hz, 1H), 7.46 (t, *J* = 2.1 Hz, 1H), 7.37 – 7.28 (m, 3H), 7.12 – 7.07 (m, 1H), 7.06 – 7.01 (m, 3H), 6.73 (ddd, *J* = 8.2, 2.4, 0.8 Hz, 1H), 4.19 (t, 2H), 4.15 (t, 2H), 3.99 – 3.91 (m, 4H). ^{13}C NMR (101 MHz, MeOD) δ 159.05, 158.49, 158.26, 155.87, 153.67, 150.37, 147.18, 141.85, 130.87, 130.72, 124.48, 120.08, 118.39, 115.23, 114.02, 110.48, 107.76, 103.58, 71.91, 71.61, 61.42, 61.22. LCMS (Finnigan, 10 → 90%): t_r = 5.56 min, m/z: 434.2. HRMS $[C_{24}H_{23}N_3O_5 + H]^+$: 434.17105 calculated, 434.1709 found.

2,2'-((4-((4-Methoxyphenyl)amino)quinazoline-6,7-diyl)bis(oxy))bis(ethan-1-ol) (27)

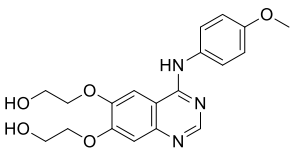

The title compound was synthesized from **71** (42 mg, 92 µmol) according to general procedure B (reaction time: 1.5 h). The crude was loaded onto Celite and purified by silica gel column chromatography (7 – 10% MeOH/DCM) to afford the product (15.4 mg, 41.5 µmol, 45%). ^{1}H NMR (500 MHz, MeOD) δ 8.35 (s, 1H), 7.74 (s, 1H), 7.52 – 7.48 (m, 2H), 7.14 (s, 1H), 6.97 – 6.94 (m, 2H), 4.27 – 4.20 (m, 4H), 4.02 – 3.97 (m, 4H), 3.82 (s, 3H). ^{13}C NMR (126 MHz, MeOD) δ 158.83, 158.30, 155.76, 152.90, 150.10, 144.93, 131.87, 126.29, 114.88, 109.84, 106.53, 103.90, 71.60, 71.37, 61.03, 60.82, 55.84. LCMS (Finnigan, 10 → 90%): t_r = 4.30 min, m/z: 372.1. HRMS $[C_{19}H_{21}N_3O_5 + H]^+$: 372.15540 calculated, 372.1555 found.

2,2'-((4-((4-Phenoxyphenyl)amino)quinazoline-6,7-diyl)bis(oxy))bis(ethan-1-ol) (28)

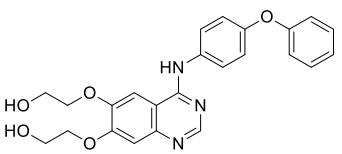

The title compound was synthesized from **72** (31.5 mg, 60.9 µmol) according to general procedure B (reaction time: 1 h). The crude was purified by silica gel column chromatography (5 – 10% MeOH/DCM) to afford the product (21 mg, 48 µmol, 80%). ^{1}H NMR (400 MHz, MeOD) δ 8.38 (s, 1H), 7.69 (s, 1H), 7.62 – 7.57 (m, 2H),

7.35 – 7.29 (m, 2H), 7.12 (s, 1H), 7.10 – 7.05 (m, 1H), 7.05 – 6.99 (m, 4H), 4.25 – 4.19 (m, 4H), 4.02 – 3.96 (m, 4H). ^{13}C NMR (101 MHz, MeOD) δ 158.17, 158.07, 155.03, 154.65, 153.50, 149.47, 146.75, 134.62, 130.25, 125.48, 123.72, 119.81, 119.09, 110.04, 107.53, 103.37, 71.23, 70.94, 60.86, 60.63. LCMS (Finnigan, 10 → 90%): t_r = 5.52 min, m/z: 434.2. HRMS [$C_{24}H_{23}N_3O_5$ + H]$^+$: 434.17105 calculated, 434.1713 found.

2,2'-((4-((4-(Benzyloxy)phenyl)amino)quinazoline-6,7-diyl)bis(oxy))bis(ethan-1-ol) (29)

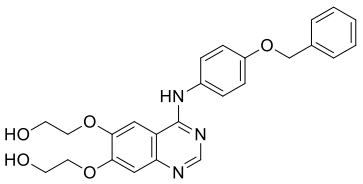

The title compound was synthesized from **73** (19 mg, 36 µmol) according to general procedure B (reaction time: 1 h). The crude was purified by silica gel column chromatography (5 – 10% MeOH/DCM) to afford the product (13 mg, 29 µmol, 81%). ^{1}H NMR (400 MHz, MeOD) δ 8.32 (s, 1H), 7.69 (s, 1H), 7.51 – 7.47 (m, 2H), 7.45 – 7.41 (m, 2H), 7.39 – 7.33 (m, 2H), 7.32 – 7.27 (m, 1H), 7.11 (s, 1H), 7.03 – 6.99 (m, 2H), 5.08 (s, 2H), 4.26 – 4.19 (m, 4H), 4.02 – 3.96 (m, 4H). ^{13}C NMR (101 MHz, MeOD) δ 158.50, 156.94, 155.11, 153.62, 149.55, 146.64, 137.83, 132.39, 129.13, 128.54, 128.10, 125.97, 115.83, 110.07, 107.52, 103.56, 71.34, 71.04, 70.90, 60.92, 60.71. LCMS (Fleet, 10 → 90%): t_r = 4.79 min, m/z: 448.3. HRMS [$C_{25}H_{25}N_3O_5$ + H]$^+$: 448.18670 calculated, 448.1870 found.

2,2'-((4-((1*H*-Pyrazol-4-yl)amino)quinazoline-6,7-diyl)bis(oxy))bis(ethan-1-ol) (30)

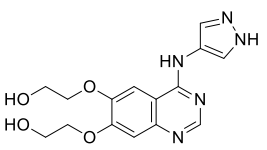

102 (30 mg, 60 µmol) was mixed in MeOH (2 mL). 0.16 M HCl in dioxane was prepared by diluting 12 M HCl (aq.). in dioxane of which 0.4 mL was added to the reaction mixture. The mixture was stirred for 3 h and subsequently concentrated. The title compound was synthesized from the remaining solids according to general procedure B (reaction time: 2 h). Since the product was soluble in water, the crude reaction mixture was concentrated directly and purified twice by silica gel column chromatography (first 30% MeOH/DCM, then, 20% MeOH (containing 10% sat. NH_4OH (aq.))/DCM) to afford the product (13.5 mg, 40.7 µmol, 68%). ^{1}H NMR (400 MHz, D_2O) δ 8.17 (s, 1H), 7.51 (s, 2H), 6.88 (s, 1H), 6.41 (s, 1H), 3.90 – 3.79 (m, 8H). ^{13}C NMR (101 MHz, D_2O) δ 155.38, 154.49, 149.56, 148.41, 134.43, 127.07 (br), 120.02, 106.51, 102.75, 100.58, 71.34, 71.27, 60.02, 59.93. LCMS (Finnigan, 0 → 50%): t_r = 5.10 min, m/z: 332.2. HRMS [$C_{15}H_{17}N_5O_4$ + H]$^+$: 332.13533 calculated, 332.1358 found.

2,2'-((4-((1-Methyl-1*H*-pyrazol-4-yl)amino)quinazoline-6,7-diyl)bis(oxy))bis(ethan-1-ol) (31)

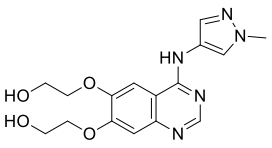

The title compound was synthesized from **103** (32 mg, 75 µmol) according to general procedure B (reaction time: 2 h). Since the product was soluble in water, the crude reaction mixture was concentrated directly and purified by silica gel column chromatography (5 – 10% MeOH (containing 10% sat. NH_4OH (aq.))/DCM) to afford the product (23.7 mg, 68.6 µmol, 92%). ^{1}H NMR (400 MHz, DMSO) δ 10.10 (s, 1H), 8.51 (s, 1H), 8.24 (s, 1H), 7.95 (s, 1H), 7.75 (s, 1H), 7.18 (s, 1H), 5.00 (br s, 2H), 4.20 (t, *J* = 5.2 Hz, 2H), 4.16 (t, *J* = 4.9 Hz, 2H), 3.86 (s, 3H), 3.85 – 3.79 (m, 4H). ^{13}C NMR (101 MHz, DMSO) δ 155.25, 153.79, 152.52, 148.34, 144.27, 131.22, 122.77, 122.02, 108.40, 106.84, 103.45, 70.80, 70.45, 59.30, 59.24, 38.83. LCMS (Fleet, 0 → 50%): t_r = 4.76 min, m/z: 346.3. HRMS [$C_{16}H_{19}N_5O_4$ + H]$^+$: 346.15098 calculated, 346.1516 found.

2,2'-((4-((1-Ethyl-1*H*-pyrazol-4-yl)amino)quinazoline-6,7-diyl)bis(oxy))bis(ethan-1-ol) (32)

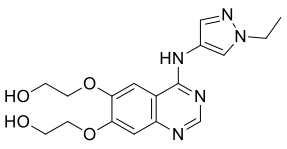

The title compound was synthesized from **104** (33 mg, 74 µmol) according to general procedure B (reaction time: 2 h). The crude reaction mixture was concentrated directly and purified by silica gel column chromatography (5 – 10% MeOH/DCM) to afford the product (22 mg, 61 µmol, 82%). ^{1}H NMR (400 MHz, MeOD) δ 8.45 (s, 1H), 8.20 (d, *J* = 0.7 Hz, 1H), 7.72 (d, *J* = 0.7 Hz, 1H), 7.62 (s, 1H), 7.06 (s, 1H), 4.23 – 4.14 (m, 6H), 4.02 – 3.94 (m, 4H), 1.49 (t, *J* = 7.3 Hz, 3H). ^{13}C NMR (101 MHz, MeOD) δ 156.88, 154.89, 153.76, 149.48, 145.98, 132.15, 122.86, 122.64, 109.82, 107.38, 103.21, 71.29, 71.02, 60.93, 60.73, 47.80, 15.82.

LCMS (Fleet, 0 → 50%): t_r = 5.09 min, m/z: 360.3. HRMS $[C_{17}H_{21}N_5O_4 + H]^+$: 360.16663 calculated, 360.1671 found.

2,2'-((4-((1-Benzyl-1*H*-pyrazol-4-yl)amino)quinazoline-6,7-diyl)bis(oxy))bis(ethan-1-ol) (33)

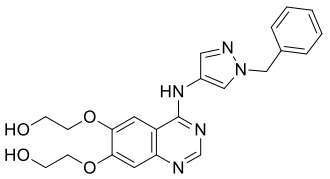

The title compound was synthesized from **105** (40 mg, 79 µmol) according to general procedure B (reaction time: 2 h). The crude reaction mixture was concentrated directly and purified by silica gel column chromatography (3 – 10% MeOH (containing 10% sat. NH_4OH (aq.))/DCM) to afford the product (28 mg, 66 µmol, 84%). ^{1}H NMR (400 MHz, MeOD) δ 8.46 (s, 1H), 8.25 (s, 1H), 7.79 (d, *J* = 0.8 Hz, 1H), 7.65 (s, 1H), 7.35 – 7.26 (m, 3H), 7.26 – 7.21 (m, 2H), 7.09 (s, 1H), 5.31 (s, 2H), 4.24 – 4.16 (m, 4H), 4.01 – 3.95 (m, 4H). ^{13}C NMR (101 MHz, MeOD) δ 156.70, 154.91, 153.54, 149.49, 145.58, 137.15, 132.51, 129.31, 128.59, 128.03, 123.37, 123.30, 109.74, 107.14, 103.20, 71.23, 70.99, 60.85, 60.65, 56.63. LCMS (Finnigan, 0 → 50%): t_r = 7.17 min, m/z: 422.3. HRMS $[C_{22}H_{23}N_5O_4 + H]^+$: 422.18228 calculated, 422.1821 found.

2,2'-((4-((1-Phenethyl-1*H*-pyrazol-4-yl)amino)quinazoline-6,7-diyl)bis(oxy))bis(ethan-1-ol) (34)

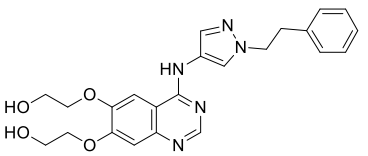

The title compound was synthesized from **106** (31 mg, 60 µmol) according to general procedure B (reaction time: 1 h). The crude reaction mixture was concentrated directly and purified by silica gel column chromatography (4 – 10% MeOH (containing 10% sat. NH_4OH (aq.))/DCM) to afford the product (21 mg, 48 µmol, 81%). ^{1}H NMR (400 MHz, MeOD) δ 8.26 (s, 1H), 7.87 (d, *J* = 0.7 Hz, 1H), 7.74 (d, *J* = 0.5 Hz, 1H), 7.41 (s, 1H), 7.26 – 7.20 (m, 2H), 7.19 – 7.14 (m, 1H), 7.12 – 7.08 (m, 2H), 6.94 (s, 1H), 4.30 (t, *J* = 7.1 Hz, 2H), 4.19 – 4.08 (m, 4H), 4.00 – 3.97 (m, 2H), 3.97 – 3.93 (m, 2H), 3.10 (t, *J* = 7.1 Hz, 2H). ^{13}C NMR (101 MHz, MeOD) δ 157.03, 154.90, 153.94, 149.46, 146.04, 139.27, 132.98, 129.75, 129.55, 127.63, 124.30, 122.82, 109.75, 107.55, 103.26, 71.63, 71.41, 61.10, 60.95, 54.54, 37.46. LCMS (Finnigan, 10 → 90%): t_r = 4.84 min, m/z: 436.3. HRMS $[C_{23}H_{25}N_5O_4 + H]^+$: 436.19793 calculated, 436.1981 found.

2,2'-((4-((1-(3-Phenylpropyl)-1*H*-pyrazol-4-yl)amino)quinazoline-6,7-diyl)bis(oxy))bis(ethan-1-ol) (35)

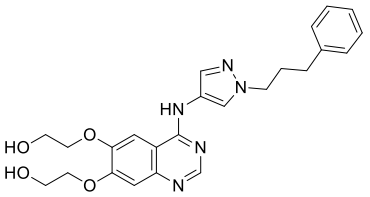

The title compound was synthesized from **108** (40.8 mg, 76.5 µmol) according to general procedure B (reaction time: 1 h). The crude reaction mixture was concentrated directly and purified by silica gel column chromatography (4 – 10% MeOH (containing 10% sat. NH_4OH (aq.))/DCM) to afford the product (31.4 mg, 69.9 µmol, 91%). ^{1}H NMR (400 MHz, MeOD) δ 8.41 (s, 1H), 8.21 (s, 1H), 7.76 (s, 1H), 7.52 (s, 1H), 7.29 – 7.21 (m, 2H), 7.21 – 7.11 (m, 3H), 7.00 (s, 1H), 4.18 (t, *J* = 4.4 Hz, 2H), 4.17 – 4.08 (m, 4H), 4.01 – 3.91 (m, 4H), 2.64 – 2.55 (m, 2H), 2.16 (p, *J* = 7.2 Hz, 2H). ^{13}C NMR (101 MHz, MeOD) δ 157.19, 155.58, 154.06, 150.17, 146.10, 142.34, 132.66, 129.50, 129.47, 127.09, 123.98, 123.48, 110.01, 107.51, 103.44, 71.87, 71.59, 61.41, 61.23, 52.61, 33.63, 33.15. LCMS (Finnigan, 10 → 90%): t_r = 5.18 min, m/z: 450.3. HRMS $[C_{24}H_{27}N_5O_4 + H]^+$: 450.21358 calculated, 450.21345 found.

2,2'-((4-((1-(2-Chlorobenzyl)-1*H*-pyrazol-4-yl)amino)quinazoline-6,7-diyl)bis(oxy))bis(ethan-1-ol) (36)

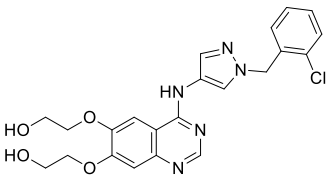

The title compound was synthesized from **107** (42 mg, 78 µmol) according to general procedure B (reaction time: 2 h). The crude reaction mixture was concentrated directly and purified by silica gel column chromatography (2 – 20% MeOH (containing 10% sat. NH_4OH (aq.))/DCM) to afford the product (30 mg, 66 µmol, 85%). ^{1}H NMR (400 MHz, DMSO) δ 9.69 (s, 1H), 8.46 (s, 1H), 8.34 (d, *J* = 0.7 Hz, 1H), 7.81 (d, *J* = 0.7 Hz, 1H), 7.79 (s, 1H), 7.50 (dd, *J* = 7.4, 1.8

Hz, 1H), 7.38 – 7.30 (m, 2H), 7.18 (s, 1H), 7.01 (dd, *J* = 7.1, 2.2 Hz, 1H), 5.47 (s, 2H), 4.99 (t, *J* = 5.4 Hz, 1H), 4.94 (t, *J* = 5.4 Hz, 1H), 4.20 – 4.14 (m, 4H), 3.84 (q, *J* = 5.3 Hz, 2H), 3.80 (q, *J* = 5.2 Hz, 2H). ^{13}C NMR (101 MHz, DMSO) δ 155.15, 153.53, 153.26, 148.16, 146.30, 135.18, 132.08, 131.90, 129.69, 129.57, 129.40, 127.55, 122.65, 122.22, 108.60, 108.18, 102.96, 70.72, 70.34, 59.37, 59.26, 52.69. LCMS (Fleet, 10 → 90%): t_r = 4.16 min, m/z: 456.3. HRMS $[C_{22}H_{22}ClN_5O_4 + H]^+$: 456.14331 calculated, 456.14322 found.

2,2'-((4-((1-(3-Fluorobenzyl)-1*H*-pyrazol-4-yl)amino)quinazoline-6,7-diyl)bis(oxy))bis(ethan-1-ol) (37)

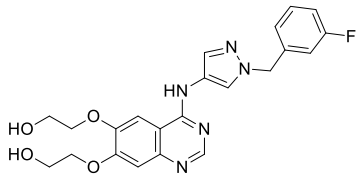

The title compound was synthesized from **109** (35 mg, 67 µmol) according to general procedure B (reaction time: 1 h). The crude reaction mixture was concentrated directly and purified by silica gel column chromatography (4 – 10% MeOH (containing 10% sat. NH_4OH (aq.))/DCM) to afford the product (25.5 mg, 58.0 µmol, 87%). ^{1}H NMR (400 MHz, DMSO) δ 9.69 (s, 1H), 8.47 (s, 1H), 8.37 (s, 1H), 7.79 (s, 1H), 7.78 (d, *J* = 0.7 Hz, 1H), 7.40 (td, *J* = 8.0, 6.1 Hz, 1H), 7.18 (s, 1H), 7.16 – 7.02 (m, 3H), 5.39 (s, 2H), 4.99 (t, *J* = 5.4 Hz, 1H), 4.94 (t, *J* = 5.4 Hz, 1H), 4.20 – 4.14 (m, 4H), 3.84 (q, *J* = 5.5 Hz, 2H), 3.80 (q, *J* = 5.2 Hz, 2H). ^{13}C NMR (101 MHz, DMSO) δ 162.17 (d, $J_{(C–F)}$ = 243.9 Hz), 155.15, 153.54, 153.26, 148.16, 146.28, 140.75 (d, $J_{(C–F)}$ = 7.3 Hz), 131.81, 130.58 (d, $J_{(C–F)}$ = 8.3 Hz), 123.54 (d, $J_{(C–F)}$ = 2.7 Hz), 122.69, 122.01, 114.38 (d, $J_{(C–F)}$ = 20.9 Hz), 114.21 (d, $J_{(C–F)}$ = 21.8 Hz), 108.60, 108.17, 102.99, 70.72, 70.35, 59.37, 59.27, 54.32. LCMS (Finnigan, 10 → 90%): t_r = 4.73 min, m/z: 440.3. HRMS $[C_{22}H_{22}FN_5O_4 + H]^+$: 440.17286 calculated, 440.17262 found.

2,2'-((4-((1-(3-Methylbenzyl)-1*H*-pyrazol-4-yl)amino)quinazoline-6,7-diyl)bis(oxy))bis(ethan-1-ol) (38)

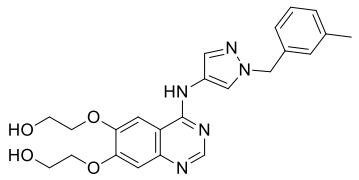

The title compound was synthesized from **110** (38.8 mg, 74.7 µmol) according to general procedure B (reaction time: 1 h). The crude reaction mixture was concentrated directly and purified by silica gel column chromatography (4 – 10% MeOH (containing 10% sat. NH_4OH (aq.))/DCM) to afford the product (29 mg, 67 µmol, 89%). ^{1}H NMR (400 MHz, DMSO) δ 9.66 (s, 1H), 8.45 (s, 1H), 8.29 (d, *J* = 0.7 Hz, 1H), 7.78 (s, 1H), 7.75 (d, *J* = 0.7 Hz, 1H), 7.24 (t, *J* = 7.5 Hz, 1H), 7.17 (s, 1H), 7.12 – 7.03 (m, 3H), 5.31 (s, 2H), 4.99 (t, *J* = 5.4 Hz, 1H), 4.94 (t, *J* = 5.4 Hz, 1H), 4.20 – 4.13 (m, 4H), 3.84 (q, *J* = 5.4 Hz, 2H), 3.80 (q, *J* = 5.2 Hz, 2H), 2.28 (s, 3H). ^{13}C NMR (101 MHz, DMSO) δ 155.14, 153.51, 153.29, 148.13, 146.28, 137.72, 137.68, 131.46, 128.47, 128.25, 128.16, 124.73, 122.57, 121.72, 108.59, 108.18, 102.97, 70.71, 70.34, 59.37, 55.06, 21.02. LCMS (Fleet, 10 → 90%): t_r = 4.16 min, m/z: 436.3. HRMS $[C_{23}H_{25}N_5O_4 + H]^+$: 436.19793 calculated, 436.19809 found.

2,2'-((4-((1-(4-Chlorobenzyl)-1*H*-pyrazol-4-yl)amino)quinazoline-6,7-diyl)bis(oxy))bis(ethan-1-ol) (39)

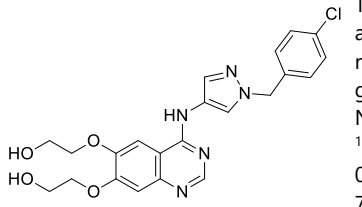

The title compound was synthesized from **111** (40 mg, 74 µmol) according to general procedure B (reaction time: 1 h). The crude reaction mixture was concentrated directly and purified by silica gel column chromatography (4 – 10% MeOH (containing 10% sat. NH_4OH (aq.))/DCM) to afford the product (30 mg, 66 µmol, 89%). ^{1}H NMR (400 MHz, DMSO) δ 9.79 (s, 1H), 8.48 (s, 1H), 8.36 (d, *J* = 0.7 Hz, 1H), 7.82 (s, 1H), 7.79 (d, *J* = 0.7 Hz, 1H), 7.43 – 7.39 (m, 2H), 7.30 – 7.25 (m, 2H), 7.18 (s, 1H), 5.36 (s, 2H), 5.01 (br s, 2H), 4.17 (q, *J* = 5.3 Hz, 4H), 3.84 (t, *J* = 5.2 Hz, 2H), 3.80 (t, *J* = 4.8 Hz, 2H). ^{13}C NMR (101 MHz, DMSO) δ 155.18, 153.65, 153.07, 148.25, 145.70, 136.89, 132.28, 131.81, 129.45, 128.55, 122.62, 121.98, 108.56, 107.79, 103.09, 70.77, 70.41, 59.38, 59.29, 54.24. LCMS (Finnigan, 10 → 90%): t_r = 5.10 min, m/z: 456.2. HRMS $[C_{22}H_{22}ClN_5O_4 + H]^+$: 456.14331 calculated, 456.1434 found.

2,2'-((4-((1-(4-Methylbenzyl)-1*H*-pyrazol-4-yl)amino)quinazoline-6,7-diyl)bis(oxy))bis(ethan-1-ol) (40)

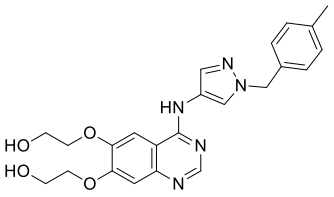

The title compound was synthesized from **112** (36 mg, 69 µmol) according to general procedure B (reaction time: 1 h). The crude reaction mixture was concentrated directly and purified by silica gel column chromatography (4 – 10% MeOH (containing 10% sat. NH_4OH (aq.))/DCM) to afford the product (26.5 mg, 60.9 µmol, 88%). ^{1}H NMR (400 MHz, DMSO) δ 9.72 (s, 1H), 8.47 (s, 1H), 8.28 (d, *J* = 0.8 Hz, 1H), 7.79 (s, 1H), 7.76 (d, *J* = 0.7 Hz, 1H), 7.23 – 7.07 (m, 5H), 5.29 (s, 2H), 5.06 – 4.89 (br m, 2H), 4.19 – 4.14 (m, 4H), 3.84 (t, *J* = 5.0 Hz, 2H), 3.80 (t, *J* = 4.8 Hz, 2H), 2.27 (s, 3H). ^{13}C NMR (101 MHz, DMSO) δ 155.17, 153.60, 153.19, 148.21, 145.93, 136.88, 134.77, 131.45, 129.11, 127.66, 122.55, 121.69, 108.58, 107.95, 103.04, 70.76, 70.39, 59.40, 59.30, 54.91, 20.74. LCMS (Finnigan, 10 → 90%): t_r = 4.97 min, m/z: 436.3. HRMS [$C_{23}H_{25}N_5O_4$ + H]$^+$: 436.19793 calculated, 436.1983 found.

2,2'-((4-((1-(4-Methoxybenzyl)-1*H*-pyrazol-4-yl)amino)quinazoline-6,7-diyl)bis(oxy))bis(ethan-1-ol) (41)

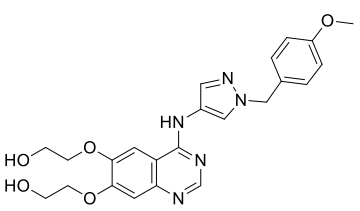

The title compound was synthesized from **113** (41 mg, 77 µmol) according to general procedure B (reaction time: 1 h). The crude reaction mixture was concentrated directly and purified by silica gel column chromatography (5 – 10% MeOH (containing 10% sat. NH_4OH (aq.))/DCM) to afford the product (30 mg, 66 µmol, 87%). ^{1}H NMR (400 MHz, DMSO) δ 9.71 (s, 1H), 8.47 (s, 1H), 8.27 (d, *J* = 0.7 Hz, 1H), 7.79 (s, 1H), 7.75 (d, *J* = 0.7 Hz, 1H), 7.27 – 7.22 (m, 2H), 7.17 (s, 1H), 6.93 – 6.88 (m, 2H), 5.26 (s, 2H), 5.11 – 4.88 (br m, 2H), 4.19 – 4.14 (m, 4H), 3.84 (t, *J* = 5.1 Hz, 2H), 3.80 (t, *J* = 4.8 Hz, 2H), 3.72 (s, 3H). ^{13}C NMR (101 MHz, DMSO) δ 158.85, 155.18, 153.60, 153.20, 148.21, 145.95, 131.40, 129.67, 129.21, 122.53, 121.51, 113.95, 108.59, 107.97, 103.04, 70.76, 70.39, 59.40, 59.30, 55.14, 54.64. LCMS (Finnigan, 10 → 90%): t_r = 4.70 min, m/z: 452.3. HRMS [$C_{23}H_{25}N_5O_5$ + H]$^+$: 452.19285 calculated, 452.1931 found.

***N*-(1*H*-Indazol-6-yl)-6,7-dimethoxyquinazolin-4-amine (42)**

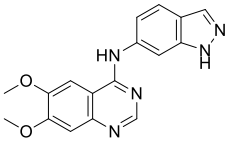

The title compound was synthesized from 1*H*-indazol-6-amine according to general procedure D (reaction time: 16 h). The crude was purified by automated column chromatography (10 – 40% EtOAc/pentane) to afford the product (52.9 mg, 165 µmol, 74%). ^{1}H NMR (400 MHz, DMSO) δ 13.02 (br s, 1H), 9.59 (s, 1H), 8.54 (s, 1H), 8.35 – 8.33 (m, 1H), 8.02 (d, *J* = 1.0 Hz, 1H), 7.90 (s, 1H), 7.73 (dd, *J* = 8.6, 0.7 Hz, 1H), 7.48 (dd, *J* = 8.7, 1.8 Hz, 1H), 7.20 (s, 1H), 3.98 (s, 3H), 3.93 (s, 3H). ^{13}C NMR (101 MHz, DMSO) δ 156.47, 154.28, 152.88, 148.98, 147.01, 140.53, 137.85, 133.36, 120.12, 119.31, 117.07, 109.13, 107.25, 101.99, 101.97, 56.30, 55.83. LCMS (Fleet, 10 → 90%): t_r = 3.54 min, m/z: 322.3. HRMS [$C_{17}H_{15}N_5O_2$ + H]$^+$: 322.12985 calculated, 322.12969 found.

***N*-(1*H*-Indazol-5-yl)-6,7-dimethoxyquinazolin-4-amine (43)**

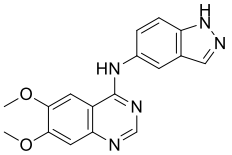

The title compound was synthesized from 1*H*-indazol-5-amine according to general procedure D (reaction time: 16 h). The crude was purified by automated column chromatography (1 – 20% EtOAc/pentane). The residue was suspended in a mixture of MeOH (1 mL) and DCM (2 mL) after which the mixture was warmed to ~50°C and subsequently cooled down. The suspension was filtered and the solids were collected to afford the product (38.6 mg, 120 µmol, 54%). ^{1}H NMR (400 MHz, DMSO) δ 13.08 (s, 1H), 9.56 (s, 1H), 8.42 (s, 1H), 8.14 (d, *J* = 1.8 Hz, 1H), 8.09 (t, *J* = 1.2 Hz, 1H), 7.87 (s, 1H), 7.64 (dd, *J* = 8.9, 1.9 Hz, 1H), 7.58 (d, *J* = 8.8 Hz, 1H), 7.17 (s, 1H), 3.96 (s, 3H), 3.93 (s, 3H). ^{13}C NMR (101 MHz, DMSO) δ 156.98, 154.13, 153.18, 148.82, 146.83, 137.40, 133.48, 132.21, 124.03, 122.92, 113.86, 109.87, 108.84, 107.20, 102.00, 56.22, 55.79. LCMS (Fleet, 10 → 90%): t_r = 3.39 min, m/z: 322.3. HRMS [$C_{17}H_{15}N_5O_2$ + H]$^+$: 322.12985 calculated, 322.12974 found.

_N_-(1_H_-Benzo[d]imidazol-5-yl)-6,7-dimethoxyquinazolin-4-amine (44)

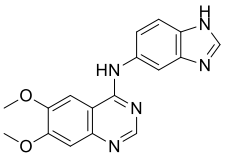

The title compound was synthesized from 1*H*-benzo[*d*]imidazol-5-amine according to general procedure D (reaction time: 16 h). The crude was purified by automated column chromatography (25 – 55% EtOAc/DCM) to afford the product (34.6 mg, 108 µmol, 48%). ^{1}H NMR (500 MHz, DMSO) δ 12.47 (br s, 1H), 9.55 (s, 1H), 8.44 (s, 1H), 8.22 (s, 1H), 8.14 (br s, 1H), 7.89 (s, 1H), 7.62 (br s, 1H), 7.50 (d, *J* = 8.6 Hz, 1H), 7.18 (s, 1H), 3.96 (s, 3H), 3.93 (s, 3H). ^{13}C NMR (126 MHz, DMSO) δ 156.77, 154.12, 153.11, 148.82, 146.85, 142.19 (br), 139.69 (br), 134.24 (br), 133.38 (br), 119.20 (br), 118.50 (br), 117.78 (br), 113.82 (br), 111.10 (br), 108.91, 107.21, 105.79 (br), 102.04, 56.23, 55.79. LCMS (Fleet, 0 → 50%): t_r = 4.68 min, m/z: 322.3. HRMS $[C_{17}H_{15}N_5O_2 + H]^+$: 322.12985 calculated, 322.12980 found.

_N_-(2-Chloropyrimidin-4-yl)-6,7-dimethoxyquinazolin-4-amine (45)

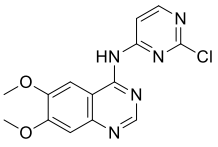

A microwave tube was charged with 4-chloro-6,7-dimethoxyquinazoline (100 mg, 0.445 mmol), Cs_2CO_3 (435 mg, 1.34 mmol), xantphos (38.6 mg, 66.7 µmol), 2-chloropyrimidin-4-amine (69.2 mg, 0.534 mmol) and DMF (2 mL). N_2 was bubbled through the mixture for 30 sec after which $Pd(OAc)_2$ (10 mg, 45 µmol) was added. N_2 was bubbled through the mixture for 10 sec after which the vial was sealed and the mixture was stirred at 90°C for 16 h. The mixture was diluted in EtOAc (20 mL) and filtered over Celite. The filtrate was diluted in EtOAc (20 mL) and poured into H_2O (40 mL) and brine (1 mL). The organic layer was separated, washed with brine (40 mL) and isolated. The water layer was extracted with EtOAc (15 mL) and the combined organic layers were concentrated as such. The crude was purified by automated column chromatography (30 – 50% EtOAc/DCM) to afford the product (95.4 mg, 300 µmol, 67%). ^{1}H NMR (500 MHz, DMSO) δ 11.03 (s, 1H), 8.72 (s, 1H), 8.56 (d, *J* = 5.9 Hz, 1H), 8.51 (d, *J* = 5.9 Hz, 1H), 8.02 (s, 1H), 7.28 (s, 1H), 3.97 (s, 3H), 3.95 (s, 3H). ^{13}C NMR (126 MHz, DMSO) δ 160.82, 159.97, 159.00, 155.14, 154.93, 151.82, 149.58, 148.06, 110.02, 109.29, 106.97, 102.10, 56.33, 56.01. LCMS (Finnigan, 10 → 90%): t_r = 5.53 min, m/z: 318.1. HRMS $[C_{14}H_{12}ClN_5O_2 + H]^+$: 318.07523 calculated, 318.07521 found.

_N_-(2-(1_H_-Pyrazol-1-yl)pyrimidin-4-yl)-6,7-dimethoxyquinazolin-4-amine (46)

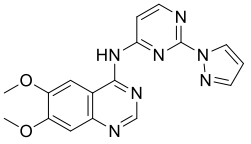

To an oven dried flask was added NaH (60% in mineral oil, 32.7 mg, 818 µmol) and dioxane (2 mL). 1*H*-pyrazole (68.5 mg, 1.01 mmol) was carefully added after which the mixture was stirred for 1 h. Of this mixture, 0.5 mL was added to a microwave tube charged with **45** (30 mg, 94 µmol). The vial was sealed, heated to 90°C and stirred for 72 h. The mixture was poured into H_2O (10 mL) and the product extracted with EtOAc (2x10 mL) and then with 10% MeOH/EtOAc (4x10 mL). The combined organic layers were concentrated as such. The crude was loaded onto Celite and purified by automated column chromatography (0 – 3% MeOH/EtOAc) to afford the product (23.1 mg, 66.1 µmol, 70%). ^{1}H NMR (400 MHz, DMSO) δ 10.86 (br s, 1H), 8.71 (s, 1H), 8.67 (dd, *J* = 2.6, 0.6 Hz, 1H), 8.64 (d, *J* = 5.8 Hz, 1H), 8.32 (d, *J* = 5.3 Hz, 1H), 8.01 (s, 1H), 7.85 (dd, *J* = 1.5, 0.6 Hz, 1H), 7.26 (s, 1H), 6.59 (dd, *J* = 2.6, 1.6 Hz, 1H), 3.98 (s, 3H), 3.95 (s, 3H). ^{13}C NMR (101 MHz, DMSO) δ 160.54 (br), 158.77, 155.28, 155.12, 155.08, 151.87 (br), 149.41, 148.01, 142.74, 129.40, 110.22, 108.49, 108.41, 106.95, 102.40, 56.29, 55.99. LCMS (Finnigan, 10 → 90%): t_r = 3.82 min, m/z: 350.3. HRMS $[C_{17}H_{15}N_7O_2 + H]^+$: 350.13600 calculated, 350.13593 found.

_N_-(2-(1_H_-Pyrrol-1-yl)pyrimidin-4-yl)-6,7-dimethoxyquinazolin-4-amine (47)

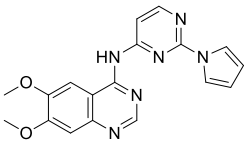

To an oven dried flask was added NaH (60% in mineral oil, 64.9 mg, 1.62 mmol) and dioxane (0.5 mL). 1*H*-pyrrole (250 µL, 3.60 mmol) was carefully added after which the mixture was stirred at 50°C for 1 h. Of this mixture, 0.5 mL was added to a microwave tube charged with **45** (74.8 mg, 235 µmol). The vial was sealed, heated to 100°C and stirred for 16 h. The mixture was poured into H_2O (20 mL) and the product extracted with EtOAc (3x20 mL). The combined organic layers were concentrated as such. The crude was loaded onto Celite and purified by silica gel column chromatography (10 – 100% EtOAc/DCM) to afford the product (31.3 mg, 89.8 µmol,

38%). ^{1}H NMR (500 MHz, DMSO) δ 10.54 (br s, 1H), 8.71 (s, 1H), 8.58 (d, *J* = 5.8 Hz, 1H), 8.22 (d, *J* = 5.9 Hz, 1H), 7.96 (s, 1H), 7.80 (t, *J* = 2.4 Hz, 2H), 7.27 (s, 1H), 6.34 – 6.30 (m, 2H), 3.99 (s, 3H), 3.95 (s, 3H). ^{13}C NMR (126 MHz, DMSO) δ 160.08, 158.80, 155.25, 155.10, 155.05, 151.98, 149.45, 148.02, 118.70, 111.55, 110.09, 107.27, 107.01, 102.28, 56.36, 56.00. LCMS (Fleet, 10 → 90%): t_r = 4.83 min, m/z: 349.3. HRMS $[C_{18}H_{16}N_6O_2 + H]^+$: 349.14075 calculated, 349.14069 found.

N-(2-(1*H*-Pyrazol-1-yl)pyrimidin-4-yl)-6,7-bis(2-methoxyethoxy)quinazolin-4-amine (48)

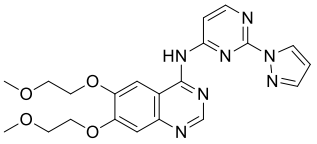

114 (100 mg, 246 µmol), 1*H*-pyrazole (17.6 mg, 259 µmol) and K_2CO_3 (68.1 mg, 493 µmol) were mixed dioxane (1 mL) after which the mixture was heated to 95°C and stirred for 140 h. The mixture poured into H_2O (20 mL) and the product extracted with EtOAc (3x20 mL). The combined organic layers were dried over Na_2SO_4, filtered and concentrated. The crude was loaded onto Celite and purified by automated column chromatography (2 – 10% MeOH/DCM). The residue was dissolved in DCM (0.5 mL), heated to 40°C for 10 min and subsequently cooled to 0°C. Heptane (0.5 mL) was added and the mixture was stirred for 20 min at 0°C. The solids were collected by filtration and washed with ice cold DCM (0.1 mL) to afford the product (20 mg, 46 µmol, 19%). ^{1}H NMR (400 MHz, DMSO) δ 10.83 (s, 1H), 8.72 (s, 1H), 8.68 (dd, *J* = 2.7, 0.8 Hz, 1H), 8.66 (d, *J* = 5.9 Hz, 1H), 8.36 (d, *J* = 5.8 Hz, 1H), 8.05 (s, 1H), 7.86 (dd, *J* = 1.6, 0.7 Hz, 1H), 7.31 (s, 1H), 6.60 (dd, *J* = 2.6, 1.6 Hz, 1H), 4.37 – 4.28 (m, 4H), 3.81 – 3.73 (m, 4H), 3.37 (s, 3H), 3.35 (s, 3H). ^{13}C NMR (101 MHz, DMSO) δ 160.44, 158.85, 155.34, 155.14, 154.38, 152.02, 148.66, 147.97, 142.77, 129.42, 110.13, 108.49, 108.45, 107.90, 103.33, 70.04, 70.02, 68.39, 68.24, 58.41, 58.38. LCMS (Fleet, 10 → 90%): t_r = 4.03 min, m/z: 438.3. HRMS $[C_{21}H_{23}N_7O_4 + H]^+$: 438.18843 calculated, 438.18818 found.

N-(3-(1*H*-Pyrazol-1-yl)phenyl)-6,7-bis(2-methoxyethoxy)quinazolin-4-amine (49)

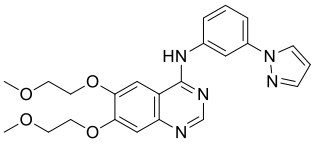

The title compound was synthesized from 4-chloro-6,7-bis(2-methoxyethoxy)quinazoline (45.2 mg, 144 µmol) and **116** (23.0 mg, 144 µmol) according to general procedure A (reaction time: 2 h). The crude was purified by automated column chromatography (2 – 10% MeOH/DCM) to afford the product (28 mg, 64 µmol, 45%). ^{1}H NMR (400 MHz, DMSO) δ 9.62 (s, 1H), 8.51 (s, 1H), 8.50 (dd, *J* = 2.6, 0.6 Hz, 1H), 8.34 (t, *J* = 2.1 Hz, 1H), 7.92 (s, 1H), 7.87 (ddd, *J* = 7.9, 2.2, 1.2 Hz, 1H), 7.77 (dd, *J* = 1.8, 0.5 Hz, 1H), 7.55 (ddd, *J* = 8.1, 2.1, 1.1 Hz, 1H), 7.49 (t, *J* = 8.0 Hz, 1H), 7.23 (s, 1H), 6.56 (dd, *J* = 2.5, 1.7 Hz, 1H), 4.33 – 4.26 (m, 4H), 3.81 – 3.77 (m, 2H), 3.77 – 3.73 (m, 2H), 3.37 (s, 3H), 3.35 (s, 3H). ^{13}C NMR (101 MHz, DMSO) δ 156.28, 153.67, 152.85, 148.16, 147.01, 140.92, 140.71, 139.93, 129.45, 127.79, 119.69, 112.95, 112.22, 109.00, 108.18, 107.90, 103.17, 70.15, 70.08, 68.40, 68.07, 58.43, 58.38. LCMS (Fleet, 10 → 90%): t_r = 4.34 min, m/z: 436.3. HRMS $[C_{23}H_{25}N_5O_4 + H]^+$: 436.19793 calculated, 436.19760 found.

2-((4-Chloro-7-(2-methoxyethoxy)quinazolin-6-yl)oxy)ethyl acetate (50)

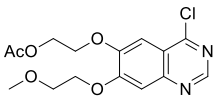

The title compound was synthesized as described in **Chapter 2** (compound 43)

2-((4-((3-Ethynylphenyl)amino)-7-(2-methoxyethoxy)quinazolin-6-yl)oxy)ethyl acetate (51)

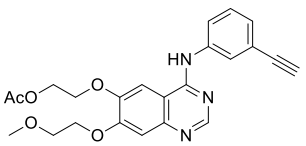

The title compound was synthesized as described in **Chapter 2** (compound 44)

2-((7-(2-Methoxyethoxy)-4-(phenylamino)quinazolin-6-yl)oxy)ethyl acetate (52)

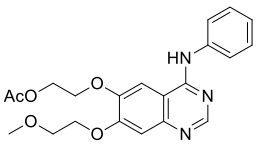

The title compound was synthesized from **50** (31.3 mg, 91.9 µmol) and aniline (9.3 µL, 102 µmol) according to general procedure A (reaction time: 1.25 h). The crude was purified by automated column chromatography (1 – 10% MeOH/DCM) to afford the product (36.1 mg, 90.8 µmol, 99%). ^{1}H NMR (400 MHz, MeOD) δ 8.32 (s, 1H), 7.70 (d, *J* = 7.6 Hz, 2H), 7.64 (s, 1H), 7.37 (t, *J* = 7.9 Hz, 2H), 7.15 (t, *J* = 7.4 Hz, 1H), 7.05 (s, 1H), 4.52 – 4.45 (m, 2H), 4.37 – 4.29 (m, 2H), 4.26 – 4.19 (m, 2H), 3.85 – 3.77 (m, 2H), 3.45 (s, 3H), 2.07 (s, 3H). ^{13}C NMR (101 MHz, MeOD) δ 172.67, 158.50, 155.84, 154.01, 149.92, 147.40, 140.20, 129.76, 125.47, 124.10, 110.41, 108.21, 104.43, 71.71, 69.68, 68.50, 63.80, 59.49, 20.77.

2-((7-(2-Methoxyethoxy)-4-(naphthalen-2-ylamino)quinazolin-6-yl)oxy)ethyl acetate (53)

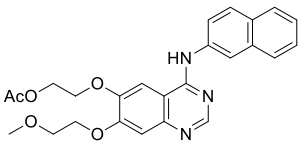

The title compound was synthesized from **50** (29.4 mg, 86.3 µmol) and naphthalen-2-amine (14.5 mg, 101 µmol) according to general procedure A (reaction time: 1.5 h). The crude was purified by automated column chromatography (1 – 10% MeOH/DCM) to afford the product (36.7 mg, 82.0 µmol, 95%). ^{1}H NMR (400 MHz, MeOD) δ 8.39 (s, 1H), 8.14 (s, 1H), 7.75 – 7.63 (m, 5H), 7.43 – 7.34 (m, 2H), 6.88 (s, 1H), 4.50 – 4.45 (m, 2H), 4.36 – 4.31 (m, 2H), 4.16 – 4.11 (m, 2H), 3.77 – 3.72 (m, 3H), 3.43 (s, 3H), 2.08 (s, 3H). LCMS (Finnigan, 0 → 50%): t_r = 8.80 min, m/z: 448.2.

((4-(Ethoxycarbonyl)-1,2-phenylene)bis(oxy))bis(ethane-2,1-diyl) diacetate (54)

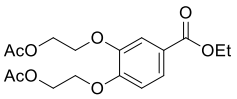

Ethyl 3,4-dihydroxybenzoate (7.00 g, 38.4 mmol) and K_2CO_3 (21.24 g, 10.98 mmol) were mixed in dry DMF (35 mL). 2-bromoethyl acetate (12.8 mL, 8.23 mmol) was added and the mixture was stirred at 100°C for 2 h. The mixture was poured into H_2O (150 mL) and the product extracted with EtOAc (3x150 mL). The combined organic layers were washed with brine (100 mL), dried with over Na_2SO_4, filtered and concentrated. The crude was purified by silica gel column chromatography (25 – 40% Et_2O/pentane) to afford the product (8.40 g, 23.7 mmol, 62%). ^{1}H NMR (400 MHz, $CDCl_3$) δ 7.63 (dd, *J* = 8.4, 2.0 Hz, 1H), 7.54 (d, *J* = 2.0 Hz, 1H), 6.86 (d, *J* = 8.5 Hz, 1H), 4.43 – 4.35 (m, 4H), 4.28 (q, *J* = 7.1 Hz, 2H), 4.24 – 4.18 (m, 4H), 2.04 (s, 3H), 2.03 (s, 3H), 1.32 (t, *J* = 7.1 Hz, 3H). ^{13}C NMR (101 MHz, $CDCl_3$) δ 170.89, 170.86, 166.04, 152.60, 148.02, 124.32, 123.85, 115.83, 113.21, 67.55, 67.07, 62.80, 62.56, 60.86, 20.81, 20.79, 14.34. LCMS (Finnigan, 10 → 50%): t_r = 10.09 min, m/z: 355.0.

Ethyl 3,4-dimethoxybenzoate (55)

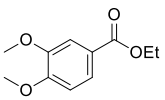

Ethyl 3,4-dihydroxybenzoate (2.00 g, 11.0 mmol) and K_2CO_3 (6.00 g, 43.9 mmol) were mixed in DMF (10.9 mL). Iodomethane (4.8 mL, 77 mmol) was added and the mixture stirred at 100°C for 1.25 h. The mixture was poured into H_2O (50 mL) and the product extracted with DCM (3x100 mL). The combined organic layers were washed with brine (100 mL), dried over Na_2SO_4, filtered and concentrated. The crude was purified by silica gel column chromatography (5 – 20% MeOH/DCM) to afford the product (2.24 g, 10.7 mmol, 97%). ^{1}H NMR (400 MHz, $CDCl_3$) δ 7.46 (dd, *J* = 8.4, 2.0 Hz, 1H), 7.34 (d, *J* = 2.0 Hz, 1H), 6.66 (d, *J* = 8.5 Hz, 1H), 4.15 (q, *J* = 7.1 Hz, 2H), 3.72 (s, 3H), 3.70 (s, 3H), 1.18 (t, *J* = 7.2 Hz, 3H). ^{13}C NMR (101 MHz, $CDCl_3$) δ 165.83, 152.47, 148.16, 123.05, 122.56, 111.46, 109.80, 60.31, 55.47, 55.46, 13.99. LCMS (Finnigan, 10 → 90%): t_r = 6.46 min, m/z: 211.0.

((4-(Ethoxycarbonyl)-5-nitro-1,2-phenylene)bis(oxy))bis(ethane-2,1-diyl) diacetate (56)

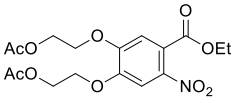

54 (8.40 g, 23.7 mmol) was dissolved in acetic anhydride (65 mL) and cooled down to 0°C. Copper(II) nitrate trihydrate (14.5 g, 60.0 mmol) was added and the mixture was stirred at 0°C for 1 h. The mixture was then allowed to warm to RT after which a mild exothermic reaction (NO_2 escapes) was observed. After TLC analysis showed completion of the reaction, the mixture was diluted with water (30 mL) and the product extracted with DCM (3x150 mL). The combined organic layers were washed with 1 M $NaHCO_3$ (400 mL, until pH 7) and brine (100 mL), and subsequently dried over Na_2SO_4, filtered and

concentrated. The crude was purified by silica gel column chromatography (40 – 60% Et_2O/pentane) to afford the product (5.80 g, 14.5 mmol, 62%). ^1H NMR (400 MHz, $CDCl_3$) δ 7.47 (s, 1H), 7.10 (s, 1H), 4.47 – 4.41 (m, 4H), 4.37 – 4.25 (m, 6H), 2.07 (s, 3H), 2.07 (s, 3H), 1.31 (t, *J* = 7.1 Hz, 3H). ^{13}C NMR (101 MHz, $CDCl_3$) δ 170.82, 165.52, 151.97, 149.74, 141.56, 122.46, 113.32, 109.61, 67.82, 67.69, 62.54, 62.33, 62.30, 20.84, 13.82. Regioselectivity was confirmed by ^1H-^1H-NOESY NMR analysis. LCMS (Finnigan, 10 → 90%): t_r = 7.09 min, m/z: not observed.

Ethyl 4,5-dimethoxy-2-nitrobenzoate (57)

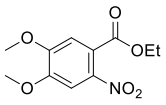

55 (1.00 g, 4.76 mmol) was dissolved in acetic anhydride (12.5 mL) and cooled down to 0°C. Copper(II) nitrate trihydrate (2.91 g, 12.0 mmol) was added and the mixture was stirred at 0°C for 2 h after which TLC analysis showed completion of the reaction. The mixture was poured into 1 M $NaHCO_3$ (aq.) (20 mL) and the product extracted with DCM (3x25mL). The combined organic layers were washed with brine (50 mL), dried over Na_2SO_4, filtered and concentrated at 80°C. The residue was coevaporated with toluene several times to remove the remaining acetic anhydride. The crude was purified by silica gel column chromatography (10 – 30% EtOAc/pentane) to afford the product (862 mg, 3.38 mmol, 71%). ^1H NMR (400 MHz, $CDCl_3$) δ 7.30 (s, 1H), 6.93 (s, 1H), 4.21 (q, *J* = 7.2 Hz, 2H), 3.83 (s, 3H), 3.83 (s, 3H), 1.20 (t, *J* = 7.2 Hz, 3H). ^{13}C NMR (101 MHz, $CDCl_3$) δ 165.43, 152.20, 150.04, 140.86, 121.56, 110.45, 106.64, 62.08, 56.33, 56.27, 13.48. Regioselectivity was confirmed by ^1H-^1H-NOESY NMR analysis after subsequent step (compound **59**). LCMS (Finnigan, 10 → 90%): t_r = 6.83 min, m/z: no mass observed.

((4-Amino-5-(ethoxycarbonyl)-1,2-phenylene)bis(oxy))bis(ethane-2,1-diyl) diacetate (58)

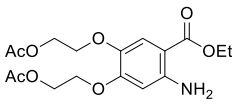

56 (5.80 g, 14.5 mmol) was dissolved in degassed MeOH (45 mL). 5% Pt/C (0.58 g) was added and the atmosphere was exchanged for H_2. The mixture was vigorously stirred for 2.75 h while bubbling H_2 through the mixture. The atmosphere was exchanged for N_2, the mixture was filtered over Celite and concentrated to afford the product (5.10 g, 13.8 mmol, 95%). ^1H NMR (400 MHz, MeOD) δ 7.37 (s, 1H), 6.30 (s, 1H), 4.84 (br s, 2H), 4.42 – 4.37 (m, 2H), 4.33 – 4.29 (m, 2H), 4.25 (q, *J* = 7.1 Hz, 2H), 4.17 – 4.13 (m, 2H), 4.09 – 4.04 (m, 2H), 2.05 (app. s, 6H), 1.33 (t, *J* = 7.1 Hz, 3H). ^{13}C NMR (101 MHz, MeOD) δ 172.67, 172.57, 168.84, 156.66, 150.42, 139.85, 120.45, 103.44, 101.57, 70.54, 67.63, 64.49, 63.73, 61.05, 20.80, 20.75, 14.76. LCMS (Finnigan, 10 → 90%): t_r = 6.25 min, m/z: 370.0.

Ethyl 2-amino-4,5-dimethoxybenzoate (59)

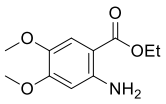

57 (1.84 g, 7.21 mmol) was dissolved in degassed MeOH (20 mL). 5% Pt/C (288 mg) was added and the atmosphere was exchanged for H_2. The mixture was vigorously stirred for 45 min while bubbling H_2 through the mixture. The atmosphere was exchanged for N_2, after which the mixture was filtered over Celite and concentrated. The crude was purified by automated column chromatography (40 – 60% Et_2O/pentane) to afford the product (1.11 g, 4.94 mmol, 69%). ^1H NMR (400 MHz, $CDCl_3$) δ 7.26 (s, 1H), 6.09 (s, 1H), 5.58 (s, 2H), 4.26 (q, *J* = 7.1 Hz, 2H), 3.78 (s, 3H), 3.78 (s, 3H), 1.33 (t, *J* = 7.2 Hz, 3H). ^{13}C NMR (101 MHz, $CDCl_3$) δ 167.75, 154.69, 147.15, 140.40, 112.68, 102.18, 99.29, 60.03, 56.38, 55.66, 14.45. LCMS (Finnigan, 10 → 90%): t_r = 5.04 min, m/z: 225.9.

((4-Oxo-3,4-dihydroquinazoline-6,7-diyl)bis(oxy))bis(ethane-2,1-diyl) diacetate (60)

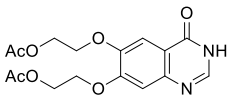

58 (5.09 g, 13.8 mmol) was dissolved in formamide (7.3 mL) and ammonium formate (0.902 g, 14.3 mmol) was added. The mixture was stirred at 160°C for 5.5 h and subsequently poured into H_2O (100 mL). The product was extracted with DCM (3x150 mL) and the combined organic layers were washed with brine (100 mL), dried over Na_2SO_4, filtered and concentrated. The crude was purified by silica gel column chromatography (1 – 3% MeOH/DCM) to afford the product (1.30 g, 3.71 mmol, 27%), which was slightly contaminated with side-product in which one of the acetyl groups had been substituted by a formyl group. ^1H NMR (400 MHz, MeOD) δ 7.95 (s, 1H), 7.60 (s, 1H), 7.12 (s, 1H), 4.52 – 4.45 (m, 4H), 4.37 – 4.29 (m, 4H), 2.08 (app. s, 6H). ^{13}C NMR (101 MHz, MeOD) δ 172.22, 172.17, 162.07, 155.44, 149.27, 145.68,

144.36, 116.86, 109.61, 108.48, 67.97, 67.74, 63.34, 63.12, 20.95, 20.93. LCMS (Finnigan, 10 → 90%): t_r = 4.22 min, m/z: 351.1.

6,7-Dimethoxyquinazolin-4(3*H*)-one (61)

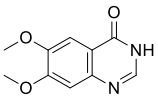

59 (1.01 g, 4.51 mmol) and ammonium formate (284 mg, 4.51 mmol) were mixed in formamide (2.4 mL) after which the mixture was heated to 160°C, stirred for 5.5 h and continued to stir at 120°C for 16 h. The mixture was poured into H_2O (50 mL) which was extracted DCM (4x50 mL). The water layer was concentrated and the residue suspended in MeOH (10 mL). The suspension was heated to about 60°C and immediately filtered as such to afford the product (360 mg, 1.75 mmol, 39%). ^{1}H NMR (400 MHz, DMSO) δ 12.03 (br s, 1H), 7.99 (s, 1H), 7.44 (s, 1H), 7.13 (s, 1H), 3.90 (s, 3H), 3.86 (s, 3H). ^{13}C NMR (101 MHz, DMSO) δ 160.12, 154.48, 148.57, 144.91, 143.91, 115.62, 108.04, 104.91, 55.97, 55.72. LCMS (Finnigan, 0 → 50%): t_r = 5.33 min, m/z: 207.2.

((4-Chloroquinazoline-6,7-diyl)bis(oxy))bis(ethane-2,1-diyl) diacetate (62)

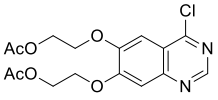

60 (500 mg, 1.43 mmol) was mixed in $POCl_3$ (2.8 ml, 30 mmol). The mixture was stirred at 105°C for 2 h and subsequently concentrated. The residue was dissolved in DCM (100 mL) and poured into H_2O (100 mL). The organic layer was separated and the water layer washed with DCM (3x100 mL). The combined organic layers were washed with brine (100 mL), dried over Na_2SO_4, filtered and concentrated. The crude was purified by silica gel column chromatography (0 – 3 % MeOH/DCM) to afford the product (440 mg, 1.19 mmol, 84%). ^{1}H NMR (400 MHz, $CDCl_3$) δ 8.84 (s, 1H), 7.40 (s, 1H), 7.30 (s, 1H), 4.56 – 4.51 (m, 4H), 4.39 – 4.35 (m, 4H), 2.11 (s, 3H), 2.10 (s, 3H). ^{13}C NMR (101 MHz, $CDCl_3$) δ 170.97, 170.90, 159.28, 155.96, 152.75, 150.58, 149.02, 119.62, 108.40, 104.64, 67.37, 67.22, 62.35, 62.07, 20.96, 20.93. LCMS (Finnigan, 10 → 90%): t_r = 5.98 min, m/z: 369.0.

4-Chloro-6,7-dimethoxyquinazoline (63)

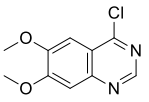

61 (285 mg, 1.38 mmol) was mixed in $POCl_3$ (2.7 mL) and the mixture was stirred at 105°C for 1.5 h. Subsequently, the mixture was concentrated, diluted in DCM (100 mL) and carefully poured into H_2O (100 mL). The organic layer was separated and the water layer extracted with DCM (3x100 mL). The combined organic layers were washed with brine (200 mL), dried over Na_2SO_4, filtered and concentrated. The crude was purified by silica gel column chromatography (1 – 3% MeOH/DCM) to afford the product (42.5 mg, 189 µmol, 14%). ^{1}H NMR (300 MHz, DMSO) δ 8.84 (s, 1H), 7.35 (s, 1H), 7.30 (s, 1H), 4.05 (app. s, 6H). ^{13}C NMR (75 MHz, $CDCl_3$) δ 159.12, 156.82, 152.59, 151.50, 149.14, 119.62, 106.98, 102.72, 56.73, 56.54. LCMS (Finnigan, 10 → 90%): t_r = 5.46 min, m/z: 225.2.

((4-((3-Ethynylphenyl)amino)quinazoline-6,7-diyl)bis(oxy))bis(ethane-2,1-diyl) diacetate (64)

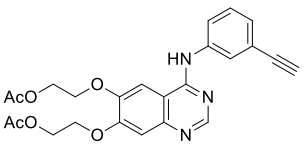

The title compound was synthesized from **62** (39.6 mg, 107 µmol) and 3-ethynylaniline (13.4 µL, 119 µmol) according to general procedure A (reaction time: 1.5 h). The crude was purified by silica gel column chromatography (8% MeOH/DCM) to afford the product (39 mg, 87 µmol, 81%). ^{1}H NMR (400 MHz, $CDCl_3$) δ 8.68 (s, 1H), 7.98 (t, *J* = 1.9 Hz, 1H), 7.87 (ddd, *J* = 8.2, 2.3, 1.1 Hz, 1H), 7.73 (s, 1H), 7.55 (s, 1H), 7.35 (t, *J* = 7.9 Hz, 1H), 7.26 (dt, *J* = 7.7, 1.3 Hz, 1H), 7.23 (s, 1H), 4.54 – 4.48 (m, 4H), 4.37 – 4.29 (m, 4H), 3.09 (s, 1H), 2.16 (s, 3H), 2.11 (s, 3H). ^{13}C NMR (101 MHz, $CDCl_3$) δ 171.88, 171.01, 156.41, 154.06, 153.99, 148.16, 147.66, 139.13, 129.14, 127.68, 124.73, 121.86, 109.51, 109.36, 102.88, 83.57, 77.48, 66.95, 66.66, 62.33, 61.41, 21.14, 21.02. LCMS (Finnigan, 10 → 90%): t_r = 5.62 min, m/z: 450.1.

((4-((3-Chlorophenyl)amino)quinazoline-6,7-diyl)bis(oxy))bis(ethane-2,1-diyl) diacetate (65)

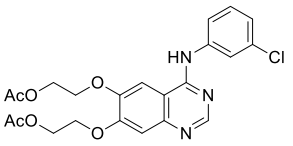

The title compound was synthesized from **62** (40.0 mg, 108 µmol) and 3-chloroaniline (12.7 µL, 120 µmol) according to general procedure A (reaction time: 1 h). The crude was purified by silica gel column chromatography (1 – 10% MeOH/DCM) to afford the product (39 mg, 85 µmol, 78%). ^{1}H NMR (400 MHz, $CDCl_3$) δ 8.69 (s, 1H), 8.02 (t, *J* = 2.0 Hz, 1H), 7.77 (br s, 1H), 7.75 (ddd, *J* = 8.3, 2.2, 1.0 Hz, 1H), 7.61 (s, 1H), 7.32 (t, *J* = 8.1 Hz, 1H), 7.25 (s, 1H), 7.11 (ddd, *J* = 8.0, 2.1, 0.9 Hz, 1H), 4.55 – 4.51 (m, 4H), 4.42 – 4.31 (m, 4H), 2.19 (s, 3H), 2.12 (s, 3H). ^{13}C NMR (126 MHz, $CDCl_3$) δ 171.85, 171.00, 156.41, 154.06, 153.71, 148.23, 147.22, 140.28, 134.56, 129.99, 123.89, 121.38, 119.31, 109.49, 108.91, 103.02, 66.92, 66.67, 62.26, 61.46, 21.09, 20.96. LCMS (Finnigan, 10 → 90%): t_r = 5.68 min, m/z: 460.1.

((4-((3-Ethylphenyl)amino)quinazoline-6,7-diyl)bis(oxy))bis(ethane-2,1-diyl) diacetate (66)

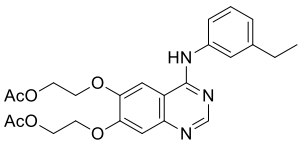

The title compound was synthesized from 62 (30.0 mg, 81.3 µmol) and 3-ethylaniline (11.1 µL, 89.5 µmol) according to general procedure A (reaction time 1.5 h). The crude was purified by silica gel column chromatography (0 – 2% MeOH/DCM) to afford the product (28 mg, 62 µmol, 76%). ^{1}H NMR (400 MHz, $CDCl_3$) δ 8.66 (s, 1H), 7.78 (s, 1H), 7.63 (dd, *J* = 8.0, 1.3 Hz, 1H), 7.54 (t, *J* = 1.8 Hz, 1H), 7.49 (s, 1H), 7.29 (t, *J* = 7.8 Hz, 1H), 7.21 (s, 1H), 6.98 (d, *J* = 7.6 Hz, 1H), 4.52 – 4.44 (m, 4H), 4.32 – 4.24 (m, 4H), 2.66 (q, *J* = 7.6 Hz, 2H), 2.12 (s, 3H), 2.09 (s, 3H), 1.24 (t, *J* = 7.6 Hz, 3H). ^{13}C NMR (101 MHz, $CDCl_3$) δ 171.58, 170.99, 156.75, 154.27, 153.90, 148.06, 147.58, 145.32, 138.78, 129.03, 123.98, 121.24, 119.23, 109.54, 109.28, 103.29, 66.93, 66.87, 62.32, 61.74, 28.98, 21.05, 20.97, 15.56. LCMS (Finnigan, 10 → 90%): t_r = 5.91 min, m/z: 454.1.

((4-((3-Isopropylphenyl)amino)quinazoline-6,7-diyl)bis(oxy))bis(ethane-2,1-diyl) diacetate (67)

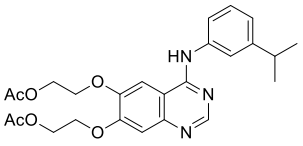

The title compound was synthesized from **62** (30.0 mg, 81.3 µmol) and 3-ethylaniline (12.1 mg, 89.5 µmol) according to general procedure A (reaction time: 1.5 h). The crude was purified by silica gel column chromatography (0 – 2% MeOH/DCM) to afford the product (28.8 mg, 61.6 µmol, 76%). ^{1}H NMR (400 MHz, $CDCl_3$) δ 8.66 (s, 1H), 7.72 (ddd, *J* = 8.1, 2.3, 1.0 Hz, 1H), 7.67 (s, 1H), 7.53 (t, *J* = 1.7 Hz, 1H), 7.50 (s, 1H), 7.32 (t, *J* = 7.8 Hz, 1H), 7.22 (s, 1H), 7.02 (dt, *J* = 7.6, 1.4 Hz, 1H), 4.55 – 4.45 (m, 4H), 4.35 – 4.28 (m, 4H), 2.93 (hept, *J* = 6.9 Hz, 1H), 2.14 (s, 3H), 2.10 (s, 3H), 1.27 (d, *J* = 6.9 Hz, 6H). ^{13}C NMR (101 MHz, $CDCl_3$) δ 171.65, 171.01, 156.69, 154.32, 153.90, 150.00, 148.05, 147.63, 138.79, 129.06, 122.56, 119.72, 119.32, 109.54, 109.38, 103.21, 66.90, 66.88, 62.35, 61.66, 34.24, 24.09, 21.09, 21.00. LCMS (Finnigan, 10 → 90%): t_r = 6.23 min, m/z: 468.1.

((4-([1,1'-Biphenyl]-3-ylamino)quinazoline-6,7-diyl)bis(oxy))bis(ethane-2,1-diyl) diacetate (68)

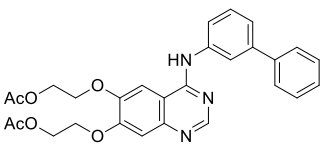

The title compound was synthesized from **62** (30.0 mg, 81.3 µmol) and [1,1'-biphenyl]-3-amine (15.1 mg, 89.2 µmol) according to general procedure A (reaction time: 1.5 h). The crude was purified by silica gel column chromatography (0 – 5% MeOH/DCM) to afford the product (39 mg, 78 µmol, 96%). ^{1}H NMR (400 MHz, $CDCl_3$) δ 8.68 (s, 1H), 8.01 – 7.91 (m, 2H), 7.87 (d, *J* = 7.1 Hz, 1H), 7.62 – 7.56 (m, 3H), 7.48 – 7.39 (m, 3H), 7.38 – 7.31 (m, 2H), 7.21 (s, 1H), 4.52 – 4.44 (m, 4H), 4.33 – 4.24 (m, 4H), 2.12 (s, 3H), 2.09 (s, 3H). ^{13}C NMR (101 MHz, $CDCl_3$) δ 171.71, 170.99, 156.71, 154.16, 153.92, 148.10, 147.51, 142.11, 140.90, 139.36, 129.50, 128.85, 127.57, 127.22, 122.94, 120.52, 120.40, 109.57, 109.21, 103.11, 66.89, 66.73, 62.30, 61.55, 21.07, 20.97. LCMS (Finnigan, 10 → 90%): t_r = 6.38 min, m/z: 502.1.

((4-((3-Methoxyphenyl)amino)quinazoline-6,7-diyl)bis(oxy))bis(ethane-2,1-diyl) diacetate (69)

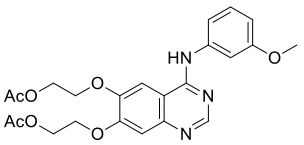

The title compound was synthesized from **62** (40.0 mg, 108 µmol) and 3-methoxyaniline (13.4 mg, 108 µmol) according to general procedure A (reaction time: 3 h). The crude was purified by silica gel column chromatography (0 – 2% MeOH/DCM) to afford the product (49.0 mg, 108 µmol, 99%). ^{1}H NMR (400 MHz, $CDCl_3$) δ 8.67 (s, 1H), 7.99 (br s, 1H), 7.55 (s, 1H), 7.54 (t, *J* = 2.1 Hz, 1H), 7.36 – 7.32 (m, 1H), 7.31 – 7.25 (m, 1H), 7.22 (s, 1H), 6.69 (ddd, *J* = 8.0, 2.5, 1.1 Hz, 1H), 4.54 – 4.44 (m, 4H), 4.33 – 4.26 (m, 4H), 3.83 (s, 3H), 2.14 (s, 3H), 2.11 (s, 3H). ^{13}C NMR (101 MHz, $CDCl_3$) δ 171.61, 170.98, 160.21, 156.67, 153.95, 153.94, 148.12, 147.26, 140.08, 129.77, 113.94, 109.62, 109.54, 109.01, 107.72, 103.21, 66.88, 66.83, 62.29, 61.65, 55.40, 21.06, 20.97. LCMS (Finnigan, 10 → 90%): t_r = 5.36 min, m/z: 456.1.

((4-((3-Phenoxyphenyl)amino)quinazoline-6,7-diyl)bis(oxy))bis(ethane-2,1-diyl) diacetate (70)

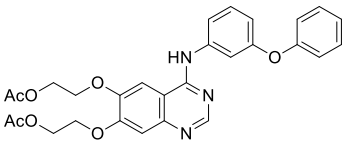

The title compound was synthesized from **62** (25 mg, 68 µmol) and 3-phenoxyaniline (12.6 mg, 68.0 µmol) according to general procedure A (reaction time 1.5 h). The crude was purified by silica gel column chromatography (2% MeOH/DCM) to afford the product (32 mg, 62 µmol, 91%). ^{1}H NMR (400 MHz, $CDCl_3$) δ 8.64 (s, 1H), 7.95 (s, 1H), 7.62 (dd, *J* = 8.1, 1.7 Hz, 1H), 7.54 (s, 1H), 7.52 (t, *J* = 1.7 Hz, 1H), 7.36 – 7.29 (m, 3H), 7.20 (s, 1H), 7.11 – 7.06 (m, 1H), 7.06 – 7.02 (m, 2H), 6.76 (dd, *J* = 8.1, 2.3 Hz, 1H), 4.49 (t, 2H), 4.44 (t, *J* = 5.7 Hz, 2H), 4.31 – 4.23 (m, 4H), 2.08 (s, 3H), 2.06 (s, 3H). ^{13}C NMR (101 MHz, $CDCl_3$) δ 171.71, 170.98, 157.89, 157.08, 156.48, 154.00, 153.91, 148.10, 147.51, 140.44, 130.07, 129.83, 123.48, 119.19, 116.11, 114.16, 111.86, 109.57, 109.16, 103.04, 66.88, 66.73, 62.29, 61.52, 21.01, 20.96. LCMS (Finnigan, 10 → 90%): t_r = 6.44 min, m/z: 518.1.

((4-((4-Methoxyphenyl)amino)quinazoline-6,7-diyl)bis(oxy))bis(ethane-2,1-diyl) diacetate (71)

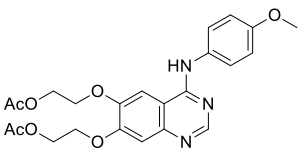

The title compound was synthesized from **62** (40.0 mg, 108 µmol) and 4-methoxyaniline (13.4 mg, 108 µmol) according to general procedure A (reaction time: 3 h). The crude was purified by silica gel column chromatography (3% MeOH/DCM) to afford the product (42.7 mg, 93.7 µmol, 86%). ^{1}H NMR (400 MHz, MeOD) δ 8.35 (s, 1H), 7.72 (s, 1H), 7.51 – 7.46 (m, 2H), 7.12 (s, 1H), 6.95 – 6.91 (m, 2H), 4.53 – 4.48 (m, 4H), 4.38 – 4.33 (m, 4H), 3.81 (s, 3H), 2.10 (app. s, 6H). ^{13}C NMR (101 MHz, MeOD) δ 172.27, 172.12, 158.44, 157.71, 154.80, 153.67, 149.07, 146.40, 131.85, 125.83, 114.68, 110.07, 108.08, 104.64, 67.89, 67.45, 63.25, 63.05, 55.77, 20.98, 20.96. LCMS (Finnigan, 10 → 90%): t_r = 5.27 min, m/z: 456.1.

((4-((4-Phenoxyphenyl)amino)quinazoline-6,7-diyl)bis(oxy))bis(ethane-2,1-diyl) diacetate (72)

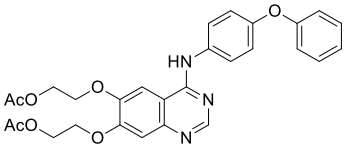

The title compound was synthesized from **62** (30.0 mg, 81.4 µmol) and 4-phenoxyaniline (15.1 mg, 81.5 µmol) according to general procedure A (reaction time: 2 h). The crude was purified by silica gel column chromatography (0 – 2% MeOH/DCM) to afford the product (34.3 mg, 66.3 µmol, 81%). ^{1}H NMR (400 MHz, $CDCl_3$) δ 8.63 (s, 1H), 7.98 (br s, 1H), 7.73 – 7.68 (m, 2H), 7.55 (s, 1H), 7.35 – 7.29 (m, 2H), 7.21 (s, 1H), 7.11 – 7.06 (m, 1H), 7.05 – 6.99 (m, 4H), 4.52 – 4.47 (m, 2H), 4.46 (t, *J* = 5.7 Hz, 2H), 4.32 – 4.25 (m, 4H), 2.12 (s, 3H), 2.09 (s, 3H). ^{13}C NMR (101 MHz, $CDCl_3$) δ 171.65, 170.99, 157.50, 156.78, 154.01, 153.96, 153.68, 148.11, 147.19, 134.14, 129.84, 123.58, 123.27, 119.57, 118.72, 109.37, 109.00, 103.25, 66.89, 66.85, 62.28, 61.63, 21.08, 20.97. LCMS (Finnigan, 10 → 90%): t_r = 6.33 min, m/z: 518.1.

((4-((4-(Benzyloxy)phenyl)amino)quinazoline-6,7-diyl)bis(oxy))bis(ethane-2,1-diyl) diacetate (73)

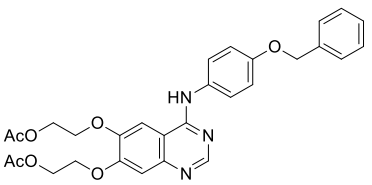

The title compound was synthesized from **62** (31.5 mg, 85.4 µmol) and 4-(benzyloxy)aniline hydrochloride (20.2 mg, 85.7 µmol) according to general procedure A (reaction time: 2 h). The crude was purified by silica gel column chromatography (0 – 3% MeOH/DCM) to afford the product (35 mg, 66 µmol, 77%). ^{1}H NMR (400 MHz, $CDCl_3$) δ 8.60 (s, 1H), 7.93 (br s, 1H), 7.60 – 7.55 (m, 2H), 7.48 (s, 1H), 7.45 – 7.40 (m, 2H), 7.40 – 7.35 (m, 2H), 7.34 – 7.29 (m, 1H), 7.18 (s, 1H), 6.97 (d, *J* = 9.0 Hz, 2H), 5.04 (s, 2H), 4.50 – 4.45 (m, 2H), 4.42 (t, *J* = 5.5 Hz, 2H), 4.28 – 4.24 (m, 2H), 4.22 (t, *J* = 5.5 Hz, 2H), 2.09 (s, 3H), 2.08 (s, 3H). ^{13}C NMR (101 MHz, $CDCl_3$) δ 171.47, 170.96, 157.09, 155.94, 154.17, 153.75, 148.02, 147.18, 137.03, 131.80, 128.67, 128.07, 127.54, 124.19, 115.34, 109.33, 109.03, 103.50, 70.37, 67.02, 66.85, 62.28, 61.85, 21.02, 20.94. LCMS (Finnigan, 10 → 90%): t_r = 6.37 min, m/z: 532.1.

((4-((3-Bromophenyl)amino)quinazoline-6,7-diyl)bis(oxy))bis(ethane-2,1-diyl) diacetate (74)

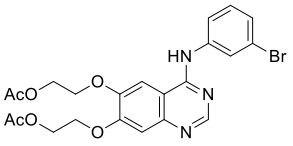

The title compound was synthesized from **62** (300 mg, 814 µmol) and 3-bromoaniline (96.8 µL, 891 µmol) according to general procedure A (reaction time: 1.5 h). The crude was purified by silica gel column chromatography (0 – 2% MeOH/DCM) to afford the product (289 mg, 573 µmol, 71%). ^{1}H NMR (400 MHz, MeOD) δ 8.43 (s, 1H), 8.01 – 7.98 (m, 1H), 7.72 – 7.62 (m, 2H), 7.27 – 7.21 (m, 2H), 7.11 (s, 1H), 4.54 – 4.46 (m, 4H), 4.40 – 4.30 (m, 4H), 2.10 (s, 3H), 2.09 (s, 3H). ^{13}C NMR (101 MHz, MeOD) δ 172.39, 172.27, 157.83, 155.14, 153.68, 149.50, 147.29, 141.28, 130.78, 127.63, 125.93, 122.85, 121.63, 110.46, 108.37, 104.37, 68.11, 67.67, 63.41, 63.22, 20.95, 20.92. LCMS (Finnigan, 10 → 90%): t_r = 5.82 min, m/z: 504.0.

((4-((2'-Methyl-[1,1'-biphenyl]-3-yl)amino)quinazoline-6,7-diyl)bis(oxy))bis(ethane-2,1-diyl) diacetate (75)

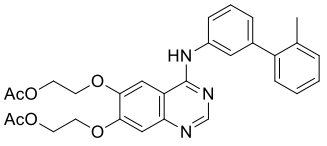

The title compound was synthesized from **74** (40 mg, 79 µmol) according to general procedure C using *o*-tolylboronic acid. The crude was purified by silica gel column chromatography (1 – 5% MeOH/DCM) to afford the product (26 mg, 50 µmol, 64%). ^{1}H NMR (400 MHz, $CDCl_3$) δ 8.67 (s, 1H), 7.89 – 7.85 (m, 2H), 7.74 (t, *J* = 1.8 Hz, 1H), 7.57 (s, 1H), 7.45 (t, *J* = 7.9 Hz, 1H), 7.29 – 7.24 (m, 5H), 7.12 (dt, *J* = 7.6, 1.1 Hz, 1H), 4.54 – 4.47 (m, 4H), 4.36 – 4.29 (m, 4H), 2.34 (s, 3H), 2.13 (s, 3H), 2.11 (s, 3H). ^{13}C NMR (101 MHz, $CDCl_3$) δ 171.72, 171.00, 156.62, 154.17, 153.95, 148.12, 147.52, 142.85, 141.63, 138.66, 135.50, 130.48, 129.83, 128.84, 127.50, 125.88, 125.08, 122.41, 119.95, 109.55, 109.27, 103.11, 66.92, 66.79, 62.33, 61.56, 21.07, 21.00, 20.66. LCMS (Finnigan, 10 → 90%): t_r = 6.74 min, m/z: 516.1.

((4-((3'-Methyl-[1,1'-biphenyl]-3-yl)amino)quinazoline-6,7-diyl)bis(oxy))bis(ethane-2,1-diyl) diacetate (76)

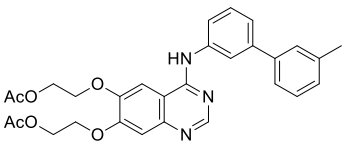

The title compound was synthesized from **74** (35 mg, 69 µmol) according to general procedure C using *m*-tolylboronic acid. The crude was purified by silica gel column chromatography (1 – 3% MeOH/DCM) to afford the product (24.6 mg, 47.7 µmol, 69%). ^{1}H NMR (400 MHz, $CDCl_3$) δ 8.68 (s, 1H), 7.94 (t, *J* = 2.0 Hz, 1H), 7.90 (ddd, *J* = 8.1, 2.3, 1.1 Hz, 1H), 7.87 (s, 1H), 7.58 (s, 1H), 7.46 (t, *J* = 7.9 Hz, 1H), 7.45 – 7.38 (m, 2H), 7.36 (ddd, *J* = 7.7, 1.8, 1.1 Hz, 1H), 7.32 (td, *J* = 7.3, 1.1 Hz, 1H), 7.24 (s, 1H), 7.21 – 7.13 (m, 1H), 4.54 – 4.46 (m, 4H), 4.37 – 4.28 (m, 4H), 2.42 (s, 3H), 2.15 (s, 3H), 2.11 (s, 3H). ^{13}C NMR (101 MHz, $CDCl_3$) δ 171.75, 171.01, 156.70, 154.16, 153.95, 148.12, 147.50, 142.31, 140.94, 139.31, 138.45, 129.49, 128.79, 128.35, 128.04, 124.39, 123.05, 120.45, 120.39, 109.56, 109.27, 103.10, 66.93, 66.75, 62.34, 61.54, 21.69, 21.11, 21.01. LCMS (Fleet, 10 → 90%): t_r = 5.96 min, m/z: 516.2.

2,2'-((4-((3-Bromophenyl)amino)quinazoline-6,7-diyl)bis(oxy))bis(ethan-1-ol) (77)

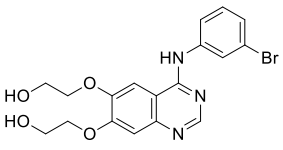

The title compound was synthesized from **74** (360 mg, 714 µmol) according to general procedure B (reaction time: 1 h). The crude was purified by silica gel column chromatography (4 – 8% MeOH/DCM) to afford the product (292 mg, 695 µmol, 97%). ^{1}H NMR (400 MHz, MeOD) δ 8.39 (s, 1H), 8.09 – 8.03 (m, 1H), 7.74 – 7.68 (m, 1H), 7.60 (s, 1H), 7.28 – 7.23 (m, 2H), 7.04 (s, 1H), 4.22 (t, 2H), 4.17 (t, 2H), 4.01 – 3.94 (m, 4H). ^{13}C NMR (101 MHz, MeOD) δ 158.08, 155.93, 153.73, 150.44, 147.49, 142.06, 131.15, 127.72, 126.13, 123.06, 121.95, 110.49, 107.92, 103.45, 71.94, 71.63, 61.45, 61.24. LCMS (Finnigan, 10 → 90%): t_r = 4.82 min, m/z: 420.1.

4-Nitro-1-(tetrahydro-2*H*-pyran-2-yl)-1*H*-pyrazole (78)

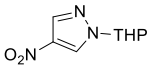

4-Nitro-1*H*-pyrazole (50.0 mg, 0.442 mmol) was dissolved in dry DCM (0.2 mL). 3,4-dihydro-2*H*-pyran (202 µL, 2.21 mmol) and 4-methylbenzenesulfonic acid monohydrate (4.2 mg, 0.022 mmol) were added and the mixture was stirred for 1 h. The mixture was poured into H_2O (20 mL) and the product extracted with DCM (3x20 mL). The combined organic layers were washed with brine (20 mL), dried over Na_2SO_4, filtered and concentrated. The crude was purified by silica gel column chromatography (10 – 30% EtOAc/pentane) and used as such in subsequent reaction (yield: 100 mg). ^{1}H NMR (400 MHz, $CDCl_3$) δ 8.33 (s, 1H), 8.04 (s, 1H), 5.36 (dd, *J* = 9.0, 2.8 Hz, 1H), 4.07 – 4.00 (m, 1H), 3.73 – 3.64 (m, 1H), 2.16 – 2.08 (m, 1H), 2.01 – 1.89 (m, 2H), 1.71 – 1.58 (m, 3H). ^{13}C NMR (101 MHz, $CDCl_3$) δ 135.42, 127.09, 88.38, 67.80, 30.61, 24.67, 21.59 (the quaternary carbon was not observed). LCMS (Finnigan, 10 → 90%): t_r = 5.67 min, m/z: no mass observed.

1-Methyl-4-nitro-1*H*-pyrazole (79)

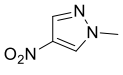

The title compound was synthesized from 4-nitro-1*H*-pyrazole (80.0 mg, 707 µmol) and iodomethane (52.9 µL, 849 µmol) according to general procedure E (1.4 M, at RT) to afford the product (88.0 mg, 692 µmol, 98%). ^{1}H NMR (400 MHz, $CDCl_3$) δ 8.12 (s, 1H), 7.99 (s, 1H), 3.93 (s, 3H). ^{13}C NMR (101 MHz, $CDCl_3$) δ 135.72, 129.28, 40.11 (the quaternary carbon was not observed).

1-Ethyl-4-nitro-1*H*-pyrazole (80)

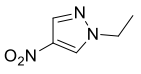

The title compound was synthesized from 4-nitro-1*H*-pyrazole (80.0 mg, 707 µmol) and iodoethane (67.9 µL, 849 µmol) according to general procedure E (1.4 M, at RT) to afford the product (98.0 mg, 694 µmol, 98%). ^{1}H NMR (400 MHz, $CDCl_3$) δ 8.14 (s, 1H), 7.98 (s, 1H), 4.17 (q, *J* = 7.3 Hz, 2H), 1.47 (t, *J* = 7.3 Hz, 3H). ^{13}C NMR (101 MHz, $CDCl_3$) δ 135.52, 127.82, 48.36, 14.87 (the quaternary carbon was not observed).

1-Benzyl-4-nitro-1*H*-pyrazole (81)

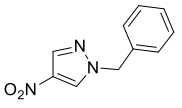

The title compound was synthesized from 4-nitro-1*H*-pyrazole (80.0 mg, 707 µmol) and benzyl bromide (101 µL, 849 µmol) according to general procedure E (1.4 M, at RT) to afford the product (144 mg, 707 µmol, quant.). ^{1}H NMR (400 MHz, $CDCl_3$) δ 8.08 (s, 1H), 8.05 (s, 1H), 7.41 – 7.33 (m, 3H), 7.30 – 7.25 (m, 2H), 5.29 (s, 2H). ^{13}C NMR (101 MHz, $CDCl_3$) δ 135.96 (br), 135.82, 134.05, 129.16, 128.95, 128.49, 128.24, 57.19.

4-Nitro-1-phenethyl-1*H*-pyrazole (82)

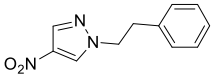

The title compound was synthesized from 4-nitro-1*H*-pyrazole (100 mg, 884 µmol) and (2-bromoethyl)benzene (145 µL, 1061 µmol) according to general procedure E (1.5 M, at 90°C) to afford the product (192 mg, 884 µmol, quant.). ^{1}H NMR (400 MHz, $CDCl_3$) δ 8.06 (s, 1H), 7.82 (s, 1H), 7.32 – 7.18 (m, 3H), 7.07 – 7.02 (m, 2H), 4.35 (t, *J* = 7.0 Hz, 2H), 3.17 (t, *J* = 7.0 Hz, 2H). ^{13}C NMR (101 MHz, $CDCl_3$) δ 136.77, 135.90, 135.33 (br), 128.86, 128.81, 128.56, 127.18, 54.83, 36.07.

4-Nitro-1-(3-phenylpropyl)-1*H*-pyrazole (83)

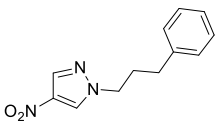

The title compound was synthesized from 4-nitro-1*H*-pyrazole (100 mg, 884 µmol) and (3-bromopropyl)benzene (122 µL, 804 µmol, 0.91 eq.) according to general procedure E (1.3 M, at 85°C, using 3 eq. of K_2CO_3) to afford the product (180 mg, 778 µmol, 97%). ^{1}H NMR (400 MHz, $CDCl_3$) δ 8.08 (d, *J* = 0.7 Hz, 1H), 8.07 (d, *J* = 0.7 Hz, 1H), 7.33 – 7.28 (m, 2H), 7.24 – 7.19 (m, 1H), 7.19 – 7.15 (m, 2H), 4.14 (t, *J* = 7.1 Hz, 2H), 2.65 (t, *J* = 7.5 Hz, 2H), 2.25 (p, *J* = 7.3 Hz, 2H). ^{13}C NMR (101 MHz, $CDCl_3$) δ 139.98, 135.77, 135.62 (br), 128.67, 128.54, 128.38, 126.43, 52.62, 32.37, 30.98.

1-(2-Chlorobenzyl)-4-nitro-1*H*-pyrazole (84)

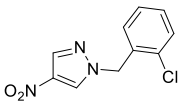

The title compound was synthesized from 4-nitro-1*H*-pyrazole (80.0 mg, 707 µmol) and 1-(bromomethyl)-2-chlorobenzene (83.0 µL, 641 µmol, 0.91 eq.) according to general procedure E (0.4 M, at RT, using 1.05 eq. of K_2CO_3) to afford the product (150 mg, 631 µmol, 97%). ^{1}H NMR (400 MHz, $CDCl_3$) δ 8.15 (s, 1H), 8.08 (s, 1H), 7.45 (dd, *J* = 7.8, 1.4 Hz, 1H), 7.39 – 7.25 (m, 3H), 5.44 (s, 2H). ^{13}C NMR (101 MHz, $CDCl_3$) δ 136.10, 136.06 (br), 133.97, 131.77, 130.93, 130.74, 130.19, 128.92, 127.72, 54.74.

1-(3-Fluorobenzyl)-4-nitro-1*H*-pyrazole (85)

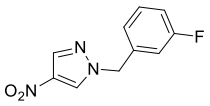

The title compound was synthesized from 4-nitro-1*H*-pyrazole (100 mg, 884 µmol) and 1-(bromomethyl)-3-fluorobenzene (108 µL, 884 µmol) according to general procedure E (1.5 M, at RT, using 3 eq. of K_2CO_3) to afford the product (194 mg, 877 µmol, 99%). ^{1}H NMR (400 MHz, $CDCl_3$) δ 8.14 (s, 1H), 8.07 (s, 1H), 7.39 – 7.32 (m, 1H), 7.10 – 7.00 (m, 2H), 6.97 (dt, *J* = 9.4, 1.9 Hz, 1H), 5.30 (s, 2H). ^{13}C NMR (101 MHz, $CDCl_3$) δ 163.00 (d, $J_{(C–F)}$ = 248.0 Hz), 136.54 (d, $J_{(C–F)}$ = 7.7 Hz), 136.23 (br), 136.11, 130.95 (d, $J_{(C–F)}$ = 8.3 Hz), 128.69, 123.80 (d, $J_{(C–F)}$ = 3.1 Hz), 116.05 (d, $J_{(C–F)}$ = 21.0 Hz), 115.19 (d, $J_{(C–F)}$ = 22.3 Hz).

1-(3-Methylbenzyl)-4-nitro-1*H*-pyrazole (86)

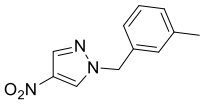

The title compound was synthesized from 4-nitro-1*H*-pyrazole (80.0 mg, 707 µmol) and 1-(bromomethyl)-3-methylbenzene (87.0 µL, 644 µmol, 0.91 eq.) according to general procedure E (0.4 M, at RT, using 1.05 eq. of K_2CO_3) to afford the product (138 mg, 635 µmol, 99%). ^{1}H NMR (400 MHz, $CDCl_3$) δ 8.07 (s, 1H), 8.06 (s, 1H), 7.31 – 7.26 (m, 1H), 7.21 – 7.17 (m, 1H), 7.12 – 7.07 (m, 2H), 5.26 (s, 2H), 2.36 (s, 3H). ^{13}C NMR (101 MHz, $CDCl_3$) δ 139.19, 136.07, 135.91, 133.87, 129.89, 129.19, 129.11, 128.45, 125.48, 57.38, 21.39.

1-(4-Chlorobenzyl)-4-nitro-1*H*-pyrazole (87)

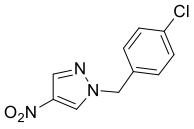

The title compound was synthesized from 4-nitro-1*H*-pyrazole (110 mg, 973 µmol) and 1-(bromomethyl)-4-chlorobenzene (182 mg, 884 µmol, 0.91 eq.) according to general procedure E (1.8 M, at RT, using 1.1 eq. of K_2CO_3) to afford the product (208 mg, 875 µmol, 99%). ^{1}H NMR (400 MHz, $CDCl_3$) δ 8.10 (s, 1H), 8.06 (s, 1H), 7.37 – 7.33 (m, 2H), 7.25 – 7.20 (m, 2H), 5.28 (s, 2H). ^{13}C NMR (101 MHz, $CDCl_3$) δ 136.19 (br), 136.10, 135.10, 132.61, 129.68, 129.46, 128.52, 56.56.

1-(4-Methylbenzyl)-4-nitro-1*H*-pyrazole (88)

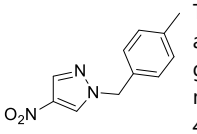

The title compound was synthesized from 4-nitro-1*H*-pyrazole (110 mg, 973 µmol) and 1-(bromomethyl)-4-methylbenzene (164 mg, 884 µmol, 0.91 eq.) according to general procedure E (1.8 M, at RT, using 1.1 eq. of K_2CO_3) to afford the product (192 mg, 884 µmol, quant.). ^{1}H NMR (400 MHz, $CDCl_3$) δ 8.06 (s, 1H), 8.05 (s, 1H), 7.20 (s, 4H), 5.25 (s, 2H), 2.35 (s, 3H). ^{13}C NMR (101 MHz, $CDCl_3$) δ 139.00, 135.91 (br), 135.78, 130.92, 129.86, 128.38, 128.33, 57.03, 21.13.

1-(4-Methoxybenzyl)-4-nitro-1*H*-pyrazole (89)

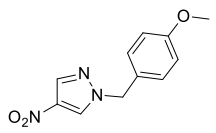

The title compound was synthesized from 4-nitro-1*H*-pyrazole (110 mg, 973 µmol) and 1-(chloromethyl)-4-methoxybenzene (110 µL, 884 µmol, 0.91 eq.) according to general procedure E (1.8 M, at RT, using 1.1 eq. of K_2CO_3) to afford the product (205 mg, 879 µmol, 99%). ^{1}H NMR (400 MHz, $CDCl_3$) δ 8.04 (d, *J* = 0.8 Hz, 1H), 8.01 (d, *J* = 0.8 Hz, 1H), 7.24 – 7.19 (m, 2H), 6.89 – 6.85 (m, 2H), 5.19 (s, 2H), 3.75 (s, 3H). ^{13}C NMR (101 MHz, $CDCl_3$) δ 159.91, 135.72 (br), 135.63, 129.82, 128.18, 125.86, 114.38, 56.56, 55.14.

1-(Tetrahydro-2*H*-pyran-2-yl)-1*H*-pyrazol-4-amine (90)

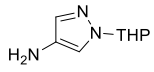

78 (100 mg) was dissolved in degassed MeOH (3 mL). 5% Pt/C (17.7 mg) was added and the atmosphere was exchanged for H_2. The mixture was vigorously stirred for 2 h while bubbling H_2 through the mixture. The atmosphere was exchanged for N_2, the mixture was filtered over Celite and subsequently concentrated. The crude was purified by silica gel column chromatography (10% MeOH (containing 10% sat. NH_4OH (aq.))/DCM) to afford the product (52.0 mg, 311 µmol, 74% over two steps). ^{1}H NMR (400 MHz, $CDCl_3$) δ 7.19 (s, 1H), 7.17 (s, 1H), 5.22 (dd, *J* = 9.6, 2.4 Hz, 1H), 4.04 – 3.97 (m, 1H), 3.68 – 3.60 (m, 1H), 2.88 (s, 2H), 2.08 – 1.94 (m, 3H), 1.68 – 1.53 (m, 3H). ^{13}C NMR (101 MHz, $CDCl_3$) δ 132.09, 129.42, 116.35, 87.87, 67.77, 30.22, 25.03, 22.61.

1-Methyl-1*H*-pyrazol-4-amine (91)

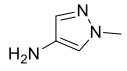

The title compound was synthesized from **79** (88.0 mg, 692 µmol) according to general procedure F (reaction time: 2 h) to afford the product (58.0 mg, 596 µmol, 86%). ^{1}H NMR (400 MHz, MeOD) δ 7.15 (s, 1H), 7.11 (s, 1H), 3.75 (s, 3H). ^{13}C NMR (101 MHz, MeOD) δ 131.75, 130.39, 121.44, 38.79.

1-Ethyl-1*H*-pyrazol-4-amine (92)

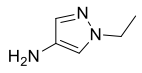

The title compound was synthesized from **80** (98.0 mg, 694 µmol) according to general procedure F (reaction time: 2 h) to afford the product (65.0 mg, 585 µmol, 84%). ^{1}H NMR (400 MHz, MeOD) δ 7.19 (d, *J* = 1.0 Hz, 1H), 7.12 (d, *J* = 0.9 Hz, 1H), 4.02 (q, *J* = 7.3 Hz, 2H), 1.37 (t, *J* = 7.3 Hz, 3H). ^{13}C NMR (101 MHz, MeOD) δ 131.63, 130.20, 119.83, 47.73, 16.01.

1-Benzyl-1*H*-pyrazol-4-amine (93)

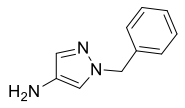

81 (144 mg, 707 µmol) and iron powder (300 mg, 5.37 mmol) were mixed in MeOH (10 mL) and AcOH (4.5 mL). The mixture was stirred at 60°C for 2 h after which the hot mixture was filtered over Celite and concentrated. The residue was diluted in 1 M $NaHCO_3$ (aq.) (30 mL) and the product extracted with EtOAc (3x25 mL). The combined organic layers were concentrated as such. The crude was purified by silica gel column chromatography (1 – 3% MeOH (containing 10% sat. NH_4OH (aq.))/DCM) to afford the product as a mixture of 1-benzyl-1H-pyrazol-4-amine and N-(1-benzyl-1H-pyrazol-4-yl)acetamide (40 mg). This mixture was dissolved in MeOH (1 mL) and 37% HCl (aq.) (0.3 mL) and stirred for 7 h. The mixture was concentrated and the residue diluted with 1 M $NaHCO_3$ (aq.) (30 mL). The product was extracted with DCM (3x20 mL). The combined organic layers were washed with brine (20 mL), dried over Na_2SO_4 and concentrated. The crude was purified by silica gel column chromatography (1 – 2% MeOH in DCM) to afford the product (20.0 mg, 115 µmol, 16%). ^{1}H NMR (400 MHz, $CDCl_3$) δ 7.35 – 7.25 (m, 3H), 7.20 – 7.16 (m, 3H), 6.96 (d, *J* = 0.9 Hz, 1H), 5.17 (s, 2H), 2.77 (br s, 2H). ^{13}C NMR (101 MHz, $CDCl_3$) δ 137.02, 131.46, 129.43, 128.82, 128.00, 127.63, 118.48, 56.28. LCMS (Finnigan, 0 → 50%): t_r = 5.00 min, m/z: 174.1.

1-Phenethyl-1*H*-pyrazol-4-amine (94)

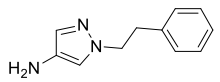

The title compound was synthesized from **82** (60.0 mg, 276 µmol) according to general procedure F (reaction time: 1 h) to afford the product (35.0 mg, 187 µmol, 68%). ^{1}H NMR (400 MHz, $CDCl_3$) δ 7.31 – 7.19 (m, 3H), 7.16 (d, *J* = 0.8 Hz, 1H), 7.12 – 7.07 (m, 2H), 6.82 (d, *J* = 0.8 Hz, 1H), 4.20 (t, *J* = 7.4 Hz, 2H), 3.10 (t, *J* = 7.5 Hz, 2H), 2.71 (br s, 2H). ^{13}C NMR (101 MHz, $CDCl_3$) δ 138.31, 131.35, 128.80, 128.63, 128.60, 126.67, 118.79, 53.75, 37.00. LCMS (Finnigan, 10 → 50%): t_r = 4.38 min, m/z: 188.1.

1-(3-Phenylpropyl)-1*H*-pyrazol-4-amine (95)

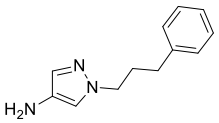

The title compound was synthesized from **83** (127 mg, 549 µmol) according to general procedure F (reaction time: 2 h) to afford the product (110 mg, 547 µmol, quant.). ^{1}H NMR (400 MHz, $CDCl_3$) δ 7.31 – 7.22 (m, 2H), 7.19 – 7.13 (m, 4H), 6.96 (d, *J* = 0.9 Hz, 1H), 3.98 (t, *J* = 7.0 Hz, 2H), 2.83 (br s, 2H), 2.58 (t, *J* = 7.4 Hz, 2H), 2.12 (p, *J* = 7.2 Hz, 2H). ^{13}C NMR (101 MHz, $CDCl_3$) δ 141.00, 131.01, 128.68, 128.44, 128.43, 126.03, 118.39, 51.45, 32.62, 31.79. LCMS (Finnigan, 0 → 50%): t_r = 6.70 min, m/z: 202.1.

1-(2-Chlorobenzyl)-1*H*-pyrazol-4-amine (96)

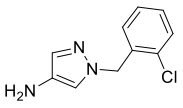

The title compound was synthesized from **84** (75.0 mg, 316 µmol) according to general procedure G to afford the product (60.0 mg, 289 µmol, 92%). ^{1}H NMR (400 MHz, MeOD) δ 7.41 (dd, *J* = 7.8, 1.5 Hz, 1H), 7.31 – 7.24 (m, 3H), 7.22 (d, *J* = 0.8 Hz, 1H), 6.92 (dd, *J* = 7.3, 1.9 Hz, 1H), 5.32 (s, 2H). ^{13}C NMR (101 MHz, MeOD) δ 136.18, 133.88, 132.62, 130.56, 130.53, 130.50 (br), 130.39, 128.40, 121.25, 54.04. LCMS (Finnigan, 10 → 90%): t_r = 4.06 min, m/z: 208.1.

1-(3-Fluorobenzyl)-1*H*-pyrazol-4-amine (97)

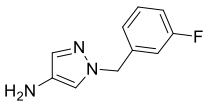

The title compound was synthesized from **85** (126 mg, 570 µmol) according to general procedure G (using 32 eq. NH_4Cl) to afford the product (69.0 mg, 361 µmol, 63%). ^{1}H NMR (400 MHz, $CDCl_3$) δ 7.33 – 7.23 (m, 1H), 7.19 (s, 1H), 7.02 – 6.91 (m, 3H), 6.84 (dt, *J* = 9.6, 2.1 Hz, 1H), 5.16 (s, 2H), 2.87 (br s, 2H). ^{13}C NMR (101 MHz, $CDCl_3$) δ 162.99 (d, $J_{(C–F)}$ = 246.6 Hz), 139.60 (d, $J_{(C–F)}$ = 7.2 Hz), 131.69, 130.30 (d, $J_{(C–F)}$ = 8.2 Hz), 129.64, 122.92 (d, $J_{(C–F)}$ = 2.9 Hz), 118.42, 114.84 (d, $J_{(C–F)}$ = 21.1 Hz), 114.33 (d, $J_{(C–F)}$ = 22.0 Hz), 55.52 (d, $J_{(C–F)}$ = 1.5 Hz). LCMS (Finnigan, 0 → 50%): t_r = 5.63 min, m/z: 192.1.

1-(3-Methylbenzyl)-1*H*-pyrazol-4-amine (98)

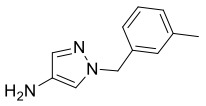

The title compound was synthesized from **86** (115 mg, 529 µmol) according to general procedure G to afford the product (98.0 mg, 523 µmol, 99%). ^{1}H NMR (400 MHz, MeOD) δ 7.35 (d, *J* = 0.8 Hz, 1H), 7.25 (d, *J* = 0.8 Hz, 1H), 7.19 (t, *J* = 7.6 Hz, 1H), 7.09 (d, *J* = 7.6 Hz, 1H), 7.02 (s, 1H), 6.98 (d, *J* = 8.0 Hz, 1H), 5.17 (s, 2H), 2.29 (s, 3H). ^{13}C NMR (101 MHz, MeOD) δ 139.55, 138.31, 132.58, 129.61, 129.60, 129.14, 127.76 (br), 125.60, 121.80, 56.69, 21.38. LCMS (Finnigan, 10 → 50%): t_r = 4.98 min, m/z: 188.1.

1-(4-Chlorobenzyl)-1*H*-pyrazol-4-amine (99)

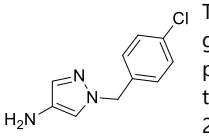

The title compound was synthesized from **87** (80.0 mg, 337 µmol) according to general procedure G (using 5 eq. of iron powder and 32 eq. NH_4Cl). The crude was purified by automated column chromatography (0 – 10% MeOH/DCM) to afford the product (23.5 mg, 113 µmol, 34%). ^{1}H NMR (400 MHz, $CDCl_3$) δ 7.31 – 7.27 (m, 2H), 7.19 (d, *J* = 0.9 Hz, 1H), 7.13 – 7.08 (m, 2H), 6.97 (d, *J* = 0.9 Hz, 1H), 5.14 (s, 2H), 2.65 (br s, 2H). ^{13}C NMR (101 MHz, $CDCl_3$) δ 135.59, 133.91, 131.74, 129.65, 129.01, 128.95, 118.39, 55.55. LCMS (Finnigan, 0 → 50%): t_r = 6.53 min, m/z: 208.1.

1-(4-Methylbenzyl)-1*H*-pyrazol-4-amine hydrochloride (100)

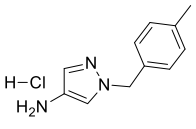

The title compound was synthesized from **88** (73.0 mg, 337 µmol) according to general procedure G (using 5 eq. of iron powder and 32 eq. NH_4Cl). The crude was diluted in a mixture of 0.5 M HCl (aq.) (10 mL) and DCM (10 mL). The organic layer was separated and the water layer extracted with DCM (10 mL). The water layer was concentrated to afford the product (29.3 mg, 156 µmol, 47%). ^{1}H NMR (400 MHz, MeOD) δ 7.97 (s, 1H), 7.64 (s, 1H), 7.20 – 7.12 (m, 4H), 5.30 (s, 2H), 2.30 (s, 3H). ^{13}C NMR (101 MHz, MeOD) δ 139.24, 134.73, 134.43, 130.39, 128.93, 126.62, 114.18, 57.10, 21.13. LCMS (Finnigan, 0 → 50%): t_r = 6.27 min, m/z: 188.1.

1-(4-Methoxybenzyl)-1*H*-pyrazol-4-amine (101)

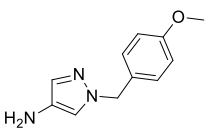

The title compound was synthesized from 89 (78.0 mg, 336 µmol) according to general procedure G (using 5 eq. of iron powder and 32 eq. NH_4Cl). The crude was purified by automated column chromatography (0 – 10% MeOH/DCM) to afford the product (25.0 mg, 123 µmol, 37%). ^{1}H NMR (400 MHz, $CDCl_3$) δ 7.16 (d, *J* = 0.8 Hz, 1H), 7.15 – 7.12 (m, 2H), 6.93 (d, *J* = 0.8 Hz, 1H), 6.87 – 6.83 (m, 2H), 5.09 (s, 2H), 3.77 (s, 3H), 2.72 (br s, 2H). ^{13}C NMR (101 MHz, $CDCl_3$) δ 159.39, 131.32, 129.30, 129.17, 128.97, 118.26, 114.17, 55.77, 55.36. LCMS (Finnigan, 0 → 50%): t_r = 5.74 min, m/z: 204.1.

((4-((1-(Tetrahydro-2*H*-pyran-2-yl)-1*H*-pyrazol-4-yl)amino)quinazoline-6,7-diyl)bis(oxy))bis(ethane-2,1-diyl) diacetate (102)

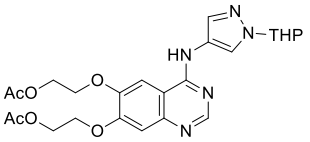

The title compound was synthesized from **62** (30.0 mg, 81.4 µmol) and **90** (13.7 mg, 81.9 µmol) according to general procedure A (also DIPEA (21.0 µL, 122 µmol) was added, reaction time: 6 h). The crude was purified by silica gel column chromatography (2% MeOH/DCM) to afford the product (30 mg, 60 µmol, 74%). ^{1}H NMR (400 MHz, $CDCl_3$) δ 8.67 (s, 2H), 8.48 (s, 1H), 7.66 (s, 1H), 7.55 (s, 1H), 7.18 (s, 1H), 5.35 (d, *J* = 9.9 Hz, 1H), 4.49 – 4.42 (m, 2H), 4.36 (t, *J* = 5.0 Hz, 2H), 4.29 – 4.22 (m, 2H), 4.09 (t, *J* = 5.1 Hz, 2H), 4.00 (d, *J* = 11.3 Hz, 1H), 3.63 (t, *J* = 10.0 Hz, 1H), 2.23 – 2.12 (m, 1H), 2.09 – 1.98 (m, 8H), 1.72 – 1.52 (m, 3H). ^{13}C NMR (101 MHz, $CDCl_3$) δ 171.52, 170.95, 155.75, 154.33, 153.68, 148.07, 146.84, 132.15, 122.81, 120.52, 109.33, 108.98, 103.33, 88.12, 67.92, 66.94, 66.87, 62.29, 62.00, 30.33, 24.99, 22.63, 20.99, 20.92. LCMS (Fleet, 10 → 90%): t_r = 4.34 min, m/z: 500.2.

((4-((1-Methyl-1*H*-pyrazol-4-yl)amino)quinazoline-6,7-diyl)bis(oxy))bis(ethane-2,1-diyl) diacetate (103)

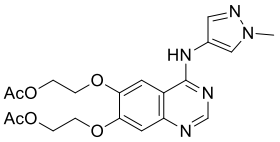

The title compound was synthesized from **62** (30.0 mg, 81.4 µmol) and **91** (9.5 mg, 98 µmol) according to general procedure A (reaction time: 2 h). The crude was purified by silica gel column chromatography (2 – 5% MeOH/DCM) to afford the product (32 mg, 75 µmol, 92%). ^{1}H NMR (500 MHz, MeOD) δ 8.48 (s, 1H), 8.17 (s, 1H), 7.59 (s, 1H), 7.58 (s, 1H), 7.08 (s, 1H), 4.46 – 4.42 (m, 4H), 4.28 – 4.24 (m, 4H), 3.86 (s, 3H), 2.05 (s, 3H), 2.05 (s, 3H). ^{13}C NMR (126 MHz, MeOD) δ 171.67, 171.35, 156.01, 153.79, 148.19, 146.15, 131.34, 123.29, 122.41, 109.42, 108.11, 103.77, 67.27, 66.80, 62.66, 62.44, 39.04, 20.82, 20.77. LCMS (Finnigan, 10 → 90%): t_r = 4.43 min, m/z: 430.1.

((4-((1-Ethyl-1*H*-pyrazol-4-yl)amino)quinazoline-6,7-diyl)bis(oxy))bis(ethane-2,1-diyl) diacetate (104)

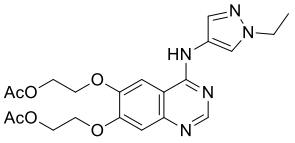

The title compound was synthesized from **62** (30.0 mg, 81.4 µmol) and **92** (10.9 mg, 98.1 µmol) according to general procedure A (reaction time: 2 h). The crude was purified by silica gel column chromatography (5% MeOH/DCM) to afford the product (33 mg, 74 µmol, 91%). ^{1}H NMR (500 MHz, $CDCl_3$) δ 8.45 (s, 1H), 8.18 (s, 1H), 7.56 (s, 1H), 7.55 (s, 1H), 7.04 (s, 1H), 4.42 – 4.37 (m, 4H), 4.25 – 4.19 (m, 4H), 4.09 (q, *J* = 7.3 Hz, 2H), 2.01 (s, 3H), 2.01 (s, 3H), 1.42 (t, *J* = 7.1 Hz, 3H). ^{13}C NMR (126 MHz, $CDCl_3$) δ 171.56, 171.22, 155.85, 153.72, 153.67, 148.07, 146.02, 130.96, 122.09, 121.49, 109.30, 108.02, 103.66, 67.15, 66.69, 62.53, 62.32, 47.20, 20.71, 20.67, 15.33. LCMS (Finnigan, 10 → 90%): t_r = 4.66 min, m/z: 444.1.

((4-((1-Benzyl-1*H*-pyrazol-4-yl)amino)quinazoline-6,7-diyl)bis(oxy))bis(ethane-2,1-diyl) diacetate (105)

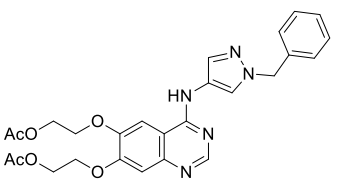

The title compound was synthesized from **62** (30.0 mg, 81.4 µmol) and **93** (15.5 mg, 89.5 µmol) according to general procedure A (reaction time: 2 h). The crude was purified by silica gel column chromatography (1 – 3% MeOH/DCM) to afford the product (40 mg, 79 µmol, 97%). ^{1}H NMR (400 MHz, $CDCl_3$) δ 8.65 (s, 1H), 8.56 (br s, 1H), 8.28 (s, 1H), 7.64 (s, 1H), 7.51 (s, 1H), 7.31 – 7.15 (m, 6H),

5.27 (s, 2H), 4.48 – 4.43 (m, 2H), 4.36 (t, *J* = 5.4 Hz, 2H), 4.29 – 4.22 (m, 2H), 4.07 (t, *J* = 5.4 Hz, 2H), 2.06 (s, 3H), 2.06 (s, 3H). ^{13}C NMR (101 MHz, $CDCl_3$) δ 171.60, 170.97, 155.67, 154.35, 153.64, 148.00, 146.88, 136.53, 131.69, 128.87, 128.15, 127.74, 122.75, 122.23, 109.29, 109.03, 103.20, 66.88, 66.85, 62.28, 61.89, 56.53, 21.02, 20.94. LCMS (Finnigan, 10 → 90%): t_r = 5.50 min, m/z: 506.1.

((4-((1-Phenethyl-1*H*-pyrazol-4-yl)amino)quinazoline-6,7-diyl)bis(oxy))bis(ethane-2,1-diyl) diacetate (106)

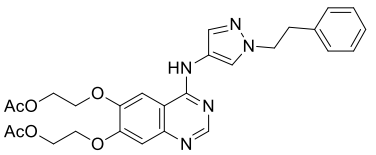

The title compound was synthesized from **62** (30.0 mg, 81.4 µmol) and **94** (15.3 mg, 81.7 µmol) according to general procedure A (reaction time: 1 h). The crude was purified by silica gel column chromatography (0 - 5% MeOH/DCM) to afford the product (31 mg, 60 µmol, 73%). ^{1}H NMR (400 MHz, MeOD) δ 8.44 (s, 1H), 8.04 (d, *J* = 0.7 Hz, 1H), 7.75 (d, *J* = 0.7 Hz, 1H), 7.66 (s, 1H), 7.27 – 7.11 (m, 5H), 7.10 (s, 1H), 4.52 – 4.46 (m, 4H), 4.38 – 4.29 (m, 6H), 3.15 (t, *J* = 7.3 Hz, 2H), 2.08 (s, 3H), 2.08 (s, 3H). ^{13}C NMR (101 MHz, MeOD) δ 172.34, 172.24, 156.93, 154.71, 154.26, 149.18, 146.61, 138.73, 132.37, 129.40, 129.24, 127.32, 123.51, 122.87, 110.16, 108.44, 104.45, 68.07, 67.62, 63.43, 63.22, 54.47, 37.50, 20.94, 20.92. LCMS (Finnigan, 0 → 90%): t_r = 6.33 min, m/z: 520.2.

((4-((1-(2-Chlorobenzyl)-1*H*-pyrazol-4-yl)amino)quinazoline-6,7-diyl)bis(oxy))bis(ethane-2,1-diyl) diacetate (107)

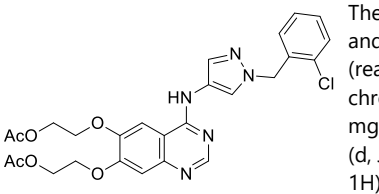

The title compound was synthesized from **62** (30.0 mg, 81.4 µmol) and **96** (16.9 mg, 81.4 µmol) according to general procedure A (reaction time: 1 h). The crude was purified by silica gel column chromatography (2 – 4% MeOH/DCM) to afford the product (42 mg, 78 µmol, 96%). ^{1}H NMR (400 MHz, $CDCl_3$) δ 8.66 (s, 1H), 8.33 (d, *J* = 0.7 Hz, 1H), 8.30 (br s, 1H), 7.72 (d, *J* = 0.8 Hz, 1H), 7.52 (s, 1H), 7.35 (dd, *J* = 7.7, 1.4 Hz, 1H), 7.22 – 7.13 (m, 3H), 7.02 (dd, *J* = 7.5, 1.8 Hz, 1H), 5.42 (s, 2H), 4.51 – 4.47 (m, 2H), 4.42 (t, *J* = 5.6 Hz, 2H), 4.32 – 4.26 (m, 2H), 4.19 – 4.12 (m, 2H), 2.10 (s, 3H), 2.08 (s, 3H). ^{13}C NMR (101 MHz, $CDCl_3$) δ 171.75, 170.99, 155.66, 154.38, 153.70, 148.02, 146.94, 134.43, 133.14, 132.07, 129.69, 129.51, 127.36, 122.72, 122.67, 109.25, 109.13, 103.09, 66.90, 66.87, 62.32, 61.76, 53.90, 21.10, 20.98. LCMS (Finnigan, 10 → 90%): t_r = 5.86 min, m/z: 540.0.

((4-((1-(3-Phenylpropyl)-1*H*-pyrazol-4-yl)amino)quinazoline-6,7-diyl)bis(oxy))bis(ethane-2,1-diyl) diacetate (108)

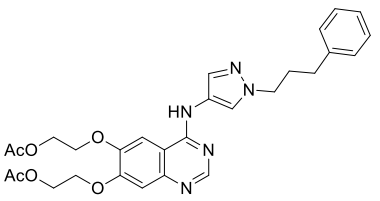

The title compound was synthesized from **62** (30.0 mg, 81.4 µmol) and **95** (16.4 mg, 81.5 µmol) according to general procedure A (reaction time: 1.5 h). The crude was purified by silica gel column chromatography (1 – 4% MeOH/DCM) to afford the product (40.8 mg, 76.5 µmol, 94%). ^{1}H NMR (400 MHz, $CDCl_3$) δ 8.79 – 8.62 (m, 2H), 8.28 (d, *J* = 0.7 Hz, 1H), 7.65 (d, *J* = 0.7 Hz, 1H), 7.60 (s, 1H), 7.28 – 7.23 (m, 2H), 7.22 – 7.13 (m, 4H), 4.50 – 4.45 (m, 2H), 4.40 (t, *J* = 5.3 Hz, 2H), 4.30 – 4.25 (m, 2H), 4.17 – 4.09 (m, 4H), 2.62 (t, *J* = 7.6 Hz, 2H), 2.21 (p, *J* = 7.4 Hz, 2H), 2.08 (s, 3H), 2.08 (s, 3H). ^{13}C NMR (101 MHz, $CDCl_3$) δ 171.60, 170.99, 155.74, 154.32, 153.67, 148.03, 146.77, 140.82, 131.21, 128.55, 128.49, 126.19, 122.15, 122.13, 109.30, 108.91, 103.31, 66.96, 66.84, 62.27, 61.94, 51.89, 32.73, 31.83, 21.01, 20.92. LCMS (Finnigan, 10 → 90%): t_r = 6.05 min, m/z: 534.2.

((4-((1-(3-Fluorobenzyl)-1*H*-pyrazol-4-yl)amino)quinazoline-6,7-diyl)bis(oxy))bis(ethane-2,1-diyl) diacetate (109)

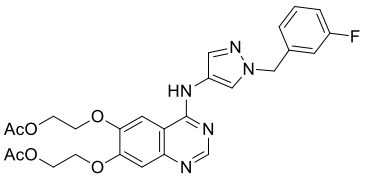

The title compound was synthesized from **62** and **97** (15.6 mg, 81.6 µmol) according to general procedure A (reaction time: 1.5 h). The crude was purified by silica gel column chromatography (1 – 4% MeOH/DCM) to afford the product (35 mg, 67 µmol, 82%). ^{1}H NMR (400 MHz, $CDCl_3$) δ 8.65 (s, 1H), 8.64 (br s, 1H), 8.33 (s, 1H), 7.65 (d, *J* = 0.8 Hz, 1H), 7.53 (s, 1H), 7.26 – 7.19 (m, 1H), 7.18 (s, 1H), 6.97 (ddd, *J* = 7.6, 1.7, 0.9 Hz, 1H), 6.94 – 6.88 (m, 1H), 6.86 (dt, *J* = 9.5, 1.9 Hz, 1H), 5.27 (s, 2H), 4.47 – 4.43 (m, 2H), 4.37 (t, *J* = 5.4 Hz, 2H), 4.27 – 4.23 (m, 2H), 4.08 (t, *J* = 5.5 Hz, 2H), 2.06 (s, 3H), 2.06 (s, 3H). ^{13}C NMR (101 MHz, $CDCl_3$) δ 171.64, 170.98, 163.01 (d, $J_{(C–F)}$ = 246.9 Hz), 155.64, 154.28, 153.70, 148.04, 146.82, 139.12 (d, $J_{(C–F)}$ = 7.2 Hz), 131.88, 130.44 (d, $J_{(C–F)}$ = 8.3 Hz), 123.15 (d, $J_{(C–F)}$ = 2.9 Hz), 122.94, 122.29, 115.07 (d, $J_{(C–F)}$ = 21.1 Hz), 114.52 (d, $J_{(C–F)}$ = 22.1 Hz), 109.28, 108.95, 103.21, 66.90, 66.86, 62.26, 61.87, 55.83 (d, $J_{(C–F)}$ = 1.8 Hz), 21.01, 20.92. LCMS (Finnigan, 10 → 90%): t_r = 5.64 min, m/z: 524.1.

((4-((1-(3-Methylbenzyl)-1*H*-pyrazol-4-yl)amino)quinazoline-6,7-diyl)bis(oxy))bis(ethane-2,1-diyl) diacetate (110)

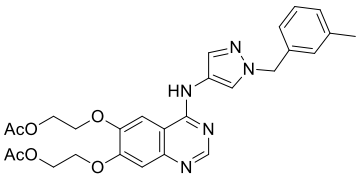

The title compound was synthesized from **62** (30.0 mg, 81.4 µmol) and **98** (15.3 mg, 81.7 µmol) according to general procedure A (reaction time: 1 h). The crude was purified by silica gel column chromatography (1 – 4% MeOH/DCM) to afford the product (38.8 mg, 74.7 µmol, 92%). ^{1}H NMR (400 MHz, $CDCl_3$) δ 8.65 (s, 1H), 8.32 (br s, 1H), 8.28 (d, *J* = 0.7 Hz, 1H), 7.67 (d, *J* = 0.8 Hz, 1H), 7.49 (s, 1H), 7.21 – 7.12 (m, 2H), 7.09 – 7.00 (m, 3H), 5.25 (s, 2H), 4.50 – 4.46 (m, 2H), 4.41 (t, *J* = 5.5 Hz, 2H), 4.31 – 4.27 (m, 2H), 4.12 (t, *J* = 5.6 Hz, 2H), 2.25 (s, 3H), 2.09 (s, 3H), 2.08 (s, 3H). ^{13}C NMR (101 MHz, $CDCl_3$) δ 171.71, 170.99, 155.64, 154.36, 153.66, 147.98, 146.91, 138.65, 136.44, 131.70, 128.94, 128.78, 128.56, 124.87, 122.65, 122.20, 109.25, 109.11, 103.11, 66.88, 62.32, 61.83, 56.60, 21.42, 21.08, 20.97. LCMS (Finnigan, 10 → 90%): t_r = 5.84 min, m/z: 520.1.

((4-((1-(4-Chlorobenzyl)-1*H*-pyrazol-4-yl)amino)quinazoline-6,7-diyl)bis(oxy))bis(ethane-2,1-diyl) diacetate (111)

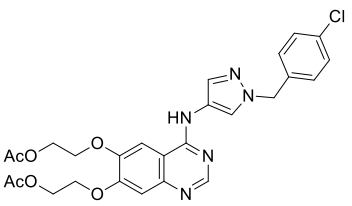

The title compound was synthesized from **62** (30.0 mg, 81.4 µmol) and **99** (16.9 mg, 81.4 µmol) according to general procedure A (reaction time: 2 h). The crude was purified by silica gel column chromatography (0 – 5% MeOH/DCM) to afford the product (40 mg, 74 µmol, 91%). ^{1}H NMR (400 MHz, MeOD) δ 8.45 (s, 1H), 8.31 (d, *J* = 0.7 Hz, 1H), 7.77 (d, *J* = 0.7 Hz, 1H), 7.63 (s, 1H), 7.30 – 7.25 (m, 2H), 7.20 – 7.16 (m, 2H), 7.07 (s, 1H), 5.28 (s, 2H), 4.50 – 4.45 (m, 4H), 4.33 – 4.28 (m, 4H), 2.08 (s, 3H), 2.07 (s, 3H). ^{13}C NMR (101 MHz, MeOD) δ 172.32, 172.22, 156.77, 154.71, 154.20, 149.18, 146.52, 136.24, 134.53, 132.72, 129.65, 129.51, 123.75, 123.42, 110.11, 108.35, 104.33, 68.05, 67.61, 63.42, 63.20, 55.87, 20.94, 20.92. LCMS (Finnigan, 10 → 90%): t_r = 5.94 min, m/z: 540.1.

((4-((1-(4-Methylbenzyl)-1*H*-pyrazol-4-yl)amino)quinazoline-6,7-diyl)bis(oxy))bis(ethane-2,1-diyl) diacetate (112)

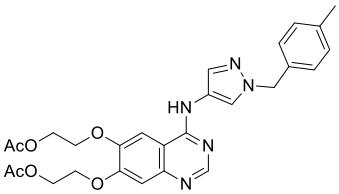

The title compound was synthesized from **62** (30.0 mg, 81.4 µmol) and **100** (18.2 mg, 81.4 µmol) according to general procedure A (reaction time: 6 h). The crude was purified by automated column chromatography (0 – 5% MeOH/DCM) to afford the product (36 mg, 69 µmol, 85%). ^{1}H NMR (400 MHz, $CDCl_3$) δ 8.64 (s, 1H), 8.57 (br s, 1H), 8.26 (d, *J* = 0.7 Hz, 1H), 7.62 (d, *J* = 0.7 Hz, 1H), 7.48 (s, 1H), 7.18 (s, 1H), 7.13 – 7.09 (m, 2H), 7.08 – 7.04 (m, 2H), 5.23 (s,

2H), 4.49 – 4.44 (m, 2H), 4.36 (t, *J* = 5.4 Hz, 2H), 4.29 – 4.24 (m, 2H), 4.06 (t, *J* = 5.4 Hz, 2H), 2.26 (s, 3H), 2.07 (s, 3H), 2.06 (s, 3H). ^{13}C NMR (101 MHz, $CDCl_3$) δ 171.59, 170.98, 155.66, 154.31, 153.61, 147.97, 146.80, 137.94, 133.46, 131.62, 129.52, 127.82, 122.68, 122.14, 109.29, 108.98, 103.20, 66.90, 66.85, 62.30, 61.94, 56.34, 21.18, 21.02, 20.94. LCMS (Finnigan, 10 → 90%): t_r = 5.85 min, m/z: 520.1.

((4-((1-(4-Methoxybenzyl)-1*H*-pyrazol-4-yl)amino)quinazoline-6,7-diyl)bis(oxy))bis(ethane-2,1-diyl) diacetate (113)

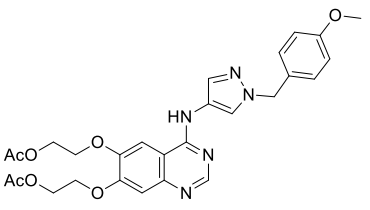

The title compound was synthesized from **62** (30.0 mg, 81.4 µmol) and **101** (16.6 mg, 81.7 µmol) according to general procedure A (reaction time: 1.5 h). The crude was purified by automated column chromatography (0 – 5% MeOH/DCM) to afford the product (41 mg, 77 µmol, 94%). ^{1}H NMR (400 MHz, $CDCl_3$) δ 8.64 (s, 1H), 8.62 (s, 1H), 8.24 (d, *J* = 0.6 Hz, 1H), 7.61 (d, *J* = 0.8 Hz, 1H), 7.47 (s, 1H), 7.18 – 7.12 (m, 3H), 6.79 – 6.74 (m, 2H), 5.19 (s, 2H), 4.48 – 4.43 (m, 2H), 4.35 (t, *J* = 5.3 Hz, 2H), 4.25 (t, 2H), 4.03 (t, *J* = 5.3 Hz, 2H), 3.71 (s, 3H), 2.06 (s, 3H), 2.05 (s, 3H). ^{13}C NMR (101 MHz, $CDCl_3$) δ 171.57, 170.97, 159.46, 155.67, 154.32, 153.60, 147.97, 146.83, 131.61, 129.30, 128.46, 122.67, 122.03, 114.19, 109.30, 108.98, 103.19, 66.89, 66.83, 62.28, 61.97, 56.04, 55.31, 21.00, 20.93. LCMS (Finnigan, 10 → 90%): t_r = 6.18 min, m/z: 536.2.

N-(2-Chloropyrimidin-4-yl)-6,7-bis(2-methoxyethoxy)quinazolin-4-amine (114)

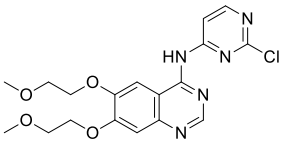

4-Chloro-6,7-bis(2-methoxyethoxy)quinazoline (1.50 g, 4.80 mmol), Cs_2CO_3 (4.69 g, 14.4 mmol), xantphos (416 mg, 0.719 mmol) and 2-chloropyrimidin-4-amine (746 mg, 5.76 mmol) were mixed in DMF (22 mL). N_2 was bubbled through the mixture for 1 min after which $Pd(OAc)_2$ (108 mg, 0.48 mmol) was added. N_2 was bubbled through the mixture for 30 sec after which the mixture was heated to 90°C and stirred for 16 h. The mixture was filtered over Celite and subsequently concentrated. The residue was suspended in EtOAc (100 mL) and poured into H_2O (100 mL) and brine (10 mL). The organic layer was separated and the water layer extracted with EtOAc (50 mL). The combined organic layers were washed with brine (100 mL) and subsequently isolated. The water layer was extracted with EtOAc (50 mL) and the combined organic layers were dried over Na_2SO_4, filtered and concentrated. The crude was purified by silica gel column chromatography (1% MeOH/EtOAc) to afford the product (1.23 g, 3.03 mmol, 63%). ^{1}H NMR (500 MHz, DMSO) δ 11.01 (s, 1H), 8.71 (s, 1H), 8.57 (d, *J* = 5.9 Hz, 1H), 8.53 (d, *J* = 5.8 Hz, 1H), 8.04 (s, 1H), 7.30 (s, 1H), 4.34 – 4.28 (m, 4H), 3.80 – 3.77 (m, 2H), 3.76 – 3.73 (m, 2H), 3.37 (s, 3H), 3.35 (s, 3H). ^{13}C NMR (126 MHz, DMSO) δ 160.79, 159.97, 158.99, 154.91, 154.39, 151.83, 148.77, 147.91, 109.98, 109.33, 107.91, 102.95, 69.97, 68.34, 68.23, 58.37, 58.34, 40.11, 40.02, 39.95, 39.85, 39.78, 39.69, 39.61, 39.52, 39.35, 39.19, 39.02.

1-(3-Nitrophenyl)-1*H*-pyrazole (115)

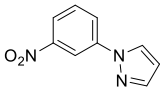

An oven dried microwave tube was charged with 1*H*-pyrazole (33.7 mg, 495 µmol), 1-bromo-3-nitrobenzene (150 mg, 743 µmol), ethyl 2-oxocyclohexane-1-carboxylate (7.9 µl, 50 µmol), Cs_2CO_3 (323 mg, 990 µmol) and dry MeCN (1 mL). Argon was bubbled through the mixture for 30 sec after which copper(I) oxide (7.1 mg, 50 µmol) was added. The microwave tube was sealed, the mixture was heated to 82°C and stirred for 16 h. The mixture was poured into H_2O (10 mL) and the product extracted with EtOAc (3x10 mL). The combined organic layers were washed with brine (10 mL), dried over Na_2SO_4, filtered and concentrated. The crude was purified by automated column chromatography (10 – 50% EtOAc/heptane) to afford the product (51.0 mg, 270 µmol, 55%). ^{1}H NMR (400 MHz, DMSO) δ 8.73 (dd, *J* = 2.7, 0.6 Hz, 1H), 8.64 (t, *J* = 2.2 Hz, 1H), 8.32 (ddd, *J* = 8.2, 2.2, 0.9 Hz, 1H), 8.13 (ddd, *J* = 8.3, 2.2, 0.9 Hz, 1H), 7.84 (dd, *J* = 1.7, 0.5 Hz, 1H), 7.78 (t, *J* = 8.2 Hz, 1H), 6.62 (dd, *J* = 2.6, 1.8 Hz, 1H). ^{13}C NMR (101 MHz, DMSO) δ 148.62, 142.05, 140.36, 131.13, 128.57, 124.13, 120.52, 112.75, 108.83. LCMS (Finnigan, 10 → 90%): t_r = 7.49 min, m/z: 190.1.

3-(1*H*-Pyrazol-1-yl)aniline (116)

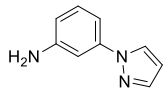

115 (28.0 mg, 148 µmol) was dissolved in EtOH/H_2O (30:1, 3.3 mL) after which iron powder (41.3 mg, 444 µmol) and NH_4Cl (41.3 mg, 740 µmol) were added. The mixture was heated to 80°C, stirred for 2.5 h and subsequently filtered over Celite. The filtrate was diluted in 10% MeOH/DCM (10 mL) and poured into 1 M $NaHCO_3$ (10 mL). The organic layer was separated and the water layer extracted with DCM (2x10 mL). The combined organic layers were washed with brine (10 mL), dried over Na_2SO_4, filtered and concentrated to afford the product (23.0 mg, 144 µmol, 98%). ^{1}H NMR (400 MHz, DMSO) δ 8.29 (dd, *J* = 1.9, 0.6 Hz, 1H), 7.66 (d, *J* = 1.8 Hz, 1H), 7.11 – 7.06 (m, 2H), 6.91 (ddd, *J* = 7.9, 2.2, 0.9 Hz, 1H), 6.50 (ddd, *J* = 8.0, 2.2, 0.9 Hz, 1H), 6.47 (dd, *J* = 2.5, 1.8 Hz, 1H), 5.56 (br s, 2H). ^{13}C NMR (101 MHz, DMSO) δ 149.51, 140.61, 140.38, 129.80, 127.41, 112.10, 107.40, 105.92, 104.19. LCMS (Fleet, 0 → 20%): t_r = 6.34 min, m/z: 160.1.

References

1. Dominguez-Brauer, C., Thu, K. L., Mason, J. M., Blaser, H., Bray, M. R. & Mak, T. W. Targeting Mitosis in Cancer: Emerging Strategies. *Mol. Cell* **60**, 524–536 (2015).
2. Kops, G. J. P. L., Weaver, B. A. A. & Cleveland, D. W. On the road to cancer: aneuploidy and the mitotic checkpoint. *Nat. Rev. Cancer* **5**, 773–785 (2005).
3. Musacchio, A. & Salmon, E. D. The spindle-assembly checkpoint in space and time. *Nat. Rev. Mol. Cell Biol.* **8**, 379–393 (2007).
4. Siemeister, G., Mengel, A., Fernández-Montalván, A. E., Bone, W., Schröder, J., Zitzmann-Kolbe, S., Briem, H., Prechtl, S., Holton, S. J., Mönning, U., von Ahsen, O., Johanssen, S., Cleve, A., Pütter, V., Hitchcock, M., von Nussbaum, F., Brands, M., Ziegelbauer, K. & Mumberg, D. Inhibition of BUB1 Kinase by BAY 1816032 Sensitizes Tumor Cells toward Taxanes, ATR, and PARP Inhibitors *In Vitro* and *In Vivo*. *Clin. Cancer Res.* **25**, 1404–1414 (2019).
5. Ling, J., Johnson, K. A., Miao, Z., Rakhit, A., Pantze, M. P., Hamilton, M., Lum, B. L. & Prakash, C. Metabolism and excretion of erlotinib, a small molecule inhibitor of epidermal growth factor receptor tyrosine kinase, in healthy male volunteers. *Drug Metab. Dispos.* **34**, 420–426 (2006).
6. Yarden, Y. & Sliwkowski, M. X. Untangling the ErbB signalling network. *Nat. Rev. Mol. Cell Biol.* **2**, 127–137 (2001).
7. Dancey, J. & Sausville, E. A. Issues and progress with protein kinase inhibitors for cancer treatment. *Nat. Rev. Drug Discov.* **2**, 296–313 (2003).
8. Dowell, J., Minna, J. D. & Kirkpatrick, P. Erlotinib hydrochloride. *Nat. Rev. Drug Discov.* **4**, 13–14 (2005).
9. Park, J. H., Liu, Y., Lemmon, M. A. & Radhakrishnan, R. Erlotinib binds both inactive and active conformations of the EGFR tyrosine kinase domain. *Biochem. J.* **448**, 417–423 (2012).
10. van Linden, O. P. J., Kooistra, A. J., Leurs, R., de Esch, I. J. P. & de Graaf, C. KLIFS: A Knowledge-Based Structural Database To Navigate Kinase–Ligand Interaction Space. *J. Med. Chem.* **57**, 249–277 (2014).
11. Roskoski, R. Properties of FDA-approved small molecule protein kinase inhibitors. *Pharmacol. Res.* **144**, 19–50 (2019).
12. Seeliger, D. & de Groot, B. L. Ligand docking and binding site analysis with PyMOL and Autodock/Vina. *J. Comput. Aided Mol. Des.* **24**, 417–422 (2010).
13. Trott, O. & Olson, A. J. AutoDock Vina: Improving the speed and accuracy of docking with a new scoring function, efficient optimization, and multithreading. *J. Comput. Chem.* **31**, 455–461 (2010).
14. The PyMOL Molecular Graphics System, Version 2.3.0 Schrödinger, LLC.
15. Word, J. M., Lovell, S. C., Richardson, J. S. & Richardson, D. C. Asparagine and glutamine: using hydrogen atom contacts in the choice of side-chain amide orientation11Edited by J. Thornton. *J. Mol. Biol.* **285**, 1735–1747 (1999).
16. Zhang, Y., Ding, K., Liao, J., Wang, Y. & Chen, P. Coupling compounds of nsaid anti-inflammatory and analgesic drugs and egfr kinase inhibitors, synthesis methods and applications thereof. US20160175453A1 (2016).
17. Wang, X., Ju, T., Li, X. & Cao, X. Regioselective Alkylation of Catechols via Mitsunobu Reactions. *Synlett* **2010**, 2947–2949 (2010).
18. Gregson, S. J., Howard, P. W., Gullick, D. R., Hamaguchi, A., Corcoran, K. E., Brooks, N. A., Hartley, J. A., Jenkins, T. C., Patel, S., Guille, M. J. & Thurston, D. E. Linker Length Modulates DNA Cross-Linking Reactivity and Cytotoxic Potency of C8/C8′ Ether-Linked C2- *exo* -Unsaturated Pyrrolo[2,1- *c*][1,4]benzodiazepine (PBD) Dimers. *J. Med. Chem.* **47**, 1161–1174 (2004).
19. Pawar, V. G., Sos, M. L., Rode, H. B., Rabiller, M., Heynck, S., van Otterlo, W. A. L., Thomas, R. K. & Rauh, D. Synthesis and Biological Evaluation of 4-Anilinoquinolines as Potent Inhibitors of Epidermal Growth Factor Receptor. *J. Med. Chem.* **53**, 2892–2901 (2010).
20. Jordan, A. M., Begum, H., Fairweather, E., Fritzl, S., Goldberg, K., Hopkins, G. V., Hamilton, N. M., Lyons, A. J., March, H. N., Newton, R., Small, H. F., Vishwanath, S., Waddell, I. D., Waszkowycz, B., Watson, A. J. & Ogilvie, D. J. Anilinoquinazoline inhibitors of the RET kinase domain—Elaboration of the 7-position. *Bioorg. Med. Chem. Lett.* **26**, 2724–2729 (2016).
21. Damkaci, F., Alawaed, A. & Vik, E. N-Picolinamides as ligands for Ullmann-type CN coupling reactions. *Tetrahedron Lett.* **57**, 2197–2200 (2016).
22. Jiang, Y., Xu, L., Zhou, C. & Ma, D. Chapter 1. Cu-Catalyzed Ullmann-Type C–Heteroatom Bond Formation: The Key Role of Dinucleating Ancillary Ligands. in *Catalysis Series* (ed. Ribas, X.) 1–45 (Royal Society of Chemistry, 2013).

4

Hit optimization of benzimidazoles towards highly potent BUB1 inhibitors

Introduction

Millions of people are diagnosed with cancer worldwide each year.[1] In 2020 the number of new cases was estimated to be 19.3 million and about 10 million cancer-related deaths were reported.[1] In a healthy individual, cell division is tightly controlled and homeostasis of cell number is thereby ensured.[2] One of the hallmarks of cancer includes uncontrolled cell proliferation, which may involve aberrant signaling of receptor tyrosine kinases.[2] Insights into these molecular mechanisms have led to the development of small molecule inhibitors that target these receptor tyrosine kinases and thereby block cell proliferation.[3] However, new molecular targets are urgently needed for cancer types that do not respond well to the currently available anti-cancer therapies. Budding uninhibited by benzimidazole 1 (BUB1) kinase has recently emerged as such a potential target for anti-cancer therapy.[4–6]

BUB1 plays an important role in the spindle assembly checkpoint (SAC), which is a safety mechanism during the prometaphase of mitosis. The SAC induces a mitotic arrest when chromosomes are not yet, or not properly, attached to the mitotic spindle.[7] This arrest is crucial for genomic integrity since mitotic progression with unattached chromosomes can result in aneuploidy which subsequently may contribute to tumorigenesis.[5] Many cancer cells have a weakened spindle assembly checkpoint and interference with these diminished checkpoints, for example by pharmacological inhibition of SAC proteins, has been hypothesized as a strategy to kill cancer cells.[4,5]

BUB1 participates in SAC signaling by recruiting several SAC proteins to unattached kinetochores.[8–11] Kinetochores, which are located at the centromeres of sister chromatids, are thought to catalyze mitotic checkpoint complex (MCC) formation.[12] The MCC is an inhibitor of the anaphase promoting complex/cyclosome (APC/C) and inhibition of APC/C results in a mitotic arrest.[12] BUB1 has been found to phosphorylate histone H2A[13], but the relevance of its kinase activity in SAC function has been debated.[14–16] Recently, the first BUB1 inhibitor, BAY1816032 (**Figure 4.1A,B**), was published and its potential as anti-cancer agent was investigated in a mouse xenograft model of human triple-negative breast cancer.[6] BAY1816032 was found to synergistically inhibit tumor growth when combined with paclitaxel, but did not exhibit efficacy as a single agent.[6] Of interest, residual BUB1 activity may be sufficient for a functional SAC[17], which suggests that more potent BUB1 inhibitors could act as single agents.

In **Chapter 2**, the results of a high-throughput screening campaign, to identify novel BUB1 inhibitors, are described. AT-9283 (**1**) (**Figure 4.1A**) was the most potent hit with a half maximal inhibitory concentration (IC_{50}) of 219 nM. AT-9283 has been investigated in several phase I clinical trials in patients with leukemia, solid tumors and non-Hodgkin's lymphoma[18–21] and as such may represent an excellent starting point for a new drug discovery program. AT-9283 potently inhibits multiple kinases, including FGFR1-3, VEGFR1-3, FLT3, PDGFRα, JAK2-3 and ABL.[22] AT-9283 is also a potent inhibitor of Aurora kinase (Aurora) A and B, which

both have an important role during mitosis. Aurora A participates in centrosome maturation, separation and bipolar spindle assembly. Aurora B is responsible for correcting erroneous kinetochore-microtubule attachments, contributes to SAC signaling and is involved in cytokinesis.[23–28] The binding mode of AT-9283 in Aurora A is shown in **Figure 4.1C** and involves three hydrogen bonds between the benzimidazole-pyrazole scaffold and amide backbones of hinge amino acids Glu211 and Ala213.[22] In addition, the urea linker adopts a cis/trans configuration, which causes the cyclopropyl group to bind in the front pocket of Aurora A. The gatekeeper residue of Aurora A, Leu210, is relatively large and thereby hinders access to its back pocket (**Figure 4.1C**). In contrast, BUB1 has a small gatekeeper residue (Gly866) and this feature can be exploited by inhibitors to target its back pocket (**Figure 4.1B**), which will contribute to their selectivity for BUB1. In this chapter, the structure-activity relationship (SAR) of AT-9283 (**1**) on BUB1 kinase activity was systematically investigated by changing its molecular structure. This resulted in the discovery of novel and highly potent BUB1 inhibitors.

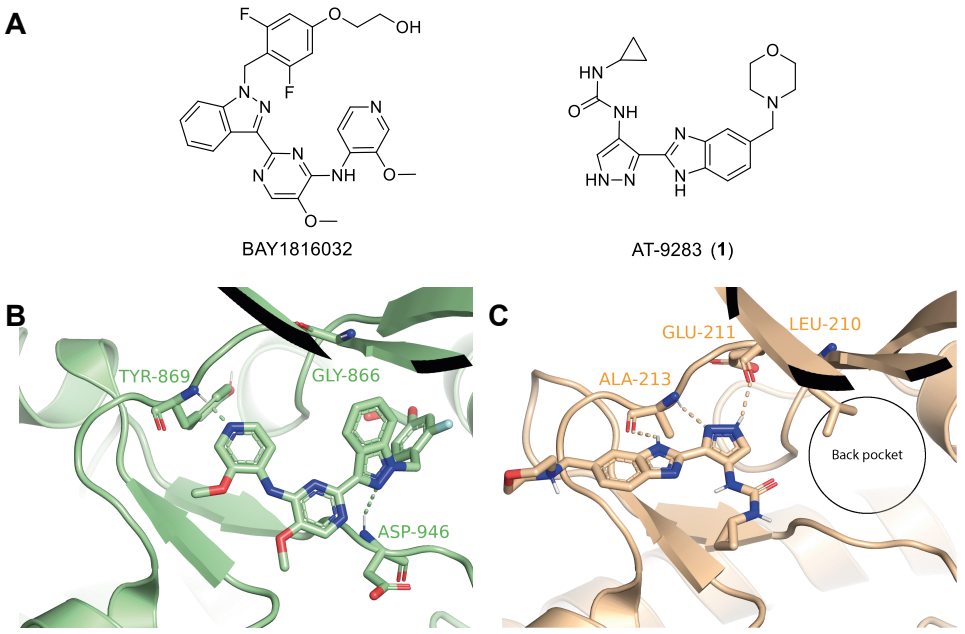

Figure 4.1 | (A) Chemical structures of BAY1816032 and AT-9283 (**1**). **(B)** Crystal structure of BAY1816032 bound to BUB1 (PDB code: 6F7B).[6] **(C)** Crystal structure of AT-9283 bound to Aurora A (PDB code: 2W1G).[22] Hydrogen bonds are indicated by dashed lines.

Results & Discussion

Biochemical evaluation of structural analogues 2 – 60 of AT-9283

To study the structure-activity relationship (SAR) of AT-9283 (**1**), analogues **2** – **60** were synthesized by employing different synthetic routes (see Experimental section). Compounds **2** – **60** were subsequently evaluated in a biochemical fluorescence polarization assay to

determine the half maximal inhibitory concentrations (IC_{50}) as described in **Chapter 2**. The data are reported in **Table 4.1** – **Table 4.6** and activities are expressed as pIC_{50} ± SEM (N=2, n=2).

To tune the activity towards BUB1 and to dial out potency for Aurora A, the cyclopropyl urea of **1** was replaced with a 2-chloro-4-aminopyrimidine as bioisoster, in which the chlorine was hypothesized to be oriented towards the back pocket of BUB1 and functioned as a synthetic handle to introduce substituents. Surprisingly, synthetic intermediate 2-chloropyrimidine **2** already showed a 3-fold increase in potency compared to compound **1** (**Table 4.1**). A disjunctive approach was applied to identify essential functional groups that constitute the pharmacophore of compound **2**. Removal of the morpholine (**3**) reduced potency 2.5-fold, which suggested that the morpholine does not only act as a solubilizer, but may also have important interactions with BUB1. Substituting the benzimidazole of **3** for a phenyl amide (**4**) was not tolerated and reduced potency over 30-fold. Methyl amide **5** further reduced potency and similarly, compound **6**, which completely lacked the benzimidazole was inactive. Overall, the benzimidazole was found to be crucial for activity, probably due to hydrogen bond formation between the benzimidazole –NH and the hinge region of BUB1 and also the morpholine contributed to the potency.

The SAR of the 2-chloropyrimidine in **3** was systematically investigated by evaluation of compound **7** – **14** (**Table 4.2**). Removal of the chlorine (**7**), one (**8**, **9**) or two nitrogens (**10**) of the pyrimidine moiety significantly reduced the potency or led to a completely inactive compound. Addition of an extra chlorine at the 5-position (**12**), but not at the 6-position (**11**), was tolerated. Introducing electron donating groups at the 5-position, such as a methyl (**13**) or methoxy group (**14**), significantly increased potency. Altogether, this suggested that the 2-chloropyrimidine substituent has favorable hydrophobic interactions with the back pocket, the pyrimidine nitrogens may form hydrogen bond interactions and the pyrimidine ring could form pi-pi or pi-sigma interactions with for example amino acids present in the β-strands 1–3.

Table 4.1 | Half maximal inhibitory concentrations (expressed as pIC_{50} ± SEM) of **1** – **6** determined by a fluorescence polarization assay on BUB1 kinase activity (N=2, n=2).

ID	Structure	pIC_{50} ± SEM	app. K_i (nM)[a]	cLogP[b]	LipE[c]	tPSA[d]	MW[e]
1	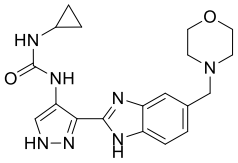	6.66 ± 0.02	77	0.4	6.7	102	381
2	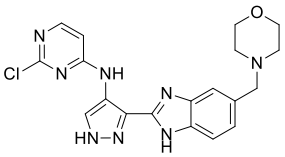	7.13 ± 0.01	26	1.6	5.9	98	411
3	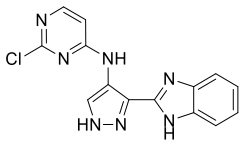	6.73 ± 0.03	66	2.1	5.1	86	312
4	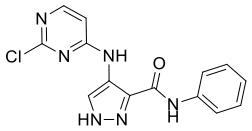	5.23 ± 0.04	2070	1.9	3.8	90	315
5	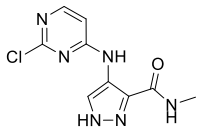	< 5	–	0.2	–	90	253
6	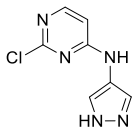	< 5	–	0.7	–	61	196

[a] Apparent K_i ; [b] cLogP, calculated by DataWarrior (v.5.2.1); [c] Lipophilic efficiency, defined as $\mathrm{LipE} = \mathrm{app.\,p}K_i - \mathrm{cLogP}$; [d] Topological polar surface area (Å^2), calculated by Chemdraw (v.19.1); [e] Molecular weight (g/mol).

Table 4.2 | Half maximal inhibitory concentrations (expressed as pIC_{50} ± SEM) of **7** – **14** determined by a fluorescence polarization assay on BUB1 kinase activity (N=2, n=2).

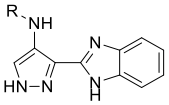

ID	R =	pIC_{50} ± SEM	app. K_i (nM)[a]	cLogP[b]	LipE[c]
3	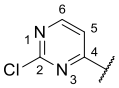	6.73 ± 0.03	66	2.1	5.1
7	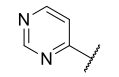	5.87 ± 0.04	474	1.2	5.1
8	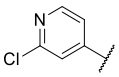	5.71 ± 0.03	685	2.1	4.0
9	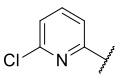	5.20 ± 0.03	2228	2.5	3.2
10	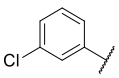	< 5	–	3.0	–
11	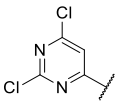	5.61 ± 0.07	865	2.8	3.3
12	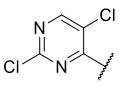	6.56 ± 0.02	96	2.7	4.4
13	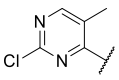	7.60 ± 0.02	9	2.4	5.6
14	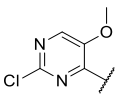	7.52 ± 0.01	11	2.0	6.0

[a] Apparent K_i ; [b] cLogP, calculated by DataWarrior (v.5.2.1); [c] Lipophilic efficiency, defined as $\mathrm{LipE} = \mathrm{app.\,p}K_i - \mathrm{cLogP}$.

To explore the size of the back pocket, the activity of compounds **15** – **25** (**Table 4.3**) was evaluated. Substitution of the chlorine with an acetylene (**15**) retained potency, whereas substitution with a larger phenyl ring (**16**) reduced potency about 3-fold. Compounds with a phenoxy (**17**) or benzyloxy (**18**) group were tolerated, but not with a phenethyloxy group (**19**), which suggested that a flexible ether linker is allowed, but that its length should not be too large. Substituting phenoxy analogue **17** with a chlorine on the *ortho*-, *meta*- or *para*-position (**23** – **25**) further reduced potency. Similarly, replacing the chlorine of **2** with small heteroaryl groups, such as pyrazole (**20**) or thiophenes (**21**, **22**) showed on average a 10-fold decrease in potency as well.

Table 4.3 | Half maximal inhibitory concentrations (expressed as pIC_{50} ± SEM) of **15** – **25** determined by a fluorescence polarization assay on BUB1 kinase activity (N=2, n=2).

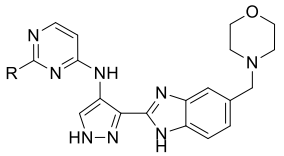

ID	R =	pIC_{50} ± SEM	app. K_i (nM)[a]	cLogP[b]	LipE[c]	tPSA[d]	MW[e]
2		7.13 ± 0.01	26	1.6	5.9	98	411
15		6.96 ± 0.03	39	0.8	6.6	98	400
16		6.61 ± 0.04	86	2.4	4.6	98	453
17	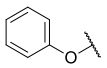	6.45 ± 0.01	125	2.6	4.3	107	469
18	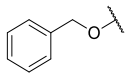	6.41 ± 0.04	138	2.5	4.3	107	483
19	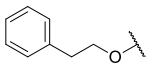	5.67 ± 0.02	758	2.9	3.2	107	497
20		6.08 ± 0.03	294	0.6	5.9	114	442
21		6.28 ± 0.02	184	2.2	4.5	98	459
22		6.11 ± 0.02	272	2.5	4.1	98	459
23	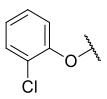	6.01 ± 0.02	347	3.2	3.3	107	503
24	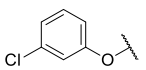	6.18 ± 0.02	234	3.2	3.5	107	503
25	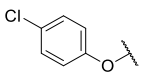	6.09 ± 0.03	289	3.2	3.4	107	503

[a] Apparent K_i ; [b] cLogP, calculated by DataWarrior (v.5.2.1); [c] Lipophilic efficiency, defined as $\mathrm{LipE} = \mathrm{app.}\, pK_i - \mathrm{cLogP}$; [d] Topological polar surface area (Å^2), calculated by Chemdraw (v.19.1); [e] Molecular weight (g/mol).

Based on the activity of phenylpyrimidine **16** (Table 4.3), a series of substituted phenylpyrimidines (**26** – **43**) was explored (Table 4.4). For synthetic reasons, this series was initially based on the scaffold lacking the morpholine group. Compared to **16**, unsubstituted phenyl **26** showed a 5-fold decrease in potency upon removal of the morpholine. Substituting the phenyl ring with either electron withdrawing or electron donating groups at

the *para* position (**27** – **30**) further decreased the potency. The presence of small lipophilic groups at the *ortho* (**31**, **32**) or *meta* position (**34**, **35**) retained or gained potency, respectively, whereas compounds with a methoxy-substituent at the *ortho* (**33**) or *meta* (**36**) position lost or retained potency, respectively. A *meta*-pyridyl (**37**) was also not allowed and neither a larger lipophilic isopropyl-substituent (**38**) or a 3,5-dichloro-substitution (**39**) were tolerated. In addition, introduction of fused rings (**40** – **43**) did not improve potency.

Table 4.4 | Half maximal inhibitory concentrations (expressed as pIC_{50} ± SEM) of **26** – **43** determined by a fluorescence polarization assay on BUB1 kinase activity (N=2, n=2).

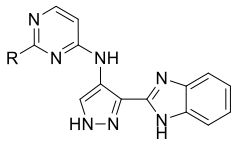

ID	R =	pIC_{50} ± SEM	app. K_i (nM)[a]	ID	R =	pIC_{50}	app. K_i (nM)[a]
26		5.91 ± 0.03	435	**35**	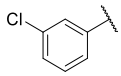	6.37 ± 0.05	151
27	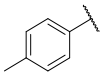	5.74 ± 0.05	643	**36**	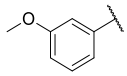	6.08 ± 0.07	290
28	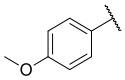	5.54 ± 0.03	1016	**37**		< 5	–
29	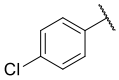	5.19 ± 0.05	2306	**38**	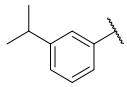	5.08 ± 0.04	2923
30	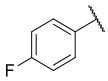	< 5	–	**39**	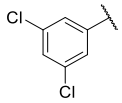	< 5	–
31		5.99 ± 0.03	362	**40**	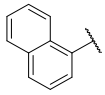	5.98 ± 0.02	370
32		6.05 ± 0.02	314	**41**	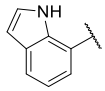	< 5	–
33		5.59 ± 0.03	908	**42**	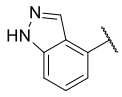	5.64 ± 0.04	809
34	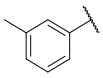	6.32 ± 0.03	167	**43**	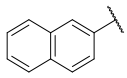	5.21 ± 0.06	2182

[a] Apparent K_i

Next, *meta*-substituents were further explored and introduced to the original benzimidazole-morpholine scaffold (**44** – **50**, Table 4.5). Substituting phenyl **16** with a chlorine (**44**) or acetylene (**45**) at position 3, significantly increased the potency. Strong electron withdrawing groups at this position (**46**, **47**) resulted in a substantial drop in activity. Introduction of an additional fluorine at position 2 in compound **48** or **49** increased the potency 10-fold, thereby providing single digit nanomolar potent inhibitors. Of note, changing the position of the fluorine to position 6 (**50**) boosted potency even further with a 25-fold increase compared to **16**.

Table 4.5 | Half maximal inhibitory concentrations (expressed as pIC_{50} ± SEM) of **44** – **50** determined by a fluorescence polarization assay on BUB1 kinase activity (N=2, n=2).

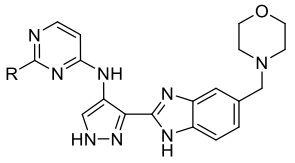

ID	R =	pIC_{50} ± SEM	app. K_i (nM)[a]	cLogP[b]	LipE[c]	tPSA[d]	MW[e]
16	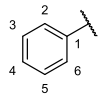	6.61 ± 0.04	86	2.4	4.6	98	453
44	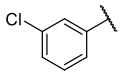	7.08 ± 0.02	29	3.0	4.5	98	487
45	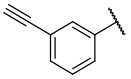	7.57 ± 0.01	10	2.5	5.5	98	477
46	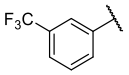	6.03 ± 0.03	329	3.3	3.2	98	521
47	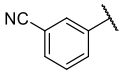	6.24 ± 0.02	201	2.3	4.4	122	478
48	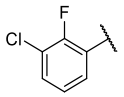	7.63 ± 0.02	8	3.1	4.9	98	505
49	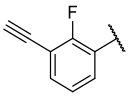	7.89 ± 0.01	5	2.6	5.7	98	495
50	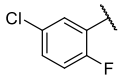	8.03 ± 0.01	3	3.1	5.4	98	505

[a] Apparent K_i ; [b] cLogP, calculated by DataWarrior (v.5.2.1); [c] Lipophilic efficiency, defined as $\mathrm{LipE} = \mathrm{app.\,p}K_i - \mathrm{cLogP}$; [d] Topological polar surface area (Å^2), calculated by Chemdraw (v.19.1); [e] Molecular weight (g/mol).

Finally, a series of compounds (**51** – **60**, **Table 4.6**) with mono-, di- and trisubstituted phenyl groups was investigated on the 5-methoxypyrimidine moiety, since this was the most potent scaffold (based on **Table 4.2** and **Table 4.5**). Compounds **51** – **57** showed a 2- to 10-fold increased potency compared to their corresponding analogues **44** – **50**. Compounds with a trifluoromethyl or nitril at position 3 (**53**, **54**) showed the lowest activity among this series, which may be attributed to their strong electron withdrawing property. Potencies of molecules with chlorine (**51**) or acetylene (**52**) at position 3 were high and could be further increased by introducing a fluorine at position 6 (**57**, **58**), but not at position 2 (**55**, **56**). Accordingly, the activities of difluorophenyl substituted **59** and **60** were similar to monofluorophenyl substituted **57** and **58**, respectively. Of note, the most active compounds identified here (**57** – **60**) showed activities near the detection limit (pIC_{50} of 8.79) of the biochemical assay. Overall, this series of substituted phenyl-5-methoxypyrimidines showed several inhibitors with pIC_{50} values near 8 or higher and compound **58** was the most potent inhibitor in this study.

Crystal structure of 58 bound to BUB1

To investigate the binding mode of **58**, the crystal structure of this inhibitor bound to the kinase domain of human BUB1 was determined at 2.1 Å resolution. The inhibitor was well defined by the electron density (**Figure 4.2A**). Compound **58** binds in the ATP-pocket of BUB1 and interacts with the hinge region via multiple hydrogen bonds. The benzimidazole forms a hydrogen bond with the backbone carbonyl of hinge amino acid Tyr869 and hydrophobic interactions were observed with the side chains of Leu793 and Ile924 (**Figure 4.2B**). Two more hydrogen bonds are formed between the pyrazole and hinge residues Tyr869 and Glu867. In addition, the hydrophobic side chains of Val819 and Ile924 interact with the pyrazole. The amine between the pyrazole and pyrimidine forms an intramolecular hydrogen bond with the benzimidazole nitrogen which favors the planar conformation of the molecule. The pyrimidine is sandwiched between the hydrophobic side chains of Ile945 and Val801 and the *N*1 nitrogen forms a water-mediated hydrogen bond with Lys821. The substituted phenyl ring occupies the so called gate area[29] which is located between residues of the DFG-motif (DLG in BUB1), the conserved lysine in β-sheet 3 (Lys821) and the gatekeeper residue (Gly866). The phenyl ring interacts with several residues in close proximity to this area, such as Lys821, Met850 and Phe852. Due to the small size of BUB1's gatekeeper residue (Gly866), a small pocket is available which is occupied by the acetylene moiety (**Figure 4.2D**). This allows for non-polar interactions with Val819, Lys821, Met850, Phe852 and Leu864 and explains the potency increase upon substituting the phenyl ring with this acetylene. The fluorine interacts with aforementioned water molecule, the –NH of DLG-Asp946 as well as with the alkyl side chain of Ile945. To classify **58** to a specific type of kinase inhibitor, the regulatory (R) spine was inspected, which is a spatial motif that consist of four non-consecutive hydrophobic residues.[30] Previous crystallography studies of ADP bound to BUB1's kinase domain revealed that both unphosphorylated[31] and pSer969[32] BUB1 had an assembled R-spine. This indicated that BUB1 is a constitutively active kinase.[32] Compound

58 was found to preserve this assembled R-spine upon BUB1 binding (**Figure 4.2C**) and can therefore be classified as a type I inhibitor.[33]

Table 4.6 | Half maximal inhibitory concentrations (expressed as pIC_{50} ± SEM) of **51** – **60** determined by a fluorescence polarization assay on BUB1 kinase activity (N=2, n=2).

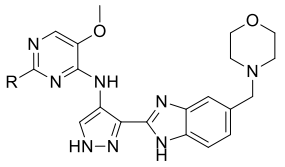

ID	R =	pIC_{50} ± SEM	app. K_i (nM)[a]	cLogP[b]	LipE[c]	tPSA[d]	MW[e]
51	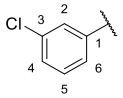	7.96 ± 0.02	3.9	3.0	5.4	107	517
52	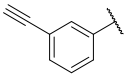	8.37 ± 0.02	1.5	2.5	6.2	107	507
53	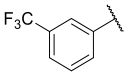	6.80 ± 0.03	55	3.2	4.0	107	551
54	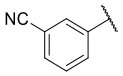	7.24 ± 0.04	20	2.2	5.5	131	508
55	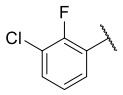	7.98 ± 0.02	3.7	3.1	5.3	107	535
56	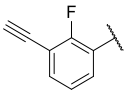	8.34 ± 0.02	1.6	2.6	6.1	107	525
57	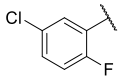	8.57 ± 0.02	0.94	3.1	5.9	107	535
58	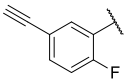	8.68 ± 0.02	0.74	2.6	6.4	107	525
59	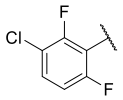	8.62 ± 0.03	0.84	3.2	5.8	107	553
60	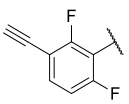	8.64 ± 0.02	0.80	2.7	6.3	107	543

[a] Apparent K_i ; [b] cLogP, calculated by DataWarrior (v.5.2.1); [c] Lipophilic efficiency, defined as $\mathrm{LipE} = \mathrm{app.\,p}K_i - \mathrm{cLogP}$; [d] Topological polar surface area (Å^2), calculated by Chemdraw (v.19.1); [e] Molecular weight (g/mol).

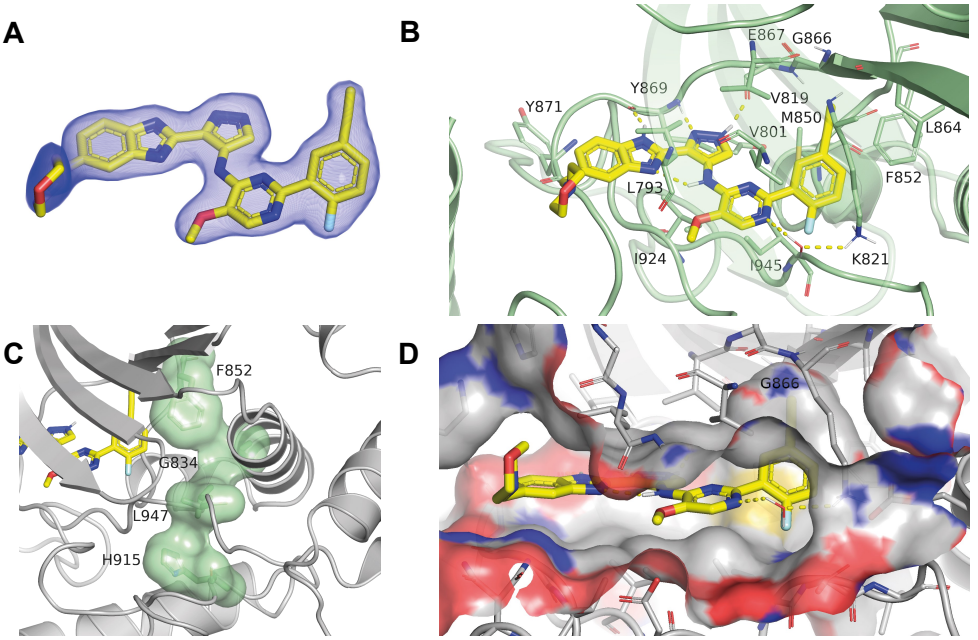

Figure 4.2 | Crystal structure of 58 bound to the kinase domain of human BUB1. **(A)** $2mF_o$-DF_c electron density map of **58** contoured at 1.0 σ. **(B)** Crystal structure of **58** bound to BUB1. Hydrogen bonds are visualized by dashed lines (yellow) and a water molecule is represented by small sticks. β-sheets 1–3 are semi-transparent for visualization purposes. **(C)** Representation of the surface around the R-spine amino acids of BUB1 reveals an intact R-spine. **(D)** Representation of the surface around amino acids within 8 Å from **58**.

Conclusion

In this chapter, the structure-activity relationship of AT-9283 (**1**) on BUB1 kinase inhibition was investigated by the synthesis and biochemical evaluation of 59 analogues based on its structure. Replacement of the cyclopropyl urea of AT-9283 (**1**) by a 2-chloro-4-aminopyrimidine (compound **2**) increased potency. The benzimidazole moiety was found to be crucial for activity and forms a hydrogen bond with the backbone of hinge amino acid Tyr869 of BUB1. In addition, the *N*1 nitrogen of the pyrimidine ring was crucial for activity and forms a water-mediated hydrogen bond with the side chain of Lys821. Substituting the chlorine of the 2-chloro-4-aminopyrimidine **2** with a phenyl ring and optimization of its substitution pattern increased potency significantly. Overall, five compounds (**56** – **60**) matched or exceeded the activity of BAY1816032. Among these compounds, **58** was the most active BUB1 inhibitor found in this study and a crystal structure of this molecule revealed that **58** can be classified as a type I inhibitor.[33] A summary of the activities and physicochemical properties of compound **58**, AT-9283 (**1**) and BAY1816032 is shown in **Table 4.7**. Compound **58** is 100-fold more active compared to original hit **1**. Compound **58** showed excellent activity (apparent K_i = 0.74 nM) and favorable physicochemical properties (cLogP = 2.6, LipE = 6.4, tPSA = 107 Å^2) which are in a similar range or better than the published[6] BUB1 inhibitor BAY1816032.

Table 4.7 | Properties of initial hit **1**, BAY1816032 and optimized hit **58**.

ID	R =	pIC_{50} ± SEM	app. K_i (nM)[a]	cLogP[b]	LipE[c]	tPSA[d]	MW[e]
1	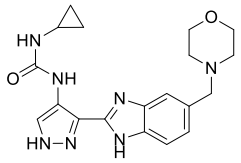	6.66 ± 0.02	77	0.4	6.7	102	381
BAY-1816032	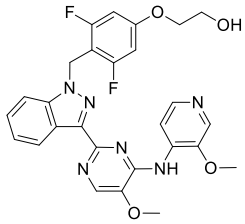	8.34 ± 0.03	1.6	2.9	5.8	113	535
58	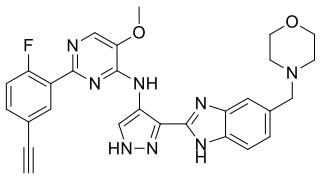	8.68 ± 0.02	0.74	2.6	6.4	107	525

[a] Apparent K_i ; [b] cLogP, calculated by DataWarrior (v.5.2.1); [c] Lipophilic efficiency, defined as $\mathrm{LipE} = \mathrm{app.\,p}K_i - \mathrm{cLogP}$; [d] Topological polar surface area (Å^2), calculated by Chemdraw (v.19.1); [e] Molecular weight (g/mol).

Acknowledgements

Jessica Domínguez Alfaro is kindly acknowledged for her contribution with regard to compound synthesis and biochemical testing, and Hans van den Elst for HPLC purifications and HRMS measurements. From the Netherlands Cancer Institute (NKI), Misbha Ud Din Ahmad is kindly acknowledged for protein production, crystallization, data collection, structure solution and refinement, Robbie Joosten for final structure refinement, Patrick Celie and Danique Ammerlaan for help in the framework of the Oncode facility Proteins4Oncode and Anastassis Perrakis for supervision.

Experimental – Biochemistry

Biochemical evaluation of BUB1 inhibitors

Assays were performed in 384-well plates (Greiner, black, flat bottom, 781076) by sequential addition (final concentrations are indicated) of inhibitor (5 µL, 0.3 nM – 1 µM or 3 nM – 10 µM), BUB1/BUB3 (5 µL, 3.26 nM, Carna Biosciences (05-187), lot: 15CBS-0644 D), ATP (5 µL, 15 µM) and BUB1/BUB3 substrate (5 µL, 75 nM, Carna Biosciences (05-187MSSU)), all as 4x working solutions. The final concentration of DMSO was 1%. Assay reactions were stopped by addition of IMAP progressive binding reagent (20 µL, 1200x diluted (see below), Molecular Devices (R8155), lot: 3117896). Each assay included the following controls: (i) a background control (treated with vehicle instead of inhibitor and BUB1/BUB3 substrate), (ii) MIN controls (treated with 5 µM BAY1816032 (MedChem Express) as inhibitor, defined as 0% BUB1 activity) and (iii) MAX controls (treated with vehicle instead of inhibitor, defined as 100% BUB1 activity). All inhibitors were tested in two separate assays and all inhibitor concentrations were tested in duplicate per assay (N=2, n=2).

For each assay, assay buffer (AB) was freshly prepared and consisted of 20 mM HEPES (prepared by diluting 1 M HEPES, pH 7.2), 5 mM $MgCl_2$, 0.01% (v/v) Tween-20 and 1 mM DTT. Stocks of inhibitors (in DMSO) were diluted in AB to obtain 4x working solutions (4% DMSO) and 5 µL was added to the assay plate. BUB1/BUB3 (3.26 µM (486 µg/mL) in storage buffer) was diluted in AB to obtain 13.0 nM of which 5 µL was added to all wells of the assay plate. The assay plate was centrifuged (1 min, 200 *g*) and incubated at RT for 30 min. ATP (4 mM in MilliQ) was diluted in AB to obtain 60 µM of which 5 µL was added to each well. BUB1/BUB3 substrate (1 mM) was diluted in 20 mM HEPES (prepared by diluting 1 M HEPES (pH 7.2) in MilliQ) to obtain 80 µM (this solution was freshly prepared every assay) and further diluted in AB to obtain 300 nM after which 5 µL was added to each well of the assay plate except for background control wells. The assay plate was centrifuged (1 min, 200 *g*) and incubated at RT in the dark for 180 min. IMAP progressive binding buffer A (5x) and IMAP progressive binding buffer B (5x) were mixed in a ratio to obtain 30% buffer A and 70% buffer B, which was subsequently diluted 5x in MilliQ. IMAP progressive binding reagent was diluted 600x in aforementioned mixture of buffer A and B (to obtain a 2x working solution) of which 20 µL was added to each well of the assay plate. The assay plate was centrifuged (1 min, 200 *g*) and incubated at RT in the dark for 90 min. Fluorescence polarization was measured on a CLARIOstar plate reader using the following settings: (i) optic settings → excitation = F: 482-16, dichroic = F: LP 504, emission = F: 530-40, (ii) optic = top optic, (iii) speed/precision = maximum precision, (iv) focus adjustment was performed for every assay and (v) gain adjustment was done by setting the target mP value to 35 mP for one of the MIN control wells. Data was normalized between MIN and MAX controls and data was plotted using GraphPad Prism 8.0 using "Nonlinear regression (curve fit)" and "log(inhibitor) vs. normalized response – Variable slope" to determine pIC_{50} values. The Cheng-Prusoff equation was used to calculate K_i values using 8.13 µM as the apparent K_M of ATP (determined as described in the experimental section of **Chapter 2**).

Protein production

The synthetic construct for BUB1, spanning the residues 725-1085, was ordered from GeneArt (Thermo Fisher). The construct was subcloned in pET-NKI-His-3C-LIC vector[34] for expression in Sf9 cells. Recombinant bacmid for transfection was generated according to the protocols in the Invitrogen manual (Bac-to-Bac® Baculovirus Expression Systems). For expression, 3 L of Sf9 cells were transfected with the P1 virus. The cultures were grown at 27°C for 72 hours. Cells were harvested by centrifugation at 1200 *g* for 10 min and pellets were stored at -20°C. All the steps of the protein purification were carried out at 4 °C. The cell pellet was resuspended in lysis buffer (40 mM HEPES (pH 7.5), 500 mM NaCl, 1 mM TCEP) supplemented with protease inhibitor tablet (Roche). Cells were lysed by sonication (5 sec ON/ 15 sec OFF; 50% amplitude; 150 sec). The lysate was centrifuged at 53,000 *g* for 45 min. The supernatant was incubated with 1 mL of Ni-Sepharose beads on a rotator for 1 h. The beads were washed with 50 mL of washing buffer (40 mM HEPES (pH 7.5), 1 M NaCl, 20 mM imidazole, 1 mM TCEP). The NaCl concentration of the beads was reduced to 100 mM by washing with buffer containing 40 mM HEPES (pH 7.5) and 1 mM TCEP and the protein was eluted with the elution buffer (40 mM HEPES (pH 7.5), 100 mM NaCl, 500 mM imidazole, 1 mM TCEP). The elution fractions containing the protein were pooled together and the

His-tag was cleaved by incubation overnight with 3C-protease. The protein was filtered through a 0.22 µm filter, the NaCl concentration was reduced to 50 mM by dilution with buffer containing 40 mM HEPES pH 7.5 and 1 mM TCEP, and the protein was loaded on a 6 mL ResourceQ anion exchange column. The protein eluted in the flowthrough which was concentrated and loaded onto a Superdex S75 10/300 Increase column, equilibrated with buffer containing 20 mM HEPES (pH 7.5), 150 mM NaCl and 1 mM TCEP. Peak fractions were analyzed by SDS-PAGE, pooled together and concentrated to 14.2 mg/mL.

Crystallization, data collection, structure solution and refinement

Protein was mixed with **58** (1:2 molar ratio, protein:compound), incubated at room temperature for 5 min and briefly centrifuged before setting up the plates. Crystals were obtained in 0.1 M Tris (pH 7.0), 19% PEG 6000 and 0.2 M $CaCl_2$. Crystals were cryoprotected in mother liquor containing 20% glycerol before flash cooling in liquid N_2. Data were collected at the MASSIF-1 beamline at the European synchrotron radiation facility (ESRF). The structure was solved by molecular replacement using BUB1 (PDB: 6F7B)[6] as the search model. Molecular replacement and initial refinement was done by the MOLREP[35] program of the ccp4i2 suite[36]. The CIF and the PDB files for the ligands were generated from the SMILES strings by AceDRG[37]. Ligand fitting was done in Coot[38] and subsequent refinement cycles were carried out in REFMAC[39]. Data collection and refinement statistics are reported in **Table 4.8**. Figures were generated using PyMOL[40].

Table 4.8 | Data collection and structure refinement statistics for human BUB1 kinase domain-**58** complex.

Data Collection[a]	
Wavelength (Å)	0.965
Resolution (Å)	46.52-2.10 (2.16-2.10)
Space Group	P 2_1 2 2_1
Unit Cell a, b, c (Å)	50.27, 59.32, 122.77
Unit Cell α, β, γ (°)	90, 90, 90
$CC_{1/2}$	0.998 (0.536)
R_{merge}	0.044 (0.572)
<I/σ(I)>	16.6 (2.0)
Completeness (%)	99.3 (99.2)
Multiplicity	3.8 (3.6)
Refinement	
Reflections work/test (nr)	20813/1111
Atoms protein/ligand/other (nr)	2803/39/91
B-factors protein/ligand/other ($Å^2$)	50/42/48
R_{work}/R_{free}[b] (%)	20.4/24.9
rmsZ bond lengths/bond angles[b]	0.260/0.519
Model validation	
Ramachandran plot, preferred/outliers[c] (%)	97.3/0.0
Ramachandran Z-score[d]	-0.11 ± 0.50
Rotamers preferred/outliers (%)[c]	96.4/0.3
Rotamer Z-score[d]	-1.06 ± 0.52
Clashscore (%-ile)[c]	99
MolProbity score (%-ile)[c]	100

[a] Values in parenthesis describe the highest resolution shell, [b] As reported by Refmac, [c] As reported by MolProbity, [d] As reported by Tortoize.

Experimental – Chemistry

Synthetic routes

The synthesis of **2** (Scheme 4.1) started from **61**, which is an intermediate for the synthesis of AT-9283 (**1**) and was synthesized as described in Chapter 2.[22] The amines of **61** were protected by SEM groups resulting in the formation of four separable regioisomers (Scheme 4.1). All of these regioisomers could be used in subsequent reactions. The nitro group of **62** was reduced to an amine, which was subsequently used for a nucleophilic aromatic substitution with 2,4-dichloropyrimidine to form **64**. The SEM groups were removed under acidic conditions and required a second reaction with ethylenediamine to completely remove the *N*-hydroxymethyl intermediate[41] to obtain **2**. Intermediate **64** was used to synthesize substituted pyrimidines **15** – **22** by employing series of transformations. A Sonogashira reaction was used to introduce a TMS-protected acetylene (**65**). Suzuki couplings led to the formation of phenylpyrimidine **66** and thiophenes **71** and **72**. Nucleophilic aromatic substitutions were used to synthesize **67** – **70**. Corresponding deprotection methods yielded **15** – **22**.

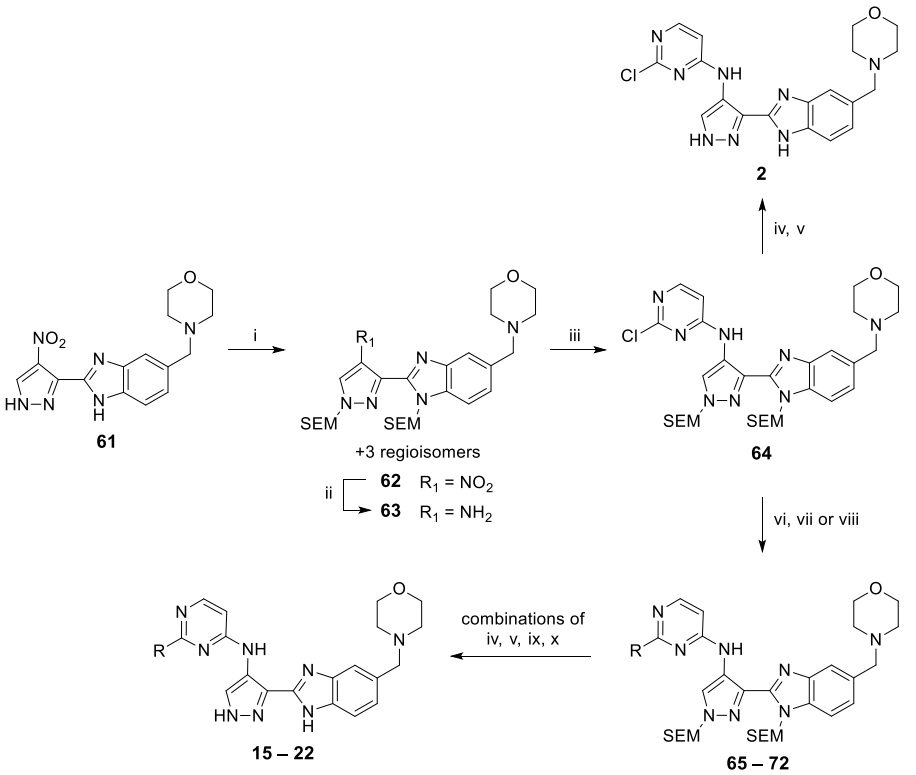

Scheme 4.1 | Synthesis of 2 and 15 – 22. Reagents and conditions: **i)** SEM-Cl, DIPEA, DCM, 0°C → RT, 60%. **ii)** 10% Pd/C, MeOH, 72 – 99%. **iii)** 2,4-dichloropyrimidine, DIPEA, EtOH, 40°C, 54%. **iv)** TFA, DCM. **v)** ethylenediamine, DCM/MeOH (1:1), 50°C. **vi)** ethynyltrimethylsilane, Et_3N, $PdCl_2(PPh_3)_2$, CuI, 89°C, 17%. **vii)** phenylboronic acid (for **66**), thiophene-3-boronic acid pinacol ester (for **71**) or thiophene-2-boronic acid pinacol ester (for **72**), K_2CO_3, Pd(dppf)Cl_2·DCM, dioxane/H_2O (4:1), 90°C. **viii)** phenol (for **67**), benzyl alcohol (for **68**), phenethyl alcohol (for **69**) or 1*H*-pyrazole (for **70**), NaH, dioxane, 0 → 90°C, 44 – 71%. **ix)** TBAF, THF, RT or 80°C (sealed tube). **x)** HCl (in dioxane), EtOH or DCM, 50°C (sealed tube).

Next, compound **3**, which lacked the morpholine group, was synthesized as depicted in Scheme 4.2. Benzene-1,2-diamine was coupled to 4-nitro-1*H*-pyrazole-3-carboxylic acid and subsequently cyclized to form benzimidazole **73**. *N*-SEM protection resulted in the formation of two separable regioisomers and by applying the reaction sequence as described for the synthesis of **2** (Scheme 4.1), compound **3** was obtained. Aminopyrazole **75** and chloropyrimidine **76** were used for the synthesis of a small library

of analogues (**7** – **14** and **26** – **43**, respectively). Synthesis of **7** – **14** proceeded via **77** – **84** by performing either Buchwald-Hartwig aminations or nucleophilic aromatic substitutions with **75** followed by SEM deprotection. For the synthesis of **26** – **43**, Suzuki couplings with **76** provided intermediates **85** – **102** and subsequent SEM deprotection afforded the desired products.

Compound **4** and **5**, in which the benzimidazole was substituted by amides, were synthesized as depicted in **Scheme 4.3** and started with esterification of 4-nitro-1*H*-pyrazole-3-carboxylic to obtain **103**. *N*-SEM protection and subsequent SEM-switch procedure[42] led to the formation of one SEM-protected regioisomer (**104**). Nitro reduction and nucleophilic aromatic substitution formed chloropyrimidine **106**. Mild ester hydrolysis[43] resulted in the formation of **107** of which the carboxylic acid was coupled to different amines to form **4** and **5** after SEM deprotection. A part of this reaction sequence was performed to synthesize compound **6** (**Scheme 4.4**), which completely lacked the benzimidazole.

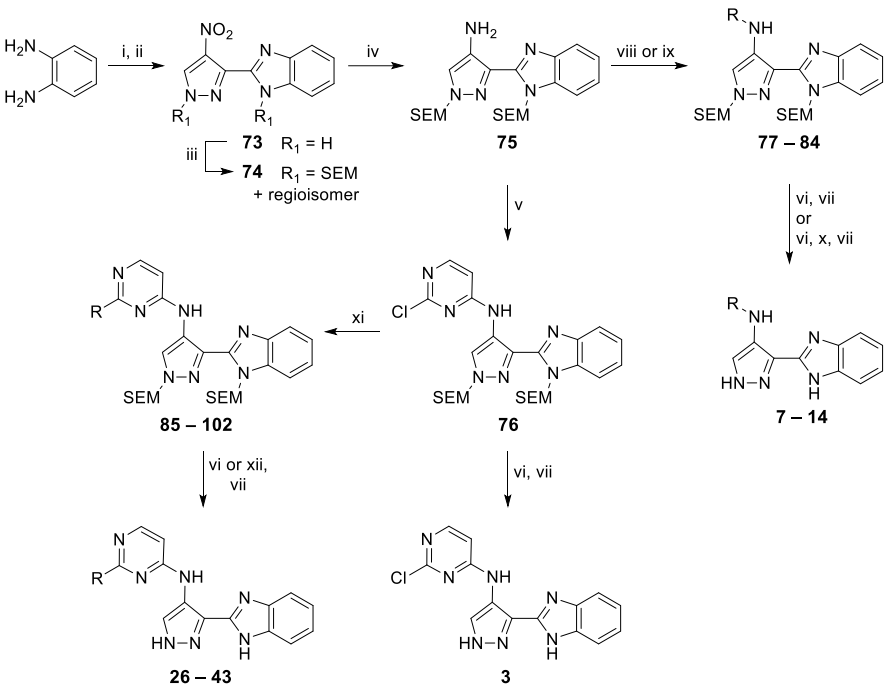

Scheme 4.2 | Synthesis of 3, 7 – 14 and 26 – 43. Reagents and conditions: **i)** 4-nitro-1*H*-pyrazole-3-carboxylic acid, EDC·HCl, HOBt, DMF. **ii)** AcOH, 118°C, 70%. **iii)** SEM-Cl, DIPEA, DCM, 0°C → RT, 81%. **iv)** 10% Pd/C, MeOH, 95%. **v)** 2,4-dichloropyrimidine, DIPEA, EtOH, 40°C, 74%. **vi)** TFA, DCM. **vii)** ethylenediamine, DCM/MeOH (1:1), RT or 50°C, 20% – quant. **viii)** corresponding (hetero)aryl halide, xantphos, Cs_2CO_3, $Pd(OAc)_2$, DMF, 90°C, 34 – 76%. **ix)** corresponding chloropyrimidine, DIPEA, EtOH, 40°C or 50°C, 45 – 63%. **x)** HCl (aq.), MeOH. **xi)** corresponding boronic acid (pinacol ester), K_2CO_3, $Pd(dppf)Cl_2$·DCM, dioxane/H2O (4:1), 90°C, 18 – 92%. **xii)** TBAF, THF, 80°C (sealed tube).

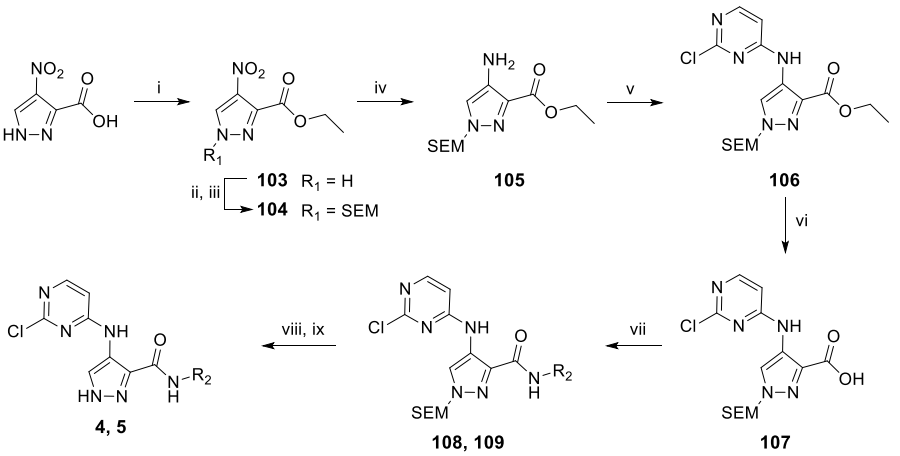

Scheme 4.3 | Synthesis of 4 and 5. Reagents and conditions: **i)** $SOCl_2$, EtOH, 0°C – RT, 96%. **ii)** SEM-Cl, DIPEA, DCM, 0°C – RT. **iii)** SEM-Cl (5 mol%), MeCN, 95°C, microwave irradiation, 83%. **iv)** 10% Pd/C, EtOH, 99%. **v)** 2,4-dichloropyrimidine, DIPEA, EtOH, 70°C, 90%. **vi)** Et_3N, LiBr, MeCN/H2O (50:1), quant. **vii)** aniline (for **108**) or methylamine (33 wt. % in EtOH, for **109**), EDC·HCl, DCM, 58 – 75%. **viii)** TFA, DCM. **ix)** ethylenediamine, DCM/MeOH (1:1), 50°C, 46 – 52%.

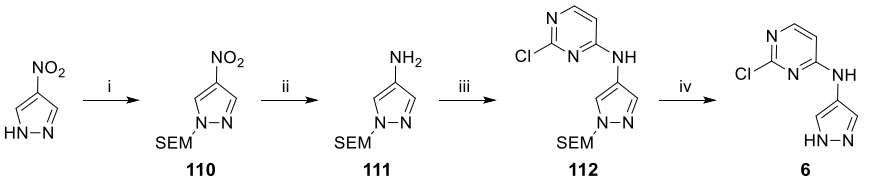

Scheme 4.4 | Synthesis of 6. Reagents and conditions: **i)** SEM-Cl, DIPEA, DCM, 0°C – RT, quant. **ii)** 10% Pd/C, MeOH, 82%. **iii)** 2,4-dichloropyrimidine, DIPEA, EtOH, 64%. **iv)** TFA, DCM, 86%.

Alternatively to the synthetic route as depicted in **Scheme 4.1**, a small library of analogues (**23** – **25** and **44** – **58**) containing the morpholine group was synthesized according to **Scheme 4.5**. The ester of **104** (synthesized as depicted in **Scheme 4.3**) was saponified, coupled to 4-(morpholinomethyl)benzene-1,2-diamine (synthesized as described in **Chapter 2**) and cyclized to form benzimidazole **113**. Nitro reduction and subsequent nucleophilic aromatic substitution with either 2,4-dichloropyrimidine or 2,4-dichloro-5-methoxypyrimidine yielded **115** and **126**, respectively. From these two intermediates, either Suzuki couplings or nucleophilic aromatic substitutions were performed to obtain substituted pyrimidines. Of these substituted pyrimidines, 3-chlorophenyl analogues **123**, **127**, **131** and **133** were also subjected to a Stille coupling to transform the chlorine into a TMS protected acetylene to form **124**, **128**, **132** and **134**.[44,45] SEM or TMS and SEM group deprotection of intermediates **116** – **125** and **127** – **134** resulted in the formation of **23** – **25** and **44** – **58**. Synthesis of **59** and **60** was performed according to **Scheme 4.6** and started from **105** (synthesized as depicted in **Scheme 4.3**) to which a 2-chloro-5-methoxypyrimidine was introduced. Subsequent coupling of the chloro-difluorophenyl proved to be challenging due to deboronation of the boronic acid and therefore required different Suzuki coupling conditions[46] to yield **137**. Analogous to the synthetic route as depicted in **Scheme 4.5**, compound **59** and **60** were subsequently obtained.

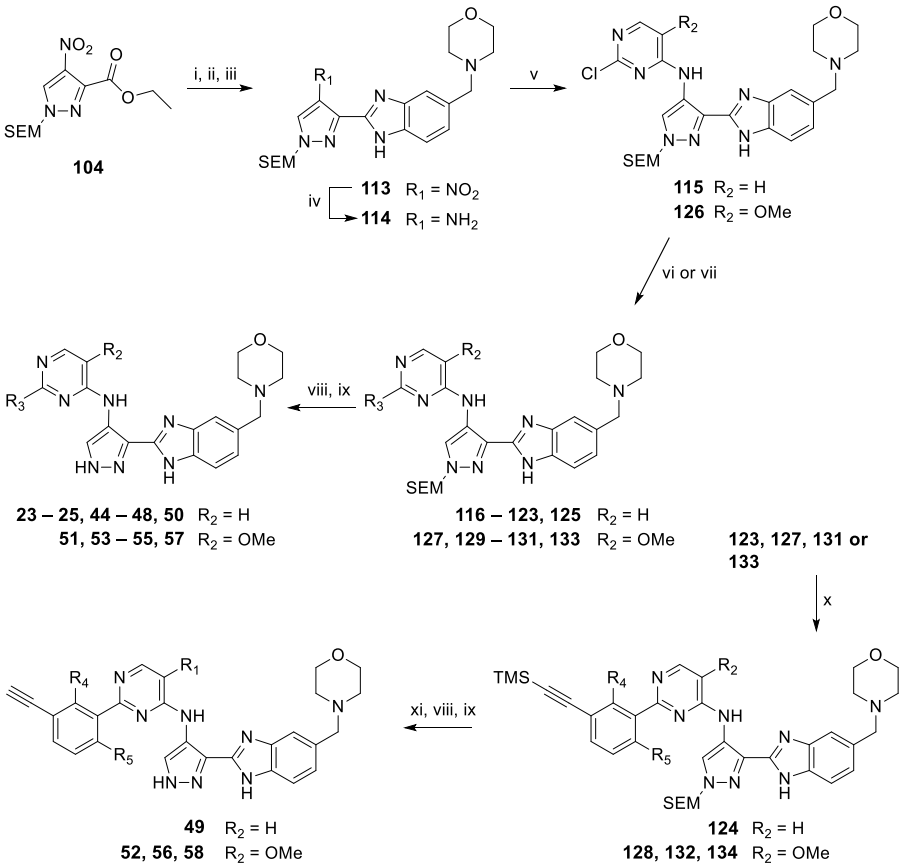

Scheme 4.5 | Synthesis of 23 – 25 and 44 – 58. Reagents and conditions: **i)** LiOH, MeOH/H2O (1:1). **ii)** 4-(morpholinomethyl)benzene-1,2-diamine (synthesized in **Chapter 2**, compound 28), EDC·HCl, HOBt, DMF. **iii)** AcOH, 118°C, 58%. **iv)** 10% Pd/C, MeOH, 97%. **v)** 2,4-dichloropyrimidine (for **115**) or 2,4-dichloro-5-methoxypyrimidine (for **126**), DIPEA, EtOH, RT or 40°C, 66 – 70%. **vi)** corresponding boronic acid (pinacol ester), K_2CO_3, Pd(dppf)Cl_2·DCM, dioxane/H2O (4:1), 90°C, 28 – 82%. **vii)** 2-chlorophenol (for **116**), 3-chlorophenol (for **117**) or 4-chlorophenol (for **118**), K_2CO_3, dioxane, 120°C (sealed tube), 81 – 91%. **vii)** TFA, DCM. **ix)** ethylenediamine, DCM/MeOH (1:1), RT or 50°C, 44 – 90%. **x)** trimethyl((tributylstannyl)ethynyl)silane, XPhos, $Pd_2(dba)_3$, THF, 135°C (sealed tube), 78 – 96%. **xi)** TBAF, THF.

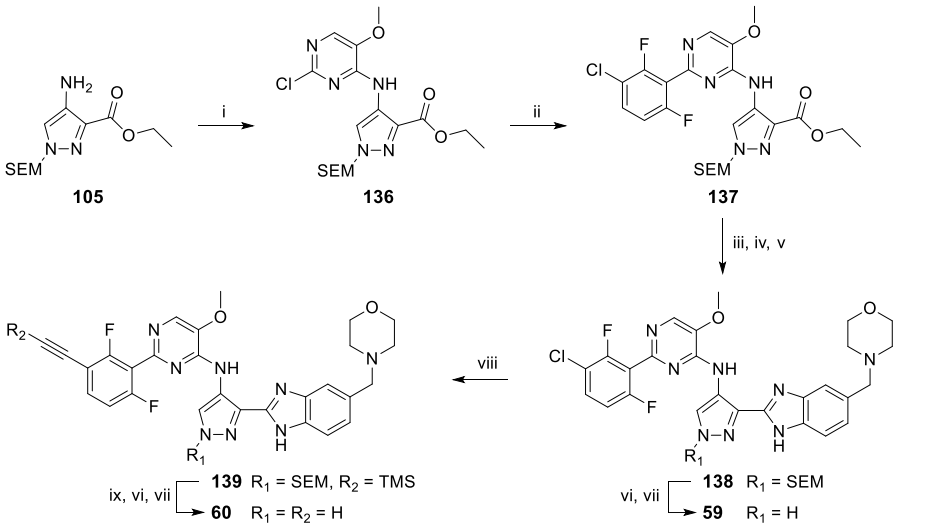

Scheme 4.6 | Synthesis of 59 and 60. Reagents and conditions: **i)** 2,4-dichloro-5-methoxypyrimidine, DIPEA, EtOH, 50°C, 78%. **ii)** (3-chloro-2,6-difluorophenyl)boronic acid, K_2CO_3, XPhos Pd G2, THF/H2O (1:2). **iii)** LiOH, MeOH/H2O (1:1), DCM, 65°C. **iv)** 4-(morpholinomethyl)benzene-1,2-diamine (synthesized in **Chapter 2**, compound 28), EDC·HCl, HOBt, DMF. **v)** AcOH, 118°C, 9% over two steps. **vi)** TFA, DCM. **vii)** ethylenediamine, DCM/MeOH (1:1), 88 – 95%. **viii)** trimethyl((tributylstannyl)ethynyl)silane, XPhos, $Pd_2(dba)_3$, THF, 135°C (sealed tube), quant. **ix)** TBAF, THF.

General procedures

All reagents were purchased from chemical suppliers (Fluorochem, Sigma-Aldrich, Merck, Fisher Scientific) and used without further purification. Solvents (Honeywell, VWR, Biosolve) indicated with "dry" were stored on activated 3 Å (EtOH) or 4 Å (other solvents) molecular sieves (8 to 12 mesh, Acros Organics). Solvents indicated by "degassed" were sonicated while bubbling N_2 through the solvent for 20 min. All reactions were performed at room temperature (RT) under a nitrogen atmosphere, unless stated otherwise. Microwave reactions were performed in a Biotage Initiator+ reactor. Reactions were monitored by thin layer chromatography (TLC, silica gel 60, UV_{254}, Macherey-Nagel, ref: 818333) and compounds were visualized by UV absorption (254 nm and/or 366 nm) or spray reagent (permanganate (5 g/L $KMnO_4$, 25 g/L K_2CO_3)) followed by heating. Alternatively, reactions were monitored by liquid chromatography-mass spectrometry (LCMS), either on a Thermo Finnigan (Thermo Finnigan LCQ Advantage MAX ion-trap mass spectrometer (ESI+) coupled to a Surveyor HPLC system (Thermo Finnigan) equipped with a Nucleodur C18 Gravity column (50x4.6 mm, 3 µm particle size, Macherey-Nagel)) or a Thermo Fleet (Thermo LCQ Fleet ion-trap mass spectrometer (ESI+) coupled to a Vanquish UHPLC system). LCMS eluent consisted of MeCN in 0.1% TFA (aq.) and LCMS methods were as follows: 0.5 min cleaning with starting gradient, 8 min using specified gradient (linear), 2 min cleaning with 90% MeCN in 0.1% TFA (aq.). LCMS data is reported as follows: instrument (Finnigan or Fleet), gradient (% MeCN in 0.1% TFA (aq.)), retention time (t_r) and mass (as m/z: $[M+H]^+$). Purity of final compounds was determined to be ≥ 95% by integrating UV intensity of spectra generated by either of the LCMS instruments. ^1H and ^{13}C NMR spectra were recorded on a Bruker AV300 (300 and 75 MHz, respectively), Bruker AV400 (400 and 101 MHz, respectively), Bruker AV500 (500 and 126 MHz, respectively) or Bruker AV600 (600 and 150 MHz, respectively) NMR spectrometer. NMR samples were prepared in deuterated chloroform, methanol or DMSO. Chemical shifts are given in ppm (δ) relative to residual protonated solvent signals ($CDCl_3$ → δ 7.260 (^1H), δ 77.160 (^{13}C), MeOD → δ 3.310 (^1H), δ 49.000 (^{13}C), DMSO → δ 2.500 (^1H), δ 39.520 (^{13}C)). Data was processed by using MestReNova (v. 14) and is reported as follows: chemical shift (δ), multiplicity, coupling constant (*J* in Hz) and integration. Multiplicities are abbreviated as follows: s = singlet, br s = broad singlet, d = doublet, dd = doublet of doublets, ddd = doublet of doublet of doublets, td = triplet of doublets, t = triplet, dt = doublet of triplets, q = quartet, hept = heptet, m = multiplet, br m = broad multiplet. For some molecules about 1:1 rotamer and/or tautomer peaks were observed, resulting in extra splitting of peaks. For these compounds, chemical shifts were

reported as ranges and multiplicity was denoted by "2x", followed by the multiplicities specified above (i.e. 2x d = twice a doublet). The reported coupling constant corresponds to either of the multiplet peaks (of note, coupling constants were the same for both multiplet peaks). Purification was done either by manual silica gel column chromatography (using 40-63 µm, 60 Å silica gel, Macherey-Nagel) or automated flash column chromatography on a Biotage Isolera machine (using pre-packed cartridges with 40-63 µm, 60 Å silica gel (4, 12, 25 or 40 g), Screening Devices). High-performance liquid chromatography (HPLC) purifications were performed on either an Agilent 1200 preparative HPLC system (equipped with a Gemini C18 column (250x10 mm, 5 µm particle size, Phenomenex) coupled to a 6130 quadrupole mass spectrometer) or a Waters Acquity UPLC system (equipped with a Gemini C18 column (150x21 mm, 5 µm particle size, Phenomenex) coupled to a SQ mass spectrometer). Specified gradients for HPLC purifications (MeCN in 0.2% TFA (aq.)) were linear (5 mL/min for 12 min (Agilent) or 25 mL/min for 10 min (Waters)). High resolution mass spectrometry (HRMS) spectra were recorded through direct injection of a 1 µM sample either on a Thermo Scientific Q Exactive Orbitrap equipped with an electrospray ion source in positive mode coupled to an Ultimate 3000 system (source voltage = 3.5 kV, capillary temperature = 275 °C, resolution R = 240,000 at m/z 400, external lock, mass range m/z = 150-2000) or on a Synapt G2-Si high definition mass spectrometer (Waters) equipped with an electrospray ion source in positive mode (ESI-TOF) coupled to a NanoEquity system with Leu-enkephalin (m/z = 556.2771) as internal lock mass. The eluent for HRMS measurements consisted of a 1:1 (v/v) mixture of MeCN in 0.1% formic acid (aq.) using a flow of 25 mL/min. Compound names were generated by ChemDraw (v. 19.1.21).

General procedure A – SEM deprotection

SEM-protected amine starting material was dissolved in DCM (2 mL) after which TFA (2 mL) was added dropwise. The mixture was stirred for the indicated time and subsequently concentrated under a flow of N_2. The mixture was suspended in EtOAc (25 mL) and poured into 1 M $NaHCO_3$ (aq.) (20 mL). The organic layer was separated and the water layer extracted with EtOAc (1 or 2x25 mL). The combined organic layers were concentrated as such, suspended/dissolved in 1:1 MeOH/DCM (2 mL) and transferred to a microwave vial. Ethylenediamine (50 µL, 746 µmol) was added after which the vial was sealed and the mixture was stirred at 50°C for 30 – 60 min. The mixture was poured into H_2O (20 mL) and when required, brine (0.5 – 1 mL) was added, and the product extracted with EtOAc (2x20 mL). The combined organic layers were concentrated as such. Purification was performed as indicated.

General procedure B – SEM deprotection

SEM-protected amine starting material was dissolved in DCM (0.5 mL) after which TFA (0.5 mL) was added dropwise. The mixture was stirred for the indicated time and subsequently quenched by addition of sat. $NaHCO_3$ (aq.) (20 mL). The product was extracted with EtOAc (2x20 mL) and the combined organic layers were concentrated as such. The mixture was suspended/dissolved in 1:1 MeOH/DCM (3 mL) and ethylenediamine (50 µL, 746 µmol) was added after which the mixture was stirred for 1 h. The mixture was poured into H_2O (20 mL) and when required, brine (1 mL) was added, and the product extracted with EtOAc (2x20 mL). The combined organic layers were concentrated as such. Purification was performed as indicated.

General procedure C – SEM deprotection

A microwave vial was charged with SEM-protected amine starting material dissolved in DCM (± 0.2 M) after which HCl (4 M in dioxane, 24 eq.) was added and the vial was sealed. The mixture was stirred at 50°C for the indicated time and subsequently concentrated. The mixture was dissolved in $CHCl_3$ (20 mL) and poured into 1 M $NaHCO_3$ (aq.) (20 mL). The organic layer was separated and the water layer extracted with $CHCl_3$ (20 mL). The combined organic layers were concentrated as such and purified as indicated.

General procedure D – TMS and SEM deprotection

TMS- and SEM-protected starting material was dissolved in TBAF (1 M in THF, 0.5 mL) and the mixture was stirred for 1.5 h. The mixture was poured into H_2O (20 mL) and brine (1 mL), and the intermediate extracted with EtOAc (2x15 mL). The combined organic layers were concentrated as such. The intermediate was dissolved in DCM (0.5 mL) after which TFA (0.5 mL) was added dropwise. The mixture

was stirred for the indicated time and subsequently quenched by addition of sat. $NaHCO_3$ (aq.) (15 mL). The product was extracted with EtOAc (2x15 mL) and the combined organic layers were concentrated as such. The mixture was suspended/dissolved in 1:1 MeOH/DCM (3 mL) and ethylenediamine (50 µL, 746 µmol) was added after which the mixture was stirred for 1 h. The mixture was poured into H_2O (20 mL) and when required, brine (1 mL) was added, and the product extracted with EtOAc (2x15 mL). The combined organic layers were concentrated as such. Purification was performed as indicated.

General procedure E – Buchwald coupling

A microwave vial was charged with **75** (150 mg, 326 µmol), Cs_2CO_3 (319 mg, 979 µmol), xantphos (28.3 mg, 48.9 µmol), indicated (hetero)aryl halide (359 µmol) and DMF (1.5 mL). N_2 was bubbled through the mixture for 1 min after which $Pd(OAc)_2$ (7.3 mg, 33 µmol) was added. N_2 was bubbled through the mixture for 30 sec after which the vial was sealed and the mixture was stirred at 90°C for 16 h. The mixture was diluted in EtOAc (15 mL) and filtered over Celite. The filtrate was diluted in EtOAc (15 mL) and poured into H_2O (30 mL) and brine (2 mL). The organic layer was isolated and the water layer extracted with EtOAc (30 mL). The combined organic layers were washed with brine (30 mL) and concentrated as such. Purification was performed as indicated.

General procedure F – Suzuki coupling

A microwave vial was charged with **76** (300 mg, 524 µmol), K_2CO_3 (290 mg, 2.10 mmol), corresponding boronic acid (786 µmol) and $Pd(dppf)Cl_2$·DCM (30 mg, 37 µmol) after which the vial was sealed. The tube was evacuated and backfilled with argon (3x) via a Schlenk setup after which degassed 4:1 dioxane/H_2O (2.6 mL) was added. The mixture was heated to 90°C, stirred for 16 h and subsequently poured into H_2O (30 mL). The product was extracted with EtOAc (2x30 mL) and the combined organic layers were concentrated as such. Purification was performed as indicated.

General procedure G – Suzuki coupling

A microwave vial was charged with 2-chloropyrimidine analogue (1 eq.), K_2CO_3 (4 eq.), corresponding boronic acid (pinacol ester) (1.02 – 1.5 eq.) and 4:1 dioxane/H_2O (0.2 M). N_2 was bubbled through the mixture for 1 min after which $Pd(dppf)Cl_2$·DCM (0.07 eq.) was added. N_2 was bubbled through the mixture for 30 sec after which the vial was sealed. The mixture was heated to 90°C, stirred for indicated time and subsequently poured into H_2O (20 mL) and when required, brine (1 mL) was added. The product was extracted with DCM (2x20 mL) and the combined organic layers were concentrated as such. Purification was performed as indicated.

General procedure H – Stille coupling

A microwave vial was charged with chlorophenyl analogue (1 eq.), XPhos (0.6 eq.) and $Pd_2(dba)_3$ (0.15 eq.). THF (0.15 M) was added and N_2 was bubbled through the mixture for 30 sec after which the vial was sealed and trimethyl((tributylstannyl)ethynyl)silane (1.5 eq.) was added via syringe. The vial was put into a heating block and the top of the vial was covered with cotton and aluminum foil. The mixture was heated to 135°C and stirred for 1 h. The mixture was cooled down to RT and filtered over a pre-wetted mixture of K_2CO_3/silica gel (~750 mg/10 mL). Elution was done by EtOAc (10 mL) and subsequently 5% MeOH/EtOAc (4x10 mL). Product containing fractions were concentrated and purified as indicated.

General procedure I – Nucleophilic aromatic substitution

A microwave vial was charged with **115** (90.0 mg, 166 µmol), K_2CO_3 (46.0 mg, 333 µmol) and dry dioxane (0.2 mL) after which corresponding phenol analogue (1.05 eq.) was added. The vial was sealed, stirred at 120°C for 16 h and subsequently poured into H_2O (20 mL). The product was extracted with DCM (2x20 mL) and the combined organic layers were concentrated as such. Purification was done by automated column chromatography (0 – 25% MeOH/DCM) to afford the product.

1-Cyclopropyl-3-(3-(5-(morpholinomethyl)-1*H*-benzo[*d*]imidazol-2-yl)-1*H*-pyrazol-4-yl)urea (1)

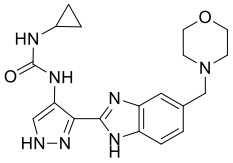

The title compound was synthesized as described in **Chapter 2** (compound 1).

2-Chloro-*N*-(3-(5-(morpholinomethyl)-1*H*-benzo[*d*]imidazol-2-yl)-1*H*-pyrazol-4-yl)pyrimidin-4-amine (2)

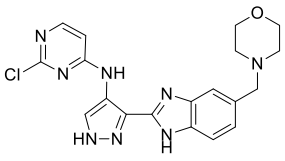

64 (77.0 mg, 115 µmol) was dissolved in DCM (1 mL) after which TFA (1 mL) was added and the mixture was stirred for 16 h. The mixture was concentrated under a flow of N_2, suspended in $CHCl_3$ (20 mL) and poured into sat. $NaHCO_3$ (aq.) (20 mL). The organic layer was separated, the water layer extracted with $CHCl_3$ (2x20 mL) and the combined organic layers were concentrated as such. The crude was dissolved in 1:1 MeOH/DCM (1 mL) and transferred to a microwave vial. Ethylenediamine (50 µL, 746 µmol) was added after which the vial was sealed and the mixture was stirred at 50°C for 1 h. The mixture was poured into H_2O (20 mL) and the product extracted with $CHCl_3$ (2x15 mL). The combined organic layers were concentrated as such. The crude was purified by automated column chromatography (2 – 15% MeOH/DCM) to afford the product (22.4 mg, 54.5 µmol, 48%). ^{1}H NMR (500 MHz, MeOD) δ 8.37 (br s, 1H), 8.05 (d, *J* = 6.0 Hz, 1H), 7.71 – 7.42 (br m, 2H), 7.22 (d, *J* = 8.2 Hz, 1H), 6.86 (d, *J* = 5.9 Hz, 1H), 3.71 – 3.66 (m, 4H), 3.61 (s, 2H), 2.53 – 2.45 (m, 4H). ^{13}C NMR (126 MHz, MeOD) δ 161.50, 156.76, 148.86, 144.09, 134.27, 132.68, 126.01, 125.62, 122.23, 121.96, 120.76, 119.16, 113.36, 112.05, 107.18, 67.71, 64.71, 54.61 (not all quaternary carbons were observed). LCMS (Fleet, 0 → 50%): t_r = 4.74 min, m/z: 411.3. HRMS $[C_{19}H_{19}ClN_8O + H]^+$: 411.14431 calculated, 411.1444 found.

***N*-(3-(1*H*-Benzo[*d*]imidazol-2-yl)-1*H*-pyrazol-4-yl)-2-chloropyrimidin-4-amine (3)**

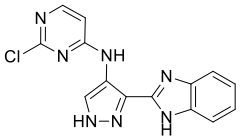

76 (58.0 mg, 101 µmol) was treated as described for the preparation of compound **2**. The crude was purified by automated column chromatography (30% EtOAc/DCM) to afford the product (8.5 mg, 27 µmol, 29%). ^{1}H NMR (500 MHz, DMSO) δ 13.51 (br s, 2H), 10.29 (br s, 1H), 8.34 (s, 1H), 8.21 (d, *J* = 5.9 Hz, 1H), 7.69 – 7.62 (m, 2H), 7.32 – 7.25 (m, 2H), 7.04 (br s, 1H). ^{13}C NMR (126 MHz, DMSO) δ 160.14 (br), 159.57, 156.93 (br), 146.40 (br), 136.91 (br), 130.98 (br), 122.90, 121.68 (br), 120.59, 114.89 (br), 106.63 (br). LCMS (Finnigan, 0 → 90%): t_r = 4.82 min, m/z: 312.1. HRMS $[C_{14}H_{10}ClN_7 + H]^+$: 312.07590 calculated, 312.0764 found.

4-((2-Chloropyrimidin-4-yl)amino)-*N*-phenyl-1*H*-pyrazole-3-carboxamide (4)

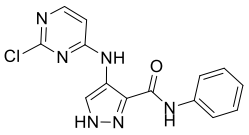

The title compound was synthesized from **108** (76.3 mg, 171 µmol) according to general procedure A (reaction time: 3 h). The crude was purified by automated column chromatography (15 – 55% EtOAc/DCM) to afford the product (28 mg, 89 mmol, 52%). ^{1}H NMR (400 MHz, DMSO) δ 13.50 (br s, 1H), 10.26 (s, 1H), 9.69 (br s, 1H), 8.35 (s, 1H), 8.16 (d, *J* = 5.9 Hz, 1H), 7.84 (d, *J* = 7.3 Hz, 2H), 7.36 – 7.30 (m, 2H), 7.22 – 7.05 (m, 2H). ^{13}C NMR (101 MHz, DMSO) δ 161.86 (br), 160.21 (br), 159.44, 156.77 (br), 138.42, 133.55 (br), 128.60, 123.76, 122.55 (br), 121.42 (br), 120.55, 106.68 (br). LCMS (Fleet, 10 → 90%): t_r = 5.91 min, m/z: 315.2. HRMS $[C_{14}H_{11}ClN_6O + H]^+$: 315.07556 calculated, 315.07550 found.

4-((2-Chloropyrimidin-4-yl)amino)-*N*-methyl-1*H*-pyrazole-3-carboxamide (5)

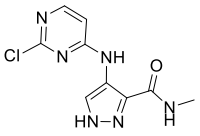

The title compound was synthesized from **109** (46.1 mg, 120 µmol) according to general procedure A (reaction time: 4 h). The crude was loaded onto Celite and purified by automated column chromatography (15 – 100% EtOAc/DCM) to afford the product (14 mg, 55 µmol, 46%). ^{1}H NMR (500 MHz, DMSO) δ 13.21 (br s, 1H), 9.76 (br s, 1H), 8.37 – 8.30 (m, 1H), 8.25 (s, 1H), 8.14 (d, *J* = 5.9 Hz, 1H), 7.06 (br s,

1H), 2.78 (d, *J* = 4.5 Hz, 3H). ^{13}C NMR (126 MHz, DMSO) δ 163.62, 159.92 (br), 159.43, 156.65 (br), 133.17 (br), 121.99, 120.81 (br), 106.59 (br), 25.29. LCMS (Fleet, 10 → 90%): t_r = 3.47 min, m/z: 253.2. HRMS $[C_9H_9ClN_6O + H]^+$: 253.05991 calculated, 253.05970 found.

2-Chloro-*N*-(1*H*-pyrazol-4-yl)pyrimidin-4-amine (6)

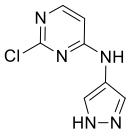

112 (70.0 mg, 215 µmol) was dissolved in DCM (1 mL) after which TFA (1 mL) was added dropwise. The mixture was stirred for 2 h and subsequently concentrated under a flow of N_2. The mixture was dissolved in $CHCl_3$ (20 mL) and poured into 1 M $NaHCO_3$ (aq.) (20 mL). The organic layer was separated and the water layer extracted with $CHCl_3$ (2x20 mL) and subsequently with EtOAc (2x20 mL). The combined organic layers were concentrated as such and purified by automated column chromatography (5% MeOH/DCM) to afford the product (36.0 mg, 184 µmol, 86%). ^{1}H NMR (500 MHz, MeOD) δ 7.97 (d, *J* = 6.0 Hz, 1H), 7.84 (br s, 2H), 6.56 (d, *J* = 6.0 Hz, 1H). ^{13}C NMR (126 MHz, MeOD) δ 162.01, 161.54, 156.20, 127.09 (br), 122.67, 106.35. LCMS (Finnigan, 0 → 90%): t_r = 4.22 min, m/z: 196.1. HRMS $[C_7H_6ClN_5 + H]^+$: 196.03845 calculated, 196.0387 found.

N-(3-(1*H*-Benzo[*d*]imidazol-2-yl)-1*H*-pyrazol-4-yl)pyrimidin-4-amine (7)

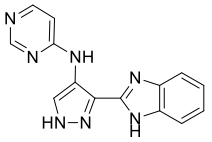

The title compound was synthesized from **77** (59.2 mg, 110 µmol) according to general procedure A (reaction time: 2 h). The crude was purified by automated column chromatography (25 – 55% EtOAc/DCM) to afford the product (27.8 mg, 80.3 µmol, 52%). ^{1}H NMR (500 MHz, DMSO) δ 13.09 (br s, 2H), 10.06 (br s, 1H), 8.72 (d, *J* = 0.8 Hz, 1H), 8.48 (s, 1H), 8.32 (d, *J* = 6.0 Hz, 1H), 7.67 – 7.58 (m, 2H), 7.25 – 7.20 (m, 2H), 7.07 (dd, *J* = 5.9, 1.2 Hz, 1H). ^{13}C NMR (126 MHz, DMSO) δ 158.38, 158.25, 155.22, 147.46, 130.68 (br), 122.21, 121.70, 120.21 (br), 114.68 (br), 107.17 (br) (not all quaternary carbons were observed). LCMS (Finnigan, 0 → 50%): t_r = 4.81 min, m/z: 278.3. HRMS $[C_{14}H_{11}N_7 + H]^+$: 278.11487 calculated, 278.11462 found.

N-(3-(1*H*-Benzo[*d*]imidazol-2-yl)-1*H*-pyrazol-4-yl)-2-chloropyridin-4-amine (8)

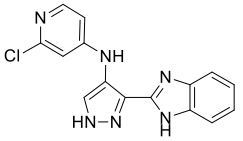

The title compound was synthesized from **78** (142 mg, 248 µmol) according to general procedure A (reaction time: 3 h). The crude was purified by automated column chromatography (70 – 100% EtOAc/DCM) to afford the product (49.5 mg, 159 µmol, 64%). ^{1}H NMR (500 MHz, DMSO) δ 13.45 (br s, 1H), 12.96 (br s, 1H), 9.36 (s, 1H), 8.28 (s, 1H), 8.01 (d, *J* = 5.6 Hz, 1H), 7.78 – 7.44 (br m, 2H), 7.24 – 7.17 (m, 2H), 6.99 – 6.92 (m, 2H). ^{13}C NMR (126 MHz, DMSO) δ 152.83, 151.38, 149.67, 146.94, 143.20 (br), 133.76 (br), 133.44, 122.61 (br), 121.75, 121.37, 118.68 (br), 111.54 (br), 108.67, 107.18. LCMS (Finnigan, 0 → 50%): t_r = 5.52 min, m/z: 311.2. HRMS $[C_{15}H_{11}ClN_6 + H]^+$: 311.08065 calculated, 311.08044 found.

N-(3-(1*H*-Benzo[*d*]imidazol-2-yl)-1*H*-pyrazol-4-yl)-6-chloropyridin-2-amine (9)

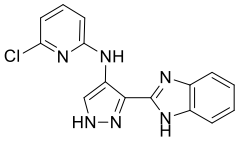

The title compound was synthesized from **79** (102 mg, 178 µmol) according to general procedure A (reaction time: 3 h). The crude was purified by automated column chromatography (15 – 50% EtOAc/DCM) to afford the product (29.6 mg, 95.2 µmol, 54%). ^{1}H NMR (500 MHz, DMSO) δ 13.06 (br s, 2H), 9.91 (br s, 1H), 8.36 (s, 1H), 7.64 (dd, *J* = 8.2, 7.5 Hz, 1H), 7.61 (br s, 2H), 7.26 – 7.19 (m, 2H), 7.00 (d, *J* = 8.2 Hz, 1H), 6.82 (d, *J* = 7.5 Hz, 1H). ^{13}C NMR (126 MHz, DMSO) δ 154.26, 148.29, 147.71, 140.34, 130.10 (br), 122.92, 122.15, 118.49 (br), 112.74, 108.64 (not all quaternary carbons were observed). LCMS (Finnigan, 10 → 90%): t_r = 5.06 min, m/z: 311.2. HRMS $[C_{15}H_{11}ClN_6 + H]^+$: 311.08065 calculated, 311.08054 found.

3-(1*H*-Benzo[*d*]imidazol-2-yl)-*N*-(3-chlorophenyl)-1*H*-pyrazol-4-amine (10)

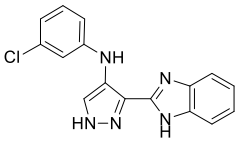

80 (125 mg, 219 µmol) was dissolved in DCM (2 mL) after which TFA (2 mL) was added and the mixture was stirred for 2.5 h. The mixture was concentrated under a flow of N_2 and subsequently dissolved in a mixture of 2 M HCl (aq.) (3 mL) and MeOH (3 mL). The mixture was stirred for 2 h and subsequently concentrated under a flow of N_2 to about half of the volume. The mixture was poured into 1 M $NaHCO_3$ (aq.) (30 mL) and the product extracted with EtOAc (2x20 mL). The combined organic layers were concentrated as such after which the mixture was dissolved in 1:1 MeOH/DCM (2 mL) and transferred to a microwave vial. Ethylenediamine (50 µL, 746 µmol) was added after which the vial was sealed and the mixture was stirred at 50°C for 1 h. The mixture was poured into H_2O (20 mL) and the product extracted with EtOAc (2x20 mL). The combined organic layers were concentrated as such and purified by automated column chromatography (25 – 60% EtOAc/DCM) to afford the product (31.6 mg, 102 µmol, 47%). ^{1}H NMR (500 MHz, MeOD) δ 7.81 (s, 1H), 7.64 – 7.55 (br m, 2H), 7.24 – 7.19 (m, 2H), 7.14 (t, *J* = 8.1 Hz, 1H), 7.00 (t, *J* = 2.1 Hz, 1H), 6.92 (ddd, *J* = 8.2, 2.3, 0.7 Hz, 1H), 6.72 (ddd, *J* = 7.9, 1.9, 0.8 Hz, 1H). ^{13}C NMR (126 MHz, MeOD) δ 148.34 (br), 147.46, 135.98, 133.30 (br), 131.44, 126.39, 123.62, 120.06 (br), 119.50, 115.81 (br), 115.09, 113.80. LCMS (Fleet, 10 → 90%): t_r = 4.77 min, m/z: 310.3. HRMS [$C_{16}H_{12}ClN_5$ + H]$^+$: 310.08540 calculated, 310.08534 found.

***N*-(3-(1*H*-Benzo[*d*]imidazol-2-yl)-1H-pyrazol-4-yl)-2,6-dichloropyrimidin-4-amine (11)**

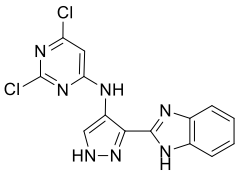

The title compound was synthesized from **81** (94.6 mg, 156 µmol) according to general procedure A (reaction time: 4 h). The crude was purified by automated column chromatography (25 – 55% EtOAc/DCM) to afford the product (27.8 mg, 80.3 µmol, 52%). ^{1}H NMR (500 MHz, DMSO) δ 13.16 (br s, 2H), 10.61 (br s, 1H), 8.33 (s, 1H), 7.80 – 7.46 (br m, 2H), 7.34 (br s, 1H), 7.26 – 7.19 (m, 2H). ^{13}C NMR (126 MHz, DMSO) δ 160.48, 158.85, 157.73, 146.94, 142.86 (br), 133.76 (br), 131.54, 122.67 (br), 121.97 (br), 121.20, 120.30, 118.63 (br), 111.59 (br), 105.07. LCMS (Fleet, 10 → 90%): t_r = 4.32 min, m/z: 346.3. HRMS [$C_{14}H_9Cl_2N_7$ + H]$^+$: 346.03693 calculated, 346.03665 found.

***N*-(3-(1*H*-Benzo[*d*]imidazol-2-yl)-1*H*-pyrazol-4-yl)-2,5-dichloropyrimidin-4-amine (12)**

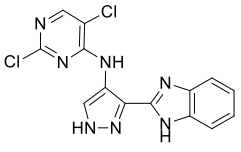

The title compound was synthesized from **82** (103 mg, 169 µmol) according to general procedure A (reaction time: 2.5 h). The crude was purified by automated column chromatography (twice, first 20 – 50% EtOAc/DCM, second 1 – 10% MeOH/DCM) to afford the product (35.5 mg, 103 µmol, 61%). ^{1}H NMR (500 MHz, DMSO) δ 13.29 (br s, 2H), 11.42 (s, 1H), 8.39 (s, 1H), 8.35 (s, 1H), 7.69 (d, *J* = 7.1 Hz, 1H), 7.52 (d, *J* = 7.0 Hz, 1H), 7.28 – 7.19 (m, 2H). ^{13}C NMR (126 MHz, DMSO) δ 157.28, 154.96, 154.29, 147.14, 142.44, 133.47, 130.98, 122.91, 121.93, 120.65, 119.87, 118.46, 114.02, 111.61. LCMS (Fleet, 10 → 90%): t_r = 5.20 min, m/z: 346.3. HRMS [$C_{14}H_9Cl_2N_7$ + H]$^+$: 346.03693 calculated, 346.03683 found.

***N*-(3-(1*H*-Benzo[*d*]imidazol-2-yl)-1*H*-pyrazol-4-yl)-2-chloro-5-methylpyrimidin-4-amine (13)**

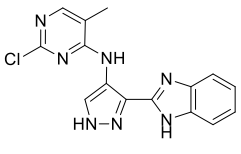

The title compound was synthesized from **83** (57.5 mg, 98.1 µmol) according to general procedure B (reaction time: 5 h). The crude was loaded onto Celite and purified by automated column chromatography (20 – 50% EtOAc/DCM) to afford the product (21.7 mg, 66.6 µmol, 68%). ^{1}H NMR (400 MHz, DMSO) δ 13.21 (br s, 2H), 10.76 (br s, 1H), 8.35 (s, 1H), 8.10 – 8.08 (2x s, 1H), 7.70 – 7.48 (br m, 2H), 7.27 – 7.20 (m, 2H), 2.34 – 2.31 (2x s, 3H). ^{13}C NMR (101 MHz, DMSO) δ 158.41, 157.34, 155.28, 147.55, 142.44 (br), 133.86 (br), 130.67, 122.42 (br), 121.59, 119.66, 118.11 (br), 114.18, 111.75 (br), 12.61. LCMS (Fleet, 10 → 90%): t_r = 4.13 min, m/z: 326.3. HRMS [$C_{15}H_{12}ClN_7$ + H]$^+$: 326.09155 calculated, 326.09140 found.

_N_-(3-(1_H_-Benzo[_d_]imidazol-2-yl)-1_H_-pyrazol-4-yl)-2-chloro-5-methoxypyrimidin-4-amine (14)

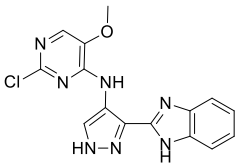

The title compound was synthesized from **84** (104 mg, 172 µmol) according to general procedure B (reaction time: 5.5 h). The crude was loaded onto Celite and purified by automated column chromatography (20 – 50% EtOAc/DCM) to afford the product (48.7 mg, 142 µmol, 83%). ^{1}H NMR (400 MHz, DMSO) δ 13.24 (br s, 2H), 10.93 (br s, 1H), 8.40 (s, 1H), 7.96 (s, 1H), 7.72 (br s, 1H), 7.52 (br s, 1H), 7.28 – 7.21 (m, 2H), 4.08 (s, 3H). ^{13}C NMR (101 MHz, DMSO) δ 150.99, 149.93, 147.34, 142.69, 139.89, 134.58, 133.59, 130.89, 122.83, 121.90, 121.07, 119.51, 118.52, 111.60, 56.89. LCMS (Fleet, 10 → 90%): t_r = 3.96 min, m/z: 342.3. HRMS [$C_{15}H_{12}ClN_7O$ + H]$^+$: 342.08646 calculated, 342.08629 found.

2-Ethynyl-_N_-(3-(5-(morpholinomethyl)-1_H_-benzo[_d_]imidazol-2-yl)-1_H_-pyrazol-4-yl)pyrimidin-4-amine (15)

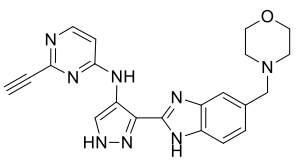

65 (19.1 mg, 26.1 µmol) was dissolved in TBAF (1 M in THF, 0.5 mL) and stirred for 2.5 h. The mixture was poured into H_2O (10 mL) and the intermediate extracted with 10% MeOH/EtOAc (3x4 mL). The combined organic layers were concentrated as such and subsequently dissolved in DCM (1.2 mL) after which TFA (0.3 mL) was added dropwise. The mixture was stirred for 6 h, subsequently poured into 1 M $NaHCO_3$ (aq.) (10 mL) and the product extracted with 10% MeOH/EtOAc (3x3 mL). The combined organic layers were concentrated as such and purified by automated column chromatography (2 – 14% MeOH/DCM) to afford the product (5.5 mg, 14 µmol, 53%). ^{1}H NMR (500 MHz, MeOD) δ 8.48 (br s, 1H), 8.18 (d, J = 6.1 Hz, 1H), 7.76 – 7.42 (br m, 2H), 7.25 (d, J = 8.2 Hz, 1H), 6.95 (d, J = 6.1 Hz, 1H), 3.72 – 3.68 (m, 4H), 3.66 (s, 1H), 3.64 (s, 2H), 2.54 – 2.47 (m, 4H). ^{13}C NMR (126 MHz, MeOD) δ 160.22, 155.23, 152.51, 149.02, 132.70 (br), 125.67 (br), 122.62, 121.89, 120.58 (br), 119.05 (br), 113.49 (br), 112.13 (br), 108.11, 83.10, 82.70, 76.34, 67.73, 64.73, 54.63 (not all quaternary carbons were observed). LCMS (Fleet, 0 → 50%): t_r = 4.25 min, m/z: 401.3. HRMS [$C_{21}H_{20}N_8O$ + H]$^+$: 401.18328 calculated, 401.18305 found.

_N_-(3-(5-(Morpholinomethyl)-1_H_-benzo[_d_]imidazol-2-yl)-1_H_-pyrazol-4-yl)-2-phenylpyrimidin-4-amine (16)

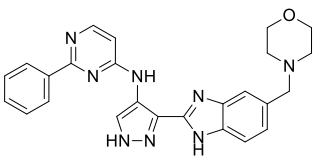

The title compound was synthesized from **66** (29.8 mg, 41.8 µmol) according to general procedure C (reaction time: 4.5 h). The crude was purified by automated column chromatography (3 – 15% MeOH/DCM) to afford the product (8.6 mg, 19 µmol, 46%). ^{1}H NMR (500 MHz, MeOD) δ 8.64 (s, 1H), 8.30 (d, J = 5.9 Hz, 1H), 8.29 – 8.25 (m, 2H), 7.70 (br s, 1H), 7.51 – 7.43 (m, 4H), 7.27 – 7.20 (br m, 1H), 6.81 (d, J = 5.9 Hz, 1H), 3.71 (t, J = 4.4 Hz, 4H), 3.64 (s, 2H), 2.58 – 2.43 (m, 4H). ^{13}C NMR (126 MHz, MeOD) δ 165.28, 159.50, 154.94, 148.06, 143.62, 143.08, 138.77, 133.85, 133.18, 132.33, 131.57, 131.14, 130.86, 128.86, 128.48, 125.47, 124.61, 122.71, 120.80, 120.08, 118.65, 112.57, 111.40, 106.03, 67.10, 64.16, 53.80. LCMS (Finnigan, 0 → 50%): t_r = 5.53 min, m/z: 453.1. HRMS [$C_{25}H_{24}N_8O$ + H]$^+$: 453.21458 calculated, 453.2146 found.

_N_-(3-(5-(Morpholinomethyl)-1_H_-benzo[_d_]imidazol-2-yl)-1_H_-pyrazol-4-yl)-2-phenoxypyrimidin-4-amine (17)

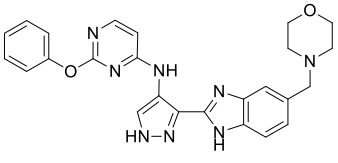

The title compound was synthesized from **67** (28.0 mg, 38.4 µmol) according to general procedure C (reaction time: 6 h). The crude was dissolved in 1:1 MeOH/DCM (1 mL) and transferred to a microwave vial. Ethylenediamine (50 µL, 746 µmol) was added after which the vial was sealed and the mixture was stirred at 50°C for 40 min. The mixture was poured into H_2O (20 mL) and the product extracted with $CHCl_3$ (2x20 mL). The combined organic layers were concentrated as such and purified by automated column chromatography (2 – 15% MeOH/DCM) to afford the product (7.5 mg, 16 µmol, 42%). ^{1}H NMR (500 MHz, $CDCl_3$) δ 11.21 – 10.75 (br m, 2H), 10.11 (s, 1H), 8.11 (d, J = 5.5 Hz, 1H), 7.70 (s, 1H), 7.54 (d, J = 15.5 Hz, 1H), 7.41 – 7.29 (m, 3H), 7.24 – 7.13 (m, 4H), 6.51 – 6.43 (2x d, J = 5.4 Hz, 1H),

3.79 – 3.52 (m, 6H), 2.56 – 2.39 (m, 4H). ^{13}C NMR (126 MHz, $CDCl_3$) δ 165.83, 160.33, 156.95, 153.50, 147.26 (br), 143.40, 142.78, 133.18, 133.05, 132.21, 132.01, 131.21 (br), 129.63, 125.20, 124.37, 122.63, 122.52, 120.72 (br), 119.94, 118.83, 111.69, 110.72, 102.41 (br), 67.09, 66.95, 63.89, 63.85, 53.70. LCMS (Finnigan, 0 → 50%): t_r = 5.88 min, m/z: 469.1. HRMS $[C_{25}H_{24}N_8O_2 + H]^+$: 469.20950 calculated, 469.2097 found.

2-(Benzyloxy)-*N*-(3-(5-(morpholinomethyl)-1*H*-benzo[*d*]imidazol-2-yl)-1*H*-pyrazol-4-yl)pyrimidin-4-amine (18)

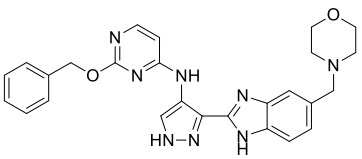

A microwave vial was charged with **68** (55 mg, 74 µmol) and TBAF (1 M in THF, 0.5 mL) was added. The vial was sealed and the mixture was stirred at 80°C for 7 days. The mixture was poured into H_2O (20 mL) and the product extracted with 10% MeOH/$CHCl_3$ (2x20 mL). The combined organic layers were concentrated as such, dissolved in 1:1 MeOH/DCM (1 mL) and transferred to a microwave vial. Ethylenediamine (50 µL, 746 µmol) was added after which the vial was sealed and the mixture was stirred at 50°C for 1 h. The mixture was poured into H_2O (20 mL) and the product extracted with $CHCl_3$ (2x20 mL). The combined organic layers were concentrated as such and purified by automated column chromatography (twice, 0 – 10% MeOH/EtOAc) to afford the product (6.9 mg, 14 µmol, 19%). ^{1}H NMR (600 MHz, MeOD) δ 8.30 (s, 1H), 8.03 (d, *J* = 5.9 Hz, 1H), 7.66 (br s, 1H), 7.50 (br s, *J* = 1.2 Hz, 1H), 7.47 – 7.44 (m, 2H), 7.38 – 7.34 (m, 2H), 7.31 – 7.28 (m, 1H), 7.24 (d, *J* = 8.1 Hz, 1H), 6.58 (d, *J* = 5.9 Hz, 1H), 5.45 (s, 2H), 3.72 – 3.68 (m, 4H), 3.65 (s, 2H), 2.55 – 2.48 (m, 4H). ^{13}C NMR (151 MHz, MeOD) δ 166.08, 161.99, 156.83, 148.77, 137.90, 129.32, 128.74, 128.32, 125.85, 125.12, 122.55, 121.55, 120.43, 119.15, 113.16, 111.85, 102.12, 69.69, 67.52, 64.56, 54.34. LCMS (Fleet, 0 → 50%): t_r = 5.48 min, m/z: 483.4. HRMS $[C_{26}H_{26}N_8O_2 + H]^+$: 483.22515 calculated, 483.22509 found.

***N*-(3-(5-(Morpholinomethyl)-1*H*-benzo[*d*]imidazol-2-yl)-1*H*-pyrazol-4-yl)-2-phenethoxypyrimidin-4-amine (19)**

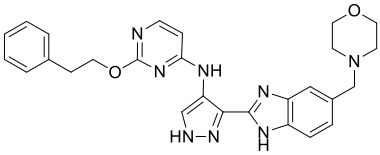

69 (30 mg, 40 µmol) was dissolved in DCM (1 mL) after which TFA (1 mL) was added dropwise and the mixture was stirred for 2.5 h. The mixture was concentrated under a flow of N_2, dissolved in 5% MeOH/DCM (20 mL), poured into 1 M $NaHCO_3$ (aq.) (20 mL) and the layers were separated. The water layer was extracted with 5% MeOH/DCM (20 mL) and the combined organic layers were concentrated as such. The mixture was dissolved in 1:1 MeOH/DCM (1 mL) and transferred to a microwave vial. Ethylenediamine (50 µL, 746 µmol) was added after which the vial was sealed and the mixture was stirred at 50°C for 80 min. The mixture was poured into H_2O (20 mL) and the product extracted with 5% MeOH/DCM (2x20 mL). The combined organic layers were concentrated as such and purified by HPLC (Agilent, 19 – 25% MeCN in 0.2% TFA (aq.)). The fractions were concentrated and traces of TFA were removed by coevaporation with 1:1 MeCN/H_2O (20 mL). The residue was dissolved in $CHCl_3$ (20 mL) and poured into 1 M $NaHCO_3$ (aq.) (20 mL). The organic layer was separated and the water layer extracted with $CHCl_3$ (20 mL). The combined organic layers were washed with brine (30 mL), dried over Na_2SO_4, filtered and concentrated to afford the product (8.6 mg, 17 µmol, 44%). ^{1}H NMR (500 MHz, $CDCl_3$) δ 11.46 – 11.12 (br m, 1H), 10.00 (s, 1H), 8.39 (s, 1H), 7.99 (d, *J* = 5.2 Hz, 1H), 7.70 (d, *J* = 5.8 Hz, 1H), 7.40 – 7.22 (m, 6H), 7.23 – 7.14 (m, 2H), 6.36 – 6.30 (m, 1H), 4.50 (t, *J* = 7.3 Hz, 2H), 3.74 – 3.64 (m, 4H), 3.63 – 3.55 (m, 2H), 3.08 (t, *J* = 7.3 Hz, 2H), 2.52 – 2.41 (m, 4H). ^{13}C NMR (126 MHz, $CDCl_3$) δ 165.26, 160.63, 156.33, 147.25 (br), 143.46, 142.85, 138.20, 133.29, 132.37, 131.91, 131.26 (br), 129.13, 128.63, 126.63, 125.19, 124.31, 122.82, 120.71 (br), 119.91, 118.82, 111.73, 110.75, 101.68, 67.87, 67.05, 66.95, 63.88, 53.71, 35.51. LCMS (Fleet, 0 → 50%): t_r = 5.76 min, m/z: 497.4. HRMS $[C_{27}H_{28}N_8O_2 + H]^+$: 497.24080 calculated, 497.24093 found.

N-(3-(5-(Morpholinomethyl)-1*H*-benzo[*d*]imidazol-2-yl)-1*H*-pyrazol-4-yl)-2-(1*H*-pyrazol-1-yl)pyrimidin-4-amine (20)

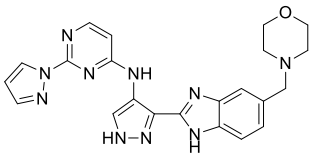

70 (60 mg, 85 µmol) was dissolved in DCM (1 mL) after which TFA (1 mL) was added dropwise and the mixture was stirred for 3 h. The mixture was concentrated under a flow of N_2, dissolved in $CHCl_3$ (20 mL) and poured into 1 M $NaHCO_3$ (aq.) (20 mL). The organic layer was separated and the water layer extracted with $CHCl_3$ (20 mL). The combined organic layers were concentrated as such, dissolved in 1:1 MeOH/DCM (1 mL) and transferred to a microwave vial. Ethylenediamine (50 µL, 746 µmol) was added after which the vial was sealed and the mixture was stirred at 50°C for 1 h. The mixture was poured into H_2O (20 mL) and the product extracted with $CHCl_3$ (2x20 mL). The combined organic layers were concentrated as such and purified by automated column chromatography (2 – 15% MeOH/DCM) to afford the product (16.5 mg, 37.3 µmol, 44%). ^{1}H NMR (500 MHz, MeOD) δ 8.60 (br s, 1H), 8.54 (d, *J* = 2.5 Hz, 1H), 8.22 (d, *J* = 5.9 Hz, 1H), 7.78 – 7.77 (m, 1H), 7.67 (br s, 1H), 7.45 (br s, 1H), 7.22 (d, *J* = 8.0 Hz, 1H), 6.77 (d, *J* = 5.8 Hz, 1H), 6.50 (dd, *J* = 2.6, 1.7 Hz, 1H), 3.72 – 3.68 (m, 4H), 3.63 (s, 2H), 2.55 – 2.46 (m, 4H). ^{13}C NMR (126 MHz, MeOD) δ 160.31 (br), 156.08, 155.93 (br), 147.96 (br), 143.61 (br), 143.35, 143.05 (br), 133.92 (br), 133.27 (br), 132.37 (br), 131.74 (br), 131.18 (br), 129.55, 125.53 (br), 124.67 (br), 122.11 (br), 121.41 (br), 120.08 (br), 118.66 (br), 112.65 (br), 111.47 (br), 108.70, 105.74 (br), 67.11, 64.17, 53.82. LCMS (Fleet, 0 → 50%): t_r = 4.78 min, m/z: 443.3. HRMS $[C_{22}H_{22}N_{10}O + H]^+$: 443.20508 calculated, 443.20488 found.

N-(3-(5-(Morpholinomethyl)-1*H*-benzo[*d*]imidazol-2-yl)-1*H*-pyrazol-4-yl)-2-(thiophen-3-yl)pyrimidin-4-amine hydrochloride (21)

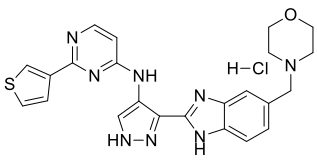

71 (43.2 mg, 60.0 µmol) was dissolved in EtOH (0.5 mL) and HCl (4 M in dioxane, 0.5 mL) was added. The mixture was stirred at 50°C for 16 h. The reaction was concentrated under a flow of N_2, subsequently 2 M K_2CO_3 (2 mL) was added and the mixture was stirred for 30 min. The mixture was diluted with DCM (10 mL) and H_2O (10 mL), the organic layer was separated and subsequently concentrated as such. The crude was purified by HPLC (Agilent, 13 – 19% MeCN in 0.2% TFA (aq.)) after which the fractions were concentrated and traces of TFA were removed by coevaporation with 1:1 MeCN/H_2O (3x20 mL). The residue was dissolved in 1:1 MeCN/H_2O (2x40 mL) to which 0.4 mL HCl (2 M aq.) was added and subsequently concentrated to afford the product as HCl salt (14.8 mg, 32.3 µmol, 54%). ^{1}H NMR (500 MHz, MeOD) δ 8.46 (s, 1H), 8.37 (s, 1H), 8.25 (d, *J* = 4.5 Hz, 1H), 8.17 (s, 1H), 7.86 (d, *J* = 6.1 Hz, 1H), 7.80 (d, *J* = 6.3 Hz, 1H), 7.60 (d, *J* = 4.1 Hz, 1H), 7.58 – 7.53 (m, 1H), 7.32 (d, *J* = 4.0 Hz, 1H), 4.55 (s, 2H), 4.05 – 3.89 (m, 4H), 3.31 – 3.21 (m, 4H). ^{13}C NMR (126 MHz, MeOD) δ 162.80, 155.49, 145.12, 143.67, 133.98, 133.36, 132.64, 130.50, 130.43, 129.39, 127.65, 127.51, 126.81, 119.69, 118.55, 115.54, 106.94, 64.41, 60.91, 52.42. LCMS (Finnigan, 0 → 50%): t_r = 5.44 min, m/z: 459.1. HRMS $[C_{23}H_{23}ClN_8OS + H]^+$: 459.17100 calculated, 459.1712 found.

N-(3-(5-(Morpholinomethyl)-1*H*-benzo[*d*]imidazol-2-yl)-1*H*-pyrazol-4-yl)-2-(thiophen-2-yl)pyrimidin-4-amine hydrochloride (22)

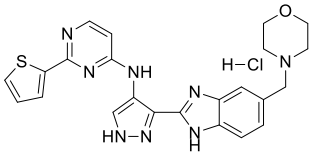

72 (59.6 mg, 82.8 µmol) was dissolved in EtOH (0.5 mL) and HCl (4 M in dioxane, 0.5 mL) was added. The mixture was stirred at 50°C for 16 h. The reaction was concentrated under a flow of N_2, subsequently 2 M K_2CO_3 (2 mL) was added and the mixture was stirred for 30 min. The mixture was diluted with DCM (10 mL) and H_2O (10 mL), the organic layer was separated and subsequently concentrated as such. The crude was purified by HPLC (Agilent, 13 – 19% MeCN in 0.2% TFA (aq.)) after which the fractions were concentrated and traces of TFA were removed by coevaporation with 1:1 MeCN/H_2O (3x20 mL). The residue was dissolved in 1:1 MeCN/H_2O (2x40 mL) to which 0.4 mL HCl (2 M aq.) was added and subsequently concentrated to afford the product as HCl salt (21.7 mg, 47.3 µmol, 57%). ^{1}H NMR (500 MHz, MeOD) δ 8.37 (s, 1H), 8.24 (d, *J* = 5.1 Hz, 1H), 8.20 – 8.12 (m, 2H), 7.87 (s, 2H), 7.81 – 7.76 (m, 1H), 7.26 (d, *J* = 5.0 Hz, 1H), 7.24 – 7.20 (m, 1H), 4.56 (s, 2H), 4.05 – 3.97 (m, 2H), 3.96 – 3.87 (m, 2H), 3.33 –

3.21 (m, 4H). ^{13}C NMR (126 MHz, MeOD) δ 162.45, 155.24, 145.39, 143.75, 136.75, 135.01, 133.72, 133.41, 133.04, 130.70, 130.44, 127.53, 119.83, 118.69, 115.63, 106.79, 64.50, 61.06, 52.53. LCMS (Finnigan, 0 → 50%): t_r = 5.54 min, m/z: 459.1. HRMS [$C_{23}H_{23}ClN_8OS$ + H]$^+$: 459.17100 calculated, 459.1710 found.

2-(2-Chlorophenoxy)-*N*-(3-(5-(morpholinomethyl)-1*H*-benzo[*d*]imidazol-2-yl)-1*H*-pyrazol-4-yl)pyrimidin-4-amine (23)

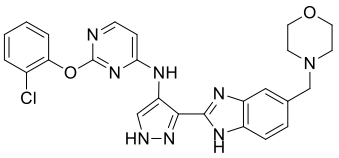

The title compound was synthesized from **116** (95.5 mg, 151 µmol) according to general procedure B (reaction time: 4 h). The crude was purified by automated column chromatography (0 – 50% MeOH/DCM) to afford the product (38.1 mg, 75.8 µmol, 50%). ^{1}H NMR (400 MHz, DMSO) δ 13.15 (br s, 1H), 13.03 – 12.94 (2x s, 1H), 10.35 – 10.14 (2x s, 1H), 8.19 – 8.15 (2x d, *J* = 5.8 Hz, 1H), 7.69 – 7.62 (m, 2H), 7.53 – 7.28 (m, 5H), 7.20 – 7.11 (2x dd, *J* = 8.3, 1.5 Hz, 1H), 6.88 – 6.79 (2x d, *J* = 5.8 Hz, 1H), 3.59 – 3.51 (m, 6H), 2.40 – 2.30 (m, 4H). ^{13}C NMR (101 MHz, DMSO) δ 164.42, 159.96 (br), 157.22 (br), 149.01, 147.58 (br), 147.45 (br), 142.85, 142.12, 133.65, 132.75, 132.57, 131.34, 130.58 (br), 130.29, 128.66, 127.04, 126.77, 124.76, 124.16, 123.21, 121.34, 121.25, 119.46 (br), 118.90, 118.00, 111.66, 111.03, 102.80 (br), 66.27, 62.99, 62.92, 53.25, 53.21. LCMS (Fleet, 10 → 90%): t_r = 3.43 min, m/z: 503.2. HRMS [$C_{25}H_{23}ClN_8O_2$ + H]$^+$: 503.17053 calculated, 503.17069 found.

2-(3-Chlorophenoxy)-*N*-(3-(5-(morpholinomethyl)-1*H*-benzo[*d*]imidazol-2-yl)-1*H*-pyrazol-4-yl)pyrimidin-4-amine (24)

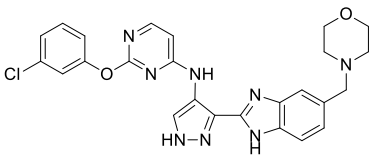

The title compound was synthesized from **117** (85.8 mg, 135 µmol) according to general procedure B (reaction time: 3 h). The crude was purified by automated column chromatography (2 – 40% MeOH/DCM) to afford the product (46 mg, 91 µmol, 67%). ^{1}H NMR (400 MHz, DMSO) δ 13.22 (br s, 1H), 13.00 (br s, 1H), 10.40 – 10.18 (2x s, 1H), 8.17 (d, *J* = 5.8 Hz, 1H), 7.67 – 7.62 (m, 1H), 7.57 (br s, 1H), 7.52 (t, *J* = 8.1 Hz, 1H), 7.44 (t, *J* = 2.2 Hz, 1H), 7.42 (br s, 1H), 7.39 (dd, *J* = 7.9, 1.8 Hz, 1H), 7.26 (dd, *J* = 7.9, 2.1 Hz, 1H), 7.20 – 7.12 (m, 1H), 6.87 – 6.78 (2x d, *J* = 5.8 Hz, 1H), 3.58 – 3.51 (m, 6H), 2.39 – 2.30 (m, 4H). ^{13}C NMR (101 MHz, DMSO) δ 164.86, 160.01 (br), 157.09 (br), 153.86, 147.58 (br), 147.48 (br), 142.87, 142.14, 133.68, 133.58, 132.77, 132.58, 131.35, 131.02, 130.65 (br), 125.34, 124.16, 123.22, 122.72, 121.35 (br), 121.25, 119.65 (br), 118.90, 118.00, 111.68, 111.04, 102.89 (br), 66.28, 62.97, 53.24. LCMS (Fleet, 10 → 90%): t_r = 3.50 min, m/z: 503.2. HRMS [$C_{25}H_{23}ClN_8O_2$ + H]$^+$: 503.17053 calculated, 503.17040 found.

2-(4-Chlorophenoxy)-*N*-(3-(5-(morpholinomethyl)-1*H*-benzo[*d*]imidazol-2-yl)-1*H*-pyrazol-4-yl)pyrimidin-4-amine (25)

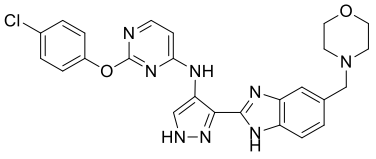

The title compound was synthesized from **118** (95.5 mg, 151 µmol) according to general procedure B (reaction time: 3 h). The crude was purified by automated column chromatography (2 – 14% MeOH/DCM) to afford the product (59.6 mg, 118 µmol, 79%). ^{1}H NMR (400 MHz, DMSO) δ 13.24 (br s, 1H), 13.01 (br s, 1H), 10.39 – 10.18 (2x s, 1H), 8.15 (d, *J* = 5.8 Hz, 1H), 7.71 (br s, 1H), 7.67 – 7.63 (m, 1H), 7.55 – 7.50 (m, 2H), 7.46 – 7.40 (m, 1H), 7.33 – 7.27 (m, 2H), 7.16 (t, *J* = 8.8 Hz, 1H), 6.85 – 6.77 (2x d, *J* = 5.8 Hz, 1H), 3.59 – 3.51 (m, 6H), 2.39 – 2.31 (m, 4H). ^{13}C NMR (101 MHz, DMSO) δ 164.88, 160.12 (br), 157.02 (br), 151.89, 147.61 (br), 147.50 (br), 142.88, 142.15, 133.68, 132.78, 132.59, 131.36, 130.68 (br), 129.52, 129.27, 124.17, 124.07, 123.23, 121.40, 121.31, 119.69 (br), 118.90, 118.01, 111.69, 111.05, 102.84 (br), 66.28, 63.01, 62.96, 53.25, 53.23. LCMS (Fleet, 10 → 90%): t_r = 3.44 min, m/z: 503.2. HRMS [$C_{25}H_{23}ClN_8O_2$ + H]$^+$: 503.17053 calculated, 503.17050 found.

_N_-(3-(1_H_-Benzo[_d_]imidazol-2-yl)-1_H_-pyrazol-4-yl)-2-phenylpyrimidin-4-amine (26)

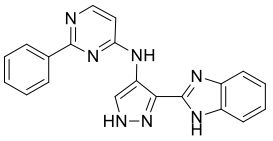

The title compound was synthesized from **85** (114 mg, 186 µmol) according to general procedure A (reaction time: 4.5 h). The crude was loaded onto Celite and purified by silica gel column chromatography (2 – 4% MeOH/DCM) to afford the product (50.6 mg, 143 µmol, 77%). ^{1}H NMR (400 MHz, DMSO) δ 13.20 (br s, 2H), 10.20 (br s, 1H), 8.63 (br s, 1H), 8.46 (d, *J* = 5.8 Hz, 1H), 8.44 – 8.39 (m, 2H), 7.75 (br s, 1H), 7.65 – 7.45 (m, 4H), 7.29 – 7.20 (m, 2H), 7.01 (d, *J* = 5.8 Hz, 1H). ^{13}C NMR (101 MHz, DMSO) δ 163.42, 158.66, 155.68, 147.55, 142.92 (br), 138.11, 133.65 (br), 130.86 (br), 130.51, 128.59, 127.77, 122.53 (br), 121.84, 119.80, 118.57 (br), 111.56 (br), 105.74 (br). LCMS (Fleet, 10 → 90%): t_r = 3.08 min, m/z: 354.3. HRMS [$C_{20}H_{15}N_7$ + H]$^+$: 354.14617 calculated, 354.14637 found.

_N_-(3-(1_H_-Benzo[_d_]imidazol-2-yl)-1_H_-pyrazol-4-yl)-2-(_p_-tolyl)pyrimidin-4-amine (27)

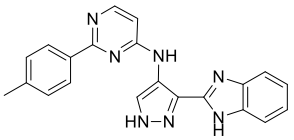

The title compound was synthesized from **86** (100 mg, 190 µmol) according to general procedure A (reaction time: 3 h). The crude was loaded onto Celite and purified by silica gel column chromatography (2% MeOH/DCM) to afford the product (40.0 mg, 106 µmol, 56%). ^{1}H NMR (400 MHz, DMSO) δ 13.19 (br s, 2H), 10.15 (br s, 1H), 8.60 (s, 1H), 8.43 (d, *J* = 5.8 Hz, 1H), 8.32 – 8.28 (m, 2H), 7.65 (br s, 2H), 7.37 – 7.33 (m, 2H), 7.28 – 7.22 (m, 2H), 6.98 (d, *J* = 5.8 Hz, 1H), 2.39 (s, 3H). ^{13}C NMR (101 MHz, DMSO) δ 163.47, 158.61, 155.65 (br), 147.52 (br), 142.68 (br), 140.23, 135.43, 134.07 (br), 130.77 (br), 129.20, 127.75, 122.21 (br), 121.89, 119.71 (br), 118.27 (br), 111.60 (br), 105.45 (br), 21.05. LCMS (Fleet, 10 → 90%): t_r = 3.35 min, m/z: 368.3. HRMS [$C_{21}H_{17}N_7$ + H]$^+$: 368.16182 calculated, 368.16204 found.

_N_-(3-(1_H_-Benzo[_d_]imidazol-2-yl)-1_H_-pyrazol-4-yl)-2-(4-methoxyphenyl)pyrimidin-4-amine (28)

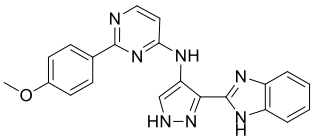

The title compound was synthesized from **87** (110 mg, 171 µmol) according to general procedure A (reaction time: 3 h), using 10% MeOH/EtOAc as organic layers in the work-up. The crude was purified by silica gel column chromatography (2% MeOH/DCM) to afford the product (66 mg, 171 µmol, quant.). ^{1}H NMR (400 MHz, DMSO) δ 13.35 (br s, 1H), 13.06 (br s, 1H), 10.16 (br s, 1H), 8.61 (br s, 1H), 8.41 (d, *J* = 5.8 Hz, 1H), 8.39 – 8.35 (m, 2H), 7.83 – 7.73 (br m, 1H), 7.58 – 7.50 (br m, 1H), 7.28 – 7.21 (m, 2H), 7.12 – 7.06 (m, 2H), 6.93 (d, *J* = 5.9 Hz, 1H), 3.84 (s, 3H). ^{13}C NMR (101 MHz, DMSO) δ 163.27, 161.30, 158.55, 155.64 (br), 147.60, 142.94, 133.66, 130.82 (br), 130.60, 129.41, 122.72, 121.97, 121.79, 119.65, 118.56, 113.90, 111.53, 104.92 (br), 55.29. LCMS (Fleet, 10 → 90%): t_r = 3.26 min, m/z: 384.3. HRMS [$C_{21}H_{17}N_7O$ + H]$^+$: 384.15673 calculated, 384.15699 found.

_N_-(3-(1_H_-Benzo[_d_]imidazol-2-yl)-1_H_-pyrazol-4-yl)-2-(4-chlorophenyl)pyrimidin-4-amine (29)

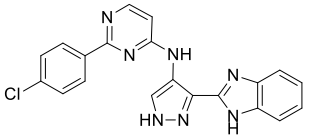

The title compound was synthesized from **88** (141 mg, 218 µmol) according to general procedure A (reaction time: 5 h). The crude was purified by HPLC (Waters, 15 – 25% MeCN in 0.2% TFA (aq.)) after which the fractions were concentrated and traces of TFA were removed by coevaporation with 1:1 MeCN/H_2O (20 mL). The residue was dissolved in EtOAc (20 mL) and poured into 1 M $NaHCO_3$ (aq.) (20 mL). The organic layer was separated and the water layer extracted with EtOAc (20 mL). The combined organic layers were washed with brine (30 mL), dried over Na_2SO_4, filtered and concentrated to afford the product (24 mg, 62 µmol, 28%). ^{1}H NMR (500 MHz, DMSO) δ 12.74 (br s, 2H), 10.25 (br s, 1H), 8.56 (br s, 1H), 8.44 (d, *J* = 5.8 Hz, 1H), 8.42 – 8.39 (m, 2H), 7.66 – 7.62 (m, 2H), 7.61 – 7.57 (m, 2H), 7.25 – 7.21 (m, 2H), 7.01 (d, *J* = 5.8 Hz, 1H). ^{13}C NMR (126 MHz, DMSO) δ 162.40, 158.68, 155.60 (br), 147.52, 138.38 (br), 136.91, 135.32, 130.65 (br), 129.50, 128.63, 122.10, 121.64, 120.42 (br), 114.94 (br), 105.96 (br). LCMS (Fleet, 10 → 90%): t_r = 3.72 min, m/z: 388.3. HRMS [$C_{20}H_{14}ClN_7$ + H]$^+$: 388.10720 calculated, 388.10714 found.

_N_-(3-(1_H_-Benzo[_d_]imidazol-2-yl)-1_H_-pyrazol-4-yl)-2-(4-fluorophenyl)pyrimidin-4-amine (30)

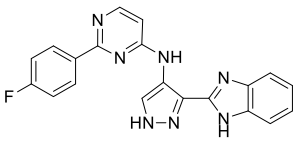

The title compound was synthesized from **89** (125 mg, 198 µmol) according to general procedure A (reaction time: 3 h). The crude was purified by HPLC (Waters, 15 – 25% MeCN in 0.2% TFA (aq.)) after which the fractions were concentrated and traces of TFA were removed by coevaporation with 1:1 MeCN/H_2O (20 mL). The residue was dissolved in EtOAc (20 mL) and poured into 1 M $NaHCO_3$ (aq.) (20 mL). The organic layer was separated and the water layer extracted with EtOAc (20 mL). The combined organic layers were washed with brine (30 mL), dried over Na_2SO_4, filtered and concentrated to afford the product (18.5 mg, 49.8 µmol, 25%). ^{1}H NMR (500 MHz, DMSO) δ 13.36 (s, 1H), 13.05 (br s, 1H), 10.19 (s, 1H), 8.58 (s, 1H), 8.46 (d, _J_ = 5.8 Hz, 1H), 8.45 – 8.42 (m, 2H), 7.65 (br s, 2H), 7.36 (t, _J_ = 8.8 Hz, 2H), 7.26 – 7.22 (m, 2H), 7.00 (d, _J_ = 5.8 Hz, 1H). ^{13}C NMR (126 MHz, DMSO) δ 164.75, 162.78, 162.46, 158.65, 155.60 (br), 147.49, 142.49 (br), 134.53, 133.94 (br), 130.91 (br), 130.10, 130.04, 122.23 (br), 121.70, 119.82, 118.05 (br), 115.53, 115.36, 111.62 (br), 105.61 (br). LCMS (Fleet, 10 → 90%): t_r = 3.42 min, m/z: 372.3. HRMS $[C_{20}H_{14}FN_7 + H]^+$: 372.13675 calculated, 372.13647 found.

_N_-(3-(1_H_-Benzo[_d_]imidazol-2-yl)-1_H_-pyrazol-4-yl)-2-(_o_-tolyl)pyrimidin-4-amine (31)

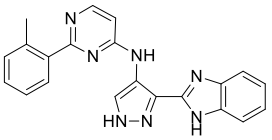

The title compound was synthesized from **90** (177 mg, 281 µmol) according to general procedure A (reaction time: 2 h). The crude was loaded onto Celite and purified by automated column chromatography (40 – 70% EtOAc/DCM) to afford the product (75.2 mg, 205 µmol, 73%). ^{1}H NMR (500 MHz, DMSO) δ 13.16 (br s, 2H), 10.19 (br s, 1H), 8.47 – 8.43 (m, 2H), 7.80 (dd, _J_ = 7.2, 1.4 Hz, 1H), 7.77 – 7.49 (br m, 2H), 7.38 – 7.29 (m, 3H), 7.28 – 7.22 (m, 2H), 7.00 (d, _J_ = 5.9 Hz, 1H), 2.52 (s, 3H). ^{13}C NMR (126 MHz, DMSO) δ 166.47, 158.41 (br), 155.27 (br), 147.59 (br), 142.94 (br), 139.19, 136.38, 133.74 (br), 130.98, 129.92, 128.86, 125.71, 122.16 (br), 121.95, 119.79 (br), 118.50 (br), 111.63 (br), 104.79 (br), 20.80 (not all quaternary carbons were observed). LCMS (Fleet, 10 → 90%): t_r = 3.21 min, m/z: 368.3. HRMS $[C_{21}H_{17}N_7 + H]^+$: 368.16182 calculated, 368.16163 found.

_N_-(3-(1_H_-Benzo[_d_]imidazol-2-yl)-1_H_-pyrazol-4-yl)-2-(2-chlorophenyl)pyrimidin-4-amine (32)

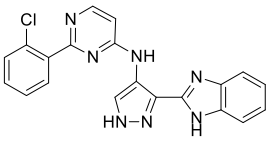

The title compound was synthesized from **91** (120 mg, 185 µmol) according to general procedure A (reaction time: 4.5 h). The crude was loaded onto Celite and purified by silica gel column chromatography (2 – 4% MeOH/DCM) to afford the product (48.1 mg, 124 µmol, 67%). ^{1}H NMR (400 MHz, DMSO) δ 13.14 (br s, 2H), 10.22 (br s, 1H), 8.50 (s, 1H), 8.47 (d, _J_ = 5.9 Hz, 1H), 7.80 – 7.75 (m, 1H), 7.65 (br s, 2H), 7.62 – 7.58 (m, 1H), 7.52 – 7.44 (m, 2H), 7.27 – 7.21 (m, 2H), 7.08 (d, _J_ = 6.0 Hz, 1H). ^{13}C NMR (101 MHz, DMSO) δ 164.33, 158.21 (br), 155.43 (br), 147.49 (br), 138.55, 131.68, 131.37, 130.72 (br), 130.46, 130.26, 127.17, 122.26 (br), 121.72, 120.23 (br), 105.83 (not all quaternary carbons were observed, neither were two –CH's of the benzimidazole). LCMS (Fleet, 10 → 90%): t_r = 3.01 min, m/z: 388.3. HRMS $[C_{20}H_{14}ClN_7 + H]^+$: 388.10720 calculated, 388.10741 found.

_N_-(3-(1_H_-Benzo[_d_]imidazol-2-yl)-1_H_-pyrazol-4-yl)-2-(2-methoxyphenyl)pyrimidin-4-amine (33)

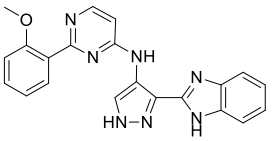

The title compound was synthesized from **92** (110 mg, 171 µmol) according to general procedure A (reaction time: 3 h). The crude was purified by silica gel column chromatography (2 – 3% MeOH/DCM) to afford the product (60.0 mg, 156 µmol, 91%). ^{1}H NMR (400 MHz, DMSO) δ 13.43 – 12.94 (br m, 2H), 10.07 (s, 1H), 8.67 (s, 1H), 8.44 (d, _J_ = 5.8 Hz, 1H), 7.76 (d, _J_ = 7.4 Hz, 2H), 7.53 (br s, 1H), 7.46 (ddd, _J_ = 8.3, 7.3, 1.8 Hz, 1H), 7.27 – 7.22 (m, 2H), 7.20 (dd, _J_ = 8.4, 1.0 Hz, 1H), 7.07 (td, _J_ = 7.5, 1.0 Hz, 1H), 7.00 (d, _J_ = 5.9 Hz, 1H), 3.87 (s, 3H). ^{13}C NMR (101 MHz, DMSO) δ 164.51, 157.98 (br), 157.48, 155.44 (br), 147.69, 142.96 (br), 133.68 (br), 131.33, 130.70, 130.51 (br), 128.73, 122.65 (br), 122.13, 121.78 (br), 120.23, 120.14, 118.53 (br), 112.34, 111.50 (br), 104.95 (br), 55.57. LCMS (Fleet, 10 → 90%): t_r = 3.22 min, m/z: 384.3. HRMS $[C_{21}H_{17}N_7O + H]^+$: 384.15673 calculated, 384.15685 found.

***N*-(3-(1*H*-Benzo[*d*]imidazol-2-yl)-1*H*-pyrazol-4-yl)-2-(*m*-tolyl)pyrimidin-4-amine (34)**

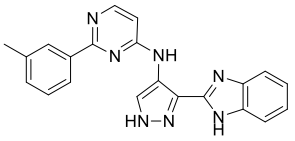

The title compound was synthesized from **93** (120 mg, 191 µmol) according to general procedure A (reaction time: 4 h). The crude was loaded onto Celite and purified by silica gel chromatography (3 – 5% MeOH/DCM) to afford the product (59.5 mg, 162 µmol, 85%). ^{1}H NMR (400 MHz, DMSO) δ 13.59 – 12.82 (br m, 2H), 10.18 (br s, 1H), 8.63 (br s, 1H), 8.45 (d, *J* = 5.9 Hz, 1H), 8.26 – 8.18 (m, 2H), 7.77 (br s, 1H), 7.57 (br s, 1H), 7.43 (t, *J* = 7.6 Hz, 1H), 7.33 (d, *J* = 7.5 Hz, 1H), 7.30 – 7.21 (m, 2H), 6.99 (d, *J* = 5.8 Hz, 1H), 2.43 (s, 3H). ^{13}C NMR (101 MHz, DMSO) δ 163.55, 158.65 (br), 155.65 (br), 147.58 (br), 142.94 (br), 138.11, 137.64, 133.69 (br), 131.15, 130.86 (br), 128.48, 128.41, 124.99, 122.55 (br), 121.90, 119.78 (br), 118.59 (br), 111.58 (br), 105.63 (br), 21.24. LCMS (Fleet, 10 → 90%): t_r = 3.33 min, m/z: 368.3. HRMS [$C_{21}H_{17}N_7$ + H]$^+$: 368.16182 calculated, 368.16206 found.

***N*-(3-(1*H*-Benzo[*d*]imidazol-2-yl)-1*H*-pyrazol-4-yl)-2-(3-chlorophenyl)pyrimidin-4-amine (35)**

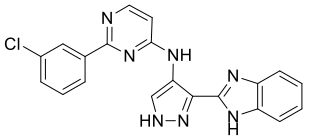

The title compound was synthesized from **94** (111 mg, 171 µmol) according to general procedure A (reaction time: 4 h), using 10% MeOH/EtOAc as organic layers in the work-up. The crude was purified by HPLC (Waters, 15 – 25% MeCN in 0.2% TFA (aq.)) after which the fractions were concentrated and traces of TFA were removed by coevaporation with 1:1 MeCN/H_2O (20 mL). The residue was dissolved in EtOAc (20 mL) and poured into 1 M $NaHCO_3$ (aq.) (20 mL). The organic layer was separated and the water layer extracted with EtOAc (20 mL). The combined organic layers were washed with brine (30 mL), dried over Na_2SO_4, filtered and concentrated to afford the product (53.0 mg, 137 µmol, 80%). ^{1}H NMR (500 MHz, DMSO) δ 13.53 – 12.90 (br m, 2H), 10.21 (br s, 1H), 8.56 (br s, 1H), 8.46 (d, *J* = 5.8 Hz, 1H), 8.37 – 8.32 (m, 2H), 7.76 (br s, 1H), 7.62 – 7.57 (m, 2H), 7.53 (br s, 1H), 7.27 – 7.21 (m, 2H), 7.04 (d, *J* = 5.8 Hz, 1H). ^{13}C NMR (126 MHz, DMSO) δ 161.99, 158.72 (br), 155.62 (br), 147.45, 142.93 (br), 140.18, 133.63 (br), 133.44, 131.03 (br), 130.56, 130.25, 127.32, 126.29, 122.68 (br), 121.79 (br), 121.57, 119.87, 118.53 (br), 111.51 (br), 106.32 (br). LCMS (Fleet, 10 → 90%): t_r = 3.66 min, m/z: 388.3. HRMS [$C_{20}H_{14}ClN_7$ + H]$^+$: 388.10720 calculated, 388.10706 found.

***N*-(3-(1*H*-Benzo[*d*]imidazol-2-yl)-1*H*-pyrazol-4-yl)-2-(3-methoxyphenyl)pyrimidin-4-amine (36)**

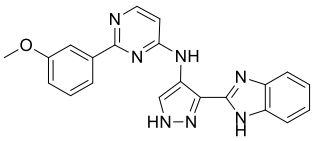

The title compound was synthesized from **95** (184 mg, 286 µmol) according to general procedure A (reaction time: 2 h). The crude was loaded onto Celite and purified by automated column chromatography (30 – 60% EtOAc/DCM) to afford the product (76.8 mg, 200 µmol, 70%). ^{1}H NMR (500 MHz, DMSO) δ 13.23 (br s, 2H), 10.21 (br s, 1H), 8.64 (br s, 1H), 8.46 (d, *J* = 5.8 Hz, 1H), 8.03 (d, *J* = 7.7 Hz, 1H), 7.99 – 7.97 (m, 1H), 7.75 (br s, 1H), 7.61 (br s, 1H), 7.46 (t, *J* = 7.9 Hz, 1H), 7.29 – 7.23 (m, 2H), 7.09 (dd, *J* = 8.1, 2.5 Hz, 1H), 7.00 (d, *J* = 5.8 Hz, 1H), 3.88 (s, 3H). ^{13}C NMR (126 MHz, DMSO) δ 163.21, 159.47, 158.62 (br), 155.59 (br), 147.56 (br), 142.92 (br), 139.63, 133.79 (br), 130.91 (br), 129.61, 122.21 (br), 121.89, 120.15, 119.78 (br), 118.56 (br), 116.31, 112.76, 111.49 (br), 105.80 (br), 55.09. LCMS (Fleet, 10 → 90%): t_r = 3.44 min, m/z: 384.3. HRMS [$C_{21}H_{17}N_7O$ + H]$^+$: 384.15673 calculated, 384.15663 found.

***N*-(3-(1*H*-Benzo[*d*]imidazol-2-yl)-1*H*-pyrazol-4-yl)-2-(pyridin-3-yl)pyrimidin-4-amine (37)**

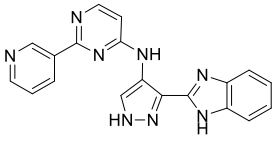

The title compound was synthesized from **96** (148 mg, 240 µmol) according to general procedure A (reaction time: 4 h), using 10% MeOH/EtOAc as organic layers in the work-up. The crude was purified by silica gel column chromatography (3 – 5% MeOH/DCM) to afford the product (17 mg, 48 µmol, 20%). ^{1}H NMR (400 MHz, DMSO) δ 13.20 (br s, 2H), 10.24 (br s, 1H), 9.53 (dd, *J* = 2.2, 0.9 Hz, 1H), 8.73 (dd, *J* = 4.8, 1.7 Hz, 1H), 8.68 (dt, *J* = 8.0, 1.9 Hz, 1H), 8.59 (br s, 1H), 8.48 (d, *J* = 5.9 Hz, 1H), 7.64 (br s, 2H), 7.58 (ddd, *J* = 7.9, 4.7, 0.9 Hz, 1H), 7.26 – 7.21 (m, 2H), 7.07 (d, *J* = 5.9 Hz, 1H). ^{13}C NMR (101 MHz, DMSO) δ 161.81, 158.70, 155.65 (br), 151.16, 148.98, 147.37 (br), 143.05 (br), 135.16, 133.43, 130.80 (br), 123.77, 122.24 (br), 121.54,

120.36 (br), 118.67 (br), 111.80 (br), 106.40 (br) (not all quaternary carbons were observed). LCMS (Fleet, 10 → 90%): t_r = 2.62 min, m/z: 355.3. HRMS $[C_{19}H_{14}N_8 + H]^+$: 355.14142 calculated, 355.14143 found.

***N*-(3-(1*H*-Benzo[*d*]imidazol-2-yl)-1*H*-pyrazol-4-yl)-2-(3-isopropylphenyl)pyrimidin-4-amine (38)**

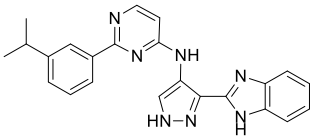

The title compound was synthesized from **97** (72.4 mg, 110 µmol) according to general procedure A (reaction time: 2 h). The crude was loaded onto Celite and purified by automated column chromatography (20 – 55% EtOAc/DCM) to afford the product (35.5 mg, 89.8 µmol, 81%). ^{1}H NMR (500 MHz, DMSO) δ 13.24 (br s, 2H), 10.19 (br s, 1H), 8.63 (br s, 1H), 8.46 (d, *J* = 5.8 Hz, 1H), 8.30 (t, *J* = 1.8 Hz, 1H), 8.22 (dt, *J* = 7.6, 1.5 Hz, 1H), 7.66 (br s, 2H), 7.45 (t, *J* = 7.6 Hz, 1H), 7.39 (dt, *J* = 7.7, 1.5 Hz, 1H), 7.28 – 7.22 (m, 2H), 7.01 (d, *J* = 5.9 Hz, 1H), 3.01 (hept, *J* = 6.9 Hz, 1H), 1.29 (d, *J* = 6.9 Hz, 6H). ^{13}C NMR (126 MHz, DMSO) δ 163.61, 158.60, 155.66 (br), 148.56, 147.55, 142.89 (br), 138.15, 133.73 (br), 130.83 (br), 128.75, 128.56, 125.53, 125.39, 122.22 (br), 121.91, 119.68 (br), 118.50 (br), 111.57 (br), 105.68 (br), 33.51, 23.98. LCMS (Fleet, 10 → 90%): t_r = 4.11 min, m/z: 396.3. HRMS $[C_{23}H_{21}N_7 + H]^+$: 396.19312 calculated, 396.19308 found.

***N*-(3-(1*H*-Benzo[*d*]imidazol-2-yl)-1*H*-pyrazol-4-yl)-2-(3,5-dichlorophenyl)pyrimidin-4-amine (39)**

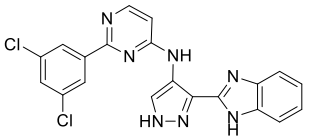

The title compound was synthesized from **98** (128 mg, 188 µmol) according to general procedure A (reaction time: 2 h). The crude was purified by HPLC (Agilent, 25 – 31% MeCN in 0.2% TFA (aq.)) after which the fractions were concentrated and traces of TFA were removed by coevaporation with 1:1 MeCN/H_2O (20 mL). The residue was dissolved in EtOAc (20 mL) and poured into 1 M $NaHCO_3$ (aq.) (20 mL). The organic layer was separated and the water layer extracted with EtOAc (20 mL). The combined organic layers were washed with brine (30 mL), dried over Na_2SO_4, filtered and concentrated to afford the product (35.4 mg, 83.8 µmol, 45%). ^{1}H NMR (400 MHz, DMSO) δ 13.43 (s, 1H), 13.04 (br s, 1H), 10.20 (br s, 1H), 8.46 (s, 1H), 8.41 (d, *J* = 5.9 Hz, 1H), 8.22 (d, *J* = 2.0 Hz, 2H), 7.70 (t, *J* = 2.0 Hz, 1H), 7.62 (br s, 2H), 7.28 – 7.19 (m, 2H), 7.01 (d, *J* = 5.9 Hz, 1H). ^{13}C NMR (101 MHz, DMSO) δ 160.69, 158.72, 155.49 (br), 147.40, 142.78 (br), 141.42, 134.44, 133.64 (br), 131.16 (br), 129.69, 126.09, 122.23 (br), 121.38, 119.92, 118.55 (br), 111.54 (br), 106.78 (br). LCMS (Finnigan, 10 → 90%): t_r = 5.15 min, m/z: 422.4. HRMS $[C_{20}H_{13}Cl_2N_7 + H]^+$: 422.06823 calculated, 422.06827 found.

***N*-(3-(1*H*-Benzo[*d*]imidazol-2-yl)-1*H*-pyrazol-4-yl)-2-(naphthalen-1-yl)pyrimidin-4-amine (40)**

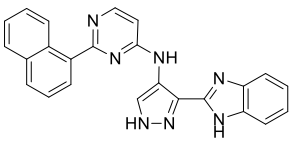

The title compound was synthesized from **99** (134 mg, 201 µmol) according to general procedure A (reaction time: 2 h). The crude was purified by automated column chromatography (20 – 55% EtOAc/DCM) to afford the product (49.3 mg, 122 µmol, 61%). ^{1}H NMR (500 MHz, DMSO) δ 13.15 (br s, 2H), 10.27 (br s, 1H), 8.77 – 8.72 (m, 1H), 8.56 (d, *J* = 5.9 Hz, 1H), 8.42 (s, 1H), 8.09 – 8.05 (m, 2H), 8.04 – 7.99 (m, 1H), 7.74 (br s, 2H), 7.66 (dd, *J* = 8.2, 7.1 Hz, 1H), 7.59 – 7.55 (m, 2H), 7.29 – 7.24 (m, 2H), 7.11 (d, *J* = 5.9 Hz, 1H). ^{13}C NMR (126 MHz, DMSO) δ 165.78, 158.37 (br), 155.55 (br), 147.57 (br), 142.97 (br), 136.79, 133.80 (br), 133.64, 130.85 (br), 130.49, 129.78, 128.48, 128.41, 126.46, 126.10, 125.90, 125.34, 122.47 (br), 121.87, 119.89 (br), 118.55 (br), 111.55 (br), 105.33 (br). LCMS (Fleet, 10 → 90%): t_r = 3.52 min, m/z: 404.3. HRMS $[C_{24}H_{17}N_7 + H]^+$: 404.16182 calculated, 404.16171 found.

***N*-(3-(1*H*-Benzo[*d*]imidazol-2-yl)-1*H*-pyrazol-4-yl)-2-(1*H*-indol-7-yl)pyrimidin-4-amine (41)**

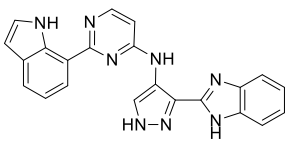

A microwave vial was charged with **100** (92.6 mg, 142 µmol) after which TBAF (1 M in THF, 2.5 mL) and ethylenediamine (28.6 µL, 425 µmol) were added. The mixture heated to 80°C, stirred for 2 days and subsequently poured into H_2O (20 mL). The product was extracted with EtOAc (2x20 mL) and the combined organic layers were concentrated as such. The mixture was dissolved in 1:1 MeOH/DCM (2 mL) and transferred to a microwave vial. Ethylenediamine (50 µL, 746 µmol) was added after which the vial was sealed and the

mixture was stirred at 50°C for 1 h. The mixture was poured into H_2O (20 mL) and the product extracted with EtOAc (2x20 mL). The combined organic layers were concentrated as such, the crude was loaded onto Celite and purified by automated column chromatography (25 – 100% EtOAc/DCM) to afford the product (16.5 mg, 42.0 µmol, 30%). ^{1}H NMR (400 MHz, DMSO) δ 13.40 (br s, 1H), 13.05 (br s, 1H), 11.57 (br s, 1H), 10.14 (br s, 1H), 8.65 (br s, 1H), 8.53 (d, *J* = 5.9 Hz, 1H), 8.30 (dd, *J* = 7.5, 1.1 Hz, 1H), 7.78 (d, *J* = 7.6 Hz, 1H), 7.75 (br s, 1H), 7.53 (br s, 1H), 7.47 (t, *J* = 2.8 Hz, 1H), 7.29 – 7.20 (m, 3H), 6.98 (br s, 1H), 6.57 (dd, *J* = 3.1, 2.1 Hz, 1H). ^{13}C NMR (101 MHz, DMSO) δ 164.17, 158.70 (br), 155.22 (br), 147.43 (br), 143.04 (br), 134.39, 133.72 (br), 131.46 (br), 129.23, 126.06, 123.35, 122.74 (br), 121.78 (br), 121.57 (br), 121.43, 120.68, 120.58 (br), 118.88, 118.62 (br), 111.55 (br), 105.11 (br), 101.47. LCMS (Fleet, 10 → 90%): t_r = 3.77 min, m/z: 393.3. HRMS [$C_{22}H_{16}N_8$ + H]$^+$: 393.15707 calculated, 393.15677 found.

N-(3-(1*H*-Benzo[*d*]imidazol-2-yl)-1*H*-pyrazol-4-yl)-2-(1*H*-indazol-4-yl)pyrimidin-4-amine (42)

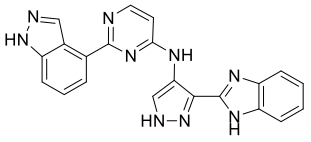

The title compound was synthesized from **101** (101 mg, 155 µmol) according to general procedure A (reaction time: 2.5 h). The crude was loaded onto Celite and purified by automated column chromatography (60 – 100% EtOAc/DCM) to afford the product (36.5 mg, 92.8 µmol, 60%). ^{1}H NMR (500 MHz, DMSO) δ 13.66 – 12.82 (br m, 3H), 10.22 (br s, 1H), 8.87 (br s, 1H), 8.59 (br s, 1H), 8.57 (d, *J* = 5.8 Hz, 1H), 8.23 (d, *J* = 7.2 Hz, 1H), 7.77 (br s, 1H), 7.75 (d, *J* = 8.3 Hz, 1H), 7.58 (br s, 1H), 7.55 (dd, *J* = 8.3, 7.2 Hz, 1H), 7.29 – 7.22 (m, 2H), 7.04 (d, *J* = 5.9 Hz, 1H). ^{13}C NMR (126 MHz, DMSO) δ 164.02, 158.77, 155.86 (br), 147.54, 143.00 (br), 140.85, 135.20, 133.71 (br), 131.23, 125.79, 122.65 (br), 121.80, 121.16, 121.11, 120.10, 118.56 (br), 112.58, 111.58 (br), 105.48 (br). LCMS (Fleet, 10 → 90%): t_r = 2.83 min, m/z: 394.3. HRMS [$C_{21}H_{15}N_9$ + H]$^+$: 394.15232 calculated, 394.15214 found.

N-(3-(1*H*-Benzo[*d*]imidazol-2-yl)-1*H*-pyrazol-4-yl)-2-(naphthalen-2-yl)pyrimidin-4-amine (43)

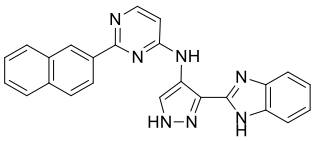

The title compound was synthesized from **102** (68.5 mg, 103 µmol) according to general procedure A (reaction time: 2 h). The crude was loaded onto Celite and purified by automated column chromatography (25 – 100% EtOAc/DCM) to afford the product (30.8 mg, 76.3 µmol, 74%). ^{1}H NMR (500 MHz, DMSO) δ 13.23 (br s, 2H), 10.23 (br s, 1H), 9.00 (s, 1H), 8.72 (br s, 1H), 8.53 (dd, *J* = 8.7, 1.8 Hz, 1H), 8.51 (d, *J* = 5.8 Hz, 1H), 8.17 – 8.12 (m, 1H), 8.07 (d, *J* = 8.6 Hz, 1H), 8.02 – 7.96 (m, 1H), 7.67 (br s, 2H), 7.62 – 7.55 (m, 2H), 7.28 – 7.23 (m, 2H), 7.05 (d, *J* = 5.8 Hz, 1H). ^{13}C NMR (126 MHz, DMSO) δ 163.44, 158.76 (br), 155.74 (br), 147.56 (br), 142.82 (br), 135.56, 134.10, 133.87 (br), 132.84, 130.92 (br), 129.08, 128.06, 127.81, 127.65, 127.22, 126.49, 124.98, 122.27 (br), 121.83, 119.98 (br), 118.48 (br), 111.59 (br), 105.76 (br). LCMS (Finnigan, 10 → 90%): t_r = 4.53 min, m/z: 404.4. HRMS [$C_{24}H_{17}N_7$ + H]$^+$: 404.16182 calculated, 404.16163 found.

2-(3-Chlorophenyl)-*N*-(3-(5-(morpholinomethyl)-1*H*-benzo[*d*]imidazol-2-yl)-1*H*-pyrazol-4-yl)pyrimidin-4-amine (44)

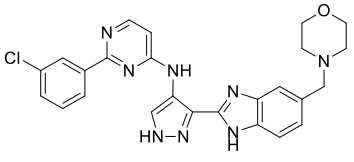

The title compound was synthesized from **119** (87.3 mg, 141 µmol) according to general procedure A (reaction time: 1.5 h). The crude was purified by automated column chromatography (0 – 10% MeOH/EtOAc) to afford the product (53.6 mg, 110 µmol, 78%). ^{1}H NMR (500 MHz, DMSO) δ 13.73 – 12.63 (br m, 2H), 10.22 (br s, 1H), 8.55 (s, 1H), 8.44 (d, *J* = 5.8 Hz, 1H), 8.35 – 8.33 (m, 2H), 7.67 – 7.44 (m, 4H), 7.17 (dd, *J* = 8.3, 0.9 Hz, 1H), 7.02 (d, *J* = 5.9 Hz, 1H), 3.58 – 3.55 (m, 4H), 3.54 (s, 2H), 2.40 – 2.32 (m, 4H). ^{13}C NMR (126 MHz, DMSO) δ 162.02, 158.70, 155.56 (br), 147.54 (br), 142.27 (br), 140.20, 133.70 (br), 133.45, 132.07 (br), 130.92 (br), 130.48, 130.21, 127.35, 126.28, 123.61 (br), 121.62, 119.80 (br), 118.04 (br), 111.54 (br), 106.31 (br), 66.27, 62.98, 53.22. LCMS (Fleet, 10 → 90%): t_r = 3.19 min, m/z: 487.3. HRMS [$C_{25}H_{23}ClN_8O$ + H]$^+$: 487.17561 calculated, 487.17545 found.

2-(3-Ethynylphenyl)-*N*-(3-(5-(morpholinomethyl)-1*H*-benzo[*d*]imidazol-2-yl)-1*H*-pyrazol-4-yl)pyrimidin-4-amine (45)

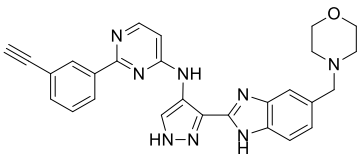

The title compound was synthesized from **120** (44.0 mg, 64.8 µmol) according to general procedure D (reaction time: 2 h). The crude was purified by automated column chromatography (0 – 10% MeOH/EtOAc) to afford the product (13.7 mg, 28.7 µmol, 44%). ^{1}H NMR (500 MHz, DMSO) δ 13.40 (br s, 1H), 13.02 (br s, 1H), 10.20 (br s, 1H), 8.55 (br s, 1H), 8.46 (d, *J* = 5.8 Hz, 1H), 8.44 – 8.41 (m, 2H), 7.67 (br s, 1H), 7.65 (dt, *J* = 7.6, 1.5 Hz, 1H), 7.58 (t, *J* = 7.7 Hz, 1H), 7.45 (br s, 1H), 7.18 (d, *J* = 8.2 Hz, 1H), 7.04 (d, *J* = 5.9 Hz, 1H), 4.30 (s, 1H), 3.61 – 3.54 (m, 6H), 2.44 – 2.32 (m, 4H). ^{13}C NMR (126 MHz, DMSO) δ 162.40, 158.74 (br), 155.65 (br), 147.48 (br), 142.91 (br), 142.19 (br), 138.49, 133.73 (br), 133.57, 132.54 (br), 131.32 (br), 130.88 (br), 130.77, 129.18, 128.26, 124.11 (br), 123.19 (br), 122.04, 121.64 (br), 119.98 (br), 118.96 (br), 118.01 (br), 111.67 (br), 111.04 (br), 106.37 (br), 83.35, 81.09, 66.27, 62.97, 53.24 (not all quaternary carbons were observed). LCMS (Fleet, 10 → 90%): t_r = 3.13 min, m/z: 477.3. HRMS $[C_{27}H_{24}N_8O + H]^+$: 477.21458 calculated, 477.21467 found.

***N*-(3-(5-(Morpholinomethyl)-1*H*-benzo[*d*]imidazol-2-yl)-1*H*-pyrazol-4-yl)-2-(3-(trifluoromethyl)phenyl)pyrimidin-4-amine (46)**

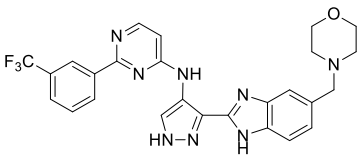

The title compound was synthesized from **121** (112 mg, 173 µmol) according to general procedure A (reaction time: 2.5 h). The crude was purified by automated column chromatography (0 – 10% MeOH/EtOAc) to afford the product (62.6 mg, 120 µmol, 70%). ^{1}H NMR (400 MHz, DMSO) δ 13.59 – 12.90 (br m, 2H), 10.26 (br s, 1H), 8.68 – 8.63 (m, 2H), 8.54 (br s, 1H), 8.45 (d, *J* = 5.8 Hz, 1H), 7.86 (d, *J* = 7.7 Hz, 1H), 7.76 (t, *J* = 8.0 Hz, 1H), 7.63 (br s, 1H), 7.50 (br s, 1H), 7.16 (d, *J* = 8.2 Hz, 1H), 7.03 (d, *J* = 5.9 Hz, 1H), 3.58 – 3.54 (m, 4H), 3.53 (s, 2H), 2.40 – 2.30 (m, 4H). ^{13}C NMR (101 MHz, DMSO) δ 161.86, 158.75, 155.59 (br), 147.56 (br), 142.95 (br), 142.25 (br), 139.01, 133.76 (br), 132.49 (br), 131.48, 130.98 (br), 129.85, 129.58, 129.27, 128.95, 128.35, 126.96 (br), 126.92 (br), 126.89 (br), 126.85 (br), 125.65, 124.20 (br), 124.04 (br), 124.00 (br), 123.97 (br), 123.93 (br), 123.39 (br), 122.94, 121.62, 119.83 (br), 118.91 (br), 118.05 (br), 111.65 (br), 111.08 (br), 106.48 (br), 66.28, 63.00, 53.25. LCMS (Fleet, 10 → 90%): t_r = 3.60 min, m/z: 521.25. HRMS $[C_{26}H_{23}F_3N_8O + H]^+$: 521.20197 calculated, 521.20212 found.

3-(4-((3-(5-(Morpholinomethyl)-1*H*-benzo[*d*]imidazol-2-yl)-1*H*-pyrazol-4-yl)amino)pyrimidin-2-yl)benzonitrile (47)

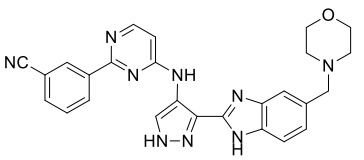

122 (100 mg, 165 mmol) was dissolved in DCM (1 mL) after which TFA (0.33 mL) was added dropwise. The mixture was stirred for 7.5 h and subsequently sat. $NaHCO_3$ (aq.) (10 mL) was added. The mixture was poured into H_2O (10 mL) and the product extracted with EtOAc (2x20 mL). The combined organic layers were concentrated as such and suspended in 1:1 MeOH/DCM (5 mL). Ethylenediamine (50 µL, 746 µmol) was added after which the mixture was stirred for 30 min. The mixture was poured into H_2O (20 mL), the product extracted with DCM (20 mL) and subsequently with 5% MeOH/DCM (20 mL). The combined organic layers were concentrated as such. The crude was purified by automated column chromatography (1 – 20% MeOH/DCM) to afford the product (34.5 mg, 72.2 µmol, 44%). ^{1}H NMR (400 MHz, DMSO) δ 13.39 (s, 1H), 13.03 – 12.96 (2x s, 1H), 10.35 – 10.16 (2x s, 1H), 8.69 – 8.62 (m, 2H), 8.56 (br s, 1H), 8.47 – 8.42 (2x d, *J* = 5.9 Hz, 1H), 7.96 (dt, *J* = 7.7, 1.5 Hz, 1H), 7.73 (t, *J* = 8.1 Hz, 1H), 7.69 – 7.64 (m, 1H), 7.47 – 7.42 (m, 1H), 7.21 – 7.13 (2x dd, *J* = 8.3, 1.5 Hz, 1H), 7.07 – 6.99 (2x d, *J* = 5.9 Hz, 1H), 3.61 – 3.51 (m, 6H), 2.43 – 2.31 (m, 4H). ^{13}C NMR (101 MHz, DMSO) δ 161.50, 158.72, 155.52 (br), 147.68 (br), 147.55 (br), 142.95, 142.23, 139.14, 133.87, 133.71, 132.82, 132.49 (br), 132.24, 131.24 (br), 131.06, 129.96, 124.14, 123.18, 121.52, 121.42, 120.02 (br), 118.93, 118.78, 118.03, 111.82, 111.68, 111.05, 106.62 (br), 66.26, 63.01, 62.93, 53.25, 53.20. LCMS (Fleet, 10 → 90%): t_r = 3.04 min, m/z: 478.2. HRMS $[C_{26}H_{23}N_9O + H]^+$: 478.20983 calculated, 478.21008 found.

2-(3-Chloro-2-fluorophenyl)-*N*-(3-(5-(morpholinomethyl)-1*H*-benzo[*d*]imidazol-2-yl)-1*H*-pyrazol-4-yl)pyrimidin-4-amine (48)

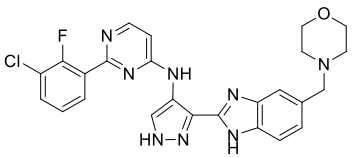

The title compound was synthesized from **123** (86.8 mg, 137 µmol) according to general procedure B (reaction time: 3 h). The crude was purified by automated column chromatography (0 – 10% MeOH/EtOAc) to afford the product (56.1 mg, 111 µmol, 81%). ^{1}H NMR (500 MHz, DMSO) δ 13.31 (br s, 1H), 12.99 (br s, 1H), 10.40 – 10.16 (br m, 1H), 8.55 (s, 1H), 8.46 (d, *J* = 5.8 Hz, 1H), 8.08 – 8.03 (m, 1H), 7.71 (ddd, *J* = 8.3, 6.7, 1.7 Hz, 1H), 7.68 (s, 1H), 7.45 (br s, 1H), 7.35 (td, *J* = 7.9, 1.0 Hz, 1H), 7.21 – 7.13 (br m, *J* = 8.4 Hz, 1H), 7.10 – 7.03 (br m, 1H), 3.61 – 3.51 (m, 6H), 2.42 – 2.31 (m, 4H). ^{13}C NMR (126 MHz, DMSO) δ 161.16, 161.12, 158.28, 156.74, 155.42 (br), 154.71, 147.62 (br), 142.95 (br), 142.22 (br), 133.72 (br), 132.81 (br), 132.53 (br), 131.90, 131.32 (br), 130.75 (br), 130.53, 128.47, 128.39, 125.15, 125.11, 124.10 (br), 123.17 (br), 121.70 (br), 121.15, 121.01, 119.82 (br), 118.89 (br), 117.99 (br), 111.66 (br), 111.03 (br), 106.25 (br), 66.27, 62.98, 53.23. LCMS (Fleet, 10 → 90%): t_r = 3.07 min, m/z: 505.3. HRMS $[C_{25}H_{22}ClFN_8O + H]^+$: 505.16619 calculated, 505.16584 found.

2-(3-Ethynyl-2-fluorophenyl)-*N*-(3-(5-(morpholinomethyl)-1*H*-benzo[*d*]imidazol-2-yl)-1*H*-pyrazol-4-yl)pyrimidin-4-amine (49)

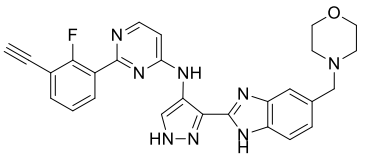

The title compound was synthesized from **124** (74.7 mg, 107 µmol) according to general procedure D (reaction time with TFA: 4 h). The crude was purified by automated column chromatography (0 – 10% MeOH/EtOAc) to afford the product (33.7 mg, 68.1 µmol, 64%). ^{1}H NMR (400 MHz, DMSO) δ 13.31 (br s, 1H), 13.02 (br s, 1H), 10.25 (br s, 1H), 8.56 (s, 1H), 8.47 (d, *J* = 5.9 Hz, 1H), 8.13 (td, *J* = 7.6, 1.8 Hz, 1H), 7.71 (ddd, *J* = 8.0, 6.4, 1.8 Hz, 1H), 7.66 (br s, 1H), 7.46 (br s, 1H), 7.36 (t, *J* = 7.7 Hz, 1H), 7.18 (d, *J* = 8.3 Hz, 1H), 7.08 (d, *J* = 5.9 Hz, 1H), 4.59 (s, 1H), 3.59 – 3.53 (m, 6H), 2.42 – 2.32 (m, 4H). ^{13}C NMR (101 MHz, DMSO) δ 162.15, 161.31, 161.27, 159.58, 158.27, 155.48 (br), 147.58 (br), 142.89 (br), 142.20 (br), 135.27, 133.73 (br), 132.83 (br), 132.56, 132.54, 131.35 (br), 130.51 (br), 127.24, 127.15, 124.56, 124.51, 124.11 (br), 123.29 (br), 121.74, 120.02 (br), 118.90 (br), 118.07 (br), 111.69 (br), 111.55, 111.38, 111.04 (br), 106.16 (br), 86.59, 86.55, 77.03, 77.02, 66.28, 62.99, 53.25. LCMS (Fleet, 10 → 90%): t_r = 3.01 min, m/z: 495.2. HRMS $[C_{27}H_{23}FN_8O + H]^+$: 495.20516 calculated, 495.20496 found.

2-(5-Chloro-2-fluorophenyl)-*N*-(3-(5-(morpholinomethyl)-1*H*-benzo[*d*]imidazol-2-yl)-1*H*-pyrazol-4-yl)pyrimidin-4-amine (50)

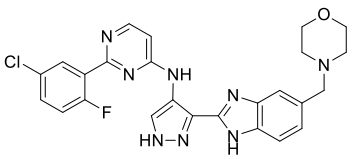

The title compound was synthesized from **125** (65.5 mg, 103 µmol) according to general procedure B (reaction time: 4 h). The crude was purified by automated column chromatography (0 – 10% MeOH/EtOAc) to afford the product (41.3 mg, 81.7 µmol, 79%). ^{1}H NMR (400 MHz, DMSO) δ 13.09 (br s, 2H), 10.28 (br s, 1H), 8.55 (s, 1H), 8.46 (d, *J* = 5.9 Hz, 1H), 8.09 (dd, *J* = 6.6, 2.8 Hz, 1H), 7.61 (ddd, *J* = 8.8, 4.0, 2.8 Hz, 1H), 7.55 (br s, 2H), 7.44 (dd, *J* = 10.8, 8.8 Hz, 1H), 7.17 (dd, *J* = 8.3, 1.5 Hz, 1H), 7.07 (d, *J* = 5.9 Hz, 1H), 3.59 – 3.52 (m, 6H), 2.41 – 2.32 (m, 4H). ^{13}C NMR (101 MHz, DMSO) δ 160.65, 160.60, 160.49, 158.28, 157.97, 155.42 (br), 147.59, 131.94 (br), 131.53, 131.44, 130.92, 130.90, 130.66 (br), 128.33, 128.30, 128.19, 123.62 (br), 121.69, 119.99 (br), 119.16, 118.91, 106.35 (br), 66.28, 62.99, 53.25 (not all quaternary carbons were observed, neither were two –CH's of the benzimidazole). LCMS (Fleet, 10 → 90%): t_r = 3.04 min, m/z: 505.2. HRMS $[C_{25}H_{22}ClFN_8O + H]^+$: 505.16619 calculated, 505.16603 found.

2-(3-Chlorophenyl)-5-methoxy-*N*-(3-(5-(morpholinomethyl)-1*H*-benzo[*d*]imidazol-2-yl)-1*H*-pyrazol-4-yl)pyrimidin-4-amine (51)

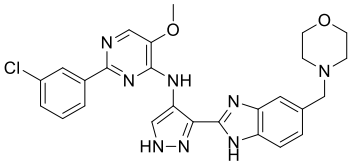

The title compound was synthesized from **127** (50 mg, 77 µmol) according to general procedure B (reaction time: 5.5 h). The crude was purified by automated column chromatography (1 – 20% MeOH/EtOAc) to afford the product (34.4 mg, 66.5 µmol, 86%). ^{1}H NMR (500 MHz, DMSO) δ 13.67 – 12.76 (br m, 2H), 10.72 (br s, 1H), 8.61 (s, 1H), 8.31 – 8.25 (m, 2H), 8.19 (s, 1H), 7.64 (br s, 1H), 7.57 – 7.50 (m, 2H), 7.45 (br s, 1H), 7.21 – 7.17 (br m, 1H), 4.14 (s, 3H), 3.61 – 3.53 (m, 6H), 2.42 – 2.33 (m, 4H). ^{13}C NMR (126 MHz, DMSO) δ 154.03, 149.70, 147.62 (br), 142.87 (br), 142.11 (br), 140.27, 139.76, 133.69 (br), 133.51, 133.38, 132.78 (br), 132.57 (br), 131.39 (br), 130.84 (br), 130.48, 129.22, 126.77, 125.76, 124.14 (br), 123.20 (br), 121.70, 119.00 (br), 118.90 (br), 117.99 (br), 111.71 (br), 111.11 (br), 66.28, 62.96, 56.62, 53.25. LCMS (Fleet, 10 → 90%): t_r = 3.79 min, m/z: 517.3. HRMS [$C_{26}H_{25}ClN_8O_2$ + H]$^+$: 517.18618 calculated, 517.18628 found.

2-(3-Ethynylphenyl)-5-methoxy-*N*-(3-(5-(morpholinomethyl)-1*H*-benzo[*d*]imidazol-2-yl)-1*H*-pyrazol-4-yl)pyrimidin-4-amine (52)

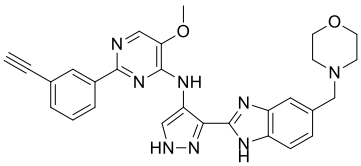

The title compound was synthesized from **128** (52.9 mg, 74.6 µmol) according to general procedure D (reaction time with TFA: 5 h). The crude was purified by automated column chromatography (1 – 15% MeOH/EtOAc) to afford the product (30.1 mg, 59.4 µmol, 80%). ^{1}H NMR (400 MHz, DMSO) δ 13.39 (br s, 1H), 13.03 (br s, 1H), 10.81 – 10.61 (2x s, 1H), 8.65 – 8.62 (2x s, 1H), 8.39 – 8.36 (m, 2H), 8.23 – 8.20 (2x s, 1H), 7.68 – 7.62 (m, 1H), 7.59 (dt, *J* = 7.6, 1.6 Hz, 1H), 7.57 – 7.53 (m, 1H), 7.49 – 7.43 (m, 1H), 7.25 – 7.15 (2x d, *J* = 8.2 Hz, 1H), 4.29 (s, 1H), 4.17 – 4.12 (2x s, 3H), 3.61 – 3.53 (m, 6H), 2.42 – 2.33 (m, 4H). ^{13}C NMR (101 MHz, DMSO) δ 154.46, 149.72, 147.70 (br), 147.61 (br), 142.87, 142.12, 139.69, 138.56, 133.68 (br), 133.61, 132.78 (br), 132.60, 131.39 (br), 130.84 (br), 130.22, 129.10, 127.76, 124.17 (br), 123.20 (br), 121.96, 121.75, 118.91 (br), 118.00 (br), 111.69 (br), 111.09 (br), 83.54, 80.93, 66.28, 62.96, 56.68, 56.60, 53.25. LCMS (Fleet, 10 → 90%): t_r = 3.68 min, m/z: 507.3. HRMS [$C_{28}H_{26}N_8O_2$ + H]$^+$: 507.22515 calculated, 507.22522 found.

5-Methoxy-*N*-(3-(5-(morpholinomethyl)-1*H*-benzo[*d*]imidazol-2-yl)-1*H*-pyrazol-4-yl)-2-(3-(trifluoromethyl)phenyl)pyrimidin-4-amine (53)

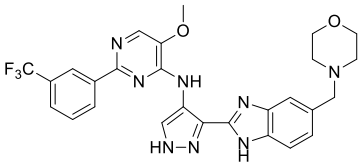

The title compound was synthesized from **129** (74.0 mg, 109 µmol) according to general procedure B (reaction time: 7 h). The crude was purified by automated column chromatography (1 – 20% MeOH/EtOAc) to afford the product (52.4 mg, 95.2 µmol, 88%). ^{1}H NMR (400 MHz, DMSO) δ 13.66 – 12.74 (br m, 2H), 10.74 (s, 1H), 8.63 – 8.56 (m, 3H), 8.19 (s, 1H), 7.82 – 7.78 (m, 1H), 7.73 (t, *J* = 7.7 Hz, 1H), 7.67 – 7.60 (br m, 1H), 7.48 – 7.42 (br m, 1H), 7.23 – 7.14 (br m, 1H), 4.14 (s, 3H), 3.62 – 3.52 (m, 6H), 2.43 – 2.30 (m, 4H). ^{13}C NMR (101 MHz, DMSO) δ 153.88, 149.75, 147.63 (br), 142.90 (br), 142.15 (br), 139.87, 139.07, 133.71 (br), 133.44, 132.81 (br), 132.58 (br), 131.38 (br), 130.93, 129.83 (br), 129.79, 129.51, 129.20, 128.88, 128.43, 125.93 (br), 125.90 (br), 125.86 (br), 125.83 (br), 125.73, 124.16 (br), 123.42 (br), 123.39 (br), 123.34 (br), 123.30 (br), 123.21 (br), 123.02, 121.71, 118.94 (br), 118.00 (br), 111.70 (br), 111.10 (br), 66.29, 62.98, 56.61, 53.26. LCMS (Fleet, 10 → 90%): t_r = 4.22 min, m/z: 551.3. HRMS [$C_{27}H_{25}F_3N_8O_2$ + H]$^+$: 551.21253 calculated, 551.21229 found.

3-(5-Methoxy-4-((3-(5-(morpholinomethyl)-1*H*-benzo[*d*]imidazol-2-yl)-1*H*-pyrazol-4-yl)amino)pyrimidin-2-yl)benzonitrile (54)

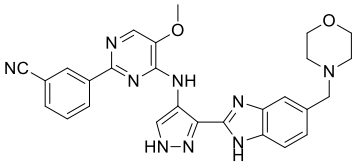

The title compound was synthesized from **130** (62.4 mg, 97.8 µmol) according to general procedure B (reaction time: 7 h). The crude was purified by automated column chromatography (1 – 20% MeOH/EtOAc) to afford the product (44.6 mg, 87.9 µmol, 90%). ^{1}H NMR (400 MHz, DMSO) δ 13.50 – 12.66 (br m, 2H), 10.71 (s, 1H), 8.60 (s, 1H), 8.60 – 8.55 (m, 2H), 8.14 (s, 1H), 7.87 (dt, *J* = 7.7, 1.4 Hz, 1H), 7.67 (t, *J* = 7.8 Hz, 1H), 7.62 (br s, 1H), 7.45 (br s, 1H), 7.22 – 7.14 (m, 1H), 4.13 (s, 3H), 3.61 – 3.53 (m, 6H), 2.43 – 2.32 (m, 4H). ^{13}C NMR (101 MHz, DMSO) δ 153.43, 149.71, 147.61 (br), 142.85 (br), 142.17 (br), 139.89, 139.18, 133.69 (br), 133.31, 132.82, 132.53 (br), 131.67, 131.44 (br), 130.80 (br), 130.42, 129.83, 124.14 (br), 123.21 (br), 121.60, 119.25 (br), 118.94, 118.01 (br), 111.71, 111.08 (br), 66.30, 62.99, 56.60, 53.27. LCMS (Fleet, 10 → 90%): t_r = 3.66 min, m/z: 508.2. HRMS [$C_{27}H_{25}N_9O_2$ + H]$^+$: 508.22040 calculated, 508.22051 found.

2-(3-Chloro-2-fluorophenyl)-5-methoxy-*N*-(3-(5-(morpholinomethyl)-1*H*-benzo[*d*]imidazol-2-yl)-1*H*-pyrazol-4-yl)pyrimidin-4-amine (55)

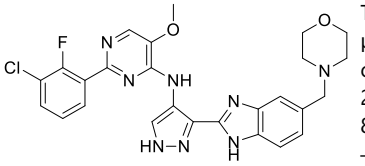

The title compound was synthesized from **131** (60.3 mg, 90.6 µmol) according to general procedure B (reaction time: 4 h). The crude was purified by automated column chromatography (2 – 20% MeOH/EtOAc) to afford the product (42.1 mg, 78.7 µmol, 87%). ^{1}H NMR (400 MHz, DMSO) δ 13.72 – 12.72 (br m, 2H), 10.74 – 10.68 (2x s, 1H), 8.60 (s, 1H), 8.23 (s, 1H), 8.05 (td, *J* = 7.8, 1.6 Hz, 1H), 7.70 – 7.60 (m, 2H), 7.48 – 7.42 (m, 1H), 7.33 (td, *J* = 7.9, 1.0 Hz, 1H), 7.24 – 7.14 (m, 1H), 4.18 – 4.12 (2x s, 3H), 3.60 – 3.53 (m, 6H), 2.41 – 2.33 (m, 4H). ^{13}C NMR (101 MHz, DMSO) δ 156.79, 154.26, 152.83, 152.78, 149.38, 147.68, 147.59, 142.89, 142.15, 139.41, 133.71, 133.58, 132.81, 132.56, 131.37, 131.18, 130.57, 130.29, 130.28, 128.37, 128.28, 125.09, 125.04, 124.16, 123.20, 121.77, 121.17, 120.98, 119.37 (br), 118.93, 117.99, 111.71, 111.09, 66.29, 62.97, 56.64, 56.57, 53.26. LCMS (Fleet, 10 → 90%): t_r = 3.70 min, m/z: 535.3. HRMS [$C_{26}H_{24}ClFN_8O_2$ + H]$^+$: 535.17675 calculated, 535.17673 found.

2-(3-Ethynyl-2-fluorophenyl)-5-methoxy-*N*-(3-(5-(morpholinomethyl)-1*H*-benzo[*d*]imidazol-2-yl)-1*H*-pyrazol-4-yl)pyrimidin-4-amine (56)

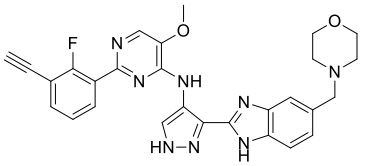

The title compound was synthesized from **132** (85.7 mg, 118 µmol) according to general procedure D (reaction time with TFA: 3 h). The crude was purified by automated column chromatography (1 – 20% MeOH/EtOAc) to afford the product (50.2 mg, 95.7 µmol, 81%). ^{1}H NMR (400 MHz, DMSO) δ 13.32 (s, 1H), 13.02 (s, 1H), 10.73 – 10.66 (2x s, 1H), 8.64 – 8.61 (2x s, 1H), 8.27 – 8.22 (2x s, 1H), 8.13 (td, *J* = 7.7, 1.8 Hz, 1H), 7.68 – 7.63 (m, 2H), 7.47 – 7.43 (m, 1H), 7.34 (t, *J* = 7.8 Hz, 1H), 7.23 – 7.16 (2x dd, *J* = 8.2, 1.5 Hz, 1H), 4.58 (s, 1H), 4.17 – 4.13 (2x s, 3H), 3.60 – 3.55 (m, 6H), 2.42 – 2.33 (m, 4H). ^{13}C NMR (101 MHz, DMSO) δ 161.95, 159.38, 152.98, 152.94, 149.34, 147.72, 147.62, 142.87, 142.13, 139.34, 134.53, 133.69, 133.65, 132.78, 132.58, 132.31, 132.28, 131.38, 130.74, 127.09, 127.00, 124.45, 124.41, 124.16, 123.19, 121.77, 119.13, 118.92, 117.99, 111.69, 111.51, 111.34, 111.08, 86.41, 86.38, 77.19, 77.17, 66.38, 66.28, 62.96, 56.65, 56.57, 53.26, 53.24. LCMS (Fleet, 10 → 90%): t_r = 3.61 min, m/z: 525.3. HRMS [$C_{28}H_{25}FN_8O_2$ + H]$^+$: 525.21573 calculated, 525.21579 found.

2-(5-Chloro-2-fluorophenyl)-5-methoxy-*N*-(3-(5-(morpholinomethyl)-1*H*-benzo[*d*]imidazol-2-yl)-1*H*-pyrazol-4-yl)pyrimidin-4-amine (57)

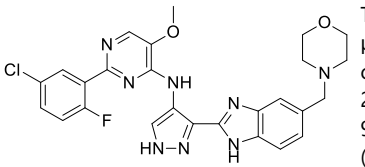

The title compound was synthesized from **133** (56.6 mg, 85.1 µmol) according to general procedure B (reaction time: 7 h). The crude was purified by automated column chromatography (1 – 20% MeOH/EtOAc) to afford the product (40.9 mg, 76.5 µmol, 90%). ^{1}H NMR (400 MHz, DMSO) δ 13.61 – 12.81 (br m, 2H), 10.70 (s, 1H), 8.61 – 8.60 (2x s, 1H), 8.22 (s, 1H), 8.07 (dd, *J* = 6.7, 2.8 Hz,

1H), 7.68 – 7.59 (br m, 1H), 7.55 (ddd, *J* = 8.8, 4.0, 2.8 Hz, 1H), 7.45 (br s, 1H), 7.41 (dd, *J* = 10.9, 8.8 Hz, 1H), 7.24 – 7.14 (br m, 1H), 4.15 (s, 3H), 3.61 – 3.53 (m, 6H), 2.42 – 2.32 (m, 4H). ^{13}C NMR (101 MHz, DMSO) δ 160.27, 157.76, 152.33, 152.28, 149.35, 147.64 (br), 142.89 (br), 142.14 (br), 139.43, 133.70 (br), 133.54, 132.80 (br), 132.58 (br), 131.40, 130.72, 130.63, 130.60, 130.58, 128.24, 128.21, 128.20, 128.09, 124.17 (br), 123.22 (br), 121.76, 119.12, 118.87, 118.00 (br), 111.71 (br), 111.09 (br), 66.29, 62.98, 56.61, 53.26. LCMS (Fleet, 10 → 90%): t_r = 3.68 min, m/z: 535.2. HRMS [$C_{26}H_{24}ClFN_8O_2$ + H]$^+$: 535.17675 calculated, 535.17674 found.

2-(5-Ethynyl-2-fluorophenyl)-5-methoxy-*N*-(3-(5-(morpholinomethyl)-1*H*-benzo[*d*]imidazol-2-yl)-1*H*-pyrazol-4-yl)pyrimidin-4-amine (58)

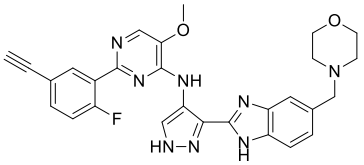

The title compound was synthesized from **134** (86.1 mg, 118 µmol) according to general procedure D (reaction time with TFA: 5 h). The crude was purified by automated column chromatography (1 – 20% MeOH/EtOAc) to afford the product (46.9 mg, 89.4 µmol, 75%). ^{1}H NMR (500 MHz, DMSO) δ 13.31 (br s, 1H), 13.02 (br s, 1H), 10.74 – 10.65 (2x s, 1H), 8.63 – 8.60 (2x s, 1H), 8.25 – 8.22 (2x s, 1H), 8.18 (dd, *J* = 7.5, 2.3 Hz, 1H), 7.68 – 7.60 (m, 2H), 7.48 – 7.43 (m, 1H), 7.40 (dd, *J* = 11.1, 8.5 Hz, 1H), 7.21 (2x dd, *J* = 8.2, 1.5 Hz, 1H), 4.24 (s, 1H), 4.18 – 4.13 (2x s, 3H), 3.62 – 3.53 (m, 6H), 2.43 – 2.32 (m, 4H). ^{13}C NMR (126 MHz, DMSO) δ 161.29, 159.26, 152.66, 152.63, 149.37, 147.70, 147.60, 142.88, 142.13, 139.38, 134.73, 134.34, 134.27, 133.69, 133.63, 132.79, 132.58, 131.38, 130.76, 127.08, 126.99, 124.16, 123.20, 121.80, 119.10, 118.92, 118.07, 118.04, 117.99, 117.84, 117.65, 111.69, 111.08, 82.37, 80.75, 66.28, 62.96, 56.65, 56.57, 53.26. LCMS (Fleet, 10 → 90%): t_r = 3.59 min, m/z: 525.2. HRMS [$C_{28}H_{25}FN_8O_2$ + H]$^+$: 525.21573 calculated, 525.21586 found.

2-(3-Chloro-2,6-difluorophenyl)-5-methoxy-*N*-(3-(5-(morpholinomethyl)-1*H*-benzo[*d*]imidazol-2-yl)-1*H*-pyrazol-4-yl)pyrimidin-4-amine (59)

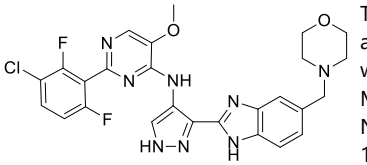

The title compound was synthesized from 137 (10 mg, 15 µmol) according to general procedure B (reaction time: 5 h). The crude was purified by automated column chromatography (1 – 15% MeOH/EtOAc) to afford the product (7.1 mg, 13 µmol, 88%). ^{1}H NMR (600 MHz, DMSO) δ 13.41 – 12.84 (br m, 2H), 10.72 (br s, 1H), 8.36 (s, 1H), 8.26 (s, 1H), 7.77 (td, *J* = 8.7, 5.5 Hz, 1H), 7.71 – 7.57 (br m, 1H), 7.52 – 7.40 (br m, 1H), 7.34 (td, *J* = 9.0, 1.7 Hz, 1H), 7.23 – 7.18 (br m, 1H), 4.17 (s, 3H), 3.61 – 3.56 (m, 6H), 2.43 – 2.36 (m, 4H). ^{13}C NMR (151 MHz, DMSO) δ 159.49, 159.46, 157.84, 157.80, 156.10, 156.05, 154.43, 154.38, 149.50, 148.65, 147.52 (br), 142.04 (br), 139.64, 134.67 (br), 133.56, 132.77 (br), 131.43 (br), 130.84, 130.77, 124.11 (br), 123.15 (br), 121.50, 119.14 (br), 119.07, 118.95, 118.94, 118.82, 117.97 (br), 116.06, 116.03, 115.94, 115.91, 113.36, 113.34, 113.20, 113.18, 111.67 (br), 111.05 (br), 66.25, 62.91, 56.66, 53.23. LCMS (Fleet, 10 → 90%): t_r = 3.80 min, m/z: 553.3. HRMS [$C_{26}H_{23}ClF_2N_8O_2$ + H]$^+$: 553.16733 calculated, 553.16754 found.

2-(3-Ethynyl-2,6-difluorophenyl)-5-methoxy-*N*-(3-(5-(morpholinomethyl)-1*H*-benzo[*d*]imidazol-2-yl)-1*H*-pyrazol-4-yl)pyrimidin-4-amine (60)

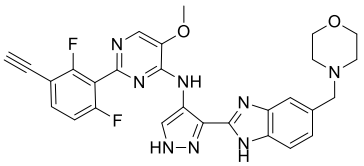

The title compound was synthesized from 138 (24 mg, 32 µmol) according to general procedure D (reaction time with TFA: 5 h). The crude was purified by automated column chromatography (1 – 15% MeOH/EtOAc) to afford the product (16.6 mg, 30.6 µmol, 95%). ^{1}H NMR (400 MHz, DMSO) δ 13.38 – 12.90 (br m, 2H), 10.72 (s, 1H), 8.36 (s, 1H), 8.26 (s, 1H), 7.73 (td, *J* = 8.2, 6.1 Hz, 1H), 7.69 – 7.60 (br m, 1H), 7.49 – 7.41 (br m, 1H), 7.31 (td, *J* = 8.9, 1.3 Hz, 1H), 7.25 – 7.16 (br m, 1H), 4.57 (s, 1H), 4.17 (s, 3H), 3.64 – 3.53 (m, 6H), 2.44 – 2.33 (m, 4H). ^{13}C NMR (101 MHz, DMSO) δ 161.99, 161.92, 161.33, 161.27, 159.46, 159.39, 158.81, 158.75, 149.50, 148.72, 147.55 (br), 142.88 – 142.61 (m), 142.16 – 142.02 (m), 139.61, 134.45, 134.35, 133.67 (br), 133.58, 132.76 (br), 132.62 (br), 131.43 (br), 130.73 (br), 124.15 (br), 123.19 (br), 121.56, 119.18 (br), 118.93 (br), 118.27, 118.09, 118.01 (br), 117.90, 112.86, 112.82, 112.63, 112.60, 111.70 (br), 111.11 (br), 107.21, 107.17, 107.04, 107.00, 86.36, 76.02, 66.27,

62.94, 56.67, 53.25. LCMS (Fleet, 10 → 90%): t_r = 3.69 min, m/z: 543.3. HRMS $[C_{28}H_{24}F_2N_8O_2 + H]^+$: 543.20630 calculated, 543.20646 found.

4-((2-(4-Nitro-1*H*-pyrazol-3-yl)-1*H*-benzo[*d*]imidazol-5-yl)methyl)morpholine (61)

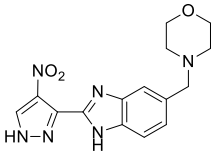

The title compound was synthesized as described in **Chapter 2** (compound 29)

4-((2-(4-Nitro-1-((2-(trimethylsilyl)ethoxy)methyl)-1*H*-pyrazol-3-yl)-1-((2-(trimethylsilyl)ethoxy)methyl)-1*H*-benzo[*d*]imidazol-5-yl)methyl)morpholine (62) & 3 regioisomers

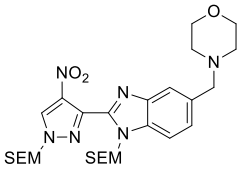

61 (3.07 g, 9.35 mmol) was suspended in dry DCM (45 mL) and cooled down to 0°C. DIPEA (5.1 mL, 29 mmol) was added after which SEM-Cl (3.56 mL, 20.1 mmol) was added dropwise. The mixture was left to stir at 0°C and allowed to warm to RT overnight. The mixture was poured into 0.05 M $NaHCO_3$ (aq.) (150 mL) and the product extracted with DCM (2x100 mL). The combined organic layers were washed with brine (200 mL) and the layers were separated. The brine layer was extracted with DCM (30 mL) after which the combined organic layers were dried over Na_2SO_4, filtered and concentrated. The crude was purified several times either by manual or automated column chromatography to separate all four regioisomers (total yield: 3.26 g, 5.54 mmol, 60%). NMR data (sorted on descending isomer lipophilicity as determined by TLC analysis): Regioisomer 1 – yield (1.34 g, 2.28 mmol, 25%). ^{1}H NMR (500 MHz, $CDCl_3$) δ 8.29 (s, 1H), 7.79 (d, *J* = 8.3 Hz, 1H), 7.61 (s, 1H), 7.39 (dd, *J* = 8.4, 1.3 Hz, 1H), 5.83 – 5.40 (br m, 2H), 5.32 (br s, 2H), 3.75 – 3.70 (m, 4H), 3.67 (s, 2H), 3.62 (br s, 2H), 3.43 – 3.36 (m, 2H), 2.56 – 2.45 (m, 4H), 0.89 – 0.72 (m, 4H), -0.05 (s, 9H), -0.08 (s, 9H). ^{13}C NMR (126 MHz, $CDCl_3$) δ 142.58, 139.22, 136.37, 136.13, 135.38, 135.30, 131.10, 125.13, 120.56, 111.35, 79.55, 74.39, 68.22, 67.14, 67.05, 63.81, 53.82, 17.94, 17.83, -1.33, -1.42. LCMS (Finnigan, 10 → 90%): t_r = 7.89 min, m/z: 589.1. Regioisomer 2 – yield (765 mg, 1.30 mmol, 14%). ^{1}H NMR (500 MHz, $CDCl_3$) δ 8.28 (s, 1H), 7.78 (s, 1H), 7.57 (d, *J* = 8.4 Hz, 1H), 7.45 (dd, *J* = 8.4, 1.2 Hz, 1H), 5.77 – 5.38 (br m, 2H), 5.31 (br s, 2H), 3.74 – 3.70 (m, 4H), 3.65 (s, 2H), 3.60 (br s, 2H), 3.42 – 3.35 (m, 2H), 2.52 – 2.46 (m, 4H), 0.87 – 0.72 (m, 4H), -0.06 (s, 9H), -0.09 (s, 9H). ^{13}C NMR (126 MHz, $CDCl_3$) δ 143.24, 139.27, 136.31, 136.11, 134.47, 133.60, 131.05, 126.36, 121.20, 110.85, 79.53, 74.45, 68.17, 67.12, 67.01, 63.57, 53.71, 17.89, 17.77, -1.38, -1.46. LCMS (Finnigan, 10 → 90%): t_r = 8.00 min, m/z: 589.1. Regioisomer 3 – yield (502 mg, 0.853 mmol, 9%). ^{1}H NMR (500 MHz, $CDCl_3$) δ 8.48 (s, 1H), 7.75 (d, *J* = 8.3 Hz, 1H), 7.55 (s, 1H), 7.31 (dd, *J* = 8.3, 1.3 Hz, 1H), 5.51 (s, 2H), 5.50 (s, 2H), 3.72 – 3.68 (m, 4H), 3.68 – 3.64 (m, 2H), 3.63 (s, 2H), 3.36 – 3.31 (m, 2H), 2.50 – 2.42 (m, 4H), 0.97 – 0.92 (m, 2H), 0.76 – 0.71 (m, 2H), -0.02 (s, 9H), -0.15 (s, 9H). ^{13}C NMR (126 MHz, $CDCl_3$) δ 143.02, 142.38, 137.77, 135.63, 135.12, 134.29, 130.01, 124.66, 120.26, 111.10, 82.14, 73.76, 68.47, 67.04, 66.36, 63.79, 53.69, 17.90, 17.65, -1.36, -1.48. LCMS (Finnigan, 10 → 90%): t_r = 7.53 min, m/z: 589.1. Regioisomer 4 – yield (649 mg, 1.10 mmol, 12%). ^{1}H NMR (500 MHz, $CDCl_3$) δ 8.49 (s, 1H), 7.76 (s, 1H), 7.53 (d, *J* = 8.4 Hz, 1H), 7.38 (dd, *J* = 8.4, 1.2 Hz, 1H), 5.51 (s, 2H), 5.50 (s, 2H), 3.71 – 3.68 (m, 4H), 3.68 – 3.64 (m, 2H), 3.63 (s, 2H), 3.36 – 3.31 (m, 2H), 2.50 – 2.44 (m, 4H), 0.98 – 0.93 (m, 2H), 0.77 – 0.72 (m, 2H), -0.01 (s, 9H), -0.15 (s, 9H). ^{13}C NMR (126 MHz, $CDCl_3$) δ 143.15, 143.09, 137.79, 135.69, 134.31, 132.95, 129.99, 125.68, 121.13, 110.56, 82.19, 73.88, 68.53, 67.09, 66.40, 63.64, 53.64, 17.94, 17.65, -1.33, -1.46. LCMS (Finnigan, 10 → 90%): t_r = 7.70 min, m/z: 589.1.

3-(5-(Morpholinomethyl)-1-((2-(trimethylsilyl)ethoxy)methyl)-1*H*-benzo[*d*]imidazol-2-yl)-1-((2-(trimethylsilyl)ethoxy)methyl)-1*H*-pyrazol-4-amine (63)

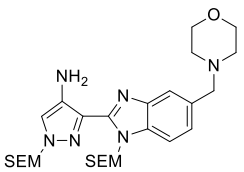

62 (502 mg, 853 µmol) was dissolved in degassed MeOH (10 mL). 10% Pd/C (60 mg) was added and the atmosphere was exchanged for H_2. The reaction was vigorously stirred for 3.5 h while bubbling H_2 through the mixture. The atmosphere was exchanged for N_2, the mixture was filtered over Celite and concentrated to afford the product, which was used as such in subsequent

reaction (471 mg, 853 µmol, 99%). LCMS (Finnigan, 10 → 90%): t_r = 6.59 min, m/z: 559.1.

2-Chloro-*N*-(3-(5-(morpholinomethyl)-1-((2-(trimethylsilyl)ethoxy)methyl)-1*H*-benzo[*d*]imidazol-2-yl)-1-((2-(trimethylsilyl)ethoxy)methyl)-1*H*-pyrazol-4-yl)pyrimidin-4-amine (64)

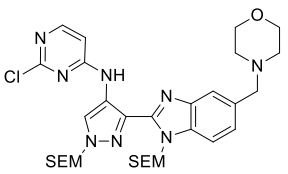

63 (471 mg, 843 µmol) was dissolved in EtOH (2 mL) after which DIPEA (450 µL, 2.69 mmol) and 2,4-dichloropyrimidine (119 mg, 801 µmol) were added. The mixture was stirred at 40°C for 3 days and subsequently poured into H_2O (50 mL). The product was extracted with DCM (2x50 mL) and the combined organic layers were washed with brine (100 mL), dried over Na_2SO_4, filtered and concentrated. The crude was purified by silica gel column chromatography (1 – 4% MeOH/DCM) to afford the product (305 mg, 455 µmol, 54%). ^{1}H NMR (500 MHz, $CDCl_3$) δ 11.00 (s, 1H), 8.57 (s, 1H), 8.11 (d, *J* = 5.8 Hz, 1H), 7.70 (d, *J* = 8.2 Hz, 1H), 7.56 (s, 1H), 7.32 (dd, *J* = 8.3, 1.4 Hz, 1H), 6.68 (d, *J* = 5.8 Hz, 1H), 6.26 (s, 2H), 5.50 (s, 2H), 3.75 – 3.69 (m, 4H), 3.69 – 3.60 (m, 6H), 2.54 – 2.44 (m, 4H), 0.99 – 0.94 (m, 2H), 0.90 – 0.85 (m, 2H), 0.00 (s, 9H), -0.12 (s, 9H). ^{13}C NMR (126 MHz, $CDCl_3$) δ 160.95, 159.52, 156.33, 146.84, 141.60, 135.03, 133.84, 131.70, 124.71, 124.39, 121.18, 118.78, 111.47, 106.27, 81.29, 73.92, 67.17, 67.10, 66.15, 63.87, 53.76, 17.96, 17.83, -1.29, -1.34. LCMS (Finnigan, 10 → 90%): t_r = 8.73 min, m/z: 671.1.

***N*-(3-(5-(Morpholinomethyl)-1-((2-(trimethylsilyl)ethoxy)methyl)-1*H*-benzo[*d*]imidazol-2-yl)-1-((2-(trimethylsilyl)ethoxy)methyl)-1H-pyrazol-4-yl)-2-((trimethylsilyl)ethynyl)pyrimidin-4-amine (65)**

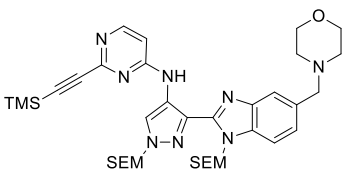

A microwave vial was charged with **64** (104 mg, 155 µmol) and Et_3N (1 mL). N_2 was bubbled through the mixture for 1 min after which $PdCl_2(PPh_3)_2$ and Cu(I)I were added. N_2 was bubbled through the mixture for 30 sec after which ethynyltrimethylsilane (100 µL, 722 µmol) was added and the vial was sealed. The mixture was heated to 89°C and stirred for 5 h. Ethynyltrimethylsilane (50 µL, 361 µmol) was added via syringe and the mixture was stirred at 90°C for 16 h. The mixture was diluted in MeOH (15 mL), filtered over Celite and subsequently concentrated. The crude was purified by automated column chromatography (0 – 10% MeOH/EtOAc) to afford the product (19.1 mg, 26.1 µmol, 17%). ^{1}H NMR (500 MHz, $CDCl_3$) δ 8.16 (d, *J* = 6.0 Hz, 1H), 8.05 (br s, 1H), 7.76 (br s, 1H), 7.72 (s, 1H), 7.44 (d, *J* = 8.3 Hz, 1H), 7.39 (dd, *J* = 8.4, 1.3 Hz, 1H), 6.49 (d, *J* = 6.0 Hz, 1H), 5.54 (s, 2H), 5.38 (s, 2H), 3.73 – 3.69 (m, 4H), 3.63 (s, 2H), 3.58 – 3.49 (m, 4H), 2.52 – 2.43 (m, 4H), 0.98 – 0.92 (m, 2H), 0.79 – 0.73 (m, 2H), 0.24 (s, 9H), -0.06 (s, 9H), -0.09 (s, 9H). ^{13}C NMR (126 MHz, $CDCl_3$) δ 156.37, 152.04, 143.31, 142.29, 134.75, 134.56, 133.52, 125.97, 120.95, 110.24, 102.89, 92.42, 79.05, 73.79, 67.68, 67.30, 67.13, 63.58, 53.70, 17.99, 17.95, -0.30, -1.34, -1.42 (not all quaternary carbons were observed). LCMS (Finnigan, 10 → 90%): t_r = 6.64 min, m/z: 661.2.

N-(3-(5-(Morpholinomethyl)-1-((2-(trimethylsilyl)ethoxy)methyl)-1*H*-benzo[*d*]imidazol-2-yl)-1-((2-(trimethylsilyl)ethoxy)methyl)-1*H*-pyrazol-4-yl)-2-phenylpyrimidin-4-amine (66)

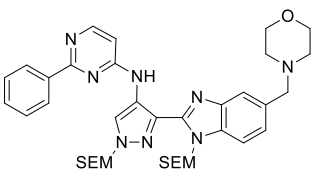

A microwave vial was charged with **64** (65.8 mg, 98.0 µmol), phenylboronic acid (20.3 mg, 167 µmol), K_2CO_3 (4.7 M (aq.), 83 µL, 392 µmol) and dioxane (0.33 mL). N_2 was bubbled through the mixture for 1 min after which $Pd(dppf)Cl_2$·DCM (4.0 mg, 4.9 µmol) was added. N_2 was bubbled through the mixture for 30 sec after which the vial was sealed. The mixture was heated to 90°C, stirred for 3.5 h and subsequently poured into H_2O (20 mL). The product was extracted with DCM (2x20 mL) and the combined organic layers were washed with brine (40 mL), dried over Na_2SO_4, filtered and concentrated. The crude was purified by automated column chromatography (50 – 100% EtOAc/pentane) to afford the product (34.2 mg, 47.9 µmol, 49%). ^{1}H NMR (400 MHz, $CDCl_3$) δ 10.72 (s, 1H), 8.79 (s, 1H), 8.44 – 8.38 (m, 3H), 7.75 (d, *J* = 8.2 Hz, 1H), 7.58 (s, 1H), 7.56 – 7.48 (m, 3H), 7.35 (dd, *J* = 8.3, 1.4 Hz, 1H), 6.74 (d, *J* = 5.8 Hz, 1H), 6.30 (s, 2H), 5.56 (s, 2H), 3.77 – 3.73 (m, 4H), 3.72 – 3.62 (m, 6H), 2.54 – 2.48 (m, 4H), 1.02 – 0.96 (m, 2H), 0.92 – 0.87 (m, 2H), -0.01 (s, 9H), -0.10 (s, 9H). ^{13}C NMR (101 MHz, $CDCl_3$) δ 164.85, 158.81, 155.36, 147.17, 141.86, 138.87, 135.14, 133.62, 131.67, 130.41,

128.60, 128.22, 125.52, 124.69, 120.44, 118.90, 111.51, 106.05, 81.46, 73.99, 67.20, 67.15, 66.14, 63.96, 53.80, 18.01, 17.92, -1.24, -1.29. LCMS (Finnigan, 10 → 90%): t_r = 7.03 min, m/z: 713.3.

_N_-(3-(5-(Morpholinomethyl)-1-((2-(trimethylsilyl)ethoxy)methyl)-1_H_-benzo[_d_]imidazol-2-yl)-1-((2-(trimethylsilyl)ethoxy)methyl)-1_H_-pyrazol-4-yl)-2-phenoxypyrimidin-4-amine (67)

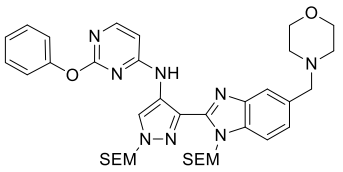

NaH (60% in mineral oil, 46 mg, 1.15 mmol) was suspended in dioxane (4 mL) and cooled down to 0°C. Phenol (116 mg, 1.23 mmol) was carefully added (H_2 evolution) and the mixture was allowed to warm to RT and stirred for 30 min. Of this mixture, 400 µL was added to a microwave vial charged with **64** (27.6 mg, 41.1 µmol) after which the vial was sealed and the mixture was stirred at 100°C for 16 h. Extra sodium phenolate was prepared freshly as described above, of which 100 µL was added to the mixture which was continued to stir at 100°C for 24 h. The mixture was poured into 1 M $NaHCO_3$ (aq.) (20 mL) and the product extracted with DCM (2x20 mL). The combined organic layers were concentrated as such and purified by automated column chromatography (0 – 15% MeOH/DCM) to afford the product (18 mg, 24.7 µmol, 60%). ^{1}H NMR (500 MHz, $CDCl_3$) δ 10.76 (s, 1H), 8.19 (d, _J_ = 5.8 Hz, 1H), 7.73 (s, 1H), 7.56 – 7.45 (m, 4H), 7.36 – 7.31 (m, 2H), 7.30 – 7.27 (m, 2H), 6.52 (d, _J_ = 5.8 Hz, 1H), 6.23 (s, 2H), 5.19 (s, 2H), 3.76 – 3.71 (m, 4H), 3.66 (s, 2H), 3.59 – 3.55 (m, 2H), 3.54 – 3.50 (m, 2H), 2.55 – 2.45 (m, 4H), 0.94 – 0.89 (m, 2H), 0.88 – 0.83 (m, 2H), -0.00 (s, 9H), -0.13 (s, 9H). ^{13}C NMR (126 MHz, $CDCl_3$) δ 166.10, 160.02, 157.35, 153.79, 147.16, 142.48, 134.32, 131.71, 129.76, 125.20, 124.60, 123.03, 121.44, 119.76, 110.78, 102.42, 80.96, 74.03, 67.16, 66.95, 66.06, 63.85, 53.75, 17.95, 17.87, -1.21, -1.33. LCMS (Finnigan, 10 → 90%): t_r = 7.37 min, m/z: 729.2.

2-(Benzyloxy)-_N_-(3-(5-(morpholinomethyl)-1-((2-(trimethylsilyl)ethoxy)methyl)-1_H_-benzo[_d_]imidazol-2-yl)-1-((2-(trimethylsilyl)ethoxy)methyl)-1_H_-pyrazol-4-yl)pyrimidin-4-amine (68)

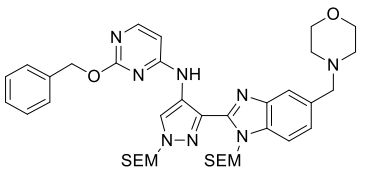

NaH (60% in mineral oil, 90.0 mg, 2.25 mmol) was suspended in dioxane (3 mL) and cooled down to 0°C. Benzyl alcohol (250 µL, 2.41 mmol) was carefully added (H_2 evolution) and the mixture was allowed to warm to RT and stirred for 2 h. Of this mixture, 300 µL was added to a microwave vial charged with **64** (80.9 mg, 120 µmol) after which the vial was sealed and the mixture was stirred at 90°C for 16 h. The mixture was poured into H_2O (20 mL) and brine (0.5 mL), and the product extracted with DCM (2x20 mL). The combined organic layers were concentrated as such and purified by automated column chromatography (1 – 10% MeOH/DCM) to afford the product (63.3 mg, 85.2 µmol, 71%). ^{1}H NMR (400 MHz, $CDCl_3$) δ 8.12 (br s, 1H), 8.05 (br s, 1H), 8.01 (d, _J_ = 5.8 Hz, 1H), 7.65 (d, _J_ = 8.3 Hz, 1H), 7.46 – 7.40 (m, 3H), 7.35 – 7.30 (m, 2H), 7.30 – 7.26 (m, 2H), 6.21 (d, _J_ = 5.8 Hz, 1H), 5.52 (s, 2H), 5.35 (s, 2H), 5.34 (s, 2H), 3.74 – 3.67 (m, 4H), 3.61 (s, 2H), 3.54 – 3.46 (m, 4H), 2.53 – 2.41 (m, 4H), 0.93 – 0.86 (m, 2H), 0.78 – 0.70 (m, 2H), -0.09 (s, 9H), -0.10 (s, 9H). ^{13}C NMR (101 MHz, $CDCl_3$) δ 165.11, 162.37 (br), 157.83 (br), 142.48, 142.37, 136.83, 135.17, 134.75 (br), 134.53, 128.42, 127.91, 127.86, 124.89, 124.49 (br), 119.84, 110.94, 99.29 (br), 78.83, 73.75, 68.68, 67.38, 67.12, 67.06, 63.74, 53.72, 17.99, 17.87, -1.40, -1.46. LCMS (Finnigan, 10 → 90%): t_r = 6.82 min, m/z: 743.3.

_N_-(3-(5-(Morpholinomethyl)-1-((2-(trimethylsilyl)ethoxy)methyl)-1_H_-benzo[_d_]imidazol-2-yl)-1-((2-(trimethylsilyl)ethoxy)methyl)-1_H_-pyrazol-4-yl)-2-phenethoxypyrimidin-4-amine (69)

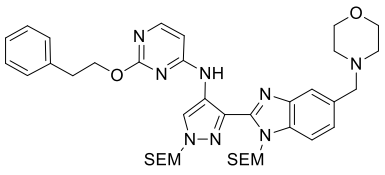

NaH (60% in mineral oil, 120 mg, 3.02 mmol) was suspended in dioxane (6 mL), phenethyl alcohol (400 µL, 3.34 mmol) was carefully added and the mixture was stirred at 45°C for 3 h. The mixture was cooled down to RT and 300 µL was added to a microwave vial charged with **64** (61.3 mg, 91.3 µmol) after which the vial was sealed and the mixture was stirred at 90°C for 16 h. The mixture was poured into H_2O (20 mL) and the product extracted with DCM (2x20 mL). The combined organic layers were concentrated as such and purified by automated column chromatography (50 – 100% EtOAc/pentane) to afford the product (30.6 mg, 40.4 µmol, 44%). ^{1}H NMR (400 MHz, $CDCl_3$) δ 10.72 (s, 1H), 8.57 (s, 1H), 8.11 (d, _J_ = 5.7 Hz, 1H), 7.75

(s, 1H), 7.54 (d, *J* = 8.3 Hz, 1H), 7.38 – 7.30 (m, 5H), 7.26 – 7.22 (m, 1H), 6.46 (d, *J* = 5.8 Hz, 1H), 6.27 (s, 2H), 5.45 (s, 2H), 4.61 (t, *J* = 7.5 Hz, 2H), 3.77 – 3.71 (m, 4H), 3.67 (s, 2H), 3.66 – 3.57 (m, 4H), 3.19 (t, *J* = 7.5 Hz, 2H), 2.55 – 2.47 (m, 4H), 0.98 – 0.90 (m, 2H), 0.93 – 0.84 (m, 2H), -0.01 (s, 9H), -0.11 (s, 9H). ^{13}C NMR (101 MHz, $CDCl_3$) δ 165.42, 160.49, 156.54, 147.18, 142.49, 138.32, 134.32, 132.80, 131.60, 129.13, 128.62, 126.57, 125.22, 125.20, 120.69, 119.79, 110.73, 101.95, 81.26, 74.02, 67.77, 67.14, 67.09, 66.08, 63.84, 53.73, 35.52, 17.94, 17.85, -1.25, -1.33. LCMS (Finnigan, 10 → 90%): t_r = 7.75 min, m/z: 757.3.

_N_-(3-(5-(Morpholinomethyl)-1-((2-(trimethylsilyl)ethoxy)methyl)-1_H_-benzo[_d_]imidazol-2-yl)-1-((2-(trimethylsilyl)ethoxy)methyl)-1_H_-pyrazol-4-yl)-2-(1_H_-pyrazol-1-yl)pyrimidin-4-amine (70)

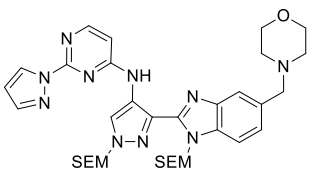

NaH (60% in mineral oil, 74 mg, 1.85 mmol) was suspended in dioxane (2 mL) and cooled down to 0°C. 1*H*-Pyrazole (155 mg, 2.28 mmol) was carefully added (H_2 evolution) and the mixture was allowed to warm to RT and stirred for 1.5 h. Of this mixture, 300 µL was added to a microwave vial charged with **64** (136 mg, 203 µmol) after which the vial was sealed and the mixture was stirred at 90°C for 45 min. The mixture was poured into H_2O (20 mL) and the product extracted with DCM (2x20 mL). The combined organic layers were concentrated as such and purified by automated column chromatography (70 – 100% EtOAc/pentane, then 0 – 10% MeOH/EtOAc) to afford the product (78.2 mg, 111 µmol, 55%). ^{1}H NMR (500 MHz, $CDCl_3$) δ 10.98 (s, 1H), 8.86 (s, 1H), 8.56 – 8.52 (m, 1H), 8.29 (d, *J* = 5.8 Hz, 1H), 7.84 – 7.80 (m, 1H), 7.76 – 7.74 (m, 1H), 7.54 (d, *J* = 8.3 Hz, 1H), 7.33 (dd, *J* = 8.3, 1.4 Hz, 1H), 6.69 (d, *J* = 5.8 Hz, 1H), 6.48 (dd, *J* = 2.6, 1.6 Hz, 1H), 6.27 (s, 2H), 5.55 (s, 2H), 3.76 – 3.70 (m, 4H), 3.72 – 3.65 (m, 2H), 3.66 (s, 2H), 3.65 – 3.59 (m, 2H), 2.50 (s, 4H), 1.01 – 0.94 (m, 2H), 0.91 – 0.85 (m, 2H), -0.02 (s, 9H), -0.12 (s, 9H). ^{13}C NMR (126 MHz, $CDCl_3$) δ 159.45, 156.01, 147.12, 143.05, 142.40, 134.28, 132.84, 131.67, 128.80, 125.20, 124.97, 121.25, 119.71, 110.72, 108.15, 105.21, 81.36, 74.00, 67.19, 67.09, 66.08, 63.79, 53.69, 17.92, 17.83, -1.30, -1.37. LCMS (Finnigan, 10 → 90%): t_r = 8.03 min, m/z: 703.2.

_N_-(3-(5-(Morpholinomethyl)-1-((2-(trimethylsilyl)ethoxy)methyl)-1_H_-benzo[_d_]imidazol-2-yl)-1-((2-(trimethylsilyl)ethoxy)methyl)-1_H_-pyrazol-4-yl)-2-(thiophen-3-yl)pyrimidin-4-amine (71)

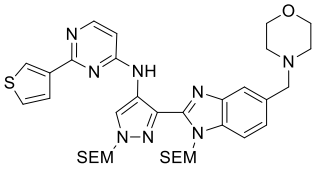

A microwave vial was charged with **64** (75.0 mg, 112 µmol), thiophene-3-boronic acid pinacol ester (27.5 mg, 134 µmol), K_2CO_3 (61.8 mg, 447 µmol), dioxane (0.8 mL) and H_2O (0.2 mL). N_2 was bubbled through the mixture for 1 min after which Pd(dppf)Cl_2·DCM (6.5 mg, 8.0 µmol) was added. N_2 was bubbled through the mixture for 30 sec after which the vial was sealed and the mixture was stirred at 100°C for 6 h. The mixture was diluted in 1:1:1 EtOAc/H_2O/brine (9 mL) and filtered over Celite. The mixture was poured into H_2O (10 mL) and EtOAc (10 mL) and the layers were separated. The organic layer was washed with brine (10 mL), dried over Na_2SO_4, filtered and concentrated. The crude was purified by automated column chromatography (0 – 10% MeOH/DCM) and used as such in subsequent reaction (yield: 43.2 mg). LCMS m/z: 719.3.

_N_-(3-(5-(Morpholinomethyl)-1-((2-(trimethylsilyl)ethoxy)methyl)-1_H_-benzo[_d_]imidazol-2-yl)-1-((2-(trimethylsilyl)ethoxy)methyl)-1_H_-pyrazol-4-yl)-2-(thiophen-2-yl)pyrimidin-4-amine (72)

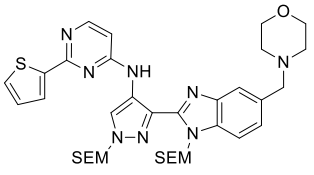

A microwave vial was charged with **64** (75.0 mg, 112 µmol), thiophene-2-boronic acid pinacol ester (27.5 mg, 134 µmol), K_2CO_3 (61.8 mg, 447 µmol), dioxane (0.8 mL) and H_2O (0.2 mL). N_2 was bubbled through the mixture for 1 min after which Pd(dppf)Cl_2·DCM (6.5 mg, 8.0 µmol) was added. N_2 was bubbled through the mixture for 30 sec after which the vial was sealed and the mixture was stirred at 100°C for 6 h. The mixture was poured into H_2O (10 mL) and the product extracted with DCM (10 mL). The organic layer was concentrated as such and purified by automated column chromatography (0 – 10% MeOH/DCM) and used as such in subsequent reaction (yield: 59.6 mg). LCMS (Finnigan, 10 → 90%): t_r = 7.31 min, m/z: 719.3.

2-(4-Nitro-1*H*-pyrazol-3-yl)-1*H*-benzo[*d*]imidazole (73)

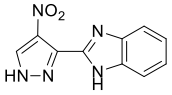

Benzene-1,2-diamine (9.39 g, 87.0 mmol), 4-nitro-1H-pyrazole-3-carboxylic acid (13.6 g, 87.0 mmol), EDC·HCl (16.7 g, 87.0 mmol) and HOBt (11.7 g, 87.0 mmol) were mixed in DMF (140 mL) and stirred for 18 h. The mixture was concentrated at 60°C after which AcOH (110 mL) was added and the reaction was stirred at 118°C for 75 min. Sat. $NaHCO_3$ (aq.) (440 mL) was added carefully while the mixture was stirred vigorously. The mixture was stirred for 1 h, filtered and the solids were washed with H_2O (2x50 mL). The solids were collected and traces of water were removed by coevaporation with MeOH to afford the product (14.0 g, 60.9 mmol, 70%). ^{1}H NMR (400 MHz, DMSO) δ 14.55 (br s, 1H), 13.01 (br s, 1H), 8.84 (br s, 1H), 7.74 – 7.67 (m, 2H), 7.33 – 7.24 (m, 2H). ^{13}C NMR (101 MHz, DMSO) δ 158.83, 141.58, 135.26, 134.13, 132.96, 122.89, 115.69 (br). LCMS (Finnigan, 0 → 90%): t_r = 4.51 min, m/z: 230.1.

2-(4-Nitro-1-((2-(trimethylsilyl)ethoxy)methyl)-1*H*-pyrazol-3-yl)-1-((2-(trimethylsilyl)ethoxy)methyl)-1*H*-benzo[*d*]imidazole (74)

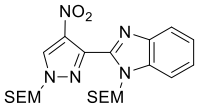

73 (10.0 g, 43.6 mmol) was suspended in DCM (220 mL) and cooled down to 0°C. DIPEA (22.8 mL, 131 mmol) was added after which SEM-Cl (17 mL, 96 mmol) was added dropwise. The mixture was stirred at 0°C for 15 min and then allowed to warm to RT and stirred for 1.5 h. The mixture was poured into 0.05 M $NaHCO_3$ (aq.) (300 mL) and the organic layer was separated. The water layer was extracted with DCM (150 mL) after which the combined organic layers were washed with brine (300 mL). The brine layer was extracted with DCM (100 mL) after which the organic layers were combined, dried over Na_2SO_4, filtered and concentrated. The crude was purified by silica gel chromatography (twice, 0 – 3% MeOH/DCM) to afford both regioisomers in pure form (total yield: 17.2 g, 35.2 mmol, 81%). NMR data (sorted on descending isomer lipophilicity): Regioisomer 1 – yield (8.45 g, 17.3 mmol, 40%). ^{1}H NMR (400 MHz, $CDCl_3$) δ 8.30 (s, 1H), 7.86 (dd, *J* = 7.3, 1.0 Hz, 1H), 7.65 – 7.62 (m, 1H), 7.44 (td, *J* = 7.7, 1.3 Hz, 1H), 7.39 (td, *J* = 7.7, 1.3 Hz, 1H), 5.75 – 5.40 (br m, 2H), 5.39 – 5.29 (br m, 2H), 3.70 – 3.54 (br m, 2H), 3.44 – 3.36 (m, 2H), 0.90 – 0.70 (m, 4H), -0.05 (s, 9H), -0.08 (s, 9H). ^{13}C NMR (101 MHz, $CDCl_3$) δ 143.11, 139.14, 136.31, 136.11, 135.19, 131.04, 124.92, 123.60, 120.90, 111.13, 79.52, 74.38, 68.15, 67.00, 17.86, 17.76, -1.40, -1.47. LCMS (Finnigan, 10 → 90%): t_r = 10.86 min, m/z: 490.0. Regioisomer 2 – yield (8.78 g, 17.9 mmol, 41%). ^{1}H NMR (400 MHz, $CDCl_3$) δ 8.49 (s, 1H), 7.85 (dd, *J* = 7.1, 1.4 Hz, 1H), 7.60 (dd, *J* = 7.0, 1.3 Hz, 1H), 7.41 – 7.32 (m, 2H), 5.53 (s, 2H), 5.52 (s, 2H), 3.72 – 3.65 (m, 2H), 3.39 – 3.32 (m, 2H), 1.00 – 0.94 (m, 2H), 0.79 – 0.73 (m, 2H), 0.00 (s, 9H), -0.13 (s, 9H). ^{13}C NMR (101 MHz, $CDCl_3$) δ 143.03, 142.98, 137.81, 135.71, 135.04, 129.99, 124.23, 123.20, 120.73, 110.85, 82.21, 73.84, 68.55, 66.43, 17.95, 17.68, -1.32, -1.45. LCMS (Finnigan, 10 → 90%): t_r = 9.48 min, m/z: 490.0.

1-((2-(Trimethylsilyl)ethoxy)methyl)-3-(1-((2-(trimethylsilyl)ethoxy)methyl)-1*H*-benzo[*d*]imidazol-2-yl)-1*H*-pyrazol-4-amine (75)

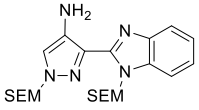

74 (8.78 g, 17.9 mmol) was dissolved in degassed MeOH (220 mL). 10% Pd/C (900 mg) was added and the atmosphere was exchanged for H_2. The reaction was vigorously stirred for 5.5 h while bubbling H_2 through the mixture. The atmosphere was exchanged for N_2, the mixture was filtered over Celite and concentrated to afford the product (7.87 g, 17.1 mmol, 95%). ^{1}H NMR (400 MHz, $CDCl_3$) δ 7.78 – 7.72 (m, 1H), 7.60 – 7.54 (m, 1H), 7.32 – 7.26 (m, 2H), 7.21 (s, 1H), 6.23 (s, 2H), 5.36 (s, 2H), 4.75 (s, 2H), 3.64 – 3.55 (m, 4H), 0.96 – 0.91 (m, 2H), 0.91 – 0.85 (m, 2H), -0.01 (s, 9H), -0.10 (s, 9H). ^{13}C NMR (101 MHz, $CDCl_3$) δ 147.51, 143.12, 135.09, 133.80, 131.81, 123.01, 122.63, 119.29, 115.95, 110.77, 81.07, 73.88, 66.78, 65.80, 17.92, 17.85, -1.29, -1.36. LCMS (Finnigan, 10 → 90%): t_r = 8.61 min, m/z: 460.1.

2-Chloro-*N*-(1-((2-(trimethylsilyl)ethoxy)methyl)-3-(1-((2-(trimethylsilyl)ethoxy)methyl)-1*H*-benzo[*d*]imidazol-2-yl)-1*H*-pyrazol-4-yl)pyrimidin-4-amine (76)

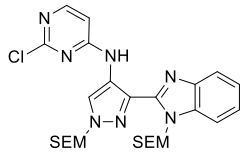

75 (6.00 g, 13.1 mmol) was dissolved in EtOH (14 mL). DIPEA (6.8 mL, 39 mmol) and 2,4-dichloropyrimidine (2.33 g, 15.7 mmol) were added after which the mixture was stirred at 40°C for 2 days. 2,4-dichloropyrimidine (388 mg, 2.61 mmol) was added and the mixture was stirred for another day at 40°C. The mixture was poured into H_2O (200 mL) and the product extracted with DCM (2x200 mL). The combined organic layers were concentrated as such and purified by silica gel column chromatography (10 – 20% EtOAc/pentane) to afford the product (5.53 g, 9.66 mmol, 74%). ^{1}H NMR (500 MHz, $CDCl_3$) δ 11.03 (s, 1H), 8.57 (s, 1H), 8.11 (d, *J* = 5.8 Hz, 1H), 7.79 – 7.74 (m, 1H), 7.62 – 7.58 (m, 1H), 7.36 – 7.31 (m, 2H), 6.67 (d, *J* = 5.8 Hz, 1H), 6.26 (s, 2H), 5.50 (s, 2H), 3.69 – 3.65 (m, 2H), 3.65 – 3.61 (m, 2H), 1.00 – 0.95 (m, 2H), 0.91 – 0.86 (m, 2H), 0.01 (s, 9H), -0.11 (s, 9H). ^{13}C NMR (126 MHz, $CDCl_3$) δ 160.90, 159.46, 156.28, 146.67, 142.15, 134.88, 131.60, 124.41, 123.72, 123.20, 121.14, 119.15, 111.06, 106.26, 81.26, 73.89, 67.15, 66.09, 17.90, 17.80, -1.29, -1.37. LCMS (Finnigan, 50 → 90%): t_r = 11.35 min, m/z: 572.1.

***N*-(1-((2-(Trimethylsilyl)ethoxy)methyl)-3-(1-((2-(trimethylsilyl)ethoxy)methyl)-1*H*-benzo[*d*]imidazol-2-yl)-1*H*-pyrazol-4-yl)pyrimidin-4-amine (77)**

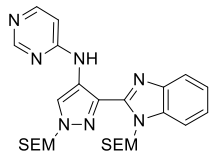

The title compound was synthesized according to general procedure E using 4-chloropyrimidine hydrochloride (54.2 mg, 359 µmol). The crude was purified by automated column chromatography (0 – 3% MeOH/EtOAc) to afford the product (59.2 mg, 110 µmol, 34%). ^{1}H NMR (400 MHz, $CDCl_3$) δ 10.69 (s, 1H), 8.81 – 8.80 (m, 1H), 8.70 (s, 1H), 8.31 (dd, *J* = 5.9, 0.5 Hz, 1H), 7.83 – 7.77 (m, 1H), 7.64 – 7.58 (m, 1H), 7.37 – 7.31 (m, 2H), 6.81 (dd, *J* = 6.0, 1.3 Hz, 1H), 6.29 (s, 2H), 5.51 (s, 2H), 3.69 – 3.60 (m, 4H), 0.99 – 0.94 (m, 2H), 0.91 – 0.86 (m, 2H), -0.00 (s, 9H), -0.11 (s, 9H). ^{13}C NMR (101 MHz, $CDCl_3$) δ 158.80, 158.39, 154.80, 146.99, 142.41, 135.03, 131.61, 125.30, 123.67, 123.18, 120.89, 119.26, 111.10, 108.01, 81.32, 73.99, 67.13, 66.11, 17.97, 17.86, -1.25, -1.33. LCMS (Finnigan, 10 → 90%): t_r = 7.80 min, m/z: 538.1.

6-Chloro-*N*-(1-((2-(trimethylsilyl)ethoxy)methyl)-3-(1-((2-(trimethylsilyl)ethoxy)methyl)-1*H*-benzo[*d*]imidazol-2-yl)-1*H*-pyrazol-4-yl)pyridin-2-amine (79)

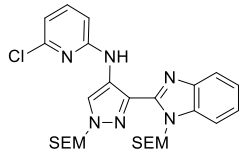

The title compound was synthesized according to general procedure E using 2,6-dichloropyrimidine (53.1 mg, 359 µmol). The crude was purified by automated column chromatography (15 – 35% EtOAc/pentane) to afford the product (102 mg, 178 µmol, 55%). ^{1}H NMR (500 MHz, $CDCl_3$) δ 8.08 (s, 1H), 8.06 (s, 1H), 7.74 – 7.70 (m, 1H), 7.44 – 7.40 (m, 1H), 7.35 (t, *J* = 7.7 Hz, 1H), 7.30 – 7.25 (m, 2H), 6.66 (dd, *J* = 7.5, 0.4 Hz, 1H), 6.59 (dd, *J* = 8.2, 0.4 Hz, 1H), 5.53 (s, 2H), 5.41 (s, 2H), 3.54 – 3.44 (m, 4H), 0.95 – 0.88 (m, 2H), 0.77 – 0.71 (m, 2H), -0.08 (s, 9H), -0.09 (s, 9H). ^{13}C NMR (126 MHz, $CDCl_3$) δ 156.02, 149.75, 143.00, 142.62, 139.79, 134.87, 134.06, 125.74, 124.19, 123.27, 122.10, 119.85, 113.71, 110.77, 105.82, 78.74, 73.78, 67.13, 66.92, 17.81, -1.47, -1.49. LCMS (Finnigan, 50 → 90%): t_r = 7.79 min, m/z: 571.0.

2-Chloro-*N*-(1-((2-(trimethylsilyl)ethoxy)methyl)-3-(1-((2-(trimethylsilyl)ethoxy)methyl)-1*H*-benzo[*d*]imidazol-2-yl)-1*H*-pyrazol-4-yl)pyridin-4-amine (78)

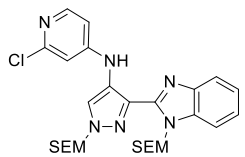

The title compound was synthesized according to general procedure E using 2-chloro-4-iodopyridine (86.0 mg, 359 µmol). The crude was purified by automated column chromatography (25 – 60% EtOAc/pentane) to afford the product (142 mg, 248 µmol, 76%). ^{1}H NMR (500 MHz, $CDCl_3$) δ 9.00 (s, 1H), 7.94 (d, *J* = 5.7 Hz, 1H), 7.61 (s, 1H), 7.49 – 7.45 (m, 1H), 7.20 – 7.17 (m, 1H), 7.14 – 7.09 (m, 2H), 6.79 (d, *J* = 2.1 Hz, 1H), 6.71 (dd, *J* = 5.8, 2.1 Hz, 1H), 5.46 (s, 2H), 5.21 (s, 2H), 3.47 – 3.42 (m, 2H), 3.30 – 3.25 (m, 2H), 0.75 – 0.70 (m, 2H), 0.69 – 0.65 (m, 2H), -0.14 (s, 18H). ^{13}C NMR (126 MHz, $CDCl_3$) δ 153.57, 152.54, 149.85, 142.20, 141.69, 134.17, 134.14, 124.36, 124.25, 123.77, 123.28, 118.93, 110.96, 107.55, 107.03, 78.67, 73.67, 67.05, 66.90, 17.72, 17.69, -1.54, -1.58. LCMS (Finnigan, 50 → 90%): t_r = 5.82 min, m/z: 571.2.

_N_-(3-Chlorophenyl)-1-((2-(trimethylsilyl)ethoxy)methyl)-3-(1-((2-(trimethylsilyl)ethoxy)methyl)-1_H_-benzo[_d_]imidazol-2-yl)-1_H_-pyrazol-4-amine (80)

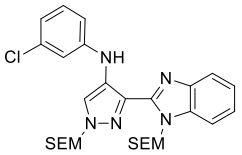

The title compound was synthesized according to general procedure E using 1-chloro-3-iodobenzene (44.4 µL, 359 µmol) which was added just before sealing the microwave vial. The crude was purified by automated column chromatography (10 – 40% EtOAc/pentane) to afford the product (140 mg, 245 µmol, 75%). ^{1}H NMR (400 MHz, $CDCl_3$) δ 9.50 (s, 1H), 7.87 – 7.80 (m, 1H), 7.76 (s, 1H), 7.64 – 7.58 (m, 1H), 7.38 – 7.31 (m, 2H), 7.22 (t, _J_ = 8.0 Hz, 1H), 7.13 (t, _J_ = 2.0 Hz, 1H), 7.01 (dd, _J_ = 8.1, 2.1 Hz, 1H), 6.85 (dd, _J_ = 7.6, 1.5 Hz, 1H), 6.27 (s, 2H), 5.49 (s, 2H), 3.72 – 3.60 (m, 4H), 1.03 – 0.96 (m, 2H), 0.94 – 0.88 (m, 2H), 0.04 (s, 9H), -0.08 (s, 9H). ^{13}C NMR (101 MHz, $CDCl_3$) δ 146.94, 144.85, 142.60, 135.14, 135.01, 131.73, 130.40, 129.36, 123.45, 122.96, 119.37, 119.31, 115.49, 114.92, 113.86, 110.88, 81.39, 73.92, 67.09, 66.01, 17.94, 17.88, -1.24, -1.33. LCMS (Finnigan, 10 → 90%): t_r = 10.86 min, m/z: 570.1.

2,6-Dichloro-_N_-(1-((2-(trimethylsilyl)ethoxy)methyl)-3-(1-((2-(trimethylsilyl)ethoxy)methyl)-1_H_-benzo[_d_]imidazol-2-yl)-1_H_-pyrazol-4-yl)pyrimidin-4-amine (81)

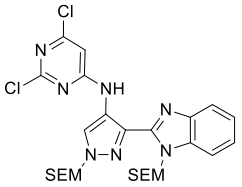

75 (150 mg, 326 µmol) was dissolved in EtOH (0.45 mL). DIPEA (170 µL, 979 µmol) and 2,4,6-trichloropyrimidine (48.8 µL, 424 µmol) were added after which the mixture was stirred at 40°C for 2.5 h. The mixture was poured into H_2O (30 mL) and the product extracted with DCM (2x30 mL). The combined organic layers were concentrated as such and purified by automated column chromatography (5 – 25% Et_2O/pentane) to afford the product (94.6 mg, 156 µmol, 48%). ^{1}H NMR (400 MHz, $CDCl_3$) δ 11.24 (s, 1H), 8.50 (s, 1H), 7.80 – 7.72 (m, 1H), 7.61 – 7.56 (m, 1H), 7.37 – 7.31 (m, 2H), 6.68 (s, 1H), 6.24 (s, 2H), 5.49 (s, 2H), 3.72 – 3.59 (m, 4H), 1.04 – 0.94 (m, 2H), 0.94 – 0.84 (m, 2H), 0.02 (s, 9H), -0.10 (s, 9H). ^{13}C NMR (101 MHz, $CDCl_3$) δ 160.22, 159.83, 159.01, 146.45, 142.00, 134.82, 131.64, 124.11, 123.82, 123.28, 121.27, 119.18, 111.05, 104.57, 81.31, 73.89, 67.23, 66.14, 17.91, 17.82, -1.28, -1.36. LCMS (Finnigan, 70 → 90%): t_r = 12.06 min, m/z: 606.1.

2,5-Dichloro-_N_-(1-((2-(trimethylsilyl)ethoxy)methyl)-3-(1-((2-(trimethylsilyl)ethoxy)methyl)-1_H_-benzo[_d_]imidazol-2-yl)-1_H_-pyrazol-4-yl)pyrimidin-4-amine (82)

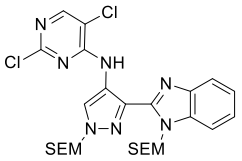

75 (150 mg, 326 µmol) was dissolved in EtOH (0.45 mL). DIPEA (170 µL, 979 µmol) and 2,4,5-trichloropyrimidine (48.6 µL, 424 µmol) were added after which the mixture was stirred at 40°C for 5.5 h. The mixture was poured into H_2O (30 mL) and the product extracted with DCM (2x30 mL). The combined organic layers were concentrated as such and purified by automated column chromatography (1 – 20% EtOAc/pentane) to afford the product (103 mg, 169 µmol, 52%). ^{1}H NMR (400 MHz, $CDCl_3$) δ 11.87 (s, 1H), 8.47 (s, 1H), 8.05 (s, 1H), 7.72 – 7.66 (m, 1H), 7.61 – 7.54 (m, 1H), 7.36 – 7.28 (m, 2H), 6.23 (s, 2H), 5.47 (s, 2H), 3.71 – 3.59 (m, 4H), 1.03 – 0.94 (m, 2H), 0.94 – 0.81 (m, 2H), 0.01 (s, 9H), -0.10 (s, 9H). ^{13}C NMR (101 MHz, $CDCl_3$) δ 158.12, 155.37, 153.77, 146.32, 142.05, 134.79, 132.08, 123.90, 123.78, 123.18, 121.00, 119.23, 114.59, 110.98, 81.30, 73.86, 67.20, 66.09, 17.92, 17.83, -1.28, -1.34. LCMS (Finnigan, 10 → 90%): t_r = 10.15 min, m/z: 606.1.

2-Chloro-5-methyl-_N_-(1-((2-(trimethylsilyl)ethoxy)methyl)-3-(1-((2-(trimethylsilyl)ethoxy)methyl)-1_H_-benzo[_d_]imidazol-2-yl)-1_H_-pyrazol-4-yl)pyrimidin-4-amine (83)

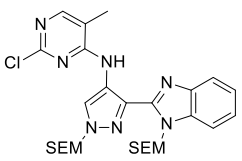

A microwave vial was charged with **75** (100 mg, 218 µmol) which was dissolved in EtOH (0.2 mL). DIPEA (114 µL, 653 µmol) and 2,4-dichloro-5-methylpyrimidine (46.1 mg, 283 µmol) were added after which the vial was sealed and stirred at 50°C for 7 days. The mixture was poured into H_2O (30 mL) and the product extracted with DCM (2x20 mL). The combined organic layers were concentrated as such. The crude was purified by automated column chromatography (10 – 25% EtOAc/pentane) to afford the product (57.5 mg, 98.1 µmol, 45%). ^{1}H NMR (400 MHz, $CDCl_3$) δ 11.22 (s, 1H), 8.56 (s, 1H), 7.91 (s, 1H), 7.71 – 7.64 (m, 1H), 7.64 – 7.55 (m, 1H), 7.39 – 7.28 (m, 2H), 6.27 (s, 2H), 5.50 (s, 2H), 3.71 – 3.57 (m, 4H), 2.32 (s, 3H), 1.01 – 0.94 (m, 2H), 0.93 –

0.86 (m, 2H), 0.01 (s, 9H), -0.10 (s, 9H). ^{13}C NMR (101 MHz, $CDCl_3$) δ 158.78, 158.46, 155.11, 146.83, 142.10, 134.81, 131.80, 124.85, 123.76, 123.18, 120.86, 118.95, 113.91, 111.12, 81.30, 73.92, 67.16, 66.11, 17.94, 17.84, 13.30, -1.27, -1.34. LCMS (Finnigan, 70 → 90%): t_r = 8.94 min, m/z: 586.3.

2-Chloro-5-methoxy-*N*-(1-((2-(trimethylsilyl)ethoxy)methyl)-3-(1-((2-(trimethylsilyl)ethoxy)methyl)-1*H*-benzo[*d*]imidazol-2-yl)-1*H*-pyrazol-4-yl)pyrimidin-4-amine (84)

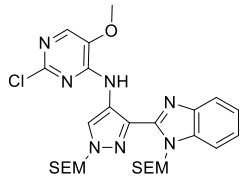

75 (125 mg, 272 µmol) was dissolved in EtOH (0.3 mL). DIPEA (142 µL, 816 µmol) and 2,4-dichloro-5-methoxypyrimidine (63.3 mg, 353 µmol) were added after which the mixture was stirred at 50°C for 4 days. The mixture was poured into H_2O (20 mL) and the product extracted with DCM (2x20 mL). The combined organic layers were concentrated as such and purified by automated column chromatography (10 – 25% EtOAc/pentane) to afford the product (104 mg, 172 µmol, 63%). ^{1}H NMR (400 MHz, $CDCl_3$) δ 11.33 (s, 1H), 8.55 (s, 1H), 7.73 – 7.68 (m, 1H), 7.60 (s, 1H), 7.60 – 7.56 (m, 1H), 7.36 – 7.29 (m, 2H), 6.25 (s, 2H), 5.46 (s, 2H), 3.99 (s, 3H), 3.68 – 3.58 (m, 4H), 0.99 – 0.93 (m, 2H), 0.90 – 0.85 (m, 2H), -0.01 (s, 9H), -0.12 (s, 9H). ^{13}C NMR (101 MHz, $CDCl_3$) δ 151.45, 151.25, 146.62, 142.30, 140.15, 134.89, 133.40, 131.92, 124.26, 123.59, 123.02, 120.78, 119.14, 111.02, 81.22, 73.85, 67.08, 65.99, 56.49, 17.88, 17.78, -1.32, -1.39. LCMS (Finnigan, 70 → 90%): t_r = 11.57 min, m/z: 602.3.

2-Phenyl-*N*-(1-((2-(trimethylsilyl)ethoxy)methyl)-3-(1-((2-(trimethylsilyl)ethoxy)methyl)-1*H*-benzo[*d*]imidazol-2-yl)-1*H*-pyrazol-4-yl)pyrimidin-4-amine (85)

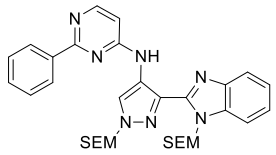

The title compound was synthesized according to general procedure F using phenylboronic acid. The crude was purified by silica gel column chromatography (40 – 50% Et_2O/pentane) to afford the product (57 mg, 93 µmol, 18%). ^{1}H NMR (500 MHz, $CDCl_3$) δ 10.77 (s, 1H), 8.77 (s, 1H), 8.44 – 8.40 (m, 3H), 7.85 – 7.81 (m, 1H), 7.63 – 7.59 (m, 1H), 7.56 – 7.49 (m, 3H), 7.38 – 7.34 (m, 2H), 6.72 (d, *J* = 5.8 Hz, 1H), 6.29 (s, 2H), 5.54 (s, 2H), 3.74 – 3.69 (m, 2H), 3.68 – 3.63 (m, 2H), 1.04 – 0.98 (m, 2H), 0.96 – 0.87 (m, 2H), 0.01 (s, 9H), -0.08 (s, 9H). ^{13}C NMR (126 MHz, $CDCl_3$) δ 164.66, 158.69, 155.08, 146.90, 142.35, 142.23, 142.20, 138.68, 134.95, 131.53, 131.44, 130.37, 128.53, 128.18, 125.43, 123.57, 123.09, 120.36, 119.22, 111.00, 105.98, 81.37, 73.90, 67.12, 66.03, 17.91, 17.84, -1.29, -1.37. LCMS (Finnigan, 70 → 90%): t_r = 3.55 min, m/z: 614.4.

2-(*o*-Tolyl)-*N*-(1-((2-(trimethylsilyl)ethoxy)methyl)-3-(1-((2-(trimethylsilyl)ethoxy)methyl)-1*H*-benzo[*d*]imidazol-2-yl)-1*H*-pyrazol-4-yl)pyrimidin-4-amine (90)

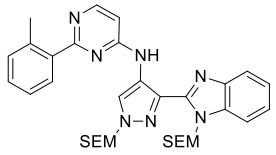

The title compound was synthesized from **76** (200 mg, 349 µmol) and *o*-tolylboronic acid (71.3 mg, 524 µmol) according to general procedure G (reaction time 1.5 h). The crude was purified by automated column chromatography (40 – 60% EtOAc/pentane) to afford the product (177 mg, 281 µmol, 80%). ^{1}H NMR (400 MHz, $CDCl_3$) δ 8.92 (br s, 1H), 8.39 (d, *J* = 5.9 Hz, 1H), 8.14 (br s, 1H), 7.80 (d, *J* = 7.3 Hz, 1H), 7.75 – 7.68 (m, 1H), 7.42 – 7.36 (m, 1H), 7.34 – 7.25 (m, 5H), 6.61 (d, *J* = 5.9 Hz, 1H), 5.55 (s, 2H), 5.38 (s, 2H), 3.56 – 3.45 (m, 4H), 2.56 (s, 3H), 0.93 – 0.87 (m, 2H), 0.80 – 0.73 (m, 2H), -0.07 (s, 9H), -0.09 (s, 9H). ^{13}C NMR (101 MHz, $CDCl_3$) δ 167.43, 160.34, 155.89, 142.74, 142.35, 138.70, 136.94, 134.78, 134.67, 131.09, 130.20, 128.99, 125.68, 124.60, 124.32, 123.34, 119.60, 110.81, 78.71, 73.72, 67.17, 66.96, 21.22, 17.77, -1.53 (not all quaternary carbons were observed, neither was one –CH of the pyrimidine). LCMS (Finnigan, 50 → 90%): t_r = 5.18 min, m/z: 628.3.

2-(2-Chlorophenyl)-*N*-(1-((2-(trimethylsilyl)ethoxy)methyl)-3-(1-((2-(trimethylsilyl)ethoxy)methyl)-1*H*-benzo[*d*]imidazol-2-yl)-1*H*-pyrazol-4-yl)pyrimidin-4-amine (91)

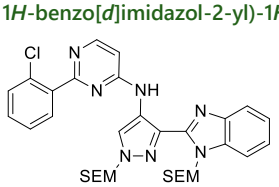

The title compound was synthesized according to general procedure F using 2-chlorophenylboronic acid. The crude was purified by silica gel column chromatography (40 – 50% Et_2O/pentane) to afford the product (268 mg, 413 µmol, 79%). ^{1}H NMR (300 MHz, $CDCl_3$) δ 10.82 (s, 1H), 8.80 (s, 1H), 8.45 (d, *J* = 5.9 Hz, 1H), 7.87 – 7.78 (m, 2H), 7.66 – 7.58 (m, 1H), 7.57

– 7.50 (m, 1H), 7.44 – 7.31 (m, 4H), 6.79 (d, *J* = 5.9 Hz, 1H), 6.30 (s, 2H), 5.47 (s, 2H), 3.69 – 3.59 (m, 4H), 0.99 – 0.85 (m, 4H), -0.02 (s, 9H), -0.10 (s, 9H). ^{13}C NMR (75 MHz, $CDCl_3$) δ 165.14, 158.24, 155.06, 147.01, 142.41, 138.80, 135.00, 132.49, 131.86, 131.61, 130.62, 130.02, 126.80, 125.12, 123.58, 123.11, 121.31, 119.23, 111.06, 106.06, 81.27, 73.96, 67.11, 66.04, 17.93, 17.86, -1.33, -1.36. LCMS (Finnigan, 70 → 90%): t_r = 3.72 min, m/z: 648.4.

2-(2-Methoxyphenyl)-*N*-(1-((2-(trimethylsilyl)ethoxy)methyl)-3-(1-((2-(trimethylsilyl)ethoxy)methyl)-1*H*-benzo[*d*]imidazol-2-yl)-1*H*-pyrazol-4-yl)pyrimidin-4-amine (92)

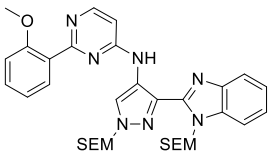

The title compound was synthesized according to general procedure F using 2-methoxyphenylboronic acid. The crude was purified by silica gel column chromatography (70 – 100% EtOAc/pentane) to afford the product (300 mg, 466 µmol, 89%). ^{1}H NMR (500 MHz, $CDCl_3$) δ 8.53 (br s, 1H), 8.39 (s, 1H), 8.35 (d, *J* = 5.9 Hz, 1H), 7.75 – 7.69 (m, 2H), 7.42 – 7.35 (m, 2H), 7.31 – 7.25 (m, 2H), 7.04 – 6.97 (m, 2H), 6.54 (d, *J* = 5.9 Hz, 1H), 5.51 (s, 2H), 5.37 (s, 2H), 3.88 (s, 3H), 3.52 – 3.43 (m, 4H), 0.86 (t, *J* = 8.2 Hz, 2H), 0.75 – 0.70 (m, 2H), -0.12 (s, 9H), -0.13 (s, 9H). ^{13}C NMR (126 MHz, $CDCl_3$) δ 165.31, 157.69, 155.72, 142.88, 142.37, 134.80, 134.50, 131.70, 130.78, 128.44, 124.34, 123.42, 120.48, 119.83, 111.74, 110.80, 78.74, 73.76, 67.23, 66.99, 55.85, 17.85, 17.81, -1.51, -1.52 (not all quaternary carbons were observed, neither was one –CH of the pyrimidine). LCMS (Finnigan, 50 → 90%): t_r = 5.24 min, m/z: 644.3.

2-(*m*-Tolyl)-*N*-(1-((2-(trimethylsilyl)ethoxy)methyl)-3-(1-((2-(trimethylsilyl)ethoxy)methyl)-1*H*-benzo[*d*]imidazol-2-yl)-1*H*-pyrazol-4-yl)pyrimidin-4-amine (93)

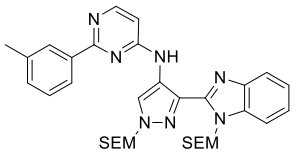

The title compound was synthesized according to general procedure F using *m*-tolylboronic acid. The crude was purified by silica gel chromatography (20 – 40% Et_2O/pentane) to afford the product (286 mg, 456 µmol, 87%). ^{1}H NMR (300 MHz, $CDCl_3$) δ 10.74 (s, 1H), 8.79 (s, 1H), 8.42 (d, *J* = 5.8 Hz, 1H), 8.27 (s, 1H), 8.23 (d, *J* = 7.8 Hz, 1H), 7.87 – 7.78 (m, 1H), 7.66 – 7.57 (m, 1H), 7.44 (t, *J* = 7.6 Hz, 1H), 7.39 – 7.30 (m, 3H), 6.70 (d, *J* = 5.8 Hz, 1H), 6.29 (s, 2H), 5.52 (s, 2H), 3.76 – 3.63 (m, 4H), 2.50 (s, 3H), 1.07 – 0.97 (m, 2H), 0.97 – 0.85 (m, 2H), 0.02 (s, 9H), -0.08 (s, 9H). ^{13}C NMR (75 MHz, $CDCl_3$) δ 164.79, 158.64, 155.16, 146.92, 142.37, 138.70, 137.97, 134.95, 131.53, 131.09, 128.91, 128.41, 125.46, 125.28, 123.52, 123.04, 120.41, 119.21, 110.97, 105.85, 81.37, 73.90, 67.09, 65.74, 21.66, 17.92, 17.84, -1.30, -1.37. LCMS (Finnigan, 70 → 90%): t_r = 4.15 min, m/z: 628.4.

2-(3-Chlorophenyl)-*N*-(1-((2-(trimethylsilyl)ethoxy)methyl)-3-(1-((2-(trimethylsilyl)ethoxy)methyl)-1*H*-benzo[*d*]imidazol-2-yl)-1*H*-pyrazol-4-yl)pyrimidin-4-amine (94)

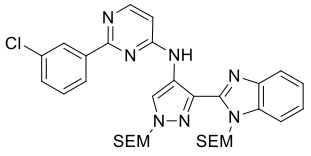

The title compound was synthesized according to general procedure F using 3-chlorophenylboronic acid. The crude was purified by silica gel column chromatography (45% EtOAc/pentane) and used as such in subsequent reaction (yield: 258 mg). LCMS (Finnigan, 70 → 90%): t_r = 2.86 min, m/z: 648.3.

2-(3-Methoxyphenyl)-*N*-(1-((2-(trimethylsilyl)ethoxy)methyl)-3-(1-((2-(trimethylsilyl)ethoxy)methyl)-1*H*-benzo[*d*]imidazol-2-yl)-1*H*-pyrazol-4-yl)pyrimidin-4-amine (95)

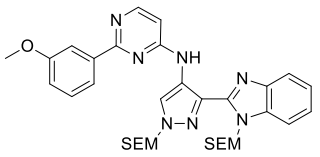

The title compound was synthesized from **76** (200 mg, 349 µmol) and 3-methoxyphenylboronic acid (80.0 mg, 524 µmol) according to general procedure G (reaction time 1.5 h). The crude was purified by automated column chromatography (40 – 60% EtOAc/pentane) to afford the product (184 mg, 286 µmol, 82%).^{1}H NMR (400 MHz, $CDCl_3$) δ 9.32 (br s, 1H), 8.39 (d, *J* = 5.8 Hz, 1H), 8.27 (br s, 1H), 8.08 – 8.01 (m, 2H), 7.69 – 7.63 (m, 1H), 7.37 (t, *J* = 7.9 Hz, 1H), 7.35 – 7.29 (m, 1H), 7.28 – 7.19 (m, 2H), 7.03 (dd, *J* = 8.1, 2.6 Hz, 1H), 6.66 (d, *J* = 5.8 Hz, 1H), 5.54 (s, 2H), 5.38 (s, 2H), 3.88 (s, 3H), 3.55 – 3.49 (m, 3H), 3.47 – 3.40 (m, 2H), 0.91 – 0.82 (m, 2H), 0.79 – 0.70 (m, 2H), -0.08 (s, 8H), -0.11 (s, 9H). ^{13}C NMR (101 MHz,

$CDCl_3$) δ 164.18, 160.51, 159.74, 156.07, 142.55, 142.25, 139.46, 134.58, 134.44, 129.33, 124.61, 124.28, 123.28, 120.65, 119.26, 117.04, 112.55, 110.89, 78.61, 73.64, 66.99, 66.91, 55.25, 17.70, -1.57 (not all quaternary carbons were observed, neither was one –CH of the pyrimidine). LCMS (Finnigan, 50 → 90%): t_r = 5.38 min, m/z: 644.3.

2-(3-Isopropylphenyl)-*N*-(1-((2-(trimethylsilyl)ethoxy)methyl)-3-(1-((2-(trimethylsilyl)ethoxy)methyl)-1*H*-benzo[*d*]imidazol-2-yl)-1*H*-pyrazol-4-yl)pyrimidin-4-amine (97)

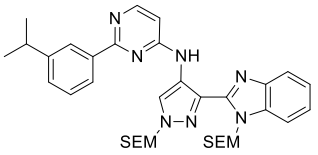

The title compound was synthesized from **76** (170 mg, 297 µmol), 3-isopropylphenylboronic acid (68.0 mg, 445 µmol), K_2CO_3 (165 mg, 1.19 mmol) and Pd(dppf)Cl_2·DCM (17 mg, 21 µmol) according to general procedure F (reaction time: 2 h). The crude was purified by silica gel column chromatography (40 – 60% EtOAc/pentane) to afford the product (89.6 mg, 137 µmol, 46%). ^{1}H NMR (400 MHz, $CDCl_3$) δ 10.76 (s, 1H), 8.84 (s, 1H), 8.44 (d, *J* = 5.8 Hz, 1H), 8.33 (t, *J* = 1.6 Hz, 1H), 8.23 (dt, *J* = 7.7, 1.4 Hz, 1H), 7.85 – 7.79 (m, 1H), 7.65 – 7.59 (m, 1H), 7.46 (t, *J* = 7.6 Hz, 1H), 7.40 – 7.33 (m, 3H), 6.75 (d, *J* = 5.9 Hz, 1H), 6.32 (s, 2H), 5.54 (s, 2H), 3.72 – 3.61 (m, 4H), 3.06 (hept, *J* = 6.8 Hz, 1H), 1.37 (d, *J* = 6.9 Hz, 6H), 1.02 – 0.93 (m, 2H), 0.93 – 0.86 (m, 2H), -0.01 (s, 9H), -0.11 (s, 9H). ^{13}C NMR (101 MHz, $CDCl_3$) δ 164.98, 158.76, 155.15, 149.15, 147.03, 142.46, 138.67, 135.07, 131.71, 128.93, 128.65, 126.30, 125.85, 125.56, 123.69, 123.21, 120.65, 119.32, 111.12, 105.95, 81.50, 74.04, 67.17, 66.14, 34.37, 24.25, 18.00, 17.91, -1.24, -1.31. LCMS (Finnigan, 70 → 90%): t_r = 5.70 min, m/z: 656.5.

2-(Pyridin-3-yl)-*N*-(1-((2-(trimethylsilyl)ethoxy)methyl)-3-(1-((2-(trimethylsilyl)ethoxy)methyl)-1*H*-benzo[*d*]imidazol-2-yl)-1*H*-pyrazol-4-yl)pyrimidin-4-amine (96)

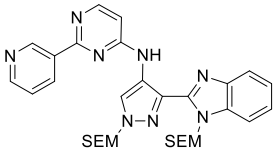

The title compound was synthesized according to general procedure F using pyridin-3-ylboronic acid. The crude was purified by silica gel column chromatography (EtOAc) to afford the product (226 mg, 367 µmol, 70%). ^{1}H NMR (300 MHz, $CDCl_3$) δ 9.54 (s, 1H), 9.34 (br s, 1H), 8.63 – 8.56 (m, 2H), 8.32 (d, *J* = 5.8 Hz, 1H), 8.19 (br s, 1H), 7.66 – 7.58 (m, 1H), 7.36 – 7.27 (m, 2H), 7.25 – 7.15 (m, 2H), 6.64 (d, *J* = 5.9 Hz, 1H), 5.49 (s, 2H), 5.34 (s, 2H), 3.52 – 3.45 (m, 2H), 3.44 – 3.35 (m, 2H), 0.85 – 0.77 (m, 2H), 0.75 – 0.66 (m, 2H), -0.13 (s, 9H), -0.17 (s, 9H). ^{13}C NMR (75 MHz, $CDCl_3$) δ 174.08, 162.38, 160.67, 156.03, 150.53, 149.37, 142.48, 142.05, 135.60, 134.61, 134.49, 133.58, 124.43, 124.34, 123.36, 123.26, 119.41, 110.83, 78.66, 73.66, 67.05, 66.99, 17.71, -1.59 (one –CH of the pyrimidine was not observed). LCMS (Finnigan, 10 → 90%): t_r = 7.77 min, m/z: 615.3.

2-(*p*-Tolyl)-*N*-(1-((2-(trimethylsilyl)ethoxy)methyl)-3-(1-((2-(trimethylsilyl)ethoxy)methyl)-1*H*-benzo[*d*]imidazol-2-yl)-1*H*-pyrazol-4-yl)pyrimidin-4-amine (86)

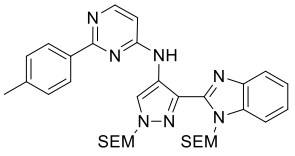

The title compound was synthesized according to general procedure F using *p*-tolylboronic acid. The crude was purified by silica gel column chromatography (20 – 80% Et_2O/pentane) to afford the product (175 mg, 279 µmol, 53%). ^{1}H NMR (300 MHz, $CDCl_3$) δ 10.72 (s, 1H), 8.78 (s, 1H), 8.41 (d, *J* = 5.8 Hz, 1H), 8.35 – 8.29 (m, 2H), 7.86 – 7.79 (m, 1H), 7.66 – 7.58 (m, 1H), 7.41 – 7.30 (m, 4H), 6.69 (d, *J* = 5.8 Hz, 1H), 6.29 (s, 2H), 5.54 (s, 2H), 3.76 – 3.62 (m, 4H), 2.46 (s, 3H), 1.06 – 0.97 (m, 2H), 0.95 – 0.88 (m, 2H), 0.02 (s, 9H), -0.08 (s, 9H). ^{13}C NMR (75 MHz, $CDCl_3$) δ 164.78, 158.69, 155.21, 146.96, 142.41, 140.46, 136.10, 134.99, 131.54, 129.28, 128.14, 125.54, 123.55, 123.08, 120.37, 119.24, 111.01, 105.71, 81.38, 73.94, 67.12, 66.03, 21.55, 17.94, 17.89, -1.27, -1.35. LCMS (Finnigan, 70 → 90%): t_r = 3.97 min, m/z: 628.4.

2-(4-Chlorophenyl)-*N*-(1-((2-(trimethylsilyl)ethoxy)methyl)-3-(1-((2-(trimethylsilyl)ethoxy)methyl)-1*H*-benzo[*d*]imidazol-2-yl)-1*H*-pyrazol-4-yl)pyrimidin-4-amine (88)

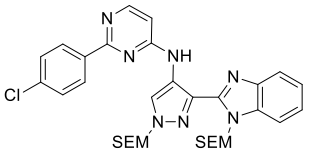

The title compound was synthesized according to general procedure F using 4-chlorophenylboronic acid. The crude was purified by silica gel column chromatography (25 – 35% EtOAc/pentane) and used as such in subsequent reaction (yield: 254 mg). LCMS (Finnigan, 70 → 90%): t_r = 2.23 min, m/z: 648.3.

2-(4-Methoxyphenyl)-*N*-(1-((2-(trimethylsilyl)ethoxy)methyl)-3-(1-((2-(trimethylsilyl)ethoxy)methyl)-1*H*-benzo[*d*]imidazol-2-yl)-1*H*-pyrazol-4-yl)pyrimidin-4-amine (87)

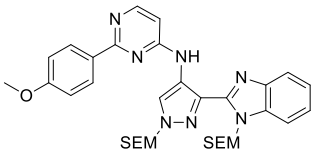

The title compound was synthesized according to general procedure F using 4-methoxyphenylboronic acid. The crude was purified by silica gel column chromatography (20% EtOAc/pentane) to afford the product (258 mg, 401 µmol, 77%). ^{1}H NMR (400 MHz, $CDCl_3$) δ 10.70 (s, 1H), 8.76 (s, 1H), 8.41 – 8.35 (m, 3H), 7.85 – 7.79 (m, 1H), 7.64 – 7.59 (m, 1H), 7.39 – 7.32 (m, 2H), 7.06 – 7.02 (m, 2H), 6.68 (d, *J* = 5.8 Hz, 1H), 6.30 (s, 2H), 5.56 (s, 2H), 3.90 (s, 3H), 3.73 – 3.68 (m, 2H), 3.68 – 3.62 (m, 2H), 1.04 – 0.97 (m, 2H), 0.94 – 0.87 (m, 2H), 0.01 (s, 9H), -0.10 (s, 9H). ^{13}C NMR (101 MHz, $CDCl_3$) δ 164.47, 161.62, 158.71, 155.21, 146.99, 142.43, 135.02, 131.57, 131.42, 129.75, 125.62, 123.61, 123.13, 120.30, 119.28, 113.89, 111.05, 105.40, 81.44, 73.98, 67.17, 66.08, 55.46, 17.97, 17.91, -1.24, -1.33. LCMS (Finnigan, 70 → 90%): t_r = 3.43 min, m/z: 644.4.

2-(4-Fluorophenyl)-*N*-(1-((2-(trimethylsilyl)ethoxy)methyl)-3-(1-((2-(trimethylsilyl)ethoxy)methyl)-1*H*-benzo[*d*]imidazol-2-yl)-1*H*-pyrazol-4-yl)pyrimidin-4-amine (89)

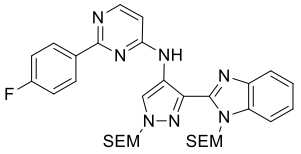

The title compound was synthesized according to general procedure F using 4-fluorophenylboronic acid. The crude was purified by silica gel column chromatography (35% EtOAc/pentane) and used as such in subsequent reaction (yield: 229 mg).

2-(Naphthalen-1-yl)-*N*-(1-((2-(trimethylsilyl)ethoxy)methyl)-3-(1-((2-(trimethylsilyl)ethoxy)methyl)-1*H*-benzo[*d*]imidazol-2-yl)-1*H*-pyrazol-4-yl)pyrimidin-4-amine (99)

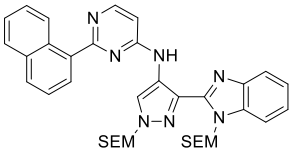

The title compound was synthesized from **76** (125 mg, 218 µmol) and naphthalen-1-boronic acid (43.2 mg, 251 µmol) according to general procedure G (reaction time 2 h). The crude was purified by automated column chromatography (40 – 60% EtOAc/pentane) to afford the product (134 mg, 201 µmol, 92%). ^{1}H NMR (400 MHz, $CDCl_3$) δ 8.89 (br s, 1H), 8.73 (d, *J* = 8.1 Hz, 1H), 8.45 (d, *J* = 5.8 Hz, 1H), 8.23 (br s, 1H), 8.04 (d, *J* = 7.1 Hz, 1H), 7.95 (d, *J* = 8.2 Hz, 1H), 7.93 – 7.89 (m, 1H), 7.78 – 7.72 (m, 1H), 7.59 – 7.55 (m, 1H), 7.54 – 7.50 (m, 2H), 7.43 – 7.38 (m, 1H), 7.33 – 7.28 (m, 2H), 6.66 (d, *J* = 5.9 Hz, 1H), 5.57 (s, 2H), 5.39 (s, 2H), 3.56 – 3.46 (m, 4H), 0.92 – 0.86 (m, 2H), 0.80 – 0.74 (m, 2H), -0.07 (s, 9H), -0.14 (s, 9H). ^{13}C NMR (101 MHz, $CDCl_3$) δ 166.86, 160.45, 156.03, 142.81, 142.35, 136.53, 134.79, 134.53, 134.02, 131.04, 130.02, 128.70, 128.30, 126.49, 126.21, 125.72, 125.10, 124.74, 124.33, 123.37, 119.76, 110.72, 78.76, 73.69, 67.27, 67.00, 17.78, 17.76, -1.53, -1.59 (not all quaternary carbons were observed, neither was one –CH of the pyrimidine). LCMS (Finnigan, 50 → 90%): t_r = 5.46 min, m/z: 664.3.

2-(1*H*-Indol-7-yl)-*N*-(1-((2-(trimethylsilyl)ethoxy)methyl)-3-(1-((2-(trimethylsilyl)ethoxy)methyl)-1*H*-benzo[*d*]imidazol-2-yl)-1*H*-pyrazol-4-yl)pyrimidin-4-amine (100)

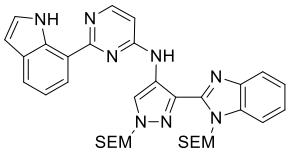

The title compound was synthesized from **76** (125 mg, 218 µmol) and indole-7-boronic acid pinacol ester (61.1 mg, 251 µmol) according to general procedure G (reaction time 16 h). The crude was purified by automated column chromatography (30 – 50% EtOAc/pentane) to afford the product (111 mg, 169 µmol, 78%). ^{1}H NMR (400 MHz, $CDCl_3$) δ 11.22 (s, 1H), 9.44 (br s, 1H), 8.46 (d, *J* = 5.9 Hz, 1H), 8.44 (dd, *J* = 7.7, 1.0 Hz, 1H), 8.14 (br s, 1H), 7.80 (d, *J* = 7.7 Hz, 1H), 7.66 – 7.60 (m, 1H), 7.33 – 7.28 (m, 1H), 7.26 – 7.17 (m, 3H), 7.09 (br s, 1H), 6.65 (d, *J* = 5.9 Hz, 1H), 6.56 (t, *J* = 2.7 Hz, 1H), 5.57 (s, 2H), 5.36 (s, 2H), 3.56 – 3.47 (m, 2H), 3.40 (dd, *J* = 8.8, 7.4 Hz, 2H), 0.84 – 0.78 (m, 2H), 0.76 – 0.70 (m, 2H), -0.10 (s, 9H), -0.15 (s, 9H). ^{13}C NMR (101 MHz, $CDCl_3$) δ 165.23, 160.43, 156.00, 142.46, 142.23, 135.32, 134.77, 134.42, 129.17, 124.49, 124.46, 123.90, 123.43, 122.55, 120.19, 119.35, 119.32, 111.00, 102.01, 78.81, 73.76, 67.07, 67.04, 17.76, 17.72, -1.53, -1.56 (not all quaternary carbons were observed). LCMS (Finnigan, 10 → 90%): t_r = 9.13 min, m/z: 653.3.

2-(1*H*-Indazol-4-yl)-*N*-(1-((2-(trimethylsilyl)ethoxy)methyl)-3-(1-((2-(trimethylsilyl)ethoxy)methyl)-1*H*-benzo[*d*]imidazol-2-yl)-1*H*-pyrazol-4-yl)pyrimidin-4-amine (101)

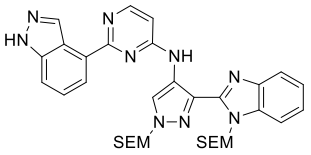

The title compound was synthesized from **76** (130 mg, 227 µmol) and indazole-4-boronic acid hydrochloride (63.1 mg, 318 µmol) according to general procedure G (reaction time 16 h). The crude was purified by automated column chromatography (40 – 100% EtOAc/pentane) to afford the product (101 mg, 155 µmol, 68%). ^{1}H NMR (500 MHz, $CDCl_3$) δ 9.00 (s, 1H), 8.89 (br s, 1H), 8.44 (d, *J* = 5.9 Hz, 1H), 8.29 – 8.12 (m, 2H), 7.76 – 7.72 (m, 1H), 7.54 (d, *J* = 8.3 Hz, 1H), 7.44 – 7.39 (m, 2H), 7.29 – 7.23 (m, 2H), 6.60 (d, *J* = 5.9 Hz, 1H), 5.57 (s, 2H), 5.42 (s, 2H), 3.60 – 3.54 (m, 2H), 3.51 – 3.44 (m, 2H), 0.88 – 0.82 (m, 2H), 0.80 – 0.75 (m, 2H), -0.10 (s, 9H), -0.17 (s, 9H) (the –NH of the benzimidazole was not observed). ^{13}C NMR (126 MHz, $CDCl_3$) δ 164.66, 160.96 (br), 156.32 (br), 142.80, 142.27, 141.00, 136.36, 135.37, 134.84, 131.55, 126.37, 124.87, 124.43, 123.52, 122.09, 121.61, 119.88, 112.37, 110.81, 103.04 (br), 78.96, 73.83, 67.29, 67.17, 17.84, -1.48, -1.54. LCMS (Finnigan, 50 → 90%): t_r = 4.10 min, m/z: 654.3.

2-(Naphthalen-2-yl)-*N*-(1-((2-(trimethylsilyl)ethoxy)methyl)-3-(1-((2-(trimethylsilyl)ethoxy)methyl)-1*H*-benzo[*d*]imidazol-2-yl)-1*H*-pyrazol-4-yl)pyrimidin-4-amine (102)

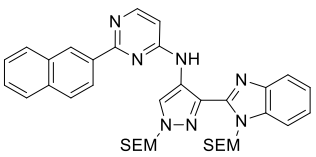

The title compound was synthesized from **76** (200 mg, 349 µmol), 2-naphthylboronic acid (90.1 mg, 524 µmol), K_2CO_3 (193 mg, 1.40 mmol) and Pd(dppf)Cl_2·DCM (20 mg, 24 µmol) according to general procedure F (reaction time: 2 h). The crude was purified by silica gel column chromatography (40 – 60% EtOAc/pentane) to afford the product (100 mg, 150 µmol, 43%). ^{1}H NMR (500 MHz, $CDCl_3$) δ 10.81 (s, 1H), 8.96 (s, 1H), 8.89 (s, 1H), 8.51 (dd, *J* = 8.6, 1.5 Hz, 1H), 8.48 (d, *J* = 5.8 Hz, 1H), 8.03 – 8.00 (m, 1H), 7.99 (d, *J* = 8.6 Hz, 1H), 7.93 – 7.88 (m, 1H), 7.87 – 7.80 (m, 1H), 7.65 – 7.60 (m, 1H), 7.57 – 7.51 (m, 2H), 7.39 – 7.34 (m, 2H), 6.78 (d, *J* = 5.8 Hz, 1H), 6.32 (s, 2H), 5.59 (s, 2H), 3.76 – 3.70 (m, 2H), 3.68 – 3.62 (m, 2H), 1.04 – 0.97 (m, 2H), 0.94 – 0.87 (m, 2H), -0.01 (s, 9H), -0.10 (s, 9H). ^{13}C NMR (126 MHz, $CDCl_3$) δ 164.76, 158.89, 155.20, 147.02, 142.48, 136.03, 135.09, 134.70, 133.43, 131.76, 129.30, 128.56, 128.24, 127.84, 127.12, 126.36, 125.55, 125.33, 123.70, 123.22, 120.61, 119.33, 111.12, 106.07, 81.57, 77.41, 77.16, 76.91, 74.06, 67.28, 66.16, 18.02, 17.98, -1.23, -1.30. LCMS (Finnigan, 70 → 90%): t_r = 5.14 min, m/z: 664.4.

2-(3,5-Dichlorophenyl)-*N*-(1-((2-(trimethylsilyl)ethoxy)methyl)-3-(1-((2-(trimethylsilyl)ethoxy)methyl)-1*H*-benzo[*d*]imidazol-2-yl)-1*H*-pyrazol-4-yl)pyrimidin-4-amine (98)

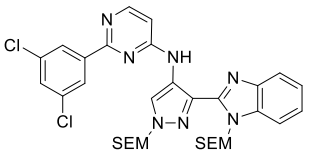

The title compound was synthesized from **76** (125 mg, 218 µmol) and 3,5-dichlorophenylboronic acid (47.9 mg, 251 µmol) according to general procedure G (reaction time 2 h). The crude was purified by automated column chromatography (25 – 45% EtOAc/pentane) to afford the product (128 mg, 188 µmol, 86%). ^{1}H NMR (400 MHz, $CDCl_3$)

δ 8.96 (br s, 1H), 8.33 (d, *J* = 5.8 Hz, 1H), 8.26 (d, *J* = 1.9 Hz, 2H), 8.14 (br s, 1H), 7.71 – 7.63 (m, 1H), 7.40 (t, *J* = 2.0 Hz, 1H), 7.38 – 7.32 (m, 1H), 7.30 – 7.22 (m, 2H), 6.63 (d, *J* = 5.8 Hz, 1H), 5.52 (s, 2H), 5.37 (s, 2H), 3.54 – 3.45 (m, 4H), 0.93 – 0.84 (m, 2H), 0.75 – 0.69 (m, 2H), -0.11 (s, 9H), -0.12 (s, 9H). ^{13}C NMR (101 MHz, $CDCl_3$) δ 162.07, 160.81 (br), 156.30 (br), 142.75, 142.21, 141.10, 140.60, 140.21, 135.11, 134.76, 134.56, 130.16, 126.59, 124.50, 124.41, 123.51, 119.70, 110.77, 78.82, 73.68, 67.38, 67.13, 17.85, 17.82, -1.49 (one –CH of the pyrimidine was not observed). LCMS (Finnigan, 70 → 90%): t_r = 7.15 min, m/z: 682.3.

Ethyl 4-nitro-1*H*-pyrazole-3-carboxylate (103)

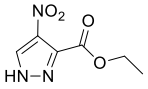

4-Nitro-1*H*-pyrazole-3-carboxylic acid (10.0 g, 63.7 mmol) was suspended in dry EtOH (160 mL) and cooled down to 0°C. $SOCl_2$ (6.0 mL, 83 mmol) was added dropwise, after which the mixture was allowed to warm to RT and stirred for 16 h. The mixture was concentrated and traces of $SOCl_2$ were removed by coevaporation with toluene (2x20 mL). The resulting solids were suspended in pentane and filtered to afford the product (11.3 g, 63.7 mmol, 96%). ^{1}H NMR (500 MHz, DMSO) δ 14.42 (br s, 1H), 8.95 (br s, 1H), 4.35 (q, *J* = 7.0 Hz, 2H), 1.29 (t, *J* = 7.1 Hz, 3H). ^{13}C NMR (126 MHz, DMSO) δ 160.81, 138.53, 133.14, 130.81, 61.83, 13.83.

Ethyl 4-nitro-1-((2-(trimethylsilyl)ethoxy)methyl)-1*H*-pyrazole-3-carboxylate (104)

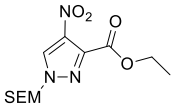

103 (15.0 g, 81.0 mmol) was suspended in DCM (81 mL). DIPEA (18.4 mL, 105 mmol) was added after which the mixture was cooled down to 0°C. SEM-Cl (15.2 mL, 85.9 mmol) was added dropwise after which the mixture was stirred at 0°C for 10 min. The reaction was allowed to warm to RT and continued to stir for 10 min. The mixture was poured into H_2O (150 mL), the layers were separated and the organic layer was washed with H_2O (75 mL). The organic layer was dried over Na_2SO_4, filtered and concentrated. The crude was split in half, transferred to a microwave vial and MeCN (8 mL) was added to each vial. Argon was bubbled through the mixture for 1 min after which SEM-Cl (357 µL, ~5 mol%) was added to each vial. The vials were sealed and heated to 95°C in a microwave reactor for 8 h. The content of both vials were combined and subsequently concentrated. The crude was purified by automated column chromatography (20 – 60% Et_2O/pentane) to afford the product (21.1 g, 67.0 mmol, 83%). ^{1}H NMR (500 MHz, $CDCl_3$) δ 8.32 (s, 1H), 5.45 (s, 2H), 4.42 (q, *J* = 7.1 Hz, 2H), 3.65 – 3.57 (m, 2H), 1.36 (t, *J* = 7.1 Hz, 3H), 0.94 – 0.87 (m, 2H), -0.04 (s, 9H). ^{13}C NMR (126 MHz, $CDCl_3$) δ 160.14, 138.98, 134.89, 129.80, 82.02, 68.33, 62.54, 17.80, 13.99, -1.46.

Ethyl 4-amino-1-((2-(trimethylsilyl)ethoxy)methyl)-1*H*-pyrazole-3-carboxylate (105)

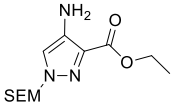

104 (4.00 g, 12.7 mmol) was dissolved in degassed EtOH (140 mL). 10% Pd/C (400 mg) was added and the atmosphere was exchanged for H_2. The reaction was vigorously stirred for 5 h while bubbling H_2 through the mixture. The atmosphere was exchanged for N_2, the mixture was filtered over Celite and concentrated to afford the product (3.57 g, 12.5 mmol, 99%). ^{1}H NMR (500 MHz, $CDCl_3$) δ 7.09 (s, 1H), 5.30 (s, 2H), 4.35 (q, *J* = 7.1 Hz, 2H), 4.09 (br s, 2H), 3.50 – 3.44 (m, 2H), 1.34 (t, *J* = 7.1 Hz, 3H), 0.86 – 0.80 (m, 2H), -0.09 (s, 9H). ^{13}C NMR (126 MHz, $CDCl_3$) δ 163.71, 135.54, 130.56, 115.82, 81.43, 66.89, 60.59, 17.79, 14.48, -1.46. LCMS (Finnigan, 10 → 90%): t_r = 5.88 min, m/z: 286.0.

Ethyl 4-((2-chloropyrimidin-4-yl)amino)-1-((2-(trimethylsilyl)ethoxy)methyl)-1*H*-pyrazole-3-carboxylate (106)

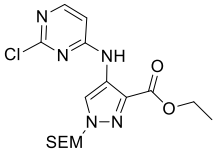

105 (3.53 g, 12.4 mmol) was dissolved in EtOH (12.4 mL). DIPEA (4.3 mL, 24.7 mmol) and 2,4-dichloropyrimidine (2.76 g, 18.6 mmol) were added after which the mixture was stirred at 70°C for 4 days. The mixture was concentrated, suspended in DCM (100 mL) and poured into H_2O (100 mL). The organic layer was separated and the water layer was extracted with DCM (50 mL). The combined organic layers were washed with brine (100 mL), dried over Na_2SO_4, filtered and concentrated. The crude was purified by silica gel column chromatography (50% Et_2O/pentane) to afford the product (4.41 g, 11.1 mmol, 90%). ^{1}H NMR (500 MHz, $CDCl_3$) δ 8.91 (s, 1H), 8.51 (s, 1H), 8.13 (d, *J* = 5.8 Hz, 1H), 6.55 (d, *J* = 5.9 Hz, 1H), 5.49 (s, 2H), 4.45 (q, *J* = 7.1 Hz, 2H), 3.63 – 3.55 (m, 2H), 1.42 (t, *J* = 7.2 Hz, 3H), 0.96 – 0.88 (m, 2H), -0.04 (s, 9H). ^{13}C NMR (126 MHz, $CDCl_3$) δ 164.47,

160.95, 159.42, 156.97, 130.53, 126.28, 121.41, 105.78, 81.78, 67.37, 61.64, 17.84, 14.47, -1.36. LCMS (Fleet, 10 → 90%): t_r = 8.29 min, m/z: 398.3.

4-((2-Chloropyrimidin-4-yl)amino)-1-((2-(trimethylsilyl)ethoxy)methyl)-1*H*-pyrazole-3-carboxylic acid (107)

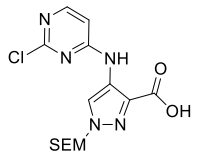

106 (250 mg, 628 µmol) was dissolved in MeCN (2.5 mL) and H_2O (50 µL). Et_3N (263 µL, 1.89 mmol) and LiBr (546 mg, 6.28 mmol) were added and the mixture was stirred for 3 days. The mixture was concentrated, suspended in DCM (30 mL) and poured into H_2O (30 mL). The pH of the water layer was adjusted (2 < pH < 5) by addition of 2 M HCl (aq.). The organic layer was separated and the water layer was extracted with DCM (30 mL). The combined organic layers were concentrated as such to afford the product (232 mg, 628 µmol, quant.). LCMS (Finnigan, 10 → 90%): t_r = 7.48 min, m/z: 370.1.

4-((2-Chloropyrimidin-4-yl)amino)-*N*-phenyl-1-((2-(trimethylsilyl)ethoxy)methyl)-1*H*-pyrazole-3-carboxamide (108)

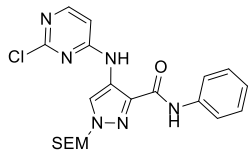

107 (85.0 mg, 230 µmol) was dissolved in DCM (0.9 mL). Aniline (25.2 µL, 276 µmol) and EDC·HCl (48.5 mg, 253 µmol) were added and the mixture was stirred for 16 h. The mixture was poured into H_2O (10 mL) and brine (1 mL), and the product extracted with DCM (2x10 mL). The combined organic layers were concentrated and purified by automated column chromatography (50 – 75% Et_2O/pentane) to afford the product (76.3 mg, 171 µmol, 75%). ^{1}H NMR (400 MHz, $CDCl_3$) δ 9.41 (s, 1H), 8.64 (s, 1H), 8.47 (s, 1H), 8.09 (d, *J* = 5.8 Hz, 1H), 7.65 – 7.60 (m, 2H), 7.39 – 7.33 (m, 2H), 7.17 – 7.11 (m, 1H), 6.53 (d, *J* = 5.8 Hz, 1H), 5.42 (s, 2H), 3.65 – 3.56 (m, 2H), 1.00 – 0.90 (m, 2H), -0.01 (s, 9H). ^{13}C NMR (101 MHz, $CDCl_3$) δ 161.86, 160.77, 159.34, 156.72, 137.08, 132.77, 129.18, 124.93, 124.71, 122.13, 119.99, 105.79, 81.22, 67.24, 17.71, -1.36. LCMS (Finnigan, 50 → 90%): t_r = 7.84 min, m/z: 445.3.

4-((2-Chloropyrimidin-4-yl)amino)-*N*-methyl-1-((2-(trimethylsilyl)ethoxy)methyl)-1*H*-pyrazole-3-carboxamide (109)

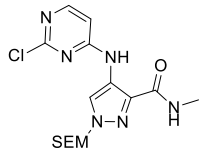

In a microwave vial, **107** (77.0 mg, 208 µmol) and EDC·HCl (47.9 mg, 250 µmol) were suspended in DCM (0.6 mL) after which methylamine (33 wt. % in EtOH, 39 µL, 312 µmol) was added. The vial was sealed and the mixture was stirred for 16 h. The mixture was poured into H_2O (10 mL) and brine (1 mL), and the product extracted with DCM (2x10 mL). The combined organic layers were concentrated as such and the crude was purified by automated column chromatography (65 – 100% Et_2O/pentane) to afford the product (46.1 mg, 120 µmol, 58%). ^{1}H NMR (400 MHz, $CDCl_3$) δ 9.52 (s, 1H), 8.42 (s, 1H), 8.08 (d, *J* = 5.9 Hz, 1H), 6.91 (q, *J* = 5.1 Hz, 1H), 6.51 (d, *J* = 5.8 Hz, 1H), 5.39 (s, 2H), 3.59 – 3.50 (m, 2H), 2.97 (d, *J* = 5.1 Hz, 3H), 0.96 – 0.86 (m, 2H), -0.04 (s, 9H). ^{13}C NMR (101 MHz, $CDCl_3$) δ 164.51, 160.84, 159.40, 156.63, 132.89, 124.46, 121.80, 105.78, 81.19, 67.14, 25.54, 17.73, -1.36. LCMS (Finnigan, 10 → 90%): t_r = 8.31 min, m/z: 383.1.

4-Nitro-1-((2-(trimethylsilyl)ethoxy)methyl)-1*H*-pyrazole (110)

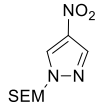

4-Nitro-1H-pyrazole (300 mg, 2.65 mmol) was dissolved in dry DCM (4.5 mL) and DIPEA (462 µL, 2.65 mmol was added. The mixture was cooled down to 0°C, SEM-Cl (510 µL, 2.92 mmol) was added dropwise and the reaction was stirred for 30 min at 0°C. The reaction was allowed to warm to RT and continued to stir for 30 min. The mixture was poured into H_2O (50 mL) and the product extracted with DCM (3x50 mL). The combined organic layers were washed with brine (50 mL), dried over Na_2SO_4, filtered and concentrated to afford the product (646 mg, 2.65 mmol, quant.). ^{1}H NMR (400 MHz, $CDCl_3$) δ 8.30 (s, 1H), 8.09 (s, 1H), 5.45 (s, 2H), 3.63 – 3.59 (m, 2H), 0.95 – 0.91 (m, 2H), -0.02 (s, 9H). ^{13}C NMR (101 MHz, $CDCl_3$) δ 136.89, 135.95, 128.57, 81.65, 68.07, 17.90, -1.36.

1-((2-(Trimethylsilyl)ethoxy)methyl)-1*H*-pyrazol-4-amine (111)

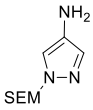

110 (330 mg, 1.36 mmol) was dissolved in degassed MeOH (14 mL). 10% Pd/C (70 mg) was added and the atmosphere was exchanged for H_2. The reaction was vigorously stirred for 3 h while bubbling H_2 through the mixture. The atmosphere was exchanged for N_2, the mixture was filtered over Celite and concentrated to afford the product (238 mg, 1.11 mmol, 82%). ^{1}H NMR (400 MHz, $CDCl_3$) δ 7.19 (d, *J* = 0.9 Hz, 1H), 7.15 (d, *J* = 0.9 Hz, 1H), 5.29 (s, 2H), 3.53 – 3.47 (m, 2H), 2.65 (br s, 2H), 0.92 – 0.85 (m, 2H), -0.03 (s, 9H). ^{13}C NMR (101 MHz, $CDCl_3$) δ 132.27, 130.07, 117.88, 80.58, 66.51, 17.93, -1.32. LCMS (Finnigan, 10 → 90%): t_r = 4.84 min, m/z: 214.0.

2-Chloro-*N*-(1-((2-(trimethylsilyl)ethoxy)methyl)-1*H*-pyrazol-4-yl)pyrimidin-4-amine (112)

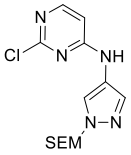

111 (220 mg, 1.03 mmol) was dissolved in EtOH (1.5 mL). DIPEA (629 µL, 3.61 mmol) and 2,4-dichloropyrimidine (180 mg, 1.21 mmol) were added. The mixture was stirred for 24 h, subsequently poured into half sat. $NaHCO_3$ (aq.) (20 mL) and the product was extracted with DCM (2x50 mL). The combined organic layers were washed with brine (100 mL), dried over Na_2SO_4, filtered and concentrated. The crude was purified by silica gel column chromatography (1% MeOH (containing 10% sat. NH_4OH (aq.))/DCM) to afford the product (214 mg, 0.665 µmol, 64%). ^{1}H NMR (400 MHz, $CDCl_3$) δ 8.04 (d, *J* = 5.9 Hz, 1H), 7.85 (br s, 2H), 7.52 (d, *J* = 0.7 Hz, 1H), 6.43 (d, *J* = 5.9 Hz, 1H), 5.40 (s, 2H), 3.60 – 3.52 (m, 2H), 0.94 – 0.84 (m, 2H), -0.05 (s, 9H). ^{13}C NMR (101 MHz, $CDCl_3$) δ 163.36 (br), 160.65, 157.28 (br), 135.88 (br), 131.93 (br), 125.13 (br), 121.30 (br), 102.85 (br), 80.85, 67.02, 17.83, -1.38. LCMS (Finnigan, 10 → 90%): t_r = 7.38 min, m/z: 326.1.

4-((2-(4-Nitro-1-((2-(trimethylsilyl)ethoxy)methyl)-1*H*-pyrazol-3-yl)-1*H*-benzo[*d*]imidazol-5-yl)methyl)morpholine (113)

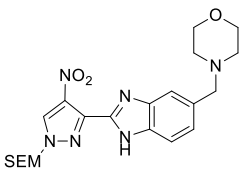

104 (2.00 g, 6.34 mmol) was suspended in a mixture of MeOH and H_2O (1:1, 12 mL), LiOH·H_2O (1.06 g, 25.3 mmol) was added and the mixture was stirred vigorously for 1.5 h. The mixture was poured into a mixture of H_2O (60 mL) and DCM (75 mL). The pH of the water layer was adjusted by addition of 2 M HCl (aq.) to pH ~2. The organic layer was separated and the water layer extracted with DCM (75 mL). The combined organic layers were dried over Na_2SO_4, filtered and concentrated to yield the free acid intermediate. The intermediate was dissolved in DMF (10 mL), after which 4-(morpholinomethyl)benzene-1,2-diamine (1.45 g, 6.98 mmol), EDC·HCl (1.22 g, 6.34 mmol) and HOBt (857 mg, 6.34 mmol) were added and the mixture was stirred for 1 h. The mixture was concentrated after which AcOH (7 mL) was added and the mixture was stirred at 118°C for 30 min. The mixture was cooled down to RT, 10 M NaOH (aq.) was added until the pH was about 8. The mixture was poured into a mixture of H_2O (60 mL) and DCM (70 mL) after which the organic layer was separated. The water layer was extracted with DCM (70 mL) and the combined organic layers were dried over Na_2SO_4, filtered and concentrated. The crude was purified by automated column chromatography twice (0 – 10% MeOH/EtOAc) to afford the product (1.69 g, 3.69 mmol, 58%). ^{1}H NMR (400 MHz, $CDCl_3$) δ 11.42 (s, 1H), 8.51 (s, 1H), 7.85 – 7.66 (br m, 1H), 7.60 – 7.44 (br m, 1H), 7.35 – 7.22 (br m, 1H), 5.53 (s, 2H), 3.70 – 3.62 (m, 6H), 3.60 (s, 2H), 2.49 – 2.38 (m, 4H), 0.97 – 0.87 (m, 2H), -0.06 (s, 9H). ^{13}C NMR (101 MHz, $CDCl_3$) δ 143.44 (br), 142.72 (br), 142.17, 136.67, 134.34 (br), 134.08, 133.41 (br), 132.80 (br), 132.56 (br), 131.56, 125.91 (br), 124.87 (br), 120.89 (br), 120.09 (br), 111.96 (br), 111.42 (br), 82.43, 68.65, 66.97, 63.60, 53.55, 17.98, -1.42. LCMS (Finnigan, 10 → 90%): t_r = 5.57 min, m/z: 459.1.

3-(5-(Morpholinomethyl)-1*H*-benzo[*d*]imidazol-2-yl)-1-((2-(trimethylsilyl)ethoxy)methyl)-1*H*-pyrazol-4-amine (114)

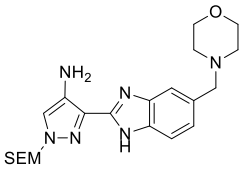

113 (1.17 g, 2.56 mmol) was dissolved in degassed MeOH (30 mL). 10% Pd/C (120 mg) was added and the atmosphere was exchanged for H_2. The reaction was vigorously stirred for 30 min while bubbling H_2 through the mixture. The atmosphere was exchanged for N_2, the mixture was filtered over Celite and concentrated to afford the product (1.07 g, 2.49 mmol, 97%). ^{1}H NMR (400 MHz, $CDCl_3$) δ 7.55 (br s, 1H), 7.50 (br s, 1H), 7.21 (dd, *J* = 8.2, 1.6 Hz, 1H), 7.18 (s, 1H), 5.29 (s, 2H), 4.18 (s, 2H), 3.76 – 3.72 (m, 4H), 3.67 (s, 2H), 3.55 – 3.49

(m, 2H), 2.58 – 2.50 (m, 4H), 0.91 – 0.85 (m, 2H), -0.06 (s, 9H) (the –NH of the benzimidazole was not observed). ^{13}C NMR (101 MHz, $CDCl_3$) δ 147.94, 131.91, 130.54 (br), 124.38 (br), 117.17, 80.90, 66.83, 66.56, 63.56, 53.29, 17.83, -1.35 (not all quaternary carbons were observed, neither were two –CH's of the benzimidazole). LCMS (Finnigan, 10 → 90%): t_r = 4.85 min, m/z: 429.2.

2-Chloro-*N*-(3-(5-(morpholinomethyl)-1*H*-benzo[*d*]imidazol-2-yl)-1-((2-(trimethylsilyl)ethoxy)methyl)-1*H*-pyrazol-4-yl)pyrimidin-4-amine (115)

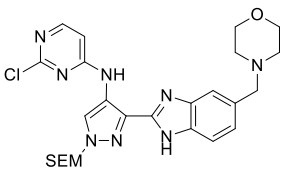

114 (445 mg, 1.04 mmol) was dissolved in EtOH (1 mL). DIPEA (0.54 mL, 3.1 mmol) and 2,4-dichloropyrimidine (232 mg, 1.56 mmol) were added and the mixture was stirred for 4 days. The mixture was poured into H_2O (75 mL) and the product extracted with DCM (2x75 mL). The combined organic layers were dried over Na_2SO_4, filtered and concentrated. The crude was purified by automated column chromatography to afford the product (371 mg, 685 µmol, 66%). ^{1}H NMR (400 MHz, $CDCl_3$) δ 10.79 – 10.63 (2x s, 1H), 10.39 – 10.30 (2x s, 1H), 8.51 – 8.47 (2x s, 1H), 8.19 – 8.15 (2x d, *J* = 5.8 Hz, 1H), 7.74 – 7.67 (m, 1H), 7.44 – 7.36 (m, 1H), 7.30 – 7.22 (2x dd, *J* = 8.3, 1.3 Hz, 1H), 6.73 – 6.68 (2x d, *J* = 5.6 Hz, 1H), 5.44 (s, 2H), 3.76 – 3.70 (m, 4H), 3.66 – 3.57 (m, 4H), 2.56 – 2.45 (m, 4H), 0.97 – 0.90 (m, 2H), -0.02 – -0.04 (2x s, 9H). ^{13}C NMR (101 MHz, $CDCl_3$) δ 160.90, 160.88, 159.55, 156.46, 147.11, 146.93, 143.26, 142.55, 133.59, 132.91, 132.23, 132.04, 131.66, 131.62, 125.28, 124.24, 123.00, 122.96, 121.91, 119.80, 118.77, 111.54, 110.74, 106.09, 81.09, 81.07, 67.11, 67.10, 67.07, 63.84, 63.77, 53.72, 53.68, 17.81, -1.33. LCMS (Fleet, 10 → 90%): t_r = 5.56 min, m/z: 541.2.

2-(2-Chlorophenoxy)-*N*-(3-(5-(morpholinomethyl)-1*H*-benzo[*d*]imidazol-2-yl)-1-((2-(trimethylsilyl)ethoxy)methyl)-1*H*-pyrazol-4-yl)pyrimidin-4-amine (116)

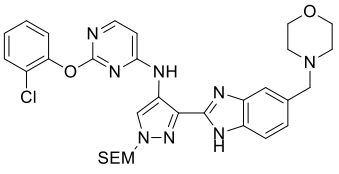

The title compound was synthesized according to general procedure I using 2-chlorophenol to afford the product (95.5 mg, 151 µmol, 91%). ^{1}H NMR (500 MHz, $CDCl_3$) δ 11.37 – 11.31 (2x s, 1H), 10.26 – 10.20 (2x s, *J* = 9.8 Hz, 1H), 8.33 – 8.30 (2x d, *J* = 5.8 Hz, 1H), 7.73 – 7.67 (m, 1H), 7.54 (dd, *J* = 8.0, 1.6 Hz, 1H), 7.47 – 7.33 (m, 3H), 7.30 – 7.24 (m, 2H), 7.24 – 7.19 (m, 1H), 6.58 – 6.52 (2x d, *J* = 5.4 Hz, 1H), 5.11 (s, 2H), 3.74 – 3.64 (m, 4H), 3.63 – 3.55 (2x s, 2H), 3.44 (t, *J* = 8.1 Hz, 2H), 2.56 – 2.38 (m, 4H), 0.92 – 0.83 (m, 2H), -0.03 – -0.05 (2x s, 9H). ^{13}C NMR (126 MHz, $CDCl_3$) δ 164.93, 160.03, 157.30, 157.28, 149.75, 147.21, 147.08, 143.26, 142.58, 133.11, 133.04, 132.25, 131.78, 131.70, 131.63, 130.54, 128.34, 128.01, 126.36, 125.00, 124.80, 124.01, 123.09, 123.04, 121.57, 119.69, 118.60, 111.83, 110.82, 102.52, 80.72, 66.99, 66.94, 66.71, 66.69, 63.79, 63.73, 53.59, 53.55, 17.77, -1.34, -1.37. LCMS (Fleet, 10 → 90%): t_r = 5.78 min, m/z: 633.2.

2-(3-Chlorophenoxy)-*N*-(3-(5-(morpholinomethyl)-1*H*-benzo[*d*]imidazol-2-yl)-1-((2-(trimethylsilyl)ethoxy)methyl)-1*H*-pyrazol-4-yl)pyrimidin-4-amine (117)

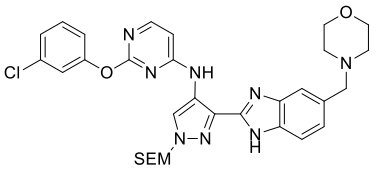

The title compound was synthesized according to general procedure I using 3-chlorophenol to afford the product (85.8 mg, 135 µmol, 81%). ^{1}H NMR (500 MHz, $CDCl_3$) δ 11.21 – 11.10 (m, 1H), 10.28 – 10.19 (m, 1H), 8.30 – 8.24 (2x d, *J* = 5.8 Hz, 1H), 7.73 – 7.68 (m, 1H), 7.48 – 7.44 (2x s, 1H), 7.43 – 7.35 (m, 2H), 7.35 – 7.33 (2x t, *J* = 2.3 Hz, 1H), 7.31 (dd, *J* = 8.0, 2.0 Hz, 1H), 7.26 – 7.22 (2x dd, *J* = 8.3, 1.5 Hz, 1H), 7.20 – 7.16 (2x dt, *J* = 8.1, 2.5 Hz, 1H), 6.58 – 6.52 (2x d, *J* = 5.8 Hz, 1H), 5.20 (s, 2H), 3.76 – 3.68 (m, 4H), 3.65 – 3.57 (2x s, 2H), 3.49 – 3.43 (m, 2H), 2.56 – 2.43 (m, 4H), 0.91 – 0.85 (m, 2H), -0.04 – -0.05 (2x s, 9H). ^{13}C NMR (126 MHz, $CDCl_3$) δ 165.46, 159.98, 159.88, 157.24, 157.21, 154.09, 147.19, 147.05, 146.92, 143.27, 142.60, 134.65, 133.19, 133.06, 132.92, 132.19, 132.04, 131.87, 131.66, 130.47, 125.49, 125.08, 124.07, 123.51, 123.00, 122.96, 122.88, 122.83, 121.76, 121.27, 119.78, 118.66, 111.68, 111.62, 110.72, 110.67, 102.63, 102.55, 80.86, 67.01, 66.97, 66.81, 66.79, 63.81, 63.75, 53.62, 17.75, -1.32. LCMS (Fleet, 10 → 90%): t_r = 5.76 min, m/z: 633.2.

2-(4-Chlorophenoxy)-*N*-(3-(5-(morpholinomethyl)-1*H*-benzo[*d*]imidazol-2-yl)-1-((2-(trimethylsilyl)ethoxy)methyl)-1*H*-pyrazol-4-yl)pyrimidin-4-amine (118)

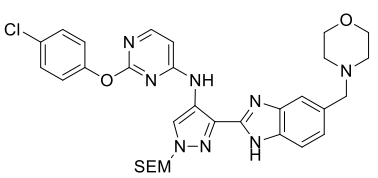

The title compound was synthesized according to general procedure I using 4-chlorophenol to afford the product (95.5 mg, 151 µmol, 91%). ^{1}H NMR (500 MHz, $CDCl_3$) δ 11.62 – 11.53 (2x s, 1H), 10.21 – 10.12 (2x s, 1H), 8.18 – 8.14 (2x d, *J* = 5.9 Hz, 1H), 7.70 – 7.64 (m, 1H), 7.44 – 7.37 (m, 3H), 7.31 (s, 1H), 7.24 – 7.16 (m, 3H), 6.57 – 6.53 (2x d, *J* = 5.8 Hz, 1H), 5.15 (s, 2H), 3.72 – 3.65 (m, 4H), 3.62 – 3.56 (2x s, 2H), 3.50 – 3.43 (m, 2H), 2.51 – 2.43 (m, 4H), 0.91 – 0.85 (m, 2H), -0.05 (s, 9H). ^{13}C NMR (126 MHz, $CDCl_3$) δ 165.46, 159.92, 159.82, 156.84, 151.96, 146.97, 146.85, 146.74, 143.07, 142.46, 133.20, 133.07, 132.67, 132.40, 132.26, 131.84, 131.38, 130.43, 129.64, 125.14, 124.39, 124.15, 124.13, 122.74, 122.70, 122.61, 122.58, 121.93, 119.67, 118.45, 111.88, 110.88, 102.45, 102.40, 80.72, 66.81, 66.76, 66.72, 63.71, 53.48, 53.44, 17.70, -1.43, -1.49. LCMS (Fleet, 10 → 90%): t_r = 5.70 min, m/z: 633.2.

2-(3-Chlorophenyl)-*N*-(3-(5-(morpholinomethyl)-1*H*-benzo[*d*]imidazol-2-yl)-1-((2-(trimethylsilyl)ethoxy)methyl)-1*H*-pyrazol-4-yl)pyrimidin-4-amine (119)

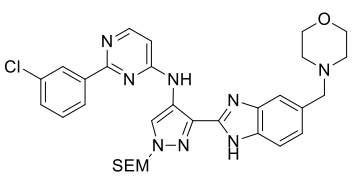

The title compound was synthesized from **115** (125 mg, 231 µmol) and 3-chlorophenylboronic acid (36.8 mg, 236 µmol) according to general procedure G (reaction time 16 h). The crude was purified by automated column chromatography (0 – 10% MeOH/EtOAc) to afford the product (87.3 mg, 141 µmol, 61%). ^{1}H NMR (500 MHz, $CDCl_3$) δ 10.96 – 10.79 (2x s, 1H), 10.14 – 10.06 (2x s, 1H), 8.58 (s, 1H), 8.41 – 8.37 (2x d, *J* = 5.9 Hz, 1H), 8.37 (s, 1H), 8.25 (d, *J* = 7.5 Hz, 1H), 7.76 – 7.71 (m, 1H), 7.45 – 7.42 (m, 1H), 7.40 (t, *J* = 7.7 Hz, 1H), 7.37 – 7.31 (m, 1H), 7.27 – 7.23 (m, 1H), 6.70 (d, *J* = 5.8 Hz, 1H), 5.43 (s, 2H), 3.79 – 3.70 (m, 4H), 3.68 – 3.60 (m, 4H), 2.57 – 2.48 (m, 4H), 0.98 – 0.93 (m, 2H), -0.05 (s, 9H). ^{13}C NMR (126 MHz, $CDCl_3$) δ 163.40, 158.67, 155.27, 147.26, 147.10, 143.42, 142.74, 140.50, 134.53, 133.18, 133.00, 132.17, 131.89, 131.64, 130.26, 129.77, 128.39, 126.21, 125.18, 124.20, 123.80, 121.18, 119.93, 118.79, 111.56, 110.64, 106.21, 81.12, 67.16, 67.00, 63.77, 63.73, 53.64, 17.81, -1.35. LCMS (Fleet, 10 → 90%): t_r = 5.44 min, m/z: 617.1.

***N*-(3-(5-(Morpholinomethyl)-1*H*-benzo[*d*]imidazol-2-yl)-1-((2-(trimethylsilyl)ethoxy)methyl)-1*H*-pyrazol-4-yl)-2-(3-((trimethylsilyl)ethynyl)phenyl)pyrimidin-4-amine (120)**

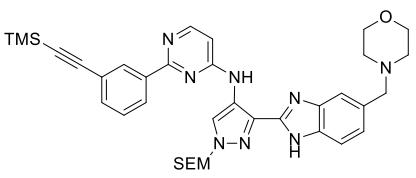

A microwave vial was charged with **115** (125 mg, 231 µmol), K_2CO_3 (128 mg, 924 µmol), 3-[(trimethylsilyl)ethynyl]phenylboronic acid pinacol ester (74.2 mg, 247 µmol) and 4:1 dioxane/H_2O (1.2 mL). N_2 was bubbled through the mixture for 1 min after which Pd(dppf)Cl_2·DCM (13.2 mg, 16.2 µmol) was added. N_2 was bubbled through the mixture for 30 sec after which the vial was sealed. The mixture was heated to 90°C and stirred for 16 h. Then, extra K_2CO_3 (64.0 mg, 462 µmol), 3-[(trimethylsilyl)ethynyl]phenylboronic acid pinacol ester (37.1 mg, 124 µmol) and Pd(dppf)Cl_2·DCM (6.7 mg, 8.0 µmol) were added, N_2 was bubbled through the mixture for 30 sec after which the vial was sealed and stirred at 90°C for another 8 h. The mixture was poured into H_2O (20 mL). The product was extracted with DCM (2x20 mL) and the combined organic layers were concentrated as such. The crude was purified by automated column chromatography (0 – 10% MeOH/EtOAc) to afford the product (44 mg, 65 µmol, 28%). ^{1}H NMR (400 MHz, $CDCl_3$) δ 10.87 – 10.70 (2x s, 1H), 10.13 – 10.06 (2x s, 1H), 8.65 (s, 1H), 8.52 (s, 1H), 8.44 – 8.39 (2x d, *J* = 5.5 Hz, 1H), 8.33 (d, *J* = 7.6 Hz, 1H), 7.77 – 7.71 (m, 1H), 7.58 (dt, *J* = 7.7, 1.4 Hz, 1H), 7.43 (t, *J* = 7.8 Hz, 1H), 7.41 – 7.35 (m, 1H), 7.26 (dd, *J* = 8.3, 1.3 Hz, 1H), 6.73 (d, *J* = 5.8 Hz, 1H), 5.48 – 5.45 (2x s, 2H), 3.78 – 3.70 (m, 4H), 3.68 – 3.59 (m, 4H), 2.57 – 2.47 (m, 4H), 0.97 – 0.91 (m, 2H), 0.28 (s, 9H), -0.06 (s, 9H). ^{13}C NMR (101 MHz, $CDCl_3$) δ 163.88, 158.72, 155.34, 147.28, 147.13, 143.42, 142.75, 138.69, 133.61, 133.20, 133.01, 132.25, 132.16, 132.00, 131.90, 131.66, 128.52, 128.16, 125.24, 124.86, 124.25, 123.87, 123.48, 121.37, 119.96, 118.82, 111.64, 110.71, 106.12, 105.13, 94.37, 81.07, 67.05, 63.82, 63.78, 53.67, 53.64, 17.82, 0.12, -1.34. LCMS (Fleet, 10 → 90%): t_r = 6.60 min, m/z: 679.2.

_N_-(3-(5-(Morpholinomethyl)-1_H_-benzo[_d_]imidazol-2-yl)-1-((2-(trimethylsilyl)ethoxy)methyl)-1_H_-pyrazol-4-yl)-2-(3-(trifluoromethyl)phenyl)pyrimidin-4-amine (121)

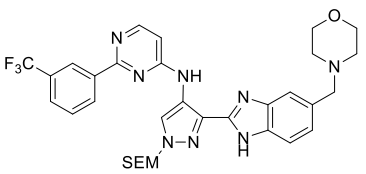

The title compound was synthesized from **115** (125 mg, 231 µmol) and (3-(trifluoromethyl)phenyl)boronic acid (46.9 mg, 247 µmol) according to general procedure G (reaction time 16 h). The crude was purified by automated column chromatography (0 – 10% MeOH/EtOAc) to afford the product (112 mg, 173 µmol, 75%). ^{1}H NMR (400 MHz, $CDCl_3$) δ 11.12 – 10.91 (2x s, 1H), 10.16 (s, 1H), 8.67 (s, 1H), 8.58 (s, 1H), 8.55 (d, _J_ = 7.8 Hz, 1H), 8.41 (d, _J_ = 5.8 Hz, 1H), 7.74 (br s, 1H), 7.72 (d, _J_ = 7.7 Hz, 1H), 7.58 (t, _J_ = 7.8 Hz, 1H), 7.41 – 7.31 (m, 1H), 7.25 (dd, _J_ = 8.1, 1.8 Hz, 1H), 6.72 (d, _J_ = 5.8 Hz, 1H), 5.41 (s, 2H), 3.79 – 3.71 (m, 4H), 3.69 – 3.58 (m, 4H), 2.60 – 2.49 (m, 4H), 0.97 – 0.90 (m, 2H), -0.06 (s, 9H). ^{13}C NMR (101 MHz, $CDCl_3$) δ 163.16, 158.64, 155.29, 147.17 (br), 147.08 (br), 143.35 (br), 142.71 (br), 139.34, 133.06 (br), 132.89 (br), 132.26 (br), 131.72, 131.57 (br), 131.27, 130.95, 130.63, 129.08, 126.85 (br), 126.81 (br), 125.70, 125.27 (br), 125.08 (br), 125.04 (br), 125.00 (br), 124.97 (br), 124.28 (br), 123.71, 122.99, 121.31, 120.00 (br), 118.77 (br), 111.75 (br), 110.74 (br), 106.39, 81.08, 67.13, 66.90, 63.67, 53.53, 17.74, -1.44. LCMS (Fleet, 10 → 90%): t_r = 5.85 min, m/z: 651.1.

3-(4-((3-(5-(Morpholinomethyl)-1_H_-benzo[_d_]imidazol-2-yl)-1-((2-(trimethylsilyl)ethoxy)methyl)-1_H_-pyrazol-4-yl)amino)pyrimidin-2-yl)benzonitrile (122)

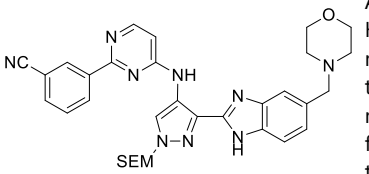

A microwave vial was charged with **115** (125 mg, 231 µmol), K_2CO_3 (128 mg, 924 µmol), (3-cyanophenyl)boronic acid (37.3 mg, 254 µmol) and 4:1 dioxane/H_2O (1.2 mL). N_2 was bubbled through the mixture for 1 min after which Pd(dppf)Cl_2·DCM (13.2 mg, 16.2 µmol) was added. N_2 was bubbled through the mixture for 30 sec after which the vial was sealed. The mixture was heated to 90°C and stirred for 5 h. Then, extra K_2CO_3 (60.0 mg, 434 µmol), (3-cyanophenyl)boronic acid (15.0 mg, 102 µmol) and Pd(dppf)Cl_2·DCM (6.0 mg, 7.3 µmol) were added, N_2 was bubbled through the mixture for 30 sec after which the vial was sealed and stirred at 90°C for another 4.5 h. The mixture was poured into H_2O (20 mL) and brine (1 mL). The product was extracted with 5% MeOH/DCM (20 mL) and DCM (3x20 mL) and the combined organic layers were concentrated as such. The crude was purified by automated column chromatography (0 – 15% MeOH/EtOAc) to afford the product (101 mg, 167 µmol, 72%). ^{1}H NMR (400 MHz, $CDCl_3$) δ 10.80 – 10.63 (2x s, 1H), 10.18 – 10.11 (2x s, 1H), 8.66 – 8.62 (2x t, _J_ = 1.7 Hz, 1H), 8.59 – 8.54 (2x dt, _J_ = 8.1, 1.5 Hz, 1H), 8.51 – 8.48 (2x s, 1H), 8.41 – 8.36 (2x d, _J_ = 5.8 Hz, 1H), 7.75 – 7.68 (m, 2H), 7.55 (t, _J_ = 7.8 Hz, 1H), 7.35 – 7.30 (m, 1H), 7.27 – 7.23 (m, 1H), 6.73 (d, _J_ = 5.8 Hz, 1H), 5.47 – 5.42 (2x s, 2H), 3.79 – 3.70 (m, 4H), 3.67 – 3.59 (m, 4H), 2.58 – 2.46 (m, 4H), 0.94 (t, _J_ = 8.2 Hz, 2H), -0.06 (s, 9H). ^{13}C NMR (101 MHz, $CDCl_3$) δ 162.50, 162.47, 158.68, 155.25, 147.18, 147.00, 143.34, 142.62, 139.76, 133.36, 132.86, 132.10, 132.01, 131.90, 131.59, 131.57, 129.30, 125.17, 124.18, 123.67, 123.61, 120.80, 119.84, 118.84, 118.75, 112.63, 111.42, 110.56, 106.60, 81.17, 67.14, 67.05, 67.00, 63.79, 63.74, 53.68, 53.64, 17.76, -1.38. LCMS (Fleet, 10 → 90%): t_r = 5.24 min, m/z: 608.3.

2-(3-Chloro-2-fluorophenyl)-_N_-(3-(5-(morpholinomethyl)-1_H_-benzo[_d_]imidazol-2-yl)-1-((2-(trimethylsilyl)ethoxy)methyl)-1_H_-pyrazol-4-yl)pyrimidin-4-amine (123)

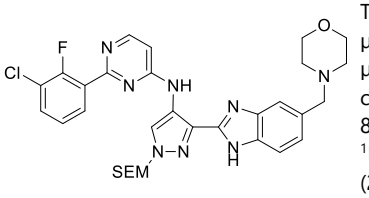

The title compound was synthesized from **115** (115 mg, 213 µmol) and (3-chloro-2-fluorophenyl)boronic acid (37.8 mg, 217 µmol) according to general procedure G (reaction time 16 h). The crude was purified by automated column chromatography (0 – 8% MeOH/EtOAc) to afford the product (104 mg, 164 µmol, 77%). ^{1}H NMR (400 MHz, $CDCl_3$) δ 10.90 – 10.75 (m, 1H), 10.16 – 10.08 (2x s, 1H), 8.72 – 8.69 (2x s, 1H), 8.46 – 8.41 (2x d, _J_ = 5.9 Hz, 1H), 8.05 – 7.99 (m, 1H), 7.77 – 7.70 (m, 1H), 7.52 – 7.46 (m, 1H), 7.33 – 7.28 (m, 1H), 7.27 – 7.22 (m, 1H), 7.20 – 7.14 (m, 1H), 6.76 (dd, _J_ = 5.9, 2.5 Hz, 1H), 5.44 – 5.41 (2x s, 2H), 3.77 – 3.70 (m, 4H), 3.67 – 3.58 (m, 4H), 2.56 – 2.45 (m, 4H), 0.98 – 0.91 (m, 2H), -0.06 – -0.07 (2x s, 9H). ^{13}C NMR (101 MHz, $CDCl_3$) δ 162.09,

162.06, 162.04, 162.02, 158.35, 157.95, 155.40, 155.21, 155.18, 147.36, 147.20, 143.40, 142.70, 133.32, 132.95, 132.09, 132.05, 131.84, 131.70, 131.66, 130.29, 130.28, 128.75, 128.66, 125.10, 124.42, 124.38, 124.12, 123.57, 123.52, 122.49, 122.31, 122.01, 121.96, 119.82, 118.75, 111.46, 110.61, 106.12, 81.05, 67.09, 67.04, 63.85, 63.79, 53.70, 53.67, 17.74, -1.40. LCMS (Fleet, 10 → 90%): t_r = 5.37 min, m/z: 635.3.

2-(2-Fluoro-3-((trimethylsilyl)ethynyl)phenyl)-*N*-(3-(5-(morpholinomethyl)-1*H*-benzo[*d*]imidazol-2-yl)-1-((2-(trimethylsilyl)ethoxy)methyl)-1*H*-pyrazol-4-yl)pyrimidin-4-amine (124)

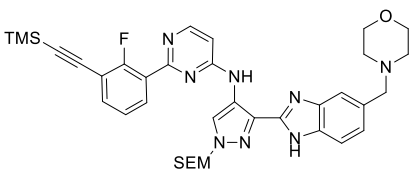

The title compound was synthesized from **123** (42 mg, 66 µmol) according to general procedure H. The crude was purified by automated column chromatography (0 – 8% MeOH/EtOAc) to afford the product (37.4 mg, 53.7 µmol, 81%). ^{1}H NMR (500 MHz, $CDCl_3$) δ 10.90 – 10.76 (2x s, 1H), 10.14 – 10.05 (2x s, 1H), 8.75 (s, 1H), 8.47 – 8.43 (2x d, *J* = 6.3 Hz, 1H), 8.12 – 8.06 (2x d, *J* = 7.3 Hz, 1H), 7.78 – 7.70 (m, 1H), 7.55 (ddd, *J* = 7.8, 6.3, 1.6 Hz, 1H), 7.36 – 7.29 (m, 1H), 7.27 – 7.23 (m, 1H), 7.18 (t, *J* = 7.7 Hz, 1H), 6.75 (d, *J* = 5.9 Hz, 1H), 5.43 (s, 2H), 3.78 – 3.71 (m, 4H), 3.69 – 3.57 (m, 4H), 2.61 – 2.45 (m, 4H), 0.96 – 0.87 (m, 2H), 0.29 (s, 9H), -0.08 (s, 9H). ^{13}C NMR (126 MHz, $CDCl_3$) δ 162.61, 162.31, 162.28, 160.54, 158.35, 155.21, 147.42, 147.27, 143.43, 142.78, 135.09, 132.98, 132.16, 131.70, 127.36, 127.29, 125.13, 124.17, 123.78, 123.74, 123.59, 122.20, 119.92, 118.78, 113.31, 113.17, 111.58, 110.67, 105.95, 100.41, 100.38, 98.16, 80.95, 66.96, 66.92, 63.73, 53.60, 17.70, 0.00, -1.38. LCMS (Fleet, 10 → 90%): t_r = 6.51 min, m/z: 697.3.

2-(5-Chloro-2-fluorophenyl)-*N*-(3-(5-(morpholinomethyl)-1*H*-benzo[*d*]imidazol-2-yl)-1-((2-(trimethylsilyl)ethoxy)methyl)-1*H*-pyrazol-4-yl)pyrimidin-4-amine (125)

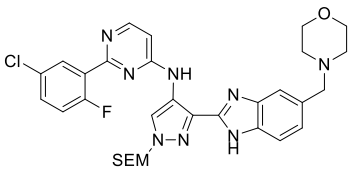

The title compound was synthesized from **115** (100 mg, 185 µmol) and (5-chloro-2-fluorophenyl)boronic acid (33.2 mg, 190 µmol) according to general procedure G (reaction time 16 h). The crude was purified by automated column chromatography (0 – 6% MeOH/EtOAc) to afford the product (65.5 mg, 103 µmol, 56%). ^{1}H NMR (400 MHz, $CDCl_3$) δ 10.76 – 10.61 (2x s, 1H), 10.17 – 10.08 (2x s, 1H), 8.71 – 8.68 (2x s, 1H), 8.45 – 8.41 (2x d, *J* = 6.2 Hz, 1H), 8.19 – 8.15 (2x dd, *J* = 6.7, 2.6 Hz, 1H), 7.76 – 7.71 (m, 1H), 7.40 – 7.35 (2x ddd, *J* = 8.6, 3.9, 2.7 Hz, 1H), 7.35 – 7.29 (m, 1H), 7.28 – 7.22 (2x dd, *J* = 8.1, 1.6 Hz, 1H), 7.16 – 7.10 (2x dd, *J* = 10.1, 8.8 Hz, 1H), 6.76 – 6.74 (2x d, *J* = 5.9 Hz, 1H), 5.45 – 5.42 (2x s, 2H), 3.79 – 3.69 (m, 4H), 3.67 – 3.57 (m, 4H), 2.57 – 2.45 (m, 4H), 0.97 – 0.90 (m, 2H), -0.05 – -0.07 (2x s, 9H). ^{13}C NMR (101 MHz, $CDCl_3$) δ 161.64, 161.61, 161.59, 161.56, 161.04, 158.52, 158.37, 155.20, 155.16, 147.36, 147.19, 143.42, 142.72, 133.39, 132.92, 132.10, 132.06, 131.70, 131.68, 131.63, 131.60, 131.20, 131.11, 129.37, 129.33, 128.42, 128.32, 125.12, 124.15, 123.64, 123.59, 121.89, 121.84, 121.82, 119.85, 118.79, 118.47, 118.22, 111.42, 110.59, 106.18, 106.15, 81.11, 67.10, 67.08, 67.06, 63.86, 63.79, 53.72, 53.69, 17.79, -1.38. LCMS (Fleet, 10 → 90%): t_r = 5.41 min, m/z: 635.2.

2-Chloro-5-methoxy-*N*-(3-(5-(morpholinomethyl)-1*H*-benzo[*d*]imidazol-2-yl)-1-((2-(trimethylsilyl)ethoxy)methyl)-1*H*-pyrazol-4-yl)pyrimidin-4-amine (126)

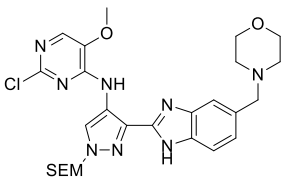

114 (1.20 g, 2.80 mmol) was dissolved in EtOH (3 mL) after which DIPEA (1.5 mL 8.4 mmol) and 2,4-dichloro-5-methoxypyrimidine (752 mg, 4.20 mmol) were added. The mixture was heated to 40°C and stirred for 6 days. The mixture was poured into H_2O (75 mL) and the product extracted with DCM (2x50 mL). The combined organic layers were concentrated as such. The crude was purified by automated column chromatography (0 – 10% MeOH/EtOAc) to afford the product (1.12 g, 1.97 mmol, 70%). ^{1}H NMR (400 MHz, $CDCl_3$) δ 10.65 – 10.59 (2x s, 1H), 10.58 – 10.49 (2x s, 1H), 8.54 – 8.48 (2x s, 1H), 7.72 – 7.66 (m, 2H), 7.43 – 7.35 (m, 1H), 7.28 – 7.24 (m, 1H), 5.45 – 5.42 (2x s, 2H), 4.06 – 4.02 (2x s, 3H), 3.76 – 3.70 (m, 4H), 3.66 – 3.62 (2x s, 2H), 3.62 – 3.56 (m, 2H), 2.55 – 2.45 (m, 4H), 0.96 – 0.90 (m, 2H), -0.03 – -0.05 (2x s, 9H). ^{13}C NMR (101 MHz, $CDCl_3$) δ 151.56, 151.54, 151.29, 147.07, 146.90,

143.48, 142.73, 140.15, 140.13, 133.70, 133.67, 133.52, 132.94, 132.09, 132.07, 132.06, 132.01, 125.29, 124.11, 122.83, 121.72, 121.67, 119.99, 118.90, 111.52, 110.65, 81.08, 81.05, 67.09, 63.92, 63.82, 56.71, 56.63, 53.74, 17.81, -1.34. LCMS (Fleet, 10 → 90%): t_r = 6.13 min, m/z: 571.1.

2-(3-Chlorophenyl)-5-methoxy-*N*-(3-(5-(morpholinomethyl)-1*H*-benzo[*d*]imidazol-2-yl)-1-((2-(trimethylsilyl)ethoxy)methyl)-1*H*-pyrazol-4-yl)pyrimidin-4-amine (127)

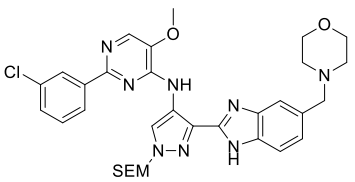

The title compound was synthesized from **126** (175 mg, 306 µmol) and (3-chlorophenyl)boronic acid (55.1 mg, 352 µmol) according to general procedure G (reaction time 16 h). The crude was purified by HPLC (Waters, 35 – 45% MeCN in 0.2% TFA (aq.)), the pH of the combined fractions was adjusted to pH ~8 using 10 M NaOH after which the mixture was concentrated. The product was dissolved in a mixture of H_2O (20 mL) and DCM (20 mL). The organic layer was separated and the water layer extracted with DCM (20 mL). The combined organic layers were dried over Na_2SO_4, filtered and concentrated to afford the product (103 mg, 159 µmol, 52%). ^{1}H NMR (400 MHz, $CDCl_3$) δ 10.89 – 10.81 (2x s, 1H), 10.47 – 10.41 (2x s, 1H), 8.61 – 8.58 (m, 1H), 8.32 – 8.29 (m, 1H), 8.20 – 8.15 (m, 1H), 7.93 – 7.88 (2x s, 1H), 7.74 – 7.69 (m, 1H), 7.41 – 7.36 (m, 2H), 7.32 – 7.27 (m, 1H), 7.27 – 7.22 (m, 1H), 5.39 (s, 2H), 4.06 – 4.03 (2x s, 3H), 3.78 – 3.70 (m, 4H), 3.68 – 3.58 (m, 4H), 2.51 (dt, *J* = 16.7, 4.7 Hz, 4H), 0.96 – 0.89 (m, 2H), -0.07 – -0.08 (2x s, 9H). ^{13}C NMR (101 MHz, $CDCl_3$) δ 155.41, 155.39, 150.21, 150.19, 147.28, 147.12, 143.60, 142.85, 140.51, 140.04, 140.02, 134.39, 134.37, 133.21, 133.01, 132.69, 132.66, 132.16, 132.02, 131.98, 131.88, 129.69, 129.25, 127.85, 125.65, 125.15, 124.01, 123.57, 120.93, 120.87, 120.02, 118.87, 111.46, 110.52, 81.07, 67.07, 67.06, 67.03, 63.91, 63.82, 56.35, 56.26, 53.71, 17.76, -1.38. LCMS (Fleet, 10 → 90%): t_r = 6.04 min, m/z: 647.3.

5-Methoxy-*N*-(3-(5-(morpholinomethyl)-1*H*-benzo[*d*]imidazol-2-yl)-1-((2-(trimethylsilyl)ethoxy)methyl)-1*H*-pyrazol-4-yl)-2-(3-((trimethylsilyl)ethynyl)phenyl)pyrimidin-4-amine (128)

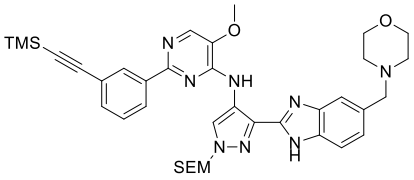

The title compound was synthesized from **127** (50 mg, 77 µmol) according to general procedure H. The crude was purified by automated column chromatography (0 – 10% MeOH/EtOAc) to afford the product (52.6 mg, 74.2 µmol, 96%). ^{1}H NMR (400 MHz, $CDCl_3$) δ 10.46 – 10.43 (2x s, 1H), 10.41 – 10.37 (2x s, 1H), 8.71 – 8.68 (2x s, 1H), 8.47 – 8.45 (2x t, *J* = 1.6 Hz, 1H), 8.29 – 8.25 (2x dt, *J* = 7.8, 1.3 Hz, 1H), 7.99 – 7.96 (2x s, 1H), 7.74 – 7.71 (m, 1H), 7.53 (dt, *J* = 7.5, 1.5 Hz, 1H), 7.41 (t, *J* = 8.1 Hz, 1H), 7.39 – 7.34 (m, 1H), 7.28 – 7.25 (m, 1H), 5.47 – 5.43 (2x s, 2H), 4.12 – 4.07 (2x s, 3H), 3.77 – 3.71 (m, 4H), 3.68 – 3.58 (m, 4H), 2.57 – 2.45 (m, 4H), 0.96 – 0.90 (m, 2H), 0.28 (s, 9H), -0.06 – -0.08 (2x s, 9H). ^{13}C NMR (101 MHz, $CDCl_3$) δ 156.03, 150.36, 150.34, 147.31, 147.14, 143.67, 142.92, 140.04, 140.03, 138.72, 133.39, 132.94, 132.69, 132.08, 132.07, 132.01, 132.00, 131.48, 128.46, 127.69, 125.24, 124.09, 123.69, 123.35, 121.17, 121.13, 120.12, 119.00, 111.42, 110.54, 105.37, 94.12, 81.12, 67.12, 67.10, 67.04, 67.02, 63.96, 63.87, 56.46, 56.38, 53.76, 0.15, -1.33. LCMS (Fleet, 10 → 90%): t_r = 7.08 min, m/z: 709.4.

5-Methoxy-*N*-(3-(5-(morpholinomethyl)-1*H*-benzo[*d*]imidazol-2-yl)-1-((2-(trimethylsilyl)ethoxy)methyl)-1*H*-pyrazol-4-yl)-2-(3-(trifluoromethyl)phenyl)pyrimidin-4-amine (129)

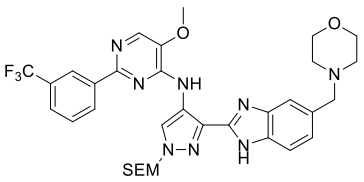

The title compound was synthesized from **126** (75.8 mg, 133 µmol) and (3-(trifluoromethyl)phenyl)boronic acid (29.0 mg, 153 µmol) according to general procedure G (reaction time 16 h). The crude was purified by automated column chromatography (0 – 10% MeOH/EtOAc) to afford the product (74.0 mg, 109 µmol, 82%). ^{1}H NMR (400 MHz, $CDCl_3$) δ 10.68 – 10.57 (2x s, 1H), 10.50 – 10.42 (2x s, 1H), 8.65 – 8.61 (m, 2H), 8.52 – 8.47 (m, 1H), 7.98 – 7.93 (2x s, 1H), 7.74 – 7.70 (m, 1H), 7.69 – 7.65 (m, 1H), 7.57 (t, *J* = 7.8 Hz, 1H), 7.37 – 7.30 (m, 1H), 7.28 – 7.23 (m, 1H), 5.40 – 5.37 (2x s, 2H), 4.09 – 4.05 (2x s, 3H), 3.78 – 3.70 (m, 4H), 3.68 – 3.58 (m, 4H),

2.58 – 2.46 (m, 4H), 0.95 – 0.90 (m, 2H), -0.06 – -0.08 (2x s, 9H). ^{13}C NMR (101 MHz, $CDCl_3$) δ 155.28, 155.26, 150.30, 150.28, 147.28, 147.12, 143.64, 142.89, 140.21, 140.19, 139.42, 133.36, 132.98, 132.80, 132.77, 132.16, 132.13, 132.12, 131.99, 130.89, 130.69, 130.57, 128.99, 125.88, 125.85, 125.80, 125.22, 124.57, 124.54, 124.50, 124.46, 124.08, 123.53, 123.10, 121.06, 121.01, 120.08, 118.95, 111.44, 110.54, 81.15, 67.11, 67.08, 63.94, 63.85, 56.42, 56.33, 53.75, 17.75, -1.43. LCMS (Fleet, 10 → 90%): t_r = 6.41 min, m/z: 681.3.

3-(5-Methoxy-4-((3-(5-(morpholinomethyl)-1*H*-benzo[*d*]imidazol-2-yl)-1-((2-(trimethylsilyl)ethoxy)methyl)-1*H*-pyrazol-4-yl)amino)pyrimidin-2-yl)benzonitrile (130)

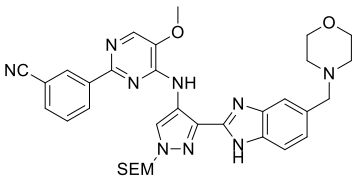

A microwave vial was charged with **126** (72,6 mg, 127 µmol), K_2CO_3 (70.3 mg, 508 µmol), (3-cyanophenyl)boronic acid (21.5 mg, 146 µmol) and 4:1 dioxane/H_2O (0.65 mL). N_2 was bubbled through the mixture for 1 min after which Pd(dppf)Cl_2·DCM (7.3 mg, 8.9 µmol) was added. N_2 was bubbled through the mixture for 30 sec after which the vial was sealed. The mixture was heated to 90°C and stirred for 16 h. Extra K_2CO_3 (70.3 mg, 508 µmol), (3-cyanophenyl)boronic acid (21.5 mg, 146 µmol), 4:1 dioxane/H_2O (0.2 mL) and Pd(dppf)Cl_2·DCM (7.3 mg, 8.9 µmol) were added and the mixture was continued to stir for another 16 h. The mixture was poured into H_2O (20 mL) and brine (2 mL). The product was extracted with DCM (2x20 mL) and the combined organic layers were concentrated as such. The crude was purified by automated column chromatography (0 – 10% MeOH/EtOAc) to afford the product (62.4 mg, 97.8 µmol, 77%). ^{1}H NMR (400 MHz, $CDCl_3$) δ 10.64 – 10.44 (m, 2H), 8.59 – 8.57 (2x t, *J* = 1.8 Hz, 1H), 8.55 – 8.53 (2x s, 1H), 8.51 – 8.47 (2x dt, *J* = 7.9, 1.4 Hz, 1H), 7.97 – 7.90 (2x s, 1H), 7.73 – 7.69 (m, 1H), 7.68 – 7.64 (2x dt, *J* = 7.7, 2.0 Hz, 1H), 7.53 (t, *J* = 7.8 Hz, 1H), 7.38 – 7.32 (m, 1H), 7.29 – 7.24 (m, 1H), 5.44 – 5.41 (2x s, *J* = 1.3 Hz, 2H), 4.11 – 4.07 (2x s, 3H), 3.77 – 3.70 (m, 4H), 3.68 – 3.58 (m, 4H), 2.57 – 2.46 (m, 4H), 0.96 – 0.90 (m, 2H), -0.06 – -0.08 (2x s, 9H). ^{13}C NMR (101 MHz, $CDCl_3$) δ 154.55, 154.52, 150.33, 150.32, 147.18, 147.01, 143.57, 142.81, 140.33, 140.31, 139.81, 133.38, 132.93, 132.67, 132.65, 132.46, 132.08, 132.00, 131.96, 131.60, 131.38, 129.24, 125.24, 124.10, 123.50, 120.67, 120.62, 120.04, 119.05, 118.91, 112.54, 111.43, 110.54, 81.17, 67.14, 67.13, 67.08, 67.05, 63.91, 63.82, 56.47, 56.38, 53.73, 17.78, -1.37. LCMS (Fleet, 10 → 90%): t_r = 5.80 min, m/z: 638.3.

2-(3-Chloro-2-fluorophenyl)-5-methoxy-*N*-(3-(5-(morpholinomethyl)-1*H*-benzo[*d*]imidazol-2-yl)-1-((2-(trimethylsilyl)ethoxy)methyl)-1*H*-pyrazol-4-yl)pyrimidin-4-amine (131)

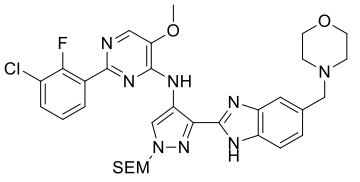

The title compound was synthesized from **126** (200 mg, 350 µmol) and (3-chloro-2-fluorophenyl)boronic acid (65.3 mg, 375 µmol) according to general procedure G (reaction time 64 h). The crude was purified by automated column chromatography (0 – 10% MeOH/EtOAc) to afford the product (160 mg, 241 µmol, 69%). ^{1}H NMR (400 MHz, $CDCl_3$) δ 10.71 – 10.58 (2x s, 1H), 10.53 – 10.45 (2x s, 1H), 8.81 – 8.75 (2x s, 1H), 8.07 – 8.04 (2x s, 1H), 8.01 (t, *J* = 7.8 Hz, 1H), 7.78 – 7.71 (m, 1H), 7.48 (t, *J* = 7.2 Hz, 1H), 7.39 – 7.31 (m, 1H), 7.31 – 7.24 (m, 1H), 7.18 (t, *J* = 7.9 Hz, 1H), 5.46 (s, 2H), 4.20 – 4.09 (2x s, 3H), 3.80 – 3.72 (m, 4H), 3.70 – 3.61 (m, 4H), 2.58 – 2.48 (m, 4H), 0.97 (t, *J* = 8.1 Hz, 2H), -0.03 (s, 9H). ^{13}C NMR (101 MHz, $CDCl_3$) δ 157.74, 155.20, 154.02, 153.97, 150.06, 150.04, 147.35, 147.18, 143.64, 142.90, 139.82, 133.30, 132.99, 132.89, 132.87, 132.14, 132.09, 131.94, 131.10, 130.00, 128.74, 128.65, 125.13, 124.31, 124.27, 124.00, 123.42, 122.44, 122.25, 121.81, 121.76, 120.04, 118.93, 111.43, 110.55, 81.06, 67.11, 67.08, 63.94, 63.85, 56.42, 56.34, 53.74, 17.75, -1.40. LCMS (Finnigan, 10 → 90%): t_r = 6.71 min, m/z: 665.1.

2-(2-Fluoro-3-((trimethylsilyl)ethynyl)phenyl)-5-methoxy-*N*-(3-(5-(morpholinomethyl)-1*H*-benzo[*d*]imidazol-2-yl)-1-((2-(trimethylsilyl)ethoxy)methyl)-1*H*-pyrazol-4-yl)pyrimidin-4-amine (132)

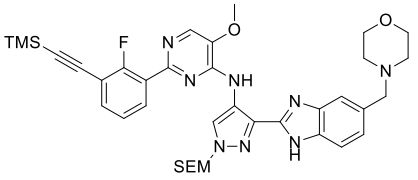

The title compound was synthesized from **131** (100 mg, 150 µmol) according to general procedure H. The crude was purified by automated column chromatography (0 – 10% MeOH/EtOAc) to afford the product (85.7 mg, 118 µmol, 78%). ^{1}H NMR (400 MHz, $CDCl_3$) δ 10.76 – 10.67 (2x s, 1H), 10.47 – 10.40 (2x s, *J* = 16.9 Hz, 1H), 8.80 – 8.77 (2x d, *J* = 1.9 Hz, 1H), 8.08 – 8.00 (m, 2H), 7.74 – 7.70 (m, 1H), 7.54 – 7.48 (m, 1H), 7.32 – 7.28 (m, 1H), 7.27 – 7.22 (m, 1H), 7.15 (td, *J* = 7.7, 1.4 Hz, 1H), 5.43 (s, 2H), 4.12 – 4.07 (2x s, 3H), 3.77 – 3.69 (m, 4H), 3.67 – 3.56 (m, 4H), 2.56 – 2.45 (m, 4H), 0.94 – 0.87 (m, 2H), 0.29 (s, 9H), -0.08 – -0.10 (2x s, 9H). ^{13}C NMR (101 MHz, $CDCl_3$) δ 162.65, 160.07, 154.25, 154.21, 150.04, 150.02, 147.38, 147.21, 143.65, 142.91, 139.72, 139.70, 134.35, 133.20, 133.01, 132.91, 132.88, 132.18, 132.17, 132.13, 131.92, 131.89, 131.83, 127.33, 127.24, 125.11, 123.98, 123.67, 123.62, 123.44, 121.97, 121.92, 121.87, 120.03, 118.92, 113.21, 113.03, 111.44, 110.55, 100.15, 100.11, 98.40, 98.38, 80.97, 67.08, 67.04, 66.90, 66.88, 63.92, 63.82, 56.38, 56.30, 53.71, 17.70, 0.03, -1.39. LCMS (Finnigan, 10 → 90%): t_r = 7.71 min, m/z: 727.3.

2-(5-Chloro-2-fluorophenyl)-5-methoxy-*N*-(3-(5-(morpholinomethyl)-1*H*-benzo[*d*]imidazol-2-yl)-1-((2-(trimethylsilyl)ethoxy)methyl)-1*H*-pyrazol-4-yl)pyrimidin-4-amine (133)

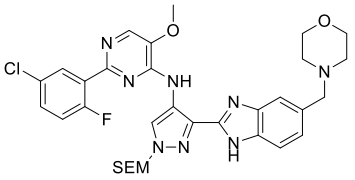

The title compound was synthesized from **126** (100 mg, 175 µmol) and (5-chloro-2-fluorophenyl)boronic acid (35.1 mg, 201 µmol) according to general procedure G (reaction time: 16 h). The crude was purified by automated column chromatography (0 – 10% MeOH/EtOAc) to afford the product (90.0 mg, 135 µmol, 77%). ^{1}H NMR (400 MHz, $CDCl_3$) δ 10.62 – 10.50 (2x s, 1H), 10.49 – 10.42 (2x s, 1H), 8.76 – 8.72 (2x d, *J* = 1.8 Hz, 1H), 8.15 – 8.11 (2x dd, *J* = 2.8, 1.9 Hz, 1H), 8.03 – 7.99 (2x s, 1H), 7.74 – 7.70 (m, 1H), 7.37 – 7.30 (m, 2H), 7.28 – 7.23 (m, 1H), 7.15 – 7.08 (2x dd, *J* = 10.3, 8.7 Hz, 1H), 5.45 – 5.42 (2x s, 2H), 4.13 – 4.09 (2x s, 3H), 3.77 – 3.70 (m, 4H), 3.66 – 3.58 (m, 4H), 2.56 – 2.45 (m, 4H), 0.96 – 0.89 (m, 2H), -0.06 – -0.07 (2x s, 9H). ^{13}C NMR (101 MHz, $CDCl_3$) δ 160.81, 158.29, 153.53, 153.48, 150.05, 150.03, 147.33, 147.16, 143.64, 142.89, 139.83, 133.34, 132.98, 132.82, 132.80, 132.12, 132.08, 132.03, 131.96, 131.38, 131.36, 130.39, 130.30, 129.23, 129.22, 129.20, 129.18, 128.40, 128.29, 125.16, 124.03, 123.47, 121.71, 121.66, 121.61, 120.06, 118.94, 118.40, 118.15, 111.42, 110.54, 81.10, 67.11, 67.08, 67.06, 63.95, 63.85, 56.42, 56.34, 53.74, 17.79, -1.38. LCMS (Fleet, 10 → 90%): t_r = 6.01 min, m/z: 665.2.

2-(2-Fluoro-5-((trimethylsilyl)ethynyl)phenyl)-5-methoxy-*N*-(3-(5-(morpholinomethyl)-1*H*-benzo[*d*]imidazol-2-yl)-1-((2-(trimethylsilyl)ethoxy)methyl)-1*H*-pyrazol-4-yl)pyrimidin-4-amine (134)

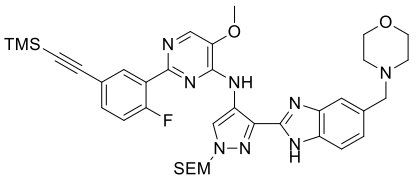

The title compound was synthesized from **133** (90.0 mg, 135 µmol) according to general procedure H. The crude was purified by automated column chromatography (0 – 10% MeOH/EtOAc) to afford the product (86.1 mg, 118 µmol, 88%). ^{1}H NMR (400 MHz, $CDCl_3$) δ 11.03 (br s, 1H), 10.59 – 10.47 (2x s, 1H), 8.79 – 8.76 (2x d, *J* = 1.9 Hz, 1H), 8.26 (dd, *J* = 7.6, 2.2 Hz, 1H), 8.05 – 8.01 (2x s, 1H), 7.73 – 7.69 (m, 1H), 7.48 (ddd, *J* = 8.5, 4.5, 2.3 Hz, 1H), 7.43 – 7.36 (m, 1H), 7.27 – 7.22 (m, 1H), 7.11 (dd, *J* = 11.1, 8.5 Hz, 1H), 5.42 (s, 2H), 4.13 – 4.06 (2x s, 3H), 3.77 – 3.71 (m, 4H), 3.71 – 3.64 (2x s, 2H), 3.62 – 3.56 (m, 2H), 2.61 – 2.49 (m, 4H), 0.96 – 0.88 (m, 2H), 0.25 (s, 9H), -0.08 (s, 9H). ^{13}C NMR (101 MHz, $CDCl_3$) δ 162.08, 159.53, 153.88, 153.83, 150.01, 147.20, 147.04, 143.56, 142.94, 139.74, 135.63, 135.60, 134.12, 134.03, 133.19, 132.82, 132.46, 132.39, 132.03, 131.99, 130.94, 127.02, 126.92, 125.31, 124.19, 123.58, 121.99, 121.94, 120.27, 119.45, 119.41, 118.92, 117.21, 116.97, 111.93, 110.80, 104.05, 94.02, 80.88, 67.04, 66.77, 63.61, 56.40, 56.32, 53.43, 53.38, 17.76, 0.05, -1.41. LCMS (Fleet, 10 → 90%): t_r = 7.07 min, m/z: 727.3.

Ethyl 4-((2-chloro-5-methoxypyrimidin-4-yl)amino)-1-((2-(trimethylsilyl)ethoxy)methyl)-1*H*-pyrazole-3-carboxylate (135)

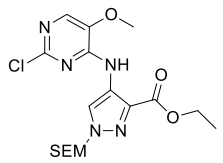

105 (1.54 g, 5.38 mmol) was dissolved in EtOH (5 mL) after which DIPEA (1.90 mL, 10.8 mmol) and 2,4-dichloro-5-methoxypyrimidine (1.45 g, 8.07 mmol) were added. The mixture heated to 40°C and stirred for 4 days and subsequently stirred at 50°C for 4 days. The mixture was poured into H_2O (75 mL) and the product extracted with DCM (2x75 mL). The organic layers were dried over Na_2SO_4, filtered and concentrated. The crude was purified by silica gel column chromatography (50% Et_2O/pentane) to afford the product (1.81 g, 4.22 mmol, 78%). ^{1}H NMR (400 MHz, $CDCl_3$) δ 9.21 (s, 1H), 8.52 (s, 1H), 7.67 (s, 1H), 5.48 (s, 2H), 4.45 (q, *J* = 7.1 Hz, 2H), 3.94 (s, 3H), 3.59 – 3.53 (m, 2H), 1.41 (t, *J* = 7.1 Hz, 3H), 0.92 – 0.86 (m, 2H), -0.06 (s, 9H). ^{13}C NMR (101 MHz, $CDCl_3$) δ 163.90, 151.14, 151.02, 139.81, 134.01, 130.84, 125.79, 121.11, 81.72, 67.27, 61.49, 56.45, 17.78, 14.42, -1.41. LCMS (Fleet, 10 → 90%): t_r = 8.76 min, m/z: 428.3.

Ethyl 4-((2-(3-chloro-2,6-difluorophenyl)-5-methoxypyrimidin-4-yl)amino)-1-((2-(trimethylsilyl)ethoxy)methyl)-1*H*-pyrazole-3-carboxylate (136)

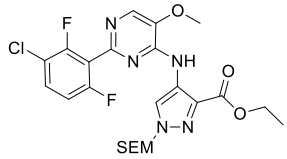

A microwave vial was charged with **135** (250 mg, 584 µmol), (3-chloro-2,6-difluorophenyl)boronic acid (169 mg, 876 µmol) and XPhos Pd G2 (92 mg, 117 µmol) after which the vial was purged with argon and subsequently sealed. Degassed THF (1 mL) and degassed 0.5 M K_3PO_4 (aq.) (2 mL) were added via syringe and the mixture was stirred for 1 h. The mixture was poured into H_2O (20 mL) and the product extracted with DCM (2x20 mL). The combined organic layers were concentrated as such. The crude was purified by automated column chromatography (50 – 80% Et_2O/pentane) to afford a mixture of starting material and product. The reaction was performed again using (3-chloro-2,6-difluorophenyl)boronic acid (113 mg, 584 µmol), XPhos Pd G2 (30 mg, 38 µmol), THF (0.5 mL) and 0.5 M K_3PO_4 (aq.) (1 mL). Performing a workup and purification as stated above, afforded a mixture of starting material and product which was subjected to another reaction using (3-chloro-2,6-difluorophenyl)boronic acid (169 mg, 876 µmol), XPhos Pd G2 (45 mg, 57 µmol) and THF (2 mL). The mixture was homogenized by stirring for 1 minute after which 1 M K_3PO_4 (aq.) (1 mL) was added and the mixture was stirred for 1 h. Performing a workup and purification as stated above, afforded a mixture of starting material and product (257 mg) which was used as such in subsequent reaction. LCMS (Fleet, 10 → 90%): t_r = 8.66 min, m/z: 540.3.

2-(3-Chloro-2,6-difluorophenyl)-5-methoxy-*N*-(3-(5-(morpholinomethyl)-1*H*-benzo[*d*]imidazol-2-yl)-1-((2-(trimethylsilyl)ethoxy)methyl)-1*H*-pyrazol-4-yl)pyrimidin-4-amine (137)

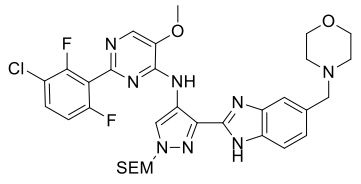

136 (257 mg, crude) was suspended in MeOH:H_2O (1:1) (2 mL) after which LiOH·H_2O (232 mg, 5.53 mmol) was added. DCM (1 mL) was added to dissolve some insoluble parts of the mixture after which the reaction was heated to 65°C and stirred for 16 h. The mixture was poured into H_2O (30 mL) and DCM (30 mL), and the pH of the water layer was adjusted by addition of 2 M HCl (aq.) to pH ~ 2. The organic layer was separated and the water layer extracted with DCM (30 mL). The combined organic layers were dried over Na_2SO_4, filtered and concentrated. To the obtained intermediate was added 4-(morpholinomethyl)benzene-1,2-diamine (143 mg, 690 µmol), EDC·HCl (109 mg, 569 µmol), HOBt (77.3 mg, 572 µmol) and DMF (1 mL) after which the reaction was stirred for 16 h. The mixture was concentrated, AcOH (1.5 mL) was added and the reaction was stirred at 118°C for 1 h. The mixture was cooled down to RT and the pH was adjusted by addition of 10 M NaOH (aq.) (until 9 > pH > 7). The mixture was poured into H_2O (40 mL) and brine (1 mL) and the product extracted with DCM (2x40 mL). The combined organic layers were concentrated as such. The crude was purified by HPLC (Waters, 39 – 42% MeCN in 0.2% TFA (aq.)), the pH of the combined fractions was adjusted to pH ~8 using 10 M NaOH after which the mixture was concentrated. The product was dissolved in a mixture of H_2O (20 mL) and DCM (15 mL). The organic layer was separated and the water layer extracted with DCM (15 mL). The combined organic layers were dried over Na_2SO_4, filtered and concentrated to afford the product (32.5 mg, 49.8 µmol, 9% over 2 steps). ^{1}H NMR (400 MHz, $CDCl_3$) δ

10.54 – 10.47 (2x s, 1H), 10.32 – 10.21 (2x s, 1H), 8.56 – 8.53 (2x s, 1H), 8.09 – 8.06 (2x s, 1H), 7.75 – 7.72 (m, 1H), 7.45 – 7.35 (m, 2H), 7.29 – 7.25 (m, 1H), 7.01 – 6.94 (m, 1H), 5.44 – 5.41 (2x s, 2H), 4.18 – 4.13 (2x s, 3H), 3.77 – 3.70 (m, 4H), 3.67 – 3.62 (2x s, 2H), 3.61 – 3.55 (m, 2H), 2.56 – 2.45 (m, 4H), 0.94 – 0.88 (m, 2H), -0.06 – -0.07 (2x s, 9H). ^{13}C NMR (101 MHz, $CDCl_3$) δ 160.65, 160.60, 158.15, 158.10, 157.71, 157.65, 155.19, 155.13, 150.37, 150.35, 149.94, 147.24, 147.07, 143.66, 142.91, 140.14, 133.51, 132.91, 132.84, 132.81, 132.11, 132.06, 132.01, 130.29, 130.20, 125.24, 124.10, 123.44, 121.56, 121.53, 120.12, 119.52, 119.34, 119.15, 119.05, 117.35, 117.17, 112.65, 112.61, 112.41, 112.37, 111.38, 110.55, 81.11, 81.10, 67.15, 67.13, 67.05, 67.03, 63.96, 63.87, 56.51, 56.44, 53.78, 17.81, -1.39. LCMS (Fleet, 10 → 90%): t_r = 6.10 min, m/z: 683.3.

2-(2,6-Difluoro-3-((trimethylsilyl)ethynyl)phenyl)-5-methoxy-*N*-(3-(5-(morpholinomethyl)-1*H*-benzo[*d*]imidazol-2-yl)-1-((2-(trimethylsilyl)ethoxy)methyl)-1*H*-pyrazol-4-yl)pyrimidin-4-amine (138)

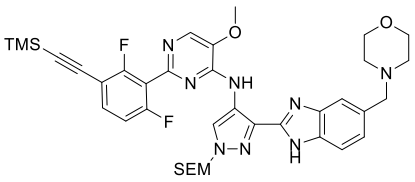

The title compound was synthesized from **137** (22 mg, 32 µmol) according to general procedure H. The crude was purified by automated column chromatography (0 – 10% MeOH/EtOAc) to afford the product (24 mg, 32 µmol, quant.). ^{1}H NMR (400 MHz, $CDCl_3$) δ 10.52 – 10.43 (2x s, 1H), 10.25 – 10.15 (2x s, 1H), 8.56 – 8.53 (2x s, 1H), 8.08 – 8.05 (2x s, *J* = 4.9 Hz, 1H), 7.76 – 7.71 (m, 1H), 7.51 – 7.45 (m, 1H), 7.43 – 7.36 (m, 1H), 7.30 – 7.25 (m, 1H), 6.99 – 6.91 (2x d, *J* = 8.8 Hz, 1H), 5.45 – 5.42 (2x s, 2H), 4.18 – 4.13 (2x s, 3H), 3.76 – 3.70 (m, 4H), 3.67 – 3.62 (2x s, 2H), 3.61 – 3.55 (m, 2H), 2.54 – 2.46 (m, 4H), 0.94 – 0.87 (m, 2H), 0.25 (s, 9H), -0.06 – -0.07 (2x s, 9H). ^{13}C NMR (101 MHz, $CDCl_3$) δ 162.89, 162.82, 162.01, 161.95, 160.34, 160.27, 159.48, 159.42, 150.36, 150.33, 150.16, 150.15, 147.27, 147.09, 143.67, 142.92, 140.06, 133.85, 133.74, 133.53, 132.91, 132.87, 132.85, 132.13, 132.06, 132.04, 132.00, 125.24, 124.11, 123.48, 121.65, 121.63, 120.13, 119.06, 118.55, 118.37, 118.20, 112.07, 112.03, 111.84, 111.81, 111.38, 110.56, 108.91, 108.87, 108.74, 108.70, 100.09, 100.05, 97.26, 97.25, 81.09, 81.07, 67.17, 67.15, 67.01, 66.99, 63.98, 63.89, 56.50, 56.43, 53.79, 17.80, -0.02, -1.35. LCMS (Fleet, 10 → 90%): t_r = 7.11 min, m/z: 745.3.

References

1. Sung, H., Ferlay, J., Siegel, R. L., Laversanne, M., Soerjomataram, I., Jemal, A. & Bray, F. Global Cancer Statistics 2020: GLOBOCAN Estimates of Incidence and Mortality Worldwide for 36 Cancers in 185 Countries. *CA. Cancer J. Clin.* **71**, 209–249 (2021).
2. Hanahan, D. & Weinberg, R. A. Hallmarks of Cancer: The Next Generation. *Cell* **144**, 646–674 (2011).
3. Zhong, L., Li, Y., Xiong, L., Wang, W., Wu, M., Yuan, T., Yang, W., Tian, C., Miao, Z., Wang, T. & Yang, S. Small molecules in targeted cancer therapy: advances, challenges, and future perspectives. *Signal Transduct. Target. Ther.* **6**, 201 (2021).
4. Dominguez-Brauer, C., Thu, K. L., Mason, J. M., Blaser, H., Bray, M. R. & Mak, T. W. Targeting Mitosis in Cancer: Emerging Strategies. *Mol. Cell* **60**, 524–536 (2015).
5. Kops, G. J. P. L., Weaver, B. A. A. & Cleveland, D. W. On the road to cancer: aneuploidy and the mitotic checkpoint. *Nat. Rev. Cancer* **5**, 773–785 (2005).
6. Siemeister, G., Mengel, A., Fernández-Montalván, A. E., Bone, W., Schröder, J., Zitzmann-Kolbe, S., Briem, H., Prechtl, S., Holton, S. J., Mönning, U., von Ahsen, O., Johanssen, S., Cleve, A., Pütter, V., Hitchcock, M., von Nussbaum, F., Brands, M., Ziegelbauer, K. & Mumberg, D. Inhibition of BUB1 Kinase by BAY 1816032 Sensitizes Tumor Cells toward Taxanes, ATR, and PARP Inhibitors *In Vitro* and *In Vivo*. *Clin. Cancer Res.* **25**, 1404–1414 (2019).
7. Musacchio, A. & Salmon, E. D. The spindle-assembly checkpoint in space and time. *Nat. Rev. Mol. Cell Biol.* **8**, 379–393 (2007).
8. Zhang, G., Kruse, T., López-Méndez, B., Sylvestersen, K. B., Garvanska, D. H., Schopper, S., Nielsen, M. L. & Nilsson, J. Bub1 positions Mad1 close to KNL1 MELT repeats to promote checkpoint signalling. *Nat. Commun.* **8**, 15822 (2017).
9. Zhang, G., Lischetti, T., Hayward, D. G. & Nilsson, J. Distinct domains in Bub1 localize RZZ and BubR1 to kinetochores to regulate the checkpoint. *Nat. Commun.* **6**, 7162 (2015).
10. Di Fiore, B., Davey, N. E., Hagting, A., Izawa, D., Mansfeld, J., Gibson, T. J. & Pines, J. The ABBA Motif Binds APC/C Activators and Is Shared by APC/C Substrates and Regulators. *Dev. Cell* **32**, 358–372 (2015).
11. Ciossani, G., Overlack, K., Petrovic, A., Huis in 't Veld, P. J., Koerner, C., Wohlgemuth, S., Maffini, S. & Musacchio, A. The kinetochore proteins CENP-E and CENP-F directly and specifically interact with distinct BUB mitotic checkpoint Ser/Thr kinases. *J. Biol. Chem.* **293**, 10084–10101 (2018).
12. Musacchio, A. & Salmon, E. D. The spindle-assembly checkpoint in space and time. *Nat. Rev. Mol. Cell Biol.* **8**, 379–393 (2007).
13. Kawashima, S. A., Yamagishi, Y., Honda, T., Ishiguro, K. & Watanabe, Y. Phosphorylation of H2A by Bub1 Prevents Chromosomal Instability Through Localizing Shugoshin. *Science* **327**, 172–177 (2010).
14. Bolanos-Garcia, V. M. & Blundell, T. L. BUB1 and BUBR1: multifaceted kinases of the cell cycle. *Trends Biochem. Sci.* **36**, 141–150 (2011).
15. Elowe, S. Bub1 and BubR1: at the Interface between Chromosome Attachment and the Spindle Checkpoint. *Mol. Cell. Biol.* **31**, 3085–3093 (2011).
16. Funabiki, H. & Wynne, D. J. Making an effective switch at the kinetochore by phosphorylation and dephosphorylation. *Chromosoma* **122**, 135–158 (2013).
17. Zhang, G., Kruse, T., Guasch Boldú, C., Garvanska, D. H., Coscia, F., Mann, M., Barisic, M. & Nilsson, J. Efficient mitotic checkpoint signaling depends on integrated activities of Bub1 and the RZZ complex. *EMBO J.* **38**, (2019).
18. Foran, J., Ravandi, F., Wierda, W., Garcia-Manero, G., Verstovsek, S., Kadia, T., Burger, J., Yule, M., Langford, G., Lyons, J., Ayrton, J., Lock, V., Borthakur, G., Cortes, J. & Kantarjian, H. A Phase I and Pharmacodynamic Study of AT9283, a Small-Molecule Inhibitor of Aurora Kinases in Patients With Relapsed/Refractory Leukemia or Myelofibrosis. *Clin. Lymphoma Myeloma Leuk.* **14**, 223–230 (2014).
19. Dent, S. F., Gelmon, K. A., Chi, K. N., Jonker, D. J., Wainman, N., Capier, C. A., Chen, E. X., Lyons, J. F. & Seymour, L. NCIC CTG IND.181: Phase I study of AT9283 given as a weekly 24 hour infusion in advanced malignancies. *Invest. New Drugs* **31**, 1522–1529 (2013).
20. Arkenau, H.-T., Plummer, R., Molife, L. R., Olmos, D., Yap, T. A., Squires, M., Lewis, S., Lock, V., Yule, M., Lyons, J., Calvert, H. & Judson, I. A phase I dose escalation study of AT9283, a small molecule inhibitor of aurora kinases, in patients with advanced solid malignancies. *Ann. Oncol.* **23**, 1307–1313 (2012).
21. Moreno, L., Marshall, L. V., Pearson, A. D. J., Morland, B., Elliott, M., Campbell-Hewson, Q., Makin, G., Halford, S. E. R., Acton, G., Ross, P., Kazmi-Stokes, S., Lock, V., Rodriguez, A., Lyons, J. F., Boddy, A. V., Griffin, M. J., Yule, M. & Hargrave, D. A Phase I Trial of AT9283 (a Selective Inhibitor of Aurora Kinases) in Children and Adolescents with Solid Tumors: A Cancer Research UK Study. *Clin. Cancer Res.* **21**, 267–273 (2015).
22. Howard, S., Berdini, V., Boulstridge, J. A., Carr, M. G., Cross, D. M., Curry, J., Devine, L. A., Early, T. R., Fazal, L., Gill, A. L., Heathcote, M., Maman, S., Matthews, J. E., McMenamin, R. L., Navarro, E. F., O'Brien, M. A., O'Reilly, M., Rees, D. C., Reule, M., Tisi, D., Williams, G., Vinković, M. & Wyatt, P. G. Fragment-Based Discovery of the Pyrazol-4-yl Urea (AT9283), a Multitargeted Kinase Inhibitor with Potent Aurora Kinase Activity. *J. Med. Chem.* **52**, 379–388 (2009).

23. Vader, G. & Lens, S. M. A. The Aurora kinase family in cell division and cancer. *Biochim. Biophys. Acta BBA - Rev. Cancer* **1786**, 60–72 (2008).
24. Lampson, M. A., Renduchitala, K., Khodjakov, A. & Kapoor, T. M. Correcting improper chromosome–spindle attachments during cell division. *Nat. Cell Biol.* **6**, 232–237 (2004).
25. Knowlton, A. L., Lan, W. & Stukenberg, P. T. Aurora B Is Enriched at Merotelic Attachment Sites, Where It Regulates MCAK. *Curr. Biol.* **16**, 1705–1710 (2006).
26. Santaguida, S., Vernieri, C., Villa, F., Ciliberto, A. & Musacchio, A. Evidence that Aurora B is implicated in spindle checkpoint signalling independently of error correction: Aurora B is directly implicated in spindle checkpoint. *EMBO J.* **30**, 1508–1519 (2011).
27. Maldonado, M. & Kapoor, T. M. Constitutive Mad1 targeting to kinetochores uncouples checkpoint signalling from chromosome biorientation. *Nat. Cell Biol.* **13**, 475–482 (2011).
28. Ruchaud, S., Carmena, M. & Earnshaw, W. C. Chromosomal passengers: conducting cell division. *Nat. Rev. Mol. Cell Biol.* **8**, 798–812 (2007).
29. van Linden, O. P. J., Kooistra, A. J., Leurs, R., de Esch, I. J. P. & de Graaf, C. KLIFS: A Knowledge-Based Structural Database To Navigate Kinase–Ligand Interaction Space. *J. Med. Chem.* **57**, 249–277 (2014).
30. Taylor, S. S. & Kornev, A. P. Protein kinases: evolution of dynamic regulatory proteins. *Trends Biochem. Sci.* **36**, 65–77 (2011).
31. Kang, J., Yang, M., Li, B., Qi, W., Zhang, C., Shokat, K. M., Tomchick, D. R., Machius, M. & Yu, H. Structure and Substrate Recruitment of the Human Spindle Checkpoint Kinase Bub1. *Mol. Cell* **32**, 394–405 (2008).
32. Lin, Z., Jia, L., Tomchick, D. R., Luo, X. & Yu, H. Substrate-Specific Activation of the Mitotic Kinase Bub1 through Intramolecular Autophosphorylation and Kinetochore Targeting. *Structure* **22**, 1616–1627 (2014).
33. Roskoski, R. Classification of small molecule protein kinase inhibitors based upon the structures of their drug-enzyme complexes. *Pharmacol. Res.* **103**, 26–48 (2016).
34. Luna-Vargas, M. P. A., Christodoulou, E., Alfieri, A., van Dijk, W. J., Stadnik, M., Hibbert, R. G., Sahtoe, D. D., Clerici, M., Marco, V. D., Littler, D., Celie, P. H. N., Sixma, T. K. & Perrakis, A. Enabling high-throughput ligation-independent cloning and protein expression for the family of ubiquitin specific proteases. *J. Struct. Biol.* **175**, 113–119 (2011).
35. Vagin, A. & Teplyakov, A. *MOLREP*: an Automated Program for Molecular Replacement. *J. Appl. Crystallogr.* **30**, 1022–1025 (1997).
36. Potterton, L., Agirre, J., Ballard, C., Cowtan, K., Dodson, E., Evans, P. R., Jenkins, H. T., Keegan, R., Krissinel, E., Stevenson, K., Lebedev, A., McNicholas, S. J., Nicholls, R. A., Noble, M., Pannu, N. S., Roth, C., Sheldrick, G., Skubak, P., Turkenburg, J., Uski, V., von Delft, F., Waterman, D., Wilson, K., Winn, M. & Wojdyr, M. *CCP* 4 *i* 2: the new graphical user interface to the *CCP* 4 program suite. *Acta Crystallogr. Sect. Struct. Biol.* **74**, 68–84 (2018).
37. Long, F., Nicholls, R. A., Emsley, P., Gražulis, S., Merkys, A., Vaitkus, A. & Murshudov, G. N. *AceDRG*: a stereochemical description generator for ligands. *Acta Crystallogr. Sect. Struct. Biol.* **73**, 112–122 (2017).
38. Emsley, P. & Cowtan, K. *Coot*: model-building tools for molecular graphics. *Acta Crystallogr. D Biol. Crystallogr.* **60**, 2126–2132 (2004).
39. Murshudov, G. N., Skubák, P., Lebedev, A. A., Pannu, N. S., Steiner, R. A., Nicholls, R. A., Winn, M. D., Long, F. & Vagin, A. A. *REFMAC* 5 for the refinement of macromolecular crystal structures. *Acta Crystallogr. D Biol. Crystallogr.* **67**, 355–367 (2011).
40. The PyMOL Molecular Graphics System, Version 2.3.0 Schrödinger, LLC.
41. Yamagishi, H., Shirakami, S., Nakajima, Y., Tanaka, A., Takahashi, F., Hamaguchi, H., Hatanaka, K., Moritomo, A., Inami, M., Higashi, Y. & Inoue, T. Discovery of 3,6-dihydroimidazo[4,5-d]pyrrolo[2,3-b]pyridin-2(1H)-one derivatives as novel JAK inhibitors. *Bioorg. Med. Chem.* **23**, 4846–4859 (2015).
42. Joo, J. M., Touré, B. B. & Sames, D. C−H Bonds as Ubiquitous Functionality: A General Approach to Complex Arylated Imidazoles via Regioselective Sequential Arylation of All Three C−H Bonds and Regioselective *N* -Alkylation Enabled by SEM-Group Transposition. *J. Org. Chem.* **75**, 4911–4920 (2010).
43. Mattsson, S., Dahlström, M. & Karlsson, S. A mild hydrolysis of esters mediated by lithium salts. *Tetrahedron Lett.* **48**, 2497–2499 (2007).
44. Dineen, T. A., Weiss, M. M., Williamson, T., Acton, P., Babu-Khan, S., Bartberger, M. D., Brown, J., Chen, K., Cheng, Y., Citron, M., Croghan, M. D., Dunn, R. T., Esmay, J., Graceffa, R. F., Harried, S. S., Hickman, D., Hitchcock, S. A., Horne, D. B., Huang, H., Imbeah-Ampiah, R., Judd, T., Kaller, M. R., Kreiman, C. R., La, D. S., Li, V., Lopez, P., Louie, S., Monenschein, H., Nguyen, T. T., Pennington, L. D., San Miguel, T., Sickmier, E. A., Vargas, H. M., Wahl, R. C., Wen, P. H., Whittington, D. A., Wood, S., Xue, Q., Yang, B. H., Patel, V. F. & Zhong, W. Design and Synthesis of Potent, Orally Efficacious Hydroxyethylamine Derived β-Site Amyloid Precursor Protein Cleaving Enzyme (BACE1) Inhibitors. *J. Med. Chem.* **55**, 9025–9044 (2012).
45. Harrowven, D. C., Curran, D. P., Kostiuk, S. L., Wallis-Guy, I. L., Whiting, S., Stenning, K. J., Tang, B., Packard, E. & Nanson, L. Potassium carbonate–silica: a highly effective stationary phase for the chromatographic removal of organotin impurities. *Chem. Commun.* **46**, 6335 (2010).
46. Kinzel, T., Zhang, Y. & Buchwald, S. L. A New Palladium Precatalyst Allows for the Fast Suzuki−Miyaura Coupling Reactions of Unstable Polyfluorophenyl and 2-Heteroaryl Boronic Acids. *J. Am. Chem. Soc.* **132**, 14073–14075 (2010).

5

Development of a cellular BUB1 target engagement assay

Introduction

Target engagement (also termed target occupancy) is a concept in drug discovery that describes the physical interaction of a small molecule with its intended protein target in a specific biological system (e.g. in living cells, animals or humans).[1] Insufficient target engagement leads to a lack of drug efficacy in preclinical and clinical studies.[1] Therefore, investigating which compound concentration is required to obtain complete target occupancy is important.[1] Several methods have recently been developed to study target engagement[2], such as thermal protein shift[3], bioluminescence resonance energy transfer (BRET)[4] and activity-based protein profiling (ABPP) assays.[5]

ABPP relies on a chemical probe that forms a covalent bond with a protein of interest. Such probes consist of a recognition element, ligation tag and an electrophilic moiety, termed 'the warhead'.[6] The recognition element provides affinity for the target (or family of targets), whereas the electrophilic moiety reacts with a nucleophilic amino acid in close proximity. The ligation handle, such as an alkyne or an azide, enables the introduction of a fluorescent or biotin reporter group using copper-catalyzed azide-alkyne cycloaddition (CuAAC, 'click'-reaction).[7,8] This allows for visualization or identification of proteins using gel-based or mass spectrometry-based proteomics methods, respectively. Broad-spectrum probes are used to investigate cellular selectivity of small molecule inhibitors across an entire protein family. For example, Zhao *et al.*[9] published XO44 as a cell permeable broad-spectrum kinase probe, which provided the cellular selectivity profile of the approved kinase drug dasatinib on 133 kinases in a cell line using competitive chemical proteomics.[5] Alternatively, tailor-made probes can be used to determine the target engagement of a single target in a competitive, gel-based ABPP assay. Van der Wel *et al.* determined, for instance, cellular target engagement of FES kinase using a highly selective probe in a chemical genetic study.[10]

Chapters 2 – 4 described the discovery of substituted quinazolines and benzimidazoles as novel and potent inhibitors of budding uninhibited by benzimidazole 1 (BUB1) kinase for the treatment of cancer. To further evaluate these compounds in living cells, a BUB1 target engagement assay is highly desirable to correlate their target occupancy with cellular effects. To this end, a tailor-made probe targeting BUB1 is required. Recently, Shindo *et al.*[11] reported NS-062 as part of a series of close analogs of afatinib (**Figure 1A**), which is a covalent inhibitor of the epidermal growth factor receptor (EGFR) approved for the treatment of non-small cell lung cancer.[12] Of interest, the alkynylated-derivative of NS-062, compound **1** (**Figure 1A**), was found to bind BUB1[12] and resembles the quinazoline inhibitors described in **Chapter 3**. In this chapter, it was investigated whether compounds from this chemical series are suitable as chemical probes for a BUB1 engagement assay.

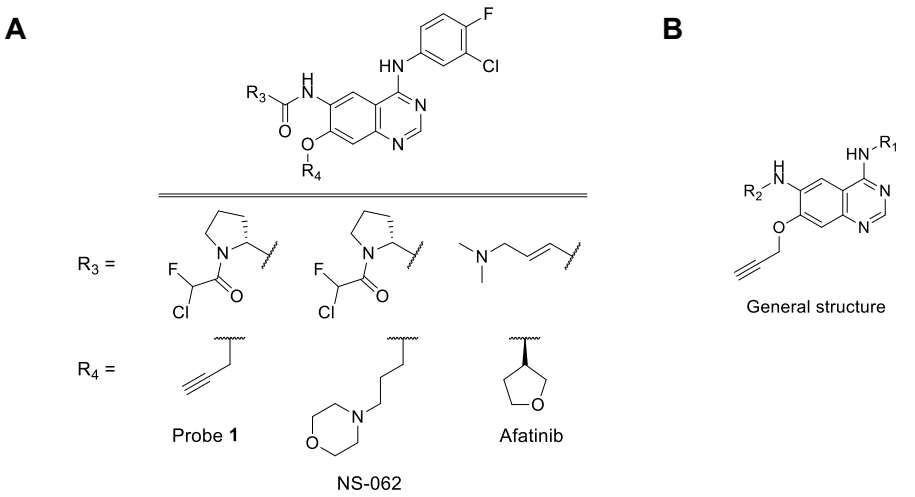

Figure 1 | (A) Chemical structures of probe **1**, NS-062 (both published by Shindo *et al.*[12]) and afatinib. **(B)** General structure of probe **1** and regions R_1 and R_2 of the quinazoline scaffold used to investigate the structure-activity relationship of **1**.

Results & Discussion

Design and synthesis of compounds 1 – 17

To study the potential of NS-062 analogues as BUB1 probes, compounds **1** – **17** were synthesized. Of note, a subset of these molecules (**1**, **3**, **4**, **8**, **10** and **12**) was previously reported.[12] Based on the biochemical activities of the quinazoline inhibitors reported in **Chapter 3**, the chloro-fluorophenyl of **1** at R_1 (**Figure 1B**) was substituted for a phenylacetylene in analogues **2**, **5**, **7**, **9**, **11** and **13** – **17**. The chloro-fluoroacetamide moiety was replaced by other warheads employed in approved kinase inhibitors, such as 2-butynamide[13] (in **5**, **6** and **14**), 4-dimethylaminocrotonamide[14] (in **7**, **8** and **15**) and an acrylamide[15] (in **9**, **10** and **16**). The chirality of the amino acid linker at R_2 (**Figure 1B**) was also investigated by substituting the D-proline for its L-enantiomer in compound **3**.[12] For analogues (**13** – **17**) glycine was used as a more flexible linker instead of a proline. Finally, to obtain negative control compounds, the warhead was replaced by an acetyl group in inhibitors **11**, **12** and **17**.[12]

Compounds **1** – **17** were synthesized as depicted in **Scheme 5.1**. Briefly, commercially available 7-fluoro-6-nitroquinazolin-4(3*H*)-one was chlorinated to obtain **18**.[16] A nucleophilic aromatic substitution with either 3-chloro-4-fluoroaniline or 3-ethynylaniline resulted in the formation of **19** and **20**, respectively.[16] Subsequent nucleophilic aromatic substitution was performed with propargyl alcohol to introduce the alkyne ligation handle.[17] Reduction of the nitro group yielded amines **23** and **24**,[17] which served as building blocks for the synthesis of **25** – **28**. The linkers were introduced by performing peptide coupling reactions using *N*-Boc-protected amino acids and pivaloyl chloride.[18] Boc deprotection yielded intermediates **29** – **32** and using acyl chlorides of the warhead or applying a peptide coupling method as mentioned above afforded the desired compounds.

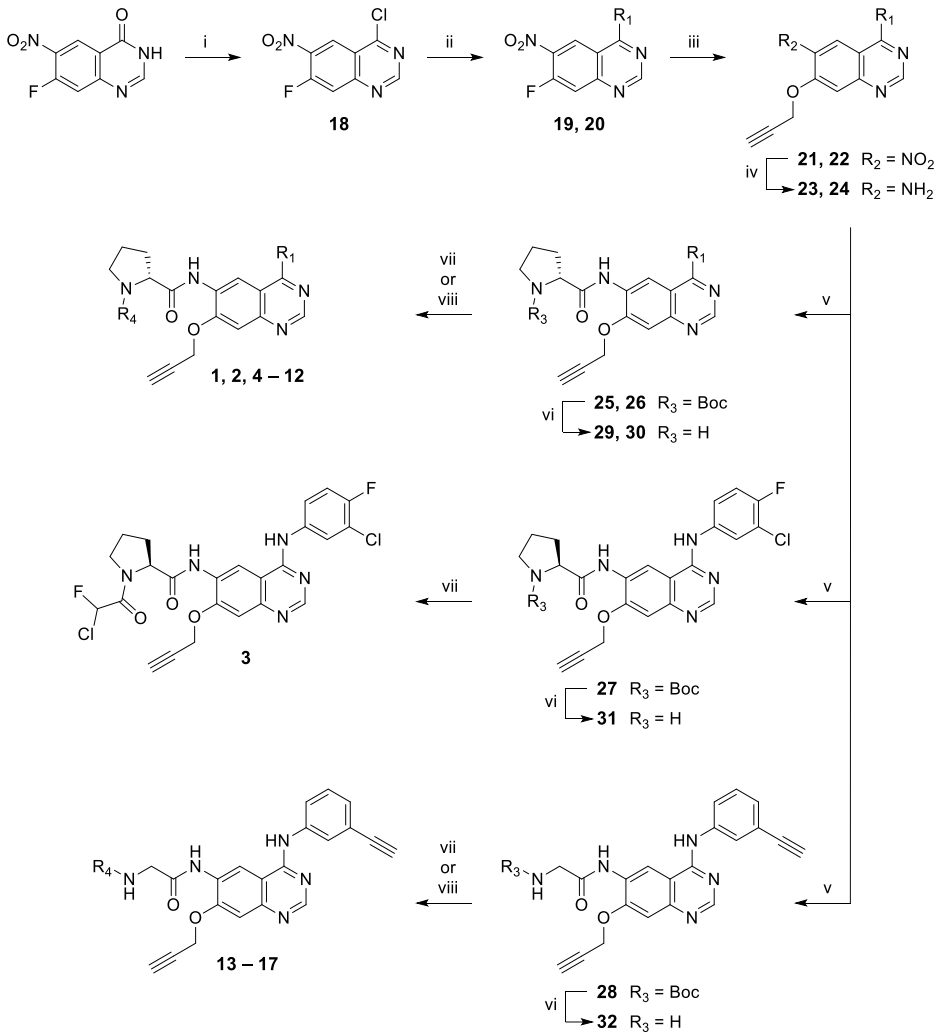

Scheme 5.1 | Synthesis of 1 – 17. Reagents and conditions: **i)** $SOCl_2$, cat. DMF, 75°C, 99%. **ii)** 3-chloro-4-fluoroaniline (for **19**) or 3-ethynylaniline (for **20**), DIPEA, 2-propanol, 37 – 81%. **iii)** propargyl alcohol, KO*t*Bu, THF, 0°C – RT, 91% – quant. **iv)** Fe, NH_4Cl, EtOH/H_2O (30:1), 80°C, 66% – quant. **v)** Boc-D-Pro-OH (for **25** and **26**), Boc-L-Pro-OH (for **27**) or Boc-Gly-OH (for **28**), PivCl, DIPEA, cat. DMF, DCM, 0°C – RT, 74 – 97%. **vi)** TFA, DCM, 56% – quant. **vii)** 2-chloro-2-fluoroacetic acid (for **1** – **3** and **13**), 2-butynoic acid (for **5**, **6** and **14**) or (*E*)-4-(dimethylamino)but-2-enoic acid·HCl (for **7**, **8** and **15**), PivCl, DIPEA, cat. DMF, DCM, 0°C – RT, 5 – 73%. **viii)** 2-chloroacetyl chloride (for **4**), acryloyl chloride (for **9**, **10** or **16**) or acetyl chloride (for **11**, **12** and **17**), DIPEA, DCM, 0°C – RT, 13 – 72%.

Biochemical evaluation of compound 1 – 17

Compounds **1** – **17** were evaluated in a biochemical fluorescence polarization BUB1 activity assay to determine the half maximal inhibitory concentrations (IC_{50}) as described in **Chapter 2**. The data reported in **Table 5.1** are expressed as pIC_{50} ± SEM (N=2, n=2). The activity of the compounds with an electrophilic warhead (**1** – **10**, **13** – **16**) were compared to corresponding control compounds (**11**, **12**, **17**). Compound **4** was the most active inhibitor with a pIC_{50} of 8.95. It was over 4000-fold more potent than negative control compound **12**, which suggested that it forms a covalent bond with BUB1. Compound **4** contained a chloroacetamide, which was the most reactive electrophilic warhead in this series of inhibitors. In line, compounds with other, less reactive warheads, such as a chloro-fluoroacetamide (**1**), 2-butynamide (**5**, **6**), dimethylaminocrotonamide (**7**, **8**) or acrylamide (**9**,**10**) were significantly less potent. Furthermore, phenylacetylene **2** showed a 5-fold reduction in potency compared to chloro-fluorophenyl **1**, which indicated that the SAR of this series was different from the quinazolines reported in **Chapter 3**. Inverting the stereochemistry of the linker from D-proline (**1**) to L-proline (**3**) dramatically reduced potency, revealing the importance of this stereocenter for BUB1 activity. D-proline was the most optimal linker, since the glycine-containing compounds (**13** – **16**) did not show any increased activity compared to their negative control (**17**).

Evaluation of compounds 1 – 17 in living cells

To assess the ability of compounds **1** – **17** to covalently label BUB1, a U2OS cell line stably overexpressing N-terminal GFP-FLAG-tagged BUB1 (U2OS-BUB1^{GFP_FLAG} cells) was generated. Briefly, U2OS-BUB1^{GFP_FLAG} cells were incubated with probes **1** – **17** at 0.1 or 1 µM for 60 min after which the cells were harvested and lysed. Probe labeled proteins were ligated to a Cy5-fluorophore using click chemistry. The proteins were resolved by sodium dodecyl sulfate polyacrylamide gel electrophoresis (SDS-PAGE) and visualized by in-gel fluorescence scanning (**Figure 5.2**). A fluorescent band at an apparent molecular weight of 175 kDa that corresponded to the BUB1^{GFP_FLAG} protein was detected for probes **1**, **2** and **4**, but not for **3** and **5** – **17**. Compounds **1** and **2** showed a similar overall labeling profile, however, the fluorescent intensity for the band at the apparent molecular weight of 175 kDa was less intense for probe **2**. This is in agreement with its reduced potency in the biochemical assay. Compound **4** was tested at 100 nM in view of its high potency. Indeed, the fluorescence intensity of the band at 175 kDa was the highest among all compounds, but significant labeling of other proteins was also observed. Of note, probe **5**, and to lesser extent compound **6**, showed strong fluorescent labeling of a protein with a lower apparent molecular weight in both U2OS-BUB1^{GFP_FLAG} (**Figure 5.2**) and non-transfected U2OS cells (**Supplementary Figure 5.1**, p.178). Taken all data together, compound **1** was selected for further evaluation as a chemical probe to study BUB1 target engagement.

Table 5.1 | Half maximal inhibitory concentrations (expressed as pIC_{50} ± SEM) of **1** – **17** determined by a fluorescence polarization assay on BUB1 kinase activity (N=2, n=2).

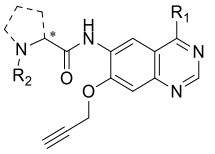

ID	R_1	Linker (*)	R_2	pIC_{50} ± SEM	ID	R_1	Linker (*)	R_2	pIC_{50} ± SEM
1	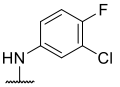	D-Pro		6.96 ± 0.04	**10**	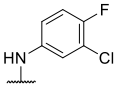	D-Pro		< 5
2	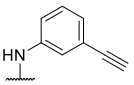	D-Pro		6.26 ± 0.06	**11**	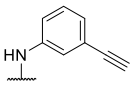	D-Pro		5.63 ± 0.04
3	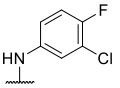	L-Pro		< 5	**12**	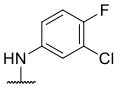	D-Pro		5.30 ± 0.04
4	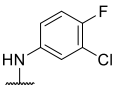	D-Pro		8.95 ± 0.05	**13**	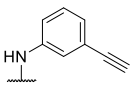	Gly		5.97 ± 0.07
5	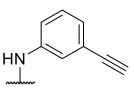	D-Pro	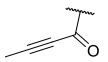	5.84 ± 0.03	**14**	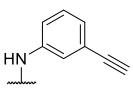	Gly	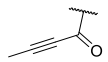	6.24 ± 0.07
6	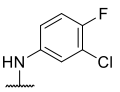	D-Pro	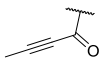	5.68 ± 0.04	**15**	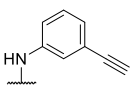	Gly	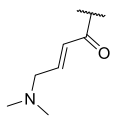	6.25 ± 0.03
7	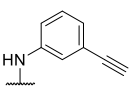	D-Pro	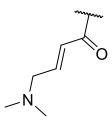	5.08 ± 0.04	**16**	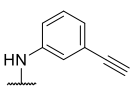	Gly		6.34 ± 0.04
8	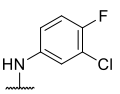	D-Pro	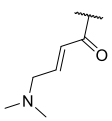	5.01 ± 0.04	**17**	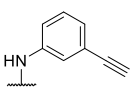	Gly		6.47 ± 0.03
9	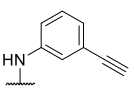	D-Pro		5.93 ± 0.02					

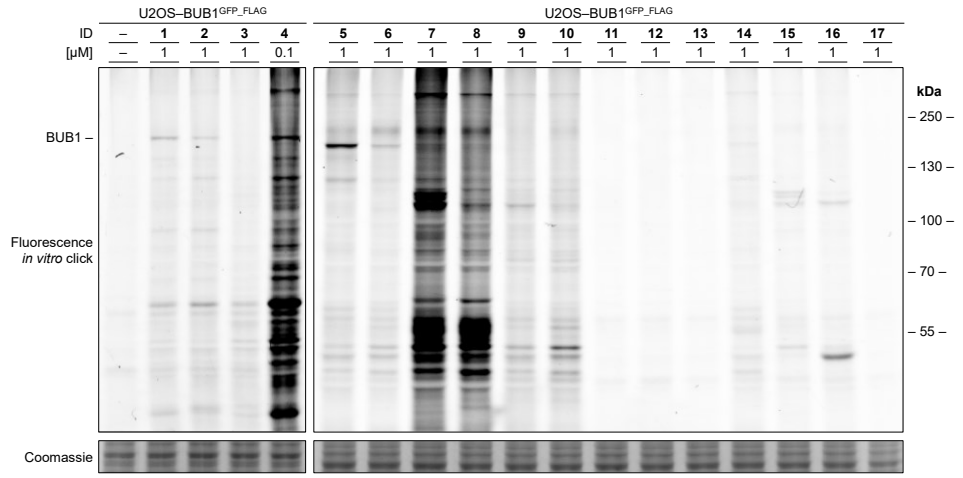

Figure 5.2 | Labeling by probes 1 – 10 and 13 – 16 and acetamide (11, 12, 17) controls. U2OS-BUB1^{GFP_FLAG} cells were incubated with probe (indicated concentration, 1 h, 37°C) after which the cells were lysed. Proteins labeled by probe were visualized by conjugation to a Cy5 fluorophore using click chemistry, SDS-PAGE and in-gel fluorescence scanning. Coomassie staining served as protein loading control.

Development of a cellular BUB1 engagement assay with probe 1.

To validate compound **1** as a BUB1 sensitive chemical probe, it was investigated which amino acid of BUB1 is responsible for the formation of a covalent bond with **1**. NS-062 covalently binds to Cys797 of EGFR (**Figure 5.3A**).[12] Based on a structural overlay of BUB1[19] and EFGR, it was hypothesized that Cys1080 of BUB1 could also react with the warhead of NS-062 and probe **1** (**Figure 5.3A**). Therefore, a C1080A point mutant was generated by site-directed mutagenesis of human BUB1 fused to an N-terminal FLAG-tag. U2OS cells were transiently transfected with wild-type (BUB1^{WT}) or mutant BUB1 (BUB1^{C1080A}) and incubated with **1**. Whereas BUB^{WT} was labeled by probe **1**, BUB1^{C1080A} was not (**Figure 5.3B**). Of note, expression of both BUB1 constructs was comparable as determined by immunoblotting against the FLAG-tag (**Figure 5.3B**). This confirmed that probe **1** specifically reacted with Cys1080. BUB1 labeling was concentration- and time-dependent (**Figure 5.3C–F**) and was optimal at 1 µM and 60 min. Finally, to study whether this probe could be used to study BUB1 target engagement, U2OS-BUB1^{GFP_FLAG} cells were pre-incubated with BAY1816032[20] at different concentrations. BAY1816032 was able to dose-dependently reduce the fluorescent labeling (**Figure 5.3G**) with an apparent target occupancy (expressed as pTE_{50}) of 6.45±0.10 (**Figure 5.3H**). Of note, the obtained pTE_{50} value is dependent on the kinetic conditions of the experiment since probe labeling occurs in a irreversible fashion, whereas BAY1816032 binds reversibly. Taken together, these results provide proof-of-principle that chemical probe **1** can be used to study BUB1 target engagement in living cells.

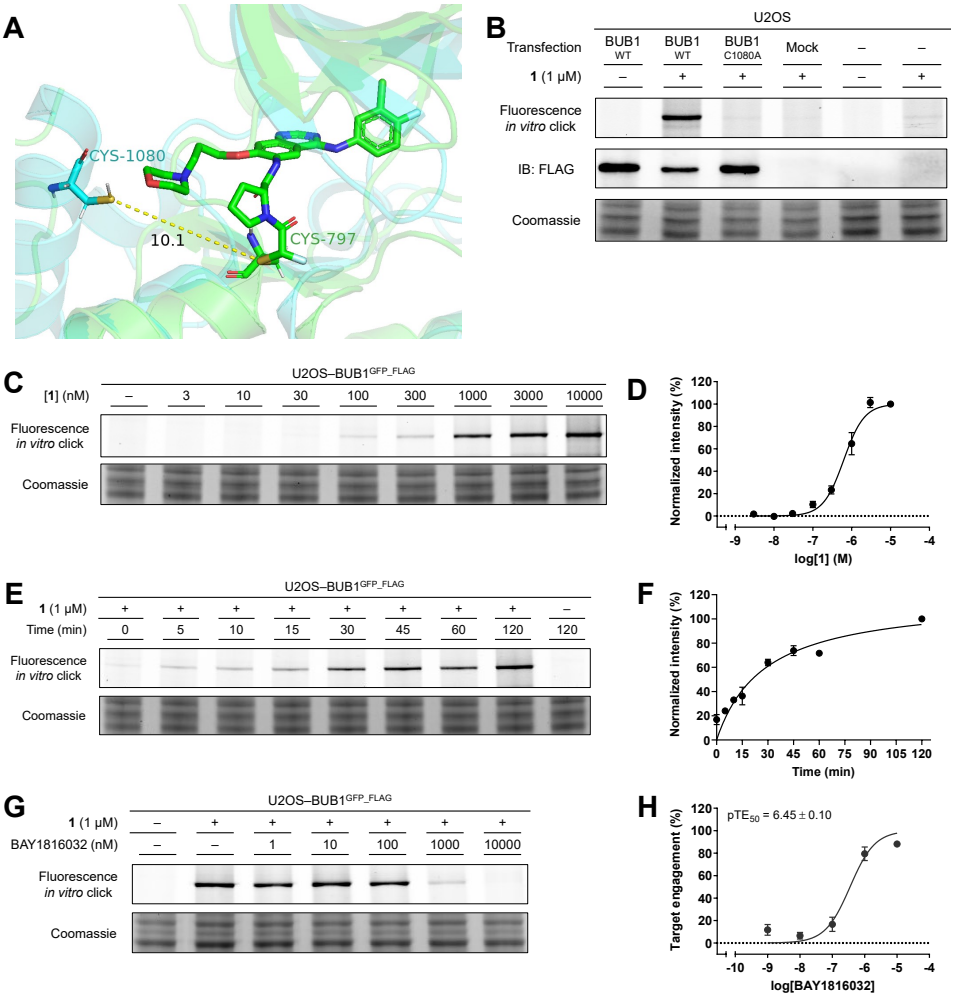

Figure 5.3 | Validation of 1 as BUB1 probe. (A) Crystal structure of NS-062 covalently bound to Cys797 of EGFR (PDB code: 5Y25, green) aligned with the crystal structure of BUB1 (PDB code: 4QPM, blue). The proposed nucleophilic amino acid of BUB1, Cys1080, is represented as sticks and its distance to Cys797 of EGFR is indicated (in angstrom, dashed line). **(B)** Labeling of $BUB1^{WT}$ but not $BUB1^{C1080A}$ in U2OS cells by **1**. U2OS cells were transfected with $BUB1^{WT}$, $BUB1^{C1080A}$ or mock control. 48 h post-transfection cells were treated with **1** (1 µM, 1 h, 37°C) after which the cells were lysed. Proteins labeled by **1** were visualized by conjugation to a Cy5 fluorophore using click chemistry, SDS-PAGE and in-gel fluorescence scanning. The top part of the gel was used for verification of protein expression by immunoblot (IB) against the N-terminal FLAG-tag, the bottom part of the gel was stained by Coomassie and served as loading control. **(C)** Representative visualization of dose-dependent labeling of GFP-FLAG-tagged BUB1 in U2OS-$BUB1^{GFP\_FLAG}$ cells by **1**. U2OS-$BUB1^{GFP\_FLAG}$ cells were incubated with vehicle (–) or **1** (indicated concentration, 1 h, 37°C) and labeling was visualized as described in (B). **(D)** Dose-response curve of **1** corresponding to experiments as performed in (C), normalized between vehicle control (–) and highest concentration of **1** (10 µM) and corrected for protein loading. Data represents mean ± SEM (N=3). **(E)** Representative visualization of time-dependent labeling of GFP-FLAG-tagged BUB1 in U2OS-$BUB1^{GFP\_FLAG}$ cells by **1**. U2OS-$BUB1^{GFP\_FLAG}$ cells were incubated with **1** (1 µM, indicated time, 37°C) and proteins labeled by **1** were visualized as described in (B). **(F)** Time-response curve of **1** corresponding to experiments as performed in (E), normalized between vehicle control (–) and longest incubation time with **1** (120 min) and corrected for protein loading. Data represents mean ± SEM (N=3). **(G)** Representative visualization of GFP-FLAG-tagged BUB1 target engagement in U2OS-$BUB1^{GFP\_FLAG}$ cells by BAY1816032. U2OS-$BUB1^{GFP\_FLAG}$ cells were pre-incubated with BAY1816032 (indicated concentration, 1 h, 37°C) followed by incubation with **1** (1 µM, 1 h, 37°C). Proteins labeled by **1** were visualized as described in (B). **(H)** Target engagement curve of BAY1816032 corresponding to experiments as performed in (G) (pTE_{50} = 6.45 ± 0.10). Data represents mean ± SEM (N=3).

Conclusion

Cellular target engagement studies are required to determine which compound concentration is sufficient to fully inhibit BUB1 activity in a living cell. Here, a series of quinazoline derivatives were designed, synthesized and tested as chemical probes of BUB1 suitable for gel-based ABPP studies. Compound **1**, which reacted with Cys1080 of BUB1, was validated as a chemical probe suitable for BUB1 engagement studies in U2OS cells. Probe **1** allows to correlate target engagement of BUB1 inhibitors with their phenotypic effects in cancer cells (**Chapter 6**). This will expand the understanding of the biological mode of action of BUB1 inhibitors and may help to further investigate BUB1 inhibitors as a potential treatment of cancer.

Acknowledgements

Tom van der Wel is kindly acknowledged for cloning and preparation of the U2OS-BUB1^{GFP_FLAG} stable cell line, Joel Rüegger for his contribution with regard to compound synthesis and biological evaluation of the probes, Bas de Man for his contribution regarding compound synthesis and biochemical evaluation and Hans van den Elst for HPLC purifications and HRMS measurements.

Experimental – Biochemistry

Biochemical evaluation of BUB1 inhibitors

Assays were performed in 384-well plates (Greiner, black, flat bottom, 781076) by sequential addition (final concentrations are indicated) of inhibitor (5 µL, 0.003 nM – 10 nM or 3 nM – 10 µM), BUB1/BUB3 (5 µL, 3.26 nM, Carna Biosciences (05-187), lot: 15CBS-0644 D), ATP (5 µL, 15 µM) and BUB1/BUB3 substrate (5 µL, 75 nM, Carna Biosciences (05-187MSSU)), all as 4x working solutions. The final concentration of DMSO was 1%. Assay reactions were stopped by addition of IMAP progressive binding reagent (20 µL, 1200x diluted (see below), Molecular Devices (R8155), lot: 3117896). Each assay included the following controls: (i) a background control (treated with vehicle instead of inhibitor and BUB1/BUB3 substrate), (ii) MIN controls (treated with 5 µM BAY1816032 (MedChem Express) as inhibitor, defined as 0% BUB1 activity) and (iii) MAX controls (treated with vehicle instead of inhibitor, defined as 100% BUB1 activity). All inhibitors were tested in two separate assays and all inhibitor concentrations were tested in duplicate per assay (N=2, n=2).

For each assay, assay buffer (AB) was freshly prepared and consisted of 20 mM HEPES (prepared by diluting 1 M HEPES, pH 7.2), 5 mM $MgCl_2$, 0.01% (v/v) Tween-20 and 1 mM DTT. Stocks of inhibitors (in DMSO) were diluted in AB to obtain 4x working solutions (4% DMSO) and 5 µL was added to the assay plate. BUB1/BUB3 (3.26 µM (486 µg/mL) in storage buffer) was diluted in AB to obtain 13.0 nM of which 5 µL was added to all wells of the assay plate. The assay plate was centrifuged (1 min, 200 *g*) and incubated at RT for 30 min. ATP (4 mM in MilliQ) was diluted in AB to obtain 60 µM of which 5 µL was added to each well. BUB1/BUB3 substrate (1 mM) was diluted in 20 mM HEPES (prepared by diluting 1 M HEPES (pH 7.2) in MilliQ) to obtain 80 µM (this solution was freshly prepared every assay) and further diluted in AB to obtain 300 nM after which 5 µL was added to each well of the assay plate except for background control wells. The assay plate was centrifuged (1 min, 200 *g*) and incubated at RT in the dark for 180 min. IMAP progressive binding buffer A (5x) and IMAP progressive binding buffer B (5x) were mixed in a ratio to obtain 30% buffer A and 70% buffer B, which was subsequently diluted 5x in MilliQ. IMAP progressive binding reagent was diluted 600x in aforementioned mixture of buffer A and B (to obtain a 2x working solution) of which 20 µL was added to each well of the assay plate. The assay plate was centrifuged (1 min, 200 *g*) and incubated at RT in the dark for 90 min. Fluorescence polarization was measured on a CLARIOstar plate reader using the following settings: (i) optic settings → excitation = F: 482-16, dichroic = F: LP 504, emission = F: 530-40, (ii) optic = top optic, (iii) speed/precision = maximum precision, (iv) focus adjustment was performed for every assay and (v) gain adjustment was done by setting the target mP value to 35 mP for one of the MIN control wells. Data was normalized between MIN and MAX controls and data was plotted using GraphPad Prism 8.0 using "Nonlinear regression (curve fit)" and "log(inhibitor) vs. normalized response – Variable slope" to determine pIC_{50} values.

General biology

DNA oligos were purchased at Integrated DNA Technologies and sequences can be found in **Supplementary Table 5.1** below. Cloning reagents were from Thermo Fisher. All cell culture disposables were from Sarstedt.

Cloning

The pDONR223-construct with full-length human cDNA of BUB1 was a gift from William Hahn & David Root (Addgene Human Kinase ORF Collection). Eukaryotic expression constructs of BUB1 were generated by PCR amplification and restriction/ligation cloning into a pcDNA3.1 vector, in frame with an N-terminal FLAG-tag or N-terminal GFP-FLAG-tag. Point mutations were introduced by site-directed mutagenesis. All plasmids were isolated from transformed XL10-Gold competent cells (prepared using *E. coli* transformation buffer set; Zymo Research) using plasmid isolation kits following the supplier's protocol (Qiagen). All sequences were verified by Sanger sequencing (Macrogen).

Supplementary Table 5.1 | List of oligonucleotide sequences.

ID	Name	Sequence
P1	FLAG-BUB1_forw	TGGTACCGCCGCCACCATGGACTACAAGGATGACGATGACAAGATGGACACCCCGGAAAA
P2	BUB1_stop_rev	TAGATCACTCGAGACCTCATTTTCGTGAACGCTTACATT
P3	BUB1_C1080A_stop_rev	TAGATCACTCGAGACCTCATTTTCGTGAACGCTTCGCTTCTAAGAGCAGTACAA
P4	XhoI-BUB1_forw	GCCCTCGAGATGGACACCCCGGAAAATGT

Cell culture

U2OS (human osteosarcoma) cells were purchased at ATCC and were tested on regular basis for mycoplasma contamination. Cultures were discarded after 2–3 months of use. Cells were cultured at 37°C under 7% CO_2 in DMEM (Sigma Aldrich, D6546) supplemented with GlutaMAX (2 mM, Thermo Fisher), 10% (v/v) heat-inactivated newborn calf serum (Seradigm), penicillin and streptomycin (200 µg/mL each, Duchefa) (complete medium). Growth medium was supplemented with G418 (600 µg/mL) (selection medium) for stable BUB1-overexpressing (U2OS-BUB1^{GFP_FLAG}) cells. Medium was refreshed every 2–3 days and cells were passaged by trypsinization twice a week at 80–90% confluence. Cell viability was assessed by Trypan Blue exclusion and cell quantification using a TC20™ Automated Cell Counter (Bio-Rad).

Generation of stable BUB1-overexpressing U2OS (U2OS-BUB1^{GFP_FLAG}) cells

One day prior to transfection, U2OS cells were transferred from confluent 10 cm dishes to 6-well plates (1:40 dilution). Before transfection, medium was refreshed (1 mL). A 3:1 (m/m) mixture of polyethyleneimine (PEI; 6 µg/well) and plasmid DNA (2 µg/well) was prepared in serum-free medium (200 µL) and incubated for 15 min at RT, after which the mixture was added dropwise to the cells. After 48 h, cells were passaged and grown in selection medium containing G418 (600 µg/mL) until the majority of cells was GFP-positive as determined by fluorescence microscopy. Cells were then single-cell diluted in 96-well plates and expanded to generate monoclonal cell lines stably overexpressing GFP-FLAG-BUB1. Expression was verified by immunoblot analysis using anti-FLAG antibody.

Overexpression of BUB1^{WT} and BUB1^{C1080A} and subsequent probe labeling

U2OS cells were seeded into 6-well plates (400,000 cells/well for transfections, 250,000 cells/well for non-transfected U2OS control) and incubated overnight to allow for cell adherence. Cell medium was aspirated and refreshed with complete medium (2 mL). A 3:1 (m/m) mixture of polyethyleneimine (PEI; 6 µg/well) and plasmid DNA (2 µg/well) was prepared in serum-free medium (200 µL) and incubated for 15 min at RT, after which the mixture was added dropwise to the cells. After 48 h, cells were treated with probe as described in "Probe labeling in living cells" (final probe concentration: 1 µM, incubation time: 1 h, lysis buffer: 60 µL for transfections, 120 µL for non-transfected cells, lysate concentration was adjusted to 1.15 mg/mL, 10 µg/lane for SDS-PAGE). After scanning fluorescence, the top part of the gel was immunoblotted as described in "Immunoblot", the bottom part of the gel was used for protein loading control as determined by Coomassie Brilliant Blue R-250 staining.

Probe labeling in living cells

U2OS-BUB1^{GFP_FLAG} or U2OS cells from 10 cm dishes with low cell density (<50% confluence) were seeded into 6-well plates (500,000 cells/well) and incubated overnight to allow for cell adherence. Probe or competitor (stock solutions in DMSO) were diluted 100x in complete medium to obtain 10x working solutions (1% DMSO). For dose-response experiments, compounds were further diluted in complete medium containing 1% DMSO. Cell medium was aspirated and complete medium (900 µL for probe labeling only, 800 µL for competition experiments) was added. Either competitor (100 µL, 10x working solution) or probe (100 µL, 10x working solution) was added and cells were incubated at 37°C for 1 h (or for indicated time in case of time-response experiments). For competition experiments, probe (100 µL, 10x working solution) was subsequently added and cells were incubated at 37°C for 1 h. Medium was aspirated and cells were washed with PBS (1 mL). Cells were harvested by trypsinization and centrifuged (500 *g*, 3 min). Pellets were washed with PBS (1 mL), centrifuged (500 *g*, 3 min) and supernatant was removed. Pellets were snap-frozen in liquid nitrogen and subsequently thawed on ice (cell pellet can optionally be stored at –80°C). Cells were lysed by suspending the pellet in 60 µL M-PER™ Mammalian Protein Extraction Reagent (Thermo Fisher), supplemented with 1x Halt™ protease inhibitor cocktail

(EDTA-free) (Thermo Fisher) and 1x Halt™ phosphatase inhibitor cocktail (Thermo Fisher), after which the samples were incubated on ice for 15 min. Samples were vortexed at medium speed and centrifuged (14,000 *g*, 10 min, 4°C). The supernatant was collected and protein concentration determined by a Quick Start™ Bradford Protein Assay (Bio-Rad). Lysates were diluted to 1.15 mg/mL in M-PER™ Mammalian Protein Extraction Reagent (lysates can optionally be snap-frozen and stored at –80°C). "Click-mix" was prepared freshly by mixing $CuSO_4$ (42 µL of 15 mM in H_2O) and sodium ascorbate (21 µL of 150 mM in H_2O) until yellow, followed by the addition of THPTA (7 µL of 15 mM in H_2O) and Cy5-N_3 (7 µL of 82.5 µM in DMSO). To 26 µL lysate was added 4 µL click-mix and samples were incubated at 37°C for 30 min. Samples were denatured by the addition of 4x Laemmli buffer (10 µL of 240 mM Tris-HCl pH 6.8, 8% w/v SDS, 40% v/v glycerol, 5% v/v β-mercaptoethanol, 0.04% v/v/ bromophenol blue) and incubated at 95°C for 3 min. Samples were resolved by sodium dodecyl sulfate polyacrylamide gel electrophoresis (SDS-PAGE) on a 7.5% polyacrylamide gel (180 V, 70 min, 10 or 20 µL/lane). Gels were scanned using Cy2, Cy3 and Cy5 multichannel settings (532/28, 602/50 and 700/50 filters, respectively) on a ChemiDoc™ MP imager (Bio-Rad). Fluorescence intensity was quantified using Image Lab 6.0.1 (Bio-Rad) and corrected for protein loading as determined by Coomassie Brilliant Blue R-250 staining. Data was plotted using GraphPad Prism 8.0.

Immunoblot

Samples were resolved by SDS-PAGE as described above and transferred to 0.2 µm polyvinylidene difluoride membranes by a Trans-Blot Turbo™ Transfer system (Bio-Rad) directly after fluorescence scanning. Membranes were washed with TBS (50 mM Tris pH 7.5, 150 mM NaCl) and blocked with 5% milk in TBS-T (50 mM Tris pH 7.5, 150 mM NaCl, 0.05% Tween-20) for 1 h at RT. Membranes were then incubated with primary antibody (monoclonal mouse anti-FLAG M2 (1:5000, Sigma Aldrich, F3156)) in 5% milk in TBS-T (overnight at 4 °C). Membranes were washed three times with TBS-T, incubated with secondary antibody (goat anti-mouse-HRP (1:5000, Santa Cruz, sc-2005)) in 5% milk in TBS-T (1 h at RT) and then washed three times with TBS-T and twice with TBS. Luminol development solution (10 mL of 1.4 mM luminol in 100 mM Tris pH 8.8 + 100 µL of 6.7 mM p-coumaric acid in DMSO + 3 µL of 30% (v/v) H_2O_2) was added after which chemiluminescence and Cy3 were detected on a ChemiDoc™ MP imager. For $BUB1^{WT}$ and $BUB1^{C1080A}$ transfections, development was performed using Clarity Max Western ECL Substrate (Bio-Rad).

Supplementary figures

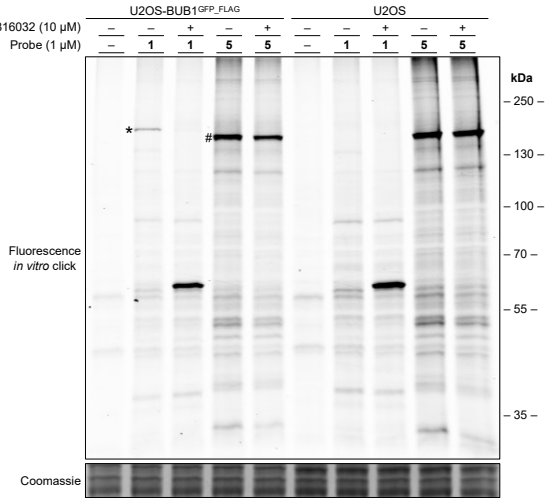

Supplementary Figure 5.1 | Competition with BAY1816032 abolishes labeling of GFP-FLAG-tagged BUB1 by **1** (*), but not the labeling of a protein with a lower apparent molecular weight by **5** (#). U2OS-$BUB1^{GFP\_FLAG}$ or U2OS cells were pre-incubated with vehicle (–) or BAY1816032 (10 µM, 1 h, 37°C) followed by incubation with vehicle (–) or indicated probe (1 µM, 1 h, 37°C). Proteins labeled by probe were visualized by conjugation to a Cy5 fluorophore using click chemistry, SDS-PAGE and in-gel fluorescence scanning. Coomassie staining served as protein loading control.

Experimental – Chemistry

General synthesis

All reagents and solvents were purchased from chemical suppliers (Fluorochem, Sigma-Aldrich, Merck, Fisher Scientific, Honeywelel, VWR, Biosolve) and used without further purification. All reactions were performed at room temperature (RT) under a nitrogen atmosphere, unless stated otherwise. Reactions were monitored by thin layer chromatography (TLC, silica gel 60, UV_{254}, Macherey-Nagel, ref: 818333) and compounds were visualized by UV absorption (254 nm and/or 366 nm) or spray reagent (permanganate (5 g/L $KMnO_4$, 25 g/L K_2CO_3)) followed by heating. Alternatively, reactions were monitored by liquid chromatography-mass spectrometry (LCMS), either on a Thermo Finnigan (Thermo Finnigan LCQ Advantage MAX ion-trap mass spectrometer (ESI+) coupled to a Surveyor HPLC system (Thermo Finnigan) equipped with a Nucleodur C18 Gravity column (50x4.6 mm, 3 µm particle size, Macherey-Nagel)) or a Thermo Fleet (Thermo LCQ Fleet ion-trap mass spectrometer (ESI+) coupled to a Vanquish UHPLC system). LCMS eluent consisted of MeCN in 0.1% TFA (aq.) and LCMS methods were as follows: 0.5 min cleaning with starting gradient, 8 min using specified gradient (linear), 2 min cleaning with 90% MeCN in 0.1% TFA (aq.). LCMS data is reported as follows: instrument (Finnigan or Fleet), gradient (% MeCN in 0.1% TFA (aq.)), retention time (t_r) and mass (as m/z: $[M+H]^+$). Purity of final compounds was determined to be ≥ 95% by integrating UV intensity of spectra generated by either of the LCMS instruments. ^1H and ^{13}C NMR spectra were recorded on a Bruker AV400 (400 and 101 MHz, respectively) or Bruker AV500 (500 and 126 MHz, respectively) NMR spectrometer. NMR samples were prepared in deuterated DMSO. Chemical shifts are given in ppm (δ) relative to residual protonated solvent signals (DMSO → δ 2.500 (^1H), δ 39.520 (^{13}C)). Data was processed by using MestReNova (v. 14) and is reported as follows: chemical shift (δ), multiplicity, coupling constant (*J* in Hz) and integration. Multiplicities are abbreviated as follows: s = singlet, br s = broad singlet, d = doublet, dd = doublet of doublets, ddd = doublet of doublet of doublets, t = triplet, dt = doublet of triplets, p = pentet, m = multiplet. For some molecules rotamer peaks were observed, resulting in extra splitting of peaks. For these compounds, chemical shifts were reported as ranges and multiplicity was denoted by "2x", followed by the multiplicities specified above (i.e. 2x d = twice a doublet). The reported coupling constant corresponds to either of the multiplet peaks (of note, coupling constants were the same for both multiplet peaks). Purification was done either by manual silica gel column chromatography (using 40-63 µm, 60 Å silica gel, Macherey-Nagel) or automated flash column chromatography on a Biotage Isolera machine (using pre-packed cartridges with 40-63 µm, 60 Å silica gel (4, 12, 25 or 40 g), Screening Devices). High-performance liquid chromatography (HPLC) purifications were performed on either an Agilent 1200 preparative HPLC system (equipped with a Gemini C18 column (250x10 mm, 5 µm particle size, Phenomenex) coupled to a 6130 quadrupole mass spectrometer) or a Waters Acquity UPLC system (equipped with a Gemini C18 column (150x21 mm, 5 µm particle size, Phenomenex) coupled to a SQ mass spectrometer). Specified gradients for HPLC purifications (MeCN in 0.2% TFA (aq.)) were linear (5 mL/min for 12 min (Agilent) or 25 mL/min for 10 min (Waters)). High resolution mass spectrometry (HRMS) spectra were recorded through direct injection of a 1 µM sample either on a Thermo Scientific Q Exactive Orbitrap equipped with an electrospray ion source in positive mode coupled to an Ultimate 3000 system (source voltage = 3.5 kV, capillary temperature = 275 °C, resolution R = 240,000 at m/z 400, external lock, mass range m/z = 150-2000) or on a Synapt G2-Si high definition mass spectrometer (Waters) equipped with an electrospray ion source in positive mode (ESI-TOF) coupled to a NanoEquity system with Leu-enkephalin (m/z = 556.2771) as internal lock mass. The eluent for HRMS measurements consisted of a 1:1 (v/v) mixture of MeCN in 0.1% formic acid (aq.) using a flow of 25 mL/min. Compound names were generated by ChemDraw (v. 19.1.21).

General procedure A – Peptide coupling

Acid derivative (3.3 eq.) was dissolved in DCM (0.15 M based on amine analogue) after which DIPEA (4 eq.) and DMF (0.1 eq.) were added. The mixture was cooled down to 0°C, pivaloyl chloride (3 eq.) was added and the mixture was stirred at 0°C for 1.5 h. Amine analogue (1 eq.) was added, the mixture was allowed to warm to RT and stirred for 16 h. The mixture was poured into 1 M $NaHCO_3$ (aq.) (50 or 100 mL) and the product extracted with DCM (3x50 or 3x100 mL). The combined organic layers were washed

with brine (100 mL), dried over Na_2SO_4, filtered and concentrated. Purification was performed as indicated.

General procedure B – Peptide coupling

Amine analogue (1 eq.) was dissolved in DCM (0.15 M) and cooled down to 0°C. DIPEA (1 eq.) and acyl chloride derivative (1 eq.) were added after which the mixture was allowed to warm to RT and stirred for 16 h. The mixture was poured into 1 M $NaHCO_3$ (aq.) (20 mL) and the product extracted with DCM (3x20 mL). The combined organic layers were washed with brine (20 mL), dried over Na_2SO_4, filtered and concentrated. Purification was performed as indicated.

(2*R*)-1-(2-Chloro-2-fluoroacetyl)-*N*-(4-((3-chloro-4-fluorophenyl)amino)-7-(prop-2-yn-1-yloxy)quinazolin-6-yl)pyrrolidine-2-carboxamide (1)

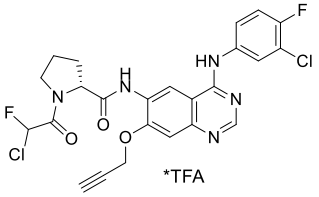

The title compound was synthesized from **29** (100 mg, 227 µmol) and 2-chloro-2-fluoroacetic acid according to general procedure A. The crude was purified by HPLC (Agilent, 35 – 38% MeCN in 0.2% TFA (aq.)) to afford the product as TFA salt (25.6 mg, 39.4 µmol, 17%). ^{1}H NMR (500 MHz, DMSO) (as a mixture of two diastereomers) δ 10.77 (br s, 1H), 9.90 – 9.82 (2x s, 1H), 9.05 – 8.93 (2x s, 1H), 8.74 (s, 1H), 8.02 – 7.98 (2x dd, *J* = 6.8, 2.6 Hz, 1H), 7.72 – 7.67 (2x ddd, *J* = 9.0, 4.6, 2.6 Hz, 1H), 7.51 – 7.45 (m, 2H), 7.27 – 7.09 (2x d, *J* = 48.5 Hz, 1H), 5.17 – 5.11 (2x d, *J* = 2.4 Hz, 2H), 4.88 – 4.79 (2x dd, *J* = 8.6, 3.3 Hz, 1H), 3.84 – 3.73 (m, 2H), 3.58 – 3.49 (m, 1H), 2.31 – 2.20 (m, 1H), 2.11 – 1.89 (m, 3H) (the spectrum was accompanied by rotamer peaks). ^{13}C NMR (126 MHz, DMSO) δ 170.29, 170.11, 161.75 (d, $J_{(C–F)}$ = 24.8 Hz), 161.71 (d, $J_{(C–F)}$ = 24.5 Hz), 158.61, 158.36, 158.11, 158.06, 157.85, 155.40, 155.34, 154.35, 153.45, 153.40, 152.75 (d, $J_{(C–F)}$ = 244.5 Hz), 152.01, 135.33, 128.51, 128.31, 125.67, 125.51, 124.43 (d, $J_{(C–F)}$ = 7.2 Hz), 124.26 (d, $J_{(C–F)}$ = 7.2 Hz), 119.00 (d, $J_{(C–F)}$ = 18.6 Hz), 118.20, 116.85, 116.72 (d, $J_{(C–F)}$ = 21.8 Hz), 115.83, 115.55, 108.36, 104.52, 104.30, 92.23 (d, $J_{(C–F)}$ = 245.7 Hz), 92.01 (d, $J_{(C–F)}$ = 245.9 Hz), 79.95, 79.87, 77.80, 77.77, 60.61, 60.43, 56.99, 46.75, 46.67, 29.38, 29.24, 24.57, 24.26 (the spectrum was accompanied by rotamer peaks). LCMS (Fleet, 10 → 90%): t_r = 5.31 min, m/z: 534.2. HRMS $[C_{24}H_{19}Cl_2F_2N_5O_3 + H]^+$: 534.09058 calculated, 534.09075 found.

(2*R*)-1-(2-Chloro-2-fluoroacetyl)-*N*-(4-((3-ethynylphenyl)amino)-7-(prop-2-yn-1-yloxy)quinazolin-6-yl)pyrrolidine-2-carboxamide (2)

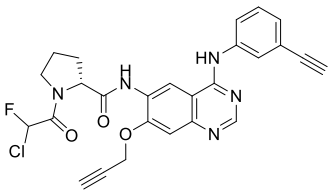

The title compound was synthesized from **30** (65.0 mg, 158 µmol) and 2-chloro-2-fluoroacetic acid according to general procedure A. The crude was purified by automated column chromatography (0 – 20% MeOH/DCM) to afford the product (3.8 mg, 7.5 µmol, 5%). ^{1}H NMR (500 MHz, DMSO) (as a mixture of two diastereomers) δ 9.84 (s, 1H), 9.73 – 9.64 (2x s, 1H), 8.89 – 8.79 (2x s, 1H), 8.55 – 8.53 (2x s, 1H), 7.99 – 7.96 (2x t, *J* = 1.9 Hz, 1H), 7.87 – 7.83 (m, 1H), 7.41 – 7.36 (m, 2H), 7.21 – 7.19 (m, 1H), 7.25 – 7.08 (2x d, *J* = 48.5 Hz, 1H), 5.11 – 5.07 (2x d, *J* = 2.4 Hz, 2H), 4.86 – 4.75 (2x dd, *J* = 8.7, 3.2 Hz, 1H), 4.17 – 4.17 (2x s, 1H), 3.84 – 3.73 (m, 1H), 3.72 – 3.71 (2x t, *J* = 2.3 Hz, 1H), 3.61 – 3.48 (m, 1H), 2.28 – 2.18 (m, 1H), 2.11 – 1.90 (m, 3H) (the spectrum was accompanied by rotamer peaks). ^{13}C NMR (126 MHz, DMSO) δ 170.14, 169.90, 161.79 (d, $J_{(C–F)}$ = 24.3 Hz), 161.73 (d, $J_{(C–F)}$ = 24.5 Hz), 157.06, 154.21, 154.08, 153.57, 152.82, 149.03, 148.69, 139.80, 139.77, 128.82, 127.25, 127.09, 126.53, 125.13, 125.08, 122.98, 122.91, 121.68, 117.07, 115.62, 109.55, 109.48, 108.32, 108.28, 92.17 (d, $J_{(C–F)}$ = 245.8 Hz), 92.09 (d, $J_{(C–F)}$ = 245.8 Hz), 83.59, 80.48, 79.38, 79.31, 78.32, 60.64, 60.47, 56.59, 46.72, 46.64, 29.41, 29.23, 24.54, 24.21 (the spectrum was accompanied by rotamer peaks). LCMS (Fleet, 10 → 90%): t_r = 5.13 min, m/z: 506.2. HRMS $[C_{26}H_{21}ClFN_5O_3 + H]^+$: 506.13897 calculated, 506.13866 found.

(2*S*)-1-(2-Chloro-2-fluoroacetyl)-*N*-(4-((3-chloro-4-fluorophenyl)amino)-7-(prop-2-yn-1-yloxy)quinazolin-6-yl)pyrrolidine-2-carboxamide (3)

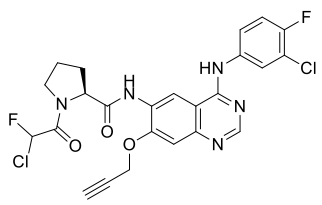

The title compound was synthesized from **31** (83.0 mg, 189 µmol) and 2-chloro-2-fluoroacetic acid according to general procedure A. The crude was purified by automated column chromatography (0 – 20% MeOH/DCM) to afford the product (42.7 mg, 79.9 µmol, 42%). ^{1}H NMR (400 MHz, DMSO) (as a mixture of two diastereomers) δ 9.93 (s, 1H), 9.71 (d, *J* = 29.3 Hz, 1H), 8.83 (d, *J* = 38.0 Hz, 1H), 8.56 – 8.51 (2x s, 1H), 8.12 – 8.05 (2x dd, *J* = 6.9, 2.6 Hz, 1H), 7.80 – 7.74 (m, 1H), 7.45 – 7.38 (m, 2H), 7.28 – 7.06 (2x d, *J* = 48.5 Hz, 1H), 5.13 – 5.05 (2x d, *J* = 2.5 Hz, 2H), 4.86 – 4.75 (2x dd, *J* = 8.5, 3.1 Hz, 1H), 3.84 – 3.70 (m, 2H), 3.61 – 3.47 (m, 1H), 2.30 – 2.16 (m, 1H), 2.11 – 1.92 (m, 3H) (the spectrum was accompanied by rotamer peaks). ^{13}C NMR (101 MHz, DMSO) δ 170.18, 169.96, 161.80 (d, $J_{(C–F)}$ = 24.6 Hz), 161.74 (d, $J_{(C–F)}$ = 24.6 Hz), 156.98, 154.08, 153.94, 153.57, 153.31 (d, $J_{(C–F)}$ = 242.9 Hz), 152.82, 148.79, 136.74, 127.39, 127.23, 123.90, 123.82, 122.79 (d, $J_{(C–F)}$ = 7.0 Hz), 122.70 (d, $J_{(C–F)}$ = 6.8 Hz), 118.73 (d, $J_{(C–F)}$ = 18.3 Hz), 116.83, 116.48 (d, $J_{(C–F)}$ = 21.3 Hz), 115.37, 109.39, 109.32, 108.25, 92.18 (d, $J_{(C–F)}$ = 246.0 Hz), 92.08 (d, $J_{(C–F)}$ = 245.9 Hz), 79.46, 79.39, 78.31, 60.64, 60.47, 56.63, 46.74, 46.66, 29.43, 29.26, 24.56, 24.24 (the spectrum was accompanied by rotamer peaks). LCMS (Fleet, 10 → 90%): t_r = 5.32 min, m/z: 534.2. HRMS $[C_{24}H_{19}Cl_2F_2N_5O_3 + H]^+$: 534.09058 calculated, 534.09040 found.

(*R*)-*N*-(4-((3-Chloro-4-fluorophenyl)amino)-7-(prop-2-yn-1-yloxy)quinazolin-6-yl)-1-(2-chloroacetyl)pyrrolidine-2-carboxamide (4)

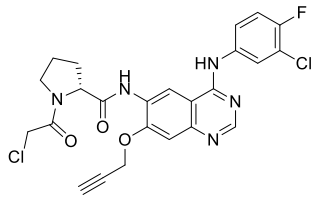

The title compound was synthesized from **29** (108 mg, 246 µmol) and 2-chloroacetyl chloride (1.5 eq.) according to general procedure B (using 1.6 eq. DIPEA). The crude was purified by automated column chromatography (0 – 20% MeOH/DCM) to afford the product (36.6 mg, 70.9 µmol, 29%). ^{1}H NMR (400 MHz, DMSO) δ 9.91 (s, 1H), 9.61 (s, 1H), 8.83 (s, 1H), 8.54 (s, 1H), 8.10 (dd, *J* = 6.9, 2.7 Hz, 1H), 7.78 (ddd, *J* = 9.0, 4.3, 2.6 Hz, 1H), 7.47 – 7.36 (m, 2H), 5.09 (d, *J* = 2.5 Hz, 2H), 4.87 – 4.72 (2x dd, *J* = 8.4, 2.6 Hz, 1H), 4.44 – 4.07 (m, 2H), 3.72 (t, *J* = 2.2 Hz, 1H), 3.71 – 3.64 (m, 1H), 3.62 – 3.55 (m, 1H), 2.23 – 2.11 (m, 1H), 2.09 – 1.87 (m, 3H) (the spectrum was accompanied by rotamer peaks). ^{13}C NMR (101 MHz, DMSO) δ 170.62, 164.81, 156.94, 154.01, 153.27 (d, *J* = 242.9 Hz), 153.19, 148.72, 136.79 (d, $J_{(C–F)}$ = 3.1 Hz), 127.37, 123.76, 122.64 (d, $J_{(C–F)}$ = 6.8 Hz), 118.72 (d, $J_{(C–F)}$ = 18.3 Hz), 116.45 (d, $J_{(C–F)}$ = 21.6 Hz), 116.04, 109.39, 108.26, 79.38, 78.31, 60.46, 56.63, 46.75, 42.89, 29.48, 24.40 (the spectrum was accompanied by rotamer peaks). LCMS (Fleet, 10 → 90%): t_r = 5.10 min, m/z: 516.1. HRMS $[C_{24}H_{20}Cl_2FN_5O_3 + H]^+$: 516.10000 calculated, 516.10012 found.

(*R*)-1-(But-2-ynoyl)-*N*-(4-((3-ethynylphenyl)amino)-7-(prop-2-yn-1-yloxy)quinazolin-6-yl)pyrrolidine-2-carboxamide (5)

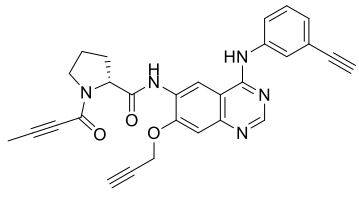

The title compound was synthesized from **30** (80.0 mg, 194 µmol) and but-2-ynoic acid according to general procedure A. The crude was purified by automated column chromatography (0 – 12% MeOH/DCM) to afford the product (58.0 mg, 121 µmol, 63%). ^{1}H NMR (400 MHz, DMSO) δ 9.86 – 9.83 (2x s, 1H), 9.82 – 9.67 (2x s, 1H), 8.89 – 8.83 (2x s, 1H), 8.56 – 8.54 (2x s, 1H), 8.00 – 7.97 (2x t, *J* = 1.9 Hz, 1H), 7.88 – 7.83 (2x ddd, *J* = 8.3, 2.2, 1.1 Hz, 1H), 7.42 – 7.35 (m, 2H), 7.23 – 7.19 (m, 1H), 5.13 – 5.08 (2x d, *J* = 2.4 Hz, 2H), 4.98 – 4.72 (2x dd, *J* = 8.7, 3.4 Hz, 1H), 4.19 – 4.18 (2x s, 1H), 3.76 – 3.67 (m, 2H), 3.49 (dd, *J* = 7.7, 6.0 Hz, 1H), 2.41 – 2.19 (m, 1H), 2.13 – 1.85 (m, 6H) (the spectrum was accompanied by rotamer peaks). ^{13}C NMR (101 MHz, DMSO) δ 171.15, 170.30, 157.04, 154.17, 154.08, 153.14, 153.00, 152.11, 152.05, 148.82, 148.74, 139.81, 139.71, 128.82, 127.30, 127.07, 126.63, 126.51, 125.30, 125.09, 123.14, 122.93, 121.68, 116.47, 115.87, 109.54, 109.50, 108.35, 108.26, 88.37, 87.94, 83.61, 83.56, 80.55, 80.50, 79.38, 79.35, 78.35, 78.32, 74.41, 74.31, 61.43, 59.29, 56.59, 56.55, 48.60, 46.08, 31.16, 29.98, 23.77, 22.87, 3.33, 3.31 (the spectrum was

accompanied by rotamer peaks). LCMS (Fleet, 10 → 90%): t_r = 4.92 min, m/z: 478.2. HRMS [$C_{28}H_{23}N_5O_3$ + H]$^+$: 478.18737 calculated, 478.18743 found.

(*R*)-1-(But-2-ynoyl)-*N*-(4-((3-chloro-4-fluorophenyl)amino)-7-(prop-2-yn-1-yloxy)quinazolin-6-yl)pyrrolidine-2-carboxamide (6)

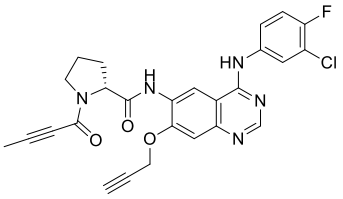

The title compound was synthesized from **29** (52.0 mg, 118 µmol) and but-2-ynoic acid according to general procedure A. The crude was purified by HPLC (Agilent, 35 – 38% MeCN in 0.2% TFA (aq.)) after which the fractions were concentrated and traces of TFA were removed by coevaporation with 1:1 MeCN/H_2O (20 mL). The residue was dissolved in DCM (15 mL) and washed with 1 M $NaHCO_3$ (aq.) (3x5 mL). The organic layer was dried over Na_2SO_4, filtered and concentrated to afford the product (6.0 mg, 12 µmol, 10%). ^{1}H NMR (500 MHz, DMSO) δ 9.89 – 9.87 (2x s, 1H), 9.81 – 9.66 (2x s, 1H), 8.85 – 8.81 (2x s, 1H), 8.54 – 8.53 (2x s, 1H), 8.11 – 8.07 (2x dd, *J* = 6.9, 2.6 Hz, 1H), 7.80 – 7.75 (2x ddd, *J* = 9.1, 4.4, 2.6 Hz, 1H), 7.45 – 7.37 (m, 2H), 5.13 – 5.07 (2x d, *J* = 2.4 Hz, 2H), 4.97 – 4.72 (2x dd, *J* = 8.7, 3.5 Hz, 1H), 3.74 – 3.68 (m, 2H), 3.48 (dd, *J* = 7.8, 6.0 Hz, 1H), 2.37 – 2.19 (m, 1H), 2.10 – 1.86 (m, 6H) (the spectrum was accompanied by rotamer peaks). ^{13}C NMR (126 MHz, DMSO) δ 171.13, 170.28, 156.90, 154.04, 153.05, 152.98 (d, $J_{(C–F)}$ = 245.8 Hz), 152.96, 152.05, 148.70, 148.64, 136.77 (d, $J_{(C–F)}$ = 3.4 Hz), 127.37, 127.15, 123.99, 123.76, 122.88 (d, $J_{(C–F)}$ = 6.8 Hz), 122.64 (d, $J_{(C–F)}$ = 6.7 Hz), 118.66 (d, $J_{(C–F)}$ = 19.5 Hz), 116.43 (d, $J_{(C–F)}$ = 21.6 Hz), 116.09, 115.58, 109.35, 109.33, 108.37, 108.27, 88.33, 87.87, 79.37, 78.30, 74.28, 61.38, 59.24, 56.58, 48.56, 46.03, 31.12, 29.94, 23.73, 22.82, 3.28. LCMS (Fleet, 10 → 90%): t_r = 5.10 min, m/z: 506.2. HRMS [$C_{26}H_{21}ClFN_5O_3$ + H]$^+$: 506.13897 calculated, 506.13910 found.

(*R*,*E*)-1-(4-(Dimethylamino)but-2-enoyl)-*N*-(4-((3-ethynylphenyl)amino)-7-(prop-2-yn-1-yloxy)quinazolin-6-yl)pyrrolidine-2-carboxamide (7)

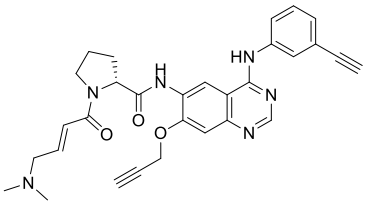

The title compound was synthesized from **30** (80.0 mg, 194 µmol) and (*E*)-4-(dimethylamino)but-2-enoic acid hydrochloride according to general procedure A (using 5 eq. DIPEA). The crude was purified by automated column chromatography (10 – 20% MeOH/DCM) to afford the product (74.0 mg, 142 µmol, 73%). ^{1}H NMR (400 MHz, DMSO) δ 9.85 (s, 1H), 9.89 – 9.69 (2x s, 1H), 8.92 – 8.84 (2x s, 1H), 8.55 – 8.53 (2x s, 1H), 7.99 (t, *J* = 1.9 Hz, 1H), 7.90 – 7.84 (2x ddd, *J* = 8.3, 2.3, 1.1 Hz, 1H), 7.41 – 7.35 (m, 2H), 7.22 – 7.18 (2x dt, *J* = 7.6, 1.3 Hz, 1H), 6.74 – 6.57 (2x dt, *J* = 15.2, 6.2 Hz, 1H), 6.52 – 6.28 (2x dt, *J* = 15.0, 1.5 Hz, 1H), 5.12 – 5.07 (2x d, *J* = 2.4 Hz, 2H), 4.98 – 4.79 (2x dd, *J* = 8.3, 3.1 Hz, 1H), 4.20 – 4.19 (2x s, 1H), 3.78 – 3.46 (m, 3H), 3.18 – 3.07 (m, 2H), 2.28 – 1.85 (m, 10H) (the spectrum was accompanied by rotamer peaks). ^{13}C NMR (101 MHz, DMSO) δ 171.42, 170.83, 163.75, 157.01, 154.25, 153.98, 153.48, 152.82, 149.02, 148.61, 141.05, 140.53, 139.84, 139.71, 128.79, 127.46, 126.88, 126.57, 126.45, 125.20, 125.04, 124.21, 124.18, 123.03, 122.88, 121.66, 117.10, 115.44, 109.57, 109.44, 108.36, 108.19, 83.61, 83.56, 80.54, 80.50, 79.47, 79.33, 78.35, 78.30, 60.07, 59.79, 59.52, 59.45, 56.61, 47.05, 46.74, 44.66, 44.58, 31.99, 29.05, 24.41, 22.34 (the spectrum was accompanied by rotamer peaks). LCMS (Fleet, 10 → 90%): t_r = 3.89 min, m/z: 523.4. HRMS [$C_{30}H_{30}N_6O_3$ + H]$^+$: 523.24522 calculated, 523.24527 found.

(*R*,*E*)-*N*-(4-((3-Chloro-4-fluorophenyl)amino)-7-(prop-2-yn-1-yloxy)quinazolin-6-yl)-1-(4-(dimethylamino)but-2-enoyl)pyrrolidine-2-carboxamide (8)

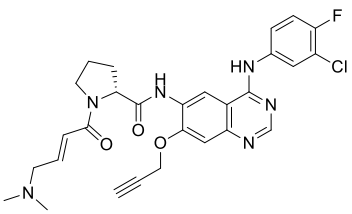

The title compound was synthesized from **29** (80.0 mg, 182 µmol) and (*E*)-4-(dimethylamino)but-2-enoic acid hydrochloride according to general procedure A (using 5 eq. DIPEA). The crude was purified by automated column chromatography (10 – 20% MeOH/DCM) to afford the product (41 mg, 74 µmol, 41%). ^{1}H NMR (400 MHz, DMSO) δ 9.91 (br s, 1H), 9.85 – 9.69 (2x s, 1H), 8.90 – 8.80 (2x s, 1H), 8.54 – 8.51 (2x s, 1H), 8.10 (dd, *J* = 6.9, 2.5 Hz, 1H), 7.77 (ddd, *J* = 9.2, 4.2, 2.5 Hz, 1H), 7.44 – 7.37 (m, 2H), 6.73 – 6.58 (2x dt, *J* = 15.1, 6.1 Hz, 1H), 6.48 – 6.22 (2x dt, *J* = 15.1, 1.4 Hz, 1H), 5.12 – 5.07 (2x d, *J* = 2.4 Hz, 2H), 4.98 – 4.78 (2x dd, *J* = 8.4, 3.1 Hz, 1H), 3.79 – 3.48 (m, 3H), 3.09 – 2.94 (m, 2H), 2.09 (d, *J* = 41.8 Hz, 10H) (the spectrum was accompanied by rotamer peaks). ^{13}C NMR (101 MHz, DMSO) δ 171.46, 170.87, 163.90, 163.87, 156.89, 154.11, 153.87, 153.26, 153.20 (d, $J_{(C–F)}$ = 242.8 Hz), 152.74, 148.50, 142.44, 141.87, 136.87, 127.55, 127.02, 123.89, 123.72, 123.30, 122.77 (d, *J* = 6.5 Hz), 122.62 (d, $J_{(C–F)}$ = 6.8 Hz), 118.66 (d, $J_{(C–F)}$ = 18.3 Hz), 116.42 (d, $J_{(C–F)}$ = 21.5 Hz), 115.10, 109.45, 108.37, 108.20, 79.49, 79.34, 78.33, 78.29, 62.49, 60.05, 59.94, 59.91, 59.76, 56.61, 47.02, 46.71, 45.15, 45.03, 31.97, 29.02, 24.41, 22.34 (the spectrum was accompanied by rotamer peaks). LCMS (Fleet, 10 → 90%): t_r = 4.02 min, m/z: 551.2. HRMS $[C_{28}H_{28}ClFN_6O_3 + H]^+$: 551.19682 calculated, 551.19663 found.

(*R*)-1-Acryloyl-*N*-(4-((3-ethynylphenyl)amino)-7-(prop-2-yn-1-yloxy)quinazolin-6-yl)pyrrolidine-2-carboxamide (9)

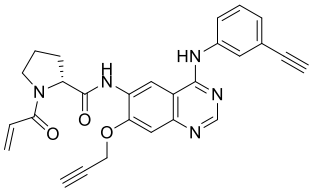

The title compound was synthesized from **30** (80.0 mg, 194 µmol) and acryloyl chloride according to general procedure B. The crude was purified by automated column chromatography (0 – 10% MeOH/DCM) to afford the product (47.0 mg, 101 µmol, 52%). ^{1}H NMR (400 MHz, DMSO) δ 9.87 – 9.82 (2x s, 1H), 9.82 – 9.67 (2x s, 1H), 8.91 – 8.77 (2x s, 1H), 8.56 – 8.53 (2x s, 1H), 7.99 (t, *J* = 1.9 Hz, 1H), 7.85 (ddd, *J* = 8.4, 2.3, 1.1 Hz, 1H), 7.41 – 7.35 (m, 2H), 7.23 – 7.18 (2x dt, *J* = 7.6, 1.3 Hz, 1H), 6.70 – 6.43 (2x dd, *J* = 16.7, 10.3 Hz, 1H), 6.24 – 6.16 (2x dd, *J* = 16.7, 2.4 Hz, 1H), 5.75 – 5.70 (2x dd, *J* = 10.3, 2.4 Hz, 1H), 5.09 (d, *J* = 2.5 Hz, 2H), 4.97 – 4.80 (2x dd, *J* = 8.5, 3.0 Hz, 1H), 4.22 – 4.17 (2x s, 1H), 3.78 – 3.48 (m, 3H), 2.42 – 1.85 (m, 4H) (the spectrum was accompanied by rotamer peaks). ^{13}C NMR (101 MHz, DMSO) δ 171.47, 170.79, 163.87, 163.81, 157.02, 154.34, 154.00, 153.76, 152.82, 149.20, 148.62, 139.83, 139.67, 129.27, 129.08, 128.83, 128.79, 127.65, 127.48, 127.45, 126.84, 126.61, 126.47, 125.18, 125.06, 123.01, 122.91, 121.69, 121.66, 117.46, 115.41, 109.56, 109.42, 108.44, 108.20, 83.61, 83.55, 80.56, 80.50, 79.35, 78.34, 78.32, 60.07, 59.75, 56.64, 56.61, 47.03, 46.75, 32.00, 29.09, 24.40, 22.29 (the spectrum was accompanied by rotamer peaks). LCMS (Fleet, 10 → 90%): t_r = 4.78 min, m/z: 466.4. HRMS $[C_{27}H_{23}N_5O_3 + H]^+$: 466.18737 calculated, 466.18736 found.

(*R*)-1-Acryloyl-*N*-(4-((3-chloro-4-fluorophenyl)amino)-7-(prop-2-yn-1-yloxy)quinazolin-6-yl)pyrrolidine-2-carboxamide (10)

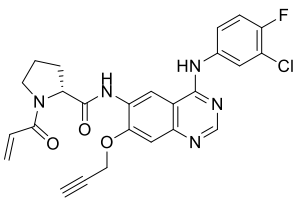

The title compound was synthesized from **29** (80.0 mg, 182 µmol) and acryloyl chloride according to general procedure B. The crude was purified by automated column chromatography (0 – 10% MeOH/DCM) to afford the product (19 mg, 38 µmol, 21%). ^{1}H NMR (400 MHz, DMSO) δ 9.90 – 9.87 (2x s, 1H), 9.83 – 9.68 (2x s, 1H), 8.90 – 8.75 (2x s, 1H), 8.55 – 8.52 (2x s, 1H), 8.09 (dd, *J* = 6.9, 2.6 Hz, 1H), 7.78 (ddd, *J* = 9.1, 4.4, 2.6 Hz, 1H), 7.45 – 7.37 (m, 2H), 6.71 – 6.43 (2x dd, *J* = 16.7, 10.3 Hz, 1H), 6.23 – 6.15 (2x dd, *J* = 16.6, 2.4 Hz, 1H), 5.75 – 5.69 (2x dd, *J* = 10.3, 2.3 Hz, 1H), 5.11 – 5.08 (2x d, *J* = 2.4 Hz, 2H), 4.97 – 4.80 (2x dd, *J* = 8.5, 2.9 Hz, 1H), 3.77 – 3.48 (m, 3H), 2.41 – 1.84 (m, 4H) (the spectrum was accompanied by rotamer peaks). ^{13}C NMR (101 MHz, DMSO) δ 171.48, 170.81, 163.86, 163.78, 156.91, 153.90, 153.67, 153.22 (d, $J_{(C–F)}$ = 242.9 Hz), 152.79, 152.10, 149.10, 148.54, 136.81 (d, $J_{(C–F)}$ = 2.9 Hz), 129.30, 129.07, 127.66, 127.54, 127.49, 126.94, 123.89, 123.74, 122.77 (d, $J_{(C–F)}$ = 6.6 Hz), 122.63 (d, $J_{(C–F)}$ = 6.9 Hz), 118.69 (d, $J_{(C–F)}$ = 17.9 Hz), 118.66 (d, $J_{(C–F)}$ = 18.3 Hz), 117.11, 116.45 (d,

$J_{(C–F)}$ = 21.5 Hz), 116.42 (d, $J_{(C–F)}$ = 21.4 Hz), 115.14, 109.41, 109.28, 108.45, 108.22, 79.38, 78.33, 78.30, 60.06, 59.73, 56.61, 47.03, 46.74, 31.99, 29.09, 24.39, 22.27 (the spectrum was accompanied by rotamer peaks). LCMS (Fleet, 10 → 90%): t_r = 4.95 min, m/z: 494.2. HRMS [$C_{25}H_{21}ClFN_5O_3$ + H]$^+$: 494.13897 calculated, 494.13893 found.

(*R*)-1-Acetyl-*N*-(4-((3-ethynylphenyl)amino)-7-(prop-2-yn-1-yloxy)quinazolin-6-yl)pyrrolidine-2-carboxamide (11)

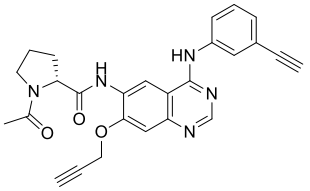

The title compound was synthesized from **30** (80.0 mg, 194 µmol) and acetyl chloride according to general procedure B. The crude was purified by HPLC (Agilent, 29 – 35% MeCN in 0.2% TFA (aq.)) after which the fractions were concentrated and traces of TFA were removed by coevaporation with 1:1 MeCN/H_2O (20 mL). The residue was dissolved in DCM (15 mL) and washed with 1 M $NaHCO_3$ (aq.) (3x5 mL). The organic layer was dried over Na_2SO_4, filtered and concentrated to afford the product (63.0 mg, 139 µmol, 72%). ^{1}H NMR (400 MHz, DMSO) δ 11.46 (br s, 1H), 10.11 – 9.90 (2x s, 1H), 9.18 – 9.01 (2x s, 1H), 8.92 – 8.88 (2x s, 1H), 7.80 – 7.78 (2x t, *J* = 1.9 Hz, 1H), 7.69 – 7.65 (m, 1H), 7.56 – 7.53 (2x s, 1H), 7.52 – 7.47 (2x t, *J* = 7.9 Hz, 1H), 7.44 – 7.40 (2x dt, *J* = 7.7, 1.4 Hz, 1H), 5.17 (d, *J* = 2.4 Hz, 2H), 4.83 – 4.72 (2x dd, *J* = 8.5, 3.0 Hz, 1H), 4.28 – 4.26 (2x s, 1H), 3.85 – 3.83 (2x t, *J* = 2.4 Hz, 1H), 3.66 – 3.39 (m, 2H), 2.21 – 1.84 (m, 7H) (the spectrum was accompanied by rotamer peaks). ^{13}C NMR (101 MHz, DMSO) δ 171.89, 171.29, 169.23, 168.68, 159.14, 159.09, 159.04, 158.78, 158.42, 158.06, 155.85, 154.54, 150.53, 150.06, 137.78, 137.28, 137.14, 136.94, 129.81, 129.69, 129.58, 129.34, 129.28, 128.92, 128.13, 128.05, 125.70, 125.65, 122.22, 122.16, 120.10, 118.60, 117.21, 115.73, 114.32, 111.42, 107.64, 107.54, 101.37, 101.06, 82.90, 82.86, 81.49, 81.43, 80.33, 80.30, 77.42, 60.68, 59.75, 57.39, 47.79, 46.48, 32.11, 29.31, 24.48, 22.61, 22.36, 22.28 (the spectrum was accompanied by rotamer peaks). LCMS (Fleet, 10 → 90%): t_r = 4.52 min, m/z: 454.2. HRMS [$C_{26}H_{23}N_5O_3$ + H]$^+$: 454.18737 calculated, 454.18728 found.

(*R*)-1-Acetyl-*N*-(4-((3-chloro-4-fluorophenyl)amino)-7-(prop-2-yn-1-yloxy)quinazolin-6-yl)pyrrolidine-2-carboxamide (12)

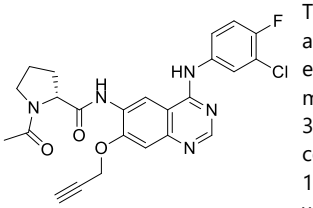

The title compound was synthesized from **29** (43 mg, 98 µmol) and acetyl chloride according to general procedure B (after 16 h of stirring, extra DIPEA (0.56 eq.) and acetyl chloride (0.56 eq.) were added and the mixture stirred for 4 h). The crude was purified by HPLC (Agilent, 30 – 32% MeCN in 0.2% TFA (aq.)) after which the fractions were concentrated and traces of TFA were removed by coevaporation with 1:1 MeCN/H_2O (20 mL). The residue was dissolved in DCM (15 mL) and washed with 1 M $NaHCO_3$ (aq.) (3x5 mL). The organic layer was dried over Na_2SO_4, filtered and concentrated to afford the product (23 mg, 48 µmol, 49%). ^{1}H NMR (400 MHz, DMSO) δ 11.42 – 11.37 (2x s, 1H), 10.09 – 9.89 (2x s, 1H), 9.16 – 8.98 (2x s, 1H), 8.91 – 8.88 (2x s, 1H), 7.96 – 7.92 (2x dd, *J* = 6.8, 2.6 Hz, 1H), 7.67 – 7.62 (2x ddd, *J* = 9.1, 4.4, 2.5 Hz, 1H), 7.58 – 7.50 (m, 2H), 5.18 – 5.16 (2x d, *J* = 2.5 Hz, 2H), 4.82 – 4.71 (2x dd, *J* = 8.6, 3.0 Hz, 1H), 3.87 – 3.84 (2x t, *J* = 2.2 Hz, 1H), 3.65 – 3.39 (m, 2H), 2.42 – 1.82 (m, 7H) (the spectrum was accompanied by rotamer peaks). ^{13}C NMR (101 MHz, DMSO) δ 171.86, 171.28, 169.15, 168.59, 158.96, 158.54, 158.19, 157.83, 154.40, 154.03, 150.24, 138.35, 137.43, 134.24 (d, $J_{(C–F)}$ = 3.4 Hz), 129.51, 128.80, 127.03, 126.97, 125.61 (d, $J_{(C–F)}$ = 7.2 Hz), 119.23 (d, $J_{(C–F)}$ = 18.8 Hz), 118.27, 116.94 (d, $J_{(C–F)}$ = 22.1 Hz), 115.45, 107.62, 101.39, 80.32, 80.29, 77.46, 77.44, 59.68, 57.33, 47.74, 46.43, 29.28, 24.44, 22.33, 22.27 (the spectrum was accompanied by rotamer peaks). LCMS (Fleet, 10 → 90%): t_r = 4.71 min, m/z: 482.2. HRMS [$C_{24}H_{21}ClFN_5O_3$ + H]$^+$: 482.13897 calculated, 482.13884 found.

2-Chloro-*N*-(2-((4-((3-ethynylphenyl)amino)-7-(prop-2-yn-1-yloxy)quinazolin-6-yl)amino)-2-oxoethyl)-2-fluoroacetamide (13)

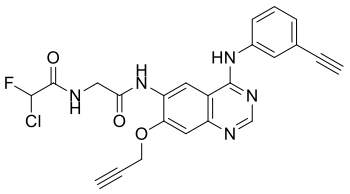

The title compound was synthesized from **32** (60.0 mg, 162 µmol) and 2-chloro-2-fluoroacetic acid according to general procedure A. The crude was purified by HPLC (Waters, 30 – 40% MeCN in 0.2% TFA (aq.)) after which the fractions were concentrated and traces of TFA were removed by coevaporation with 1:1 MeCN/H_2O (20 mL). The residue was dissolved in DCM (15 mL) and washed with 1 M $NaHCO_3$ (aq.) (3x5 mL). The organic layer was dried over Na_2SO_4, filtered and concentrated to afford the product (16 mg, 34 µmol, 21%). ^{1}H NMR (400 MHz, DMSO) δ 9.84 (s, 1H), 9.73 (s, 1H), 9.12 – 9.07 (m, 1H), 8.88 (s, 1H), 8.54 (s, 1H), 7.98 (t, *J* = 1.9 Hz, 1H), 7.84 (ddd, *J* = 8.3, 2.3, 1.1 Hz, 1H), 7.40 (s, 1H), 7.38 (t, *J* = 8.0 Hz, 1H), 7.20 (dt, *J* = 7.6, 1.3 Hz, 1H), 6.88 (d, *J* = 49.3 Hz, 1H), 5.11 (d, *J* = 2.4 Hz, 2H), 4.19 (s, 1H), 4.15 (d, *J* = 5.4 Hz, 2H), 3.76 – 3.70 (m, 1H). ^{13}C NMR (101 MHz, DMSO) δ 167.14, 164.13 (d, $J_{(C-F)}$ = 23.3 Hz), 157.00, 154.14, 152.81, 148.68, 139.76, 128.84, 126.87, 126.52, 125.05, 122.90, 121.68, 116.06, 109.50, 108.37, 93.86 (d, $J_{(C-F)}$ = 251.0 Hz), 83.59, 80.56, 79.49, 78.34, 56.47, 42.46. LCMS (Fleet, 10 → 90%): t_r = 4.76 min, m/z: 466.2. HRMS [$C_{23}H_{17}ClFN_5O_3$ + H]$^+$: 466.10767 calculated, 466.10730 found.

***N*-(2-((4-((3-Ethynylphenyl)amino)-7-(prop-2-yn-1-yloxy)quinazolin-6-yl)amino)-2-oxoethyl)but-2-ynamide (14)**

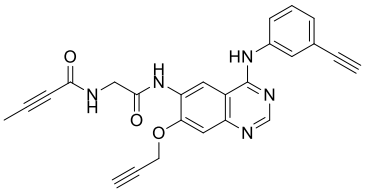

The title compound was synthesized from **32** (60.0 mg, 162 µmol) and but-2-ynoic acid according to general procedure A. The crude was loaded onto silica gel and purified by automated column chromatography (3 – 10% MeOH/DCM) to afford the product (9.0 mg, 21 µmol, 13%). ^{1}H NMR (500 MHz, DMSO) δ 9.83 (s, 1H), 9.61 (s, 1H), 8.89 – 8.85 (m, 2H), 8.53 (s, 1H), 7.98 (t, *J* = 1.9 Hz, 1H), 7.84 (ddd, *J* = 8.3, 2.3, 1.1 Hz, 1H), 7.40 – 7.36 (m, 2H), 7.20 (dt, *J* = 7.6, 1.3 Hz, 1H), 5.10 (d, *J* = 2.4 Hz, 2H), 4.20 (s, 1H), 4.03 (d, *J* = 6.1 Hz, 2H), 3.73 (t, *J* = 2.3 Hz, 1H), 1.99 (s, 3H). ^{13}C NMR (126 MHz, DMSO) δ 167.60, 156.97, 154.08, 153.08, 152.74, 148.60, 139.77, 128.83, 126.95, 126.50, 125.02, 122.87, 121.67, 115.83, 109.50, 108.31, 83.59, 83.41, 80.55, 79.47, 78.33, 75.31, 56.49, 42.63, 3.09. LCMS (Fleet, 10 → 90%): t_r = 4.50 min, m/z: 438.2. HRMS [$C_{25}H_{19}N_5O_3$ + H]$^+$: 438.15607 calculated, 438.15611 found.

(*E*)-4-(Dimethylamino)-*N*-(2-((4-((3-ethynylphenyl)amino)-7-(prop-2-yn-1-yloxy)quinazolin-6-yl)amino)-2-oxoethyl)but-2-enamide (15)

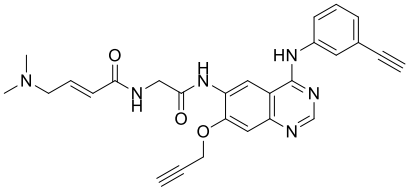

The title compound was synthesized from **32** (40.0 mg, 108 µmol) and (*E*)-4-(dimethylamino)but-2-enoic acid hydrochloride according to general procedure A (using 5 eq. DIPEA). The crude was purified by HPLC (Waters, 20–30% MeCN in 0.2% TFA (aq.)) after which the fractions were concentrated and traces of TFA were removed by coevaporation with 1:1 MeCN/H_2O (20 mL). The residue was dissolved in DCM (15 mL) and washed with 1 M $NaHCO_3$ (aq.) (3x5 mL). The organic layer was dried over Na_2SO_4, filtered and concentrated to afford the product (19 mg, 39 µmol, 37%). ^{1}H NMR (400 MHz, DMSO) δ 9.82 (s, 1H), 9.60 (s, 1H), 8.89 (s, 1H), 8.53 (s, 1H), 8.51 (t, *J* = 6.1 Hz, 1H), 7.98 (t, *J* = 1.9 Hz, 1H), 7.84 (ddd, *J* = 8.2, 2.2, 1.1 Hz, 1H), 7.42 – 7.33 (m, 2H), 7.20 (dt, *J* = 7.6, 1.3 Hz, 1H), 6.63 (dt, *J* = 15.5, 6.1 Hz, 1H), 6.17 (dt, *J* = 15.5, 1.6 Hz, 1H), 5.10 (d, *J* = 2.4 Hz, 2H), 4.19 (s, 1H), 4.10 (d, *J* = 6.0 Hz, 2H), 3.74 – 3.70 (m, 1H), 3.00 (dd, *J* = 6.2, 1.6 Hz, 2H), 2.14 (s, 6H). ^{13}C NMR (101 MHz, DMSO) δ 168.33, 165.27, 156.98, 154.06, 152.72, 148.59, 140.29, 139.79, 128.82, 127.02, 126.49, 125.49, 125.00, 122.85, 121.69, 115.66, 109.54, 108.30, 83.60, 80.52, 79.43, 78.30, 59.79, 56.52, 45.12, 42.77. LCMS (Fleet, 10 → 90%): t_r = 3.59 min, m/z: 483.2. HRMS [$C_{27}H_{26}N_6O_3$ + H]$^+$: 483.21392 calculated, 483.21389 found.

N-(2-((4-((3-Ethynylphenyl)amino)-7-(prop-2-yn-1-yloxy)quinazolin-6-yl)amino)-2-oxoethyl)acrylamide (16)

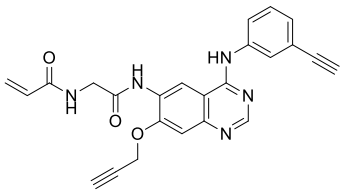

The title compound was synthesized from **32** (60.0 mg, 162 µmol) and acryloyl chloride according to general procedure B. The crude was loaded onto silica gel and purified by automated column chromatography (3 – 10% MeOH/DCM) to afford the product (9.0 mg, 21 µmol, 13%). ^{1}H NMR (500 MHz, DMSO) δ 9.83 (s, 1H), 9.64 (s, 1H), 8.89 (s, 1H), 8.60 (t, *J* = 6.0 Hz, 1H), 8.54 (s, 1H), 7.98 (t, *J* = 1.9 Hz, 1H), 7.84 (ddd, *J* = 8.3, 2.3, 1.1 Hz, 1H), 7.40 (s, 1H), 7.38 (t, *J* = 8.0 Hz, 1H), 7.20 (dt, *J* = 7.6, 1.3 Hz, 1H), 6.37 (dd, *J* = 17.1, 10.2 Hz, 1H), 6.16 (dd, *J* = 17.1, 2.1 Hz, 1H), 5.66 (dd, *J* = 10.2, 2.1 Hz, 1H), 5.10 (d, *J* = 2.4 Hz, 2H), 4.19 (s, 1H), 4.13 (d, *J* = 6.0 Hz, 2H), 3.73 (t, *J* = 2.3 Hz, 1H). ^{13}C NMR (126 MHz, DMSO) δ 168.21, 165.21, 156.98, 154.08, 152.76, 148.62, 139.78, 131.36, 128.83, 126.98, 126.50, 125.89, 125.01, 122.86, 121.68, 115.76, 109.52, 108.30, 83.60, 80.54, 79.47, 78.32, 56.52, 42.73. LCMS (Fleet, 10 → 90%): t_r = 4.30 min, m/z: 426.2. HRMS $[C_{24}H_{19}N_5O_3 + H]^+$: 426.15607 calculated, 426.15604 found.

2-Acetamido-*N*-(4-((3-ethynylphenyl)amino)-7-(prop-2-yn-1-yloxy)quinazolin-6-yl)acetamide (17)

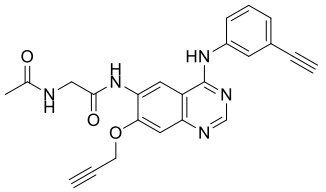

The title compound was synthesized from **32** (60.0 mg, 162 µmol) and acetyl chloride according to general procedure B. The crude was purified by HPLC (Agilent, 24 – 30% MeCN in 0.2% TFA (aq.)) after which the fractions were concentrated and traces of TFA were removed by coevaporation with 1:1 MeCN/H_2O (20 mL). The residue was dissolved in DCM (15 mL) and washed with 1 M $NaHCO_3$ (aq.) (3x5 mL). The organic layer was dried over Na_2SO_4, filtered and concentrated to afford the product (14 mg, 34 µmol, 21%). ^{1}H NMR (400 MHz, DMSO) δ 9.83 (s, 1H), 9.51 (s, 1H), 8.89 (s, 1H), 8.53 (s, 1H), 8.38 (t, *J* = 5.9 Hz, 1H), 7.98 (t, *J* = 1.9 Hz, 1H), 7.85 (ddd, *J* = 8.2, 2.2, 1.1 Hz, 1H), 7.39 (s, 1H), 7.38 (t, *J* = 8.0 Hz, 1H), 7.20 (dt, *J* = 7.6, 1.3 Hz, 1H), 5.10 (d, *J* = 2.4 Hz, 2H), 4.20 (s, 1H), 4.00 (d, *J* = 6.0 Hz, 2H), 3.74 (t, *J* = 2.3 Hz, 1H), 1.93 (s, 3H). ^{13}C NMR (101 MHz, DMSO) δ 169.96, 168.39, 156.98, 154.05, 152.67, 148.58, 139.79, 128.83, 126.97, 126.49, 125.00, 122.85, 121.68, 115.48, 109.53, 108.27, 83.59, 80.55, 79.47, 78.33, 56.58, 42.82, 22.46. LCMS (Fleet, 10 → 90%): t_r = 4.04 min, m/z: 414.2. HRMS $[C_{23}H_{19}N_5O_3 + H]^+$: 414.15607 calculated, 414.15607 found.

4-Chloro-7-fluoro-6-nitroquinazoline (18)

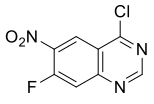

7-fluoro-6-nitroquinazolin-4(3*H*)-one (2.50 g, 12.0 mmol) was suspended in $SOCl_2$ (21.8 mL) and DMF (105 µL, 1.35 mmol). The mixture was heated to 75°C, stirred for 5 h and subsequently concentrated to afford the product (2.70 g, 11.9 mmol, 99%). ^{1}H NMR (500 MHz, DMSO) δ 8.72 (d, *J* = 8.2 Hz, 1H), 8.35 (s, 1H), 7.79 (d, *J* = 12.2 Hz, 1H). ^{13}C NMR (126 MHz, DMSO) δ 159.35, 157.68 (d, $J_{(C–F)}$ = 265.9 Hz), 153.69 (d, $J_{(C–F)}$ = 13.6 Hz), 150.18, 135.55 (d, $J_{(C–F)}$ = 9.5 Hz), 125.69, 119.32, 115.45 (d, $J_{(C–F)}$ = 21.3 Hz).

N-(3-Chloro-4-fluorophenyl)-7-fluoro-6-nitroquinazolin-4-amine (19)

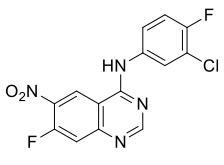

18 (1.40 g, 6.15 mmol) was mixed in 2-propanol (13.7 mL) after which DIPEA (2.15 mL, 12.3 mmol) and 3-chloro-4-fluoroaniline (895 mg, 6.15 mmol) were added. The mixture was stirred for 7 h, subsequently diluted in EtOAc (50 mL) and poured into H_2O (50 mL). The organic layer was isolated and the water layer extracted with EtOAc (2x50 mL). The combined organic layers were washed with brine (100 mL), dried over Na_2SO_4, filtered and concentrated. The crude was loaded onto silica gel and purified by automated column chromatography (25 – 75% EtOAc/pentane) to afford the product (760 mg, 2.26 mmol, 37%). ^{1}H NMR (500 MHz, DMSO) δ 10.49 (s, 1H), 9.56 (d, *J* = 7.9 Hz, 1H), 8.72 (s, 1H), 8.12 (dd, *J* = 7.0, 2.6 Hz, 1H), 7.84 (d, *J* = 12.4 Hz, 1H), 7.79 (ddd, *J* = 9.2, 4.5, 2.8 Hz, 1H), 7.48 (t, *J* = 9.1 Hz, 1H). ^{13}C NMR (126 MHz, DMSO) δ 158.38, 158.18, 156.46 (d, $J_{(C–F)}$ = 265.1 Hz), 154.04 (d, $J_{(C–F)}$ = 13.2 Hz), 153.96 (d, $J_{(C–F)}$ = 244.3 Hz), 135.53, 135.45, 124.41, 124.37, 123.13 (d, $J_{(C–F)}$ = 7.1 Hz), 119.00 (d, $J_{(C–F)}$ = 18.6 Hz), 116.77 (d, $J_{(C–F)}$ = 22.0 Hz), 115.07 (d, $J_{(C–F)}$ = 20.2 Hz), 111.27. LCMS (Fleet, 10 → 90%): t_r = 5.88 min, m/z: 337.2.

N-(3-Ethynylphenyl)-7-fluoro-6-nitroquinazolin-4-amine (20)

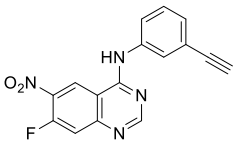

18 (2.20 g, 9.67 mmol) was mixed in 2-propanol (22 mL) after which DIPEA (3.38 mL, 19.3 mmol) and 3-ethynylaniline (985 µL, 9.67 mmol) were added. The mixture was stirred for 16 h, subsequently diluted in DCM (150 mL) and poured into H_2O (50 mL). The organic layer was isolated and the water layer extracted with DCM (2x50 mL). The combined organic layers were washed with brine (100 mL), dried over Na_2SO_4, filtered and concentrated. The crude was loaded onto silica gel and purified by automated column chromatography (25 – 75% EtOAc/pentane) to afford the product (2.40 g, 7.79 mmol, 81%). ^{1}H NMR (400 MHz, DMSO) δ 10.45 (s, 1H), 9.60 (d, *J* = 8.0 Hz, 1H), 8.72 (s, 1H), 7.99 (t, *J* = 1.8 Hz, 1H), 7.87 (ddd, *J* = 8.5, 2.2, 1.2 Hz, 1H), 7.82 (d, *J* = 12.5 Hz, 1H), 7.44 (t, *J* = 8.0 Hz, 1H), 7.29 (dt, *J* = 7.7, 1.2 Hz, 1H), 4.24 (s, 1H). ^{13}C NMR (101 MHz, DMSO) δ 158.47, 158.28, 156.44 (d, $J_{(C–F)}$ = 264.8 Hz), 154.13 (d, $J_{(C–F)}$ = 13.0 Hz), 138.61, 135.47 (d, $J_{(C–F)}$ = 10.0 Hz), 129.10, 127.73, 125.58, 124.52, 123.29, 121.93, 115.02 (d, $J_{(C–F)}$ = 19.9 Hz), 111.40, 83.25, 80.95. LCMS (Fleet, 10 → 90%): t_r = 5.38 min, m/z: 309.2.

N-(3-Chloro-4-fluorophenyl)-6-nitro-7-(prop-2-yn-1-yloxy)quinazolin-4-amine (21)

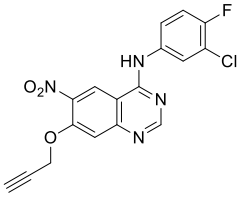

19 (730 mg, 2.17 mmol) was mixed in THF (10 mL) after which propargyl alcohol (0.5 mL, 8.67 mmol) was added. The mixture was cooled down to 0°C and potassium *tert*-butoxide (487 mg, 4.34 mmol) was added. After stirring for 5 min, the mixture was allowed to warm to RT and continued to stir for 16 h. The mixture was diluted in EtOAc (20 mL) and poured into H_2O (20 mL). The organic layer was isolated and the water layer extracted with EtOAc (2x20 mL). The combined organic layers were washed with brine (50 mL), dried over Na_2SO_4, filtered and concentrated. The crude loaded onto silica gel and purified by automated column chromatography (10 – 75% EtOAc/pentane) to afford the product (737 mg, 1.98 mmol, 91%). ^{1}H NMR (400 MHz, DMSO) δ 10.38 (br s, 1H), 9.24 (s, 1H), 8.64 (s, 1H), 8.13 (dd, *J* = 6.9, 2.6 Hz, 1H), 7.76 (ddd, *J* = 9.0, 4.3, 2.7 Hz, 1H), 7.52 (s, 1H), 7.43 (t, *J* = 9.1 Hz, 1H), 5.17 (d, *J* = 2.4 Hz, 2H), 3.77 (t, *J* = 2.3 Hz, 1H). ^{13}C NMR (101 MHz, DMSO) δ 157.86, 157.60, 153.54 (d, $J_{(C–F)}$ = 243.4 Hz), 153.15, 152.26, 138.69, 136.60, 123.88, 122.71 (d, $J_{(C–F)}$ = 6.9 Hz), 122.21, 118.87 (d, $J_{(C–F)}$ = 18.3 Hz), 116.63 (d, $J_{(C–F)}$ = 21.6 Hz), 110.98, 108.86, 79.93, 77.73, 57.43. LCMS (Fleet, 10 → 90%): t_r = 5.41 min, m/z: 373.3.

N-(3-Ethynylphenyl)-6-nitro-7-(prop-2-yn-1-yloxy)quinazolin-4-amine (22)

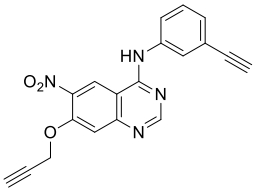

20 (2.27 g, 7.35 mmol) was mixed in THF (24 mL) after which propargyl alcohol (1.70 mL, 29.4 mmol) was added. The mixture was cooled down to 0°C and potassium *tert*-butoxide (1.65 g, 14.7 mmol) was added. After stirring for 5 min, the mixture was allowed to warm to RT and continued to stir for 22 h. The mixture was diluted in H_2O (25 mL) and filtered. The solids were collected and dried to afford the product (2.53 g, 7.35 mmol, quant.) which was used as such in subsequent reaction. ^{1}H NMR (400 MHz, DMSO) δ 10.13 (s, 1H), 9.28 (s, 1H), 8.68 (s, 1H), 8.03 (t, *J* = 1.8 Hz, 1H), 7.88 (ddd, *J* = 8.3, 2.3, 1.1 Hz, 1H), 7.56 (s, 1H), 7.42 (t, *J* = 7.9 Hz, 1H), 7.26 (dt, *J* = 7.6, 1.3 Hz, 1H), 5.19 (d, *J* = 2.4 Hz, 2H), 4.23 (s, 1H), 3.78 (t, *J* = 2.3 Hz, 1H). ^{13}C NMR (101 MHz, DMSO) δ 157.99, 157.62, 153.11, 152.24, 138.93, 138.89, 129.06, 127.29, 125.14, 122.86, 122.10, 121.88, 111.13, 108.59, 83.35, 80.83, 79.95, 77.70, 57.45. LCMS (Finnigan, 10 → 90%): t_r = 5.86 min, m/z: 345.1.

N^4-(3-Chloro-4-fluorophenyl)-7-(prop-2-yn-1-yloxy)quinazoline-4,6-diamine (23)

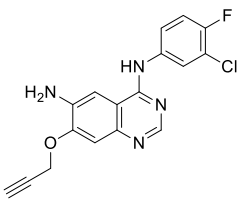

21 (717 mg, 1.92 mmol) was mixed in EtOH/H_2O (30:1, 43 mL) after which iron powder (537 mg, 9.62 mmol) and NH_4Cl (309 mg, 5.77 mmol) were added. The mixture was heated to 80°C and stirred for 2.5 h. The mixture was filtered over Celite and subsequently concentrated to afford the product (438 mg, 1.28 mmol, 66%). ^{1}H NMR (400 MHz, DMSO) δ 9.44 (s, 1H), 8.38 (s, 1H), 8.19 (dd, *J* = 6.9, 2.7 Hz, 1H), 7.81 (ddd, *J* = 9.1, 4.3, 2.7 Hz, 1H), 7.43 – 7.36 (m, 2H), 7.22 (s, 1H), 5.40 (s, 2H), 5.04 (d, *J* = 2.4 Hz, 2H), 3.73 – 3.67 (m, 1H). ^{13}C NMR (101 MHz, DMSO) δ 155.10, 152.71 (d, $J_{(C–F)}$ = 242.0 Hz), 150.39,

150.38, 144.42, 138.57, 137.49 (d, $J_{(C–F)}$ = 2.9 Hz), 122.54, 121.50 (d, $J_{(C–F)}$ = 6.7 Hz), 118.65 (d, $J_{(C–F)}$ = 18.2 Hz), 116.44 (d, $J_{(C–F)}$ = 21.6 Hz), 110.86, 107.55, 101.34, 79.04, 78.71, 56.06. LCMS (Fleet, 10 → 90%): t_r = 4.78 min, m/z: 343.3.

*N*⁴-(3-Ethynylphenyl)-7-(prop-2-yn-1-yloxy)quinazoline-4,6-diamine (24)

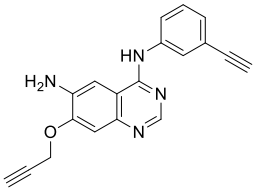

22 (140 mg, 407 µmol) was mixed in EtOH/H_2O (30:1, 9 mL) after which iron powder (114 mg, 2.03 mmol) and NH_4Cl (65.2 mg, 1.22 mmol) were added. The mixture was heated to 80°C and stirred for 2.5 h. The mixture was filtered over Celite and subsequently concentrated to afford the product (128 mg, 407 µmol, quant.). ^{1}H NMR (500 MHz, DMSO) δ 10.18 (br s, 1H), 8.56 (s, 1H), 7.95 (t, *J* = 1.9 Hz, 1H), 7.82 – 7.78 (m, 1H), 7.58 (s, 1H), 7.41 (t, *J* = 7.9 Hz, 1H), 7.29 (s, 1H), 7.26 (dt, *J* = 7.6, 1.3 Hz, 1H), 5.68 (br s, 2H), 5.07 (d, *J* = 2.4 Hz, 2H), 4.23 (s, 1H), 3.76 (t, *J* = 2.4 Hz, 1H). ^{13}C NMR (126 MHz, DMSO) δ 156.32, 151.15, 148.29, 139.67, 139.04, 129.00, 127.42, 125.73, 123.53, 121.83, 110.09, 103.63, 101.77, 83.38, 80.85, 79.52, 78.22, 56.39. LCMS (Fleet, 10 → 90%): t_r = 4.54 min, m/z: 315.2.

tert-Butyl (*R*)-2-((4-((3-chloro-4-fluorophenyl)amino)-7-(prop-2-yn-1-yloxy)quinazolin-6-yl)carbamoyl)pyrrolidine-1-carboxylate (25)

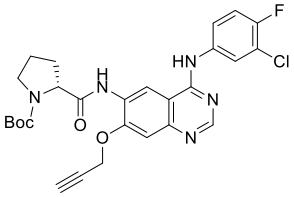

The title compound was synthesized from **23** (418 mg, 1.22 mmol) and Boc-D-Pro-OH according to general procedure A. The crude was purified by automated column chromatography (2 – 10% MeOH/DCM) to afford the product (488 mg, 0.904 mmol, 74%). ^{1}H NMR (400 MHz, DMSO) δ 9.89 (s, 1H), 9.56 – 9.45 (2x s, 1H), 8.93 – 8.88 (2x s, 1H), 8.53 (s, 1H), 8.08 (s, 1H), 7.81 – 7.73 (m, 1H), 7.42 (t, *J* = 9.2 Hz, 1H), 7.39 (s, 1H), 5.09 (d, *J* = 2.4 Hz, 2H), 4.58 – 4.44 (m, 1H), 3.75 – 3.69 (m, 1H), 3.50 – 3.38 (m, 1H), 2.37 – 2.08 (m, 1H), 2.07 – 1.81 (m, 1H), 1.43 – 1.28 (2x s, 9H) (three proline protons were not observed). LCMS (Finnigan, 10 → 90%): t_r = 6.65 min, m/z: 540.1.

tert-Butyl (*R*)-2-((4-((3-ethynylphenyl)amino)-7-(prop-2-yn-1-yloxy)quinazolin-6-yl)carbamoyl)pyrrolidine-1-carboxylate (26)

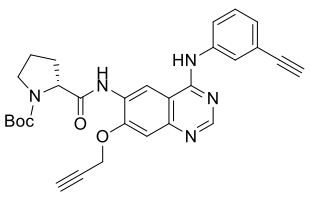

The title compound was synthesized from **24** (837 mg, 2.66 mmol) and Boc-D-Pro-OH according to general procedure A. The crude was purified by automated column chromatography (2 – 10% MeOH/DCM) to afford the product (1.32 g, 2.58 mmol, 97%). ^{1}H NMR (400 MHz, DMSO) δ 9.83 (s, 1H), 9.54 – 9.44 (2x s, 1H), 8.94 – 8.88 (2x s, 1H), 8.53 (s, 1H), 7.99 – 7.93 (m, 1H), 7.87 – 7.82 (m, 1H), 7.39 (s, 1H), 7.38 (t, *J* = 7.9 Hz, 1H), 7.20 (d, *J* = 7.6 Hz, 1H), 5.09 (d, *J* = 2.4 Hz, 2H), 4.56 – 4.45 (m, 1H), 4.19 (s, 1H), 3.75 – 3.69 (m, 1H), 3.46 – 3.38 (m, 2H), 2.31 – 2.11 (m, 1H), 2.09 – 1.80 (m, 3H), 1.44 – 1.29 (2x s, 9H). LCMS (Fleet, 10 → 90%): t_r = 5.70 min, m/z: 512.3.

tert-Butyl (*S*)-2-((4-((3-chloro-4-fluorophenyl)amino)-7-(prop-2-yn-1-yloxy)quinazolin-6-yl)carbamoyl)pyrrolidine-1-carboxylate (27)

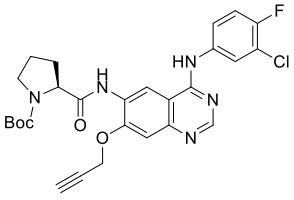

The title compound was synthesized from **23** (104 mg, 303 µmol) and Boc-L-Pro-OH according to general procedure A. The crude purified by automated column chromatography (2 – 10% MeOH/DCM) and used as such in subsequent reaction (yield: 131 mg). LCMS (Finnigan, 10 → 90%): t_r = 6.87 min, m/z: 540.2.

***tert*-Butyl (2-((4-((3-ethynylphenyl)amino)-7-(prop-2-yn-1-yloxy)quinazolin-6-yl)amino)-2-oxoethyl)carbamate (28)**

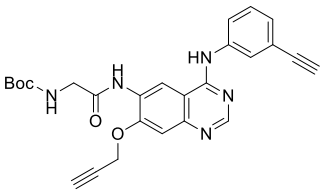

The title compound was synthesized from **24** (749 mg, 2.38 mmol) and Boc-Gly-OH according to general procedure A. The crude was loaded onto Celite and purified by automated column chromatography (2 – 10% MeOH/DCM) to afford the product (910 mg, 1.93 mmol, 81%). ^{1}H NMR (400 MHz, DMSO) δ 9.84 (s, 1H), 9.44 (s, 1H), 8.95 (s, 1H), 8.54 (s, 1H), 7.98 (t, *J* = 1.9 Hz, 1H), 7.85 (ddd, *J* = 8.3, 2.3, 1.1 Hz, 1H), 7.41 (s, 1H), 7.38 (t, *J* = 7.9 Hz, 1H), 7.30 (t, *J* = 6.1 Hz, 1H), 7.20 (dt, *J* = 7.6, 1.3 Hz, 1H), 5.11 (d, *J* = 2.4 Hz, 2H), 4.18 (s, 1H), 3.87 (d, *J* = 6.1 Hz, 2H), 3.73 (t, *J* = 2.3 Hz, 1H), 1.42 (s, 9H). ^{13}C NMR (101 MHz, DMSO) δ 168.74, 157.01, 156.05, 154.01, 152.35, 148.46, 139.80, 128.82, 127.04, 126.51, 125.07, 122.92, 121.69, 114.93, 109.60, 108.27, 83.61, 80.51, 79.47, 78.40, 78.26, 56.58, 44.06, 28.22. LCMS (Fleet, 10 → 90%): t_r = 5.31 min, m/z: 472.2.

(*R*)-*N*-(4-((3-Chloro-4-fluorophenyl)amino)-7-(prop-2-yn-1-yloxy)quinazolin-6-yl)pyrrolidine-2-carboxamide (29)

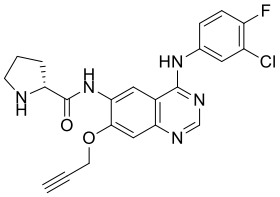

25 (468 mg, 867 µmol) was dissolved in DCM (8.6 mL) and cooled down to 0°C. TFA (2.6 mL) was added and the mixture was stirred at 0°C for 2.5 h. The mixture was quenched with 1 M $NaHCO_3$ (aq.) (50 mL) and the product extracted with DCM (3x50 mL). The combined organic layers were washed with brine (50 mL), dried over Na_2SO_4, filtered and concentrated. The crude was loaded onto silica gel and purified by automated column chromatography (0 – 10% MeOH/DCM) to afford the product (381 mg, 867 µmol, quant.). ^{1}H NMR (400 MHz, DMSO) δ 10.52 (s, 1H), 9.89 (s, 1H), 9.10 (s, 1H), 8.52 (s, 1H), 8.08 (dd, *J* = 6.9, 2.7 Hz, 1H), 7.77 (ddd, *J* = 9.1, 4.4, 2.7 Hz, 1H), 7.41 (t, *J* = 9.1 Hz, 1H), 7.40 (s, 1H), 5.14 (d, *J* = 2.4 Hz, 2H), 3.83 (dd, *J* = 9.1, 5.1 Hz, 1H), 3.75 (t, *J* = 2.3 Hz, 1H), 3.02 (dt, *J* = 10.2, 6.6 Hz, 1H), 2.84 (dt, *J* = 10.2, 6.4 Hz, 1H), 2.14 – 2.05 (m, 1H), 1.93 – 1.84 (m, 1H), 1.67 (p, *J* = 6.8 Hz, 2H) (the proline –NH was not observed). ^{13}C NMR (101 MHz, DMSO) δ 173.54, 156.89, 153.59, 153.18 (d, $J_{(C–F)}$ = 242.5 Hz), 151.50, 147.96, 136.87 (d, $J_{(C–F)}$ = 3.0 Hz), 127.28, 123.73, 122.63 (d, $J_{(C–F)}$ = 6.8 Hz), 118.65 (d, $J_{(C–F)}$ = 18.4 Hz), 116.41 (d, $J_{(C–F)}$ = 21.7 Hz), 111.36, 109.69, 108.20, 79.44, 78.19, 60.98, 56.90, 46.74, 30.37, 26.11. LCMS (Finnigan, 10 → 90%): t_r = 4.76 min, m/z: 440.2.

(*R*)-*N*-(4-((3-Ethynylphenyl)amino)-7-(prop-2-yn-1-yloxy)quinazolin-6-yl)pyrrolidine-2-carboxamide (30)

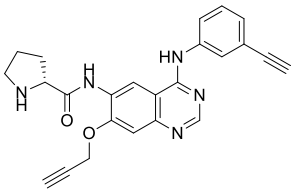

26 (1.25 g, 2.43 mmol) was dissolved in DCM (24 mL) and cooled down to 0°C. TFA (7.5 mL) was added and the mixture was stirred at 0°C for 3 h. The mixture was quenched with 1 M $NaHCO_3$ (aq.) (100 mL) and the product extracted with DCM (2x100 mL). The combined organic layers were washed with brine (100 mL), dried over Na_2SO_4, filtered and concentrated. The crude was loaded onto silica gel and purified by automated column chromatography (0 – 10% MeOH/DCM) to afford the product (561 mg, 1.36 mmol, 56%). ^{1}H NMR (400 MHz, DMSO) δ 10.51 (s, 1H), 9.83 (s, 1H), 9.11 (s, 1H), 8.52 (s, 1H), 7.96 (t, *J* = 1.9 Hz, 1H), 7.84 (ddd, *J* = 8.3, 2.3, 1.1 Hz, 1H), 7.42 – 7.32 (m, 2H), 7.20 (dt, *J* = 7.6, 1.3 Hz, 1H), 5.14 (d, *J* = 2.4 Hz, 2H), 4.19 (s, 1H), 3.84 (dd, *J* = 9.1, 5.1 Hz, 1H), 3.75 (t, *J* = 2.2 Hz, 1H), 3.02 (dt, *J* = 10.2, 6.6 Hz, 1H), 2.85 (dt, *J* = 10.2, 6.4 Hz, 1H), 2.16 – 2.04 (m, 1H), 1.96 – 1.83 (m, 1H), 1.67 (p, *J* = 6.8 Hz, 2H) (the proline –NH was not observed). ^{13}C NMR (101 MHz, DMSO) δ 173.52, 157.00, 153.69, 151.50, 148.02, 139.89, 128.80, 127.20, 126.41, 125.02, 122.88, 121.65, 111.60, 109.85, 108.17, 83.61, 80.50, 79.43, 78.21, 60.99, 56.89, 46.76, 30.38, 26.12. LCMS (Fleet, 10 → 90%): t_r = 3.63 min, m/z: 412.3.

(*S*)-*N*-(4-((3-Chloro-4-fluorophenyl)amino)-7-(prop-2-yn-1-yloxy)quinazolin-6-yl)pyrrolidine-2-carboxamide (31)

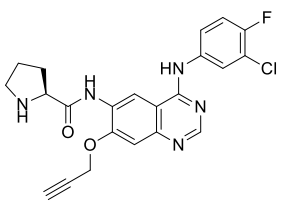

27 (120 mg, 222 µmol) was dissolved in DCM (0.7 mL) and cooled down to 0°C. TFA (0.7 mL) was added and the mixture was stirred at 0°C for 2 h. The mixture was quenched with 1 M $NaHCO_3$ (aq.) (30 mL) and the product extracted with EtOAc (3x30 mL). The combined organic layers were dried over Na_2SO_4, filtered and concentrated. The crude purified by automated column chromatography (0 – 10% MeOH/DCM) to afford the product (83.0 mg, 189 µmol, 85%). ^{1}H NMR (400 MHz, DMSO) δ 10.52 (s, 1H), 9.88 (s, 1H), 9.08 (s, 1H), 8.51 (s, 1H), 8.07 (dd, *J* = 6.9, 2.7 Hz, 1H), 7.76 (ddd, *J* = 9.1, 4.4, 2.7 Hz, 1H), 7.39 (t, *J* = 9.1 Hz, 1H), 7.38 (s, 1H), 5.13 (d, *J* = 2.4 Hz, 2H), 3.84 (dd, *J* = 9.1, 5.1 Hz, 1H), 3.74 (t, *J* = 2.3 Hz, 1H), 3.02 (dt, *J* = 10.2, 6.6 Hz, 1H), 2.85 (dt, *J* = 10.2, 6.7 Hz, 1H), 2.15 – 2.05 (m, 1H), 1.93 – 1.84 (m, 1H), 1.67 (p, *J* = 6.8 Hz, 2H) (the proline –NH was not observed). ^{13}C NMR (101 MHz, DMSO) δ 173.63, 156.94, 153.65, 153.27 (d, $J_{(C–F)}$ = 242.8 Hz), 151.59, 148.02, 136.91 (d, $J_{(C–F)}$ = 3.1 Hz), 127.31, 123.76, 122.64 (d, $J_{(C–F)}$ = 6.8 Hz), 118.75 (d, $J_{(C–F)}$ = 18.4 Hz), 116.44 (d, $J_{(C–F)}$ = 21.5 Hz), 111.50, 109.75, 108.21, 79.47, 78.22, 61.04, 56.96, 46.82, 30.45, 26.16. LCMS (Finnigan, 10 → 90%): t_r = 4,92 min, m/z: 440.2.

2-Amino-*N*-(4-((3-ethynylphenyl)amino)-7-(prop-2-yn-1-yloxy)quinazolin-6-yl)acetamide (32)

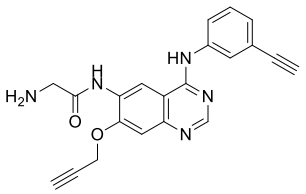

28 (810 mg, 1.72 mmol) was dissolved in DCM (8.5 mL) and cooled down to 0°C. TFA (5.2 mL) was added after which the mixture was allowed to warm to RT and stirred for 3 h. The mixture was quenched with 1 M $NaHCO_3$ (aq.) (100 mL) and DCM (100 mL) was added. The mixture was filtered and the solids were collected. From the filtrate, the layers were separated and the water layer was extracted with DCM (2x50 mL). The combined organic layers were washed with brine (100 mL), dried over Na_2SO_4, filtered and concentrated. The residue was combined with the collected solids, loaded onto silica gel and purified by automated column chromatography (0 – 5% MeOH/DCM) to afford the product (396 mg, 1.07 mmol, 62%). ^{1}H NMR (400 MHz, DMSO) δ 9.83 (s, 1H), 9.13 (s, 1H), 8.52 (s, 1H), 7.96 (t, *J* = 1.9 Hz, 1H), 7.84 (ddd, *J* = 8.2, 2.2, 1.1 Hz, 1H), 7.41 (s, 1H), 7.38 (t, *J* = 7.9 Hz, 1H), 7.20 (dt, *J* = 7.6, 1.3 Hz, 1H), 5.15 (d, *J* = 2.4 Hz, 2H), 4.19 (s, 1H), 3.74 (t, *J* = 2.3 Hz, 1H), 3.36 (s, 2H) (three –NHs were not observed). ^{13}C NMR (101 MHz, DMSO) δ 171.82, 157.00, 153.70, 151.44, 148.00, 139.87, 128.80, 127.24, 126.43, 125.07, 122.94, 121.65, 111.82, 109.82, 108.14, 83.61, 80.52, 79.49, 78.23, 56.74, 45.20. LCMS (Fleet, 10 → 90%): t_r = 3.31 min, m/z: 372.2.

References

1. Simon, G. M., Niphakis, M. J. & Cravatt, B. F. Determining target engagement in living systems. *Nat. Chem. Biol.* **9**, 200–205 (2013).
2. Schürmann, M., Janning, P., Ziegler, S. & Waldmann, H. Small-Molecule Target Engagement in Cells. *Cell Chem. Biol.* **23**, 435–441 (2016).
3. Molina, D. M., Jafari, R., Ignatushchenko, M., Seki, T., Larsson, E. A., Dan, C., Sreekumar, L., Cao, Y. & Nordlund, P. Monitoring Drug Target Engagement in Cells and Tissues Using the Cellular Thermal Shift Assay. *Science* **341**, 84–87 (2013).
4. Robers, M. B., Dart, M. L., Woodroofe, C. C., Zimprich, C. A., Kirkland, T. A., Machleidt, T., Kupcho, K. R., Levin, S., Hartnett, J. R., Zimmerman, K., Niles, A. L., Ohana, R. F., Daniels, D. L., Slater, M., Wood, M. G., Cong, M., Cheng, Y.-Q. & Wood, K. V. Target engagement and drug residence time can be observed in living cells with BRET. *Nat. Commun.* **6**, 10091 (2015).
5. Cravatt, B. F., Wright, A. T. & Kozarich, J. W. Activity-Based Protein Profiling: From Enzyme Chemistry to Proteomic Chemistry. *Annu. Rev. Biochem.* **77**, 383–414 (2008).
6. Niphakis, M. J. & Cravatt, B. F. Enzyme Inhibitor Discovery by Activity-Based Protein Profiling. *Annu. Rev. Biochem.* **83**, 341–377 (2014).
7. Kolb, H. C., Finn, M. G. & Sharpless, K. B. Click Chemistry: Diverse Chemical Function from a Few Good Reactions. *Angew. Chem. Int. Ed.* **40**, 2004–2021 (2001).
8. Rostovtsev, V. V., Green, L. G., Fokin, V. V. & Sharpless, K. B. A Stepwise Huisgen Cycloaddition Process: Copper(I)-Catalyzed Regioselective "Ligation" of Azides and Terminal Alkynes. *Angew. Chem. Int. Ed.* **41**, 2596–2599 (2002).
9. Zhao, Q., Ouyang, X., Wan, X., Gajiwala, K. S., Kath, J. C., Jones, L. H., Burlingame, A. L. & Taunton, J. Broad-Spectrum Kinase Profiling in Live Cells with Lysine-Targeted Sulfonyl Fluoride Probes. *J. Am. Chem. Soc.* **139**, 680–685 (2017).
10. van der Wel, T., Hilhorst, R., den Dulk, H., van den Hooven, T., Prins, N. M., Wijnakker, J. A. P. M., Florea, B. I., Lenselink, E. B., van Westen, G. J. P., Ruijtenbeek, R., Overkleeft, H. S., Kaptein, A., Barf, T. & van der Stelt, M. Chemical genetics strategy to profile kinase target engagement reveals role of FES in neutrophil phagocytosis. *Nat. Commun.* **11**, 3216 (2020).
11. Keating, G. M. Afatinib: A Review in Advanced Non-Small Cell Lung Cancer. *Target. Oncol.* **11**, 825–835 (2016).
12. Shindo, N., Fuchida, H., Sato, M., Watari, K., Shibata, T., Kuwata, K., Miura, C., Okamoto, K., Hatsuyama, Y., Tokunaga, K., Sakamoto, S., Morimoto, S., Abe, Y., Shiroishi, M., Caaveiro, J. M. M., Ueda, T., Tamura, T., Matsunaga, N., Nakao, T., Koyanagi, S., Ohdo, S., Yamaguchi, Y., Hamachi, I., Ono, M. & Ojida, A. Selective and reversible modification of kinase cysteines with chlorofluoroacetamides. *Nat. Chem. Biol.* **15**, 250–258 (2019).
13. Barf, T., Covey, T., Izumi, R., van de Kar, B., Gulrajani, M., van Lith, B., van Hoek, M., de Zwart, E., Mittag, D., Demont, D., Verkaik, S., Krantz, F., Pearson, P. G., Ulrich, R. & Kaptein, A. Acalabrutinib (ACP-196): A Covalent Bruton Tyrosine Kinase Inhibitor with a Differentiated Selectivity and In Vivo Potency Profile. *J. Pharmacol. Exp. Ther.* **363**, 240–252 (2017).
14. Wind, S., Schnell, D., Ebner, T., Freiwald, M. & Stopfer, P. Clinical Pharmacokinetics and Pharmacodynamics of Afatinib. *Clin. Pharmacokinet.* **56**, 235–250 (2017).
15. Cross, D. A. E., Ashton, S. E., Ghiorghiu, S., Eberlein, C., Nebhan, C. A., Spitzler, P. J., Orme, J. P., Finlay, M. R. V., Ward, R. A., Mellor, M. J., Hughes, G., Rahi, A., Jacobs, V. N., Brewer, M. R., Ichihara, E., Sun, J., Jin, H., Ballard, P., Al-Kadhimi, K., Rowlinson, R., Klinowska, T., Richmond, G. H. P., Cantarini, M., Kim, D.-W., Ranson, M. R. & Pao, W. AZD9291, an Irreversible EGFR TKI, Overcomes T790M-Mediated Resistance to EGFR Inhibitors in Lung Cancer. *Cancer Discov.* **4**, 1046–1061 (2014).
16. Tu, Y., OuYang, Y., Xu, S., Zhu, Y., Li, G., Sun, C., Zheng, P. & Zhu, W. Design, synthesis, and docking studies of afatinib analogs bearing cinnamamide moiety as potent EGFR inhibitors. *Bioorg. Med. Chem.* **24**, 1495–1503 (2016).
17. Sun, H., Ren, Y., Hou, W., Li, L., Zeng, F., Li, S., Ma, Y., Liu, X., Chen, S. & Zhang, Z. Focusing on probe-modified peptides: a quick and effective method for target identification. *Chem. Commun.* **52**, 10225–10228 (2016).
18. Shinozuka, T., Tsukada, T., Fujii, K., Tokumaru, E., Matsui, Y., Wakimoto, S., Ogata, T., Araki, K., Sawamura, R., Watanabe, N., Mori, M. & Tanaka, J. Structure–Activity Relationship Studies of 3- or 4-Pyridine Derivatives of DS-6930. *ACS Med. Chem. Lett.* **10**, 358–362 (2019).
19. Lin, Z., Jia, L., Tomchick, D. R., Luo, X. & Yu, H. Substrate-Specific Activation of the Mitotic Kinase Bub1 through Intramolecular Autophosphorylation and Kinetochore Targeting. *Structure* **22**, 1616–1627 (2014).
20. Siemeister, G., Mengel, A., Fernández-Montalván, A. E., Bone, W., Schröder, J., Zitzmann-Kolbe, S., Briem, H., Prechtl, S., Holton, S. J., Mönning, U., von Ahsen, O., Johanssen, S., Cleve, A., Pütter, V., Hitchcock, M., von Nussbaum, F., Brands, M., Ziegelbauer, K. & Mumberg, D. Inhibition of BUB1 Kinase by BAY 1816032 Sensitizes Tumor Cells toward Taxanes, ATR, and PARP Inhibitors *In Vitro* and *In Vivo*. *Clin. Cancer Res.* **25**, 1404–1414 (2019).

6

Profiling of benzimidazole-based BUB1 inhibitors

Introduction

Eukaryotic cell division proceeds through four consecutive phases, one of which is mitosis. During mitosis, duplicated genetic material must be equally divided among the newly formed daughter cells. To accurately separate sister chromatids, microtubules emanating from the spindle poles must form bi-oriented attachments with kinetochores which are located at the centromeres of these chromatids.[1] Proper attachment is important for genomic integrity since mitotic progression with attachment errors can lead to gain and loss of chromosomes. An abnormal number of chromosomes, a state referred to as aneuploidy, is thought to contribute to tumorigenesis.[2] The process of forming correct kinetochore-microtubule attachments is therefore carefully monitored by a safety mechanism called the spindle assembly checkpoint (SAC). The SAC prevents mitotic progression to the anaphase before all chromosomes are correctly attached to the mitotic spindle.[3] Proper SAC functioning is therefore crucial for cell division and survival. As a result, interfering with the SAC and impairing chromosome segregation, has emerged as potential anti-cancer strategy.[2,4] Key proteins of the SAC, including kinases such as monopolar spindle 1 (MPS1) and budding uninhibited by benzimidazole 1 (BUB1), may therefore be interesting therapeutic targets.[2,4]

Taxanes are a class of microtubule targeting drugs, including paclitaxel and docetaxel, that are used for the treatment of various types of cancer, such as ovarian, breast and non-small cell lung cancer.[5,6] Taxane-based chemotherapy is usually associated with severe adverse effects, including bone marrow suppression, peripheral neuropathy and hypersensitivity reactions.[7] Lowering taxane exposure during anti-cancer therapy is therefore desired. Previously, it has been shown that genetically reducing MPS1 levels sensitized several cancer cell lines, including U2OS cells, to low doses (1 – 10 nM) of paclitaxel.[8] In line with these findings, another report showed that the efficacy of docetaxel could be enhanced by pharmacological MPS1 inhibition using small molecule NTRC0066-0 in a mouse xenograft model of human triple-negative breast cancer.[9] Similarly, a small molecule inhibitor of BUB1, BAY1816032 (**Figure 6.1**), was reported to synergistically inhibit a panel of cancer cell lines when combined with taxanes.[10] In a mouse xenograft model this combination of BUB1 inhibition and paclitaxel showed promising anti-tumor effects. Importantly, the combination therapy reduced tumor growth, but BAY1816032 as single agent treatment did not show efficacy *in vivo*. The reason for this is currently unknown, but low amounts of BUB1 protein are thought to be sufficient for proper SAC functioning.[11] Thus, incomplete BUB1 target engagement by BAY1816032 may explain its lack of efficacy as a single agent. The discovery of novel BUB1 inhibitors with the ability to exhibit full target engagement is, therefore, desired to test this hypothesis. Improving the physicochemical properties of compounds to increase their cell permeability may contribute to better target engagement. In addition, frequent exposure to kinase inhibitors may induce mutations in the target protein which prevent inhibitor binding.[12] To overcome this acquired drug resistance, additional chemotypes are warranted.

In **Chapter 4** a series of substituted 2-phenyl-5-methoxy-*N*-(3-(5-(morpholinomethyl)-1*H*-benzo[*d*]imidazol-2-yl)-1*H*-pyrazol-4-yl)pyrimidin-4-amines were discovered as highly potent BUB1 kinase inhibitors with half maximal inhibitory concentrations (IC_{50} values) ranging from 2 – 30 nM. A subset of these molecules matched or even exceeded the biochemical potency of BAY1816032. This chapter describes the further profiling of these inhibitors in absorption, distribution, metabolism and excretion (ADME) assays, cellular BUB1 target engagement and cell proliferation. In addition, the *in vitro* selectivity profile of the most promising inhibitors was assessed and the anti-proliferative activity of one molecule was evaluated in a large panel of cancer cell lines. This led to the identification of ROB433, which showed potent BUB1 target engagement and inhibited a multitude of cancer cell lines as single agent.

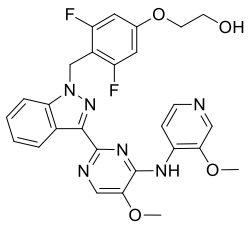

BAY1816032

Figure 6.1 | Chemical structure of BAY1816032.

Results & Discussion

Compounds **1** – **16** (**Table 6.2**) were selected for further biological profiling, because they were the most potent BUB1 inhibitors identified in **Chapter 4**.

Assessment of *in vitro* ADME properties

To investigate the drug-like properties of this chemical series, aqueous solubility and several *in vitro* ADME parameters, such as plasma and microsomal stability and plasma protein binding, were measured of a subset of these molecules (**4** – **9** and **11** – **16**, **Table 6.1**). The stability in both human and rat plasma was good for most compounds. Only compounds **4** and **8** showed a reduced plasma stability (<80% remaining after 3 h). Overall, the human and rat microsomal stability was moderate to good, except for compound **9**. The stability in mouse microsomes was significantly lower for almost all compounds. Compound **11** had the lowest clearance among all species. Of note, this compound did not contain a fluorine at the R_1 phenyl group and increasing the number of fluorine atoms on this ring seemed to lower the metabolic stability. Plasma protein binding was high for all compounds, which correlated with the low to moderate solubility of the compounds. Remarkably, compounds with a hydrogen at R_2 (**4**, **6**, **12**, **14**) were in general better soluble compared to compounds which had a methoxy group at this position (**5**, **7**, **13**, **15**). Taken together, the ADME properties of most of the compounds were acceptable to good.

Table 6.1 | Overview of biochemical pIC_{50} values as determined in **Chapter 4**, *in vitro* ADME parameters and aqueous solubility of compound **4** – **9** and **11** – **16**.

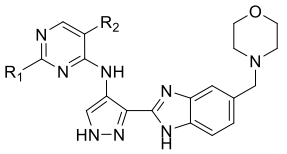

ID	R_1	R_2	pIC_{50} ± SEM	Species	Plasma stability (% remaining after 180 min)	Microsomal stability ($t_{1/2}$ (min))	Microsomal stability (Cl_{int} (µL min^{-1} mg^{-1}))	Plasma protein binding (%)	Aqueous solubility (µM)
4	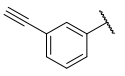		7.57 ± 0.01	Human	76	74	4.7	99.6	
				Rat	100	82	17	99.6	37
				Mouse	N.D.	16	22	N.D.	
5	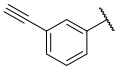		8.37 ± 0.02	Human	100	49	7.1	100	
				Rat	100	64	22	100	5.7
				Mouse	N.D.	30	11	N.D.	
6	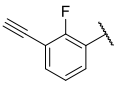		7.89 ± 0.01	Human	100	28	12	99.3	
				Rat	85	29	48	99.1	69
				Mouse	N.D.	16	22	N.D.	
7	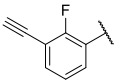		8.34 ± 0.02	Human	100	38	9.1	99.8	
				Rat	91	31	45	99.7	5.0
				Mouse	N.D.	11	33	N.D.	
8	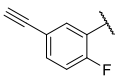		8.68 ± 0.02	Human	69	37	9.4	100	
				Rat	100	49	28	100	3.9
				Mouse	N.D.	18	20	N.D.	
9	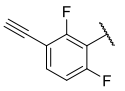		8.64 ± 0.02	Human	100	13	28	99.6	
				Rat	100	35	39	99.7	5.4
				Mouse	N.D.	8.4	41	N.D.	
11	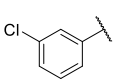		7.96 ± 0.02	Human	100	99	3.5	100	
				Rat	100	75	19	100	1.8
				Mouse	N.D.	73	4.8	N.D.	
12	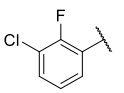		7.63 ± 0.02	Human	100	27	13	99.3	
				Rat	100	46	30	99.2	46
				Mouse	N.D.	12	28	N.D.	
13	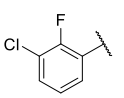		7.98 ± 0.02	Human	86	34	10	99.9	
				Rat	80	34	41	99.8	25
				Mouse	N.D.	12	30	N.D.	
14	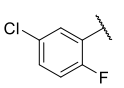		8.03 ± 0.01	Human	100	61	5.6	99.6	
				Rat	96	68	21	99.4	56
				Mouse	N.D.	19	18	N.D.	
15	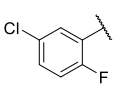		8.57 ± 0.02	Human	100	41	8.4	100	
				Rat	100	63	22	100	4.4
				Mouse	85	22	16	99.9	
16	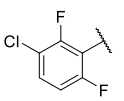		8.62 ± 0.03	Human	100	29	12	99.7	
				Rat	100	49	28	99.7	6.0
				Mouse	N.D.	6.1	57	N.D.	

N.D. = not determined

Assessment of BUB1 target engagement in living cells

To investigate whether the inhibitors engaged with BUB1 in living cells, the inhibitors were profiled in the target engagement assay developed in **Chapter 5**. Compounds **8**, **9**, **15** and **16** potently engaged with BUB1 with half maximal target occupancy concentrations (TE_{50}) of 10-30 nM (**Table 6.2**, **Supplementary Figure 6.1** (p. 207)). This was significantly better than for BAY1816032 (TE_{50} = 355 nM). Target engagement values were approximately 14-fold lower compared to corresponding biochemical pIC_{50} values. This observed reduction may be influenced by the different experimental conditions between these assays and also the cell permeability of the compounds can affect target engagement.[13] In addition, inhibitor target residence time may contribute to the observed difference, since target engagement is measured with a probe that covalently binds BUB1, whereas the inhibitors bind reversibly. BUB1 target engagement by BAY1816032 was more than 75-fold lower compared to its biochemical pIC_{50} value, which may be attributed to unfavorable cell permeability of this compound. A Pearson correlation analysis revealed a strong correlation between cellular target engagement and biochemical pIC_{50} values (**Figure 6.2A**, Pearson's r: 0.921, *p*-value: 0.0004). This indicated that target engagement was predominantly driven by the affinities of these inhibitors for BUB1. Overall, potent cellular BUB1 target engagement was observed for most compounds.

Evaluation of antiproliferative activity

Next, the effect of compounds **1** – **16** on U2OS cell proliferation was investigated by a sulforhodamine B (SRB) assay (**Table 6.2**, **Supplementary Figure 6.2**, (p. 208)).[14] SRB is an aminoxanthene dye, which binds stoichiometrically to basic amino acid residues in trichloroacetic acid (TCA)-fixed cells.[15] SRB is extracted from cells and quantified by absorbance measurements.[15] The optical density is proportional to the amount of protein, which is dependent on the number of cells.[15] U2OS cells were incubated for 72 h with different concentrations of inhibitor. To investigate synergistic effects between BUB1 inhibitors and paclitaxel[10], cells were also co-treated with a low dose (4 nM) of paclitaxel in a separate experiment. A Pearson correlation analysis revealed a strong correlation between biochemical activities and pIC_{50} values on cell proliferation (**Figure 6.2B**, Pearson's r: 0.826, *p*-value: <0.0001), however, target engagement and cell proliferation only moderately correlated and lacked statistical significance (**Figure 6.2C**, Pearson's r: 0.655, *p*-value: 0.056). This suggested that inhibition of cell proliferation was, to a large extent, dependent on BUB1 inhibition, but that off-target activity contributed to the observed effect. Compounds **8**, **9** and **16** potently inhibited cell proliferation with IC_{50} values below 100 nM. Of note, paclitaxel cotreatment only significantly increased the activity (fold-change ≥ 1.9) of compounds **1** – **4**, **10**, **12** and **14**, that showed low potency as single agent (pIC_{50} ≤ 6). The most active compound from this subset in combination with paclitaxel treatment (**12**) had a pIC_{50} of 6.45, which did not exceed the activity of the other inhibitors as single agent. Compound **9** was the most active cellular compound with a pIC_{50} of 7.46. Of note, BAY1816032 showed weak inhibitory activity as single agent (pIC_{50} = 5.07), whereas its activity was enhanced 28-fold by

cotreatment with paclitaxel. To summarize, the benzimidazole-based inhibitors showed good cellular activity, which was not further enhanced by cotreatment with paclitaxel.

Table 6.2 | Overview of compounds **1** – **16** and their biochemical half maximal inhibitory concentrations (expressed as pIC_{50} ± SEM, N=2, n=2), cellular half maximal target occupancy concentrations (expressed as pTE_{50} ± SEM, N=3) and half maximal inhibitory concentration on U2OS cell proliferation with (+) and without (-) 4 nM paclitaxel. Corresponding dose-response graphs are reported in **Supplementary Figure 6.1** (target engagement) and **Supplementary Figure 6.2** (SRB assays).

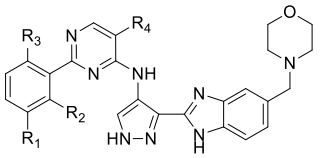

					Biochemical assay			Proliferation assay		
								- paclitaxel	+ paclitaxel	
ID	**R_1**	**R_2**	**R_3**	**R_4**	**pIC_{50} ± SEM**	**app. K_i (nM)[a]**	**pTE_{50} ± SEM**	**pIC_{50} ± SEM**	**pIC_{50} ± SEM**	**f.c.[b]**
BAY-1816032	–	–	–	–	8.34 ± 0.03	1.6	6.45 ± 0.10	5.07 ± 0.05	6.52 ± 0.03	28
1	$-CF_3$	-H	-H	-H	6.03 ± 0.03	329	< 5	~5.4[c]	6.18 ± 0.04	5.4
2	$-CF_3$	-H	-H	-OMe	6.80 ± 0.03	55	N.D.	~6.0[c]	6.32 ± 0.11	2.1
3	-CN	-H	-H	-H	6.24 ± 0.02	201	N.D.	5.56 ± 0.07	6.05 ± 0.08	3.1
4	-C≡C	-H	-H	-H	7.57 ± 0.01	9.5	6.49 ± 0.10	5.70 ± 0.04	6.03 ± 0.08	2.1
5	-C≡C	-H	-H	-OMe	8.37 ± 0.02	1.5	N.D.	6.62 ± 0.05	6.61 ± 0.07	1.0
6	-C≡C	-F	-H	-H	7.89 ± 0.01	4.6	6.24 ± 0.11	6.64 ± 0.05	6.69 ± 0.07	1.1
7	-C≡C	-F	-H	-OMe	8.34 ± 0.02	1.6	7.26 ± 0.08	6.89 ± 0.09	6.91 ± 0.10	1.0
8	-C≡C	-H	-F	-OMe	8.68 ± 0.02	0.74	7.59 ± 0.05	7.13 ± 0.03	7.15 ± 0.05	1.0
9	-C≡C	-F	-F	-OMe	8.64 ± 0.02	0.80	7.54 ± 0.08	7.46 ± 0.05	7.47 ± 0.05	1.0
10	-Cl	-H	-H	-H	7.08 ± 0.02	29	N.D.	5.56 ± 0.01	6.21 ± 0.03	4.5
11	-Cl	-H	-H	-OMe	7.96 ± 0.02	3.9	N.D.	6.26 ± 0.06	6.41 ± 0.07	1.4
12	-Cl	-F	-H	-H	7.63 ± 0.02	8.2	N.D.	5.98 ± 0.05	6.45 ± 0.13	2.9
13	-Cl	-F	-H	-OMe	7.98 ± 0.02	3.7	6.55 ± 0.13	6.73 ± 0.07	6.87 ± 0.08	1.4
14	-Cl	-H	-F	-H	8.03 ± 0.01	3.3	6.75 ± 0.18	5.92 ± 0.06	6.20 ± 0.08	1.9
15 (ROB433)	-Cl	-H	-F	-OMe	8.57 ± 0.02	0.94	7.50 ± 0.11	6.32 ± 0.06	6.48 ± 0.10	1.4
16 (ROB464)	-Cl	-F	-F	-OMe	8.62 ± 0.03	0.84	8.01 ± 0.09	7.39 ± 0.05	7.38 ± 0.05	1.0

[a] apparent K_i ; [b] fold change: increase in activity upon cotreatment with paclitaxel in the SRB assay ($IC_{50\ (+paclitaxel)}$ / $IC_{50\ (-paclitaxel)}$); [c] Due to a steep Hill slope data was reported as ambiguous according to GraphPad Prism; N.D. = not determined.

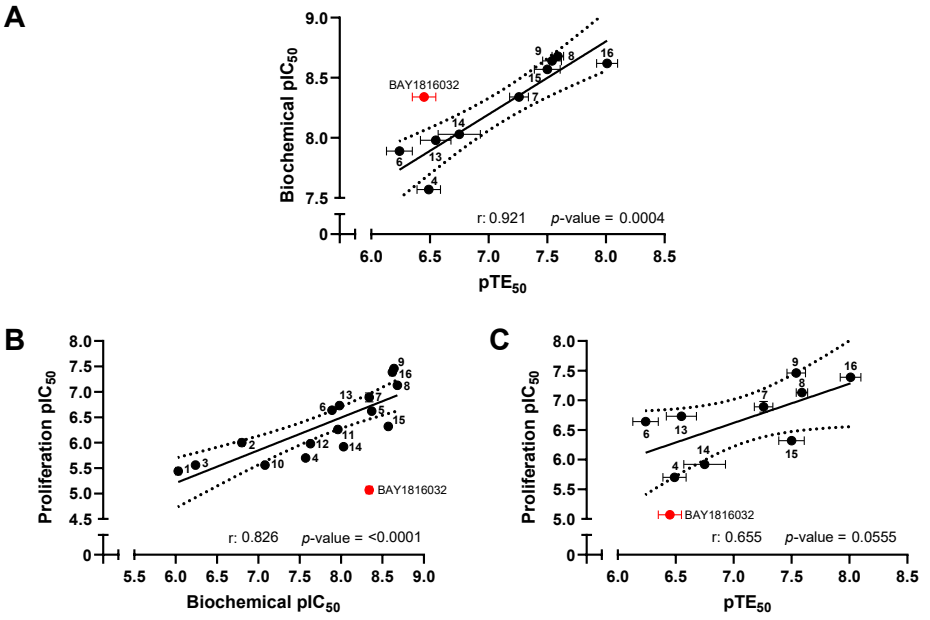

Figure 6.2 | Correlation analysis between **(A)** biochemical pIC_{50} values and pTE_{50} values, **(B)** biochemical pIC_{50} values and pIC_{50} values on cell proliferation and **(C)** pTE_{50} values and pIC_{50} values on cell proliferation. Statistics was performed using a two-tailed Pearson correlation analysis. Biochemical pIC_{50} values are displayed as mean ± SEM (N=2, n=2), pTE_{50} values as mean ± SEM (N=3) and pIC_{50} values on cell proliferation as mean ± SEM (N=2, n=3). For some data points error bars were smaller than the symbol size. Dotted lines represent 95% confidence interval of the best-fit line (solid line) as determined by linear regression analysis. Data for BAY1816032 is indicated in red and is not included in the correlation and linear regression analyses.

Selectivity profile of 15 and 16

Compound ROB433 (**15**) and ROB464 (**16**) were selected based on their biochemical, cellular and ADME profile for further profiling in a kinase selectivity assay. The selectivity profile was assessed using Thermo Fisher Scientific's SelectScreen™ biochemical kinase profiling service in a panel of 403 wild-type kinases (396 unique kinases, see Experimental section). ROB433 and ROB464 were tested at a concentration of 1 µM and 100 nM (**Supplementary Figure 6.3** (p. 209), **Supplementary Table 6.1** (p. 210)). At 1 µM, 165 and 187 kinases were inhibited (>50%) by ROB433 and ROB464, respectively. Of note, although both compounds are structurally similar, significant differences in inhibition were found for a subset of kinases (**Figure 6.3A**). At 100 nM only 49 and 44 kinases were inhibited by ROB433 and ROB464, respectively. 33 off-targets were shared between both compounds (**Figure 6.3B**). Importantly, MPS1 (also known as TTK) was not inhibited, whereas Aurora kinases A, B and C were identified as off-targets of both compounds (**Supplementary Table 6.1** (p. 210)). Other kinases involved in mitosis[4], such as CDK1, Haspin, PLK1, NEK2, NEK6 and NEK9, were not inhibited. In view of the fact that ATP levels in cells are in millimolar range[16–19] compared to micromolar ATP concentrations used in the biochemical assays, it is unknown whether these off-targets will be inhibited in a living cell. Overall, the selectivity profile of both ROB433 and ROB464 is acceptable.

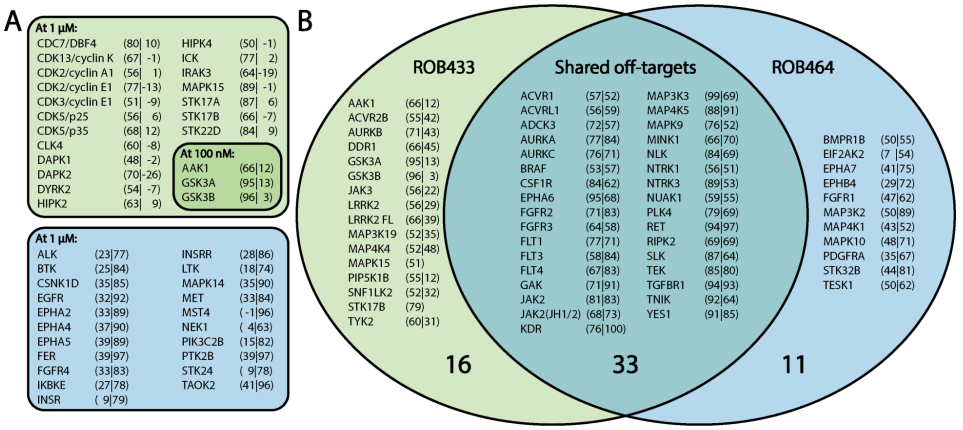

Figure 6.3 | (A) Overview of kinases for which the percentage of inhibition differed ≥50% between ROB433 and ROB464. Kinases that were more prone to inhibition by 1 µM or 100 nM of ROB433 (**15**) compared to corresponding concentrations of ROB464 (**16**) are indicated in the green boxes. Kinases more prominently inhibited by 1 µM ROB464 are indicated in the blue box. Numbers between parentheses indicate percentages of inhibition by ROB433 (left) and ROB464 (right). **(B)** Comparison of *in vitro* selectivity profile of ROB433 and ROB464 at a concentration of 100 nM. Inhibition >50% was used as cut-off. Percentages of inhibition are reported as described in (A). Kinases for which no percentage of inhibition is reported were not inhibited for more than 50% at a concentration of 1 µM and therefore not tested at a concentration of 100 nM. Large numbers indicate the total number of kinases in corresponding part of the Venn diagram.

Antiproliferative effects of ROB433 (15) among a large panel of cancer cell lines

Based on its good biochemical activity and BUB1 target engagement, combined with its acceptable microsomal stability, ROB433 was screened in the Oncolines™ panel which consists of 102 cancer cell lines originating from different tissues (**Supplementary Table 6.2** (p. 212)). Briefly, cells were treated with nine concentrations (3.16 nM – 31.6 µM) of ROB433 for 72 h. Subsequently, cell proliferation was assessed and half maximal inhibitory concentration (IC_{50}), half maximal growth inhibition concentration (GI_{50}) and half maximal lethal dose (LD_{50}) were determined (see Experimental section). ROB433 inhibited cell growth (GI_{50}) with concentrations ranging from 101 nM (for KG-1 cells) to 5.57 µM (for THP-1 cells). Cell lines for which GI_{50}, IC_{50} and LD_{50} values were high, off-target activity may contribute to inhibition of cell proliferation. Cell growth was inhibited with a mean GI_{50} value of 1.43 µM (mean IC_{50} = 1.61 µM) among all cell lines tested which suggested a favorable toxicity profile for this compound. Similar mean IC_{50} values have been published for approved kinase drugs abemaciclib, brigatinib, midostaurin and neratinib (1.71, 1.88, 1.73 and 2.10 µM, respectively) using this Oncolines™ panel.[20] Inhibitors of MPS1 kinase, which is another member of the SAC, have previously been tested in 66 cell lines of the Oncolines™ panel.[21] Among these inhibitors, Mps-BAY2b[22] and tool compound Mps1-12[23] showed similar mean IC_{50} values (1.98 and 1.41 µM, respectively) when compared to ROB433 for this subset of cell lines (mean IC_{50} = 1.63 µM). Classification of cell lines to tissue types and calculating median pIC_{50} values (**Figure 6.4A**) revealed that chronic myeloid leukemia (CML) cells were the most sensitive to ROB433 treatment (median pIC_{50} = 6.10), while non-small cell lung cancer (NSCLC) cells were the least effectively inhibited (median pIC_{50} = 5.53). Strikingly, the opposite was true for cells

treated with MPS1 inhibitors, since low sensitivity was observed for CML cells while NSCLC tissue was in the top 5 most sensitive tissue for seven out of ten MPS1 inhibitors (**Supplementary Figure 6.4**, p. 209).[21] Tissue that was sensitive to both ROB433 and MPS1 inhibitors included uterus and non-hodgkin lymphoma cells (**Supplementary Figure 6.4**, p. 209). To investigate whether certain genomic alterations were related to ROB433 sensitivity, a genomic biomarker analysis was performed on known cancer genes (see Experimental section). This revealed that ROB433 preferentially inhibited proliferation of cells that harbor a mutation in the *CTNNB1* gene (**Figure 6.4B**), which encodes for β-catenin. β-Catenin is a member of the WNT signaling pathway and its accumulation results in nuclear localization and gene transcription.[24] WNT-CTNNB1-dependent transcription ultimately modulates changes in cell behavior, such as cell proliferation.[24] Cell lines with a mutation in the *CTNNB1* gene were on average 2.7-fold more sensitive to ROB433 treatment compared to cells with wild-type *CTNNB1* (ANOVA p = 0.018). Interestingly, this sensitivity was also reported for ten previously investigated MPS1 inhibitors[21], which may be due to targeting the same biological pathway. Cells with an amplification of the *CCNE1* gene, which encodes for cyclin E1, were 2.1-fold less sensitive to ROB433 (**Figure 6.4B**, ANOVA p = 0.029). Cyclin E1 is the regulatory subunit of CDK2 and its gene amplification has been described as a mechanism of primary treatment resistance in serous ovarian cancer.[25] *CCNE1* gene amplification was found to be largely exclusive of *BRCA1/2* pathway disruption.[26] *BRCA1/2*-deficient tumors, which are deficient in homologous recombination (HR) DNA repair, can be targeted by poly (ADP-ribose) polymerase (PARP) inhibitors.[27] PARP inhibitors lead to double-strand DNA breaks which cannot be efficiently repaired in HR deficient cells.[27] It is therefore hypothesized that *CCNE1*-amplified tumors are unlikely to respond to PARP inhibitors.[28] Since BUB1 inhibitor BAY1816032 enhanced the efficacy of PARP inhibitor olaparib a mouse xenograft study[10] and given the reported function of BUB1 in DNA damage response[29], the reduced sensitivity of ROB433 in cells with *CCNE1* gene amplification may therefore be in line with aforementioned data. Overall, ROB433 was found to inhibit a multitude of cancer cell lines originating from different tissues at submicromolar concentrations.

Conclusion

In this chapter, two novel BUB1 inhibitors, ROB433 (**15**) and ROB464 (**16**), are reported. Both compounds showed drug-like *in vitro* ADME properties and inhibited U2OS cell proliferation. In contrast to BAY1816032, the antiproliferative activity of these inhibitors did not require cotreatment with paclitaxel. Potent cellular BUB1 target engagement for ROB433 and ROB464, but less potent for BAY1816032, was observed which supports the hypothesis that full BUB1 inhibition is required to induce antiproliferative activity. Notably, based on the *in vitro* selectivity profiles of ROB433 and ROB464, off-target activity may contribute to the observed cellular effects. The cellular selectivity profile, however, remains to be investigated. The antiproliferative effects of ROB433 were further explored in a large panel of cancer cell lines. ROB433 was able to inhibit a multitude of cell lines, but activity varied among different cancer tissue. Cells with a mutation in the *CTNNB1* gene were found to be more sensitive to

ROB433 treatment, whereas cells with *CCNE1* gene amplification were less affected. Sensitivity to mutations in the *CTNNB1* gene was previously reported for inhibitors of SAC kinase MPS1[21], which may be a result of targeting the same biological pathway. Overall, ROB433 and ROB464 are two novel lead BUB1 inhibitors with favorable properties and provide an excellent expansion of the currently available BUB1 inhibitor BAY1816032.

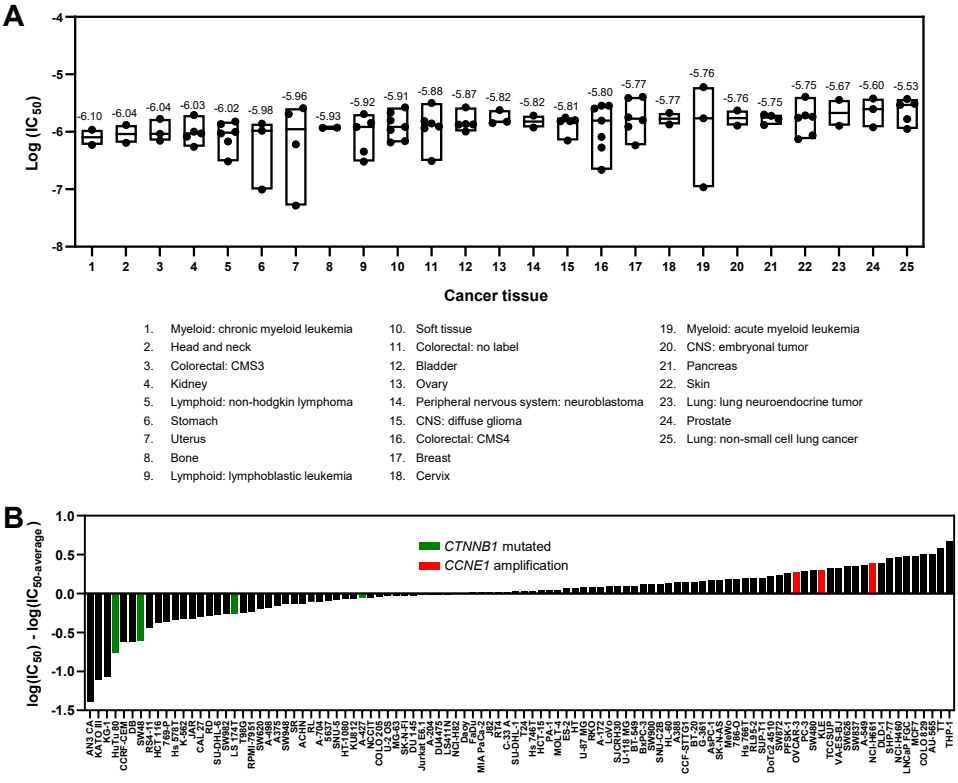

Figure 6.4 | Antiproliferative activity of ROB433 on cancer cells (A) Results of the Oncolines™ profiling service in a panel of 102 cancer cell lines originating from different tissues represented by a tissue-based boxplot (see **Supplementary Table 6.2** (p. 212) for corresponding activity data per cell line). The horizontal line inside each box represents the median log(IC_{50}) value (which is also annotated above each box). **(B)** Waterfall plot raking cell lines on sensitivity. Bars indicate differences from the average pIC_{50} value of the cell panel as: log($IC_{50\_cell\_line}$) – log($IC_{50\_average}$). Bars corresponding to cell lines harboring a *CTNNB1* mutation are indicated in green, cell lines with *CCNE1* gene amplification are indicated in red.

Acknowledgements

From Netherlands Translational Research Center (NTRC), Diep Vu is kindly acknowledged for performing the ADME and solubility assays, Martine Prinsen for conducting the Oncolines™ cell panel screen and Rogier Buijsman for supervision.

Experimental – Biochemistry

Plasma stability assay

Lithium-heparin plasma was thawed and used directly for the assay. An aliquot of 100 µL plasma in a 96-well plate was incubated in a water bath at 37°C for 10 min. Next, 1 µM of compound (max 1% DMSO) or positive control was added and the assay plate was mixed at 1500 rpm for 15 seconds. At 0, 5, 10, 15, 30, 60, 120, 180 min samples of 10 µL were taken and extracted by adding 200 µL of acetonitrile containing an internal standard. The samples were centrifuged for 30 min at 4500 rpm to pellet the precipitated protein and the supernatant was transferred to a True Taper™ 2-mL square 96-well plate (Screening Devices Cat. No. 968820) for LC–MS/MS analysis. Procaine and propantheline were incubated alongside as controls. Procaine is a reference substrate in the rat stability assays, and propantheline in mouse and human stability assays. The signal (counts) was related to the internal standard. Plasma half-life ($t_{1/2}$) was calculated from linear fitting of ln(counts) versus time in Excel. Assay runs were invalidated if $t_{1/2}$ of the controls varied more than two-fold from historical means. The maximum $t_{1/2}$ that could be reliably measured in the assay was determined by analyzing the variation in the replicates of the controls. The percentage remaining compound was calculated by setting the signal at t = 0 to 100%. In addition, %-remaining at 180 min was calculated based on the linear fit used for $t_{1/2}$. The compounds are considered stable if this percentage is higher than 80%.

Microsomal stability assay

The liver microsomal suspensions were thawed and used directly for the assay. To a 96-well plate was added 56 µL of 100 mM KH_2PO_4 (pH 7.4), 2 µL of 50 µg/mL alamethicin, 2 µL of 250 mM $MgCl_2$, 10 µL of liver microsomes and 10 µL of compound (max 1% DMSO) after which the plate was incubated in a water bath at 37°C for 10 min. Next, 20 µL of 10 mM NADPH was added and the assay plate was mixed at 1500 rpm for 15 seconds. At 0, 5, 10, 15, 30, 45, 60, 120 min samples of 10 µL were taken and extracted by adding 200 µL of acetonitrile containing an internal standard. The samples were centrifuged for 30 min at 4000 rpm to pellet the precipitated protein and the supernatant was transferred to a True Taper™ 2-mL square 96-well plate (Screening Devices Cat. No. 968820) for LC–MS/MS analysis. Dextromethorphan, propranolol and phenacetin were incubated alongside as controls. The signal (counts) was related to the internal standard. The half-life ($t_{1/2}$) was calculated from linear fitting of ln(counts) versus time in Excel. Assay runs were invalidated if $t_{1/2}$ or the CL_{int} value of the control compounds varied more than two-fold from historical means.

Plasma protein binding assay

Equilibrium dialysis was used to determine plasma protein binding. DIALYZER™ plates were used that separates a protein-containing compartment from a protein-free compartment via a semi-permeable membrane. The protein-free compartment (clear frame) of the system was filled with 150 µL PBS and the protein-containing side (blue frame) was filled with 150 µL plasma (Sera Laboratories International Ltd. (BioIVT), K_3 EDTA) containing 5 µM of compound (max. 1% DMSO). The filled wells were sealed with cap strips. The system was allowed to rotate for 17 h at 25 rpm, in an incubator at 37°C. After equilibrium had been reached, samples of 10 µL were taken from each of the compartments and extracted by adding 100 µL of acetonitrile containing an internal standard. The samples were centrifuged for 30 min at 4500 rpm to pellet the precipitated protein and the supernatant was transferred to a True Taper™ 2-mL square 96-well plate (Screening Devices Cat. No. 968820) for LC–MS/MS analysis. Tolbutamide was incubated alongside as control. Incubations and subsequent analyses were performed in duplicate. Assay runs were invalidated if the fraction unbound (fu)-value of tolbutamide varied more than two-fold from historical means. The extent of binding is reported as protein binding fraction (PB) which is calculated by PB(%) = 100*(PC – PF)/PC, where PC and PF are the compound concentrations in the protein-containing and protein-free compartments, respectively. The fraction unbound was calculated by fu = 1 – ((PC – PF) /PC).

Solubility assay

Compounds stocks (in DMSO) were diluted in an 8-point dilution series (with a factor 1.67) in DMSO to obtain 33.3x working solutions. In a clear 384-well plate, 3 µL compound from the dilution plate was

added to 10 µL PBS and the plate was mixed at 2000 rpm for 15 seconds. Next, 87 µl PBS was added to the assay plate and mixed 15 times using a Biomek NXP (final concentrations were 14.0, 23.3, 38.9, 64.8, 108, 180, and 300 µM). Absorption was measured at 620 nm using an EnVision® Multimode Plate Reader and the wells were also inspected for turbidity using a microscope. A linear relation between compound concentrations and turbidity signal was fitted and the intersection with the x-axis was determined. This intersection represents the maximal concentration of compound that is supposed to be still in solution. Insoluble compounds were also checked by visual inspection using a microscope.

Cell culture

U2OS (human osteosarcoma) cells were purchased at ATCC and were tested on regular basis for mycoplasma contamination. Cultures were discarded after 2–3 months of use. Cells were cultured at 37°C under 7% CO_2 in DMEM (Sigma Aldrich, D6546) supplemented with GlutaMAX (2 mM, Thermo Fisher), 10% (v/v) heat-inactivated newborn calf serum (Seradigm), penicillin and streptomycin (200 µg/mL each, Duchefa) (complete medium). Growth medium was supplemented with G418 (600 µg/mL) (selection medium) for culturing stable BUB1-overexpressing (U2OS-BUB1^{GFP_FLAG}) cells. U2OS-BUB1^{GFP_FLAG} cells were prepared as described in **Chapter 5**. Medium was refreshed every 2–3 days and cells were passaged by trypsinization twice a week at 80–90% confluence. Cell viability was assessed by Trypan Blue exclusion and cell quantification using a TC20™ Automated Cell Counter (Bio-Rad).

Target engagement assay

U2OS-BUB1^{GFP_FLAG} cells from 10 cm dishes with low cell density (<50% confluence) were seeded into 6-well plates (500,000 cells/well) and incubated overnight to allow for cell adherence. Inhibitor (stock solutions in DMSO) were diluted 100x in complete medium to obtain 10x working solutions (1% DMSO). Inhibitors were serially diluted in complete medium containing 1% DMSO. Cell medium was aspirated and complete medium (800 µL) was added. Either vehicle or inhibitor (100 µL, 10x working solution) was added and cells were incubated at 37°C for 1 h. Vehicle or probe (100 µL, 10x working solution) was added and cells were incubated at 37°C for 1 h. Medium was aspirated and cells were washed with PBS (1 mL). Cells were harvested by trypsinization and centrifuged (500 *g*, 3 min). Pellets were washed with PBS (1 mL), centrifuged (500 *g*, 3 min) and supernatant was removed. Pellets were snap-frozen in liquid nitrogen and subsequently thawed on ice (cell pellets can optionally be stored at –80°C). Cells were lysed by suspending the pellet in 60 µL M-PER™ Mammalian Protein Extraction Reagent (Thermo Fisher), supplemented with 1x Halt™ protease inhibitor cocktail (EDTA-free) (Thermo Fisher) and 1x Halt™ phosphatase inhibitor cocktail (Thermo Fisher), after which the samples were incubated on ice for 15 min. Samples were vortexed at medium speed and centrifuged (14,000 *g*, 10 min, 4°C). The supernatant was collected and protein concentration determined by a Quick Start™ Bradford Protein Assay (Bio-Rad). Lysates were diluted to 1.15 mg/mL in M-PER™ Mammalian Protein Extraction Reagent (lysates can optionally be snap-frozen and stored at –80°C). "Click-mix" was prepared freshly by mixing $CuSO_4$ (42 µL of 15 mM in H_2O) and sodium ascorbate (21 µL of 150 mM in H_2O) until yellow, followed by the addition of THPTA (7 µL of 15 mM in H_2O) and Cy5-N_3 (7 µL of 82.5 µM in DMSO). To 26 µL lysate was added 4 µL click-mix and samples were incubated at 37°C for 30 min. Samples were denatured by the addition of 4x Laemmli buffer (10 µL of 240 mM Tris-HCl pH 6.8, 8% w/v SDS, 40% v/v glycerol, 5% v/v β-mercaptoethanol, 0.04% v/v/ bromophenol blue) and incubated at 95°C for 3 min. Samples were resolved by sodium dodecyl sulfate polyacrylamide gel electrophoresis (SDS-PAGE) on a 7.5% polyacrylamide gel (180 V, 70 min, 10 or 20 µL/lane). Gels were scanned using Cy2, Cy3 and Cy5 multichannel settings (532/28, 602/50 and 700/50 filters, respectively) on a ChemiDoc™ MP imager (Bio-Rad). Fluorescence intensity was quantified using Image Lab 6.0.1 (Bio-Rad) and corrected for protein loading as determined by Coomassie Brilliant Blue R-250 staining. Data was plotted using GraphPad Prism 8.0.

SRB proliferation assay

Assays were performed in 96-well plates (Greiner, Cellstar, 655180) by seeding (day 0), treatment (day 1) and subsequent incubation for 72 h. Cells were fixed, stained and staining was subsequently dissolved after which absorbance was measured. Each assay included the following controls: (i) a background control (to which no cells were added), (ii) t_0 controls (separate assay plate in which cells were fixed on

day 1, defined as 0% proliferation), (iii) nontreated controls (present in each assay plate, treated with vehicle and defined as 100% proliferation). Cells were treated with different concentrations of inhibitor, inhibitor + paclitaxel (4 nM) or paclitaxel (4 nM). All inhibitors were tested in two separate assays and all inhibitor concentrations were tested in triplicate per assay (N=2, n=3).

For each assay, U2OS cells from 10 cm dishes were seeded into 96-well plates (3,000 cells/well) and subsequently incubated overnight to allow for cell adherence. Vehicle, inhibitor and paclitaxel (stock solutions in DMSO) were diluted in complete medium to obtain 2x working solutions (1% DMSO). Cell medium was replaced by fresh complete medium (50 µL), treatment was started by addition of the 2x working solutions (50 µL) and plates were incubated at 37°C for 72 h. Cell medium was replaced by fresh serum free medium (100 µL) and cells were fixed by addition of 30 µL 50% (w/v) aq. trichloroacetic acid after which the plates were incubated at 4°C for 60 min. Wells were emptied by shaking the plates upside down after which wells were washed three times with demineralized water and air-dried overnight. To each well, 60 µL of SRB solution (0.4% (w/v) in 1% aq. acetic acid) was added and plates were incubated for 30 min. The excess SRB was removed and the wells were washed three times with 1% aq. acetic acid and air-dried overnight. Bound SRB was redissolved by addition of 150 µL 10 mM TRIS (free-base) and absorbance was measured at 540 nm on a CLARIOstar plate reader. Data was normalized between t_0 and nontreated controls and plotted using GraphPad Prism 8.0 using "Nonlinear regression (curve fit)" and "log(inhibitor) vs. normalized response – Variable slope" to determine pIC_{50} values.

Kinase selectivity profiling

Assays for determination of kinase selectivity were performed by Thermo Fisher Scientific's SelectScreen™ biochemical kinase profiling service. The complete list of tested kinases and inhibition profiles are shown in **Supplementary Table 6.1** (p. 210) and detailed assay procedures are described in SelectScreen Assay Conditions documents located at www.thermofisher.com/selectscreen under "SelectScreen kinase profiling Services" and then "Technology overview". The concentration of ATP was selected to be equal to the K_M, unless stated otherwise. Assays were performed with a compound concentration of 1 µM and kinases showing >50% inhibition were assayed again at a compound concentration of 100 nM. Data obtained from SelectScreen™ kinase assays were processed using KNIME Analytics Platform[30] (v.4.3.0). Inconsistent kinase naming was corrected. Seven kinases (BRAF, MAP2K1, MAP2K2, MAP2K6, JNK3, JNK1, JNK2) were present in two screening technologies and data for these kinases were therefore averaged resulting in 396 'unique' kinases (**Supplementary Table 6.1** (p. 210)). During screening of ROB433 (**15**), the assay to determine RPS6KB2 activity was not available and was therefore not measured (resulting in 395 'unique' kinases). The "genenames" database[31,32] was used to couple kinase names to Uniprot[33] IDs and Uniprot IDs were subsequently linked to kinase names accepted by KinMap[34] to generate **Supplementary Figure 6.3** (p. 209). Phosphatidylinositol kinases (16) and sphingosine kinases (2) were not visualized in **Supplementary Figure 6.3** (p. 209) and inhibition percentages of kinases that are tested with different combinations of subunits (for example AMPK) or kinases that are tested with different cyclins (for example CDKs) were averaged for the generation of **Supplementary Figure 6.3** (p. 209).

Oncolines™ profiling

Cell proliferation

Assays for determining the antiproliferative activity of ROB433 (**15**) were performed by the Oncolines™ profiling service. Detailed assay procedures are described at https://www.oncolines.com.[35] All cell lines have been licensed from the American Type Culture Collection (ATCC) Manassas, Virginia (US). Master and working cell banks (MCB and WCB) were prepared by subculturing in ATCC-recommended media and freezing according to ATCC recommended protocols (www.atcc.org). Cell line stocks for the assays were prepared from the WCB. The MCB, WCBs and assay stocks were prepared within respectively 3, 6 and 10 passages of the ATCC vial. Solid powder of ROB433 was weighed on a calibrated balance and dissolved in DMSO. At the day of the experiment, the compound stock (10 mM) was diluted in 3.16-fold steps in DMSO to obtain a 9-point dilution series which were all further diluted 31.6 times in 20 mM sterile HEPES buffer (pH 7.4). The final DMSO concentration during incubation was 0.4% in all wells. Cells were diluted in the corresponding ATCC recommended medium and dispensed in a 384-well plate,

depending on the cell line used, at a density of 100 - 6400 cells per well in 45 µL medium. For each cell line used, the optimal cell density was used. The margins of the plate were filled with PBS. Plated cells were incubated in a humidified atmosphere of 5% CO_2 at 37°C. After 24 h, 5 µL of compound (final concentrations were between 3.16 nM – 31.6 µM) was added and plates were incubated for 72 h. At t=end, 24 µL of ATPlite 1Step™ (PerkinElmer) solution was added to each well and plates were subsequently shaken for 2 min. After 10 min of incubation in the dark, the luminescence was recorded on an Envision multimode reader (PerkinElmer). Each compound concentration was tested in duplicate and half maximal inhibitory concentration (IC_{50}), half maximal growth inhibition concentration (GI_{50}) and half maximal lethal dose (LD_{50}) were determined as visualized by the graphs below.

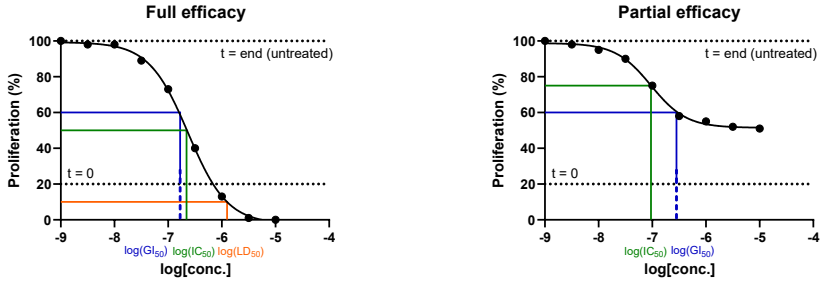

Controls cell proliferation

[t = 0 signal] – on a parallel plate, 45 µL cells were dispensed and incubated in a humidified atmosphere of 5% CO_2 at 37°C. After 24 h, 5 µL DMSO-containing HEPES buffer and 25 µL ATPlite 1Step™ solution were mixed, and luminescence measured after 10 min of incubation (=$luminescence_{t=0}$). [Reference compound] – the IC_{50} of reference compound doxorubicin is measured on a separate plate. The IC_{50} is trended. If the IC_{50} is out of specification (0.32 - 3.16 times deviating from historic average) the assay is invalidated. [Cell growth control] – the cellular doubling times of all cell lines are calculated from the t = 0 h and t = end growth signals of the untreated cells. If the doubling time is out of specification (0.5 – 2.0 times deviating from historical mean) the assay is invalidated. [t = end (untreated)] – for each cell line, the maximum luminescence was recorded after incubation until t = end without compound in the presence of 0.4% DMSO.

Drug sensitivity

The sensitivity distribution was analyzed across the tissue origin of the cell lines. The results are presented in a boxplot (**Figure 6.4A**). Tissue and disease types were annotated according to a cell line knowledge resource[36] and binned according to a widely used standardized classification[37]. Boxplots were generated for tissue types represented by at least two Oncolines™ cell lines. The large group of cell lines of colorectal origin was further divided according to a consensus classification based on gene expression.[38] These subtypes are biologically distinct and include CMS1 (MSI-immune), CMS2 (epithelial and canonical), CMS3 (epithelial and metabolic), and CMS4 (mesenchymal). Colorectal cell lines which could not significantly be assigned to a single subtype are annotated as 'No label'.

Cell genetics

The mutation status of cell lines was established from a combination of public and proprietary (NTRC) data. Based on public data (COSMIC Cancer Genome Project, version 80)[39,40], NTRC collected mutations, amplifications and deletions in established cancer driver genes that occur in Oncolines™.[41] For further validation, a selection of 23 cancer genes were sequenced by NTRC by targeted and full exome sequencing directly from the cell lines used in Oncolines™. As an extra filter, genetic changes were required to be observed with a preset frequency in patient tumor samples in COSMIC, depending on the type of genetic alteration. This discards sporadic, non-cancer-causing mutations. Cell lines were classified as having a 'wild type' or a 'mutated' genotype, where 'mutated' means: at least one allele changed by point mutation, insertion, deletion, amplification or copy number variation. Analysis was performed on genes that were mutated in at least three different Oncolines™ cell lines (98 genes in

total). A subset of the most commonly occurring and best known cancer genes (38 in total) was analyzed with type II Anova analysis in the statistical program R. For the genes which were significantly associated with drug response, genetic changes and drug sensitivities were visualized in waterfall plots.

Supplementary information

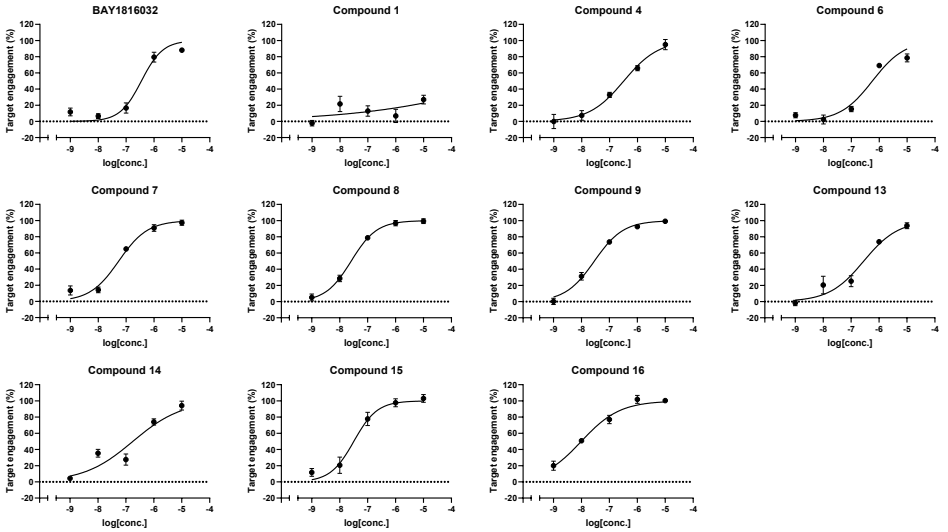

Supplementary Figure 6.1 | Dose-response curves of inhibitors on cellular BUB1 target engagement. All data were obtained using the target engagement assay as described in **Chapter 5**. U2OS-BUB1^{GFP_FLAG} cells were pre-incubated with different concentrations of indicated inhibitor (1 h, 37°C) followed by incubation with probe (1 µM, 1 h, 37°C). Cells were lysed, proteins labeled by probe were visualized by conjugation to a Cy5 fluorophore using click chemistry and samples were resolved by SDS-PAGE. In-gel fluorescence was measured, corrected for protein loading and normalized. Corresponding pTE_{50} values are reported in **Table 6.2**. Data represents mean ± SEM (N=3).

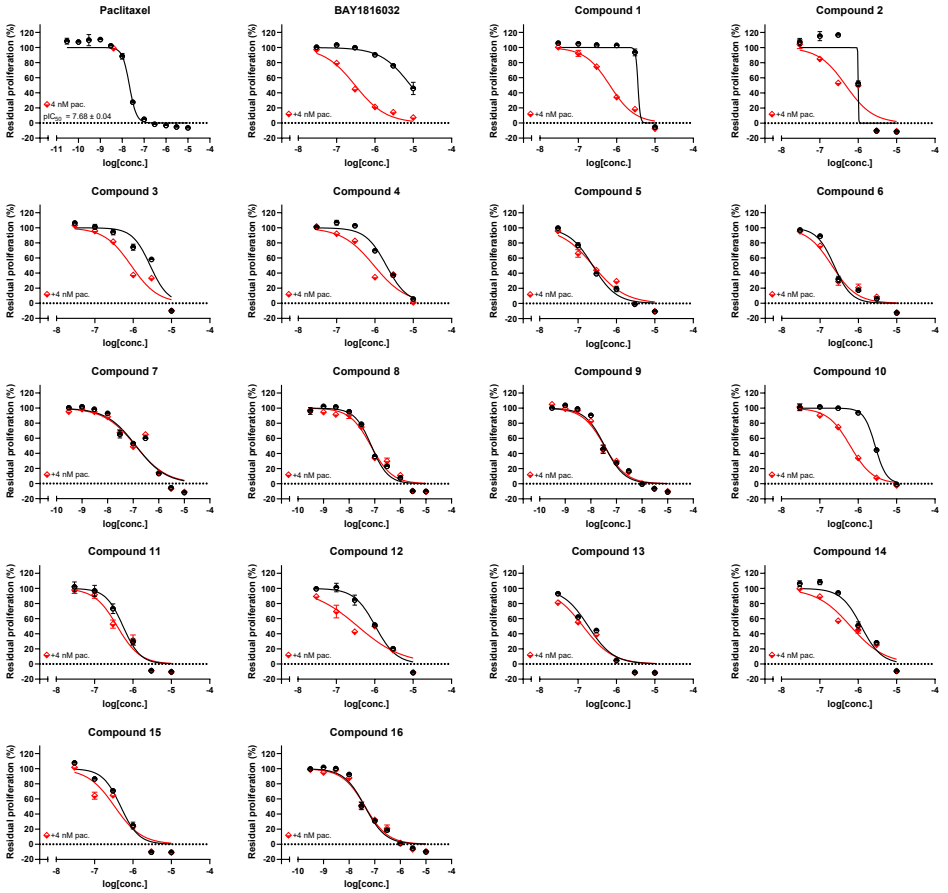

Supplementary Figure 6.2 | Dose-response curves of paclitaxel and BUB1 inhibitors on U2OS cell proliferation. All data were obtained using an SRB assay. Cells were treated with indicated inhibitor (black curves) or inhibitor + 4 nM paclitaxel (red curves) for 72 h after which cell proliferation was assessed. The effect of 4 nM of paclitaxel is indicated (red) in the graph of paclitaxel. Corresponding pIC_{50} values are reported in **Table 6.2**, except for paclitaxel which is reported in corresponding graph. Data represents mean ± SEM (at least N=2, n=3).

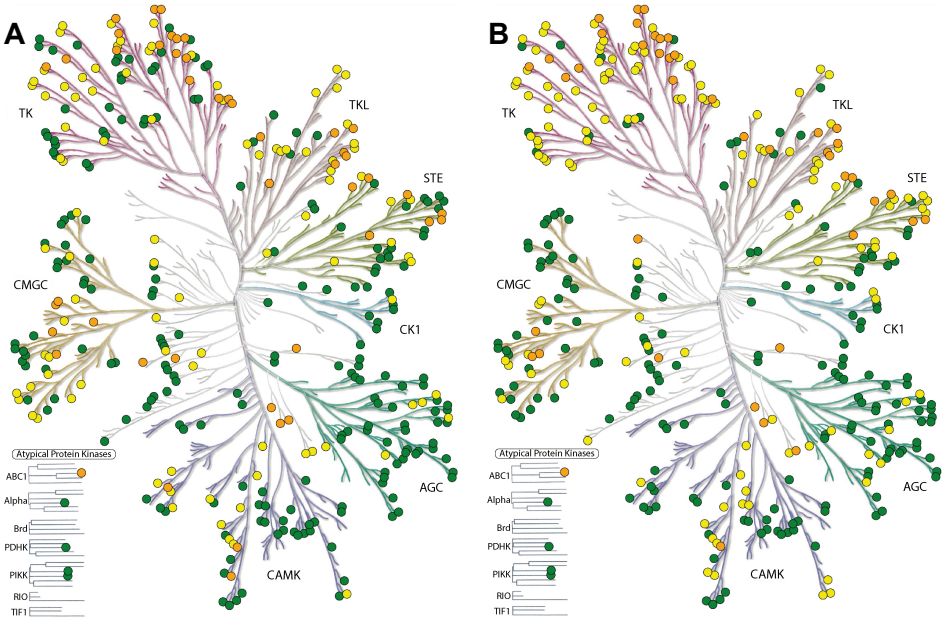

Supplementary Figure 6.3 | Representation of selectivity profiles of **(A)** ROB433 (**15**) and **(B)** ROB464 (**16**). Kinases not inhibited (≤50%) at a concentration of 1 μM are indicated in green, kinases inhibited (>50%) at 1 μM but not (≤50%) at 100 nM are indicated in yellow and kinases inhibited (>50%) at both 1 μM and 100 nM are indicated in orange. Images generated using KinMap[34], reproduced courtesy of Cell Signaling Technology, Inc. (www.cellsignal.com).

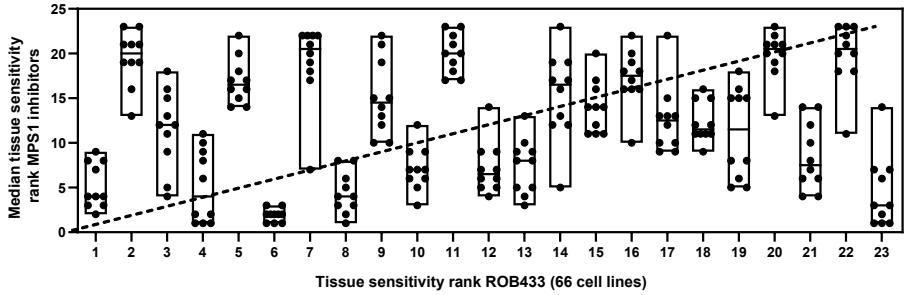

1. Uterus
2. Myeloid: chronic myeloid leukemia
3. Colorectal: CMS3
4. Lymphoid: non-hodgkin lymphoma
5. Kidney
6. Head and neck
7. Bone
8. Colorectal: CMS4
9. CNS: embryonal tumor
10. Lymphoid: lymphoblastic leukemia
11. Bladder
12. Colorectal: no label
13. CNS: diffuse glioma
14. Peripheral nervous system: neuroblastoma
15. Soft tissue
16. Pancreas
17. Cervix
18. Skin
19. Breast
20. Ovary
21. Lung: lung neuroendocrine tumor
22. Prostate
23. Lung: non-small cell lung cancer

Supplementary Figure 6.4 | Comparison of tissue sensitivity between ROB433 and MPS1 inhibitors. Previously, IC_{50} data from ten MPS1 inhibitors in 66 cell lines of the Oncolines™ profiling service was reported.[21] For each MPS1 inhibitor, IC_{50} values of cells originating from the same tissue, were averaged. Based on these averaged IC_{50} values, tissue sensitivity was ranked per compound (in which rank 1 is the most sensitive tissue). Per tissue, a box was generated in which each data point represents the rank of indicated tissue for one MPS1 inhibitor. The horizontal line inside each box represents the median rank among all ten MPS1 inhibitors within that tissue. Tissues were sorted (x-axis) based on the most sensitive tissue (=1) to ROB433 treatment among this panel of 66 cell lines. Of note, the tissue sensitivity rank of ROB433 varies slightly from that reported in **Figure 6.4A** since only data from 66 instead of 102 cell lines were included in this data set. The diagonal dashed line represents the same rank for both axes, median values close to this line therefore represents tissue with similar sensitivity to both ROB433 and MPS1 inhibitors. Median values distant to this line represent sensitivity to only either ROB433 or MPS1 inhibitors.

Supplementary Table 6.1 | Results of Thermo Fisher Scientific's SelectScreen™ biochemical kinase profiling service in a panel of 403 wild-type kinases (396 unique kinases, see Experimental section). Compound names (ROB433 (**15**) = 433 and ROB464 (**16**) = 464) and test concentrations are indicated in the column header. Only kinases that were inhibited (>50%) at a concentration of 1 µM were tested again at a concentration of 100 nM.

[µM]	433 1	433 0.1	464 1	464 0.1		[µM]	433 1	433 0.1	464 1	464 0.1		[µM]	433 1	433 0.1	464 1	464 0.1	
AAK1	92	66	58	12	•	CSNK1G1 (CK1 γ 1)	12		12			MAP2K2 (MEK2)	24		32		•
ABL1	61	38	93	28		CSNK1G2 (CK1 γ 2)	13		19			MAP2K4 (MEK4)	21		28		•
ABL2 (Arg)	68	37	88	33		CSNK1G3 (CK1 γ 3)	7		14			MAP2K5 (MEK5)	82	24	87	37	•
ACVR1 (ALK2)	94	52	94	57	•	CSNK2A1 (CK2 α 1)	2		4			MAP2K6 (MKK6)	11		30		•
ACVR1B (ALK4)	67	38	92	19		CSNK2A2 (CK2 α 2)	10		5			MAP3K10 (MLK2)	77	28	82	37	•
ACVR2A	72	19	79	30	•	DAPK1	48		-2			MAP3K11 (MLK3)	65	22	74	24	•
ACVR2B	98	55	91	42	•	DAPK2	70	37	-26		•	MAP3K14 (NIK)	56	11	11		•
ACVRL1 (ALK1)	92	59	88	56	•	DAPK3 (ZIPK)	32		7			MAP3K19 (YSK4)	88	52	98	35	
ADCK3	106	57	104	72	•	DCAMKL1 (DCLK1)	0		3			MAP3K2 (MEKK2)	95	50	97	89	•
ADRBK1 (GRK2)	4		3			DCAMKL2 (DCK2)	5		5			MAP3K3 (MEKK3)	101	69	91	99	•
ADRBK2 (GRK3)	-1		1			DDR1	89	66	96	45	•	MAP3K5 (ASK1)	-4		1		•
AKT1 (PKB α)	2		5			DDR2	77	30	90	33	•	MAP3K7/MAP3K7IP1 (TAK1-TAB1)	88	46	73	26	•
AKT2 (PKB β)	6		3			DMPK	50		74	27	•	MAP3K8 (COT)	11		10		‡
AKT3 (PKB γ)	3		9			DNAPK	3		8			MAP3K9 (MLK1)	79	34	94	20	
ALK	23		77	11		DYRK1A	21		1			MAP4K1 (HPK1)	89	43	91	52	•
AMPK (A1/B1/G1)	53	20	58	-1		DYRK1B	31		2			MAP4K2 (GCK)	40		87	12	
AMPK (A1/B1/G2)	79	33	71	30	•	DYRK2	54	13	-7		•	MAP4K3 (GLK)	68	43	74	45	•
AMPK (A1/B1/G3)	80	42	77	31	•	DYRK3	9		0			MAP4K4 (HGK)	88	52	102	48	
AMPK (A1/B2/G1)	79	35	66	21	•	DYRK4	0		-1			MAP4K5 (KHS1)	94	91	97	88	
AMPK (A1/B2/G2)	80	31	65	7		EEF2K	0		2			MAPK1 (ERK2)	6		5		
AMPK (A1/B2/G3)	71	24	69	12		EGFR (ErbB1)	32		92	26		MAPK10 (JNK3)	78	48	92	71	•
AMPK (A2/B1/G1)	68	18	80	9		EIF2AK2 (PKR)	54	7	82	54	•	MAPK11 (p38 β)	20		55	7	
AMPK (A2/B1/G2)	76	36	71	11		EPHA1	38		87	26		MAPK12 (p38 γ)	8		13		
AMPK (A2/B1/G3)	65	31	76	16		EPHA2	33		89	27		MAPK13 (p38 δ)	13		6		
AMPK (A2/B2/G1)	80	35	87	34	•	EPHA3	18		36		•	MAPK14 (p38 α)	35		90	19	‡
AMPK (A2/B2/G2)	83	42	87	42	•	EPHA4	37		90	17		MAPK14 (p38 α) Direct	31		91	23	
AMPK (A2/B2/G3)	88	35	67	14		EPHA5	39		89	20		MAPK15 (ERK7)	89	51	-1		•
ANKK1	49		54	24	•	EPHA6	92	68	92	95	•	MAPK3 (ERK1)	5		5		
AURKA (Aurora A)	98	84	100	77		EPHA7	85	41	95	75	•	MAPK7 (ERK5)	3		7		
AURKB (Aurora B)	94	71	97	43		EPHA8	52	17	90	32		MAPK8 (JNK1)	59	25	85	42	•
AURKC (Aurora C)	85	71	98	76		EPHB1	64	34	99	50		MAPK9 (JNK2)	86	52	91	76	•
AXL	72	24	89	20		EPHB2	57	8	98	33		MAPKAPK2	-6		-3		
BLK	48		88	21		EPHB3	-2		28			MAPKAPK3	-4		8		
BMPR1A (ALK3)	67	9	83	17	•	EPHB4	62	29	98	72		MAPKAPK5 (PRAK)	6		4		
BMPR1B (ALK6)	91	50	96	55	•	ERBB2 (HER2)	17		54	4		MARK1 (MARK)	23		15		
BMPR2	57	11	84	20	•	ERBB4 (HER4)	83	43	72	5		MARK2	18		12		
BMX	36		83	17		ERN1	76	15	58	16	•	MARK3	41		22		
BRAF	67	57	77	53	•	ERN2	28		19		•	MARK4	43		31		
BRSK1 (SAD1)	83	38	62	8		FER	39		97	23		MASTL	90	42	89	41	•
BRSK2	23		-12		•	FES (FPS)	32		80	8		MATK (HYL)	3		16		
BTK	25		84	11		FGFR1	92	47	100	62		MELK	68	21	89	20	
CAMK1 (CaMK1)	61	19	86	38	†	FGFR2	79	83	100	71		MERTK (cMER)	70	20	95	19	
CAMK1D (CaMKI δ)	16		58	8		FGFR3	87	58	96	64		MET (cMet)	33		84	5	
CAMK1G (CAMKI γ)	11		53	5		FGFR4	33		83	21		MINK1	98	70	102	66	
CAMK2A (CaMKII α)	9		0			FGR	83	43	97	42		MKNK1 (MNK1)	34		3		
CAMK2B (CaMKII β)	5		5			FLT1 (VEGFR1)	80	71	92	77		MKNK2 (MNK2)	38		-9		•
CAMK2D (CaMKII δ)	17		8			FLT3	94	84	96	58		MLCK2 (MLCK2)	78	26	55	9	•
CAMK2G (CaMKII γ)	5		5		•	FLT4 (VEGFR3)	94	83	99	67		MLK4	72	43	39		•
CAMK4 (CaMKIV)	-2		17			FRAP1 (mTOR)	0		-7			MST1R (RON)	45		60	8	
CAMKK1 (CAMKKA)	-1		34		•	FRK (PTK5)	24		63	8		MST4	-1		96	7	
CAMKK2 (CaMKK β)	20		4		•	FYN	67	18	90	29		MUSK	66	15	83	11	
CASK	0		4		•	FYN A	61	10	75	22	•	MYLK (MLCK)	66	16	44		•
CDC42BPA (MRCKA)	8		2			GAK	96	91	86	71	•	MYLK2 (skMLCK)	56	13	89	19	
CDC42BPB (MRCKB)	-1		2			GRK1	0		0		•	MYLK4	22		2		•
CDC42BPG (MRCKG)	22		39			GRK4	-3		-9			MYO3A (MYO3 α)	13		14		•
CDC7/DBF4	80	35	10		•	GRK5	0		0			MYO3B (MYO3 β)	45		35		•
CDK1/cyclin B	31		6			GRK6	4		-4			NEK1	4		63	-3	
CDK11 (Inactive)	4		1		•	GRK7	1		3			NEK2	10		48		
CDK11/cyclin C	4		-27		•	GSG2 (Haspin)	3		-3			NEK4	12		30		
CDK13/cyclin K	67	19	-1		•	GSK3A (GSK3 α)	99	95	78	13		NEK6	5		11		
CDK14 (PFTK1)/cyclin Y	53	7	8		•	GSK3B (GSK3 β)	101	96	71	3		NEK8	-8		-8		•
CDK16 (PCTK1)/cyclin Y	87	37	73	29	•	HCK	52	18	91	21		NEK9	9		26		
CDK17/cyclin Y	53	25	11			HIPK1 (Myak)	44		5			NIM1K	3		3		
CDK18/cyclin Y	35		3			HIPK2	63	17	9			NLK	103	69	102	84	•
CDK2/cyclin A	34		2			HIPK3 (YAK1)	49		0			NTRK1 (TRKA)	67	51	97	56	
CDK2/cyclin A1	56	17	1		•	HIPK4	50		-1			NTRK2 (TRKB)	66	28	97	39	
CDK2/cyclin E1	77	19	-13		•	HUNK	65	13	77	37	•	NTRK3 (TRKC)	91	53	101	89	
CDK2/cyclin O	77	40	34		•	ICK	77	31	2		•	NUAK1 (ARK5)	93	55	94	59	
CDK3/cyclin E1	51	7	-9		•	IGF1R	2		41			NUAK2	66	16	68	40	•
CDK4/cyclin D1	36		45		†	IKBKB (IKK β)	8		4			PAK1	15		17		
CDK4/cyclin D3	45		46		†	IKBKE (IKK epsilon)	27		78	8		PAK2 (PAK65)	5		13		
CDK5 (Inactive)	26		42		•	INSR	9		79	5		PAK3	-4		24		
CDK5/p25	56	21	6			INSRR (IRR)	28		86	17		PAK4	66	29	56	7	
CDK5/p35	68	23	12			IRAK1	42		24			PAK6	6		10		
CDK6/cyclin D1	55	15	61	6	†	IRAK3	64	31	-19		•	PAK7 (KIAA1264)	66	17	50		
CDK7/cyclin H/MNAT1	36		-1			IRAK4	10		9			PASK	2		2		
CDK8/cyclin C	15		-5		•	ITK	63	30	70	13		PDGFRA (PDGFR α)	71	35	96	67	
CDK9 (Inactive)	57	39	55	5	•	JAK1	54	15	79	11		PDGFRB (PDGFR β)	46		87	20	
CDK9/cyclin K	64	14	48		•	JAK2	95	83	100	81		PDK1	8		10		‡
CDK9/cyclin T1	85	29	62	11		JAK2 JH1 JH2	95	73	99	68		PDK1 Direct	20		58	1	
CDKL5	60	16	28			JAK3	90	56	93	22		PEAK1	54	30	93	11	
CHEK1 (CHK1)	27		20			KDR (VEGFR2)	99	100	101	76		PHKG1	6		6		
CHEK2 (CHK2)	9		7			KIT	16		43			PHKG2	4		5		
CHUK (IKK α)	34		13			KSR2	4		10			PI4K2A (PI4K2 α)	9		-3		†
CLK1	9		6			LATS2	33		63	19	•	PI4K2B (PI4K2 β)	8		3		†
CLK2	45		3			LCK	68	47	97	38		PI4KA (PI4K α)	6		3		†
CLK3	6		4			LIMK1	67	23	87	50	•	PI4KB (PI4K β)	7		-7		
CLK4	60	20	-8		•	LIMK2	77	23	91	46	•	PIK3C2A (PI3K-C2 α)	8		12		
CSF1R (FMS)	87	62	97	84		LRRK2	97	56	83	29		PIK3C2B (PI3K-C2 β)	15		82	15	†
CSK	25		60	6		LRRK2 FL	100	66	89	39		PIK3C2G (PI3K-C2 γ)	25		37		†
CSNK1A1 (CK1 α 1)	12		9			LTK (TYK1)	18		74	13		PIK3C3 (hVPS34)	6		3		
CSNK1A1L	4		8			LYN A	72	39	94	32		PIK3CA/PIK3R1 (p110 α/p85 α)	-8		0		
CSNK1D (CK1 δ)	35		85	16		LYN B	81	50	98	37		PIK3CA/PIK3R3 (p110 α/p55 γ)	7		5		†
CSNK1E (CK1 epsilon)	52	12	81	15		MAP2K1 (MEK1)	16		26		•	PIK3CB/PIK3R1 (p110 β/p85 α)	0		-10		

Supplementary Table 6.1 | (continued)

[μM]	433 1	433 0.1	464 1	464 0.1	
PIK3CB/PIK3R2 (p110 β/p85 β)	-5		-1		†
PIK3CD/PIK3R1 (p110 δ/p85 α)	14		3		
PIK3CG (p110 γ)	5		18		
PIM1	0		2		
PIM2	7		7		
PIM3	-1		7		
PIP4K2A	-6		14		†
PIP5K1A	79	37	44		†
PIP5K1B	89	55	54	12	†
PIP5K1C	95	50	55	6	†
PKMYT1	-6		14		•
PKN1 (PRK1)	4		34		
PKN2 (PRK2)	50		74	26	•
PLK1	4		1		
PLK2	4		20		
PLK3	-1		4		
PLK4	93	69	96	79	•
PRKACA (PKA)	6		46		
PRKACB (PRKAC β)	46		77	22	•
PRKACG (PRKAC γ)	61	19	82	39	•
PRKCA (PKC α)	33		15		
PRKCB1 (PKC β I)	-7		22		
PRKCB2 (PKC β II)	22		36		
PRKCD (PKC δ)	6		11		
PRKCE (PKC epsilon)	3		8		
PRKCG (PKC γ)	45		22		
PRKCH (PKC eta)	1		14		
PRKCI (PKC iota)	4		8		
PRKCN (PKD3)	31		68	12	
PRKCQ (PKC theta)	-4		14		
PRKCZ (PKC zeta)	-1		14		
PRKD1 (PKC mu)	40		66	13	
PRKD2 (PKD2)	44		70	13	
PRKG1	4		7		
PRKG2 (PKG2)	16		21		
PRKX	4		10		
PTK2 (FAK)	5		30		
PTK2B (FAK2)	39		97	49	
PTK6 (Brk)	75	14	94	43	
RET	99	97	99	94	
RIPK2	93	69	94	69	•
RIPK3	74	19	71	42	•
ROCK1	2		4		
ROCK2	2		10		
ROS1	84	32	95	25	
RPS6KA1 (RSK1)	52	8	47		
RPS6KA2 (RSK3)	67	22	51	5	
RPS6KA3 (RSK2)	36		44		
RPS6KA4 (MSK2)	20		26		
RPS6KA5 (MSK1)	16		27		
RPS6KA6 (RSK4)	65	22	66	8	
RPS6KB1 (p70S6K)	45		40		
RPS6KB2 (p70S6Kb)	N.D.	N.D.	5		
SBK1	4		14		
SGK (SGK1)	58	18	20		
SGK2	28		24		
SGKL (SGK3)	3		2		
SIK1	31		60	10	•
SIK3	25		33		•
SLK	94	64	98	87	•
SNF1LK2	81	52	87	32	
SPHK1	-3		4		
SPHK2	-5		-19		†
SRC	53	37	94	23	
SRMS (Srm)	10		45		
SRPK1	2		4		
SRPK2	2		3		
STK16 (PKL12)	90	23	61	12	•
STK17A (DRAK1)	87	23	6		•
STK17B (DRAK2)	66	79	-7		•
STK22B (TSSK2)	2		3		
STK22D (TSSK1)	84	30	9		
STK23 (MSSK1)	0		-1		
STK24 (MST3)	9		78	-3	
STK25 (YSK1)	13		55	0	
STK3 (MST2)	15		34		
STK32B (YANK2)	86	44	98	81	•
STK32C (YANK3)	54	9	87	38	•
STK33	59	11	55	10	•
STK38 (NDR)	36		29		•
STK38L (NDR2)	39		47		•
STK39 (STLK3)	24		50		•
STK4 (MST1)	18		59	6	
SYK	77	33	73	7	
TAOK1	86	44	77	49	•
TAOK2 (TAO1)	41		96	23	
TAOK3 (JIK)	33		56	19	•
TBK1	58	15	47		
TEC	8		-1		•
TEK (Tie2)	98	80	100	85	
TESK1	84	50	91	62	•
TESK2	26		44		•
TGFBR1 (ALK5)	99	93	99	94	•
TGFBR2	71	48	79	13	•
TLK1	-2		-8		•
TLK2	40		-2		•
TNIK	96	64	97	92	•
TNK1	49		82	16	
TNK2 (ACK)	22		60	10	•
TTK	33		10		•
TXK	37		84	11	
TYK2	97	60	97	31	
TYRO3 (RSE)	45		75	7	
ULK1	7		-2		•
ULK2	16		6		•
ULK3	59	22	28		•
VRK2	-1		19		•
WEE1	35		47		•
WNK1	9		10		•
WNK2	77	21	93	50	•
WNK3	50		80	20	•
YES1	98	85	100	91	
ZAK	12		9		•
ZAP70	7		9		

• LanthaScreen technology, no ATP; † = 10 μM ATP; ‡ = 100 μM ATP; N.D. = not determined.

Supplementary Table 6.2 | Results of the Oncolines™ profiling service in a panel of 102 cancer cell lines originating from different tissues. ROB433 (**15**) was tested at nine concentrations. Dose-response curves that were biphasic are indicated (•). Max eff.: maximal effect (%), pIC_{50}: half maximal inhibitory concentration, pGI_{50}: half maximal growth inhibitory concentration, pLD_{50}: half maximal lethal dose, all as –log(molar concentration) and determined as described in the Experimental section.

Cell line	ATCC ref	Tissue	Disease	pIC_{50}	Max eff. (%)	pGI_{50}	pLD_{50}
5637	HTB-9	Bladder/Urinary Tract	Bladder carcinoma	6.00	98	6.07	5.76
769-P	CRL-1933	Kidney	Renal cell carcinoma	6.26	100	6.24	5.40
786-O	CRL-1932	Kidney	Renal cell carcinoma	5.71	100	5.70	5.19
A-172	CRL-1620	CNS/Brain	Glioblastoma	5.81	100	5.89	5.34
A-204	HTB-82	Soft tissue	Embryonal rhabdomyosarcoma	5.91	100	5.99	5.37
A375	CRL-1619	Skin	Amelanotic melanoma	6.06	100	6.07	4.92
A388	CRL-7905	Skin	Squamous cell carcinoma	5.75	100	5.76	5.58
A-427	HTB-53	Lung	Lung adenocarcinoma	5.95	100	5.97	5.69
A-498	HTB-44	Kidney	Renal cell carcinoma	6.09	100	6.13	5.47
A-549	CCL-185	Lung	Lung adenocarcinoma	5.53	100	5.59	4.92
A-704	HTB-45	Kidney	Renal cell carcinoma	6.00	100	6.13	5.82
ACHN	CRL-1611	Kidney	Papillary renal cell carcinoma	6.03	100	6.05	5.59
AN3 CA	HTB-111	Uterus	Endometrial adenocarcinoma	7.28	38	<6.50	<5.50•
AsPC-1	CRL-1682	Pancreas	Pancreatic ductal adenocarcinoma	5.72	100	5.77	5.60
AU-565	CRL-2351	Breast	Breast adenocarcinoma	5.39	99	5.46	5.24
BT-20	HTB-19	Breast	Invasive ductal carcinoma	5.75	100	5.86	5.51
BT-549	HTB-122	Breast	Invasive ductal carcinoma	5.80	100	5.87	5.36
BxPC-3	CRL-1687	Pancreas	Pancreatic ductal adenocarcinoma	5.78	100	5.80	5.49
C-33 A	HTB-31	Cervix	Cervical squamous cell carcinoma	5.87	100	5.91	5.70
CAL 27	CRL-2095	Head and Neck	Tongue squamous cell carcinoma	6.19	100	6.19	5.71
CCF-STTG1	CRL-1718	CNS/Brain	Astrocytoma	5.75	98	5.78	5.62
CCRF-CEM	CCL-119	Lymphoid	Childhood T acute lymphoblastic leukemia	6.52	98	6.54	6.29
COLO 205	CCL-222	Bowel	Colon adenocarcinoma	5.94	100	5.96	5.57
COLO 829	CRL-1974	Skin	Cutaneous melanoma	5.39	100	5.43	5.24
Daoy	HTB-186	CNS/Brain	Medulloblastoma	5.89	100	5.94	5.55
DB	CRL-2289	Lymphoid	Diffuse large B-cell lymphoma	6.51	100	6.57	6.29
DLD-1	CCL-221	Bowel	Colon adenocarcinoma	5.50	100	5.52	4.94
DoTc2 4510	CRL-7920	Cervix	Cervical carcinoma	5.67	100	5.72	5.25
DU 145	HTB-81	Prostate	Prostate carcinoma	5.92	99	5.92	5.45
DU4475	HTB-123	Breast	Breast carcinoma	5.91	100	5.97	5.70
ES-2	CRL-1978	Ovary/Fallopian Tube	Ovarian clear cell adenocarcinoma	5.82	100	5.83	5.52
FaDu	HTB-43	Head and Neck	Hypopharyngeal squamous cell carcinoma	5.88	99	5.91	5.42
G-361	CRL-1424	Skin	Melanoma	5.74	100	5.77	5.59
HCT 116	CCL-247	Bowel	Colon carcinoma	6.27	98	6.22	5.31
HCT-15	CCL-225	Bowel	Colon adenocarcinoma	5.85	100	5.85	5.05
HL-60	CCL-240	Myeloid	Adult acute myeloid leukemia	5.76	100	5.79	5.63
Hs 578T	HTB-126	Breast	Invasive ductal carcinoma	6.23	100	6.30	5.72
Hs 746T	HTB-135	Esophagus/Stomach	Gastric adenocarcinoma	5.86	100	5.93	5.52
Hs 766T	HTB-134	Pancreas	Pancreatic adenocarcinoma	5.70	99	5.75	5.55
HT	CRL-2260	Lymphoid	Diffuse large B-cell lymphoma	5.82	100	5.86	5.68
HT-1080	CCL-121	Soft Tissue	Fibrosarcoma	5.97	100	5.90	5.45
HuTu 80	HTB-40	Bowel	Duodenal adenocarcinoma	6.66	100	6.65	5.53
J82	HTB-1	Bladder/Urinary Tract	Bladder carcinoma	5.87	99	5.95	5.63
JAR	HTB-144	Uterus	Gestational choriocarcinoma	6.22	100	6.25	5.48
Jurkat E6.1	TIB-152	Lymphoid	Childhood T acute lymphoblastic leukemia	5.92	100	5.96	5.63
K-562	CCL-243	Myeloid	Chronic myelogenous leukemia	6.23	100	6.26	5.50
KATO III	HTB-103	Esophagus/Stomach	Signet ring cell gastric adenocarcinoma	7.00	70	6.98	<6.00•
KG-1	CCL-246	Myeloid	Adult acute myeloid leukemia	6.97	68	7.00	<6.00•
KLE	CRL-1622	Uterus	Endometrial adenocarcinoma	5.59	100	5.75	5.42
KU812	CRL-2099	Myeloid	Chronic myelogenous leukemia	5.96	100	6.00	5.85
LNCaP FGC	CRL-1740	Prostate	Prostate carcinoma	5.42	100	5.48	5.32
LoVo	CCL-229	Bowel	Colon adenocarcinoma	5.80	100	5.91	5.28
LS 174T	CL-188	Bowel	Colon adenocarcinoma	6.15	100	6.14	5.43
LS411N	CRL-2159	Bowel	Cecum adenocarcinoma	5.91	100	5.95	5.44
MCF7	HTB-22	Breast	Invasive ductal carcinoma	5.41	100	5.47	5.32
MeWo	HTB-65	Skin	Melanoma	5.72	100	5.74	5.56
MG-63	CRL-1427	Bone	Osteosarcoma	5.93	100	5.95	5.74
MIA PaCa-2	CRL-1420	Pancreas	Pancreatic ductal adenocarcinoma	5.88	100	5.91	5.50
MOLT-4	CRL-1582	Lymphoid	Adult T acute lymphoblastic leukemia	5.85	100	5.91	5.66
NCCIT	CRL-2073	Testis	Testicular embryonal carcinoma	5.95	100	5.92	5.32
NCI-H460	HTB-177	Lung	Large cell lung carcinoma	5.43	100	5.43	4.94
NCI-H661	HTB-183	Lung	Large cell lung carcinoma	5.51	100	5.73	5.27
NCI-H82	HTB-175	Lung	Small cell lung carcinoma	5.89	100	5.92	5.61
OVCAR-3	HTB-161	Ovary/Fallopian Tube	High grade ovarian serous adenocarcinoma	5.62	100	5.79	5.39
PA-1	CRL-1572	Ovary/Fallopian Tube	Ovarian mixed germ cell tumor	5.85	100	5.88	5.66
PC-3	CRL-1435	Prostate	Prostate carcinoma	5.60	100	5.72	5.14
PFSK-1	CRL-2060	CNS/Brain	Primitive neuroectodermal tumor	5.63	99	5.64	5.46
RD	CCL-136	Soft tissue	Embryonal rhabdomyosarcoma	6.19	100	6.30	5.56
RKO	CRL-2577	Bowel	Colon carcinoma	5.82	100	5.84	5.53
RL	CRL-2261	Lymphoid	Diffuse large B-cell lymphoma	6.00	100	6.04	5.68
RL95-2	CRL-1671	Uterus	Endometrial adenosquamous carcinoma	5.69	100	5.74	5.58
RPMI-7951	HTB-66	Skin	Melanoma	6.13	100	6.19	5.58
RS4-11	CRL-1873	Lymphoid	Adult B acute lymphoblastic leukemia	6.34	100	6.36	5.89
RT4	HTB-2	Bladder/Urinary Tract	Bladder carcinoma	5.87	100	6.07	5.41
SHP-77	CRL-2195	Lung	Small cell lung carcinoma	5.45	96	5.54	5.21
SJCRH30	CRL-2061	Soft tissue	Alveolar rhabdomyosarcoma	5.80	100	5.85	5.65
SK-N-AS	CRL-2137	Peripheral Nervous System	Neuroblastoma	5.72	100	5.78	5.45

Supplementary Table 6.2 | (continued)

Cell line	ATCC ref	Tissue	Disease	pIC_{50}	Max eff. (%)	pGI_{50}	pLD_{50}
SK-N-FI	CRL-2142	Peripheral Nervous System	Neuroblastoma	5.93	99	6.06	5.62
SNU-5	CRL-5973	Esophagus/Stomach	Gastric carcinoma	5.98	100	6.14	5.42
SNU-C2B	CCL-250	Bowel	Cecum adenocarcinoma	5.78	100	5.83	5.63
SR	CRL-2262	Lymphoid	Anaplastic large cell lymphoma	6.03	99	6.05	5.73
SU-DHL-1	CRL-2955	Lymphoid	Anaplastic large cell lymphoma	5.87	100	5.88	5.58
SU-DHL-6	CRL-2959	Lymphoid	Diffuse large B-cell lymphoma	6.17	99	6.31	5.77
SUP-T1	ACC140	Lymphoid	Childhood T lymphoblastic lymphoma	5.69	100	5.71	5.52
SW48	CCL-231	Bowel	Colon adenocarcinoma	6.51	87	6.52	<5.50•
SW480	CCL-228	Bowel	Colon adenocarcinoma	5.60	100	5.61	5.41
SW620	CCL-227	Bowel	Colon adenocarcinoma	6.09	100	6.11	5.84
SW626	HTB-78	Bowel	Colon adenocarcinoma	5.55	100	5.58	5.29
SW837	CCL-235	Bowel	Rectal adenocarcinoma	5.55	99	5.66	5.07
SW872	HTB-92	Soft tissue	Liposarcoma	5.67	100	5.70	5.02
SW900	HTB-59	Lung	Squamous cell lung carcinoma	5.78	99	5.78	5.24
SW948	CCL-237	Bowel	Colon adenocarcinoma	6.04	99	6.08	5.68
SW982	HTB-93	Soft Tissue	Biphasic synovial sarcoma	6.16	99	6.21	5.55
T24	HTB-4	Bladder/Urinary Tract	Bladder carcinoma	5.87	100	5.86	5.64
T98G	CRL-1690	CNS/Brain	Glioblastoma	6.15	100	6.18	5.56
TCCSUP	HTB-5	Bladder/Urinary Tract	Bladder carcinoma	5.58	99	5.59	5.43
THP-1	TIB-202	Myeloid	Childhood acute monocytic leukemia	5.22	99	5.25	5.10
TT	CRL-1803	Thyroid	Hereditary thyroid gland medullary carcinoma	5.31	100	5.48	5.23
U-118 MG	HTB-15	CNS/Brain	Astrocytoma	5.80	100	5.83	5.60
U-2 OS	HTB-96	Bone	Osteosarcoma	5.93	100	5.99	5.65
U-87 MG	HTB-14	CNS/Brain	Glioblastoma	5.82	99	5.83	5.49
VA-ES-BJ	CRL-2138	Soft Tissue	Epithelioid sarcoma	5.57	100	5.59	5.42

References

1. Walczak, C. E., Cai, S. & Khodjakov, A. Mechanisms of chromosome behaviour during mitosis. *Nat. Rev. Mol. Cell Biol.* **11**, 91–102 (2010).
2. Kops, G. J. P. L., Weaver, B. A. A. & Cleveland, D. W. On the road to cancer: aneuploidy and the mitotic checkpoint. *Nat. Rev. Cancer* **5**, 773–785 (2005).
3. Musacchio, A. & Salmon, E. D. The spindle-assembly checkpoint in space and time. *Nat. Rev. Mol. Cell Biol.* **8**, 379–393 (2007).
4. Dominguez-Brauer, C., Thu, K. L., Mason, J. M., Blaser, H., Bray, M. R. & Mak, T. W. Targeting Mitosis in Cancer: Emerging Strategies. *Mol. Cell* **60**, 524–536 (2015).
5. Gallego-Jara, J., Lozano-Terol, G., Sola-Martínez, R. A., Cánovas-Díaz, M. & de Diego Puente, T. A Compressive Review about Taxol®: History and Future Challenges. *Molecules* **25**, 5986 (2020).
6. Weaver, B. A. How Taxol/paclitaxel kills cancer cells. *Mol. Biol. Cell* **25**, 2677–2681 (2014).
7. Markman, M. Managing taxane toxicities. *Support. Care Cancer* **11**, 144–147 (2003).
8. Janssen, A., Kops, G. J. P. L. & Medema, R. H. Elevating the frequency of chromosome mis-segregation as a strategy to kill tumor cells. *Proc. Natl. Acad. Sci.* **106**, 19108–19113 (2009).
9. Maia, A. R. R., de Man, J., Boon, U., Janssen, A., Song, J.-Y., Omerzu, M., Sterrenburg, J. G., Prinsen, M. B. W., Willemsen-Seegers, N., de Roos, J. A. D. M., van Doornmalen, A. M., Uitdehaag, J. C. M., Kops, G. J. P. L., Jonkers, J., Buijsman, R. C., Zaman, G. J. R. & Medema, R. H. Inhibition of the spindle assembly checkpoint kinase TTK enhances the efficacy of docetaxel in a triple-negative breast cancer model. *Ann. Oncol.* **26**, 2180–2192 (2015).
10. Siemeister, G., Mengel, A., Fernández-Montalván, A. E., Bone, W., Schröder, J., Zitzmann-Kolbe, S., Briem, H., Prechtl, S., Holton, S. J., Mönning, U., von Ahsen, O., Johanssen, S., Cleve, A., Pütter, V., Hitchcock, M., von Nussbaum, F., Brands, M., Ziegelbauer, K. & Mumberg, D. Inhibition of BUB1 Kinase by BAY 1816032 Sensitizes Tumor Cells toward Taxanes, ATR, and PARP Inhibitors *In Vitro* and *In Vivo*. *Clin. Cancer Res.* **25**, 1404–1414 (2019).
11. Zhang, G., Kruse, T., Guasch Boldú, C., Garvanska, D. H., Coscia, F., Mann, M., Barisic, M. & Nilsson, J. Efficient mitotic checkpoint signaling depends on integrated activities of Bub1 and the RZZ complex. *EMBO J.* **38**, (2019).
12. Lovly, C. M. & Shaw, A. T. Molecular Pathways: Resistance to Kinase Inhibitors and Implications for Therapeutic Strategies. *Clin. Cancer Res.* **20**, 2249–2256 (2014).
13. Hann, M. M. & Simpson, G. L. Intracellular drug concentration and disposition – The missing link? *Methods* **68**, 283–285 (2014).
14. Vichai, V. & Kirtikara, K. Sulforhodamine B colorimetric assay for cytotoxicity screening. *Nat. Protoc.* **1**, 1112–1116 (2006).
15. Skehan, P., Storeng, R., Scudiero, D., Monks, A., McMahon, J., Vistica, D., Warren, J. T., Bokesch, H., Kenney, S. & Boyd, M. R. New Colorimetric Cytotoxicity Assay for Anticancer-Drug Screening. *JNCI J. Natl. Cancer Inst.* **82**, 1107–1112 (1990).
16. Dragon, S., Hille, R., Götz, R. & Baumann, R. Adenosine 3′:5′-Cyclic Monophosphate (cAMP)-Inducible Pyrimidine 5′-Nucleotidase and Pyrimidine Nucleotide Metabolism of Chick Embryonic Erythrocytes. *Blood* **91**, 3052–3058 (1998).
17. Gribble, F. M., Loussouarn, G., Tucker, S. J., Zhao, C., Nichols, C. G. & Ashcroft, F. M. A Novel Method for Measurement of Submembrane ATP Concentration. *J. Biol. Chem.* **275**, 30046–30049 (2000).
18. Pathak, D., Shields, L. Y., Mendelsohn, B. A., Haddad, D., Lin, W., Gerencser, A. A., Kim, H., Brand, M. D., Edwards, R. H. & Nakamura, K. The Role of Mitochondrially Derived ATP in Synaptic Vesicle Recycling. *J. Biol. Chem.* **290**, 22325–22336 (2015).
19. Rangaraju, V., Calloway, N. & Ryan, T. A. Activity-Driven Local ATP Synthesis Is Required for Synaptic Function. *Cell* **156**, 825–835 (2014).
20. Uitdehaag, J. C. M., Kooijman, J. J., de Roos, J. A. D. M., Prinsen, M. B. W., Dylus, J., Willemsen-Seegers, N., Kawase, Y., Sawa, M., de Man, J., van Gerwen, S. J. C., Buijsman, R. C. & Zaman, G. J. R. Combined Cellular and Biochemical Profiling to Identify Predictive Drug Response Biomarkers for Kinase Inhibitors Approved for Clinical Use between 2013 and 2017. *Mol. Cancer Ther.* **18**, 470–481 (2019).
21. Zaman, G. J. R., de Roos, J. A. D. M., Libouban, M. A. A., Prinsen, M. B. W., de Man, J., Buijsman, R. C. & Uitdehaag, J. C. M. TTK Inhibitors as a Targeted Therapy for CTNNB1 (β-catenin) Mutant Cancers. *Mol. Cancer Ther.* **16**, 2609–2617 (2017).
22. Jemaà, M., Galluzzi, L., Kepp, O., Senovilla, L., Brands, M., Boemer, U., Koppitz, M., Lienau, P., Prechtl, S., Schulze, V., Siemeister, G., Wengner, A. M., Mumberg, D., Ziegelbauer, K., Abrieu, A., Castedo, M., Vitale, I. & Kroemer, G. Characterization of novel MPS1 inhibitors with preclinical anticancer activity. *Cell Death Differ.* **20**, 1532–1545 (2013).
23. Kusakabe, K., Ide, N., Daigo, Y., Itoh, T., Higashino, K., Okano, Y., Tadano, G., Tachibana, Y., Sato, Y., Inoue, M., Wada, T., Iguchi, M., Kanazawa, T., Ishioka, Y., Dohi, K., Tagashira, S., Kido, Y., Sakamoto, S., Yasuo, K., Maeda, M., Yamamoto, T., Higaki, M., Endoh, T., Ueda, K., Shiota, T., Murai, H. & Nakamura, Y. Diaminopyridine-Based Potent and Selective Mps1 Kinase Inhibitors Binding to an Unusual Flipped-Peptide Conformation. *ACS Med. Chem. Lett.* **3**, 560–564 (2012).

24. Anastas, J. N. & Moon, R. T. WNT signalling pathways as therapeutic targets in cancer. *Nat. Rev. Cancer* **13**, 11–26 (2013).
25. Etemadmoghadam, D., deFazio, A., Beroukhim, R., Mermel, C., George, J., Getz, G., Tothill, R., Okamoto, A., Raeder, M. B., AOCS Study Group, Harnett, P., Lade, S., Akslen, L. A., Tinker, A. V., Locandro, B., Alsop, K., Chiew, Y.-E., Traficante, N., Fereday, S., Johnson, D., Fox, S., Sellers, W., Urashima, M., Salvesen, H. B., Meyerson, M. & Bowtell, D. Integrated Genome-Wide DNA Copy Number and Expression Analysis Identifies Distinct Mechanisms of Primary Chemoresistance in Ovarian Carcinomas. *Clin. Cancer Res.* **15**, 1417–1427 (2009).
26. Patch, A.-M., Christie, E. L., Etemadmoghadam, D., Garsed, D. W., George, J., Fereday, S., Nones, K., Cowin, P., Alsop, K., Bailey, P. J., Kassahn, K. S., Newell, F., Quinn, M. C. J., Kazakoff, S., Quek, K., Wilhelm-Benartzi, C., Curry, E., Leong, H. S., Hamilton, A., Mileshkin, L., Au-Yeung, G., Kennedy, C., Hung, J., Chiew, Y.-E., Harnett, P., Friedlander, M., Quinn, M., Pyman, J., Cordner, S., O'Brien, P., Leditschke, J., Young, G., Strachan, K., Waring, P., Azar, W., Mitchell, C., Traficante, N., Hendley, J., Thorne, H., Shackleton, M., Miller, D. K., Arnau, G. M., Tothill, R. W., Holloway, T. P., Semple, T., Harliwong, I., Nourse, C., Nourbakhsh, E., Manning, S., Idrisoglu, S., Bruxner, T. J. C., Christ, A. N., Poudel, B., Holmes, O., Anderson, M., Leonard, C., Lonie, A., Hall, N., Wood, S., Taylor, D. F., Xu, Q., Fink, J. L., Waddell, N., Drapkin, R., Stronach, E., Gabra, H., Brown, R., Jewell, A., Nagaraj, S. H., Markham, E., Wilson, P. J., Ellul, J., McNally, O., Doyle, M. A., Vedururu, R., Stewart, C., Lengyel, E., Pearson, J. V., Waddell, N., deFazio, A., Grimmond, S. M. & Bowtell, D. D. L. Whole–genome characterization of chemoresistant ovarian cancer. *Nature* **521**, 489–494 (2015).
27. Rose, M., Burgess, J. T., O'Byrne, K., Richard, D. J. & Bolderson, E. PARP Inhibitors: Clinical Relevance, Mechanisms of Action and Tumor Resistance. *Front. Cell Dev. Biol.* **8**, 564601 (2020).
28. Etemadmoghadam, D., Weir, B. A., Au-Yeung, G., Alsop, K., Mitchell, G., George, J., Australian Ovarian Cancer Study Group, Davis, S., D'Andrea, A. D., Simpson, K., Hahn, W. C. & Bowtell, D. D. L. Synthetic lethality between CCNE1 amplification and loss of BRCA1. *Proc. Natl. Acad. Sci.* **110**, 19489–19494 (2013).
29. Yang, C., Wang, H., Xu, Y., Brinkman, K. L., Ishiyama, H., Wong, S. T. C. & Xu, B. The kinetochore protein Bub1 participates in the DNA damage response. *DNA Repair* **11**, 185–191 (2012).
30. Berthold, M. R., Cebron, N., Dill, F., Gabriel, T. R., Kötter, T., Meinl, T., Ohl, P., Thiel, K. & Wiswedel, B. KNIME - the Konstanz Information Miner: Version 2.0 and Beyond. *SIGKDD Explor Newsl* **11**, 26–31 (2009).
31. HGNC Database, HUGO Gene Nomenclature Committee (HGNC), European Molecular Biology Laboratory, European Bioinformatics Institute (EMBL-EBI), Wellcome Genome Campus, Hinxton, Cambridge CB10 1SD, United Kingdom www.genenames.org. *(accessed in April 2021)* https://www.accessdata.fda.gov/drugsatfda_docs/nda/2013/205552Orig1s000TOC.cfm.
32. Tweedie, S., Braschi, B., Gray, K., Jones, T. E. M., Seal, R. L., Yates, B. & Bruford, E. A. Genenames.org: the HGNC and VGNC resources in 2021. *Nucleic Acids Res.* **49**, D939–D946 (2021).
33. The UniProt Consortium. UniProt: the universal protein knowledgebase in 2021. *Nucleic Acids Res.* **49**, D480–D489 (2021).
34. Eid, S., Turk, S., Volkamer, A., Rippmann, F. & Fulle, S. KinMap: a web-based tool for interactive navigation through human kinome data. *BMC Bioinformatics* **18**, 16 (2017).
35. Uitdehaag, J. C. M., de Roos, J. A. D. M., van Doornmalen, A. M., Prinsen, M. B. W., de Man, J., Tanizawa, Y., Kawase, Y., Yoshino, K., Buijsman, R. C. & Zaman, G. J. R. Comparison of the Cancer Gene Targeting and Biochemical Selectivities of All Targeted Kinase Inhibitors Approved for Clinical Use. *PLoS ONE* **9**, e92146 (2014).
36. Bairoch, A. The Cellosaurus, a Cell-Line Knowledge Resource. *J. Biomol. Tech. JBT* **29**, 25–38 (2018).
37. Kundra, R., Zhang, H., Sheridan, R., Sirintrapun, S. J., Wang, A., Ochoa, A., Wilson, M., Gross, B., Sun, Y., Madupuri, R., Satravada, B. A., Reales, D., Vakiani, E., Al-Ahmadie, H. A., Dogan, A., Arcila, M., Zehir, A., Maron, S., Berger, M. F., Viaplana, C., Janeway, K., Ducar, M., Sholl, L., Dogan, S., Bedard, P., Surrey, L. F., Sanchez, I. H., Syed, A., Rema, A. B., Chakravarty, D., Suehnholz, S., Nissan, M., Iyer, G. V., Murali, R., Bouvier, N., Soslow, R. A., Hyman, D., Younes, A., Intlekofer, A., Harding, J. J., Carvajal, R. D., Sabbatini, P. J., Abou-Alfa, G. K., Morris, L., Janjigian, Y. Y., Gallagher, M. M., Soumerai, T. A., Mellinghoff, I. K., Hakimi, A. A., Fury, M., Huse, J. T., Bagrodia, A., Hameed, M., Thomas, S., Gardos, S., Cerami, E., Mazor, T., Kumari, P., Raman, P., Shivdasani, P., MacFarland, S., Newman, S., Waanders, A., Gao, J., Solit, D. & Schultz, N. OncoTree: A Cancer Classification System for Precision Oncology. *JCO Clin. Cancer Inform.* 221–230 (2021).
38. Sveen, A., Bruun, J., Eide, P. W., Eilertsen, I. A., Ramirez, L., Murumägi, A., Arjama, M., Danielsen, S. A., Kryeziu, K., Elez, E., Tabernero, J., Guinney, J., Palmer, H. G., Nesbakken, A., Kallioniemi, O., Dienstmann, R. & Lothe, R. A. Colorectal Cancer Consensus Molecular Subtypes Translated to Preclinical Models Uncover Potentially Targetable Cancer Cell Dependencies. *Clin. Cancer Res.* **24**, 794–806 (2018).
39. Tate, J. G., Bamford, S., Jubb, H. C., Sondka, Z., Beare, D. M., Bindal, N., Boutselakis, H., Cole, C. G., Creatore, C., Dawson, E., Fish, P., Harsha, B., Hathaway, C., Jupe, S. C., Kok, C. Y., Noble, K., Ponting, L., Ramshaw, C. C., Rye, C. E., Speedy, H. E., Stefancsik, R., Thompson, S. L., Wang, S., Ward, S., Campbell, P. J. & Forbes, S. A. COSMIC: the Catalogue Of Somatic Mutations In Cancer. *Nucleic Acids Res.* **47**, D941–D947 (2019).
40. Garnett, M. J., Edelman, E. J., Heidorn, S. J., Greenman, C. D., Dastur, A., Lau, K. W., Greninger, P., Thompson, I. R., Luo, X., Soares, J., Liu, Q., Iorio, F., Surdez, D., Chen, L., Milano, R. J., Bignell, G. R., Tam, A. T., Davies, H., Stevenson, J. A., Barthorpe, S., Lutz, S. R., Kogera, F., Lawrence, K., McLaren-Douglas, A., Mitropoulos, X., Mironenko, T., Thi, H., Richardson, L., Zhou, W., Jewitt, F., Zhang, T., O'Brien, P., Boisvert, J. L., Price, S., Hur, W., Yang, W., Deng, X.,

Butler, A., Choi, H. G., Chang, J. W., Baselga, J., Stamenkovic, I., Engelman, J. A., Sharma, S. V., Delattre, O., Saez-Rodriguez, J., Gray, N. S., Settleman, J., Futreal, P. A., Haber, D. A., Stratton, M. R., Ramaswamy, S., McDermott, U. & Benes, C. H. Systematic identification of genomic markers of drug sensitivity in cancer cells. *Nature* **483**, 570–575 (2012).

41. Lawrence, M. S., Stojanov, P., Mermel, C. H., Robinson, J. T., Garraway, L. A., Golub, T. R., Meyerson, M., Gabriel, S. B., Lander, E. S. & Getz, G. Discovery and saturation analysis of cancer genes across 21 tumour types. *Nature* **505**, 495–501 (2014).

7

Summary and future prospects

Cancer is the overarching term for diseases in which abnormal cells divide in an uncontrolled manner.[1] These cells can develop in and may subsequently spread to different types of tissue. Hallmarks of cancer, which are biological capabilities that are acquired during the development of a tumor, include, but are not limited to, sustaining proliferative signaling, resisting cell death and metastasis.[2] In addition, there are characteristics that enable their acquisition, including genetic instability.[2] The development of new anti-cancer drugs can therefore be aimed at one or multiple hallmarks or at characteristics that enable these hallmarks.[2] The research described in thesis covers several phases of a drug discovery program (**Figure 7.1**) aimed at the discovery of small molecule kinase inhibitors for the treatment of cancer. This chapter summarizes the work described in previous chapters and provides future directions for further optimization and applications of the inhibitors.

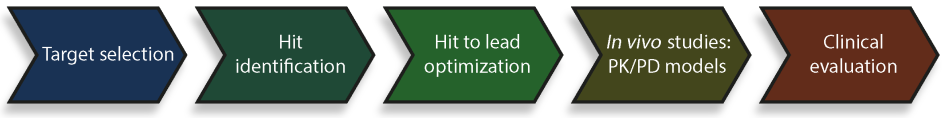

Figure 7.1 | Simplified scheme of the different phases in drug discovery.

Target selection

Protein kinases are a prominent class of drug targets for the treatment of cancer.[3] **Chapter 1** introduces the protein kinase budding uninhibited by benzimidazole 1 (BUB1) as therapeutic target. BUB1 participates in the spindle assembly checkpoint (SAC), which is a safety mechanism during mitosis that ensures correct chromosome segregation.[4] Many cancer cells suffer from a weakened SAC and interference with these diminished checkpoints to further disrupt SAC signaling is hypothesized to eventually result in cell death due to severe chromosomal instability.[5,6] Potential kinase targets of the SAC include monopolar spindle 1 (MPS1) and BUB1.[5,6] Previously, MPS1 inhibitors have been developed, some of which have entered clinical trials.[7–9] However, multiple mouse xenograft studies on MPS1 inhibitors only showed single agent efficacy when administered near the maximum tolerated dose and cotreatment with taxanes was therefore necessary to obtain the desired inhibition of tumor growth.[10–13] Novel inhibitors with good physicochemical properties that allow cellular BUB1 target engagement may result in single agent efficacy. This would make cotreatment with taxanes dispensable, which is desired in view of the fact that these agents cause severe side effects.[14] BUB1 was therefore selected as target for the discovery of novel inhibitors.

Hit identification

Chapter 2 describes the results of a high-throughput screen which was used for the discovery of novel BUB1 inhibitors. A library of 53,408 compounds, enriched with kinase inhibitors, was screened and resulted in 214 confirmed actives. After deselecting compounds that interfered with the assay readout, and dose-response experiments, a qualified hit list of 25 structurally diverse molecules was obtained. Hits **1** and **2** (**Figure 7.2**) were prioritized based on their

favorable properties such as activity, molecular weight, ligand efficiency, lipophilicity and lipophilic efficiency.[15] Both hits were resynthesized and their activities were confirmed.

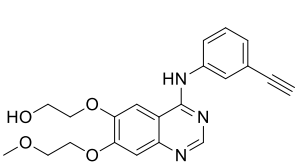

1

pIC_{50} = 6.59
MW = 379
LE = 0.33
cLogP = 2.6
LipE = 4.2

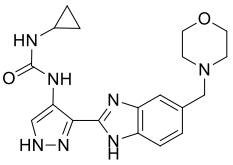

2

pIC_{50} = 6.78
MW = 381
LE = 0.34
cLogP = 0.4
LipE = 6.5

Figure 7.2 | Prioritized hits **1** and **2** of high-throughput screen and corresponding physicochemical properties. pIC_{50}: half maximal inhibitory concentrations from high-throughput dose-response assay; MW: molecular weight (g/mol); LE: ligand efficiency[15], defined as: $\mathrm{LE} = (-RT * \ln(\mathrm{app}.K_i))/\mathrm{HA}$, where HA stands for the number of 'heavy atoms' (non-hydrogen atoms); cLogP: LogP calculated by DataWarrior (v.5.2.1); LipE: lipophilic efficiency[15], defined as: $\mathrm{LipE} = \mathrm{app}.\mathrm{p}K_i - \mathrm{cLogP}$.

Hit to lead optimization

In **Chapter 3**, the structure-activity relationship (SAR) of hit **1** was investigated. Synthesis and biochemical evaluation of 48 analogues resulted in the identification of compound **3** (**Figure 7.3**). Compared to hit **1**, compound **3** which was significantly less lipophilic and due to its slightly improved potency, a 10-fold better lipophilic efficiency was obtained. The docking pose of compounds **1** and **3** in the kinase domain of BUB1 matched with the observed SAR. Whereas the quinazoline *N*1 of **1** formed a hydrogen bond with the backbone of hinge amino acid Tyr869, no hydrogen bonds were established with the hinge region in the docking pose of compound **3**. Instead, hydrogen bond formation was predicted between the pyrazole *N*2 and both Lys821 and Asp946 as well as between the pyrimidine *N*1 and Lys821.

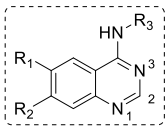

General structure

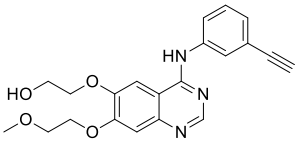

1

pIC_{50} = 6.28 ± 0.05
app.K_i = 185 nM
MW = 379
cLogP = 2.6
LipE = 4.1
tPSA = 85

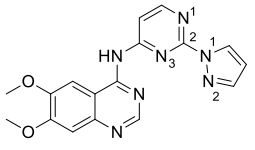

3

pIC_{50} = 6.41± 0.04
app.K_i = 136 nM
MW = 349
cLogP = 1.7
LipE = 5.1
tPSA = 96

Figure 7.3 | Chemical structures and physicochemical properties (as defined in **Figure 7.2**) of hit **1** and optimized hit **3**. pIC_{50}: half maximal inhibitory concentration, determined by the biochemical BUB1 assay; tPSA: topological polar surface area (Å^2), calculated by Chemdraw (v.19.1).

Chapter 4 describes a comprehensive structure-activity relationship (SAR) study of hit **2**. In total, 59 analogues were synthesized and biochemically evaluated. This yielded substituted 2-phenyl-5-methoxy-*N*-(3-(5-(morpholinomethyl)-1*H*-benzo[*d*]imidazol-2-yl)-1*H*-pyrazol-4-yl)pyrimidin-4-amines as highly potent BUB1 inhibitors, including compound **4** (**Figure 7.4A**), which is the most potent BUB1 inhibitor reported to date. To study the binding mode of **4**, the crystal structure of this compound bound to the kinase domain of BUB1 was elucidated (**Figure 7.4B,C**). Compound **4** binds in the ATP pocket of BUB1 leaving the regulatory (R)-spine[16] intact. This indicated that **4** can be classified as a type I inhibitor.[17] The benzimidazole-pyrazole scaffold forms three hydrogen bonds with the backbone of hinge amino acids Tyr869 and Glu867 of BUB1 (**Figure 7.4B**). An additional hydrogen bond is formed between the pyrimidine *N*1 and the side chain of Lys821 which is mediated by a water molecule. Furthermore, the morpholine is solvent exposed and the amine between the pyrazole and pyrimidine forms an intramolecular hydrogen bond with the benzimidazole nitrogen. The acetylene binds a pocket that is available due to the small size of the glycine gatekeeper residue of BUB1 (**Figure 7.4C**).

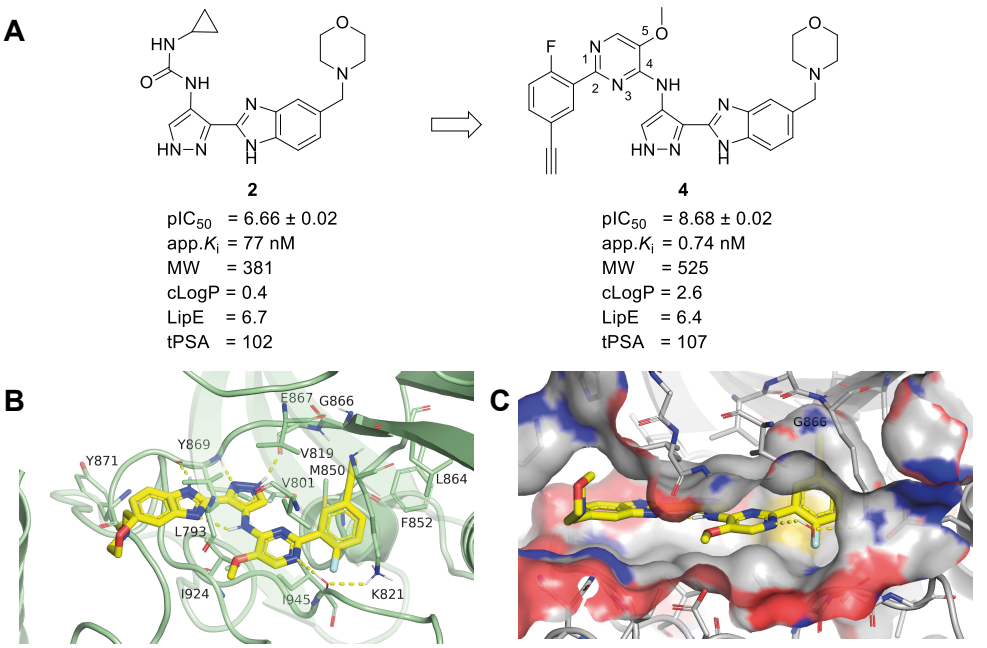

Figure 7.4 | Hit optimization and crystal structure of optimized compound 4 bound to the kinase domain of human BUB1. (A) Chemical structures and physicochemical properties (as defined in **Figure 7.3**) of hit **2** and optimized compound **4**. **(B)** Crystal structure of **4** bound to BUB1. Hydrogen bonds are visualized by dashed lines (yellow) and a water molecule is represented by small sticks. β-sheets 1–3 are semi-transparent for visualization purposes. **(C)** Representation of the surface around amino acids within 8 Å from **4**.

Chapter 5 describes the development of a cellular BUB1 target engagement assay using probe **5**[18] (**Figure 7.5**) and gel-based activity-based protein profiling (ABPP). Probe **5** as well as 16 analogues were synthesized. To study BUB1 labeling, a U2OS cell line was generated that stably overexpressed GFP-FLAG-BUB1. Labeling by all probes was evaluated in this cell

line and probe **5** was found to show the most favorable labeling profile. Mutating Cys1080 to alanine completely abolished BUB1 labeling indicating that this amino acid is responsible for the formation of a covalent bond. Labeling of BUB1 by probe **5** was dose- and time-dependent and labeling could dose-dependently be outcompeted by BUB1 inhibitor BAY1816032.[19] This provided proof-of-principle for the use of **5** as BUB1 chemical probe that allows for studying cellular BUB1 target engagement using gel-based ABPP.

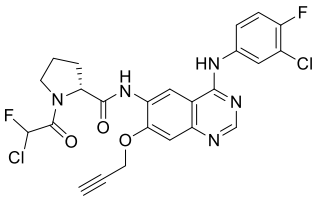

5

Figure 7.5 | Chemical structure of probe **5**.[18]

Chapter 6 focuses on further profiling a subset of the substituted 2-phenyl-5-methoxy-*N*-(3-(5-(morpholinomethyl)-1*H*-benzo[*d*]imidazol-2-yl)-1*H*-pyrazol-4-yl)pyrimidin-4-amine BUB1 inhibitors identified in **Chapter 4** to study their potential as lead candidates for therapeutic purposes. To this end, drug-likeness was studied by investigation of several *in vitro* absorption, distribution, metabolism and excretion (ADME) assays. In addition, cellular BUB1 target engagement was investigated by using the assay developed in **Chapter 5**. A strong correlation was found between biochemical pIC_{50} values and BUB1 target engagement (Pearson's r: 0.921, *p*-value: 0.0004), which suggested that cell permeability was similar among the compounds tested and that target engagement was mainly driven by the affinity for BUB1. Furthermore, the effects on U2OS cell proliferation were explored by sulforhodamine B (SRB) assays. These assays were performed with and without a low dose of paclitaxel to investigate potential synergistic effects between BUB1 inhibition and paclitaxel.[19] A moderate correlation was found between BUB1 target engagement and pIC_{50} values of the SRB assays (Pearson's r: 0.655, *p*-value: 0.056). This suggested that inhibition of cell proliferation was, to a large extent, dependent on BUB1 inhibition, but that off-target activity contributed to the observed effect. ROB433 (**6**) and ROB464 (**7**) showed the most favorable profile (**Figure 7.6**, **Table 7.1**) with good physicochemical properties, subnanomolar affinity for BUB1, good cellular BUB1 target engagement and an acceptable *in vitro* ADME profile. Therefore, kinase selectivity was assessed for these compounds. At 100 nM, ROB433 and ROB464 were selective over 346 and 352 kinases, respectively, while 49 (ROB433) and 44 (ROB464) kinases were detected as off-targets. Finally, the antiproliferative activity of ROB433 (**6**) was assessed in a panel of 102 cancer cell lines. Concentrations required for half maximal growth inhibition (GI_{50}) ranged from 101 nM (for KG-1 cells) to 5.57 µM (for THP-1 cells). The mean GI_{50} value among all cell lines was 1.43 µM, which indicated that ROB433 has a favorable cytotoxicity profile.

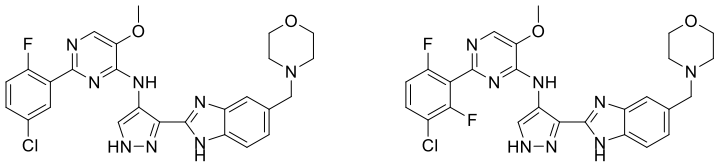

ROB433 (**6**) ROB464 (**7**)

Figure 7.6 | Chemical structures of ROB433 (**6**) and ROB464 (**7**).

Table 7.1 | Summary of physicochemical properties (as defined in **Figure 7.3**), ADME properties, aqueous solubility and activities of lead compounds ROB433 (**6**) and ROB464 (**7**).

	ROB433	**ROB464**		**ROB433**	**ROB464**
Biochemical activity (pIC_{50} ± SEM)	8.57 ± 0.02	8.62 ± 0.03	**Target engagement** (pTE_{50} ± SEM)	7.50 ± 0.11	8.01 ± 0.09
Apparent K_i (nM)	0.94	0.84	**U2OS cell proliferation** (pIC_{50} ± SEM)	6.32 ± 0.06	7.39 ± 0.05
Molecular weight (g/mol)	535	553	**Plasma stability** (% remaining after 180 min)	100 (h)* 100 (r)* 85 (m)*	100 (h) 100 (r)
cLogP	3.1	3.2	**Microsomal stability** ($t_{1/2}$ in min)	41 (h) 63 (r) 22 (m)	29 (h) 49 (r) 6.1 (m)
LipE	5.9	5.8	**Microsomal clearance** (µL/min/mg)	8.4 (h) 22 (r) 16 (m)	12 (h) 28 (r) 57 (m)
tPSA ($Å^2$)	107	107	**Plasma protein binding** (%)	100 (h) 100 (r) 99.9 (m)	99.7 (h) 99.7 (r)
			Aqueous solubility (µM)	4.4	6.0

* (h): human, (r): rat, (m): mouse

Future directions

Chapter 3 describes the optimization of hit **1** to compound **3**. Docking studies revealed a different binding mode of **3** when compared to that of hit **1**, in which the quinazoline *N1* did not form a hydrogen bond with the hinge region of BUB1. To provide evidence for this proposed binding mode, a compound lacking the quinazoline *N*1 is proposed (**Figure 7.7**). If this molecule would show similar activity, it may indeed suggest that it does not interact with the hinge region of BUB1 and its predicted binding mode may provide future directions for further analogue design.

The use of covalent drugs is an alternative approach to reversible kinase inhibition and has been shown to have several benefits.[20] Due to the formation of a covalent bond, irreversible inhibitors have high potencies due to prolonged target occupancy. In addition, when off-target binding only occurs in a reversible fashion, better selectivity can be achieved. Furthermore, covalent inhibitors might be less prone to acquired resistance, as was reported for covalent EGFR inhibition, which upon the T790M mutation improved affinity for ATP and

thereby reduced efficacy of reversible inhibitors.[21,22] **Chapter 5** describes the validation of compound **5** (**Figure 7.5**) as BUB1 probe which was found to covalently react with BUB1. Compound **5** therefore provides an excellent starting point for the development of irreversible BUB1 inhibitors. However, optimization of **5** proved challenging. Therefore, crystallization of this compound in the kinase domain of BUB1 would allow for a more rational design of novel covalent BUB1 inhibitors.

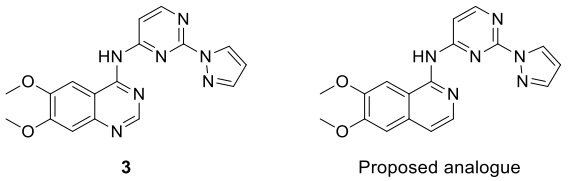

Figure 7.7 | Proposed analogue of **3** to provide evidence for its predicted binding mode.

BUB1 is known to phosphorylate histone H2A at threonine 120.[23] The importance of the enzymatic activity of BUB1 in chromosome alignment is less well established since contradicting results have been published.[24–27] In **Chapter 6**, ROB433 (**6**) and ROB464 (**7**) were identified as lead BUB1 inhibitors with good cellular BUB1 target engagement which provide opportunities to study aforementioned processes. A preliminary (N=1) study on the effects of BUB1 inhibition on H2A phosphorylation and chromosome alignment was therefore performed. To this end, human retinal pigment epithelial 1 (RPE1) cells, which are frequently used to study mitosis[28], were synchronized in the G_2 phase by CDK1 inhibitor RO-3306.[29] After drug washout, cells were treated with monastrol, which causes monopolar spindles due to inhibition of motor protein kinesin Eg5.[30] Simultaneously, cells were treated with a BUB1 inhibitor. Subsequently, another drug washout was performed to allow for bipolar spindle assembly. Cells were then treated with MG132, a proteasome inhibitor to prevent mitotic exit[31], and a BUB1 inhibitor. H2A phosphorylation was visualized by immunofluorescence staining using an anti-H2A-p-T120 antibody. In addition, chromosome alignment was investigated by staining of CENP-C, located at the inner kinetochore, tubulin and DNA.

Quantification of H2A phosphorylation (H2A-p-T120) revealed a significant reduction of H2A-p-T120 signal upon treatment with 100 nM of ROB433 and ROB464 (**Figure 7.8A,C**). This confirmed inhibition of BUB1 in a cellular system. In contrast, 300 nM of BAY1816032 was required to match these results. To study chromosomal alignment, the immunofluorescence images were used to classify cells into different phenotypes based on their extent of chromosome alignment as determined by DAPI staining of DNA. Chromosome alignment was dose-dependently impaired and more profound for ROB464 compared to ROB433 (**Figure 7.8B,C**). BAY1816032 only moderately increased chromosome alignment errors at both concentrations. Based on the observation that 100 nM ROB433 and ROB464 inhibited Aurora B *in vitro* (71 and 43%, respectively, **Chapter 6**), Aurora B may also be (partially) inhibited in living cells. To investigate this, phosphorylation of one of Aurora B's

targets, histone H3 at Ser10[32], was investigated as described above. Immunofluorescence staining by an anti-H3-p-S10 antibody revealed a significant reduction in phosphorylation of H3Ser10 (H3-p-S10) in both ROB433 and ROB464 treated cells (**Figure 7.9A,C**). This reduction was similar to cells treated with Aurora B inhibitor ZM447439[33] (2 µM). Interestingly, BAY1816032 also reduced phosphorylation of H3Ser10, whereas no *in vitro* inhibition of Aurora B was observed for this compound.[19] Previously, BUB1-mediated H2A phosphorylation has been reported to control the localization and activity of Aurora B.[27] Whether direct inhibition of Aurora B by ROB433 and ROB464 is responsible for the observed reduction of histone H3-S10 phosphorylation or that this is mediated via a reduction of H2A-T120 phosphorylation, remains to be investigated. Of note, the fractions of moderately and heavily misaligned phenotypes for ZM447439 treated cells were similar to those of ROB433 (300 nM) and ROB464 (100 nM) treated cells (**Figure 7.9B,C**).

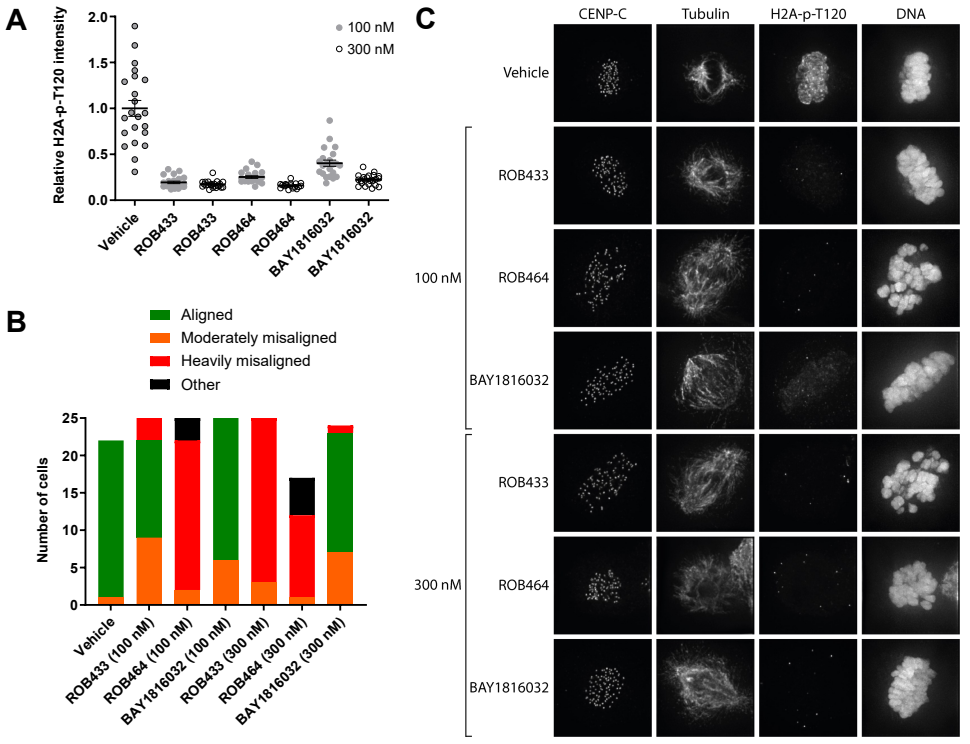

Figure 7.8 | ROB433 and ROB464 reduce phosphorylation of histone H2A-T120 and induce chromosome alignment errors in RPE1 cells. (A) Cells were synchronized by treatment with RO-3306 (5 µM, 16 h), monopolar spindles were induced by treatment with monastrol (200 µM, 2 h), bipolar spindle assembly was then allowed during treatment with MG132 (5 µM, 30 min). Drug washout was performed in between each treatment and during the treatment of monastrol and MG132 cells were cotreated with indicated inhibitor at indicated concentration. Cells were then permeabilized, fixed and immunostained with antibodies for H2A-p-T120, CENP-C and tubulin. DNA was stained by DAPI. The fluorescence intensity of H2A-p-T120 was determined in 22 cells per condition, unless fewer cells were available due to treatment-related cellular defects, and normalized to vehicle-treated cells. **(B)** Cells were treated as in (A) and classified into four different phenotypes based on chromosome alignment as determined by DNA staining: aligned, moderately misaligned, heavily misaligned or other. Phenotypes of 20-25 cells were assessed per condition, unless fewer cells were available due to treatment-related cellular defects. **(C)** Representative images corresponding to graphs in (A) and (B) based on the most predominant phenotype as assessed in (B). Data represent mean with SEM (N=1).

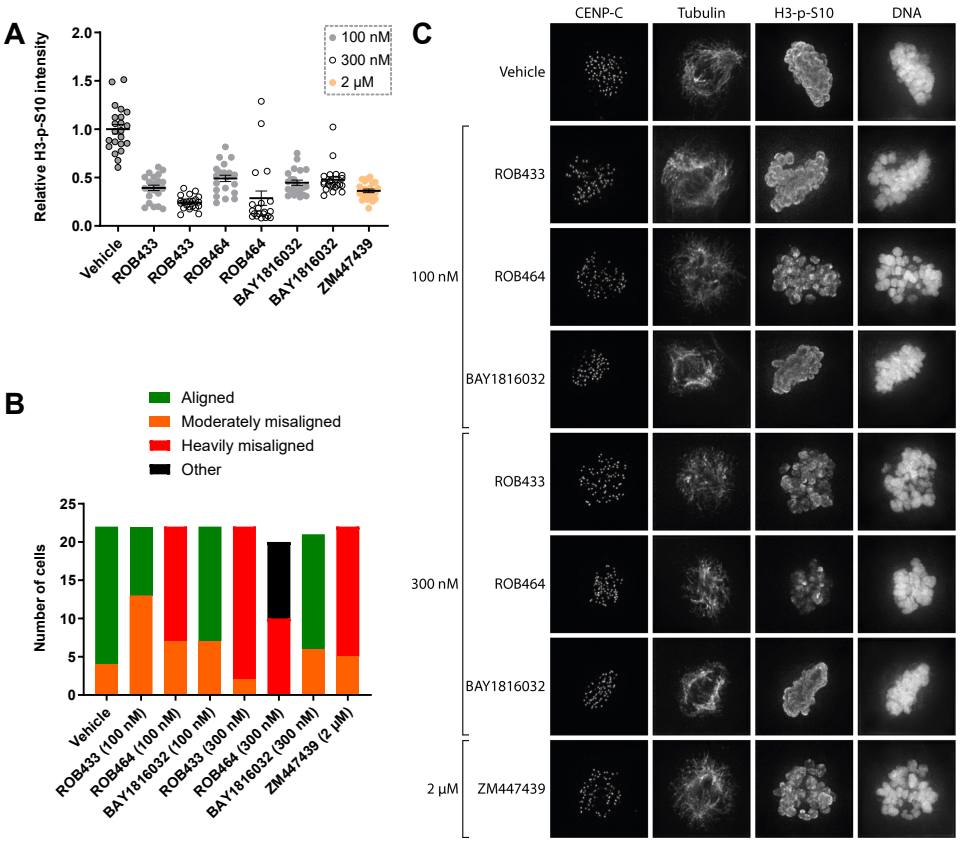

Figure 7.9 | ROB433 and ROB464 reduce phosphorylation of histone H3-S10 and induce chromosome alignment errors in RPE1 cells. (A) Cells were synchronized by treatment with RO-3306 (5 µM, 16 h), monopolar spindles were induced by treatment with monastrol (200 µM, 2 h), bipolar spindle assembly was then allowed during treatment with MG132 (5 µM, 30 min). Drug washout was performed in between each treatment and during the treatment of monastrol and MG132 cells were cotreated with indicated inhibitor at indicated concentration. Cells were then permeabilized, fixed and immunostained with antibodies for H3-p-S10, CENP-C and tubulin. DNA was stained by DAPI. The fluorescence intensity of H3-p-S10 was determined in 22 cells per condition and normalized to vehicle-treated cells. **(B)** Cells were treated as in (A) and classified into four different phenotypes based on chromosome alignment as determined by DNA staining: aligned, moderately misaligned, heavily misaligned or other. Phenotypes of 20-22 cells were assessed per condition. **(C)** Representative images corresponding to graphs in (A) and (B) based on the most predominant phenotype as assessed in (B). Data represent mean with SEM (N=1).

To further provide evidence that the observed phenotypes are attributed to BUB1 inhibition, the cellular selectivity profiles of these compounds need to be investigated. Previously, a broad-spectrum kinase probe, XO44, was published which allowed for capturing over 130 kinases from a single cell line.[34] Such probes can be used for activity-based protein profiling in a chemical proteomics setting to investigate cellular selectivity.[35]

Finally, to assess whether ROB433 and/or ROB464 are suitable for the investigation of their anti-cancer properties, measuring pharmacokinetics is required. Measuring clearance, volume of distribution, half-life, bioavailability and plasma exposure in mice will determine

whether follow-up studies can be performed in mouse xenograft models or that further optimization of these BUB1 inhibitors is required.

Concluding remarks

Research aimed at the identification of novel targets for the treatment of cancer is expanding and small molecule inhibitors fulfill an important role in this process. The research described in this thesis provides two lead inhibitors (ROB433 and ROB464) of the spindle assembly checkpoint kinase BUB1, and an assay to measure cellular BUB1 target engagement. Assessment of cellular BUB1 target occupancy, using the assay described in **Chapter 5**, will be a valuable tool for future development of BUB1 inhibitors. In addition, the series of substituted 2-phenyl-5-methoxy-*N*-(3-(5-(morpholinomethyl)-1*H*-benzo[*d*]imidazol-2-yl)-1*H*-pyrazol-4-yl)pyrimidin-4-amines described in **Chapter 4** include the most active BUB1 inhibitors known to date. Among this series, ROB433 and ROB464 showed excellent properties, including single agent inhibition of cancer cell proliferation, which allow for further evaluation of pharmacokinetic and pharmacodynamic studies *in vivo*. Both compounds hold promise for their therapeutic application in the treatment of cancers which currently lack a molecular target, such as triple-negative breast cancer.

Acknowledgements

From the Hubrecht institute, Maaike Lambers and Carlos Sacristan are kindly acknowledged for performing the immunofluorescence and chromosome alignment assays and Geert Kops for supervision.

Experimental

Cell culture

RPE1 Flp-in cells were cultured at 37°C under 5% CO_2 in Dulbecco's Modified Eagle's Medium/Nutrient Mixture F-12 Ham (DMEM/F12; Sigma D8062) supplemented with 9% (v/v) tetracycline-free fetal bovine serum (FBS), penicillin and streptomycin (50 µg/mL each; Sigma (P0781)).

Immunofluorescence staining

For chromosome alignment assays and measuring histone phosphorylation, RPE1 cells were seeded at 40% confluency in 24-well plates on 1.5H 12 mm coverslips. Cells were synchronized by treatment with RO-3306 (5 µM; Tocris (4181)) for 16 h, washed with pre-warmed DMEM/F12 five times and incubated for 2 h in DMEM/F12 with monastrol (200 µM, Tocris (1305)) and vehicle or inhibitor (indicated concentration) (final concentration (f.c.) DMSO was 0.5%). Cells were then carefully washed four times with pre-warmed DMEM/F12 and incubated for 30 min in DMEM/F12 with MG132 (5 µM, Sigma (C2211)) and vehicle or inhibitor (indicated concentration) (f.c. DMSO was 0.5%), to allow chromosome alignment. Subsequently, cells were permeabilized for 1 min with pre-warmed 0.5% Triton X-100/PHEM buffer (=PIPES (60 mM), HEPES (25 mM), $MgCl_2{\cdot}6H_2O$ (2 mM), EGTA (10 mM), pH 6.9), followed by fixation for 10 min with pre-warmed 4% paraformaldehyde/PBS. After fixation, coverslips were washed three times with PBS and blocked with 3% BSA in PBS for 1 h at RT. Primary antibodies, diluted in 3% BSA in PBS, were added to the coverslips and incubated in a dark, humidified chamber for 16 h at 4°C. Subsequently, cells were washed three times with 0.1% Triton X-100/PBS and incubated with DAPI and secondary antibodies in 3% BSA in PBS for 1 h at RT. Coverslips were washed three times with PBS and mounted onto glass slides using Prolong Gold antifade. All images were acquired on a deconvolution system (DeltaVision Elite Applied Precision/GE Healthcare) with a x100/1.40 NA UPlanSApo objective (Olympus) using SoftWorx 6.0 software (Applied Precision/GE Healthcare). Images were acquired as z-stacks at 0.2-µm intervals and deconvolved using SoftWoRx. Images were quantified using Fiji.[36] Fluorescence intensities were corrected for background signal and normalized to the average intensity of vehicle-treated cells.

Antibodies: guinea pig anti-CENP-C (1:2000, MBL PD030), mouse anti-tubulin (1:10,000, Sigma T5168), rabbit anti-H2A-p-T120 (1:1000, Active motif 39391), rabbit anti-H3-p-S10 (Millipore 06-570), Alexa Fluor 647 goat anti-guinea pig (1:1000, Invitrogen A21450), Alexa Fluor 568 goat anti-mouse (1:1000, Invitrogen A11031), Alexa Fluor 488 goat anti-rabbit (1:1000, Invitrogen A11034) or DAPI (1:1000, Sigma D9542).

References

1. NCI Dictionary of Cancer Terms. *(accessed in September 2021)* https://www.cancer.gov/publications/dictionaries/cancer-terms/def/cancer.
2. Hanahan, D. & Weinberg, R. A. Hallmarks of Cancer: The Next Generation. *Cell* **144**, 646–674 (2011).
3. Cohen, P., Cross, D. & Jänne, P. A. Kinase drug discovery 20 years after imatinib: progress and future directions. *Nat. Rev. Drug Discov.* **20**, 551–569 (2021).
4. Musacchio, A. & Salmon, E. D. The spindle-assembly checkpoint in space and time. *Nat. Rev. Mol. Cell Biol.* **8**, 379–393 (2007).
5. Dominguez-Brauer, C., Thu, K. L., Mason, J. M., Blaser, H., Bray, M. R. & Mak, T. W. Targeting Mitosis in Cancer: Emerging Strategies. *Mol. Cell* **60**, 524–536 (2015).
6. Kops, G. J. P. L., Weaver, B. A. A. & Cleveland, D. W. On the road to cancer: aneuploidy and the mitotic checkpoint. *Nat. Rev. Cancer* **5**, 773–785 (2005).
7. Mason, J. M., Wei, X., Fletcher, G. C., Kiarash, R., Brokx, R., Hodgson, R., Beletskaya, I., Bray, M. R. & Mak, T. W. Functional characterization of CFI-402257, a potent and selective Mps1/TTK kinase inhibitor, for the treatment of cancer. *Proc. Natl. Acad. Sci.* **114**, 3127–3132 (2017).
8. Wengner, A. M., Siemeister, G., Koppitz, M., Schulze, V., Kosemund, D., Klar, U., Stoeckigt, D., Neuhaus, R., Lienau, P., Bader, B., Prechtl, S., Raschke, M., Frisk, A.-L., von Ahsen, O., Michels, M., Kreft, B., von Nussbaum, F., Brands, M., Mumberg, D. & Ziegelbauer, K. Novel Mps1 Kinase Inhibitors with Potent Antitumor Activity. *Mol. Cancer Ther.* **15**, 583–592 (2016).
9. Anderhub, S. J., Mak, G. W.-Y., Gurden, M. D., Faisal, A., Drosopoulos, K., Walsh, K., Woodward, H. L., Innocenti, P., Westwood, I. M., Naud, S., Hayes, A., Theofani, E., Filosto, S., Saville, H., Burke, R., van Montfort, R. L. M., Raynaud, F. I., Blagg, J., Hoelder, S., Eccles, S. A. & Linardopoulos, S. High Proliferation Rate and a Compromised Spindle Assembly Checkpoint Confers Sensitivity to the MPS1 Inhibitor BOS172722 in Triple-Negative Breast Cancers. *Mol. Cancer Ther.* **18**, 1696–1707 (2019).
10. Kusakabe, K., Ide, N., Daigo, Y., Itoh, T., Yamamoto, T., Hashizume, H., Nozu, K., Yoshida, H., Tadano, G., Tagashira, S., Higashino, K., Okano, Y., Sato, Y., Inoue, M., Iguchi, M., Kanazawa, T., Ishioka, Y., Dohi, K., Kido, Y., Sakamoto, S., Ando, S., Maeda, M., Higaki, M., Baba, Y. & Nakamura, Y. Discovery of Imidazo[1,2- *b*]pyridazine Derivatives: Selective and Orally Available Mps1 (TTK) Kinase Inhibitors Exhibiting Remarkable Antiproliferative Activity. *J. Med. Chem.* **58**, 1760–1775 (2015).
11. Martinez, R., Blasina, A., Hallin, J. F., Hu, W., Rymer, I., Fan, J., Hoffman, R. L., Murphy, S., Marx, M., Yanochko, G., Trajkovic, D., Dinh, D., Timofeevski, S., Zhu, Z., Sun, P., Lappin, P. B. & Murray, B. W. Mitotic Checkpoint Kinase Mps1 Has a Role in Normal Physiology which Impacts Clinical Utility. *PLOS ONE* **10**, e0138616 (2015).
12. Maia, A. R. R., de Man, J., Boon, U., Janssen, A., Song, J.-Y., Omerzu, M., Sterrenburg, J. G., Prinsen, M. B. W., Willemsen-Seegers, N., de Roos, J. A. D. M., van Doornmalen, A. M., Uitdehaag, J. C. M., Kops, G. J. P. L., Jonkers, J., Buijsman, R. C., Zaman, G. J. R. & Medema, R. H. Inhibition of the spindle assembly checkpoint kinase TTK enhances the efficacy of docetaxel in a triple-negative breast cancer model. *Ann. Oncol.* **26**, 2180–2192 (2015).
13. Schulze, V. K., Klar, U., Kosemund, D., Wengner, A. M., Siemeister, G., Stöckigt, D., Neuhaus, R., Lienau, P., Bader, B., Prechtl, S., Holton, S. J., Briem, H., Marquardt, T., Schirok, H., Jautelat, R., Bohlmann, R., Nguyen, D., Fernández-Montalván, A. E., Bömer, U., Eberspaecher, U., Brüning, M., Döhr, O., Raschke, M., Kreft, B., Mumberg, D., Ziegelbauer, K., Brands, M., von Nussbaum, F. & Koppitz, M. Treating Cancer by Spindle Assembly Checkpoint Abrogation: Discovery of Two Clinical Candidates, BAY 1161909 and BAY 1217389, Targeting MPS1 Kinase. *J. Med. Chem.* **63**, 8025–8042 (2020).
14. Markman, M. Managing taxane toxicities. *Support. Care Cancer* **11**, 144–147 (2003).
15. Hopkins, A. L., Keserü, G. M., Leeson, P. D., Rees, D. C. & Reynolds, C. H. The role of ligand efficiency metrics in drug discovery. *Nat. Rev. Drug Discov.* **13**, 105–121 (2014).
16. Taylor, S. S. & Kornev, A. P. Protein kinases: evolution of dynamic regulatory proteins. *Trends Biochem. Sci.* **36**, 65–77 (2011).
17. Roskoski, R. Classification of small molecule protein kinase inhibitors based upon the structures of their drug-enzyme complexes. *Pharmacol. Res.* **103**, 26–48 (2016).
18. Shindo, N., Fuchida, H., Sato, M., Watari, K., Shibata, T., Kuwata, K., Miura, C., Okamoto, K., Hatsuyama, Y., Tokunaga, K., Sakamoto, S., Morimoto, S., Abe, Y., Shiroishi, M., Caaveiro, J. M. M., Ueda, T., Tamura, T., Matsunaga, N., Nakao, T., Koyanagi, S., Ohdo, S., Yamaguchi, Y., Hamachi, I., Ono, M. & Ojida, A. Selective and reversible modification of kinase cysteines with chlorofluoroacetamides. *Nat. Chem. Biol.* **15**, 250–258 (2019).
19. Siemeister, G., Mengel, A., Fernández-Montalván, A. E., Bone, W., Schröder, J., Zitzmann-Kolbe, S., Briem, H., Prechtl, S., Holton, S. J., Mönning, U., von Ahsen, O., Johanssen, S., Cleve, A., Pütter, V., Hitchcock, M., von Nussbaum, F., Brands, M., Ziegelbauer, K. & Mumberg, D. Inhibition of BUB1 Kinase by BAY 1816032 Sensitizes Tumor Cells toward Taxanes, ATR, and PARP Inhibitors *In Vitro* and *In Vivo*. *Clin. Cancer Res.* **25**, 1404–1414 (2019).
20. Singh, J., Petter, R. C., Baillie, T. A. & Whitty, A. The resurgence of covalent drugs. *Nat. Rev. Drug Discov.* **10**, 307–317 (2011).

21. Kwak, E. L., Sordella, R., Bell, D. W., Godin-Heymann, N., Okimoto, R. A., Brannigan, B. W., Harris, P. L., Driscoll, D. R., Fidias, P., Lynch, T. J., Rabindran, S. K., McGinnis, J. P., Wissner, A., Sharma, S. V., Isselbacher, K. J., Settleman, J. & Haber, D. A. Irreversible inhibitors of the EGF receptor may circumvent acquired resistance to gefitinib. *Proc. Natl. Acad. Sci. U. S. A.* **102**, 7665 (2005).
22. Yun, C.-H., Mengwasser, K. E., Toms, A. V., Woo, M. S., Greulich, H., Wong, K.-K., Meyerson, M. & Eck, M. J. The T790M mutation in EGFR kinase causes drug resistance by increasing the affinity for ATP. *Proc. Natl. Acad. Sci.* **105**, 2070–2075 (2008).
23. Kawashima, S. A., Yamagishi, Y., Honda, T., Ishiguro, K. & Watanabe, Y. Phosphorylation of H2A by Bub1 Prevents Chromosomal Instability Through Localizing Shugoshin. *Science* **327**, 172–177 (2010).
24. McGuinness, B. E., Anger, M., Kouznetsova, A., Gil-Bernabé, A. M., Helmhart, W., Kudo, N. R., Wuensche, A., Taylor, S., Hoog, C., Novak, B. & Nasmyth, K. Regulation of APC/C Activity in Oocytes by a Bub1-Dependent Spindle Assembly Checkpoint. *Curr. Biol.* **19**, 369–380 (2009).
25. Perera, D. & Taylor, S. S. Sgo1 establishes the centromeric cohesion protection mechanism in G2 before subsequent Bub1-dependent recruitment in mitosis. *J. Cell Sci.* **123**, 653–659 (2010).
26. Klebig, C., Korinth, D. & Meraldi, P. Bub1 regulates chromosome segregation in a kinetochore-independent manner. *J. Cell Biol.* **185**, 841–858 (2009).
27. Ricke, R. M., Jeganathan, K. B., Malureanu, L., Harrison, A. M. & van Deursen, J. M. Bub1 kinase activity drives error correction and mitotic checkpoint control but not tumor suppression. *J. Cell Biol.* **199**, 931–949 (2012).
28. Scott, S. J., Suvarna, K. S. & D'Avino, P. P. Synchronization of human retinal pigment epithelial-1 cells in mitosis. *J. Cell Sci.* **133**, jcs247940 (2020).
29. Vassilev, L. T., Tovar, C., Chen, S., Knezevic, D., Zhao, X., Sun, H., Heimbrook, D. C. & Chen, L. Selective small-molecule inhibitor reveals critical mitotic functions of human CDK1. *Proc. Natl. Acad. Sci.* **103**, 10660–10665 (2006).
30. Mayer, T. U. Small Molecule Inhibitor of Mitotic Spindle Bipolarity Identified in a Phenotype-Based Screen. *Science* **286**, 971–974 (1999).
31. Brito, D. A. & Rieder, C. L. Mitotic Checkpoint Slippage in Humans Occurs via Cyclin B Destruction in the Presence of an Active Checkpoint. *Curr. Biol.* **16**, 1194–1200 (2006).
32. Goto, H., Yasui, Y., Nigg, E. A. & Inagaki, M. Aurora-B phosphorylates Histone H3 at serine28 with regard to the mitotic chromosome condensation: H3-Ser28 phosphorylation by Aurora-B. *Genes Cells* **7**, 11–17 (2002).
33. Ditchfield, C., Johnson, V. L., Tighe, A., Ellston, R., Haworth, C., Johnson, T., Mortlock, A., Keen, N. & Taylor, S. S. Aurora B couples chromosome alignment with anaphase by targeting BubR1, Mad2, and Cenp-E to kinetochores. *J. Cell Biol.* **161**, 267–280 (2003).
34. Zhao, Q., Ouyang, X., Wan, X., Gajiwala, K. S., Kath, J. C., Jones, L. H., Burlingame, A. L. & Taunton, J. Broad-Spectrum Kinase Profiling in Live Cells with Lysine-Targeted Sulfonyl Fluoride Probes. *J. Am. Chem. Soc.* **139**, 680–685 (2017).
35. Cravatt, B. F., Wright, A. T. & Kozarich, J. W. Activity-Based Protein Profiling: From Enzyme Chemistry to Proteomic Chemistry. *Annu. Rev. Biochem.* **77**, 383–414 (2008).
36. Schindelin, J., Arganda-Carreras, I., Frise, E., Kaynig, V., Longair, M., Pietzsch, T., Preibisch, S., Rueden, C., Saalfeld, S., Schmid, B., Tinevez, J.-Y., White, D. J., Hartenstein, V., Eliceiri, K., Tomancak, P. & Cardona, A. Fiji: an open-source platform for biological-image analysis. *Nat. Methods* **9**, 676–682 (2012).

Samenvatting

Kanker is de overkoepelende term voor ziektes waarin abnormale cellen delen op een ongecontroleerde manier.[1] Deze cellen kunnen zich ontwikkelen in, en vervolgens verspreiden naar verschillende soorten weefsels. *Hallmarks* van kanker, ofwel de vermogens van een biologisch systeem die worden opgedaan tijdens de ontwikkeling van een tumor, omvatten, maar zijn niet gelimiteerd tot, de constante signalering voor celdeling, het bieden van weerstand tegen celdood en metastase.[2] Daarnaast zijn er karakteristieken die deze *hallmarks* mogelijk maken, zoals genetische instabiliteit.[2] De ontwikkeling van nieuwe anti-kanker medicijnen kan daarom worden gericht op een of meer *hallmarks* van kanker of de karakteristieken die deze *hallmarks* mogelijk maken.[2] Het onderzoek dat wordt beschreven in dit proefschrift omvat verschillende fasen van een geneesmiddelenonderzoek (**Figuur 1**) en is gericht op het ontdekken van kleine moleculen als kinaseremmers voor de behandeling van kanker.

Figuur 1 | Versimpelde weergave van de verschillende fasen van een geneesmiddelenonderzoek.

Het selecteren van een doeleiwit

Eiwitkinasen zijn een prominente klasse doeleiwitten van medicijnen voor de behandeling van kanker.[3] **Hoofdstuk 1** introduceert het eiwitkinase *budding uninhibited by benzimidazole 1* (BUB1) als therapeutisch doeleiwit. BUB1 maakt deel uit van het zogeheten *spindle assembly checkpoint* (SAC), een beveiligingsmechanisme dat correcte chromosoom segregatie verzekert tijdens mitose.[4] Veel kankercellen hebben een verzwakt SAC en de hypothese is dat het verstoren van deze verzwakte controlepunten, om zo SAC signalen te ontwrichten, uiteindelijk resulteert in celdood ten gevolgde van ernstige chromosoom instabiliteit.[5,6] Potentiële kinase doeleiwitten van het SAC omvatten *monopolar spindle 1* (MPS1) en BUB1.[5,6] In het verleden zijn MPS1 remmers ontwikkeld waarvan sommigen in klinische studies zijn onderzocht.[7–9] Echter, verschillende muis xenotransplantatie studies waarin MPS1 remmers als monotherapie werden toegediend, lieten alleen een therapeutische werking zien nabij de maximaal getolereerde dosering.[10–13] Hierdoor was een combinatiebehandeling met taxanen vereist om de gewenste remming van tumorgroei te verkrijgen.[10–13] Nieuwe remmers met goede fysicochemische eigenschappen, welke zorgen voor de cellulaire BUB1 remmer-eiwit interactie (in het Engels: *target engagement*), kunnen mogelijk een therapeutische werking hebben als monotherapie. Dit zou de combinatiebehandeling met taxanen overbodig maken, wat gewenst is gezien het feit dat deze therapeutische middelen voor ernstige bijwerkingen kunnen zorgen.[14] BUB1 is daarom gekozen als doeleiwit voor het ontwikkelen van nieuwe remmers.

Hit identificatie

Hoofdstuk 2 beschrijft de resultaten van een *high-throughput screen* (HTS) die is gebruikt voor het ontdekken van nieuwe BUB1 remmers. Een bibliotheek van 53.408 stoffen, verrijkt met kinaseremmers, is gescreend en dit resulteerde in 214 bevestigde actieve stoffen. Na het deselecteren van stoffen die interfereerden met de meetmethode, en dosis-respons experimenten, werd een lijst verkregen van 25 structureel diverse *hits*. *Hits* **1** en **2** (**Figuur 2**) werden geprioriteerd op basis van gunstige eigenschappen zoals activiteit, molecuulgewicht, ligand efficiëntie, lipofiliciteit en lipofiele efficiëntie.[15] Beide *hits* zijn opnieuw gesynthetiseerd en hun activiteit kon worden bevestigd.

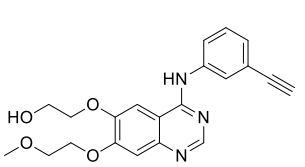

1

pIC_{50} = 6.59
MW = 379
LE = 0.33
cLogP = 2.6
LipE = 4.2

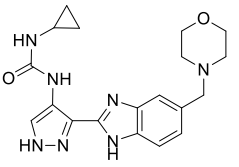

2

pIC_{50} = 6.78
MW = 381
LE = 0.34
cLogP = 0.4
LipE = 6.5

Figuur 2 | Geprioriteerde *hits* **1** en **2** van de *high-throughput screen* en bijbehorende fysicochemische eigenschappen. pIC_{50}: half-maximale inhibitie concentratie van *high-throughput* dosis-respons experiment; MW: molecuulgewicht (g/mol); LE: ligand efficiëntie[15], gedefinieerd als: $\mathrm{LE} = (-RT * \ln(\mathrm{app}.K_i))/\mathrm{HA}$, waar HA staat voor het aantal 'zware atomen' (niet-waterstof atomen); cLogP: LogP berekend door DataWarrior (v.5.2.1); LipE: lipofiele efficiëntie[15], gedefinieerd als: $\mathrm{LipE} = \mathrm{app}.\mathrm{p}K_i - \mathrm{cLogP}$.

Hit-to-lead optimalisatie

In **Hoofdstuk 3** is de structuur-activiteitsrelatie (SAR) van *hit* **1** onderzocht. De synthese en biochemische evaluatie van 48 analoga resulteerde in de identificatie van stof **3** (**Figuur 3**). In vergelijking met *hit* **1** was stof **3** aanzienlijk minder lipofiel en door zijn lichtelijk verbeterde activiteit werd een 10-voudige verbetering behaald met betrekking tot de lipofiele efficiëntie. De gemodelleerde bindingsmodi van stoffen **1** en **3** in het kinasedomein van BUB1 kwamen overeen met de geobserveerde SAR. Daar waar de *quinazoline N*1 van **1** een waterstofbrug vormde met de *backbone* (ruggengraat) van *hinge* (scharnier-) aminozuur Tyr869, werden geen waterstofbruggen vastgesteld met de *hinge* regio in de gemodelleerde bindingsmodus van stof **3**. In plaats daarvan werd een waterstofbrug voorspeld tussen de pyrazool *N*2 en zowel Lys821 als Asp946 en daarnaast ook tussen de pyrimidine *N*1 en Lys821.

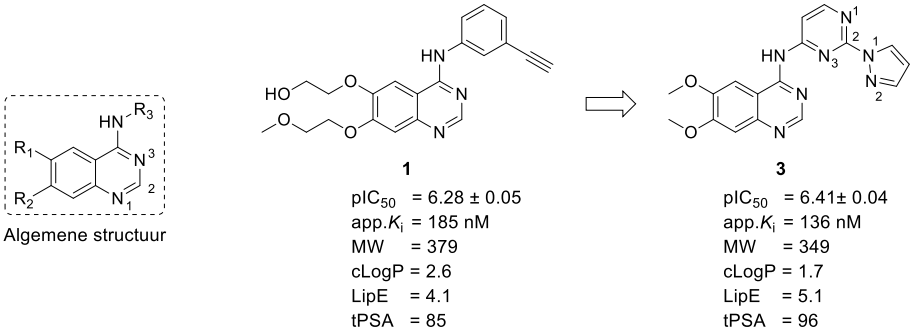

Figuur 3 | Chemische structuren en fysicochemische eigenschappen (zoals gedefinieerd in **Figuur 2**) van *hit* **1** en geoptimaliseerde *hit* **3**. pIC_{50}: half-maximale inhibitie concentratie, bepaald met de biochemische BUB1 assay; tPSA: *topological polar surface area* ($Å^2$), berekend door Chemdraw (v.19.1).

Hoofdstuk 4 beschrijft een uitgebreide structuur-activiteitsrelatie (SAR) studie van *hit* **2**. In totaal zijn er 59 analoga gesynthetiseerd en biochemisch geëvalueerd. Dit resulteerde in gesubstitueerde 2-phenyl-5-methoxy-*N*-(3-(5-(morpholinomethyl)-1*H*-benzo[*d*]imidazol-2-yl)-1*H*-pyrazol-4-yl)pyrimidin-4-amines als zeer actieve BUB1 remmers, waaronder stof **4** (**Figuur 4A**), de meest actieve BUB1 remmer die tot op heden is gerapporteerd. Om de bindingsmodus van **4** te bestuderen, is de kristalstructuur van deze stof in het kinasedomein van BUB1 opgehelderd (**Figuur 4B,C**). Stof **4** bindt in de ATP-*pocket* van BUB1 en laat de regulerende (R)-*spine*[16] intact. Dit geeft aan dat **4** kan worden geclassificeerd als type I remmer.[17] De benzimidazool-pyrazool kern vormt drie waterstofbruggen met de *backbone* van de *hinge* aminozuren Tyr869 en Glu867 van BUB1 (**Figuur 4B**). Een additionele waterstofbrug wordt gevormd tussen de pyrimidine *N*1 en de zijketen van Lys821 welke wordt gemedieerd door een watermolecuul. Verder wordt de morfoline blootgesteld aan het oplosmiddel en de amine tussen de pyrazool en pyrimidine vormt een intramoleculaire waterstofbrug met de stikstof van de benzimidazool. De acetyleen bindt een ruimte welke beschikbaar is door de kleine omvang van het glycine *gatekeeper*-residu van BUB1 (**Figuur 4C**).

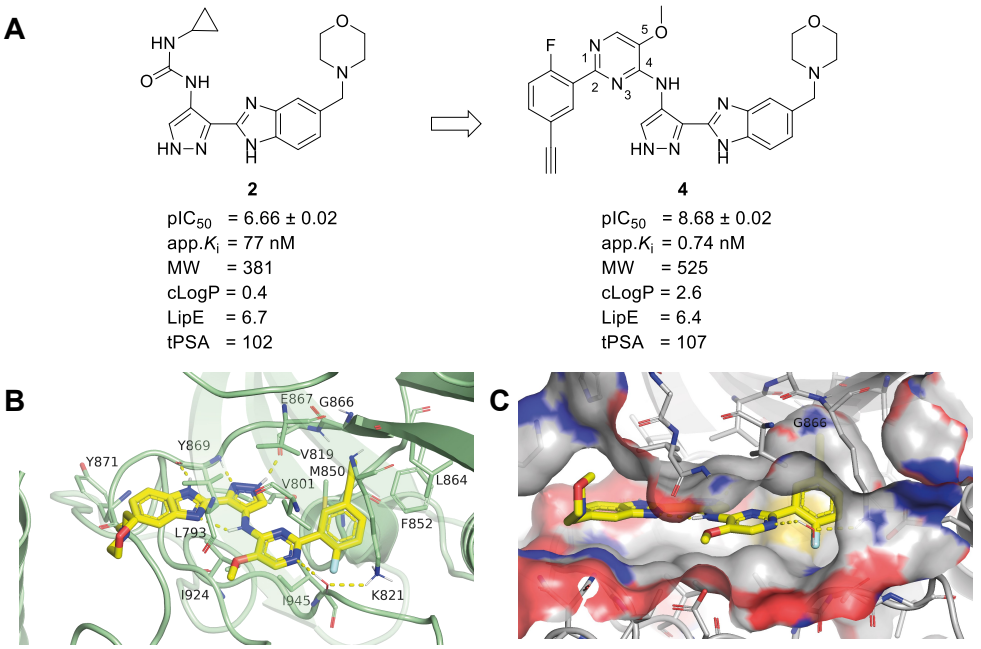

Figuur 4 | *Hit* optimalisatie en kristalstructuur van geoptimaliseerde stof 4 gebonden in het kinasedomein van humaan BUB1. (A) Chemische structuren en fysicochemische eigenschappen (zoals gedefinieerd in **Figuur 3**) van *hit* **2** en geoptimaliseerde stof **4**. **(B)** Kristalstructuur van **4** gebonden in BUB1. Waterstofbruggen zijn gevisualiseerd met stippellijnen (geel) en een watermolecuul is weergegeven als kleine stokjes. β-*sheets* 1–3 zijn semi-transparant voor visualisatiedoeleinden. **(C)** Weergave van de oppervlakken van aminozuren welke zich binnen 8 Å van **4** bevinden.

Hoofdstuk 5 beschrijft de ontwikkeling van een cellulaire methode om BUB1 *target engagement* te meten met behulp van *probe* **5**[18] (**Figuur 5**) en gel-gebaseerde, activiteit-gebaseerde eiwitprofilering (Engels: *activity-based protein profiling*, of ABPP). *Probe* **5** en 16 analoga zijn gesynthetiseerd. Om het labelen van BUB1 te onderzoeken is een U2OS cellijn gegenereerd die GFP-FLAG-BUB1 stabiel tot overexpressie brengt. De labeleigenschappen van alle *probes* werden geëvalueerd in deze cellijn en *probe* **5** liet het meest gunstige labelprofiel zien. Het muteren van Cys1080 naar alanine voorkwam het labelen van BUB1 volledig en liet zien dat dit aminozuur verantwoordelijk is voor het vormen van een covalente binding. Het labelen van BUB1 door *probe* **5** was dosis- en tijdsafhankelijk en het labelen kon dosisafhankelijk worden voorkomen door BUB1 remmer BAY1816032.[19] Dit gaf *proof-of-principle* voor het gebruik van **5** als BUB1 chemische *probe* welke het onderzoeken van BUB1 *target engagement* mogelijk maakt, gebruikmakend van gel-gebaseerde ABPP.

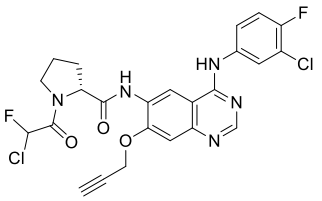

5

Figuur 5 | Chemische structuur van *probe* **5**.[18]

Hoofdstuk 6 focust op de verdere profilering van een aantal van de gesubstitueerde 2-phenyl-5-methoxy-*N*-(3-(5-(morpholinomethyl)-1*H*-benzo[*d*]imidazol-2-yl)-1*H*-pyrazol-4-yl)pyrimidin-4-amine BUB1 remmers die in **Hoofdstuk 4** zijn geïdentificeerd om hun potentieel als *lead* kandidaat voor therapeutische doeleinden te onderzoeken. Hiertoe is de *drug-likeness* ('medicijn-gelijkenis') onderzocht door middel van verschillende *in vitro* absorptie, verdeling, metabolisme en uitscheiding (Engels: *absorption, distribution, metabolism and excretion*, of ADME) *assays*. Daarnaast is cellulaire BUB1 *target engagement* onderzocht, gebruikmakend van de methode die is ontwikkeld zoals beschreven in **Hoofdstuk 5**. Er werd een sterke correlatie gevonden tussen de biochemische pIC_{50} waarden en BUB1 *target engagement* (Pearson's r: 0.921, *p*-waarde: 0.0004). Dit suggereerde dat de cel permeabiliteit van de stoffen die werden getest vergelijkbaar was en dat *target engagement* voornamelijk werd beïnvloed door de affiniteit voor BUB1. Verder werden de effecten op proliferatie van U2OS cellen onderzocht door middel van Sulforhodamine B (SRB) *assays*. Deze *assays* werden uitgevoerd met en zonder een lage dosis van paclitaxel om een potentieel synergistisch effect te onderzoeken tussen het remmen van BUB1 en paclitaxel.[19] Een minder sterke correlatie werd gevonden tussen BUB1 *target engagement* en de pIC_{50} waarden van de SRB *assays* (Pearson's r: 0.655, *p*-waarde: 0.056). Dit suggereerde dat de remming van proliferatie van cellen grotendeels afhankelijk is van BUB1 remming, maar dat *off-target* activiteit bijdraagt aan het geobserveerde effect. ROB433 (**6**) en ROB464 (**7**) lieten het meest gunstige profiel zien (**Figuur 6**, **Tabel 1**) met goede fysicochemische eigenschappen, subnanomolaire affiniteit voor BUB1, goede cellulaire BUB1 *target engagement* en een acceptabel *in vitro* ADME-profiel. De kinase selectiviteit van beiden stoffen is daarom onderzocht. Op een concentratie van 100 nM waren ROB433 en ROB464 selectief over 346 en 352 kinasen, respectievelijk, terwijl 49 (ROB433) en 44 (ROB464) kinasen werden gedetecteerd als *off-target*. Tot slot zijn de antiproliferatieve effecten van ROB433 (**6**) onderzocht in een screen op 102 kankercellijnen. De concentratie die benodigd was om half-maximale remming van celgroei te bereiken (GI_{50}) varieerde van 101 nM (voor KG-1 cellen) tot 5,57 µM (voor THP-1 cellen). De gemiddelde GI_{50}-waarde van alle cellijnen was 1.43 µM. Dit gaf aan dat ROB433 een gunstig cytotoxiciteitsprofiel heeft.

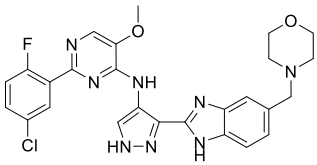

ROB433 (**6**)

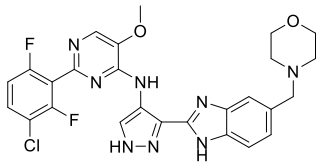

ROB464 (**7**)

Figuur 6 | Chemische structuren van ROB433 (**6**) en ROB464 (**7**).

Tabel 1 | Overzicht van fysicochemische eigenschappen (zoals gedefinieerd in **Figuur 3**), ADME eigenschappen, oplosbaarheid in water en activiteiten van *lead* stoffen ROB433 (**6**) en ROB464 (**7**).

	ROB433	**ROB464**		**ROB433**	**ROB464**
Biochemische activiteit (pIC_{50} ± SEM)	8.57 ± 0.02	8.62 ± 0.03	***Target engagement*** (pTE_{50} ± SEM)	7.50 ± 0.11	8.01 ± 0.09
Apparent K_i (nM)	0.94	0.84	**Proliferatie U2OS cellen** (pIC_{50} ± SEM)	6.32 ± 0.06	7.39 ± 0.05
Molecuulgewicht (g/mol)	535	553	**Plasma stabiliteit** (% restant na 180 min)	100 (h)* 100 (r)* 85 (m)*	100 (h) 100 (r)
cLogP	3.1	3.2	**Microsomale stabiliteit** ($t_{1/2}$ in min)	41 (h) 63 (r) 22 (m)	29 (h) 49 (r) 6.1 (m)
LipE	5.9	5.8	**Microsomale klaring** (µL/min/mg)	8.4 (h) 22 (r) 16 (m)	12 (h) 28 (r) 57 (m)
tPSA ($Å^2$)	107	107	**Plasma eiwitbinding** (%)	100 (h) 100 (r) 99.9 (m)	99.7 (h) 99.7 (r)
			Oplosbaarheid in water (µM)	4.4	6.0

* (h): humaan, (r): rat, (m): muis

Tot slot

Onderzoek dat gericht is op het identificeren van nieuwe *targets* voor de behandeling van kanker groeit en kleine moleculen als kinase remmers vervullen een belangrijke rol in dit proces. Het onderzoek dat is beschreven in dit proefschrift heeft geleid tot twee *lead* remmers (ROB433 en ROB464) van het *spindle assembly checkpoint* kinase BUB1 en een *assay* voor het meten van cellulaire BUB1 *target engagement*. Het bepalen van cellulaire BUB1 bezetting, gebruikmakend van de methode die is beschreven in **Hoofdstuk 5**, zal een belangrijk hulpmiddel zijn voor de toekomstige ontwikkeling van BUB1 remmers. Daarnaast bevat de reeks van gesubstitueerde 2-phenyl-5-methoxy-*N*-(3-(5-(morpholinomethyl)-1*H*-benzo[*d*]imidazol-2-yl)-1*H*-pyrazol-4-yl)pyrimidin-4-amines uit **Hoofdstuk 4** de meest actieve BUB1 remmers die tot op heden zijn beschreven. ROB433 en ROB464, als onderdeel van deze reeks, bezitten uitstekende eigenschappen, waaronder het remmen van de groei van kankercellen als mono-behandeling. Dit staat toe om de farmacokinetische en farmacodynamische eigenschappen van deze stoffen verder *in vivo* te onderzoeken. Beide stoffen laten potentieel zien als therapeutische toepassing voor de behandeling van

kankersoorten die op dit moment geen moleculair *target* hebben, zoals triple-negatieve borstkanker.

Bronnen

1. NCI Dictionary of Cancer Terms. *(accessed in September 2021)* https://www.cancer.gov/publications/dictionaries/cancer-terms/def/cancer.
2. Hanahan, D. & Weinberg, R. A. Hallmarks of Cancer: The Next Generation. *Cell* **144**, 646–674 (2011).
3. Cohen, P., Cross, D. & Jänne, P. A. Kinase drug discovery 20 years after imatinib: progress and future directions. *Nat. Rev. Drug Discov.* **20**, 551–569 (2021).
4. Musacchio, A. & Salmon, E. D. The spindle-assembly checkpoint in space and time. *Nat. Rev. Mol. Cell Biol.* **8**, 379–393 (2007).
5. Dominguez-Brauer, C., Thu, K. L., Mason, J. M., Blaser, H., Bray, M. R. & Mak, T. W. Targeting Mitosis in Cancer: Emerging Strategies. *Mol. Cell* **60**, 524–536 (2015).
6. Kops, G. J. P. L., Weaver, B. A. A. & Cleveland, D. W. On the road to cancer: aneuploidy and the mitotic checkpoint. *Nat. Rev. Cancer* **5**, 773–785 (2005).
7. Mason, J. M., Wei, X., Fletcher, G. C., Kiarash, R., Brokx, R., Hodgson, R., Beletskaya, I., Bray, M. R. & Mak, T. W. Functional characterization of CFI-402257, a potent and selective Mps1/TTK kinase inhibitor, for the treatment of cancer. *Proc. Natl. Acad. Sci.* **114**, 3127–3132 (2017).
8. Wengner, A. M., Siemeister, G., Koppitz, M., Schulze, V., Kosemund, D., Klar, U., Stoeckigt, D., Neuhaus, R., Lienau, P., Bader, B., Prechtl, S., Raschke, M., Frisk, A.-L., von Ahsen, O., Michels, M., Kreft, B., von Nussbaum, F., Brands, M., Mumberg, D. & Ziegelbauer, K. Novel Mps1 Kinase Inhibitors with Potent Antitumor Activity. *Mol. Cancer Ther.* **15**, 583–592 (2016).
9. Anderhub, S. J., Mak, G. W.-Y., Gurden, M. D., Faisal, A., Drosopoulos, K., Walsh, K., Woodward, H. L., Innocenti, P., Westwood, I. M., Naud, S., Hayes, A., Theofani, E., Filosto, S., Saville, H., Burke, R., van Montfort, R. L. M., Raynaud, F. I., Blagg, J., Hoelder, S., Eccles, S. A. & Linardopoulos, S. High Proliferation Rate and a Compromised Spindle Assembly Checkpoint Confers Sensitivity to the MPS1 Inhibitor BOS172722 in Triple-Negative Breast Cancers. *Mol. Cancer Ther.* **18**, 1696–1707 (2019).
10. Kusakabe, K., Ide, N., Daigo, Y., Itoh, T., Yamamoto, T., Hashizume, H., Nozu, K., Yoshida, H., Tadano, G., Tagashira, S., Higashino, K., Okano, Y., Sato, Y., Inoue, M., Iguchi, M., Kanazawa, T., Ishioka, Y., Dohi, K., Kido, Y., Sakamoto, S., Ando, S., Maeda, M., Higaki, M., Baba, Y. & Nakamura, Y. Discovery of Imidazo[1,2- *b*]pyridazine Derivatives: Selective and Orally Available Mps1 (TTK) Kinase Inhibitors Exhibiting Remarkable Antiproliferative Activity. *J. Med. Chem.* **58**, 1760–1775 (2015).
11. Martinez, R., Blasina, A., Hallin, J. F., Hu, W., Rymer, I., Fan, J., Hoffman, R. L., Murphy, S., Marx, M., Yanochko, G., Trajkovic, D., Dinh, D., Timofeevski, S., Zhu, Z., Sun, P., Lappin, P. B. & Murray, B. W. Mitotic Checkpoint Kinase Mps1 Has a Role in Normal Physiology which Impacts Clinical Utility. *PLOS ONE* **10**, e0138616 (2015).
12. Maia, A. R. R., de Man, J., Boon, U., Janssen, A., Song, J.-Y., Omerzu, M., Sterrenburg, J. G., Prinsen, M. B. W., Willemsen-Seegers, N., de Roos, J. A. D. M., van Doornmalen, A. M., Uitdehaag, J. C. M., Kops, G. J. P. L., Jonkers, J., Buijsman, R. C., Zaman, G. J. R. & Medema, R. H. Inhibition of the spindle assembly checkpoint kinase TTK enhances the efficacy of docetaxel in a triple-negative breast cancer model. *Ann. Oncol.* **26**, 2180–2192 (2015).
13. Schulze, V. K., Klar, U., Kosemund, D., Wengner, A. M., Siemeister, G., Stöckigt, D., Neuhaus, R., Lienau, P., Bader, B., Prechtl, S., Holton, S. J., Briem, H., Marquardt, T., Schirok, H., Jautelat, R., Bohlmann, R., Nguyen, D., Fernández-Montalván, A. E., Bömer, U., Eberspaecher, U., Brüning, M., Döhr, O., Raschke, M., Kreft, B., Mumberg, D., Ziegelbauer, K., Brands, M., von Nussbaum, F. & Koppitz, M. Treating Cancer by Spindle Assembly Checkpoint Abrogation: Discovery of Two Clinical Candidates, BAY 1161909 and BAY 1217389, Targeting MPS1 Kinase. *J. Med. Chem.* **63**, 8025–8042 (2020).
14. Markman, M. Managing taxane toxicities. *Support. Care Cancer* **11**, 144–147 (2003).
15. Hopkins, A. L., Keserü, G. M., Leeson, P. D., Rees, D. C. & Reynolds, C. H. The role of ligand efficiency metrics in drug discovery. *Nat. Rev. Drug Discov.* **13**, 105–121 (2014).
16. Taylor, S. S. & Kornev, A. P. Protein kinases: evolution of dynamic regulatory proteins. *Trends Biochem. Sci.* **36**, 65–77 (2011).
17. Roskoski, R. Classification of small molecule protein kinase inhibitors based upon the structures of their drug-enzyme complexes. *Pharmacol. Res.* **103**, 26–48 (2016).
18. Shindo, N., Fuchida, H., Sato, M., Watari, K., Shibata, T., Kuwata, K., Miura, C., Okamoto, K., Hatsuyama, Y., Tokunaga, K., Sakamoto, S., Morimoto, S., Abe, Y., Shiroishi, M., Caaveiro, J. M. M., Ueda, T., Tamura, T., Matsunaga, N., Nakao, T., Koyanagi, S., Ohdo, S., Yamaguchi, Y., Hamachi, I., Ono, M. & Ojida, A. Selective and reversible modification of kinase cysteines with chlorofluoroacetamides. *Nat. Chem. Biol.* **15**, 250–258 (2019).
19. Siemeister, G., Mengel, A., Fernández-Montalván, A. E., Bone, W., Schröder, J., Zitzmann-Kolbe, S., Briem, H., Prechtl, S., Holton, S. J., Mönning, U., von Ahsen, O., Johanssen, S., Cleve, A., Pütter, V., Hitchcock, M., von Nussbaum, F., Brands, M., Ziegelbauer, K. & Mumberg, D. Inhibition of BUB1 Kinase by BAY 1816032 Sensitizes Tumor Cells toward Taxanes, ATR, and PARP Inhibitors *In Vitro* and *In Vivo*. *Clin. Cancer Res.* **25**, 1404–1414 (2019).

List of publications

Patent

4-Substituted (1*H*-benzo[*d*]imidazol-2-yl)-1*H*-pyrazoles as BUB1 inhibitors useful for treating cancers

R.E.J. Bosman, C.A.A. van Boeckel, R.C. Buijsman, A.P.A. de Man, M. van der Stelt. EP22178710.4. Filing date: June 13, **2022**.

Curriculum Vitae

Rob Bosman was born on January 30th, 1993 in Delft, The Netherlands. He obtained his high school diploma (pre-university level, VWO) from the Stanislascollege Westplantsoen in Delft in 2011. He subsequently started his studies for a bachelor's degree in Molecular Science and Technology at Leiden University and Delft University of Technology. After a minor "Modern Drug Discovery" (Leiden University), he performed a research internship titled "*Development of β1i- and β5i-specific proteasome inhibitors*" in the Bio-organic Synthesis group at Leiden University. The bachelor's degree was obtained in 2014.

The same year, he started the master's program Chemistry with a specialization in "Research in Chemistry". As part of his master's program, he performed a research internship in the Molecular Physiology group at Leiden University, under the supervision of prof. dr. M. van der Stelt. This research, titled "*Development of NAPE-like photoaffinity probes for labeling NAPE-PLD*", was focused on the synthesis and biochemical evaluation of NAPE-PLD substrate-based probes using diazirines as photoactivatable groups. In 2016, Rob obtained his master's degree.

In October 2016, he started his doctoral studies in the Molecular Physiology group at Leiden University under the supervision of prof. dr. M. van der Stelt and prof. dr. C.A.A. van Boeckel. The research described in this thesis was performed in collaboration with Dr. R.C. Buijsman of Netherlands Translational Research Center (NTRC). NWO, Topsector Chemie (TKI-project 'OncoDrugs') and Oncode Institute are kindly acknowledged for financial support.

Parts of the research described in this thesis were orally presented at CHAINS (online, 2020) and the Oncode Institute Annual Scientific Meeting (NL, 2020). Posters were presented at CHAINS (NL, 2017-2019).

Dankwoord

Als onderzoek een sport zou zijn, dan is onderzoek zonder twijfel een teamsport. Wat mij betreft halen samenwerkingen met teams van verschillende disciplines het beste in een onderzoek naar boven. Daarnaast is de directe omgeving waarin een onderzoeker zich verkeerd tijdens het onderzoekstraject een belangrijke factor voor zijn/haar motivatie. Ik wil hierbij dan ook een aantal mensen bedanken die hebben bijgedragen aan de totstandkoming van dit proefschrift (in de hoop niemand te zijn vergeten 😊).

Allereerst wil ik *Mario van der Stelt* bedanken. *Mario*, jij hebt mij de mogelijkheid gegeven om te doen wat ik het leukste vind: onderzoek doen gericht op het ontwikkelen van nieuwe geneesmiddelen. Ik waardeer de vrijheid die ik heb gekregen om mijn eigen ideeën uit te werken en jij stuurde bij waar nodig. Daarnaast wil ik je bedanken voor de goede feedback die je had op posters, presentaties en mijn proefschrift, dit heeft in mijn optiek altijd waardevolle verbeteringen opgeleverd. *Stan van Boeckel*, ook jou wil ik bedanken. Met jouw input en geweldige humor was jij een waardevolle toevoeging tijdens onze werkbesprekingen.

Het project dat is beschreven in dit proefschrift is vanaf het begin af aan in nauwe samenwerking uitgevoerd met Netherlands Translational Research Center (NTRC). Allereerst wil ik mijn co-promotor *Rogier Buijsman* bedanken. Vanaf onze eerste ontmoeting, heb ik onze samenwerking altijd als zeer prettig ervaren. Je jarenlange ervaring in het veld hebben een belangrijke bijdrage geleverd aan het project. Daarnaast heeft NTRC op diverse vlakken bijgedragen aan dit project. *Jos de Man* en *Joost Uitdehaag*, bedankt voor jullie bijdrage aan de werkbesprekingen, onder meer over synthese en kristallografische data. *Diep Vu*, bedankt voor het meten van diverse ADME en oplosbaarheid assays en *Martine Prinsen* bedankt voor het uitvoeren van de Oncolines screen en het ontwikkelen van de biochemische BUB1 assay.

De zoektocht naar nieuwe remmers voor BUB1 begon bij de hit identificatie door middel van een high-throughput screen. *Willemijn Wouters*, bedankt dat je mij heb meegenomen door het hele proces van high-throughput screening in het Pivot Park Screening Centre. Dit proces heeft mij erg gefascineerd en ik vond het een zeer leuke ervaring. *Helma Rutjes* en *Stan van Boeckel*, ook jullie wil ik graag bedanken voor jullie bijdrage aan het uitvoeren van deze screen en het hit selectie proces.

Analyses zijn een belangrijk onderdeel van een onderzoek. Tijdens mijn onderzoek heb ik dan ook veelvuldig gebruik gemaakt van diverse analyseapparatuur. Allereerst wil ik *Hans van den Elst* bedanken. *Hans*, jij hebt er continu voor gezorgd dat het analyse lab in de DE3 vleugel bleef draaien (en dat doe je uiteraard nog steeds). Naast dat je altijd klaar stond om vragen te beantwoorden over alle apparatuur, heb je een belangrijke bijdrage geleverd aan het meten van hoge resolutie massa (HRMS) en het zuiveren van verbindingen. Ook onze niet-wetenschappelijke conversaties heb ik altijd als prettig ervaren. Naast de genoemde

analyses, kan de NMR ook niet ontbreken. *Fons* and *Karthick*, I would like to thank you for your support to me, but also to the students I have supervised.

As mentioned above, the working environment of a researcher is also important. Therefore, I would like to thank all current group members: *Alexander*, *Annemarieke*, *Anthe*, *Berend*, *Daan*, *Floor*, *Frans*, *Hedwich*, *Jeroen*, *Jessica*, *Joel*, *Julia*, *Laura*, *Marnix*, *Mirjam*, *Na*, *Noëlle*, *Stephan*, *Tom*, *Verena*, *Wouter* and *Xinyu*, as well as the former members of our group: *Andrea*, *Annelot*, *Bing*, *Elliot*, *Emanuele*, *Eva*, *Florian*, *Freek*, *Hans den Dulk*, *Hui*, *Juan*, *Kim*, *Marc*, *Marjolein*, *Ming*, *Natascha*, *Patrick*, *Sebastiaan*, *Sebastian*, *Timo* and *Vasu* for creating an amazing atmosphere. I very much appreciate how close we are/have been as a group and greatly enjoyed our countless lunch breaks, coffee breaks, (non-)scientific discussions and parties. You were always willing to help me out and made me really enjoy my work. In addition, I would like to thank all current and former members of the Biosyn group for being part of this great atmosphere. Ook wil ik het ondersteunende personeel bedanken. *Astrid*, *Bobby*, *Jessica*, *Nico*, *Rian* en *Richard*, bedankt voor jullie hulp en ondersteuning. In het bijzonder, *Richard*, bedankt voor het op zeer nauwkeurige wijze controleren van de experimentele hoofdstukken, ik heb dit erg gewaardeerd.

Parts of the research described in this thesis were established through collaborations with people from different labs. I would like to thank *Misbha Ud Din Ahmad*, *Robbie Joosten*, *Patrick Celie*, *Danique Ammerlaan* and *Anastassis Perrakis* from the Netherlands Cancer Institute (NKI) for their contribution to the crystallization studies which are currently exploited for further optimization of the inhibitors. In addition, *Maaike Lambers*, *Carlos Sacristan* and *Geert Kops* from the Hubrecht Institute are kindly acknowledged for their ongoing studies on exploring the effects of ROB433 and ROB464 in living cells. Furthermore, I would like to thank *Alexander Turkin* and *Emil Pot* from the Oncode Institute for their help in the patent application and Oncode Institute itself for funding.

During my PhD research, I supervised a large number of students. *Aukje*, *Bas*, *Bibi*, *Britt*, *Cesar*, *Floran*, *Jessica*, *Joel*, *Julian*, *Kevin*, *Maya*, *Na* and *Titia*, thank you all for your effort during your internships. Your contribution to this research project is very much appreciated.

Tenslotte wil ik mijn ouders, familie en vrienden bedanken voor hun support en interesse in waar ik mij de afgelopen jaren mee bezig heb gehouden. *Syl*, bedankt voor al je geruststellingen, hulp en 'begrip' voor alle lange dagen die ik heb gemaakt. "Ik ben bijna klaar" was eigenlijk nooit echt "bijna", maar gelukkig nam je mij dat vrijwel nooit kwalijk 😊.